DTIC FILE COPY

AD-A214 603

GL-TR-89-0222

SPACECRAFT ENVIRONMENTAL ANOMALIES HANDBOOK

Paul A. Robinson, Jr

Jet Propulsion Laboratory
California Institute of Technology
Mail Station 301-456
4800 Oak Grove Drive
Pasadena, CA 91109

1 August 1989

Final Report
October 1987-August 1989

APPROVED FOR PUBLIC RELEASE; DISTRIBUTION UNLIMITED

DTIC
ELECTE
NOV 24 1989
S B D

GEOPHYSICS LABORATORY
AIR FORCE SYSTEMS COMMAND
UNITED STATES AIR FORCE
HANSCOM AIR FORCE BASE, MASSACHUSETTS 01731-5000

89 11 21 134

REPORT DOCUMENTATION PAGE

Form Approved
OMB No. 0704-0188

Public reporting burden for this collection of information is estimated to average 1 hour per response, including the time for reviewing instructions, searching existing data sources, gathering and maintaining the data needed, and completing and reviewing the collection of information. Send comments regarding this burden estimate or any other aspect of this collection of information, including suggestions for reducing this burden, to Washington Headquarters Services, Directorate for Information Operations and Reports, 1215 Jefferson Davis Highway, Suite 1204, Arlington, VA 22202-4302, and to the Office of Management and Budget, Paperwork Reduction Project (0704-0188), Washington, DC 20503.

1. AGENCY USE ONLY *(Leave blank)*

2. REPORT DATE
1 August 1989

3. REPORT TYPE AND DATES COVERED
Final Report (October 1987–August 1989

4. TITLE AND SUBTITLE
SPACECRAFT ENVIRONMENTAL ANOMALIES HANDBOOK

5. FUNDING NUMBERS
282201AA
PE: 63410F

6. AUTHOR(S)
Paul A. Robinson, Jr

7. PERFORMING ORGANIZATION NAME(S) AND ADDRESS(ES)
Jet Propulsion Laboratory
California Institute of Technology
4800 Oak Grove Drive
Pasadena, CA 91109

8. PERFORMING ORGANIZATION REPORT NUMBER
Contract No.:
NAS-7-918
Task Order RE-182, Amendment 398; Task Plan 81-2472A

9. SPONSORING/MONITORING AGENCY NAME(S) AND ADDRESS(ES)
Geophysics Laboratory
Hanscom AFB, MA 01731

Contract Manager: Allen G. Rubin/PHK

10. SPONSORING/MONITORING AGENCY REPORT NUMBER
GL-TR-89-0222

11. SUPPLEMENTARY NOTES

12a. DISTRIBUTION/AVAILABILITY STATEMENT
APPROVED FOR PUBLIC RELEASE; DISTRIBUTION UNLIMITED

12b. DISTRIBUTION CODE

13. ABSTRACT *(Maximum 200 words)*

Anomalies on spacecraft can be avoided by understanding their mechanisms and causes. This handbook discusses single event upsets (SEUs), surface charging and discharging, and internal or deep dielectric charging along with methods available for the reduction or elimination of the effects they can cause in spacecraft.

Keywords: Integrated Circuits, Anomalies, Space Systems, Radiation hardening, Spacecraft [illegible]

14. SUBJECT TERMS
Spacecraft anomalies
Single-event upsets
Surface charging
Deep dielectric charging

15. NUMBER OF PAGES
293

16. PRICE CODE

17. SECURITY CLASSIFICATION OF REPORT	18. SECURITY CLASSIFICATION OF THIS PAGE	19. SECURITY CLASSIFICATION OF ABSTRACT	20. LIMITATION OF ABSTRACT
UNCLASSIFIED	UNCLASSIFIED	UNCLASSIFIED	

FOREWORD

Allen Rubin, Geophysics Laboratory

Since the earliest spaceflights, spacecraft have been plagued with problems caused by the harsh space energetic particle and hot plasma environments. Some of the sources of spacecraft anomalies have been discovered after years of investigation, and engineering solutions for mitigating the effects of environmental anomalies have been developed. Among the causes of spacecraft anomalies are surface charging and discharges (ESD), internal charging and discharges (ID), and single event upsets (SEU). The present publication brings together information about these three anomaly mechanisms and methods which have been developed to date for avoiding or minimizing their harmful effects.

Space systems are increasingly large and complex, and a greater variety of spacecraft systems are proposed as time goes on. The spacecraft engineer needs to consider these anomaly mechanisms in the design phase, that the increased utilization of space is not unduly hampered by anomalies.

This publication is a contribution to spacecraft engineering which can serve as an introduction to these three anomaly mechanisms.

DTIC COPY INSPECTED 1

Accession For
NTIS GRA&I ☑
DTIC TAB ☐
Unannounced ☐
Justification
By
Distribution/
Availability Codes
Dist | Avail and/or Special
A-1

FOREWORD

Allen Rubin, Geophysics Laboratory

Since the earliest spaceflights, spacecraft have been plagued with problems caused by the harsh space energetic particle and hot plasma environments. Some of the sources of spacecraft anomalies have been discovered after years of investigation, and engineering solutions for mitigating the effects of environmental anomalies have been developed. Among the causes of spacecraft anomalies are surface charging and discharges (ESD), internal charging and discharges (ID), and single event upsets (SEU). The present publication brings together information about these three anomaly mechanisms and methods which have been developed to date for avoiding or minimizing their harmful effects.

Space systems are increasingly large and complex, and a greater variety of spacecraft systems are proposed as time goes on. The spacecraft engineer needs to consider these anomaly mechanisms in the design phase, that the increased utilization of space is not unduly hampered by anomalies.

This publication is a contribution to spacecraft engineering which can serve as an introduction to these three anomaly mechanisms.

DTIC COPY INSPECTED 1

Accession For
NTIS GRA&I ☑
DTIC TAB ☐
Unannounced ☐
Justification
By
Distribution/
Availability Codes
Dist | Avail and/or Special
A-1

There is an old adage which says, "Fool me once shame on you, fool me twice shame on me." For some time now the satellite community has been surprised, if not fooled, by the anomalous behavior satellites have experienced from electrostatic discharge (ESD), internal discharge (ID), and single event upset (SEU) phenomena. Both the frequency and severity of these upsets have been much more troublesome than had been anticipated. Chapter 5 covers but a few of the operational impact problems which have resulted in everything from a mere nuisance to the loss of a multimillion dollar satellite.

For those who design, fabricate, and operate these complex and expensive satellite systems it is time to say, "Yes, we were fooled, but we shall not be shamed, because we are going to design and build our next generation of space assets to be immune to ESD, ID, and SEU upset phenomena."

This will require a dedicated effort on the part of everyone associated with the program. Systems architects, specification writers, mission planners, operations personnel, and all systems contractors must dedicate themselves to the idea that hardness assurance against ESD, ID, and SEU will be an integral part of their efforts. The timeliness of such a commitment is also important, for unless these principles are subscribed to at the outset of a program (with no thought to retrofits), the desired immunity is not likely to be achieved, at least not in a cost-effective way.

Robert Pruett
Radiation Consultants Inc.
October 14, 1987

ABSTRACT

Anomalies on spacecraft can be avoided by understanding their mechanisms and causes. This handbook discusses single event upsets (SEUs),. surface charging and discharging, and internal or deep dielectric charging along with methods available for the reduction or elimination of the effects they can cause in spacecraft.

ACKNOWLEDGMENTS

This text would not have been possible to assemble without the help of a lot of very talented and hard-working people. Among those are:

Billy McCormac, Paul Higbie, and the SEAREC committee for early advice and counsel;
Walther Spjeldvik for contributions on diffusion, and generally helping clarify both the subtle and obvious physics of the magnetosphere;
Myron Mandell and Ira Katz for timely response and expertise in ESD;
Ed Petersen for the use of his SEU material and helpful discussions;
Hank Garrett for sharing his expertise, experience, and encouragement;
Bruce Goldstein and Neil Divine for reviewing the text;
Professor Richard Wolf, Professor Elden Whipple, Ms. Jo Ann Joselyn, Andrei Konradi, Harold Liemohn, John Scarpulla, Carol Underwood, Frank Walker, and Hugh Anderson for providing many constructive criticisms
the large number of people who attended meetings and offered their insight, encouragement, and advice;
Living Video Text for MORE and consulting on the best ways to use it;
Bill Hall, Len Dorsky, and Bob Pruett for being helpful with the editing and structuring of the text and for being easy to work with;
Al Rubin, Col. Johnson, Col. Gaudet, Bill Hall, and Lt. Frushon for working long and hard to coordinate this task and bring it to completion;
Paula Kelly, Andrea Fellows, and Jeanne Collins for technical editing and production; and
Jaime Bermudez for accurately typing, copying, gofering, and expediting the text.

CONTRIBUTORS

William Hall
Ed Daszewski
Walther Spjeldvik
Hank Garrett
E. Hones
Paul Higbie
Members of the staff of AWS (Air Weather Service)
Peter Coakley
Al Vampola
Chris Chu
Myron Mandell
Ed Petersen
Jim Adams
Jim Pickel
Leonard Dorsky
Michael O'Brine
Daniel Wilkinson
Winfred Farthing
Dan Baker
Bob Pruett
Paul Neu
George Davenport
Tod Williamson
Al Whittlesey
Leonard Dorsky
Phil Leung
Gerry Tucker

TABLE OF CONTENTS

1.1. Importance of Engineering for Immunity 1
1.1.1. How a Satellite Failure Leads to SCATHA 1
1.1.2. Costs of a Hardening Program 2
1.1.3. System Test Plans 2
1.1.4. Successful Tests 4
1.2. Structure of this Book 4
1.2.1. Electrostatic Surface Discharges (ESD) -- Chapter 2 4
1.2.2. Internal Discharges -- Chapter 3 6
1.2.3. Single Event Upsets (SEU) -- Chapter 4 9
1.2.4. Anomalies -- Chapter 5 11
1.2.5 Engineering for Immunity -- Chapter 6 12
1.3. The Bottom Line 14

figure	title	page
1-1	Program time line	1-3
1-2	Surface discharges	1-5
1-3	Surface discharge characteristics	1-6
1-4	Internal discharges	1-7
1-5	Internal discharge characteristics	1-8
1-6	Direct ionization single event upset	1-9
1-7	Nuclear reaction induced single event upsets	1-10
1-8	Pain versus rate chart	1-12
1-9	Systems approach	1-13
1-10	Program organization	1-14

table	title	page
1-1	Single event upset causing environments	1-11

2.1. Surface Charging 1
2.1.1 Outline of chapter 2
2.1.2 Definition 2
2.2. Concerns 3
2.3 Charging Mechanism 4
2.3.1 Sheath Formation 5
2.3.2 Plasma Currents 5
2.3.3 Current Balance 5
2.3.4 Distribution functions 10
2.3.5 A Simple Analytic Approximation 11
2.3.6 System Charging Characteristics 12
2.3.6.1 Lumped-Element Modeling 12
2.4. ESD Causing Environments 12
2.4.1 The Regions of the Earth's Magnetosphere 13
2.4.1.1. Bow Shock 14
2.4.1.2. Magnetosheath 15
2.4.1.3. Magnetopause 15
2.4.1.3.1 Magnetopause Currents 15
2.4.1.3.2 Deep Magnetospheric Convection 16
2.4.1.4 Auroral Oval 17
2.4.1.4.1 Auroral Morphology -- contributed by Captain Robert Frederick, Air Weather Service 18
2.4.1.4.2 Auroral Substorms -- contributed by Captain Robert Frederick, Air Weather Service 19
2.4.1.5. Magnetotail 20
2.4.1.6. Neutral Sheet 20
2.4.1.7. Plasma Sheet 21
2.4.1.8. Plasmasphere 21
2.4.1.9. Ring Current 22
2.4.1.10. Radiation Belts 24
2.4.1.11. Currents in the Ionosphere -- contributed by Captain Robert Frederick, Air Weather Service 24
2.4.2 Geomagnetic Storms -- contributed by Captain Robert Frederick, Air Weather Service 25
2.4.2.1 Geomagnetic Indices 25
2.4.2.1.1. Dst Index 28
2.4.2.1.2. Q Index 28
2.4.2.1.3. The A and K Indices 28
2.4.2.1.3.1. AE Index 29
2.4.2.1.3.2. Ap Index 29
2.4.2.1.3.3. K, Kp Index 29
2.4.2.2 The Use of Indices 29
2.4.2.3 The Substorm Mechanism 30
2.4.2.3.1 Substorms -- contributed by E. Hones, Los Alamos National Laboratory 30
2.4.2.4 Engineering Models 32
2.4.2.4.1 Stevens' Model 32
2.4.2.4.2 Worst case Models 34
2.4.3 Spacecraft Role 36
2.5 System Discharging Characteristics 36
2.5.1 Discharge Models 37
2.5.2. Criteria for Breakdown 38
2.6 Other Plasma Interactions 40
2.6.1. Ram and Wake Effects 40
2.6.2 Radio Distortion in the Sheath 41
2.6.3 Collision Induced Ionization 41
2.6.4 Biased Surfaces 42
2.6.5 Torques and Induced Fields 44
2.7 Summary 44

figure	title	page
2-1	Spacecraft charging	2-2
2-2	Secondary electron yield	2-7
2-3	Map of the magnetosphere	2-14
2-4	Lobed structure of the magnetopshere	2-16
2-5	Plasma flows in the equatoral plane	2-17
2-6	Auroral electron intensity	2-20
2-7	The plasmasphere	2-21
2-8	Evening buldge	2-22
2-9	Geomagnetic index calculation	2-26
2-10	Plasmasheet during substorm	2-31
2-11	Steven's model	2-33
2-12	Gaseous discharges	2-38
2-13	Paschen curve	2-43

Table	title	page
2-1	Secondary emission	2-8
2-2	Photoemission	2-9
2-3	Radiation Induced Conductivity	2-10
2-4	Collision frequencies	2-18
2-5	Indices	2-27
2-6	Design environments	2-32
2-7	Worse case -- Purvis	2-34
2-8	Worse case -- pitch angle	2-34
2-9	Worse case -- perpendicular	2-35
2-10	Worse case -- least squares	2-35
2-11	Discharge models	2-37

3.1 Internal Discharges 1
3.1.1. Penetration of Electrons to Interior of Spacecraft 3
3.1.1.1. Energy Loss by Electrons 3
3.1.1.2. Electron Range, Effect of Shielding 4
3.1.2 Charge Buildup 5
3.1.2.1 Charge Leakage 6
3.1.2.2 Material Charging 7
3.1.2.3. Currents in Electrets 8
3.1.3 Maxwell-Wagner Effect 9
3.1.4 An Example -- Teflon Characteristics 9
3.2. Experimental Rates 9
3.3 Discharge Process 14
3.3.1. Buried Charge Breakdowns 15
3.3.2 Minimum Discharge 15
3.3.3 Electrode Geometry 16
3.4. Calculation of Internal Discharge Rates 17
3.4.1. Discharge Rate Depends on Incident Flux 19
3.4.2. Experimental Discharge Rates 20
3.5. Coupling to Sensitive Circuits 21
3.6. ID Causing Environments 22
3.7. Summary 25

figure	title	page
3-1	Internal charging and discharging	3-2
3-2	Stopping power of electrons	3-4
3-3	Fractional energy loss for electrons	3-4
3-4	Electron range	3-5
3-5	Electrets	3-7
3-6	Paschen curve	3-16
3-7	Internal discharge configurations	3-17
3-8	Internal discharge characteristics	3-18
3-9	Ohms law materials	3-19
3-10	Discharge rate versus flux	3-20
3-11	Laboratory simulation	3-22
3-12	Natural environments	3-23

table	title	page
3-1	Resistivity	3-11
3-2	Time to discharge	3-18
3-3	Measured pulses	3-21
3-4	Charging times	3-24

4.1. Single Event Upsets (SEUs) Due to Heavy Ions 1
4.1.1. Early History -- (Contributed by E. Petersen, NRL) 3
4.1.2. Basic Mechanism 3
4.1.3. Linear Energy Transfer (LET) 5
4.1.4. Charge Required for SEU 6
4.1.5. LET and Range 11
4.1.6. Funnelling 11
4.1.7. Current Pulse 12
4.1.8. Advancing Technology 13
4.1.9. Upset Mechanisms -- Circuit Analysis 14
4.1.9.1. Charge Storage and Dynamic RAM 15
4.1.9.2. Voltage Storage 16
4.1.9.3. Current Steering and I2L 18
4.2 Calculation of SEU Rate 18
4.2.1. Integral for Heinrich Curve 22
4.2.1.1 Environments of Concern 22
4.2.1.1.1 Cosmic Radiation 23
4.2.1.1.1.1 Universal Abundance 23
4.2.1.1.1.2 Cosmic Ray Abundance 25
4.2.1.1.1.3. Hydrogen Spectrum 27
4.2.1.1.1.4. Helium Spectra 27
4.2.1.1.1.5. Extension to Other Elements 28
4.2.1.1.1.6. The Adams Model 29
4.2.1.1.1.7. Variation With Distance From the Sun 32
4.2.1.1.2 Heavy Ions in Planetary Radiation Belts 33
4.2.1.1.2.1. Helium 34
4.2.1.1.2.2. C, N, and O 34
4.2.1.1.2.3. Anomalous Particles 34
4.2.1.1.2.4. Planetary Radiation Belt Temporal Variations 35
4.2.1.1.3 Solar Particle Events 35
4.2.1.1.3.1. Solar Flare Particles 36
4.2.1.1.3.3. Solar Proton Fluxes 38
4.2.1.1.3.4. Solar Energetic Particle Composition 40
4.2.1.1.3.5. Ionization State 42
4.2.1.2. Environment at the Spacecraft Location 43
4.2.1.2.1. Magnetic Shielding 43
4.2.1.2.2. Effect of Mass Shielding 43
4.2.2. The Sensitive Volume 44
4.2.2.1. Determining the Path Length 44
4.2.4. Part Data 46
4.2.5. Available SEU Rate Calculations 47
4.2.5.1. Petersen Approximation 47
4.2.5.2. Detailed Calculation -- Adams, 1981 47
4.2.5.3. Comparative Part Technologies 49
4.3. Single Event Upsets Due to Protons 49
4.3.1. Introduction 49
4.3.2. Semi-Empirical Proton SEU Cross-Section 50
4.3.3. Proton Upset Rate 50

figure	title	page
4-1	Progress in technology leads to single event upset concern	4-2
4-2	Single event upset diagram	4-4
4-3	Single event upset cross section	4-5
4-4	Stopping power in silicon	4-6
4-5	Charge deposited in one micron	4-7
4-6	P-N junction	4-8
4-7	Forward biased junction	4-9
4-8	Reversed biased junction	4-10

4-9	Charged track tunnel formation	4-12
4-10	Ion current pulse	4-13
4-11	Sensitivity versus feature size	4-14
4-12	Dynamic RAM storage cell	4-15
4-13	CMOS memory circuit cell	4-16
4-14	SPICE simulation of non-SEU	4-17
4-15	SPICE simulation of SEU	4-17
4-16	IIL gate circuit	4-18
4-17	LET versus energy	4-20
4-18	Universal abundance	4-24
4-19	Cosmic ray abundance	4-26
4-20	Proton spectrum	4-27
4-21	Helium spectrum	4-28
4-22	Iron spectrum	4-29
4-23	Flux versus heliocentric distance	4-33
4-24	Propagation of solar flare	4-37
4-25	Proton differential fluence	4-38
4-26	Solar flare occurrence	4-39
4-27	Peak solar flux	4-40
4-28	The cosine law	4-45
4-29	Pathlength distribution function	4-46
4-30	Rate for 2901B	4-48
4-31	Rate for SBP9989	4-49

table	title	page
4-1	Single event upset causing environments	4-23
4-2	Adams basic spectra	4-30
4-3	Adams Hydrogen to Nickel	4-31
4-4	Adams Copper to Uranium	4-32
4-5	Anomalous component	4-35
4-6	Low Z solar particle event composition	4-41
4-7	High Z	4-42
4-8	Stopping power and range for protons	4-51

5.1. Introduction 1
5.2. GPS Operations -- contributed by Michael O'Brine, Air Force 2
5.3. Voyager's Power On Resets 3
5.3.1. Effect of POR 4
5.3.2. Environmental Correlation 6
5.4. GOES 4 and 5 Anomalies -- Winfred Farthing, GSFC 7
5.5. GOES-4 Failure -- contributed by Daniel Wilkinson, National Geophysical Data Center 9
5.6. Los Alamos Anomaly Studies -- contributed by Dan Baker, ... 12
5.8 Operational Impact 12
5.8.1 Surface Charging 13
5.8.1.1. Engineering Concerns -- Discharges 13
5.8.1.2. Charged Surface Concerns 14
5.8.2. Internal Discharge 14
5.8.3. Single Event Upsets 14
5.9. Obtaining Environmental Data and Reporting Anomalies 15
5.9.1. Air Weather Service 15
5.9.1.1. Air Weather Service Support Organization 15
5.9.1.1.1. Staff Weather Officers (SWOs) 15
5.9.1.1.2. Staff Meteorologists 15
5.9.1.2. Real Time Monitoring System 15
5.9.2. NOAA Space Environmental Laboratory -- Reporting Anomalies 15
5.9.3. National Geophysical Data Center 16
5.10. Unreported Anomalies 16

figure	title	page
5-1	Command [illegible]ity	5-4
5-2	Anomaly versus high energy electrons	5-5
5-3	Jupiter's high energy electrons	5-6
5-4	Correlation of failure with anomaly	5-10
5-5	Electron count rate	5-12

table	title	page
5-1	Spacecraft and their anomalies	5-2
5-2	GOES 4 and 5 anomalies	5-8

6.1 Organizing for Success....1
6.2. Immunity to ESD....4
6.2.1. Design Assessment....4
6.2.1.3. Grounding....9
6.2.1.4. Cable Harness and Routing....10
6.2.1.5. Faraday Cage Shielding....10
6.2.2. Mitigation Techniques....11
6.2.2.1. Current Limiting....11
6.2.2.2. Filtering....11
6.2.2.3. Error Detection/Correction....11
6.2.2.4. Plasma Contactors contributed by Tod Williamson -- Hughes Research Labs 11
6.2.2.4.1. Requirements for ESD Prevention....12
6.2.2.4.2. Plasma Contactor Operation....13
6.2.2.4.3. Current Bias Relations....15
6.2.3. Methods of Circumvention....16
6.2.4. Quality Control....17
6.2.5. Cost-Effectiveness....17
6.2.6. Subsystem Guidelines....17
6.2.6.1. Solar Panel Grounding....17
6.2.6.2. Solar Panel Fabrication....17
6.2.6.3. Power System Electrical Design....18
6.2.6.4. Mechanical and Structural....18
6.2.6.5. Thermal Blankets....18
6.2.6.6. Thermal Control Louvers....19
6.2.2.7. Antenna Grounding....19
6.2.6.8. Antenna Apertures....19
6.2.6.9. Antenna Reflector Surfaces....19
6.2.6.10. Transmitters and Receivers....19
6.2.6.11. Attitude Control....19
6.2.6.12. Deployed Packages....19
6.2.6.13. Ungrounded Materials....20
6.2.6.14. Deliberate Surface Potentials....20
6.2.7. Summary -- Surface Charging....20
6.3. Immunity to Internal Discharges....21
6.3.2. Mitigation Techniques....22
6.3.3. Methods of Circumvention....22
6.4. Immunity to SEU....22
6.4.1. Available Part Data....23
6.4.1.1. JPL/NASA Ground Test Radiation Data Bank....23
6.4.1.2. IEEE Transactions on Nuclear Science....23
6.4.1.3. Defense Nuclear Agency (DNA) Hardness Assurance Advisory Committee....23
6.4.1.4. DASIAC....23
6.4.1.5. Various MIL Specs....23
6.4.2 Programs for Developing SEU Hard Parts....23
6.4.3 Fault Tolerant Solutions....23
6.4.4. Methods of Circumvention -- System Level....24
6.5 Testing....25
6.5.1. Surface Charging Testing....26
6.5.2. Internal Charging Testing....26
6.5.3. Single Event Upset Testing....27
6.5.4 How Many Tests Are Enough?....32
6.5.5. EMC Tests....33
6.5.5.1. Tests Designed Specifically for Surface Charging....39
6.5.5.2. INTELSAT VI Tests....41
6.5.5.3. Tests Designed Specifically for internal Charging....42
6.6. A Final Word....43

figure	title	page
6-1	Cause-transmission-victim	6-3
6-2	Neutralizer discharge	6-12
6-3	Plasma contactor	6-13
6-4	SPACECLAMP	6-14
6-5	25 cm plasma contactor	6-15
6-6	SPACECLAMP current	6-16
6-7	SEU test apparatus	6-28
6-8	Typical SEU test data	6-29
6-9	SEU test plan	6-30
6-10	Typical discharges	6-36
6-11	MIL-STD test configuration	6-37
6-12	INTELSAT discharge circuit	6-41
6-13	INTELSAT test setup	6-42
6-14	INTELSAT discharge trigger	6-42

table	title	page
6-1	Guidelines and standards	6-2
6-2	Recommended spacecraft surfaces	6-7
6-3	Surfaces to be avoided on spacecraft	6-8
6-4	Anomaly testing summary	6-25
6-6	SEU testing facilities	6-32

TABLE OF CONTENTS

APPENDIX 1 GENERAL REFERENCES ..... A

A1.1 Conference Proceedings ..... A

A1.2 Spacecraft Charging ..... A

A1.3 Government Documents ..... A

A1.4 Individual References ..... A

A1.5 Bibliography A1

APPENDIX 2 GLOSSARY ..... A

APPENDIX 3 MODELS AND COMMITTEES ..... A

A3.1 NASCAP Predictions -- Myron Mandell, S-Cubed, San Diego, CA ..... A

A3.1.1 Geometrical Modeling ..... A

A3.1.2 Material Properties Used in Modeling ..... A

A3.1.3 Calculations ..... A

A3.1.4 NASCAP Conclusion ..... A

A3.2 Environmental Models ..... A

A3.2.1 NASA ..... A

A3.2.2 AP8 ..... A

A3.2.3 AE4, AE5, AE6, AE7, and AE8 ..... A

A3.2.4 Orbital Integration Codes ..... A

A3.3 AFGWC ..... A

A3.4 NGDC ..... A

APPENDIX 4 AVAILABLE SENSORS AND DETECTORS ..... A

A4.1 CRRES/SPACERAD Experiment Descriptions ..... A

A4.2 SOPA Detector (Synchronous Orbit Particle Analyzer) ..... A

A4.3 Plasma Spectrometer ..... A

TABLE OF CONTENTS

A4.4 Pulse Monitor A4-3

A4.5 SSPM A4-4

A4.6 2d Plasma Analyzer A4-4

A4.7 1D Plasma Analyzer A4-5

A4.8 Internal Discharge Monitor A4-5

A4.9 FMDS: An Automatic Plasma-Contactor System for Spacecraft Potential Control A4-6

A4.9.1 FMDS Environmental Sensors A4-7

A4.9.2 FMDS Controller A4-9

A4.10 Concluding Comments A4-9

TABLE OF CONTENTS

A4.4 Pulse Monitor A4-3

A4.5 SSPM A4-4

A4.6 2d Plasma Analyzer A4-4

A4.7 1D Plasma Analyzer A4-5

A4.8 Internal Discharge Monitor A4-5

A4.9 FMDS: An Automatic Plasma-Contactor System for Spacecraft Potential Control A4-6

A4.9.1 FMDS Environmental Sensors A4-7

A4.9.2 FMDS Controller A4-9

A4.10 Concluding Comments A4-9

Chapter

1

Introduction

1.1. Importance of Engineering for Immunity

This is an endeavor to alert space system programs to the dangers of three specific sources which have caused anomalies in space systems. These three are: (1) surface charging and discharges (ESD), (2) internal charging and discharges (ID), and (3) single event upsets (SEU). Each of these, in its own way, has been crucial in one or more programs. A well-thought-out program will deal with each of these environmentally induced effects. This publication is based on the experience of many programs. Some wisely considered environmental concerns from the beginning of their planning and design; others learned the lessons of history the hard way. Some were forced to pioneer new ways of building in immunity; others proved the merit of techniques developed on prior programs.

Integrating space environmental support into a program benefits the design, implementation, test, and operation of a space system. In the early phases of a program, consideration of the environment results in good design trades for the system and a sound strategy for dealing with each effect. During implementation and test, proper environmental consideration results in realistic tests (as compared to under- or over-testing) and insures that all of the details included in the original planning are actually carried out in practice. Finally, in the operational phases of the space system, environmental operational support alerts the system to the local conditions the system is experiencing and makes planning easier and more effective. Reporting the results of each system, especially any anomalous behavior, benefits future designs and helps develop operational procedures for use by the system(s) experiencing trouble with similar environments.

As technology advances, other environmental effects may become important sources of anomalies. In the future, the experience used in developing this publication may not be directly applicable, but the general lesson of attention to the environment and alertness to its effects will, we believe, still be valid.

1.1.1. How a Satellite Failure Leads to SCATHA

One of the first DSCS satellites -- a military communications satellite -- failed. When that occurred, a massive effort was made to understand the source of the anomaly. Were enemy satellites degrading our satellite's performance, was there a basic flaw in the electronics, or were as yet unknown physics involved in producing these anomalies? While suppositions ran from one extreme to another, Sherman DeForest observed a curious phenomenon on ATS-5 and 6. During times when the magnetosphere was disturbed, his particle spectrometer observed that the entire satellite charged (DeForest, 1972). Environmental data from ATS-5 (Sharp et al., 1970)

showed that the environment could be characterized by plasmas with electron densities ≈ 0.1 to 1.0 cm^3 and temperatures characterized by kT ≈ 1 to 20 keV. It was readily concluded from this that the spacecraft potential could reach minus 10 kilovolts. At potentials of 10 kilovolts, discharges could easily be imagined, and the source of the anomalies was suspected to be those discharges. A number of investigators began piecing together parts of the puzzle. Engineers examined what effect discharges would have on satellite electronics. Space physicists investigated the environment. Material scientists examined typical spacecraft materials to determine their charging characteristics. Physicists calculated charging as a function of geometry, sunlight, and materials. By 1973 both the Air Force and NASA were aware that they had many common technology problems when operating in a space environment. In 1975 a joint program to investigate spacecraft charging was begun which included a spacecraft devoted particularly to measuring the environment and its effects. The P78-2 spacecraft (launched 30 January 1979) had two initial objectives: to measure the charging and to measure material effects (Shane, 1977). Other parts of the spacecraft charging at high altitudes (SCATHA) program included ground experiments and the development of a computer model for charging of spacecraft surfaces -- NASCAP (NASA Charging/Analyzing Program). From this effort a number of environmental interaction studies have evolved. Guidelines, rules of thumb, and specifications have resulted from some of the data collected. Other investigations have grown out of the original SCATHA effort. The Combined Release Radiation Effects satellite (CRRES) is an example of a spacecraft, like P78-2, which is designed to measure and quantify environmental interactions so that anomalous behavior of spacecraft can be understood and controlled.

Failures of complete spacecraft, such as the early DSCS failure, are unpleasant. Long investigations are costly. As George Inouye stated in a summary of his experience with DSCS, "Our experience on the DSCS satellites has been that a great deal of effort was required to identify the sources of anomalous behavior, whether internal or due to the ambient environment. In the final analysis, in spite of concentrated 'detective work,' some of the conclusions that the environment was the most likely causative source were arrived at by an elimination process rather than by a more direct approach because of the lack of diagnostic data." It is important then not only to design immunity into each new space system but to prepare for future systems by monitoring and reporting on anomalies that do develop.

1.1.2. Costs of a Hardening Program

Viewed as a whole the cost of a well integrated environmental program as part of the total system program more than offsets its cost in terms of retrofit costs, downtime, ease of use and reliability. It is estimated that to harden the shuttle would have cost about 5% of the total system cost if its threat environment had clearly defined and there was a commitment to design for immunity from the start of the program. To retrofit the shuttle after the design was complete would have cost 35% of the total system costs. A large part of the increased cost is the redesign needed to accommodate improvements required for hardening. Real cost savings can result from careful planning which includes environmental considerations from the beginning of the program.

1.1.3. System Test Plans

System test plans are approval documents required early in the program by the SPO (system program office). Figure 1-1 shows the relation of space environmental observations/forecasts to the system plans. At the start of a program the likely environmental conditions are specified as an input in the system requirements. How well the system will respond to these predicted environments or worst case environments is assessed during the preliminary and critical design reviews. Reviews by environmental specialists of actual hardware as well as designs during the implementation phase insure that design trades are carried out and problems avoided prior to testing. Environmental tests prior to launch uncover any environmental problems which were not correctly addressed. A final review of environmental requirements specified at the start of the program provides environmental updates/alerts which occurred during the program. Following launch, on-orbit checkout uses environmental predictions and real time data to qualify the system and as input to anomaly scenario planning as needed. During the useful life of the system, environmental forecasts are used, and anomalies reported. Flight experience and environmental monitoring of the real system make an important contribution to the next generation of space systems.

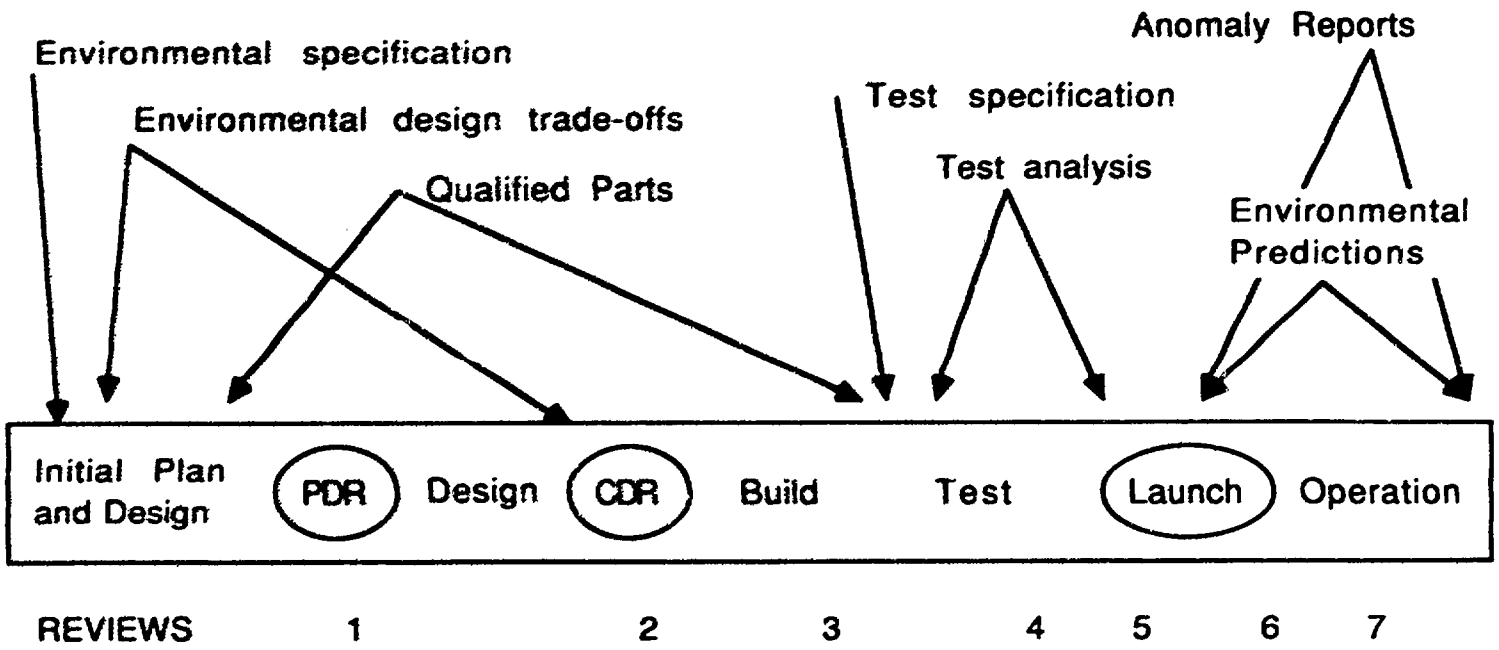

1: Preliminary Design Review
2: Critical Design Review
3: As-built Review(s)
4: Test Reviews
5: Pre-ship Review
6: Post-Launch Review
7: Anomaly Reviews

Figure 1-1. Program Plan

1.1.4. Successful Tests

The success of tests (both ground and operationally on orbit) is aided, or even hinges on, timely, accurate (to the extent possible) space environmental observations/forecasts. Appendix 3 lists both measured and predicted environmental databases available for the system developer/user. The functional effectiveness of the entire system is enhanced by the timeliness and accuracy of environmental specifications, predictions, and measurements.

The ground processing function, where output data consist of or contribute to decisions, is enhanced by factoring in (or factoring out) the known, measured, or predicted state of the environment. Appendix 3 lists sources of this kind of environmental data. By correlating certain classes of anomalies with the environment and having up to date environmental information, unexpected anomalies can be quickly categorized and resolved.

1.2. Structure of this Book

This text deals with three kinds of anomaly producing effects of a charged particle environment: surface discharges, internal discharges, and single event upsets. Various names have been given to the effects we wish to talk about: surface discharges or electrostatic discharges (ESDs), internal discharges, and single event upsets (SEUs).

Surface discharges are sometimes referred to as electrostatic discharges (ESDs) although there is not much static about ESDs. At other times surface charging is what is meant by spacecraft charging; however, spacecraft charging is many times used as a much wider term in which all phenomena involving charging are referred to. Spacecraft charging in the widest sense includes surface as well as bulk charging and discharging phenomena. For clarity in this text we have divided spacecraft charging into two parts: charge buildup and discharge on the surface of the spacecraft, and charge buildup and discharge interior to the spacecraft. This is a convenient engineering definition because it separates the environment of concern into those particles initially at low energy in the spectrum, and those with sufficient energy to penetrate the skin of the spacecraft and deposit charge inside the spacecraft. It is not a clean division from the point of view of the charge buildup and discharge processes involved because particles which penetrate the skin of the spacecraft may help buildup charge on the surface of materials interior to the spacecraft, in exactly the same manner as charges build up and discharge on the surface of the spacecraft. However, one does not need to consider charged particle transport, to first order, to calculate charge buildup on the surface of the spacecraft, while one does in considering charge buildup interior to the spacecraft.

Internal discharges are also referred to as electron caused electromagnetic pulses (ECEMP) and are the result of internal charging, deep dielectric charging, or spacecraft charging.

Single event upsets or SEUs are also called bit flips especially when soft errors are meant. By soft errors one usually means errors in the sense of wrong bit values, but not with damage to the hardware. Single event upset as used in this book refers to the change of a bit in an integrated circuit (IC) by a single particle during which no damage was done to the IC. Recent research suggests that a more descriptive name would be single particle phenomena, with single event upset, or soft error upset as a subclass of the larger phenomena. In fact certain latchups of ICs have been attributed to single heavy ions passing through a sensitive region of an IC. These developments are not included in the present text, but the reader should be aware that this field like any other dynamic area of research will change as progress is made in exploring and understanding these effects. We have tried to be consistent with our terminology, but the reader should recognize that various names will continue to be used to refer to these effects and that new names as well as new aspects of these effects will continue to be introduced into the literature.

1.2.1. Electrostatic Surface Discharges (ESD) -- Chapter 2

Chapter 2 is concerned with surface discharges. Electrostatic discharges occur when differential charging of adjacent parts of a space system exceeds the breakdown potential of those parts. Charging is produced when a solid object is immersed in a plasma (Figure 1-2). Typically potential differences on the order of 500 volts are needed to produce ESDs that are significant to an operating system (Figure 1-3). The environment which causes surface charging and eventually ESDs is primarily the plasma environment which is characterized by the electron and ion temperature and density. Near earth the ultraviolet flux from the sun plays a key role by releasing electrons from the material through a process called photoemission. The material characteristics of bulk conductivity, surface

conductivity, secondary emission properties, and photoemission properties play important roles in the charge state of the surface. In steady state, the potential of a uniform surface is determined by requiring that the net current to the surface be zero.

A number of design, assessment, test, and monitoring techniques are available to control a space system's ESDs. In some cases detailed specifications and procedures have been established which are applied to almost all systems through MIL specs; however, it is almost always wise to customize these specs to the particular threat imposed on a system. If nothing else, this insures that the effect is understood by the program affected, and that unrealistic demands are not usurping program resources.

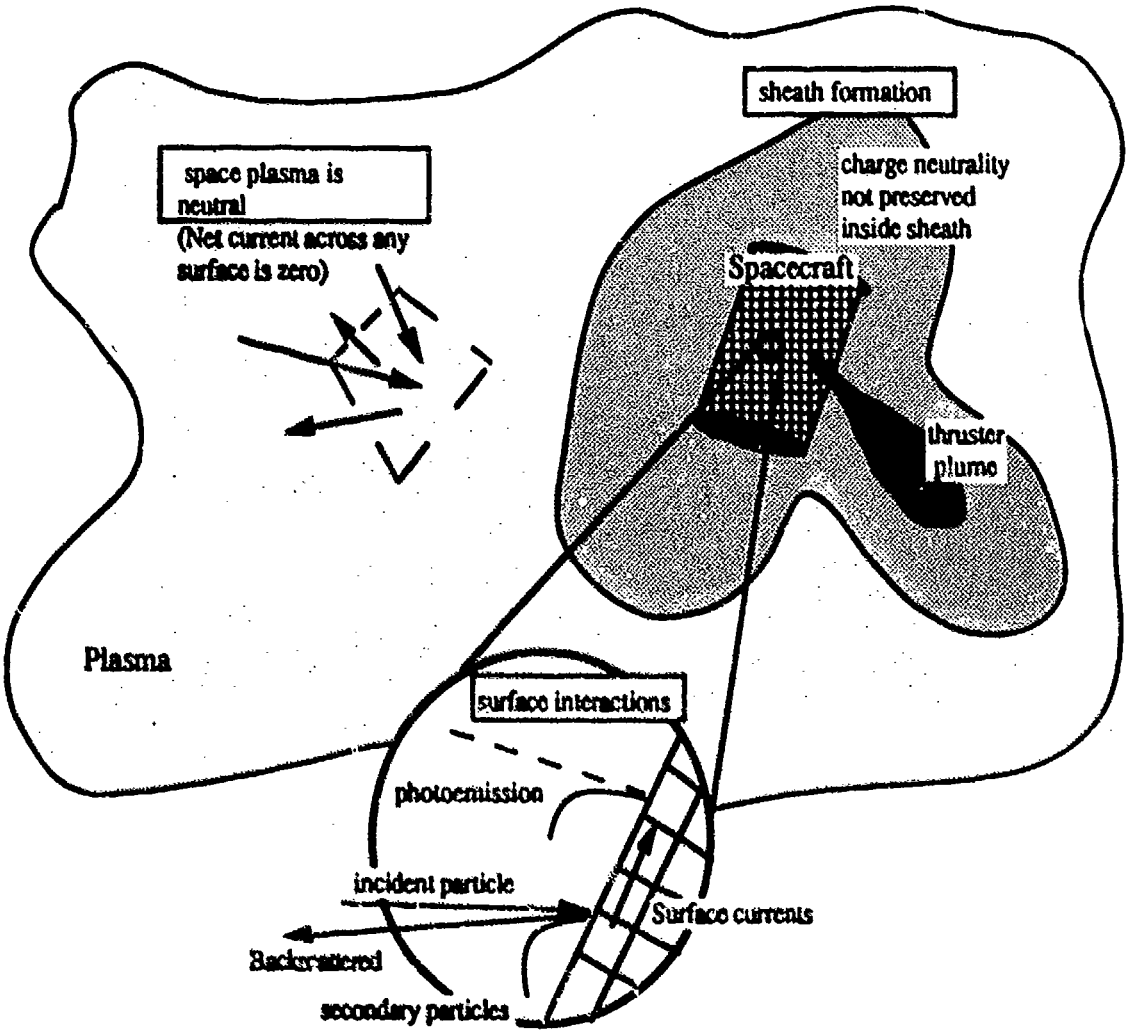

Figure 1-2. Surface Discharges Result From Charge Built Up on the Surface of the Spacecraft.

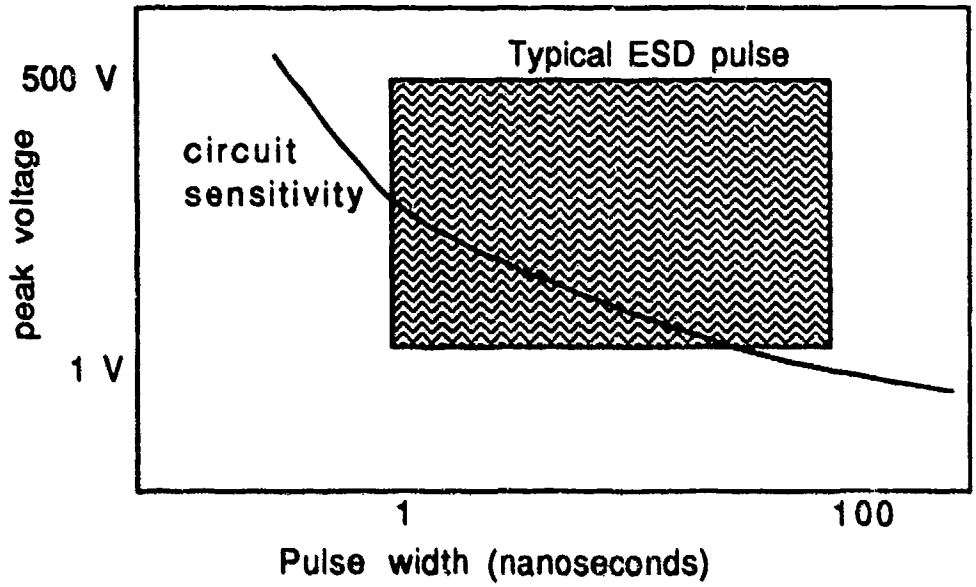

Figure 1-3. ESD Characteristics. Typical ESD pulses are generated on reasonably large surface areas and so range from 1 to several hundred volts with pulse widths in nanoseconds. When coupled to the spacecraft the signal can be stretched into microseconds.

1.2.2. Internal Discharges -- Chapter 3

Chapter 3 is concerned with internal discharges. Internal discharges are important when a system is expected to operate in an environment where penetrating radiation causes charging inside the system. The basic physics of this charging process is very similar to the plasma effects covered under ESD, but now the electrons or ions are passing through the "surface" of the spacecraft and deposit charge on and within materials inside the spacecraft (figure 1-4).

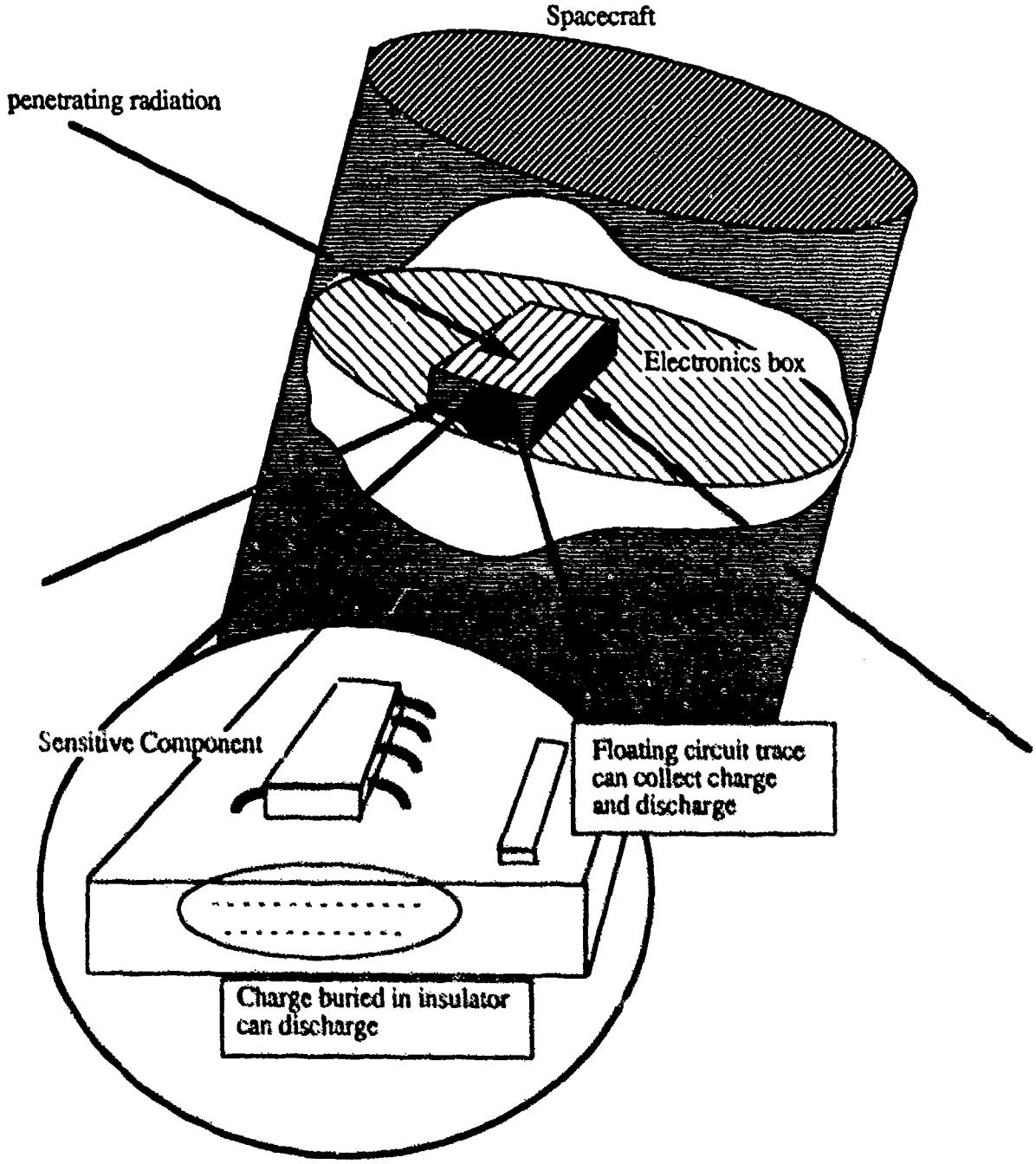

Figure 1-4. Internal Discharges Result From Charges Deposited Directly On or In Well Insulated Regions Inside the Spacecraft

Internal discharges occur when floating metal or dielectrics collect enough charge so that the electric field generated exceeds the breakdown strength from the point of the deposited charge to a nearby point. Internal discharges have been suspected as the cause of a number of spacecraft anomalies. The conditions for discharge are

dependent on the environment, the shielding provided by the spacecraft, the material which is charging, and the geometry of the charged materials. System response to internal charging de nds on the location of the discharge and the sensitivity of the circuits. Since internal discharge can occur within the circuits themselves, discharges that would go unnoticed on the exterior of a space system can be significant when they occur internally (Figure 1-5). This is an area of current research; nonetheless, various options are available for testing and circumventing the effects of internal charging. For specific missions, criteria can be generated which will eliminate or reduce internal discharge concerns.

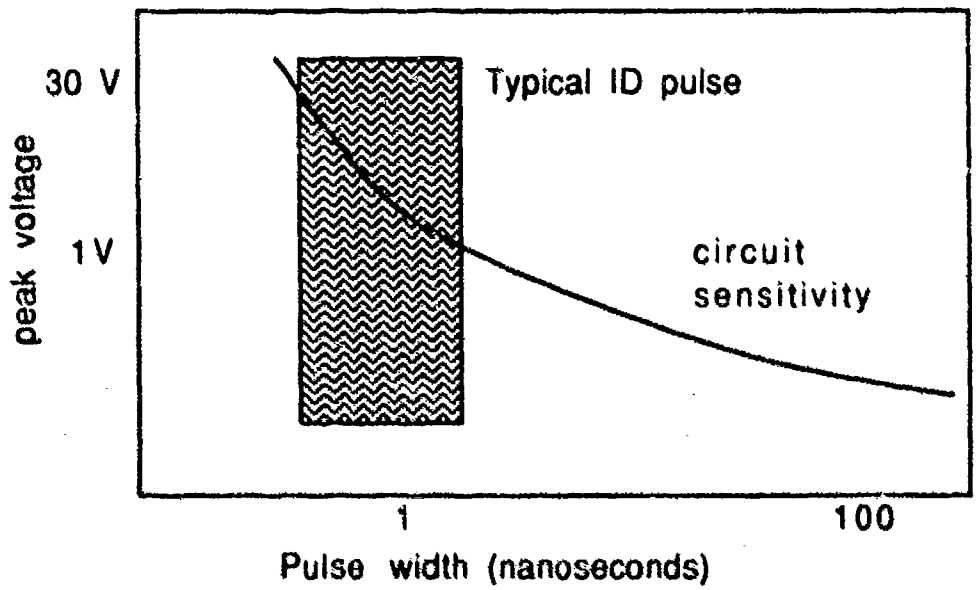

Figure 1-5. ID Characteristics. Typical ID pulses are generated on reasonably small surface areas or in small volumes of insulators and so range from 10 to several hundred millivolts with pulse width in nanoseconds.

1.2.3. Single Event Upsets (SEU) -- Chapter 4

Chapter 4 is concerned with single event upsets. Single event upsets occur in microelectronics when a single particle, usually a heavy ion or proton, deposits enough charge at a sensitive node in the circuit to cause that circuit to change state. The feature size of the electronics helps determine the sensitivity as well as the probability of a single event upset occurring. In its most simplified description, an SEU is a threshold phenomenon. If a particle deposits sufficient charge along a sensitive path in a device the event will occur. This is illustrated in Figure 1-6. In the first part a single heavy ion which is losing energy by ionizing the atoms of the material it is passing through happened to pass through a depletion region of an off transistor in a flip-flop circuit. Depending on the charge collection efficiency of the device and the response time of the flip-flop, this can cause the flip-flop to change state. In the second example in Figure 1-7, a proton causes the same reaction in the circuit by means of first causing a nuclear reaction in or very close to the sensitive region. In extreme cases, it is possible for the proton to cause the SEU directly. However, parts which are sensitive to protons directly are probably unsuitable for space applications.

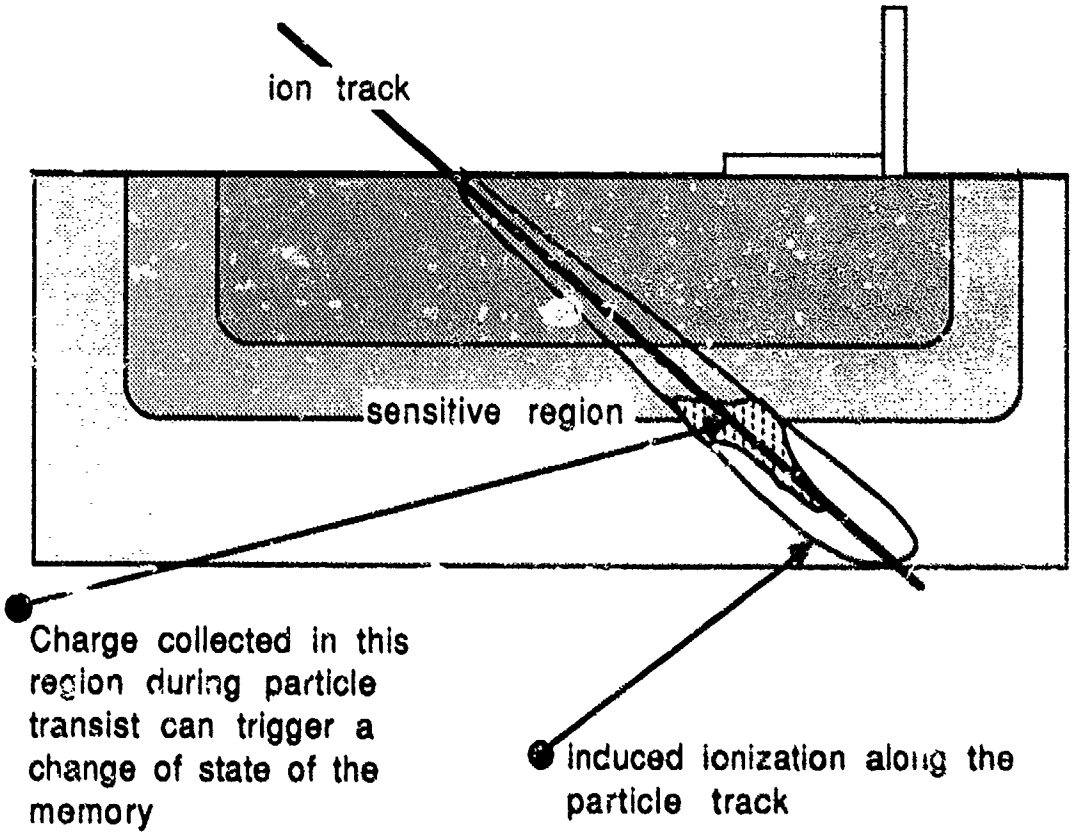

Figure 1-6. Direct Ionization SEU. Sensitive region is typically the depletion region, although charge can be collected a considerable distance from the depletion region.

Single Event Upset Mechanism
Proton induced

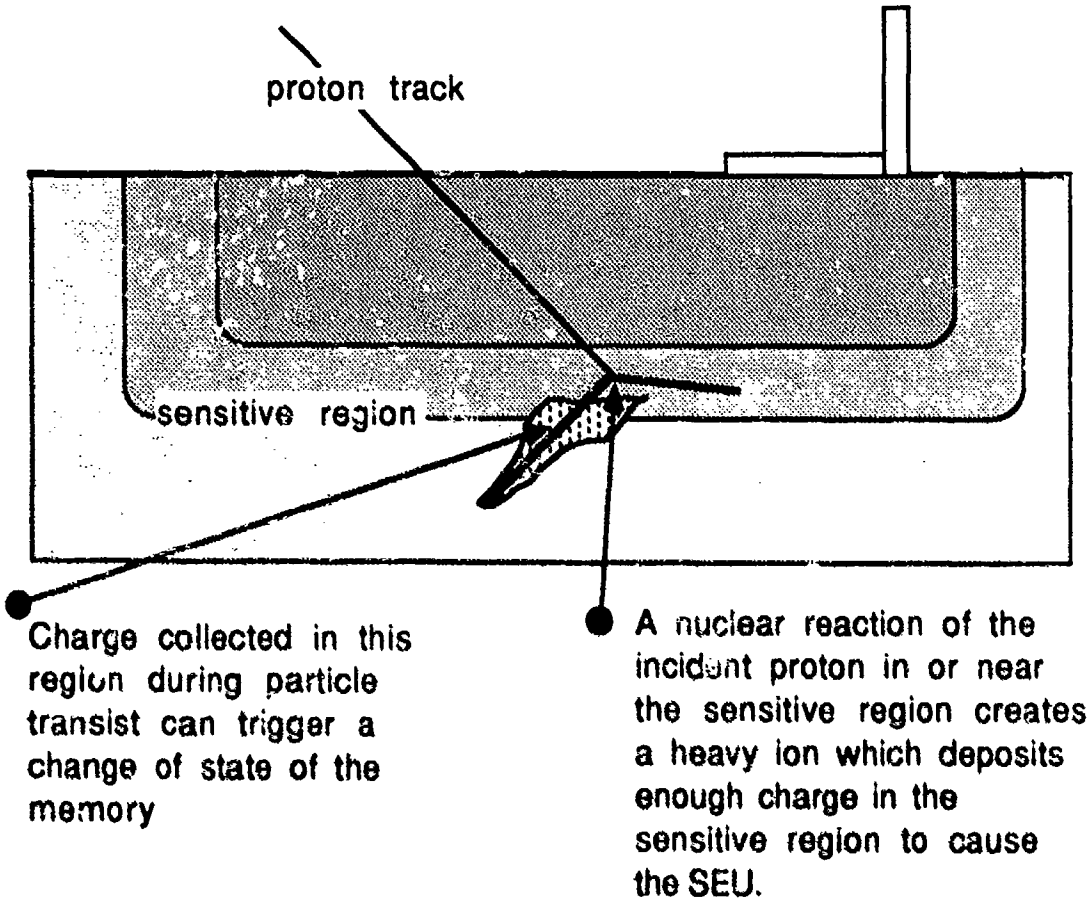

Figure 1-7. Proton Induced SEU. Sensitive region is typically the depletion region, although charge can be collected a considerable distance from the depletion region.

The determination of the SEU rate is central to the development of techniques necessary to circumvent the effects of an SEU. For example if the SEU rate is small, a simple watchdog timer may be all that is required to meet the reliability requirements of the mission. On the other hand, an SEU rate which is large compared to the data acquisition time of the mission may require a complete redesign of the electronics to meet the mission requirements.

Current progress in the design of smaller and faster ICs is, in the opinion of some technologists, leading to the use of parts which are more and more sensitive to SEUs. A considerable effort has been spent in discovering ways in which, despite the small size and fast electronics, the SEU rate can be minimized. These techniques are touched on in later chapters as a significant possibility exists that the right system engineering solution is the procurement of radiation and SEU hard parts for specific space applications.

There are a multitude of environments which must be considered in assessing the SEU rate (Table 1-1). Not only are cosmic rays, specifically the heavy ion component, to be considered, but protons and heavy ions from solar flares or in trapped radiation belts can contribute significantly to the rate during critical times of the mission. Even electrons through a nuclear reaction have been postulated as causing SEUs. Therefore it is even more important to recognize the spatial dependence of the phenomenon when considering system engineering options. The heavy ions in the earth's radiation belts are most likely amenable to a simple mass shielding solution, whereas many times it is "impossible" to shield against cosmic heavy ions. Recognizing the complexity and richness of the environment as well as the effect goes a long way in leading a program to effective and practical solutions to a possible SEU concern. Nonetheless, there are workable and effective solutions possible for many SEU concerns. Again the key is an early understanding of the problem so that intelligent solutions can be found.

Table 1-1. SEU Causing Environments

Particles	Environment	Remarks
Heavy ions	Galactic Cosmic Rays	very high energy
	Solar Flares	large flux
	Trapped Belts	large flux; lower energy
Protons	Galactic Cosmic Rays	smaller than belts
	Solar Flares	large flux
	Trapped Belts	large flux; lower energy
Alpha particles	Packaging Material	radioactive decay
	Trapped Belts	see heavy ions
	Flares	see heavy ions

1.2.4. Anomalies -- Chapter 5

No single word hides its significance and impact as well as anomaly. Perhaps it is useful and used so often simply because it conveys so little information. It could result in the total loss of a mission or could be a curious, but nonconsequential occurrence. In this book we are dealing with anomalies that occur because: a surface charged and then discharged (ESD); charge was buried inside the system (Internal Discharge); or a single particle hits a device in just the right manner to be noticed. It is certainly possible that any one of these occurrences could have serious consequences. It is also possible that nothing of significance would flow from such an occurrence. Each system individually needs to determine the impact of these environmental interactions. Chapter 5 describes some of the experience the community has gleaned in dealing with anomalies. To those pioneers who have gone before us, we give praise and thanks.

The rate, seriousness, and other characteristics of each of the anomalies described in this book will vary considerably from one program to another. What is important to all programs is that each of these phenomena can and does occur, and that design, test, and operational techniques exist which can mitigate the consequences of these phenomena. This text hopes to inspire programs to deal intelligently with the issue of environmentally produced anomalies, and to diligently report the anomalies which do occur. Significant reduction in the anomalies produced by ESD, ID, and SEU is achievable by the techniques described in this text. The difficulty of dealing with a given anomaly depends in part on the rate of its occurrence. This is illustrated in Figure 1-8 introduced by Gentry Lee when dealing with the single event upset problem which occurred on Galileo. The point is that the difficulty of dealing with a problem is a function of the rate at which it occurs and the risk one is willing to take. In this case, if the rate were low enough it could be ignored; if it were significant but small, timers or error correcting techniques

could be used; if it were high enough, none of the known techniques could be used within the constraints of power, weight, and schedule.

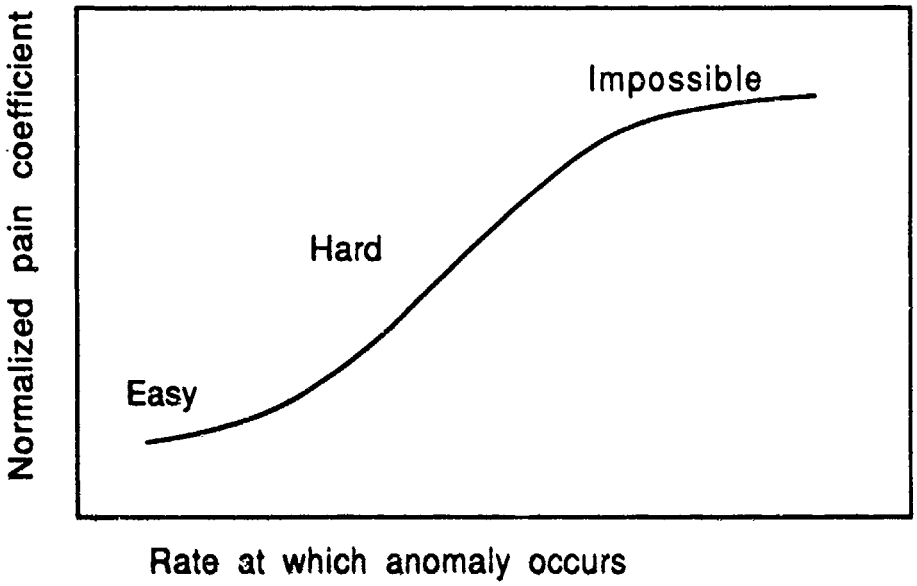

Figure 1-8. How Much Trouble an Anomaly Will Cause a Program Depends on How Often it Happens, and How Significant the Impact is. Each potential anomaly needs to be evaluated in terms of its rate of occurrence. Those which do not often occur are in general easily fixed (Gentry Lee, private communication, 1987).

1.2.5 Engineering for Immunity -- Chapter 6

Sometimes it seems that the anomaly is the center of attention. However, the reader should not lose sight of the fact that the elimination of anomalies is what is desired. Chapter 6 deals with methods used to control or eliminate the anomaly. A system that doesn't respond adversely to the environment is what is desired, no matter how interesting the phenomenon which causes anomalies may be.

In Chapter 6, methods which either eliminate or reduce surface and internal charging (primarily by: providing conductive paths and increasing the conductivity of insulating materials, decreasing the coupling from the discharge sites to the sensitive circuits through the use of a Faraday shield and filtering, reducing the flux of particles incident on the volume or area of concern through the use of shielding, or reducing the sensitivity of the victim circuit susceptibility through good EMC practice and careful part selection) are discussed. In addition some methods of actively influencing the environment to control absolute charging of the spacecraft by plasma emitters are discussed. As with all system engineering problems, care needs to be exercised to include the most appropriate engineering response for a given situation. Monitors are described in the appendix which can be used to gather information on the environment, as well as determine the health of the spacecraft and help determine the cause of any unforeseen anomalies. With the ultimate goal of engineering for immunity let's examine in detail the specific environmental interactions of concern here -- surface charging/discharging, internal discharging, and single event upsets.

It is the hope of AFGL, the authors, editors, and the SEAREC committee that this book will enable space system designers, engineers, users, and program offices to take advantage of the knowledge of the space environment and its effects on space systems in the "community." We hope this book will lead to a better understanding of the

surface charging/discharging, internal discharging, and SEU anomalies and their solutions. A complete system design depends on the independent sciences which are central to these effects, i.e., space physics, material science, device physics, and system engineering. In the limited space of this text we will not cover each area in depth, nor provide an answer book for all situations, but hope to point out the areas involved and give the readers a running start on understanding the basic issues. In fact, many areas touched on in this book are under active investigation.

In general, anomalies such as the ones we have been discussing have three distinct levels. A system approach allows the program to attack the problem on each level. No matter where the problem occurs, it must be transmitted to its victim through some medium. This is illustrated in Figure 1-9. To attack the problem at its source, one needs to modify or avoid the situation which causes the event. To attack the problem while it is being

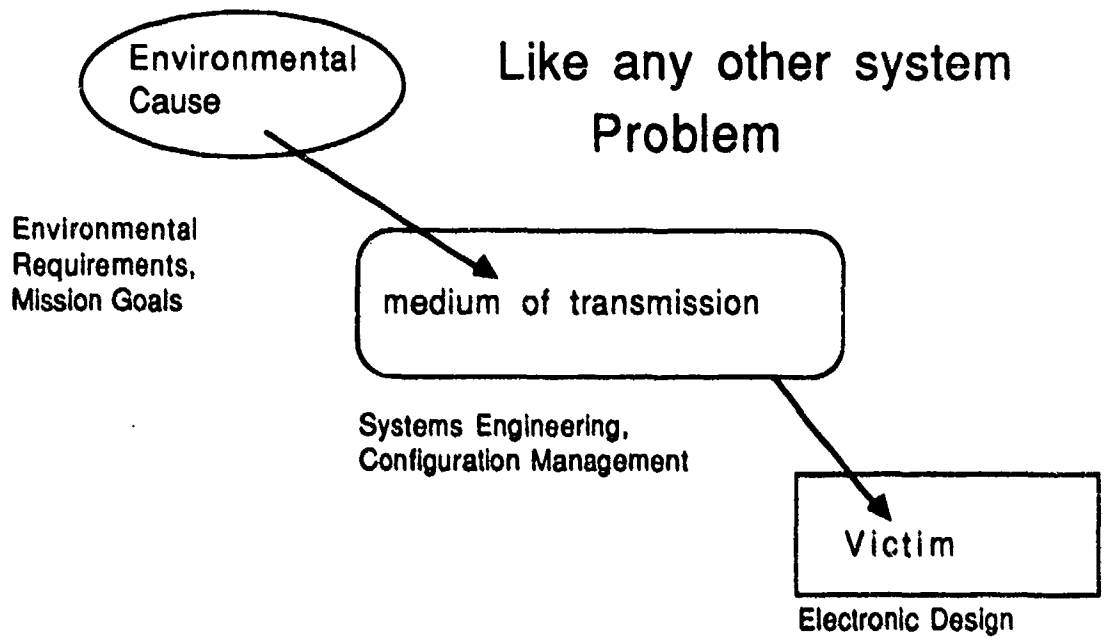

Figure 1-9. Systems Approach

transmitted to the victim, one needs to modify or eliminate the transmission path. To attack the problem at the victim, one needs to modify the sensitivity of the victim to the signal which could disrupt it.

By distributing the responsibility for finding solutions to the problems of environmentally induced anomalies across all responsible groups, a program can eliminate in a cost-effective manner the effects of these anomalies (Figure 1-10). When implemented with a supporting environmental program and provision for reporting any anomalies that do occur the result will be more reliable and cost-effective space systems.

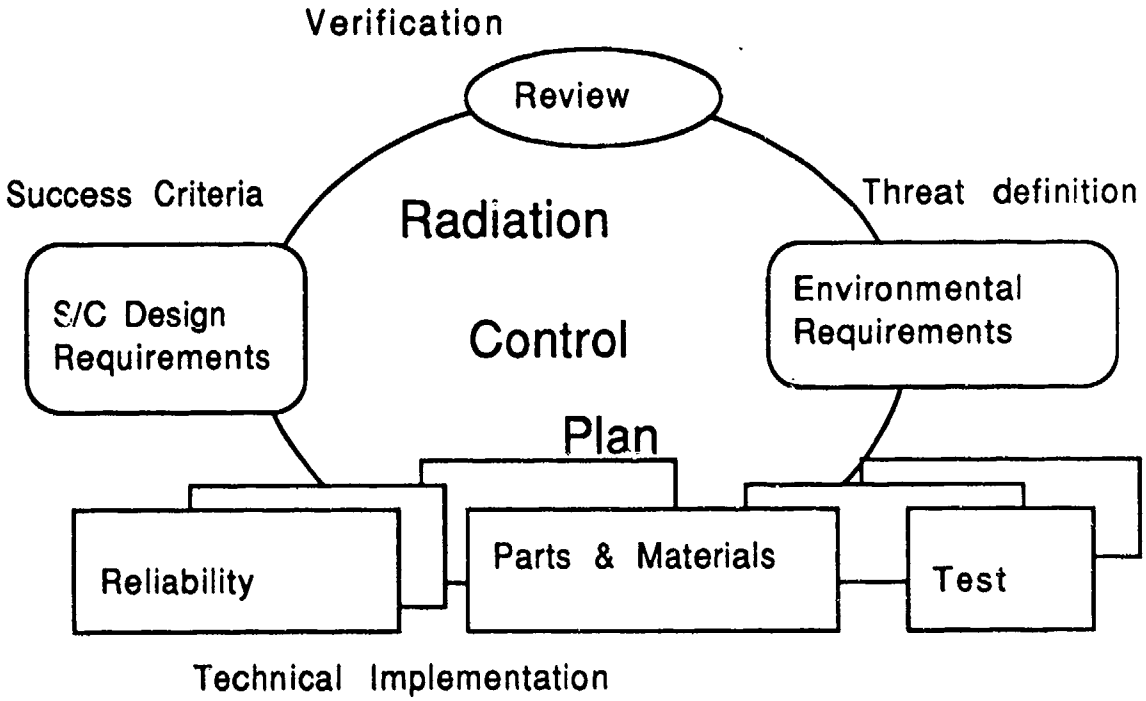

Figure 1-10. Program Organization

1.3. The Bottom Line

Ultimately, the cost of performing a mission determines whether or not the mission will be done. Ultimately the quality of the system determines whether or not the system will be used. Eliminating anomalies tends to save operational costs, make the system more user friendly, and make the system more reliable. A program which is alert to the effects and causes of anomalies from the beginning can design in immunity to those anomalies. Even a program which discovers an anomaly late in its development can deal intelligently with it and produce a system with some immunity. The costs of this effort need to be weighed against the cost of operating with the anomaly, and the usefulness of the system with or without the anomaly. Useful systems depend on doing everything possible to produce a reliable design. In the long run, environmental anomaly control is worth the added cost and effort demanded of programs in the design, implementation, and operational phases.

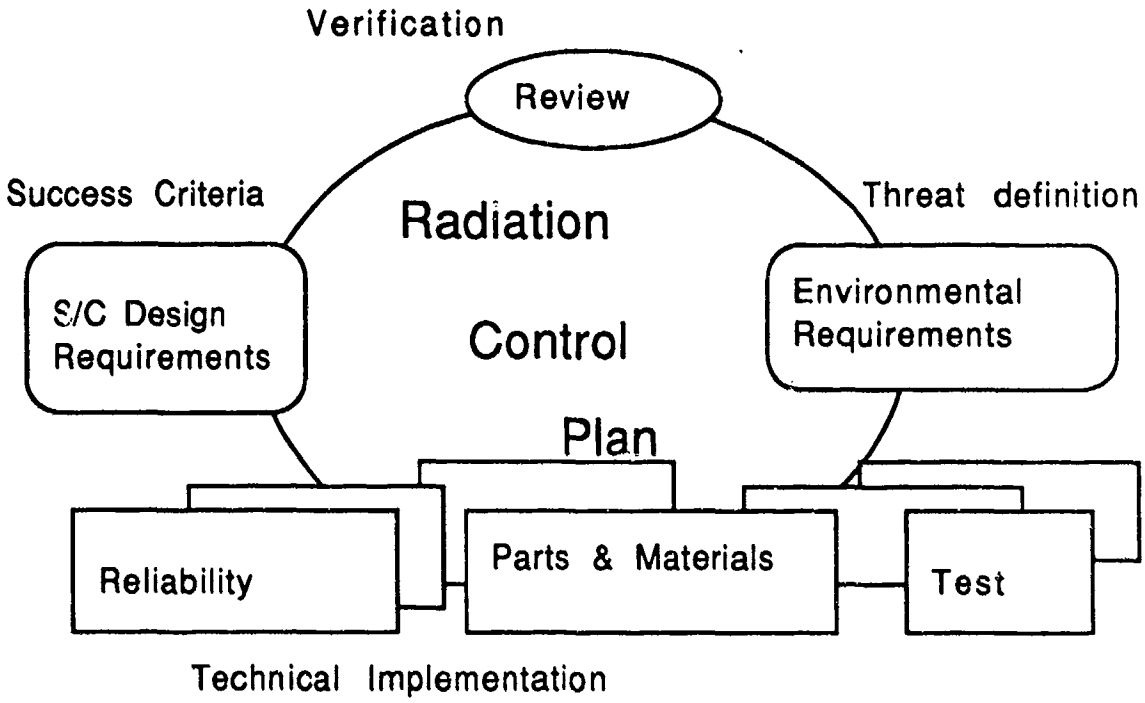

Figure 1-10. Program Organization

1.3. The Bottom Line

Ultimately, the cost of performing a mission determines whether or not the mission will be done. Ultimately the quality of the system determines whether or not the system will be used. Eliminating anomalies tends to save operational costs, make the system more user friendly, and make the system more reliable. A program which is alert to the effects and causes of anomalies from the beginning can design in immunity to those anomalies. Even a program which discovers an anomaly late in its development can deal intelligently with it and produce a system with some immunity. The costs of this effort need to be weighed against the cost of operating with the anomaly, and the usefulness of the system with or without the anomaly. Useful systems depend on doing everything possible to produce a reliable design. In the long run, environmental anomaly control is worth the added cost and effort demanded of programs in the design, implementation, and operational phases.

Chapter

2

SURFACE DISCHARGES

2.1. Surface Charging

By the occurrence of the first Spacecraft Charging Technology Conference in October 1976, there had been a number of indications that the charging of spacecraft surfaces could lead to anomalous spacecraft behavior. Operational solutions had been found for many of these anomalies once the spacecraft design deficiency was understood. Correlation of the anomaly with conditions in the magnetosphere represented a useful clue for "detective" work used to discover the cause of the anomaly -- spacecraft charging. That conference also announced to the rest of the world the SCATHA (Spacecraft Charging at High Altitudes) program which would investigate spacecraft.charging. As a result of the commercial and military importance of spacecraft charging on spacecraft operations, much work has been done in understanding the causes and cures of spacecraft charging. Spacecraft charging brought together space physicists, engineers, and scientists to discuss and review their work on the charging of spacecraft surfaces. The SCATHA program, commercial, and military interests have resulted in several guidelines on spacecraft charging. Two of the most popular ones are Purvis et al., 1984, and Vampola et al., 1985.

Spacecraft charging is the accumulation of charge on a spacecraft due to its interaction with a plasma, radiation, and particle environments. The figure below from chapter 1 illustrates some of the considerations involved in spacecraft charging. The cartoon in the left corner illustrates that the net current through a surface in the plasma is zero. This idea will be used to calculate equilibrium charge configurations for spacecraft. The upper right hand corner of the cartoon illustrates the influence of the spacecraft on the plasma. The sheath region that forms around the spacecraft is a volume strongly effected by the spacecraft. In this region the plasma is distorted by electric fields due to the charge on the spacecraft. The sheath region is easily distorted by activity on the spacecraft such as thruster firings which carry the influence of the spacecraft farther into the plasma. This region can be quite complex and depends on the motion of the spacecraft through the plasma as well as the plasma properties and the surface materials of the spacecraft. The bottom part of the cartoon focuses attention on the actual interaction at the surface of the spacecraft. The detailed atomic properties of the surface material are of prime concern locally.

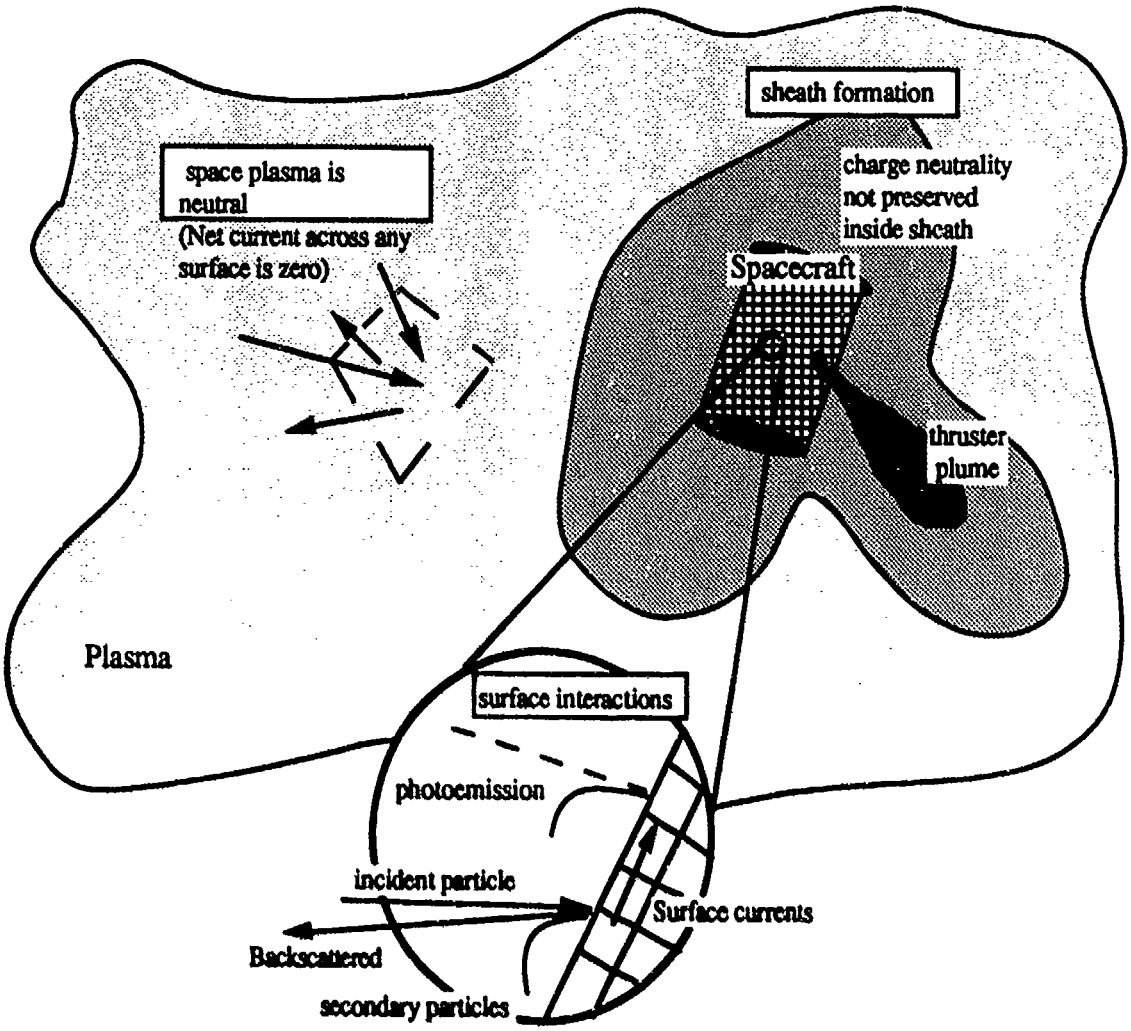

Figure 2-1: Spacecraft charging

2.1.1 Outline of chapter

This chapter is easily divided into several major areas. After the introduction (section 1) and some definitions, there is a discussion of the concerns raised in design by spacecraft charging (section 2). This is followed by a discussion of the charging mechanism (section 3). This is essentially a more detailed explanation of the charging figure above. Knowing the mechanism is important to recognizing what environments represent a threat to spacecraft operations; the environment is described in section 4. Section 5 discusses the breakdown mechanism. Section 6 covers a number or spacecraft or system effects that are related to spacecraft charging. Mitigation techniques that can be used to minimize spacecraft charging are covered in chapter 7.

2.1.2 Definition

Surface charging is defined as those phenomena associated with the buildup of charge on exposed external surfaces of spacecraft. (Spacecraft charging is a generic term for all charged particle interactions with a spacecraft.)

In this chapter our attention is directed to surface charging, that is charging of the surface of the spacecraft by its interaction with the space plasma, magnetic field, and solar radiation. In many situations this analysis is sufficient because the preponderance of particles effecting the charging state are low energy particles in the plasma environment. In this context low energy means particles that do not penetrate further than the first layer of the spacecraft, that is electrons up to about 50 keV and protons up to about .5 MeV. As illustrated in Figure 2-1, the net current across a surface in the plasma must be zero to maintain the overall charge neutrality of the plasma. If the net charge flow across a surface is not zero then charge must be building up on one side of the surface and decreasing on the other. Although this can happen for some period of time eventually a equilibrium value is reached. In a plasma charge neutrality is maintained because of strong, long range electromagnetic forces. Across an imaginary closed surface which is large enough to hold a significant amount of plasma the net current will be zero. This only requires that the there are an equal number of charges flowing across the surface in opposite directions. Any isotropic flow will met this condition of zero net current. There are many other configurations which will produce a zero net current across a surface in the plasma. However, when a solid surface (such as a spacecraft) is inserted suddenly, compensating currents are now radically changed, and for a time charge buildups on the spacecraft until the net current across the surface of the spacecraft is zero. During this period the spacecraft accumulates charge, forms a sheath, and if no discharges occur eventually reaches a equilibrium with the space plasma and radiation so that a surface drawn around the spacecraft will not have any net current flowing through it. Depending on the geometry and material properties of the spacecraft, different charge levels may occur on different surfaces. The whole potential distribution on and around the spacecraft can be quite complex. The mechanism involved in charging spacecraft will be discussed in more detail in section 2-3

Two types of surface charging can be identified. The first, absolute charging, occurs when the entire spacecraft potential is changed relative to the ambient space plasma by the encounter with the environment. For absolute charging the spacecraft potential changes as a whole -- the dielectric surface voltages are "locked" to the ground reference voltage. This type of charging occurs very rapidly (in fractions of a second), typical of the time required to charge the spacecraft to free space capacitance.

The second type, called differential charging, occurs when parts of the spacecraft are charged to different potentials relative to each other. This type of charging is more significant from an engineering point of view. In this type of charging, strong local electric fields may exist. Differential charging usually occurs slowly (in minutes) and results in one part or surface being charged to a potential different from those of other parts of the spacecraft. Differential charging can also change the absolute charging level of the spacecraft.

2.2. Concerns

The kinds of things that can go wrong when charging is allowed to go unchecked are: electrical discharges that couple into sensitive circuits, noise in data and on spacecraft systems' wiring, accelerated aging of surfaces, increased contamination of spacecraft surfaces due to the reattraction of outgased and ambient material, and the contamination of scientific and engineering charged particle data by electric fields induced by the presence of the spacecraft.

Whether or not charging/discharging is important to a given system depends on the system's objectives and constraints. The buildup of large potentials on a spacecraft relative to the ambient plasma when the spacecraft is not actively measuring an undisturbed plasma environment is not, of itself, a serious engineering concern. Spacecraft electronic systems referenced to a structural ground are not affected by a uniformly charged spacecraft. However, scientific missions, seeking to measure properties of the space environment, can be severely impacted by uncontrolled or unknown potentials on the surface of the spacecraft. The sheath formed around even a uniformed charged body influences the trajectories of particles near the body. Since the instruments we use to measure the particles and fields are mounted on the spacecraft body, the environment they are sampling is distorted by any fields induced by the presence of the spacecraft body. Here even uniform fields may represent a serious concern. For example the placement of particle sensors on the Galileo mission was influenced by small unavoidable potentials on the spacecraft surface (Leung and Robinson, 1982). Uniform charging must also been considered as a means of increasing the contamination of charged surfaces in space. Here the concern is that a charged surface will attract oppositely charged particulate matter which can then stick to the surface. Optical surfaces are particularly sensitive to contamination and raise questions for both charging and contamination analysis.

Spacecraft surfaces are not uniform in their material properties or exposure to the environment, so one would not necessarily expect to seen a uniform charge distribution over the entire spacecraft surface. Nonuniform charging can influence the measurement of the ambient plasma distribution even more severely than uniform charging (Olsen, 1980). However from an engineering point of view, differential charging that can lead to discharges is the major concern. Discharges introduce noise into the system. Occasionally this noise interrupts normal spacecraft operation, or represents a false command. This spacecraft charging effect was the motivation for the SCATHA program and needs to be included in electromagnetic compatibility (EMC) design practices in system design. In the process of breakdown it is possible to cause physical damage where the discharge occurred. Thus it is possible to change the physical characteristic (thermal properties, conductivity, optical parameters, chemical properties, etc.) where the discharge occurred. In addition the release of material from the discharge site has been suggested as a contamination source for the remainder of the spacecraft (Hall 1977).

Charging and discharging due to the interaction of the system with the natural environment raises concerns in the areas of electromagnetic compatibility, contamination control, thermal control, reliability, and science analysis.

2.3 Charging Mechanism

In most environments of engineering interest, the largest current to the the spacecraft surface is the plasma. Consider for example a plasma in "thermal equilibrium." Such a plasma easily satisfies the zero net current condition of a plasma. Even through the electrons and ions have very different velocities, for every electron traveling in one direction there is another electron traveling in the opposite direction on the average. The same is true of the protons. So an imagined volume will on the average contain equal numbers of positive and negative charge carriers. Now imagine a material which completely absorbs every charged particle that impacts it. When that solid object is inserted into the plasma, half of the electrons and protons are prevented from reaching the opposite side of the object (that is they intercept the other side of the object.). The average velocities of the electrons and protons can be calculated from the equipartition theorem,

$$\frac{1}{2}kT = \frac{1}{2}m_e v_e^2 = \frac{1}{2}m_p v_p^2 \qquad (2\text{-}1)$$

where the subscripts refer to either electrons (e) or protons (p), k is Boltzmann's constant, v is the average velocity and m is the mass. Clearly the average electron velocity is much larger than the average proton velocity. Since the current is proportional to the average velocity times the density (assumed to be the same for electrons and proton in this plasma), the electron current hitting the absorber will be higher than the proton current. Thus a negative charge will build up on the material. This will continue until the electric field produced by the accumulation of charge is sufficient to repeal electrons and attract positive ions. Thus there is a charge build up until the equilibrium condition of zero net current is reached. Real spacecraft, of course are more complex. Real plasmas may not be describable as a Maxwellian plasma. The surface of a spacecraft is made of a number of materials with different electrical properties. One of the key properties being the number of electrons released from the material when impacted by an electron or ion. This secondary emission coefficient is tabulated for a number of popular spacecraft materials later in this chapter. For real materials the secondary emission coefficient, backscattering and geometry of the material all play a role in determining the net current to the surface. In addition the electrical interconnection and geometrical relations of one part of the surface to another can play a key role.

Consider a spacecraft with two basic materials on its surface -- one a conductor, the second an insulator (for example the insulator might be the solar cell cover glass (silicon), while the antenna and exposed structure might be aluminum). The zero current balance condition needs to be applied at each surface point for the insulator. Solar cell covers at one location may see larger fluxes than another location due to distortions in the environment or produced by differential charging about the spacecraft.. While the conductors integrate currents from all surfaces that are electrically connected. Clearly with complex three dimensional geometries the determination of currents to each part of the spacecraft can be quite complex. This problem has been studied for a number of years. The computer code NASCAP (NASA Charging Analysis Program) was originally developed in support of the SCATHA (Spacecraft Charging AT High Altitudes - a joint Air Force NASA project) program to handle the geometric and material

complications inherent in realistic charging calculations. NASCAP is described in more detail in the appendix. Simplified codes based on NASCAP results also exist (N. J. Stevens, private communication, 1989)

2.3.1 Sheath Formation

When the spacecraft is at a high altitude (for example geosynchronous) the mean free path of both electrons and ions is very large compared to the dimensions of the spacecraft and individual particle trajectories are controlled mainly by the electric and magnetic fields near the spacecraft. NASCAP was written to handle spacecraft charging calculations in this regime. While at low altitudes, or when the spacecraft is moving at a velocity which is high compared to plasma velocities, particle trajectories are influenced by the presence of other plasma particles. In this case sheath formation, ram, and wake effects are very important. A second three dimensional computer code called NASCAP-LEO has been constructed to handle this situation.

In plasma physics the parameter which describes the length over which an electric field exists in a plasma (which is essentially a conducting gas) is the Debye length. In gaussian units the Debye length is

$$\lambda_D = \sqrt{\frac{kT}{4\pi ne^2}} = 743\sqrt{\frac{T}{n}}\,\text{cm}. \qquad (2\text{-}2)$$

where T is the plasma temperature in electron volts, n is the density in particles per cubic centimeters, e is the electron charge and k is Boltzmann's constant. At gyrosynchronous orbit the Debye length is long compared to the spacecraft dimensions for typical 1980's communications satellites and so the NASCAP code is a good choice. At low altitudes, the Debye length is short compared to the size of the Shuttle or the space station or even weather satellites, and consequently the LEO code is the more realistic choice.

2.3.2 Plasma Currents

The environment plays a key role in determining the electron and ion currents to and from the spacecraft surface. If the surface is insulating, the net current to each point on the surface in equilibrium is zero. If the surface is conducting, the sum of all currents to the connected conducting surfaces sums to zero. The net current to a surface is the sum of currents due to ambient electrons and ions, secondary electrons, and photoelectrons.

The density of the plasma determines the primary currents.

$$J = nq\langle v\rangle \qquad (2\text{-}3)$$

where n is the density of the plasma, q is the charge on a particle, $\langle v\rangle$ is the average velocity of the particle, and J is the current density of particles of charge q. A "thin" or tenuous plasma of less than 1 particle/cm^3 will charge the spacecraft and its surfaces more slowly than a "dense" plasma of thousands of particles per cubic centimeter with the same velocity distribution. The current density can also affect the conductivity of the material through an effect called radiation induced conductivity. The conductivity helps determine the leakage current throughout the material, and hence the likelihood of differential charging.

2.3.3 Current Balance

The equation for current balance (to calculate the equilibrium spacecraft potential, V) including secondary emission processes is

$$I_{total} = I_e + I_i + I_{e/e} + I_{e/i} + I_{bac} + I_{h\nu} \pm I_{other} \qquad (2\text{-}4)$$

Each of these currents is a function of the potential. The potential enters the equations through the dependence of the velocity on the potential. I is the total current (which will go to zero in equilibrium).

The first term is the electron current from the plasma to the surface.

$$I_e = n\,e\,\langle v \rangle = \int d^2r \int_{v=0}^{v=\infty} d^3v\, f(v,r,t)\, e\, v \cos\theta \qquad (2\text{-}5)$$

where n is the electron density, e is the charge on the electron, $\langle v \rangle$ is the average electron velocity, f is the distribution function, and theta is the angle between the normal to the surface and the velocity. This term is integrated over whatever surface "sees" any plasma. For conductors in space the appropriate surface is all of the conducting surface. For insulators each point of the surface is done individually. If f is the distribution function for electrons the next integral is over all electrons which reach the surface with a velocity of zero or greater. This will of course depend on the potential of the surface. The cosine factor accounts for the projection of the actual surface to the distribution function. The charge on the electron is e. The second current in the total current equation (2-4) is a similar integral for the ion current.

When electrons impact on a surface there is a finite probability that they will release one or more electrons from the surface. This effect, called secondary electron emission, is accounted for in the next two terms of equation 2-4. The first is the secondary emission due to incoming electrons. The second is the emitted electrons for incoming ions. The integral for electrons is

$$I_{e/e} = \int d^2r \int_{v=0}^{v=\infty} d^3v\, f(r,v,t)\, \delta(v)\, h(v,\theta) \cos\theta \qquad (2\text{-}6)$$

The integral is over the appropriate surface, but now the distribution function is weighted by a probability of emission delta that is a function of the velocity,v. In addition there is a distribution of velocities for the emitted electrons represented in this equation by h. The resulting secondary emission current is still a function of the potential of the surface. A similar expression could be written for ion secondary electron production. The total number of electrons with energy less than 50 eV, called the secondary electron yield, as a function of the incident electron energy is shown in figure 2-2. The important parameters, experimentally, are the maximum yield, the incoming electron energy at the maximum yield (E_2), and the electron energies at which the secondary yield is exactly one which are E_3 and E_1 in Figure 2-2.

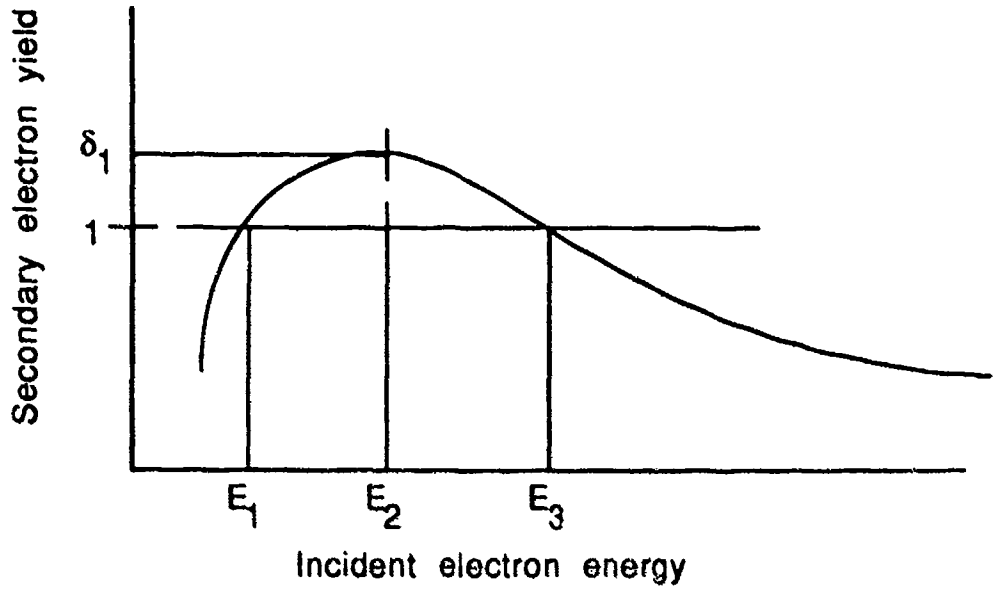

Figure 2-2. Secondary Electron Yield

Accurate measurements of the secondary yield for dielectrics which charge are difficult when a full description is desired. Katz et al. (1986) describe secondary electron emission with the following equation

$$Y(E) = \left(\frac{E}{E_3}\right)^{1-p} \qquad (2\text{-}7)$$

where the range of electrons in the material is proportional to the energy to the power p. The exponent, p, is typically between 1.5 and 2; E_3 is the energy at which the secondary yield extrapolates to unity. Some typical values are listed below in table 2-1.

Table 2.1 Secondary Emission Parameters

MATERIAL	p	E_3 (keV)	Reference
Aluminum	1.76	1.8	NASCAP
Aquadag	1.55	1.2	NASCAP
Gold	1.73	4.6	NASCAP
Kapton	1.725	1.53	Burke 1980
Lucite	1.725	3.02	Burke 1980
Magnesium	1.75	0.7	NASCAP
Mylar	1.725	2.07	Burke 1980
Nylon	1.725	3.15	Burke 1980
Polyethylene	1.725	4.02	Burke 1980
Polystyrene	1.725	2.27	Burke 1980
Polyvinyl alcohol	1.725	3.51	Burke 1980
Silver	1.74	4.0	NASCAP
SiO_2	1.86	4.8	NASCAP
SOLA	1.73	4.63	NASCAP
Teflon	1.725	4.75	Burke 1980

Characterizing the secondary emission by the two parameters in the table above can be done crudely and quickly by measuring the equilibrium potential of the surface for a sample of the material where the leakage current is kept as low as possible. The surface of the material in such a situation tends to be the electron beam energy minus E_3, the energy at which the secondary yield extrapolates to one.

Another popular fit to the experimental data is Sternglass (1957):

$$\delta(E) = 7.4\delta_1\left(\frac{E}{E_2}\right)\exp\left[-2\sqrt{\left[\frac{E}{E_2}\right]}\right] \qquad (2\text{-}8)$$

where δ_1 is the maximum secondary yield, and E_2 is the energy at which the secondary yield is at a maximum. Here $\delta(E)$ is the number of secondary electrons emitted as a function of the energy, E, of the incoming electrons.

The next term in the total current series (equation 2-4) is the current of electrons leaving the surface due to backscattered electrons. This term looks identical to the plasma current except for a factor B.

$$I_{bac} = I_e B = n\,e\,\langle v\rangle = \int d^2r \int_{v=0}^{v=\infty} d^3v\, B(v)\, f(v,r,t)\, e\, v \cos\theta \qquad (2\text{-}9)$$

When electrons impact the surface electrons of all energies are observed leaving the surface. The electrons leaving the surface fall into two major energy groups. The low energy ones (below 50 eV) are usually lumped into the secondary emission category. There is also a group which has only had one or two collisions with atoms in the surface and leave the surface at almost the incident energy. These are the backscattered electrons characterized by the function B.

If the surface is exposed to photons, there will be a photocurrent contribution to the total current. This current is represented by

$$I_{h\nu} = \int d^2r \int_0^{\infty} d\nu F(\nu) g(\nu, r) \qquad (2\text{-}10)$$

In this term the second integral is over the frequency distribution function, f, for the photons and the photoelectric yield g. For materials in orbit around the earth, this is probably the most important surface charging current. Photoemission has been characterized in a manner similar to secondary emission. Photoemission also depends on the surface condition of the material. Grard (1973b) characterized some materials of interest to spacecraft with the following parameters for solar fluxes (table 2-2).

Table 2-2 Photoemission Saturation Currents

Material	Saturation Current Density, $\mu A/m^2$	Average Energy Leaving the Surface, eV
Aluminum Oxide	42	.94
Indium Oxide	30	1.19
Gold	29	1.02
Stainless Steel	20	1.06
Graphite	4	1.02

Purely empirical, monoenergetic, or Maxwellian distributions have been used to characterize the spectra of photoelectrons. The relatively low energy (on the order of 1 eV) of most photoemitted electrons makes them particularly susceptible to the barrier effect. (The barrier effect is when the potential in front of a photoemitting surface is slightly repulsive due to a highly charged region nearby. Thus, photoemitted electrons will be repelled to the photoemitting surface, and consequently the effect of photoemission will be nullified.)

The last term in our current balance equation (equation 2-4) is meant to cover any other current we haven't mentioned. This might include any ohm's law current from the spacecraft, currents due to thruster operations, ion engine currents, ram (current collected by the spacecraft because of its motion through the plasma) or wake(the shock-like structure formed about a moving spacecraft) effects that distort the distribution functions, or anything else. One current that may play a role and is sometimes overlooked is radiatin induced conductivity.

The conductive current, j_1, can be expressed in terms of mobilities and charge densities as

$$j_2 = [g + \mu_1 \rho_1^+ + \mu_2 \rho_2^-] E \qquad (2\text{-}11)$$

The conductivity of the dielectric, g, is

$$g = e(n_1 \mu_1 + n_2 \mu_2) \qquad (2\text{-}12)$$

where n_1 is the density of intrinsic positive carriers -- both trapped and free, and n_2 is the intrinsic density for electrons. The total charge density for positive carriers is $e\, n_1 + \rho_1^+$ and for negative carriers is $e\, n_2 + \rho_2^-$.

The trap-modulated mobilities for positive and negative carriers are μ_1^+ and μ_2^-, respectively, and ρ is the generally space-dependent excess charge carrier density. The internal charge decay in dielectrics is governed by this conduction phenomenon. When exposed to a radiation field (UV, charged particle, or neutrons), the excess charge carrier density is usually increased, increasing the measured conductivity of the material. The current density can now be written as

$$J = (\Omega_0 + \Omega_1 D) E \quad (2\text{-}13)$$

if the excess carrier density is assumed to be proportional to the dose rate. Frederickson (1974), in studying photocurrents, added a term not proportional to E. Wilkenfeld et al. (1981) express the radiation induced conductivity due to electrons as a coefficient and the dose rate to a power ζ so that the combined current might be written as

$$J = J_0 + \left(\Omega_0 + \Omega_1 (D)^{\zeta}\right) \quad (2\text{-}14)$$

Some suggested values are listed below (Table 2-3)

Table 2-3 Radiation Induced Conductivity

Material	Ω_1 $s(\Omega\text{-cm-rad})^{-1}$	ζ	Dose Rate Range rads/s in Material
1 mil FEP	3.5E-17	.70	10^3 to 10^5 (Wilkenfeld et al., 1981)
Kapton H	5.9E-18 to 5.6E-17	.85 to 1.00	10^3 to 10^5 (Wilkenfeld et al., 1981)
	8.0E-17 to 7E-16	.6 to .8	(Riddel and Passenheim, 1982)
Type S Mylar	1.0E-17 to 4.5e-18	.81	10^3 to 10^5 (Wilkenfeld et al., 1981)
	8E-17 to 1.4E-16	.8	(Riddel and Passenheim, 1982)
Second surface mirrors	4E-16	.8	(Riddel and Passenheim, 1982)

In addition, there is a dependence on temperature, thickness of the sample, and type of radiation. In high dose rate situations radiation induced conductivity can be very significant.

2.3.4 Distribution functions

A great deal of effort is still needed to adequately describe the electron and ion environment around the earth. Although well behaved in limited regions of energy space, the actual distribution functions hold within them detailed descriptions of the dynamics and complexities of the magnetosphere. Simple approximations are generally inadequate to describe such richness. Nonetheless single or double maxwellian functions have been fit to measured data to help engineers and scientists deal with this complexity, but care is always needed not to push the approximation to far. Even comparisons with measurements may be misleading, as the natural binning of the instrument making the measurement may hide some important details of the physics, and make the final approximation misleading. Nonetheless, great progress has been made using double or single maxwellian

approximations to the real environments and these will probably continue as our first order approximation because of the simplifying concept of a single temperature for a distribution.

2.3.5 A Simple Analytic Approximation

For a spherical body and a Maxwell-Boltzmann distribution, the first-order current densities (the current divided by the area over which the current is collected) can be shown (Garrett, 1981) to be given by

Electrons

$$J_1 = J_{10} \exp\left(\frac{qV}{kT_1}\right) \qquad V < 0 \quad \text{(repulsive)}$$

$$J_1 = J_{10}\left[1 + \left(\frac{qV}{kT_1}\right)\right] \qquad V > 0 \quad \text{(attractive)} \qquad (2\text{-}15)$$

Ions

$$J_2 = J_{20} \exp\left(-\frac{qV}{kT_2}\right) \qquad V > 0 \quad \text{(repulsive)}$$

$$J_2 = J_{20}\left[1 - \left(\frac{qV}{kT_2}\right)\right] \qquad V < 0 \quad \text{(attractive)} \qquad (2\text{-}16)$$

where the incident (zero potential) electron and ion currents are:

$$\left.\begin{aligned} J_{10} &= \left(\frac{qN_1}{2}\right)\left(\frac{2kT_1}{\pi m_1}\right)^{1/2} \\ &\text{and} \\ J_{20} &= \left(\frac{qN_2}{2}\right)\left(\frac{2kT_2}{\pi m_2}\right) \end{aligned}\right\} \quad \text{Primary incident electron and ion currents}$$

where N_1 is the electron density and N_2 is the ion density, m_1 and m_2 are masses of electrons and ions, respectively; and q is the magnitude of the electronic charge.

Given these expressions and parameterizing the secondary and backscatter emissions, Garrett has reduced the current balance equation to an analytic expression in terms of the potential at a point. This model, called an analytic probe model, can be stated as follows:

$$I = 0 = A_1 J_{10}\{1 - SE(V,T_1,N_1) - BSE(V,T_1,N_1)\} \exp\left(\frac{qV}{kT_1}\right)$$

$$- A_2 J_{20}\{1 + SI(V,T_2,N_2)\}\left[1 - \left(\frac{qV}{kT_2}\right)\right] - A_4 J_{40}, \Phi \qquad (2\text{-}17)$$

for $V < 0$ where A_1 is the electron collection area, A_2 is the ion collection area, A_4 is the photoelectron emission area, J_{40}, is the saturation photoelectron flux, BSE the parameterization of the backscattered electrons, SE the parameterization of secondary electrons, SI the parameterization of secondary electrons from ion impact on the surface, and Φ the solar EUV flux at the spacecraft. This equation is appropriate for a small (<10 m), uniformly conducting spacecraft at geosynchronous orbit in the absence of magnetic field effects. To solve the equation, V is varied until I=0. Typical values of SI, SE, and BSE are 3, 0.4, and 0.2, respectively, for aluminum. The EUV-

created photoelectron emissions usually dominate near earth and prevent the spacecraft potential from being very negative during sunlit portions of the mission. However, in and near geosynchronous orbit during geomagnetic substorms the ambient hot electron current can control the charging process. For geosynchronous orbit, the ratio of the electron to ion current density is about 30 during a geomagnetic storm. When the spacecraft is in eclipse, these values give

$$V \approx -T_1 \quad (2\text{-}18)$$

where T_1 is in electron volts. That is, to first order in eclipse, the approximate spacecraft potential is numerically equal to the plasma temperature expressed in electron volts. Note, however, that T_1 must exceed some critical value (Olsen, 1983; Garrett, 1981), usually of the order of 1000 eV, before charging will occur because secondary electron production exceeds ambient current for low T_1.

2.3.6 System Charging Characteristics

There is much more to understanding the charge buildup on a complicated spacecraft system, than the simple calculation of the charge flowing to a surface. All of the surfaces, their interconnections and geometry play a role in the current flow to and around a spacecraft. The very simple analytic probe model just covered emphasized the plasma conditions for the current flow. Just as important are the magnetic field, the geometry, and the interconnection of the areas involved. A simple engineering approximation which begins to consider these interconnections and the geometry of the surfaces is to view the spacecraft as a collection of capacitors. The capacitance of the spacecraft body to space, for example, determines the time required for the spacecraft as a whole to reach a potential. Thermal blankets, instruments, and other parts of the systems each have a distributed capacitance, and impedance to other parts of the system. Differential charging is governed by these capacitances. Computer codes like NASCAP must consider these in calculating the charge buildup as a function of time. When circuit codes are used to simulate this process, all of the appropriate capacitances need to be modeled. What is not modeled is not simulated.

2.3.6.1 Lumped-Element Modeling

Lumped-element models have been used to define the surface charging response to environmental fluxes (Robinson and Holman, 1977; Inouye, 1976; Massaro et al., 1977; Massaro and Ling, 1979), and are currently used to predict interior structural currents resulting from surface discharges and system generated electromagnetic pulses. The basic idea of a lumped-element model is to represent spacecraft surfaces, boxes, elements, and structures as electrical circuit elements. These models can be made as simple or as complex as desired. The circuit simulation code SPICE and its clones and derivatives can be used to calculate circuit element responses. SEMCAP (Specification and Electromagnetic Compatibility Program) is a code developed by TRW specifically to calculate the effects of discharges on the Voyager spacecraft. SEMCAP is based on modeling the interbox harness cabling and input/output interface boxes and calculates the peak voltage at designated receptors.

2.4. ESD Causing Environments

Surface charging and discharging results when the environment is rich in kilovolt electrons and poor in lower energy particles. Plasmas of that distribution usually occur only during periods of dynamic change such as magnetic substorms or solar particle events. This is why spacecraft charging effects are so strongly correlated with geomagnetic indices. In addition, other situations which somehow manage to remove low energy electrons, accelerate electrons or ions in beams or other structures, create a hot plasma with a temperature on the order of kilovolts, or in some other way create a distorted plasma condition can result in charging spacecraft surfaces. This section describes some of the better known environments which should be considered in spacecraft charging analysis.

2.4.1 The Regions of the Earth's Magnetosphere

When a plasma is heated and accelerated towards the earth from the geomagnetic tail region, it rushes into synchronous orbit and bathes a spacecraft in a hot plasma, causing charging. The early observations of spacecraft charging occurred in this way. The SCATHA program was organized to investigate this effect, and many research and engineering papers have resulted from this work. Purvis et al. (1984), Garrett (1979), Whipple (1981), and others have published review articles on this subject. Most regions of the magnetosphere that are in thermal equilibrium tend to be at relatively low temperature and consequently not of concern for charging.

A full description of the magnetosphere is the goal of a great deal of current research and thought. Every four years a summary of research in the United States is given in "Contributions in Solar-Planetary Relationships, U. S. National Report to International Union of Geodesy and Geophysics." To describe the "shape" of the magnetosphere we need either the motion of all the particles near the earth or the currents and fields surrounding the earth. Tracing magnetic field lines, for example, gives us some insight into the general flow patterns of particles because individual charged particle trajectories are determined in part by the magnetic forces on the particle, but the magnetic field configuration is also the result of particle flows. So if the final magnetic field is known, it indicates the currents and flows which are both formed by the magnetic field and help to form it.

The volume around the earth called the magnetosphere can be roughly divided into the regions. Sometimes these regions overlay, or become ill-defined, but it is still useful to attempt to describe regions of the magnetosphere and the interrelations of these regions.

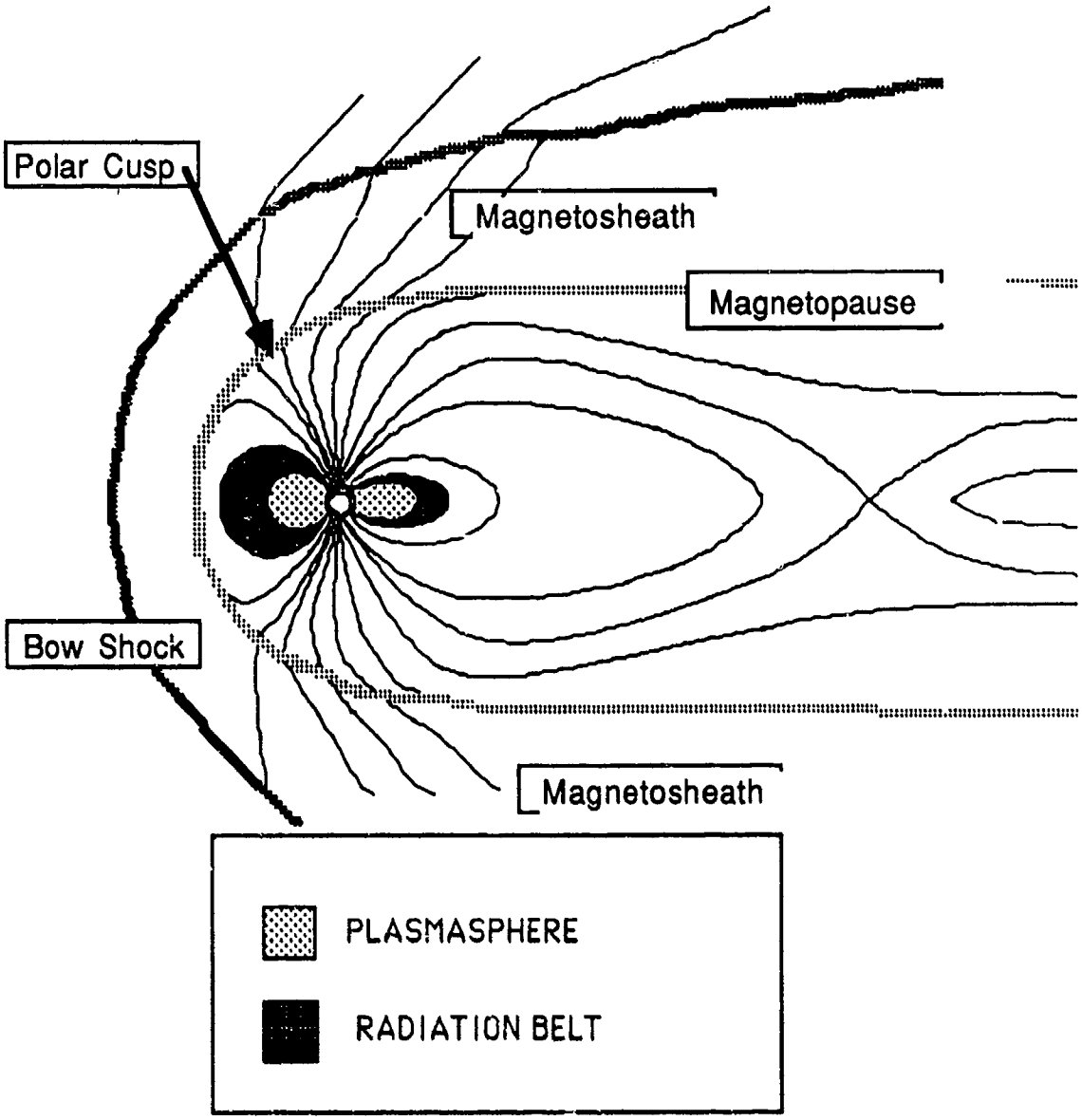

Figure 2-3. Map of the Magnetosphere

2.4.1.1. Bow Shock

Figure 2-3 is a cartoon of the near-earth region of space. The first black line coming from the left hand edge of the figure is the "bow shock." This is the boundary formed when the supersonic solar wind with its magnetic field encounters the earth's magnetic field. The solar wind is made up of plasma from the sun and a magnetic field trapped within the plasma because of the high conductivity of the plasma. The magnetic field in regions between planets is called the interplanetary magnetic field or IMF. The solar wind is supersonic (that is, the velocity of the particles in the solar wind is greater than the sound velocity in the medium) and super Alfvenic as well (that is the particles are moving faster than disturbances, Alfven waves, which propagate in magnetic fields). The magnetosphere acts like a blunt object inserted in the supersonic flow of the solar wind. The bow shock formed is much like the aerodynamic shock wave formed by a blunt object in the supersonic flow of a wind tunnel. The

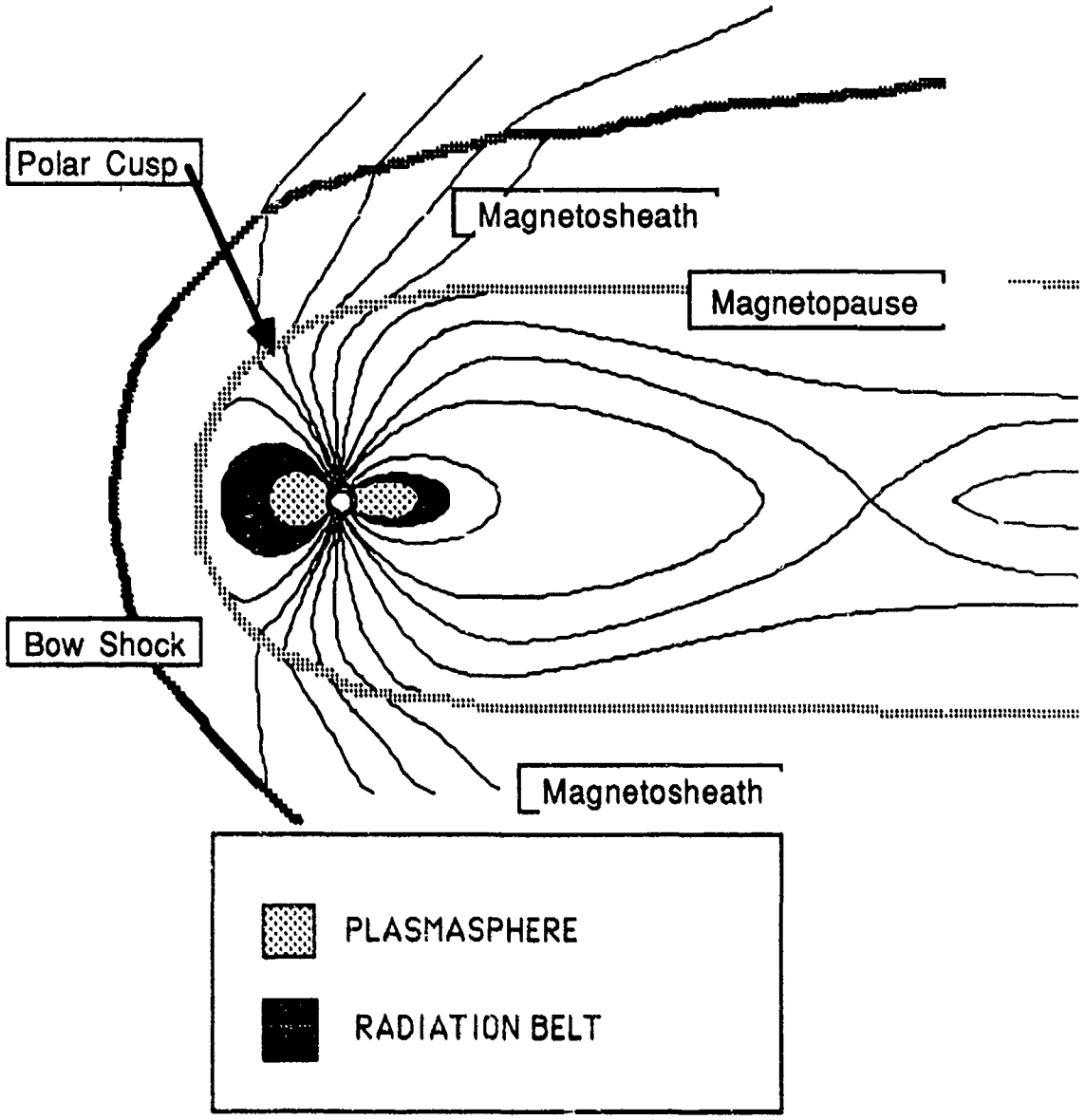

Figure 2-3. Map of the Magnetosphere

2.4.1.1. Bow Shock

Figure 2-3 is a cartoon of the near-earth region of space. The first black line coming from the left hand edge of the figure is the "bow shock." This is the boundary formed when the supersonic solar wind with its magnetic field encounters the earth's magnetic field. The solar wind is made up of plasma from the sun and a magnetic field trapped within the plasma because of the high conductivity of the plasma. The magnetic field in regions between planets is called the interplanetary magnetic field or IMF. The solar wind is supersonic (that is, the velocity of the particles in the solar wind is greater than the sound velocity in the medium) and super Alfvenic as well (that is the particles are moving faster than disturbances, Alfven waves, which propagate in magnetic fields). The magnetosphere acts like a blunt object inserted in the supersonic flow of the solar wind. The bow shock formed is much like the aerodynamic shock wave formed by a blunt object in the supersonic flow of a wind tunnel. The

shock is detached (separated) from the magnetosphere. The solar wind coming from the sun cannot pass through the earth, and is forced around the earth. So the solar wind "piles up" in front of the earth, and creates a bow shock in front of and around the earth. The particle density and field strength of the solar wind increase in front of the earth. In this region, solar wind speeds fall into the subsonic range.

2.4.1.2. Magnetosheath

The region between the undisturbed solar wind and the magnetopause (to be defined in a following paragraph) is called the magnetosheath and is characterized by considerable plasma turbulence. The IMF still dominates in the magnetosheath, but it is disturbed. The solar wind may be deflected by as much as 20°, and slowed to about 250 km/sec (subsonic) with a concurrent increase in density to as much as a factor of four. Electron and ion temperatures as high as 10^6 K (≈100 eV) have been measured. The detailed structure of the magnetosheath depends on the relative orientation of the magnetic field of the solar wind and that of the earth. In Figure 2-3, the IMF is parallel to the earth's dipole in the sense that the component of the IMF in the direction of the earth's magnetic field above the north pole of the earth is in the same direction as the earth's field there. This allows the IMF and the earth's magnetic field to coincide above the poles of the earth. Magnetic field lines which pass directly into the IMF are called "open." Thus solar particles gyrating about these lines have direct access to regions very near the earth. If the IMF reversed, the field lines shown in this figure above the earth's poles would be oppositely directed to the IMF. In the case where there is no connection between the IMF and the earth's field over the poles and the lines are said to be "closed," that is the IMF and the earth's magnetic field are counter to each other over the poles. The magnetic field lines at the equatorward edge of the auroral oval, no matter what the IMF is doing, are closed. At the poleward edge, the magnetic field lines trace back to the neutral sheet (to be defined later in this section). The noontime section of the auroral oval is indicated by the magnetic field lines which continue from the earth's magnetic field through the magnetopause and the bow shock into the undisturbed solar wind. This region is referred to as the "polar cusp."

As the plasma moves around the earth toward the tail region, the bulk velocity of the solar wind plasma in the magnetosheath increases due to the adiabatic expansion of the plasma as it expands into the region behind the earth.

2.4.1.3. Magnetopause

The major boundary separating the earth from the solar wind is the magnetopause. This boundary is where the pressure of the solar wind (primarily particle pressure, but including the "trapped magnetic field") is equal to the pressure of the earth's magnetic field and a small component of particle pressure from the earth. In the sunward direction the magnetopause occurs at approximately 10 - 12 earth radii (10 - 12 R_e). This distance varies, depending on the IMF, between 7 and 14 R_e. Experimentally, the point at which the pressure from the solar wind, primarily particles, is exactly balanced by the pressure due to the earth, primarily magnetic field, is not determined exactly. The magnetopause has a thickness, a region over which the pressures approximately balance. The magnetopause is normally 100 to 200 km thick. Just as the bow shock extends a very long distance beside and behind the earth, the magnetopause extends in a roughly cylindrical shape behind the earth. The magnetopause extends well past the orbit of the moon (60 R_e), and may extend to more than 1000 R_e.

2.4.1.3.1 Magnetopause Currents

The magnetopause allows some diffusion of solar wind particles across the boundary from the magnetosheath. This diffusion can be considered perpendicular to the magnetopause at all points. The perpendicular diffusive velocity and the orientation of the geomagnetic field determine the electric currents produced through the Lorentz force, $F = q\ V \times B$. This is illustrated in figure 2-4. In the case of the magnetopause, there is no local plasma to speak of and strong electric fields can develop to influence the penetration depths of the electrons and ions into the earth's magnetic field. Depending on the plasma densities and generated electric fields either the ions or the electrons will be the main current carriers. In the case of the solar wind with an electron velocity of 10^8 cm/s various instabilities arise producing waves, two stream instabilities, the growth of electric space charge clouds, and a

scattering or thermalizing of particles within the boundary layer instead of reflection of solar wind particles from the boundary. Interplanetary electric fields further complicate the picture. On the sunward side of the earth, the diffusive velocities and the northward oriented geomagnetic field cause a current flowing from left to right (as viewed from the sun)

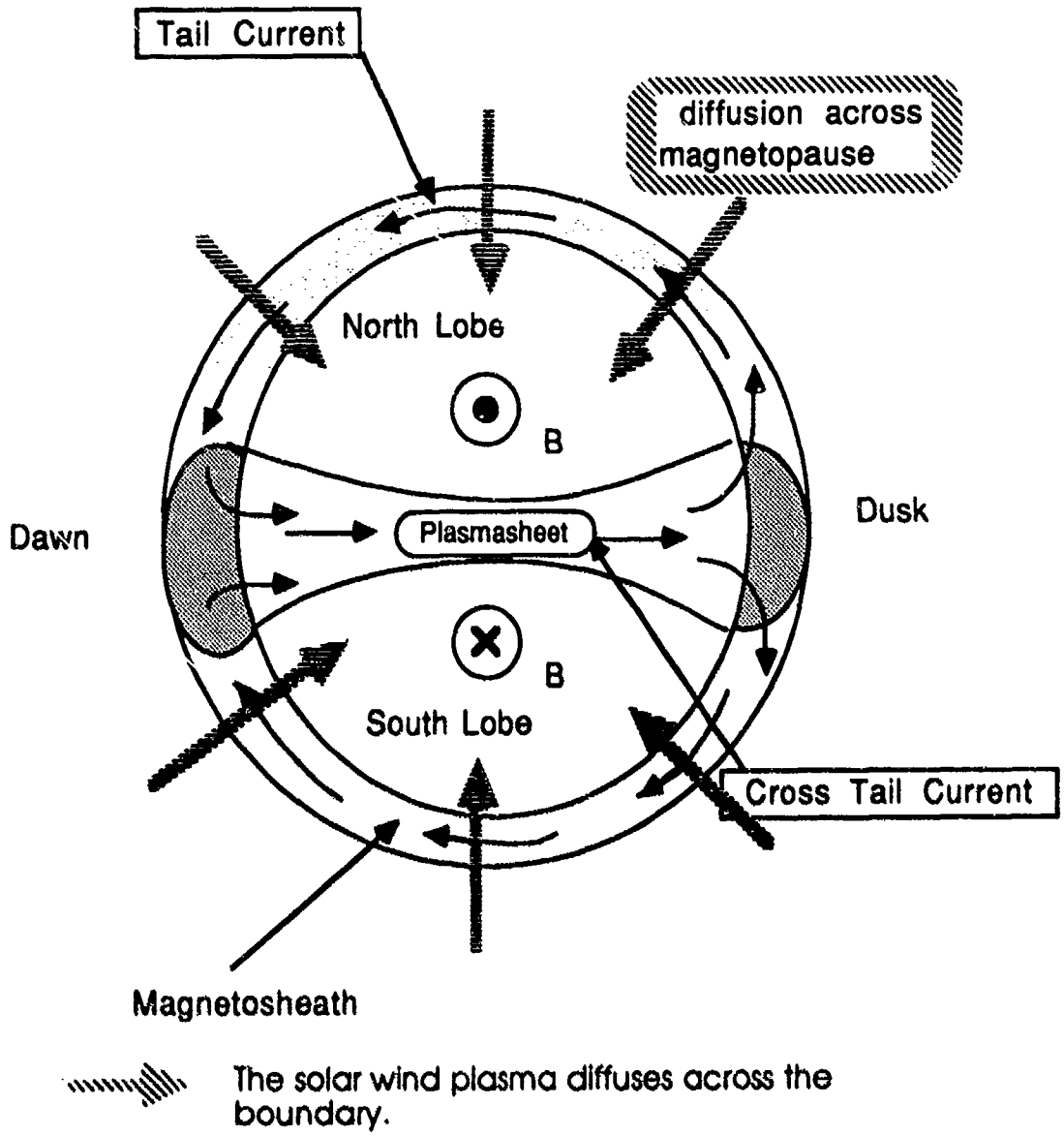

Figure 2-4. Lobed Structure in Geomagnetic Tail

2.4.1.3.2 Deep Magnetospheric Convection

On the inner surface of the magnetopause is a boundary layer of plasma which flows away from the sun, just as the plasma in the magnetosheath, but its velocity and density are less than those of the magnetosheath plasma. Both electrons and protons drift in the same direction. The orientation of the geomagnetic tail field lines (toward the earth in the north lobe, and away in the south lobe) causes electrons and protons to drift toward the center

of the magnetotail, providing a source of particles for maintaining the plasma sheet. Once the particles are near the middle of the plasma sheet, they feel the influence of both the weak net northward magnetic field in the neutral sheet and the large scale electric field across the tail. The result is a drift of electrons and protons up the center of the magnetotail toward the earth (the drift is strongest near the plane of the neutral sheet). This large scale magnetospheric circulation is called the "deep magnetospheric convection." Plasma flow in the equatorial plane is illustrated below (figure 2-5).

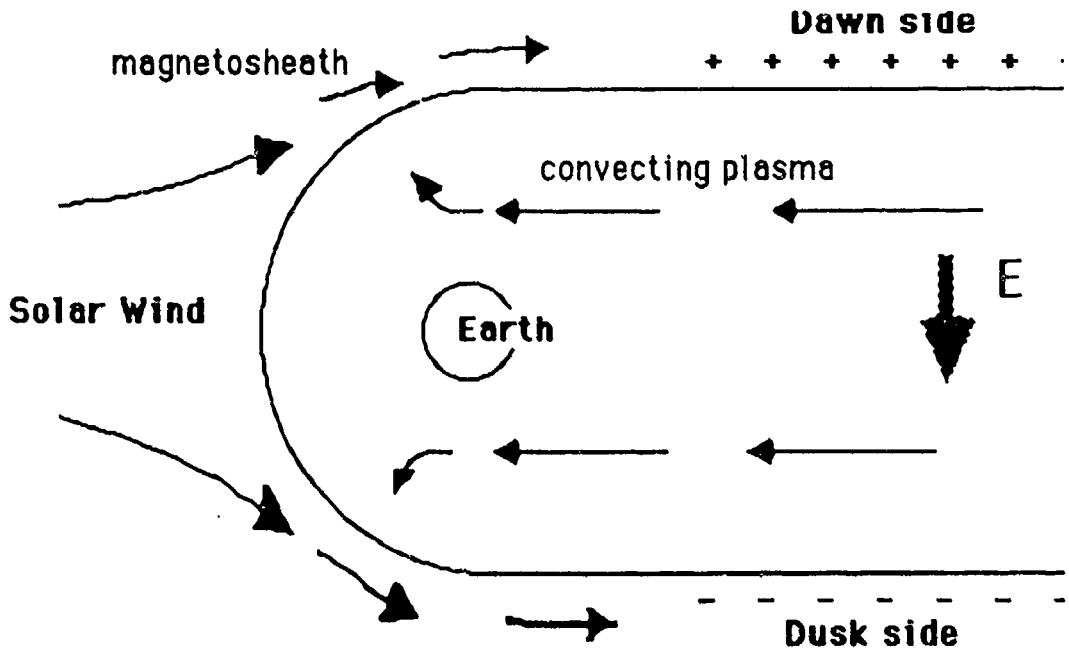

Figure 2-5. Plasma Flow in Equatorial Plane

2.4.1.4 Auroral Oval

The auroral oval is the area where electrons and ions focused by the earth's magnetic field encounter the upper atmosphere and produce aurora. The electric fields, accelerating and decelerating mechanisms in the auroral regions are still the subject of intense investigation and speculation. [Auroral injection of ionospheric particles into the magnetosphere is one mechanism under consideration when investigators consider the source of particles in the ring current and radiation belts.] The auroral oval is a transition region including both open and closed field lines. Some researchers object to using magnetic field lines in describing dynamic situations like this where the magnetic field lines are thought of as moving and twisting in a time-dependent manner. It is not always clear how fully time-dependent field lines are to be described; nonetheless, it is common to speak of open and closed field lines in dynamic situations like those in the auroral oval.

The current flow in the auroral region is quite complex. In the upper regions electrons and ions flow along the field lines. As the charged particles descend lower into the atmosphere, collisions with neutrals increase and the transport mechanisms change. Table 2-4 indicates regions where collisional effects are becoming more important. Electric fields caused by charge separation or other effects induce currents through out the auroral region.. A current called the auroral electrojet flows from east to west at heights of 80 to 100 km in what is called the E layer.

Table 2.4 Electron and proton collision frequencies

Altitude	Electrons	Ions	Comments
~300 km	$\upsilon << \omega$	$\upsilon << \omega$	Both electrons and ions move along field lines.
140 km	$\upsilon < \omega$	$\upsilon > \omega$	Electrons move along field lines Ions dominated by collisions .
80 km	$\upsilon > \omega$	$\upsilon > \omega$	Both electrons and Ions motion dominated by collisions
~ 60 km	$\upsilon >> \omega$	$\upsilon >> \omega$	Collisions dominate motion

ω is the gyration frequency; υ is the collision frequency.

2.4.1.4.1 Auroral Morphology -- contributed by Captain Robert Frederick, Air Weather Service

Visual auroras are faint, luminous phenomena seen in the night sky at high geomagnetic lattude (auroral zones). The principal source of energy for auroras is the dissipation of the kinetic energy carried by charged particles that bombard the earth's upper atmosphere. Collisions with these particles ionize and/or excite atmospheric atoms and molecules. During de-excitation or recombination, electromagnetic energy is emitted. Auroras occur simultaneously in both hemispheres with nearly identical temporal and spatial variations. The lower altitude limit of visual auroras is usually between 90 and 120 km, and they may extend hundreds of kilometers upward.

The energy emitted in the non-visible part of the spectrum greatly exceeds that in the visible range. The term "optical aurora" is used for auroral emissions from the infrared to the ultraviolet. Auroras may also emit radio noise in the VLF band (less than 30 kHz) and on rare occasions in the HF-VHF bands (3-300 MHz). However, the term "radio or radar aurora" is reserved for the auroral backscatter of radio waves from field-aligned irregularities.

Auroras also emit x-ray radiation. A continuous x-ray spectrum is produced as fast, energetic electrons are slowed by encounters with atmospheric particles (bremsstrahlung). In addition, x-rays are produced by excitation of inner shell electrons caused by collisions with these fast particles.

The visual form and intensity of auroras change rapidly. There are two general classes of auroral forms: diffuse and discrete.

(1) Diffuse auroras - usually faint, ill-defined, broad auroral luminosity with a width of at least several tens of kilometers. Diffuse auroras include the following forms:
   (a) Veil - an extensive, usually uniform luminosity covering a large fraction of the sky. A veil is frequently red and may occur as a background for other forms.
   (b) Patches - a region of luminosity with no particular shape, and no sharp, continuous lower border as found in bands and arcs.

(2) Discrete auroras - curtain-like structures with a typical horizontal width of 0.2 to 10 km, a horizontal extent of 100 to several thousand kilometers, and extending from a more or less continuous lower boundary upward (along local magnetic field lines) in height several tens to hundreds of kilometers. The curtains can occur singularly or in sets separated by dark spaces of the order of a few tens of kilometers wide. Discrete auroras include the following forms:

(a) Bands - curtains showing folds or kinks along their length; frequently quite active (especially if rayed).
(b) Arcs - curtains showing only slight curvature; usually a quiet, less bright form than the band.
(c) Rays - shafts of luminosity aligned along magnetic field lines, with a horizontal width of a few tens of meters to several kilometers and a height of a few tens to several hundred kilometers. Rays occur alone, but are most often found within arcs or bands.

2.4.1.4.2 Auroral Substorms -- contributed by Captain Robert Frederick, Air Weather Service

Auroras in the quiet auroral oval occasionally become active. The activation originates, in general, in the midnight sector and rapidly spreads into other local time sectors. A typical auroral substorm has two phases: expansive and recovery.

Expansive phase: The first indication of a substorm is usually the sudden brightening of the midnight sector quiet arcs or the sudden formation of a bright arc in the midnight sector. This is normally followed by a rapid poleward motion of the arc, causing an expanding bulge in the midnight sector. The evening side of the bulge contains a large-scale fold which travels westward along a quiet arc, and is called the "westward traveling surge." In the morning sector, the quiet arcs and diffuse auroras disintegrate into "patches" which drift rapidly eastward at nearly constant magnetic latitude.

Recovery phase: The westward traveling surge continues into the afternoon sector and eventually degenerates into irregular bands. The patches continue to drift eastward and reach the noon sector in the late recovery phase. At the end of the substorm conditions have returned to those before the onset. After about 2-3 hours the entire substorm pattern may be repeated.

Qualitatively the intensity of the substorm is directly related to:

(1) The brightness of the aurora,
(2) The complexity of the auroral forms,
(3) The areal coverage of the auroral bulge, and
(4) The duration of the substorm.

Equipment or systems required to operate in the auroral zone will experience quite high electron fluxes. Figure 2-6 shows a typical auroral electron spectrum.

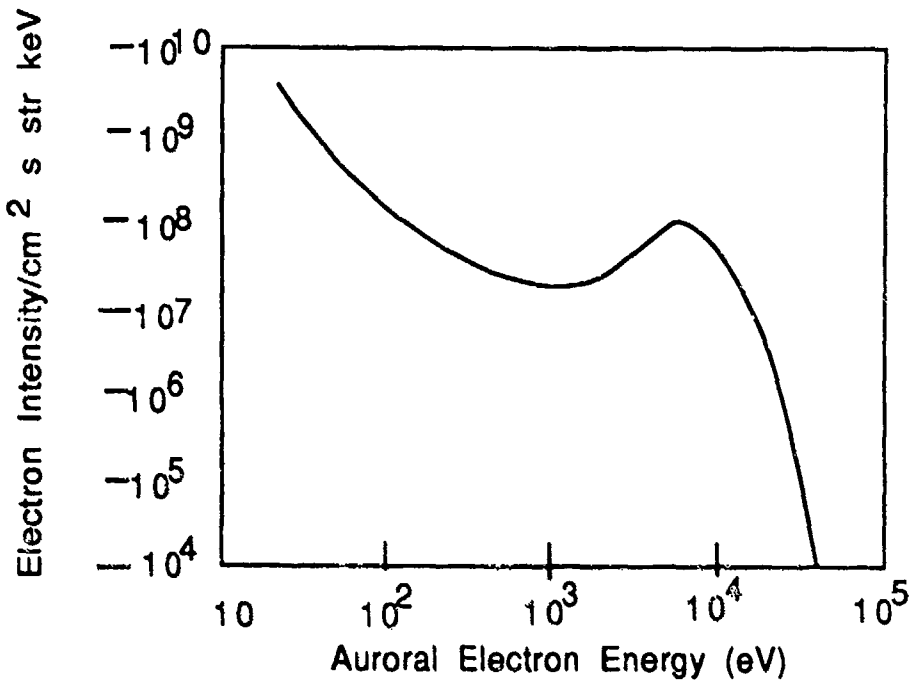

Figure 2-6 Auroral Electron Intensity at Center of an Arc

2.4.1.5. Magnetotail

The earth's magnetic field towards the sun is compressed, while the region away from the sun is stretched out. The stretched out region is called the magnetotail and extends at least 1000 earth radii, eventually becoming indistinguishable from the IMF. Beyond 8 to 10 R_E the magnetic field lines are essentially parallel to the solar wind flow, regardless of the inclination of the geomagnetic equator to the ecliptic plane. In order to sustain this structure, the tail itself has a two lobed structure where magnetic field lines from the earth are divided by a thin plasma sheet which carries a large current.separating the two regions of oppositely directed magnetic fields. This lobed structure (shown in cross section in Figure 2-4) exists for many earth radii along the geomagnetic tail.

Plasma from the solar wind can diffuse across the solar wind geomagnetic boundary into the lobed structure of the tail . The prevailing solar flow past the earth, coupled via the Lorentz force with the magnetic field which connects across the magnetopause, causes the tail current shown in figure 2-4. The sum of the northern and southern lobes' tail current flows in the cross-tail current, which flows between the two lobes in the plasma sheet area.

In the magnetotail the diffusive velocities and the orientation of the geomagnetic field (towards earth in north lobe, and away in the south lobe) set up currents along the outside of the magnetopause which flow from right to left in both lobes (as viewed from the sun) (Figure 2-4).

2.4.1.6. Neutral Sheet

The neutral sheet is the highly conductive plasma within the plasma sheet which exists between the earth directed field line in the northern lobe of the magnetotail and the anti-earth directed field lines in the southern lobe. The neutral sheet has electron and proton densities of 0.1 to 3 cm^{-3}. Electron energies range from 200 eV to over 12 keV; proton energies range from 1 to 20 keV. The neutral sheet begins about 10 R_e from the earth's center and extends along the tail in an antisolar direction.

The tail current builds up positive charge on the dawn side and negative charge on the dusk side of the magnetotail. The charge buildup on the dawn and dusk side of the magnetotail runs nearly its full length and causes

a "large scale magnetospheric electric field" across the tail. The circuit is completed by current flow from dawn to dusk across the neutral sheet.

2.4.1.7. Plasma Sheet

The plasma sheet is a large region of high energy plasma with mean energies ranging from 0.5 to 2 keV, and mean proton energies ranging from 2 to 10 keV with number densities ranging from 0.3 to 1 cm^{-3}. The distant plasma sheet begins about 30 R_e from the earth and contains the neutral sheet. It is typically 4 to 6 R_e thick. The inner plasma sheet extends inward from the distant plasma sheet (30 R_e) to about 8 R_e in the antisolar direction. The inner plasma sheet also includes the region equatorward of the auroral zone in the anti-sun direction.

2.4.1.8. Plasmasphere

The plasmasphere is a region of high energy trapped protons which corotate with the earth. (The inner Van Allen Radiation belt is included within the plasmasphere.) The plasmasphere extends from the top of the ionosphere (about 1000 kilometers altitude) to about 4 R_e (about 26000 km). Plasma densities range from 10^3 to 10^1 ions/cm^3 (see Figure 2-7).

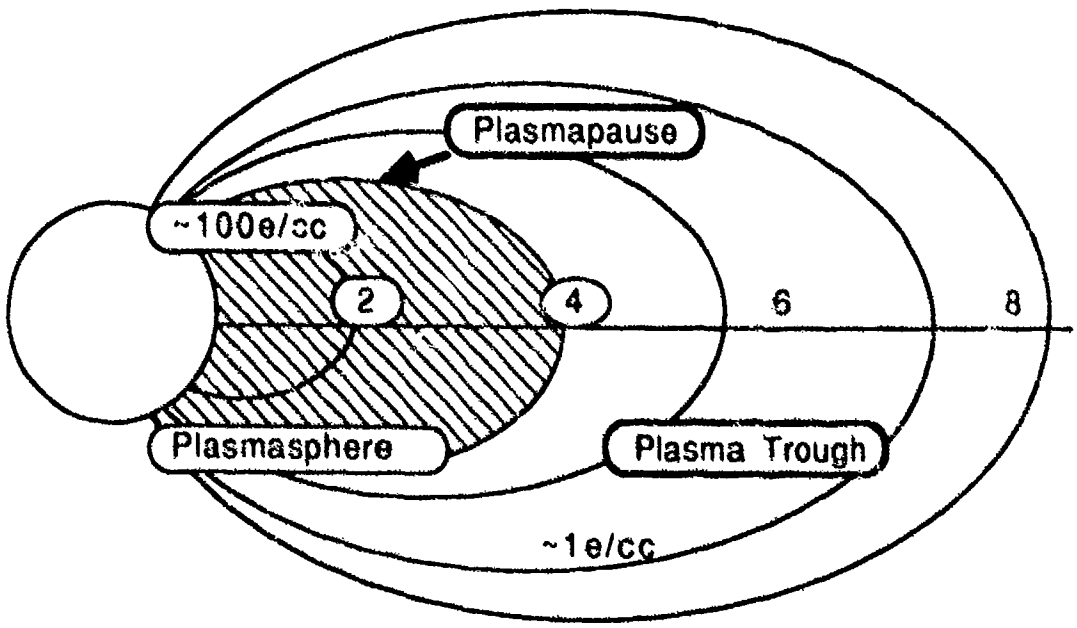

Figure 2-7.
The Plasmasphere: Configuration of the Magnetospheric Plasma
as Deduced by Whistler Measurements (Carpenter, 1966)
scale is indicated by L shell numbers

The plasmasphere is a stable region of trapped radiation. The magnetosphere plasma distribution depends on local time and the state of geomagnetic activity. When there is only moderate activity or less the plasmasphere in the sunward direction is neatly contained within a shell bounded by L=4. Outside of the L=4 shell is a region known as the plasma trough. Plasma densities in the plasma trough region vary from 1 to 10/cm^3. The boundary between these two regions is called the plasmapause. The plasmapause is about 0.15 R_e thick. The plasma density

decreases rapidly outward. The location of the plasmapause varies with local time (see figure 2-8)-- there is a pronounced bulge shortly after dusk extending out to perhaps 5 R_e. The plasmasphere corotates with the earth, and is largely populated with particles of terrestrial origin; although above 10,000 km some particles are thought to be of solar origin. The particles of solar origin are thought to have diffused across the magnetopause, found their way into the ring current, and finally been accelerated into the plasmasphere. Other particles may arise from the interaction of cosmic rays with atoms in the atmosphere.

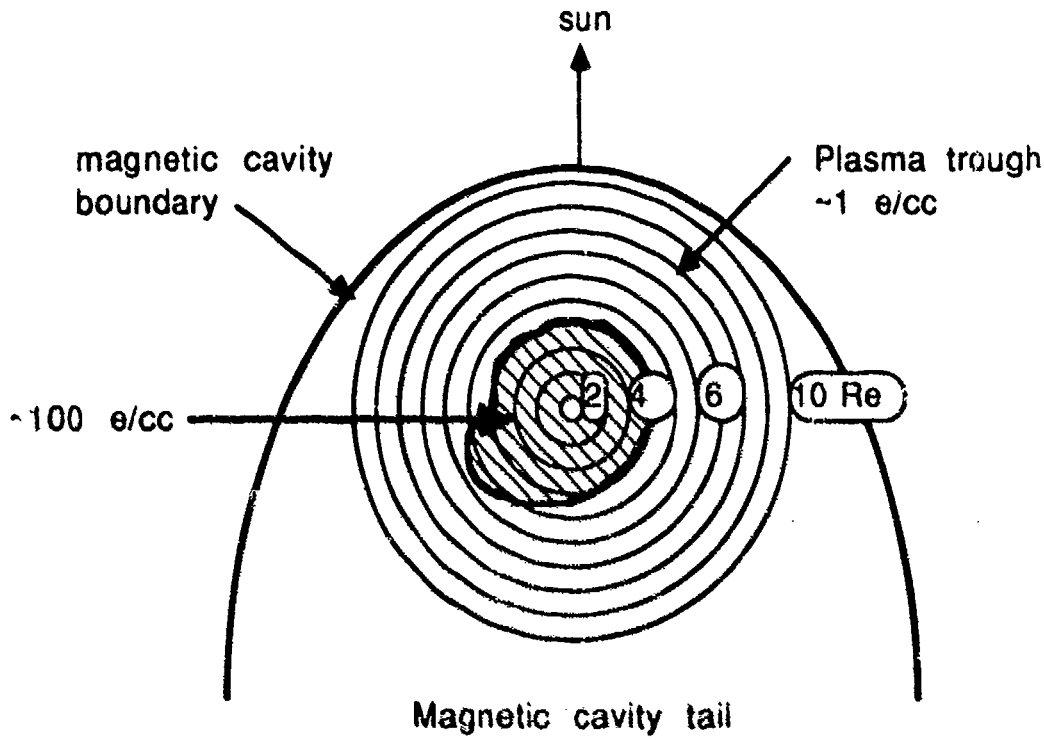

Figure 2-8. Evening Bulge in Plasmasphere. Schematic view of equatorial plane distribution of thermal ions deduced by Carpenter (1966) from Whistler data. Kp = 2 to 4

2.4.1.9. Ring Current

As charged particles deep in the magnetosphere diffuse toward the earth they encounter an increasing magnetic field strength that, combined with the large scale electric field, accelerate the particles. These particles are eventually trapped in the Outer Van Allen Radiation belt. Once inside the trapping region they drift around the earth due to the gradient and curvature of the geomagnetic field. Protons will drift westward and electrons will drift eastward, causing a net westward current called the Ring Current. This current induces a magnetic field which opposes the geomagnetic field on its earthward side, and enhances the field on the side away from the earth. On the earth side, the horizontal component of geomagnetic field at the earth's surface will be somewhat less than it would be in the absence of a ring current, especially at low and middle latitudes. During the main phase of a geomagnetic storm, the ring current is increased. The resultant decrease in the horizontal geomagnetic field can be measured at the earth's surface by magnetometers. Enhancing the ring current shifts it slightly earthward reducing the inner radius of the trapping region and shifting the auroral oval equatorward.

The ring current is inherently a global phenomenon (Williams, 1987, and the articles therein), and therefore requires an understanding of the global behavior of the magnetosphere. In its simplest terms the ring current is just

the drift of charged particles about the earth. The particle drift due to a particle gyrating about a field line at the equator is

$$\langle v_1 \rangle = \frac{\left\{ E\left(1 + \cos^2\alpha\right)\langle B \rangle \times \nabla B \right\}}{\left[qB^3 \right]} \qquad (2\text{-}19)$$

where E is the particle energy, B is the magnetic field, α is the pitch angle, and q is the charge on the particle. The symbols $\langle\,\rangle$ denote the average value. To get a notion of the magnitude of this effect, consider the case of a particle with $\alpha = 90°$ at the equator. The magnetic field for an ideal dipole will be

$$B = \frac{M}{r^3}\hat{\theta} \qquad (2\text{-}20)$$

where $\hat{\theta}$ is the unit vector in the theta direction. When $\alpha = 90°$ (pitch angle) the drift velocity due to the gradient in B is

$$\left\langle v_{90°} \right\rangle = \frac{-3Er^2}{qM}\hat{\Phi} \qquad (2\text{-}21)$$

where $\hat{\Phi}$ is the unit vector in the phi direction. The current due to the particle's drift around the earth at the position r is

$$i = \frac{q\left\langle v_{90°} \right\rangle n}{2\pi r} \qquad (2\text{-}22)$$

where n is the number of particles. The change in the magnetic field at the center of the earth due to this current is

$$B_1 = i\int \frac{ds}{r^2} = \frac{2\pi i}{r} = -\frac{3En}{M} \qquad (2\text{-}23)$$

There is another magnetic effect at the center of the earth due to the gyrating particle. The particle has a magnetic moment due to its gyration μ which is E/B where E is the kinetic energy of the particle. The contribution this makes to the field at the center of the earth is:

$$B_2 = -\frac{n\mu}{r^3} = -\frac{nE}{M} \qquad (2\text{-}24)$$

As the particles surrounding the earth distort due to inhomogenities and gradients in the local field these simple calculations lose accuracy, but still show the influence that the ring current can have on fields measured at the surface of the earth. Although it is possible to understand the perturbations of the magnetic field of the earth on the surface of the earth in terms of the distribution of particles moving in the earth's magnetic field through the equation relating current density and magnetic field, there is still "much more quantitative work ... required" [Williams, 1983] to understand the source of the ring current, and to isolate the source(s) of ring current particles.

2.4.1.10. Radiation Belts

Inside the magnetopause the earth's magnetic field dominates. Here the magnetic field lines are "closed" in the sense that they "begin and end" on the earth, as contrasted with some of the magnetic field lines we have been discussing which lead far beyond the earth. Inside the relatively undistorted region of the earth's magnetic field are the radiation belts and the plasmasphere. The radiation belts are regions of intense electron and proton fluxes trapped by the shape and magnitude of the earth's magnetic field. Actually these regions are not exclusive. The inner electron radiation belts lie within the plasmasphere.

Magnetic field lines which intersect the earth's surface below about 65° latitude are generally closed and reasonably symmetric about the earth. Charged particles injected into this region are trapped, at least briefly, by their interaction with the geomagnetic field. Electrons with energies greater than 40 keV tend to be found throughout the trapping region. Protons, however, are concentrated in two stable radiation belts. The outer Van Allen Belt has a maximum proton density at about 4 or 5 R_e (16000 to 20000 km). The protons and electrons in this belt are presumed to be of solar origin. Electrons circle the earth eastward, protons westward. The ring current is colocated with the outer Van Allen Belt.

The inner belt is part of the plasmasphere. It is more stable than the outer belt. The inner belt's peak proton intensity occurs at about 1.5 R_e (3000 km). The protons are thought to be primarily of terrestrial origin -- created by the collisions of cosmic rays with upper atmospheric air particles. Inner belt protons are high energy (MeV range). Unlike trapped particles in the outer Van Allen belt, many plasmasphere particles in the inner belt corotate with the earth.

2.4.1.11. Currents in the Ionosphere -- contributed by Captain Robert Frederick, Air Weather Service

Current flows in the ionosphere seem to be divided into two parts: the equatorial electrojet, and the auroral electrojet. The equatorial electrojet is the result of charged particles being moved along with the neutral atmosphere. The auroral electrojet is thought to be due to electric fields in response to the cross tail and field aligned currents flowing in the magnetosphere.

Charged particles in the ionosphere which are dragged along with the neutral atmosphere result in a small E-W current. This current generates very weak magnetic fields which can be detected by earth based magnetograms. The neutral atmosphere moves in response to lunar attraction, solar attraction and heating. Periodic fluctuations in magnetograms have been identified with these atmospheric motions. Lunar gravitational tides cause variations in magnetograms of only a few nanoteslas (1 nT = 10^{-5} gauss) with a period of 1/2 lunar day. These are called L-currents. Both solar gravitational tides (S_1) and solar thermotides (S_2) have a period of 1 day. The effect of solar heating (S_2) is much greater than gravitational tides (S_1). Collectively these two are referred to as Sq ("solar geomagnetically quiet day"). Solar effects cause variations of about 20 nT at midlatitudes. Changes in the ionization of the ionosphere affect the solar and lunar currents and therefore influence the measured magnetic field on the earth. Particle precipitation during geomagnetic storms, UV, and x-ray radiation from solar flares can significantly increase ionization in the ionosphere. The atmospheric dynamo currents vary in magnitude with conductivity, which in turn depends on latitude, altitude and degree of ionization.

The atmospheric "dynamo" current is greatest within ±5° of the magnetic equator in a narrow altitude band (around 20 km thick) at a height of 110 km. The current location is determined by local plasma dynamics. The collision frequency increases as the density increases. When the collision frequency is much greater than the gyrofrequency there isn't much motion of the charged particles. When the gyrofrequency is much greater than the collision frequency, charged particles move along the magnetic field lines.

The equatorial electrojet current flows toward the east by day (westward motion of electrons) and produces variations of up to 100 to 200 nT in magnetograms. The westward flow at night is nearly undetectable because of the small electron concentration at night in the E layer.

At high latitudes there is a current system connected to the magnetosphere in the auroral region. These current can vary greatly depending on the day and dusk sides, altitude, collision frequencies, and magnetospheric conditions

2.4.2 Geomagnetic Storms -- contributed by Captain Robert Frederick, Air Weather Service

Geomagnetic substorm bath spacecraft in a widely varying, complex and very interesting environment. There are two types of geomagnetic storms:

(1) Sporadic Storms - caused by mass ejections from large flares of eruptive prominences (or disappearing filaments), and

(2) Recurrent Storms - caused by high speed streams in the solar wind associated with solar sector boundaries (SSBs) or coronal holes (with open magnetic field lines). Recurrent storms show a 27 day periodicity associated with solar rotation. They are similar in morphology to sporadic storms, except they tend to have a more gradual but weaker onset, and last longer.

Both sporadic and recurrent storms ultimately depend on particle emissions from the sun, which in turn depend on the overall level of solar activity. As a result, a plot of geomagnetic activity with respect to time closely follows the solar cycle. However, the peak of geomagnetic activity tends to lag that of the sunspot cycle by about 2 years, because coronal holes are larger, stronger, and more common in the period between solar max and min.

Geomagnetic storms are identified by disturbances in magnetometer readings. In general, $K_p \geq 5$ or $A_p \geq 30$ indicates a geomagnetic storm. Magnetic index is explained in more detail later in this chapter and in Appendix 2. Geomagnetic storms seem to go through four phases.

(1) Sudden Storm Commencement (SSC) - Also known as a "sudden commencement" (SC). A geomagnetic storm begins with a sharp increase in the H component at all latitudes, almost simultaneously observed at all stations.

(2) Initial Phase (IP) - For about 1/2 hour to several hours the H component remains above pre-storm values.

(3) Main Phase (MP) - Begins with a decrease in the H component, and lasts for several hours to more than a day. Decreases of 100 to several hundred nanoteslas (nT) may occur (1 nT = 10^{-5} gauss).

(4) Recovery Phase - A slow recovery of the H component to pre-storm levels over a period of hours to several days.

2.4.2.1 Geomagnetic Indices

Geomagnetic indices were developed to monitor the variation in the magnetic field of the earth. Locally the magnetic field at any position on the earth will be characterized by three vector components, so the variation in the local magnetic field consists of three "magnetograms" which show the variation of those three components as a function of time. A number of indices have been developed which tend to emphasize one or another aspect of the magnetic activity.

For example, the "Dst" index was developed to reflect the perturbation in the magnetic field due to variations in the ring current. To do this, Dst or "Equatorial Dst" uses an average of the changes in the data of a number of low latitude stations. Please refer to Appendix 2 -- definitions under A index, a index, Dst, etc. -- for brief descriptions of the indices commonly in use. A few indices are described below.

Figure 2-9 shows how some of the indices used by the Air Weather Service of the U.S. Air Force are calculated. This also indicates how these indices are interrelated. Table 2.5 provides a quick summary.

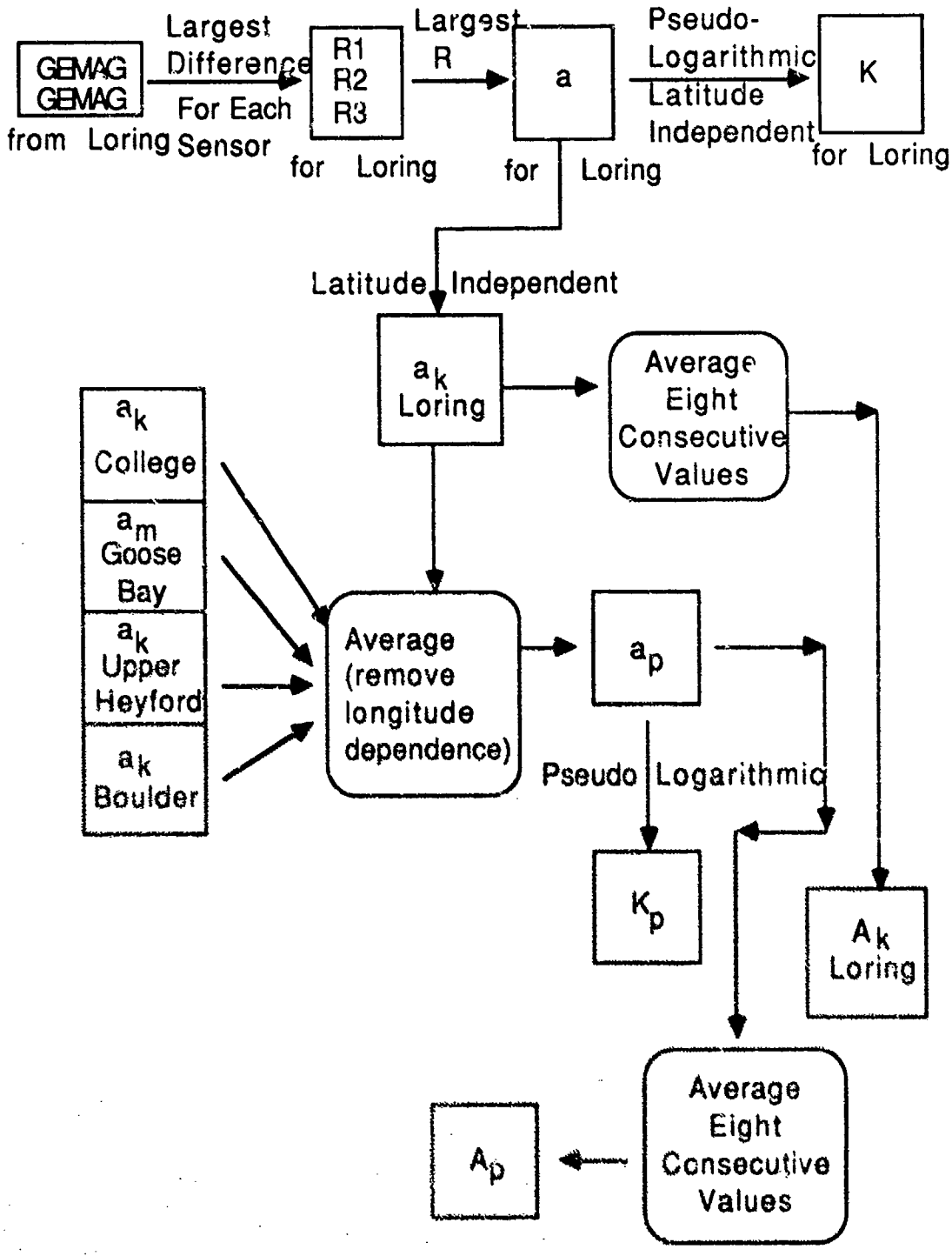

Figure 2-9. How AWS Calculates Some Indices: Flowchart of AFGWC Geomagnetic Index Calculation (Prochaska, 1980)

Table 2-5. Indices 1: Summary of Some Geomagnetic Indices (Frederick, 1985)

INDEX	RESOLUTION	ORIGIN	RANGE	UNIT
a Amplitude	3 hourly single station Lat and Longitude dependent	Range of the largest disturbance of any sensor	linear	gammas
K logarithmic amplitude	3 hourly Single station longitude dependent	Computed from "a" using a conversion factor that varies with observatory -- designed to remove latitude dependence	log 0 - 9	none
a_k equivalent amplitude	3 hourly single station longitude dependent	Computed from either a or K	linear 0 - 400	gammas
A_k	24 hour single station longitude dependent	Average of eight a_k values for a Zulu day (Note: k is often replaced by a station id	linear 0 - 400	gammas
a_p equivalent planetary amplitude	3 hourly planetary	Average of the a_k values for all reporting stations	linear 0 - 400	gammas
A_p	24 hour planetary	Average of eight a_p values for a Zulu day	linear 0 - 400	gammas

Table 2-5 . Indices 1: Summary of Some Geomagnetic Indices (Frederick, 1985) - (contd)

INDEX	RESOLUTION	ORIGIN	RANGE	UNIT
K_p	3 hourly planetary	computed from a_p	quasi-log 0 - 9 in 28 steps	none
$\sum K_p$	24 hour planetary	sum of eight K_p values for a Zulu day	quasi-log 0 - 9 in 28 steps	none
Running A_p	12 or 24 hour planetary	average of last 4 or 8 a_p values	linear 0 - 400	gammas

2.4.2.1.1. Dst Index

The Dst, also known as "equatorial Dst" or "storm time variation," index was developed to reflect the H component perturbation arising from the ring current alone. Only low latitude stations are used. Since auroral latitude stations are not included, the Dst index does not include any contribution from the Auroral Electrojet. As a result, the Dst index is not sensitive to substorms, but it is an excellent indicator for the start and end of the main phase of geomagnetic storms. The time resolution of the index is one hour.

2.4.2.1.2. Q Index

The Q, or "polar range," index is a measure of the size of the polar cap and the auroral oval surrounding it. Q is a comparison between instantaneous and quiet day measurements. Classical Q is the maximum within any 15 minute interval. In principle, since this is a direct current index, an instantaneous Q prime could be continually generated. Increase in Q prime signals the onset of a disturbance. Q is based on the relation between location of visible aurora and the magnetic field. It varies with the intensity of ionospheric currents which flow across the polar cap, and reacts strongly to geomagnetic disturbances. It is a quasi-logarithmic index computed only for observatories located poleward of 58 degrees geomagnetic latitude.

AFGWC uses a "QE (equivalent Q) index" to monitor auroral and polar disturbances. Using the formula for the relation between the auroral edge, geomagnetic local time, and Q, AWS calculates Q from auroral locations. This can be extrapolated to predict locations of the rest of the auroral oval and polar cap. Since an optical aurora is the consequence of auroral precipitation, the precipitating particles themselves can be used to estimate Q. DMSP imagery is used to specify the time and location of the equatorward boundary of the diffuse aurora. Also, DMSP measurements of precipitating particles can be used to compute the time and location of the aurora. These times and locations are used to estimate the Q value which would have caused the observed auroral oval extent.

2.4.2.1.3. The A and K Indices

The A and k indices are alternating current indices and present the highest and lowest values of the change in the magnetic field in the given direction. An ac index cannot be instantaneous, because it represents a span of values within a time interval, typically three hours. The second letter indicates the specific point of view of the index, for example, A_p -- planetary, or AE -- electrojet.

2.4.2.1.3.1. AE Index

The AE index was developed to reflect the H component perturbation arising from the auroral electrojet alone. Only auroral latitude stations (60-70 degrees) are used. When the H component magnetograms are superimposed, the maximum or most positive value, called "AU," represents the perturbation due to the eastward electrojet (afternoon sector). The minimum or most negative value is called "AL" and represents the perturbation due to the westward electrojet (midnight/morning sectors). The AE index is then given by: AE = AU - AL. The time resolution of the index is 2.5 minutes, but it is available as an hourly average. Years of AE data have been determined and are available from the world data center. Hourly averages have been published.

2.4.2.1.3.2. A_p Index

Ap is a daily index that represents the general state of planetary geomagnetic activity rather well. It includes contributions from both the ring current and auroral electrojet since the latitude range of the 13 stations used is 46 to 63 degrees geomagnetic latitude (the Gottingen index). The Gottingen A_p index is not available in real time, so AWS calculates and distributes an approximation of A_p, based on 5 real time reporting stations located between 49 and 65 degrees geomagnetic latitude. (Thule is not used due to its high geomagnetic latitude, 88 degrees.) AWS also uses a running 24 hour A_p index which equals the daily A_p only at 2400Z.

The basic index is the "amplitude (a)" index, which is a three hourly, single station index that represents the range of the largest disturbance of any magnetogram component. From this basic index a whole family of indices can be computed: 3 hourly or daily, single station or planetary, linear or logarithmic, or any combination.

2.4.2.1.3.3. K, K_p Index

K, K_p, K_m - A 3-hour dimensionless quasi-logarithmic index that provides a measure of the level of disturbance of the geomagnetic field. Without a subscript, the index refers to the deviation of the most disturbed horizontal component relative to an assumed quiet day curve for the recording site. The K index ranges from 0 (Very Quiet) to 9 (Violently Disturbed). The "p" subscript denotes a planetary, as opposed to a single station, index. K_p is generated in Gottingen, West Germany, based on the K index from 12 or 13 stations distributed around the world. The K_p index has been derived routinely since 1932. GWC estimates K_p and A_p indices using data from six North American stations. The K_p index ranges from 0° to 9°, with 27 one-third unit steps (0°, 0+, 1-, 1°, 1+, 2-, etc.). (Also see a_p in Appendix 2.) K_m is similar to K_p but based on a more symmetric global array of stations.

2.4.2.2 The Use of Indices

There are a large number of indices which are used and available. They come in either ac or dc variables, and are linear, logarithmic or semi-logarithmic. One or more may correlate well with surface charging. None is probably ideal for all environmentally produced anomalies. Since they indicate activity in the magnetosphere and since sometimes the activity of the magnetosphere causes an environment at the spacecraft which causes the anomaly, indices can be useful in determining the cause of an anomaly. However, care needs to be taken in interpreting correlations of the indices and the occurrence of the anomaly, especially the non-occurrence when the index repeats its sequence and the anomaly does not occur. There is no substitute for a detailed understanding of the response of the spacecraft system to the environment.

2.4.2.3 The Substorm Mechanism

The description below contributed by Hones is not the only model of substorms (see for example Smith 1986). Observationally based models of the substorm seem to fall into at least two classes. One (as given below) concentrate on the formation of a neutral line, and reconnection. Another class dwells on the dynamics of the plasma sheet boundary layer between the lobe region of the tail and the central plasma sheet. Although the approaches and descriptions are conceptually quite different, it is possible they are related, and represent different aspects of the complex energy storage and release in the magnetotail. In this area of active observation and theoretical research much remains to be done for a complete understanding and verification of a substorm model.

2.4.2.3.1 Substorms -- contributed by E. Hones, Los Alamos National Laboratory

Most descriptions of magnetospheric substorm activity picture a "classic" substorm process as one in which the interplanetary magnetic field (IMF) turns southward making it easier for energy to flow into the tail region of the earth's magnetotail. Earlier it was noted that the solar wind, leaving the sun, drags the solar magnetic field lines out like rubber bands into the shape of an Archimedean spiral. In a like manner, when the solar wind flows past the earth it distorts the geomagnetic field, compressing it on the day side of earth and stretching field lines far downstream on the night side. The resulting comet-like magnetic structure is called the earth's magnetosphere and its night-side magnetotail is several million kilometers long and about 250,000 kilometers in diameter. A large quantity of energy that has been acquired directly from the solar wind plasma, and thus indirectly from the sun itself, is stored in this huge magnetotail.

The solar wind has its own magnetic field, called the interplanetary magnetic field (IMF), which is actually the stretched-out solar magnetic field. The IMF strongly influences the efficiency with which the solar wind energy is coupled into the earth's magnetosphere. When the IMF has a southward component so that it is directed opposite to the earth's northward field at the subsolar surface of the magnetosphere, magnetic reconnection occurs at this surface, causing IMF field lines to become connected to earth field lines (and thus to the solid earth itself). Then, the flowing solar wind plasma is slowed, its kinetic energy being transformed into the magnetic energy of the field lines, which then become part of the magnetotail and add to the magnetic energy stored there.

Energy cannot be stored within the magnetotail indefinitely, but must be dissipated somehow. The magnetosphere achieves this dissipation of energy simply by releasing part of its magnetotail to the on-flowing solar wind. Such releases occur intermittently, at few-hour intervals, and are manifested at earth by auroral substorms. Figure 2-10 illustrates what happens in the magnetotail during this process of energy release. This figure is a cross section in the plane of this solar wind velocity vector and the earth's magnetic dipole. The shaded region is the plasma sheet which extends completely across the magnetotail's midplane (i.e., out of the paper). It contains largely solar wind plasma that has been carried into the magnetotail with the magnetic field lines. The process of energy release begins (in panel 2) with the formation of a magnetic neutral line, N', about 100,000 kilometers behind the earth. This coincides with the onset of the auroral substorm at earth. Magnetic reconnection then proceeds, severing the closed magnetic field lines of the plasma sheet until, in panel 5 (about 5 minutes after the substorm onset), all of the closed field lines have been severed (Figure 2-10), leaving a configuration of closed magnetic loops. This process continues (the dark shading in panels 6, 7, and 8) until the loops are no longer magnetically connected to earth. The closed loop configuration, called a "plasmoid," flows downstream and eventually out of the magnetotail, carrying with it a large fraction (perhaps one-half) of the previously stored energy. The great auroral and geomagnetic disturbances that characterize a substorm at earth are generated by energy given up by the earthward portions of the severed field lines as they collapse earthward.

About an hour after the sequence begins, the substorm neutral line, N', suddenly races downtail. Magnetic reconnection proceeding at this retreating neutral line accelerates cold plasma from the tail regions above and below the midplane, jetting it earthward on newly closed magnetic field lines, to reform the plasma sheet. This is the concluding phase of the substorm during which auroras at earth seem to execute a final activation and poleward movement. Panel 10 is essentially the same as panel 1: the cycle begins again.

Figure 2-10. Plasma Sheet Configuration Changes During a Substorms

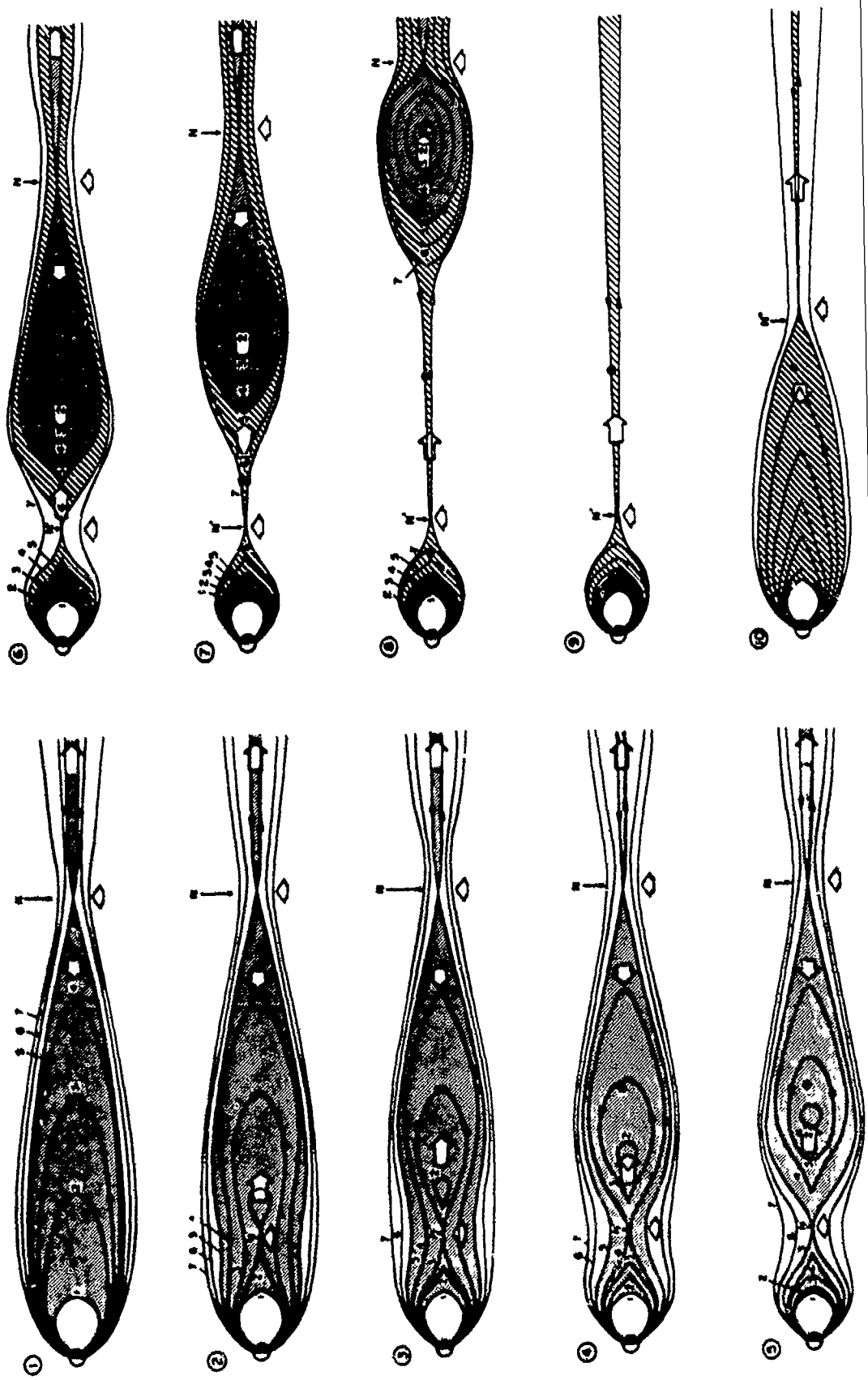

2.4.2.4 Engineering Models

No matter what the actual mechanism, there is ample proof that spacecraft are occasionally immersed in a hot plasma. This environment results in high potentials around the spacecraft, and that, as has already been discussed, can lead to engineering anomalies and perturbations of science measurements. Surface charging results from the encounter of spacecraft surfaces with a plasma environment of particles up to 50 keV. Energies above 50 keV usually penetrate beneath the surface of the spacecraft and consequently do not play a major role in surface charging. Although a full spacecraft charging analysis would include charge trapped inside the spacecraft as part of the total charge effecting the spacecraft. From an anomaly prevention and analysis point of view, the important thing is to describe the environment and how frequently it occurs so that the space systems reaction can be understood. One such useful model is described by Stevens (1982)

2.4.2.4.1 Stevens' Model

Stevens (1982) suggests a specification which does not have the characteristics of a real geomagnetic substorm but will produce a maximum stress within dielectrics. His specification is given in terms of a single Maxwellian temperature for severe and moderate substorms (Table 2-6). This temperature description was chosen because the previous analysis of satellite surface charging showed that single Maxwellian environments, although not as realistic as the double Maxwellian descriptions, produced more severe charging. He also attempted to indicate how frequently the most severe charging conditions persist. His curves are shown below (Figure 2-11). The time curve runs out to only 4000 hours since beyond that time particle temperatures drop below levels that produce charging. The ion temperature (in kV) was found to be numerically equal to 10 times the electron density (in cm^{-3}). To account for the ion composition of the substorm environment, which indicates a substantial oxygen ion population in addition to hydrogen ions, the ion density is set to be one-third of the electron density.

Stevens also recommends that both sunlight (at an angle of incidence to maximize differential charging) and eclipse charging be evaluated. He choses to describe geosynchronous orbits charging environments in terms to two simple looking curves, figure 2-11. One describes the temperature of a Maxwellian plasma, and the second describes the density of the plasma. Both curves are a function of hours per year that such a description is valid. This approach provides insight into the engineering design required for the system. The darker curves are for moderate environments, while the lighter curves are for severe environments.

Table 2-6 Design Environments (Single Maxwellian Description)

	Electrons		Ions	
Environmental condition	Temp, keV	Density, cm^{-3}	Temp, keV	Density, cm^{-3}
Moderate	8.0	2.1	21.0	0.7
Severe	11.0	1.1	11.0	0.4

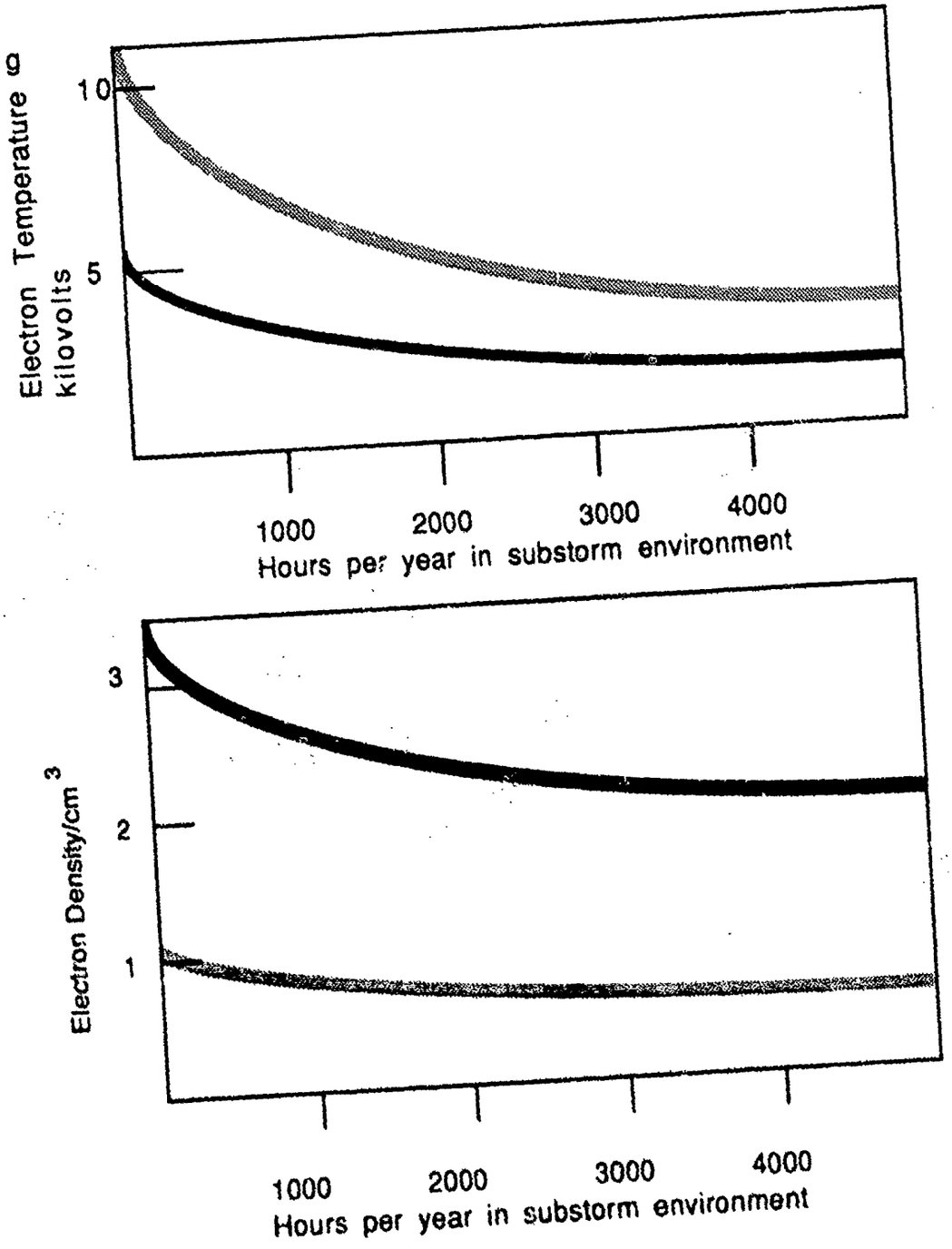

Figure 2-11. Stevens Model for Geomagnetic Substorms

2.4.2.4.2 Worst case Models

For many design considerations, it is not a detailed knowledge of the day by day environment that is the design driver; instead it is the occasional situation which results in the highest charging. If the system will survive such an environment, the assumption is that any lesser environment will not be a problem. Thus in the literature there is a great deal of attention placed on criteria for a worst case environment as well as determining what the actual worst case environment is. The charging of a surface can be simply represented if a Maxwell-Boltzmann distribution for both electrons and ions is assumed. The values given in Table 2-7 are a 90th percentile single-Maxwellian representation of the environment as proposed by Purvis et al., 1984.

Table 2-7 Worst-Case Geosynchronous Plasma Environment (Purvis et al., 1984)

Electron number density, N_1	$1.12/cm^3$
Electron temperature, T_1	1.2×10^4 eV
Ion number density, N_2	$2.36 \times 10^{-1}/cm3$
Ion temperature, T_2	2.95×10^4 eV

Gussenhoven and Mullen (1982) suggest using a real case from data taken on the SCATHA (Spacecraft Charging AT High Altitudes) satellite on 24 April 1979. Their "worst case" is chosen from sunlit charging events. In eclipse the satellite potential severely affects the ion and electron spectra inhibiting an accurate measurement of the ambient particles. In sunlight the satellite potential is much smaller since photoelectrons provide a significant amount of the current balance, and therefore the particle spectra are affected to a much lesser degree. They choose to use a double Maxwellian fit to the spectral data because it is reasonably accurate and highly usable.

The table below (Table 2-8) gives the first four moments of the ion and electron distribution function, together with T_1(average) and T_2(rms), during the "worst case" charging at ~0650 UT on 24 April. Measurements over the 100 eV to 400 keV energy range were used to construct the distribution functions. Integrations over pitch angle were used for all moments; therefore, the number and energy flux are average directional quantities. The moments for ions were calculated assuming hydrogen as the only species.

Table 2-8. Moments and Temperatures Integrated Over Pitch Angle

		Electrons	Ions
n:	(cm^{-3})	0.9	2.3
NF:	$(cm^{-2}s^{-1}sr^{-1})$	4.7×10^9	2.0×10^8
ε:	(eV/cm^3)	9.6×10^3	1.9×10^4
EF:	$(eV/cm^2 s\ sr)$	8.4×10^{13}	5.4×10^{12}
T_{AVE}:	(keV)	7.7	5.5
T_{RMS}:	(keV)	9.0	14

The same moments assuming isotropic particle distributions and using particle fluxes at 90° pitch angle are given in Table 2-9. The difference between the corresponding quantities in the two tables gives a measure of the anisotropy of the plasma.

Table 2-9. Moments and Temperatures Using Perpendicular Particles Only

		Electrons	Ions
n:	(cm^{-3})	1.5	1.4
NF:	($cm^{-2}s^{-1}sr^{-1}$)	9.2×10^9	2.1×10^8
ε:	(eV/cm^3)	2.1×10^4	2.4×10^4
EF:	(eV/cm^2 s sr)	1.9×10^{14}	7.2×10^{12}
T_{AVE}:	(keV)	10.4	12.6
T_{RMS}:	(keV)	11.3	16.8

The electron and ion densities and temperatures that characterize the double Maxwellians that represent distribution functions at the time of the sunlit charging peak are listed in Table 2-10.

Table 2-10. Worst-Case Least-Squares Particle Environment Fit (~0650 UT 24 April 79)

	n_1 (cm^{-3})	n_2 (cm^{-3})	T_1 (keV)	T_2 (keV)
Ions				
perpendicular	1.1	1.3	0.3	28.2
parallel	1.6	0.6	0.3	26.0
Electrons				
perpendicular	0.2	2.3	0.4	24.8
parallel	0.2	0.6	0.4	24.0

Gussenhoven and Mullen (1982) comment that "... the high energy electron current or density is the driver in charging spacecraft to high levels. The decrease (anti-correlation) of n_1 ...and the n_2 increase suggest that the low energy particles are being accelerated to higher energies during injection events, and that the introduction of a new higher energy population is not necessarily required. The high and low energy ion densities remain nearly constant.

each between 1 and 2 particles/cm^3 during the entire period. The high energy ion temperature stays near 28 keV and the low energy temperature, near 300 eV. (Again, caution is advised in using the low energy values)" (pp. 7–8).

2.4.3 Spacecraft Role

The critical factor determining the extent to which charging interactions must be considered in the design of a spacecraft is the mission of the spacecraft. In all spacecraft, differential charging is undesirable. For scientific spacecraft, absolute charging usually is not desired. For short missions which are repeated again and again, an average charging environment may be more appropriate than the worst case. For each spacecraft the effort should be directed toward controlling those charging effects that are detrimental to the particular mission.

Spacecraft can be divided into spinners and three axis stabilized. Both designs are concerned with stability for pointing (communications and/or observations), and getting energy from solar cells. The spinners are basically cylinders with their axis perpendicular to the line to the sun. The spinning helps provide the stability through its large angular momentum along the spin axis. Solar cells typically cover the outer surface and roughly $1/\pi$ are producing useful current at any instant. Three axis stabilized systems forego the simplicity of spin stabilization (although they may accomplish the same thing with momentum wheels), but make full use of every solar cell by pointing their "wings" directly at the sun at all times. Three axis spacecraft are much like a controlled platform in which various parts can be oriented with respect to the sun or earth, whatever is desired. Purvis et al., 1984, provide the following useful generalizations regarding the overall charging characteristics of these two species of spacecraft. (1) A spin-stabilized spacecraft usually has a low spacecraft ground potential (a few hundred volts negative). On some shaded dielectric surfaces during sunlit charging events, differential voltages of several thousand volts can occur. (2) A three-axis-stabilized spacecraft can have a rather large negative structure potential (a few thousand volts) in sunlit charging events. The dominant areas controlling charging in this case are the backs of the solar array wings. Differential charging will likely not be as large as in the spinner case.

2.5 System Discharging Characteristics

Breakdowns, or discharges, probably occur because a differential charge buildup generates an electric field that exceeds a breakdown threshold at some point. When a discharge occurs, charge is released from one part of the spacecraft to another or to space. This charge release will continue until the differential driving force no longer exists. Hence, the amount of charge released will be controlled by the total charge stored in or on the discharge site. The charge loss or current to space drives the local surface voltage to zero. Since the dielectric is capacitively coupled to the structure, the charge loss will also cause the structure potential to become less negative. In fact, the local structure could become positive with respect to the space plasma potential and begin to collect electrons from the environment (or attract back the emitted ones) to reestablish the structure potential required by the substorm conditions. The whole process can take microseconds. Multiple discharges can result as various parts of the system experience strong differential potentials as various nodes are discharged. This is especially true when the substorm plasma intensities remain high, long enough to reestablish the conditions necessary for a discharge.

For a long time it was believed that there could be a charge loss over an extended area of the dielectric. This phenomenon would have produced area-dependent charge losses capable of generating currents of hundreds of amperes. This concept was based on testing of grounded substrate samples, which produced spectacular lightning-strike photographs. The differential voltages necessary to produce this large charge-clean off type of discharge were typically in excess of 10 kV. Since spacecraft modeling and current space flight data indicate differential voltages of only 3 to 4 kV, it must be assumed that actual discharges are much milder and limited in charge loss. Without the strong differential voltages on the dielectrics, the large-area charge clean off probably will not occur.

Since breakdowns are believed to be due to differential charging, they can occur during sunlit charging events at 1 AU. Because sunlight tends to keep all illuminated surfaces near plasma potential, whereas shaded dielectric surfaces may charge strongly negatively, sunlight enhances differential charging. Eclipsed charging events, in contrast, result in a change in absolute charging for all surfaces except those weakly coupled to the structure (capacitance to structure is less than that of spacecraft to space, normally <0.2 nanofarad). Differential charging in

eclipse develops slowly and depends on differences in secondary yield or other material or configurational parameters. Transitions from full eclipse to sunlight are probably the most critical times for developing large potential differences between one part of the spacecraft and another.

2.5.1 Discharge Models

The physics of discharges on the surface of spacecraft is complex. Three types of discharges have been identified: a) punch through, b) flash-over, and c) particle emission. Punchthrough is a discharge through the material. It usually occurs at a weak point in the material and many times results in physical damage to the dielectric. Flash-over describes the situation when charge on the surface is removed due to the collapse of potential gradients across the surface. G. T. Inouye's "Brush -Fire model" attempts to describe this type of discharge. Particle emission refers to the actual ejection of a plasma from the surface of the dielectric. This has been observed by Nanevicz and others. Other models and concepts abound. Table 2-11 lists some of the current discharge models.

Table 2-11. Discharge Models

Model	Authors	References
First Principles	Beers et al.	NASA-Lewis CR159560
Brush Fire	G. T. Inouye	TRW document M2-142-80
Stettner	Stettner	AFGL-88-34
Longmire	Longmire	AFGL-TR-87-32

Figure 2-12 shows the various modes and regions of arch discharge formation in a "simple" gas. Discharges in or on a dielectric could be just as complex. In general discharges seem to have some kind of threshold. When a breakdown threshold is exceeded a discharge is possible. The transient generated by this discharge can couple with the spacecraft electronics and cause problems ranging from logic switching to complete system failure. Discharges can also cause long-term degradation of exterior surface coatings and enhance contamination of surfaces by causing the release of contaminating particles.

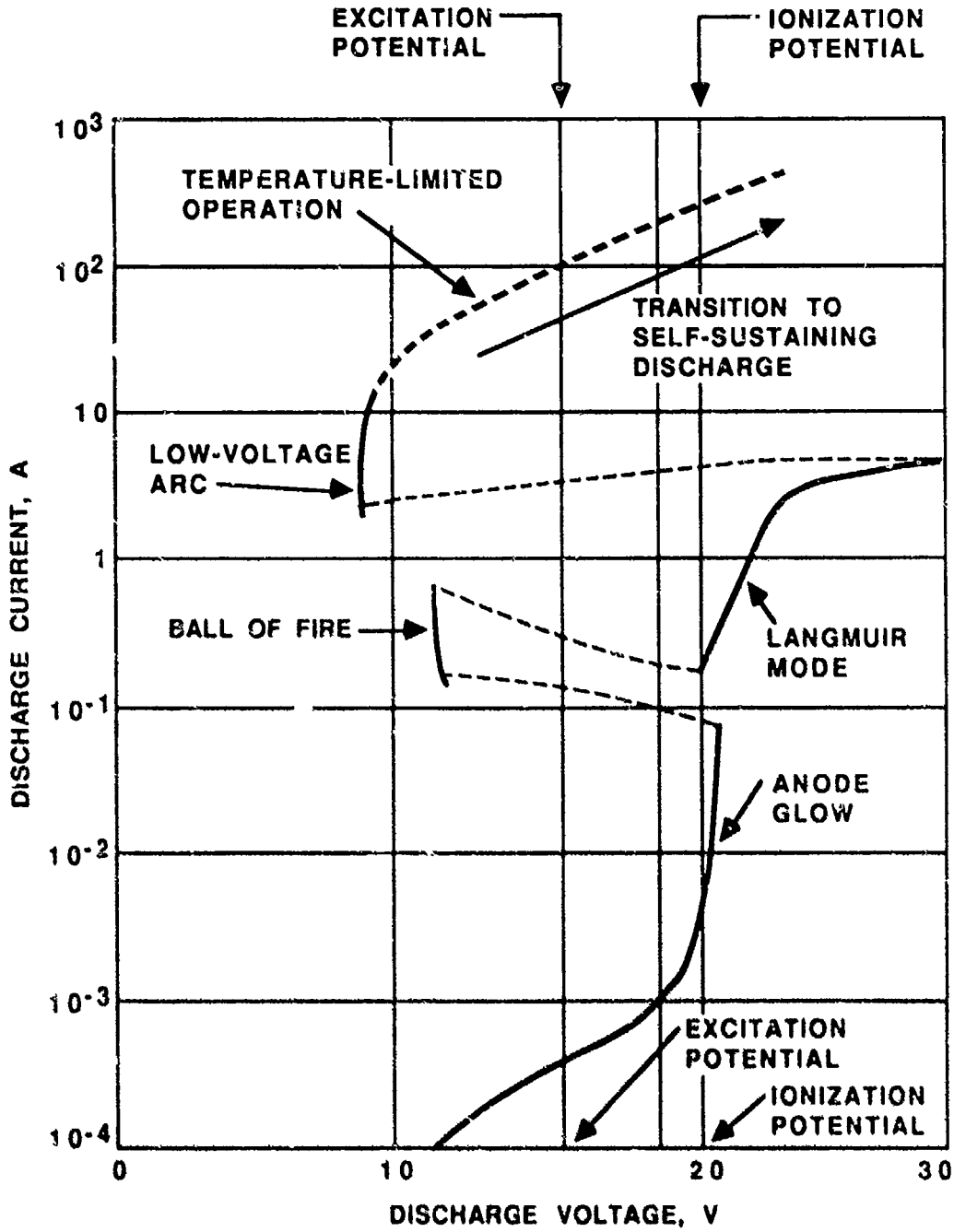

Figure 2-12. Gaseous Discharges

2.5.2. Criteria for Breakdown

The exact mechanism for breakdowns is not clearly understood. However, current thought is that if either of the following criteria is exceeded, discharges can occur:

(1) Dielectric surface voltages are greater than 500 V positive relative to an adjacent exposed conductor, or
(2) The interface between a dielectric and an exposed conductor has an electric field $>10^5$ V/cm.

Edges, points, gaps, seams, and imperfections in surface materials tend to occasion high local electric fields and hence promote the probability of discharges. These must be found by close inspection of the exterior surface of a system.

The first criterion is important in considering solar arrays in which the high secondary yield of the cover slide can result in surface voltages that are positive with respect to the metalized interconnects. This criterion can also apply to metalized dielectrics in which the metalized film, either by accident or design, is isolated from structure ground by a resistance value great enough to allow a five hundred volt potential difference. For example with an ambient space current of 1–10 nanoamperes/cm^2 a resistivity on the order of 10 MΩ-cm (essentially only capacitively coupled) yields a maximum potential difference of concern using criterion one.

The second criterion applies to those areas of a spacecraft where a strong negative voltage gradient could exist. This is usually associated with metal edges or with cracks in the dielectric exposing a conductor underneath when the charge stored on or in the dielectric is relatively unstable and could be lost.

When a discharge occurs, stored charge is redistributed. This produces a transient that couples into the spacecraft structure and possibly into the electronic systems. The computation of charge lost in any discharge is highly speculative at this time. The charge loss depends on the voltages on the spacecraft at the time that discharges occur, the path(s) the current takes, and the final state of the system after the discharge.

From an engineering point of view, Purvis et al., 1984, categorize discharges according to the amount of charge lost to a local area as follows:

$Q_{lost} < 0.5\ \mu C$--minor discharge

$0.5\ \mu C < Q_{lost} < 1.0\ \mu C$--moderate discharge

$Q_{lost} > 1.0\ \mu C$--severe discharge

The current in a discharge pulse can be approximated by square, triangular, or double exponential pulses or by a resistance-inductance-capacitance (RLC) series circuit. Purvis et al., 1984, use as an example, an RLC model:

$$I = \left(\frac{V_0}{2L}\right) \exp\left(\frac{-Rt}{2L}\right) - \frac{\exp(dt) - \exp(-dt)}{d} \quad (2\text{-}25)$$

where

$$d = \left(\frac{R}{2L}\right)^2 - \left(\frac{1}{LC}\right)^{1/2} \quad (2\text{-}26)$$

and V_0 is the surface voltage just before the discharge. The change with time of the voltage can be computed from

$$I = C\frac{dV}{dt} \quad (2\text{-}27)$$

By integrating this expression the charge loss can be determined. The resistance, inductance, and capacitance values can be adjusted to produce a desired charge loss.

Robiscoe, and co-workers (Damas and Robiscoe, 1988, Robiscoe and Sui, 1988, and Robiscoe et al. 1988) model the discharge with a LCR circuit in which the arc resistance is taken to be constant divided by the arc current. This constant alone determine the arc threshold, and the model is able to reproduce a number of experimentally known facts.

The size of the arc has been determined experimentally (Balmain and Dubous, 1979, Stettner et al., 1980) to vary as simple powers of the charged area. The total charge is proportional to the area that is charged. The pulse duration scales as a characteristic length of the charged area or as the square root of the area. The rise time of the pulse scales as the square root of the area and the current peak also scales as the square root of the area (i.e. the total charge divided by the pulse duration).

2.6 Other Plasma Interactions

Plasma interactions with a space system involve many aspects of system design. In addition to the basic charging and discharging of th system described above, there are other effects which may or may not play an important role in a given space system. The basic charging of the system can be strongly influenced by the motion of the system through the plasma. This influences the current collection and adds yet another asymetry to the problem. Spacecraft motion also allows the formation of a wake about the spacecraft. These and other effects are discussed below.

2.6.1. Ram and Wake Effects

Spacecraft in low altitude orbits (<1000 km) have orbital velocities on the order of 7 km/s. The thermal velocities of the ambient ions at 1000 km is 3 km/sec for H+, 0.8 km/sec for 0+. The movement of a spacecraft through the ionosphere produces a wake. It takes a finite time for the ions to fill in the void created behind the passing spacecraft. The electron thermal velocity at 1000 km is 180 km/sec).. The electrons tend to fill in the void behind the spacecraft but are retarded by the electrostatic field that results from charge separation at the wake. The plasma distribution around a moving spacecraft will be very complex, most likely three dimensional, and probably nonlinear. These effects are seen in plasma measurements as shifting of the spectra in energy, preferential focusing or exclusion of particles of a particular energy or direction. The spacecraft itself further contaminates measurements by electric and magnetic fields, secondaries, backscattered electrons, and photoelectrons.

The plasma sheath around objects can also trap contaminant ions, due to thrusters (ionic or chemical) or outgassing of satellite materials, and cause preferential deposition on negatively charged surfaces. Cauffman (1973) (see also Jemiola (1978) and Jemiola (1980)) has estimated that as much as 50 Å of material can be deposited on charged optical surfaces in as little as one hundred days. Adamo and Nanevicz (1980) found that the heating rate of sensors on a geosynchronous satellite apparently rose with increased charging. Such deposition may also alter secondary emission and photoelectron properties. Long duration exposures of surfaces or exposed potentials (i.e., solar arrays) may greatly enhance contamination effects over the life of a mission. Laboratory and in-situ measurements by Soop (1972 and 1973), Samir and Jew (1972), and others have delineated the main features of the plasma wake and sheath around small (a few meters in diameter) bodies under a variety of conditions. Models of the wake and sheath for small bodies have been developed by Gurevich and Dimant (1975), Parker (1978), and others for realistic conditions and simple geometries. The PDP (Plasma Diagnostics Pckage: Shawhan, 1982) may provide data to confirm predictions.

Magnetic field induced effects which are normally ignored in spacecraft ram/wake calculations may turn out to be a particularly important. It has been suggested that this constraint of charged particles to motion may become of real concern for structures larger than particle gyroradii. The magnetic field also induces anisotropies in the particle fluxes. Ambient fluxes, secondaries, beam fluxes, and charged particle wakes are all controlled to a greater or lesser extent by the magnetic field. Whipple (1965) and Parker and Murphy (1967) have analyzed some of the effects of these magnetic field induced anisotropies on spacecraft charging (see also reviews by Brundin (1963) and Gurevich et al. (1970)) and found that the electron flux can be reduced by as much as a factor of two on some surfaces.

The low energy plasma that would normally lead to low absolute vehicle potentials is absent or distorted in the depletion region behind a n object or inside the wake.. Auroral fluxes, artificial plasma beams, or the beams produced by the wake itself could induce high potentials on isolated surfaces within the depletion region. Potentials on the order of 1000 volts were observed on DMSP during passage through an auroral arc. The distortions of the ram/wake during such charging events are being studied as they may ultimately limit the potential to which an isolated body can charge (Katz et al., 1984).

2.6.2 Radio Distortion in the Sheath

Reflection: Electron density irregularities in the vicinity of an antenna and antenna feed system can distort the farfield antenna patterns, reducing the main beam efficiency and increasing the sidelobe levels. This effect is undesirable for either receiving or transmitting antennas. Severe destruction of the beam pattern occurs if the plasma density leads to a plasma frequency comparable to the wave frequency:

$$fp(MHz) = \frac{9}{10^3 \sqrt{N}} \quad (2\text{-}28)$$

where N is electron number density in cm^{-3}. Densities of 10^8 to 10^{12} cm^{-3} are necessary to severely affect the 100 MHz to 10 GHz range. Although natural polar electron densities range only up to 10^5 cm^{-3}, local ionization in the vicinity of a large space structure may be significantly higher in the ram direction or enhanced due to auroral particle bombardment.

Distortion: At lower densities, the nearfield phase pattern is modified, distorting the farfield pattern . Since the ram/wake densities are expected to be widely varying function of location and time, the farfield pattern will change with time. Ram/wake densities were observed to vary over 10^5 near the Orbiter on STS-3 and STS-4. Naturally occurring variations in the electron densities in the ionosphere due to auroral particle precipitation and auroral current systems distort radio transmission in the ionosphere.

Harmonic Distortion: The presence of plasma and plasma irregularities in the vicinity of high power transmitters could cause nonlinear effects on the signals. The nonlinear effects come about in a number of ways. If the plasma tends to rectify the signals or if irregularities cause wave energy to become trapped in a localized volume then harmonic distortions or other nonlinear effects can occur.

One of the most insidious ways in which to get high plasma densities in the region of an antenna is from a process called multipacting. If the time required for a charged particle to transit the gap between two elements of the antenna corresponds to the time required for the voltage on those elements to change sign, secondary emission from those elements may release sufficient electrons to cause one or more of the distortions described above.

2.6.3 Collision Induced Ionization

Two different types of plasma sheath formation processes are postulated for the environment above 100 km. First there are the collisional models of Medved and others that assume the dominant process is basically the result of collisions between ambient particles (nearly) elasticity scattering off the vehicle surface and the incoming ambient flux. In the center of mass frame this represents a collisional velocity twice the velocity of the vehicle relative to the gas. Since the velocity of a typical low altitude vehicle is 7-8 km/s, the kinetic energy available per particle in the center of mass frame varies from about 4.6 eV for N to 10 eV for O_2. There is close to sufficient energy therefore to ionize the ambient constituents in the vicinity of a low altitude spacecraft through collisions. At Space Station altitudes, however, this process alone will likely not account for the pronounced plasma enhancements observed.

The second mechanism, proposed by Papadopoulos (1984), invokes a plasma instability to generate the enhanced plasma sheath. Neutral particles reflected from a satellite surface at low altitudes have, as already noted, nearly enough energy to ionize the incoming flux. The high velocity of the neutrals and ions relative to the Earth's magnetic field is also sufficient to evoke the plasma critical velocity effect. Given this ionization, Papadopoulos (1984) proposed a plasma process that involves a two stream instability between the incoming ram and reflected ions. The ion instability sets up electrostatic waves which in turn heat the ambient electrons. These in turn excite the in situ and ram neutral and ion constituents. If the electrons are excited to 20 eV or higher, they allow e+X reactions. Papadopoulos proposes that this process could produce both "Shuttle Glow" and the observed enhanced ionization and temperature in the ram direction.

2.6.4 Biased Surfaces

Parker (1979), Parker (1980), Stevens (1980), McCoy, et al. (1980), and Reiff et al. (1980) have all carried out calculations of the currents to biased surfaces for large high voltage structures. They find that a major effect is to induce large voltage gradients in the plasma sheath. Negative potentials may cause preferential deposition of positively charged ion contaminants or sputtering . Chemical effects in the presence of the accelerated ions may be enhanced. Focusing or acceleration due to positive potential fields around exposed high voltage surfaces may greatly enhance electron fluxes Exposed potentials such as high voltage solar arrays may cause a variety of environmental interactions. Several of these are discussed in more detail below.

Positively ch[illegible]ed surfaces immersed in the dense Space Station plasma environment, even when insulated, can lead to substant[illegible] [illegible]20% at Space Station altitudes) power loss. Small pin holes in insulation covering positive potentials [illegible]olar array are able to attract large currents (the pinhole effect). Below about +100 V the electron return flux is about what would be expected for the area of the exposed surfaces (typically the interconnect wires between solar cells). Above about +100 V, however, a curious phenomenon is observed that can greatly enhance negative current collection for positive surfaces. When a small pinhole exists in the insulation, the flux of incident electrons accelerated by the gradients around the pinhole is of sufficient energy and intensity to generate enhanced fluxes of secondary electrons from the insulating surface. This cloud of secondaries greatly increases the apparent size of the pinhole by creating a local enhancement in the plasma that effectively defeats the insulation. Such pinholes are inevitable, except for exceptionally thick insulation, due to the flux of micrometeoroids and surface erosion. Thus power loss can occur even for insulated surfaces! Fortunately, positive surface areas on a vehicle are usually less than 1/40 of the negative surface areas. This follows because, for the same energy, the ions are 40 times or more slower than the electrons. Since the spacecraft as a whole floats with respect to the plasma, the average potential of the craft will be negative. Thus, for current balance the factor (flux * area) is constant, implying that ion collection area must be 39 times that of the electron collection area. Not discussed here, but very important in a complete understanding of this phenomenon, is the effect of the Earth's magnetic field on the collection of electrons.

Since most of the floating array surface will be negatively with respect to plasma ground most of the exposed array interconnects will collect ions. Since the solar cell coverglass is an insulator it will remain at a potential near plasma ground creating a substantial differential potential with respect to the solar array conductors. This differential has been observed to cause arcing both in laboratory experiments (Kennerud, 1974, Stevens, et al., 1978) and in space experiments (Grier and Stevens, 1979 and Grier, 1985) at relatively low potentials (-255 V in the high density plasmas associated with the Space Station). The arcing threshold is inversely related to plasma density. The susceptibility of modern space systems to such phenomena is not known, and the relative sensitivities of two different array designs to the same environment has never been studied. In particular, the variation of arcing threshold for negatively biased surfaces with ram/wake conditions, solar illumination, and high energy auroral electrons has not been determined. Since recent studies indicate that surface effects on conductors and other surface conditions may be important in initiating arcs, it is necessary to examine discharge rates as a function of exposure to atomic oxygen, and similar processes which could significantly alter surface properties. C. K. Purvis, N. T. Grier, and D. B. Synder at NASA's Lewis Research Center, as well as others, have performed experiments and constructed models aimed at determining the response of materials and configurations to charging effects.

Very high potential differences between closely spaced electrodes exposed to the plasma environment are in danger of shorting out through the plasma through the normal gaseous breakdown phenomena. The breakdowo voltage in these situations is usually expressed in terms of a Paschen curve (figure 2-13 below).

Figure 2-13 Paschen curve

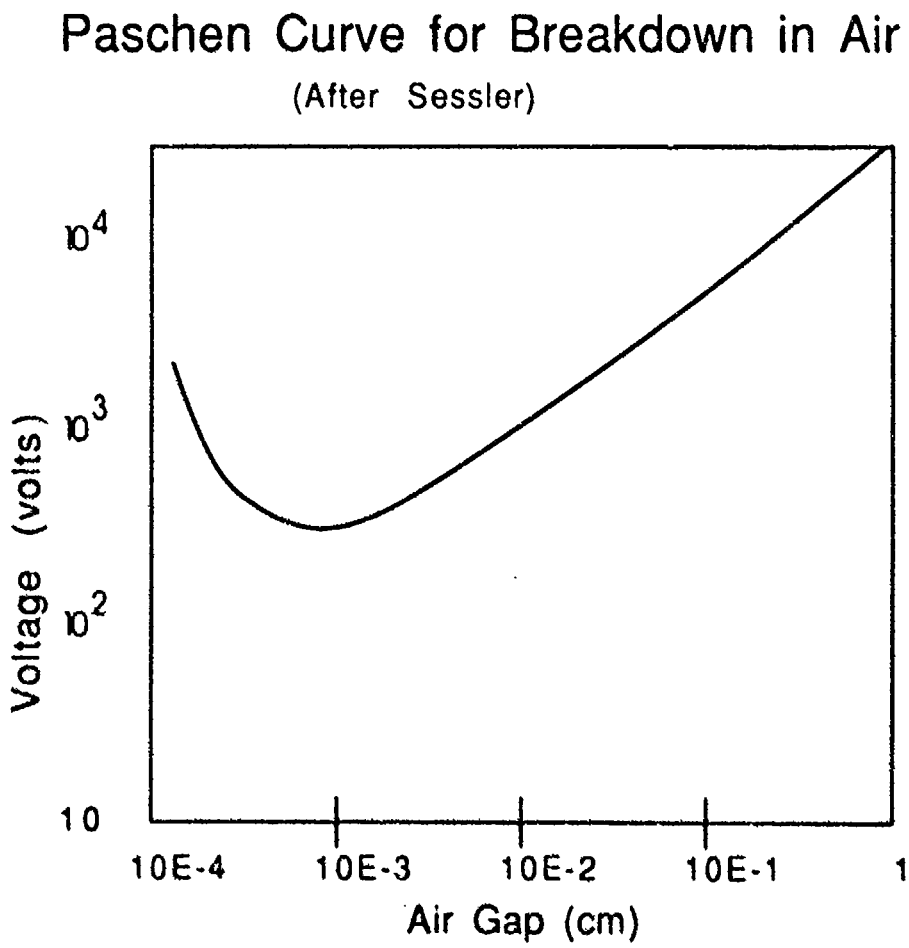

When high frequency electrodes are exposed to a plasma it is possible to generate dense electron plasmas by multiple impacts of electrons with the surfaces of the electrodes (multipacting). When the time required for a secondary electrons generated at the surface of the electrode to transit the gap between the electrodes is in resonance with the frequency of the applied voltage, secondary particles arrive at the opposing electrode just in time to create new electrons for the return trip. Under the right conditions this leads to a a rapid rise of plasma density in between the electrodes. The effects of a dense plasma in this region can be dramatic, shorting out the electrodes or blocking rf transmission.

2.6.5 Torques and Induced Fields

Torques produced by the interaction of current flows in spacecraft with the earth's magnetic field can degrade pointing accuracy. In fact, some spacecraft use this effect in their attitude control systems. The torque on the spacecraft is produced by the attempt of the magnetic moment to align itself with the ambient magnetic field. The torque is given by

$$N = \frac{1}{c}\int x \times \left(J \times B\right) d^3x \qquad (2\text{-}29)$$

where N is the torque (gaussian units), c is the speed of light, x is the position vector, J is the current density vector, and B is the external magnetic field. This integral can for many interestings cases be expressed by the simpler expression,

$$N = m \times B \qquad (2\text{-}30)$$

where m is the magnetic moment. The magnetic moment of the spacecraft is calculated by integrating over all of the current loops.

$$m = \frac{1}{2c}\int_{\text{around current loop}} x \times dl$$

$$|m| = \frac{I}{c} \times (\text{Area of loop}) \qquad (2\text{-}31)$$

where m is the magnetic moment in gaussian units. The second expression is useful when the current lies in a plane.

The magnetic field also plays a role when there is movement across the magnetic field inducing currents and electric fields in the same manner as an electric generator. These effects could be significant for large objects or tethered operations In these cases both the charging, induced currents and fields and the torques and forces on the space system will need to account for the presence of the earth's magnetic field and the motion of the space system with respect to the magnetic field.

For example a satellite at space station altitudes will see an electric field of about 0.3 volts per meter radially from the earth. The tethered satellite system (TSS) seeks to use or at least understand this effect by studying gravity gradient stabilized wires tens of kilometers long generating potential differences of kilovolts. For structures this large and with voltages and field this big, many effects will become important including the ability of the space structures to collect and maintain the currents implied in such a system.

2.7 Summary

Plasma interactions with the surface of a spacecraft can and have lead to surprising reaction in spacecraft systems and need careful attention from the beginning of the design process. However our understanding of plasma

processes is growing, spacecraft/plasma interactions are becoming understood, and there are engineering techniques (see chapter 6) available for many of the known effects. Although studied for a long time, the physics of breakdowns is not yet fully developed. Detailed description of plasma currents in the magnetosphere is an active field of research. More subtle effects of the plasma of space systems are becoming important. and the inevitable change in space system technology is focusing our attention of new aspects of charging. Spacecraft charging will continue to be an important aspect of space system design for the foreseeable future. The hard learned lessons of the past predict future progress and development as our ambitions in space grow.

Chapter

3

INTERNAL DISCHARGES

3.1 Internal Discharges

Following the discovery of surface charging and discharging in spacecraft operations, and the launch of the SCATHA spacecraft, Vampola at Aerospace, Whitlesey et al. at JPL and others began to notice anomalies that seemed to be caused by discharges but at times when no surface charging should have been present. In some cases ground simulations using large surface discharges reproduced the anomaly. In other cases no reasonable surface discharge was able to reproduce the anomaly. Finally a rough correlation of the anomaly with the high energy component of the electron spectrum was observed. This lead to a new subfield for spacecraft charging. Internal discharges result from charge stored in dielectric material or well insulated floating conductors inside the spacecraft. When these discharge they produce small but well coupled signals in nearby electronics and are suspected of causing a number of spacecraft observed anomalies. Internal discharges are particularly difficult to simulate and are correlated with markedly different environments than surface discharges just discussed in Chapter 2. In this text we are calling this phenomena internal discharges, to emphasize the idea that the charge build up in these cases occurs inside the spacecraft on floating conductors or in large volumes of dielectric. Other workers refer to the same phenomena as deep dielectric charging, or electron caused electromagnetic pulses (ECEMP). No matter what the name, good spacecraft design is needed to avoid anomalies due to charges which penetrate the surface of the space system and buildup within materials near sensitive electronics.

Internal discharges are discharges that occur inside the spacecraft due to charge buildup on and inside materials. Of most concern are large volumes of floating conductors, although charge buildup in bulk dielectrics and on the surface of good insulators can also produce unwanted effects in systems. The most graphic examples of bulk discharges in insulators are the Lichtenberg patterns produced in clear plastic samples by bombardment with electrons. Figure 3-1 emphasizes the charge buildup and discharge in a circuit board with floating lands.

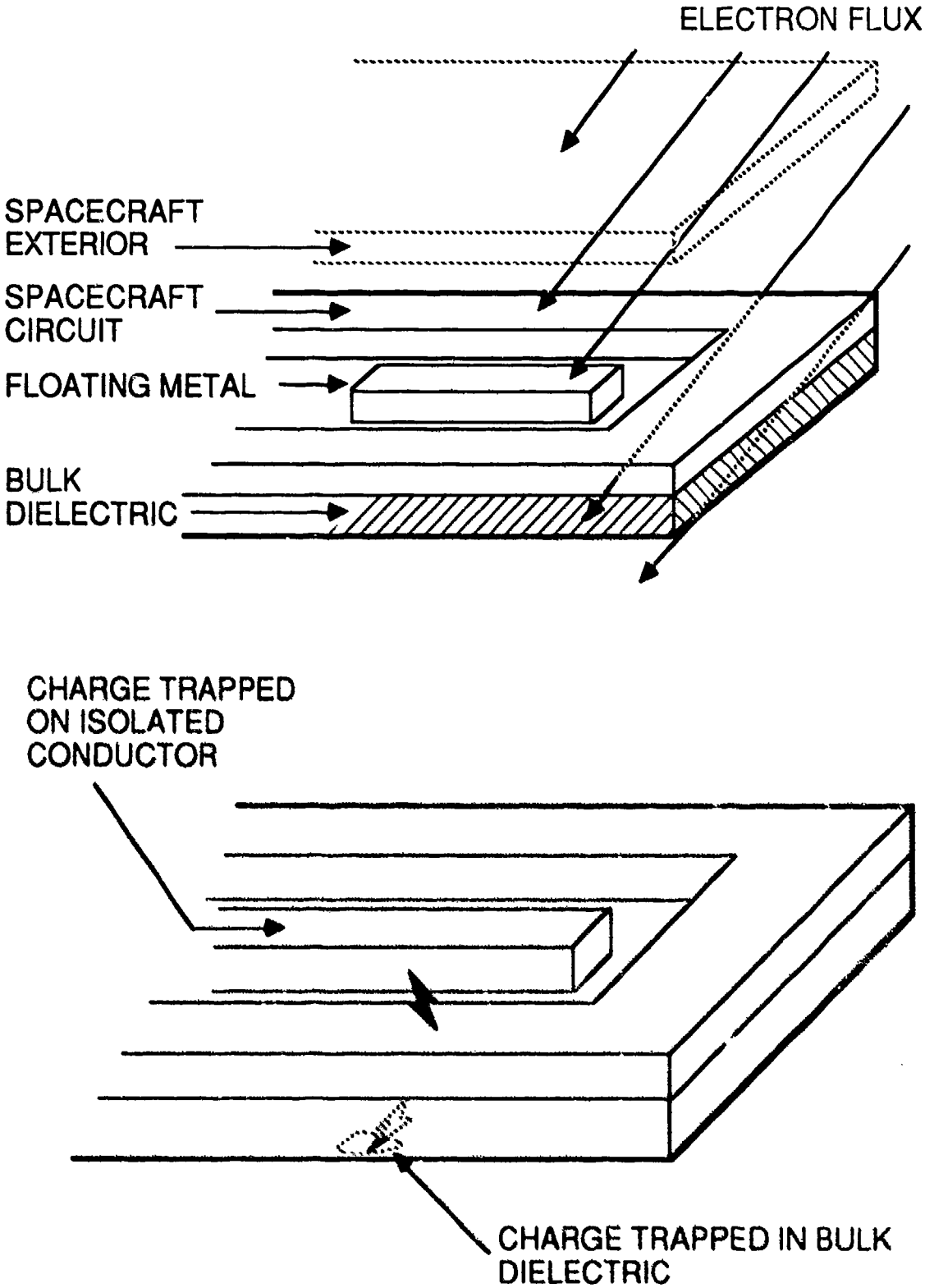

Figure 3-1. Internal Charge Buildup and Discharge

3.1.1. Penetration of Electrons to Interior of Spacecraft

The calculation of the passage of charged particles through materials involves energy loss to the primary charged particle by ionizing or exciting particles in the materials along its track, by Bremsstrahlung and other inelastic scattering processes, and by elastic nuclear scattering. Considerable effort has gone into accurately describing these processes, and comparing these calculations to measured results. For electrons the process is particularly complicated by the fact that the electron's mass is so small compared to the mass of the atom and therefore it is easy for it to have very large angle scattering events.

3.1.1.1. Energy Loss by Electrons

The energy loss per unit path length decreases with increasing electron energy with an inverse velocity squared dependence until the velocity becomes relativistic. This is followed by a broad minimum (called the "minimum ionization") with a very slow increase at higher energies. The energy loss of electrons as a result of ionization as the electron travels a distance dz in a material is:

$$\left(\frac{dE}{dx}\right) = \frac{4\pi e^4 N Z}{m_0 v_0^2}\left\{\ln\left(\frac{2 m_0 c^2}{I}\right) + \ln(\gamma - 1) + \frac{1}{2}\ln(\gamma + 1) - \frac{1}{2}\left(3 + \frac{2}{\gamma} - \frac{1}{\gamma^2}\right) + \frac{1}{16} - \frac{1}{8\gamma} + \frac{9}{16\gamma^2}\right\} \quad (3\text{-}1)$$

where γ is the relativistic factor, $1/\sqrt{1-\beta^2}$, v_0 is the incident electron's velocity, I is the ionization energy of the material, m, the rest mass of the electron, and e the charge on an electron (see van Lint et al., 1980, p. 58).

The increase at very high energies is due to the relativistic sharpening of the transverse electric field of the moving electron. This relativistic effect approaches a value of 1.3 to 1.5 times the minimum value depending on the material. The ionization loss in other materials can be estimated from the energy loss in silicon by multiplying by the ratio of Z/A. For example stopping power (dE/dx) in iron is 0.96 times that in aluminum.

For electrons of energy 10 MeV or less, ionization loss is the dominant mechanism for slowing down and stopping electrons. Above 10 MeV other processes become important. This is shown in Figures 3-2 and 3-3. There are many texts (for example Evans, 1955, or Fermi, 1950), which give detailed discussions and derivations of the transport of electrons (and other particles) in matter.

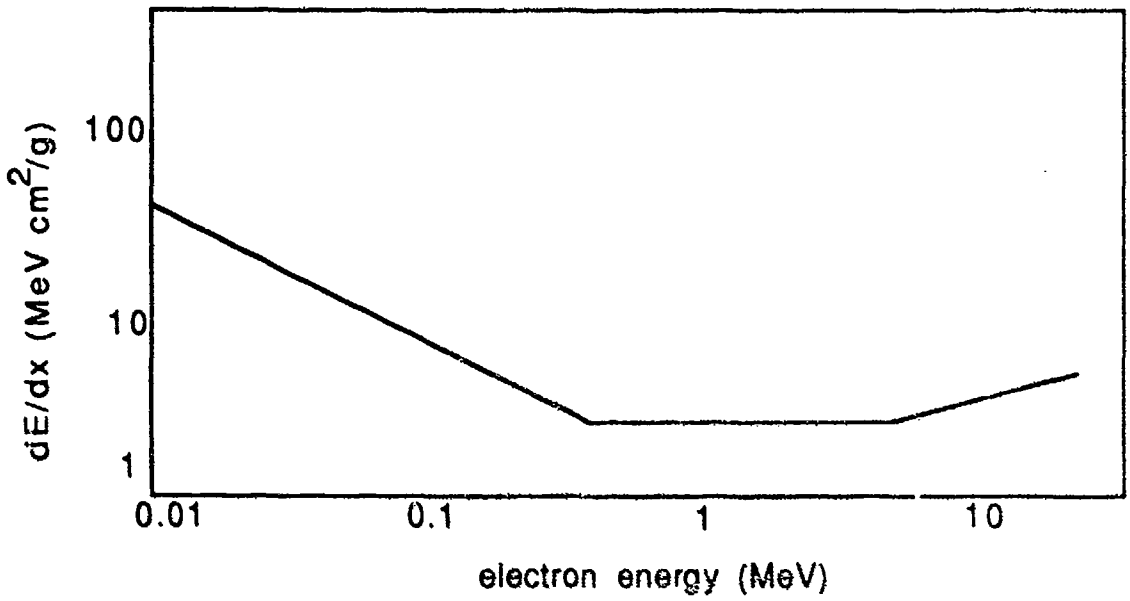

Figure 3-2. Fractional Energy Loss for Electrons in Lead (van Lint, et al., 1980)

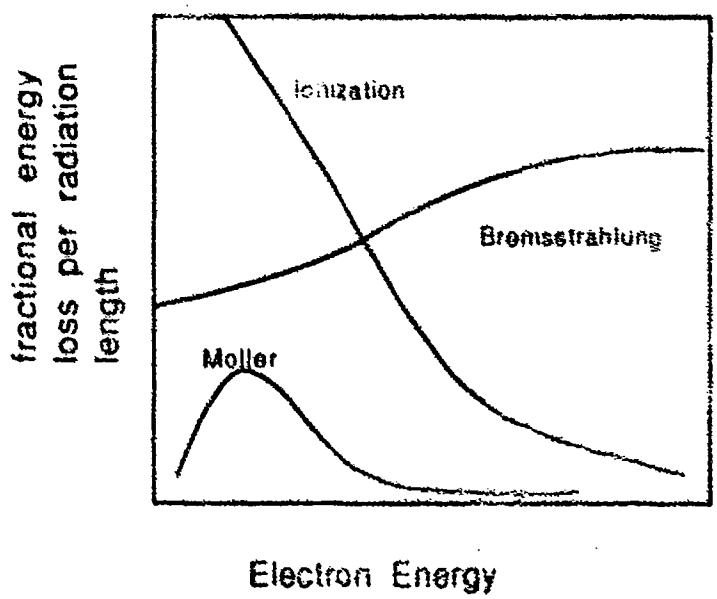

Figure 3-3. Fractional Energy Loss for Electrons in Lead (Anderson, 1981)

3.1.1.2. Electron Range, Effect of Shielding

Since internal discharges depend on particles penetrating to the place where they collect and finally discharge, shielding (if grounded) can be very effective in reducing ID. For example, increasing the shielding from 20 to 100-mil (Aluminium) will remove internal discharges as a concern for many geostationary storm environments.

Of practical interest is the range of electrons in materials. Figure 3-4 shows the empirical range energy relationship for electrons absorbed in Aluminum (Evans, 1955). Katz and Penfold, 1952, give an empirical fit,

$$R = 412\,(E)^n \quad ; \quad n = 1.265 - 0.0954 \ln E \qquad (3\text{-}2)$$

for electrons with energies greater than 0.01 MeV but less than 3 MeV, and

$$R = 530\,E - 106 \qquad (3\text{-}3)$$

for electrons between 1 and 20 MeV. The range, R, has units of mg/cm^2 in these expressions, and E is in MeV.

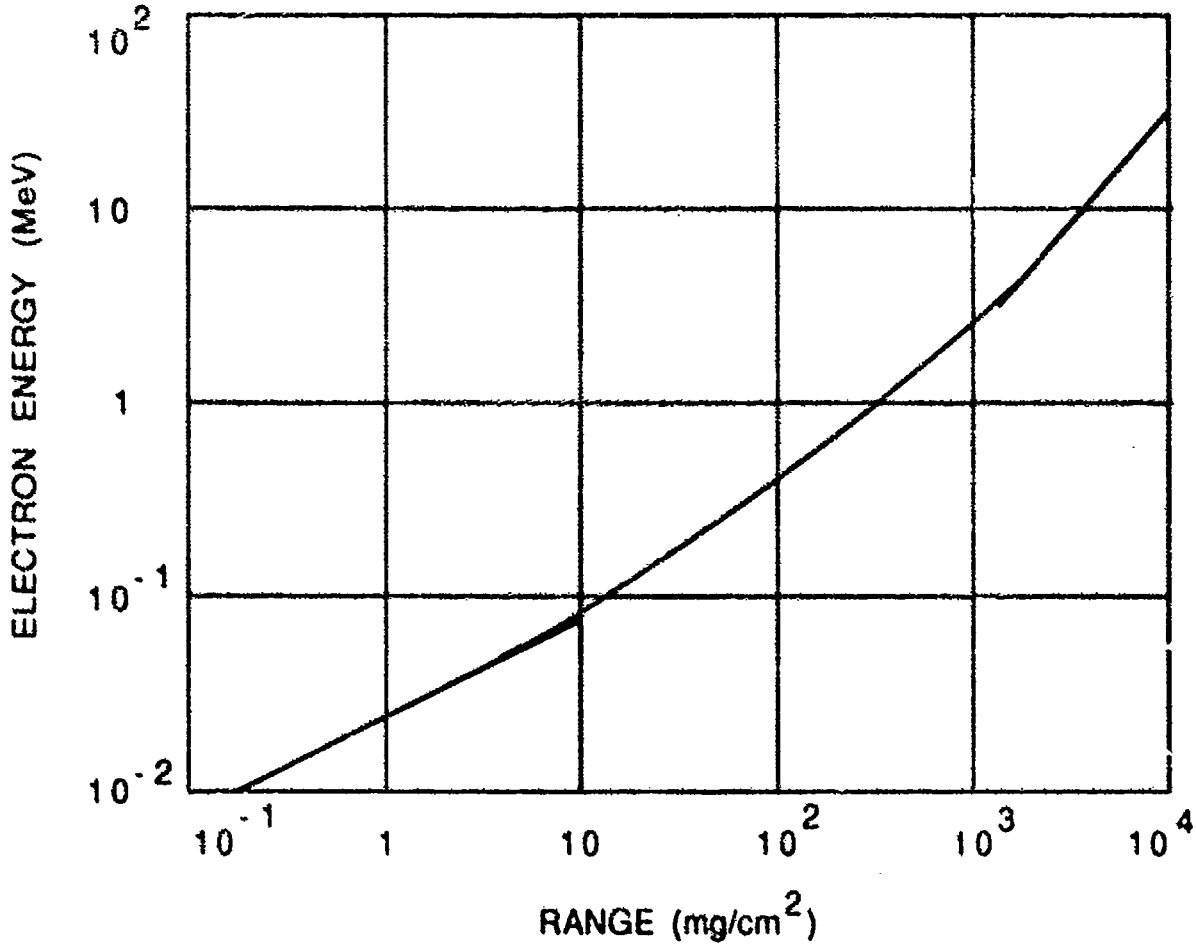

Figure 3-4. Electron Energy Versus Range in Aluminum

3.1.2 Charge Buildup

The charge buildup in or on a material can be estimated by considering all of the currents which deposit charge either in or on the material and those which transport currents away from the material or surface. The

expressions and discussion on surface charging already covered are still valid. For internal surfaces, the only difference is to calculate the incident flux by considering the effects of the shielding the spacecraft mass provides between the surface in question and the ambient environment. However, in addition one now needs to consider the charge deposited in the bulk as well.

The currents which need to be considered in calculating the charge deposited in the bulk of an insulator or isolated conductor are:

1. Incident electron and ion currents
2. Secondary emission from the surface
3. Diffusion of charge through the material
4. Charge flow due to electric fields inside the material (perhaps an Ohm's law type flow? See discussion under material charging.)

Hopefully in estimating the charge buildup, some of the above considerations can be neglected. For example in many cases the ions do not penetrate very far into the interior of the spacecraft and only electrons need be considered. If the surface of the insulator is covered with a conductor the boundary condition is established by the potential of the metal surface. Suppose we have a planar piece of ungrounded metal which is collecting charge rapidly, so that we can neglect the leakage from the plate through the insulator. The charge buildup will be determined by the capacitance of the plate $Q = C\,V$, where $C \approx \kappa_0 \kappa A/d$, κ is the dielectric constant of the material, κ_0 is the dielectric constant ($8.8542 * 10^{-12}$ farads/meter), V is the voltage across the material, $V \approx E \times d$, d is a typical thickness of the material and E is the electric field across the material.

Typically, a good insulator will have a breakdown threshold electric field on the order of 10^6 V/cm. Specific geometries and dielectric properties will increase or decrease that value by factors of 3 or 4. The charge required to cause a breakdown if none of the charge leaks off will be

$$\frac{Q}{A} = \varepsilon_0 \varepsilon E = \varepsilon\ 8.8 \times 10^{-14} \text{ farads/cm} \times 10^6 \text{ V/cm} \qquad (3\text{-}4)$$

where ε is somewhere between 1 and 10, so that the fluence required will be

$$\frac{q}{A} = 5.5 * 10^{11} \frac{\varepsilon}{\text{cm}^2} \qquad (3\text{-}5)$$

3.1.2.1 Charge Leakage

Low flux laboratory tests have shown that dielectrics do not charge and discharge all the time. One conclusion is that dielectrics inside satellites must charge to some steady state potential where the charging current is balanced by leakage terms. Leakage terms can be included in the above analysis by considering the voltage as a function of time including the leakage term.

$$V(t) = \frac{A}{C} \int j\,dt - \frac{1}{C} \int i(\text{leakage})\,dt \qquad (3\text{-}6)$$

In the case of a simple Ohm's law material, i(leakage) is the voltage divided by R, the resistance. R is proportional to 1/conductivity. The conductivity is determined by its ambient conductivity plus any radiation-induced terms and field-induced terms. In general, there can be a voltage dependence for the conductivity. This formulation can be expressed in a more pleasing form mathematically as follows

$$\frac{dV}{dt} = \frac{A}{C} j(t) - \frac{V(t)}{CR} = \frac{j(t) \cdot d}{\varepsilon\,\varepsilon_0} - \frac{V(t)\,\sigma(j,V)}{\varepsilon\,\varepsilon_0} \qquad (3\text{-}7)$$

The expression relates the change in voltage based on the incoming current and the leakage. For steady state, dV/dt = 0, the equations simplify.

Laboratory tests also show decharges long after the charging beam has been turned off. This implies that a simple Ohm's law behavior is inadequate.

3.1.2.2 Material Charging

Charge buildup within a material such as Teflon can be viewed as follows. The charge on a surface due to incident charges from outside the material is calculated by considering secondary emission, etc. (as outlined in the discussion of surface charging). The electric fields inside the material will depend on any external fields, the surface charge (as a boundary condition), the polarization of the dielectric, and any space charge left within the bulk of the dielectric itself. The boundary conditions will play a significant role in determining the field across the dielectric. A dielectric body which includes trapped charge is called an electret (Gerhard-Multhaupt, 1987). In some cases the trapped charge in an electret is of opposite signs and the net charge is zero. In figure 3-5 Sessler (1980) points out some of the configurations of planar electrets.

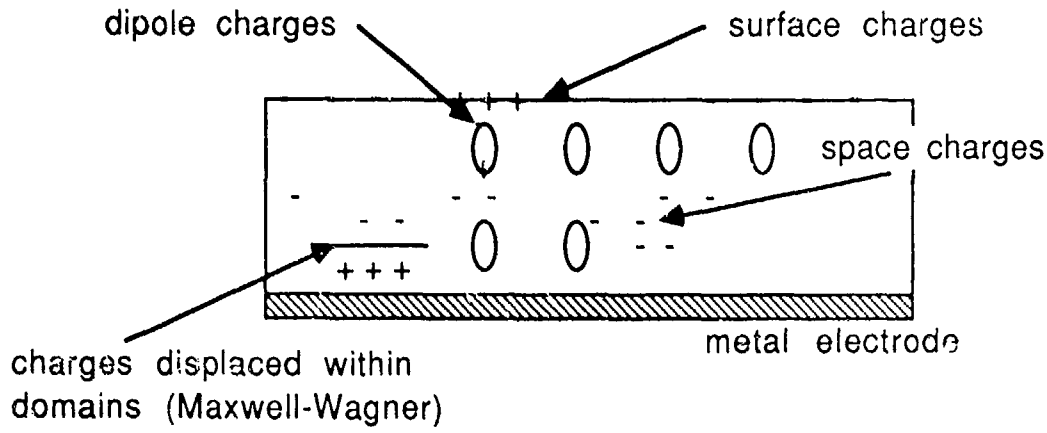

Schematic cross-section of some planar electrode and dielectric configurations involving excess charge and polarization

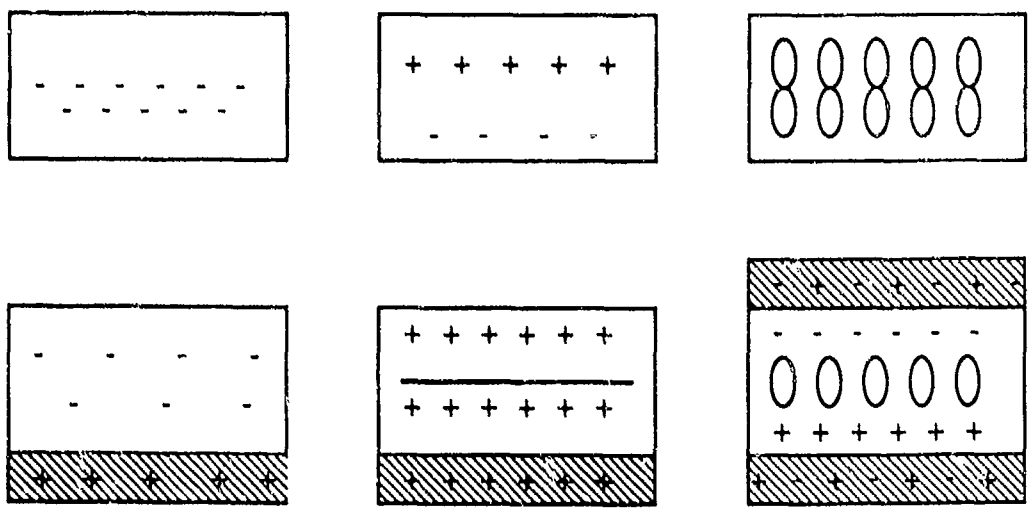

Figure 3-5. Electrets: Excess Charge and Polarization in a Dielectric

3.1.2.3. Currents in Electrets

Currents flow in an electret because of time and space variations in electric fields, and electret charges. Following the discussion of Sessler (1980), the current is easily divided into conductive and displacement components. Conductive currents are the physical motion of charges through the material. The conductive-current density is related to the real charge density ρ_1 by the continuity equation:

$$\frac{\partial \rho_1(x,t)}{\partial t} = -\frac{\partial j_1(x,t)}{\partial x} \quad \text{for planar geometry} \qquad (3\text{-}8)$$

The real charge density ρ is related to the electric field by Poisson's equation,

$$\nabla \cdot \mathbf{D} = \rho_1 \qquad (3\text{-}9)$$

The total charge density is made up of two parts, the real charge density, ρ_1, and the dipole polarization or microscopic charge displacement component, ρ_2

$$\rho = \rho_1 + \rho_2 \qquad \text{and} \qquad \sigma = \sigma_1 + \sigma_2 \qquad (3\text{-}10)$$

for surface charge densities. The dipole polarization component is related to that part of the polarization of the material, the "frozen-in component due to ... microscopic charge displacement" (Sessler, 1980)

$$\rho_2 = -\nabla \cdot \mathbf{P}_2 \qquad (3\text{-}11)$$

where total polarization, P, is divided into two parts, the instantaneous, P_1, and the quasi-permanent component, P_2

$$\mathbf{P} = \mathbf{P}_1 + \mathbf{P}_2 \quad ; \quad \mathbf{P}_1 = \varepsilon_0(\varepsilon - 1)\,\mathbf{E} \qquad (3\text{-}12)$$

Displacement currents are due to inductive effects.

$$j_2 = \varepsilon_0 \varepsilon \frac{\partial E}{\partial t} + \frac{\partial P_2}{dt} \qquad (3\text{-}13)$$

The total current density is $j = j_1 + j_2$. (3-14)

The conductive current, j_1, is expressed in terms of mobilities and charge densities as

$$j_2 = \left[g + \mu_1 \rho_1^{+} + \mu_2 \rho_2^{-}\right] E \qquad (3\text{-}15)$$

The conductivity of the dielectric, g, is

$$g = e(n_1 \mu_1 + n_2 \mu_2) \qquad (3\text{-}16)$$

where n_1 is the density of intrinsic positive carriers -- both trapped and free, and n_2 is the intrinsic density for electrons. The total charge density for positive carriers is

$$e\, n_1 + \rho_1^{+}$$

and for negative carriers

$$e\, n_2 + \rho_2^-$$

The trap-modulated mobilities for positive and negative carriers are μ_1^+ and μ_2^- respectively. One reason to break up the expressions in this way is to separate out the physical components where g is the conductivity of the dielectric, and ρ is the generally space dependent excess charge carrier density. The internal charge decay in dielectrics is governed by this conduction phenomenon. In substances capable of quasi-permanent charge storage, the mobilities are trap-modulated. If an electron is trapped near the bottom of the conduction band and moves between extended states by quantum-mechanical hopping, the process requires no thermal activation and leads to relatively high mobilities (10 $cm^2/(V \cdot s)$). If the electron is trapped below the "mobility edge" it needs thermal energy to perform the hopping process and the mobility is typically four orders of magnitude less. So-called deep traps have even smaller mobilities, 1E-10 to 1E-17 $cm^2/(Vs)$.

3.1.3 Maxwell-Wagner Effect

In heterogeneous materials consisting of different components or phases, such as paints, it is possible for the components to have different dielectric constants and conductivities. In that case charges can accumulate near the interfaces between components. When such a sample is heated and subjected to a field these charges can be frozen in if the field is maintained during cooling. Subsequent thermally stimulated discharging (TSD) of the sample will show an excess charge peak when the trapped charge is neutralized by conduction across the interface. (See the discussion by van Turnout in Sessler (1980) for comparison of a simple model with experimental results.)

Such an effect also appears in uniform samples when radiation-induced conductivity dissipates electrons non-uniformly. In irradiated dielectrics Maxwell-Wagner distributions can be implanted without temperature changes and external electric fields by penetrating charged particles.

3.1.4 An Example -- Teflon Characteristics

Teflon refers to either PTFE (Polytetrafluoroethylene), PFA (Tetrafluoroethylene-perfluoromethoxylethylene copolymer), or FEP (Tetraflouroethylene-hexa-flouropropylene copolymer). It is a combination of crystalline and amorphous regions. It has no piezoelectric or pyroelectric properties, and so is typical of many spacecraft dielectrics, and it has been extensively studied (see Sessler, 1980, and the references therein). The intrinsic resistivity, 1/g, is very high, $\approx 10^{22}$ ohm-cm. This is because both the mobility is small and the density of intrinsic carriers, n, is small. The dielectric relaxation time, $\varepsilon\varepsilon_0/g$, is approximately 10^9 s. In Teflon, transit time measurements over periods of the order of one microsecond yield mobilities of 5 E-5 cm^2/Vs and hole mobilities an order of magnitude greater. Both of these mobilities obey an exponential temperature dependence suggesting shallow trapping centers. The temperature dependence of "free mobility" is typically T^{-1} to T^{-2}. The Schubweg, that is the distance over which a carrier drifts under the influence of an electric field before it disappears by recombination, is about 0.1 micron at a few 10^5 V/cm in FEP, and 6 microns in Mylar (PET -- Polyethylene terephthalate) for an electric field of 8 x 10^5 V/cm and is proportional to the electric field. Holes in FEP have a Schubweg of about 100 microns for electric fields on the order of 10^5 V/cm.

3.2. Experimental Rates

Experimentally, dielectrics have been observed to charge to a steady state condition without discharge. This condition is referred to as a saturation potential. Other materials have been observed to continue discharging after all external fluxes have been removed. For those materials in which a saturation potential describes the material well, no discharges have been observed below 0.3 pA/centimeter squared. At that current density it will take 74 hours to reach a total deposited charge density of 5.5×10^{11} electrons/cm^2.

The time that dielectrics store charge is characteristic of the time constants for leakage. Typical spacecraft dielectrics store charge for periods ranging between hours and days.

ceramic	0.5 hour
polyimide	2 hours
Teflon	12 hours
Fiberglass FR4	>24 hours

Whenever the time to accumulate 5.5×10^{11} electrons/cm^2 is less than the typical decay period of the material and configuration, internal discharges are possible. To be absolutely sure there will be no discharges, measurements of the materials and configurations of interest are highly desirable. Variations in material and breakdown threshold could decrease the fluence required by a factor of ten or more. Table 3-1 lists typical resistivities which can be used to estimate charge buildup.

Table 3-1. Resistivity Table

TITLE	DESCRIPTION	RESISTIVITY	REFERENCE
ALUMINA	—	10^{11} TO 10^{14} ohm-cm (23 deg C)	CRC, 1977
ALUMINUM	—	2.6548 microhm-cm (20 deg C)	CRC, 1977
AMBER	—	—	CRC, 1977
BRASS	(RED CAST)	11 microhm-cm 7 microhms-cm (20 deg C)	CRC, 1977
CARBON	—	1375.0 microhm-cm (0 deg C)	CRC, 1977
COPPER	—	1.6730 microhms-cm (20 deg C) 1.71 microhms-cm (20 deg C)	CRC, 1977
CROSS-LINKED POLY-STYRENE	—	10^{16} ohm-cm	COTTS AND REYES, 1985
DELRIN	ACETAL POLY (OXYMETHY-LENE)	10^{15} ohm-cm	COTTS AND REYES, 1985
EPOXY	—	4×10^{16} ohm-cm	COTTS AND REYES, 1985
GLASS	SEE INDIVIDUAL DESCRIPTIONS	10^{12} TO 10^{16}	—
HARD RUBBER	—	—	—
IRON	—	9.71 microhms-cm (20 deg C)	CRC, 1977
KAPTON	POLYIMIDE	10^{14} TO 10^{16} ohm-cm	COTTS AND REYES, 1985

Table 3-1. Resistivity Table (Cont'd)

TITLE	DESCRIPTION	RESISTIVITY	REFERENCE
KAPTON H	POLYIMIDE	10^{13} TO 10^{15} ohm-cm	COTTS AND REYES, 1985
LEAD	—	20.6448 microhm-cm (20 deg C)	CRC, 1977
MERCURY	—	96.4 microhm-cm (50 deg C)	CRC, 1977
MICA	A) SHEET B) MOULDED	A) 10^{11} TO 10^{15} ohm-cm B) 10^{13} ohm-cm	KAYE, 1986
MYLAR	HUMIDITY SENSITIVE POLYETHYLENE TEREPHTHALATE (PET)	6.4×10^{9} TO 10^{18} ohm-cm	COTTS AND REYES, 1985
NICHROME	—	100 microhms-cm (20 deg C)	CRC, 1977
NYLON	(66) POLY (HEXAMETHYLENE ADIPAMIDE) HUMIDITY SENSITIVE	—	COTTS AND REYES, 1985
PARAFFIN	— —	— 10^{15} TO 10^{19} ohm-cm (20 deg C)	COTTS AND REYES, 1985 CRC, 1977
POLYETHYLENE	—	10^{15} TO 10^{20} ohm-cm 10^{16}	COTTS AND REYES, 1985
POLYACRYLONITRILE	(PAN)	10^{-2} TO 10^{7}	COTTS AND REYES, 1985
POLYAMIDEIMIDE	—	1×10^{17}	COTTS AND REYES, 1985

Table 3-1. Resistivity Table (Cont'd)

TITLE	DESCRIPTION	RESISTIVITY	REFERENCE
POLY-CARBON-ATE	POLY (OXY-CARBONYLOXY -1, 4-PHENY-LENE ISOPRO-PYLIDENE-1, 4-PHENYLENE (LEXAN)	$>10^{17}$ ohm-cm	COTTS AND REYES, 1985
POLY-OLEFIN	POLY (ETHY-LENE-CROPY-LENE) THER-MOFIT)	1×10^{14}	COTTS AND REYES, 1985
POLY-STYRENE	—	10^{17} ohms-cm	COTTS AND REYES, 1985
POLY-URETHANE	(SOLITHINE 113)	2.5×10^{14} ohms-cm	COTTS AND REYES, 1985
PVF-2	POLY (VINYL-IDINE-FLUOR-IDE) (KYNAR)	2×10^{15} ohms-cm	COTTS AND REYES, 1985
SILICA GLASS GE CLEAR	—	4,000-30,000 megohm-cm (350 deg C)	CRC, 1977
SILICA GLASS PYREX	—	4 TO 2,500 megohms-cm (350 deg C)	CRC, 1977
SILICONES	—	7×10^{13} TO 10^{15}	COTTS AND REYES, 1985
SILVER	—	1.59 microhms-cm (20 deg C)	CRC, 1977
SULPHUR	YELLOW	2×10^{23} microhms-cm (20 deg C)	CRC, 1977
TEFLON	POLY TETRA-FLUOROETHY-LENE PTFE	8×10^{16} ohms-cm 10^{13} TO 10^{17} ohms-cm	COTTS AND REYES, 1985
TITANIUM DIOXIDE	—	10^{13} TO 10^{18} ohms-cm (23 deg C)	CRC, 1977

Table 3-1. Resistivity Table (Cont'd)

TITLE	DESCRIPTION	RESISTIVITY	REFERENCE
TUNGSTEN	—	5.65 microhms-cm (300 K)	CRC, 1977
VITON	POLY (VYNIL-IDINE FLUOR-IDE CO-HEXA-FLUOROPRO-PYLENE)	2×10^{13} ohms-cm	COTTS AND REYES, 1985
WOOD	(PARAFFINED)	10^{8} TO 10^{19} ohms-cm	KAYE, 1986

3.3 Discharge Process

Without a discharge, most internal electronics and devices do not experience harmful effects. When a breakdown occurs, a sharp pulse of electromagnetic energy is released which can couple into the electronics and cause malfunction, noise or even burn-out of the electronics. The discharge process is not understood precisely. It involves the release of energy built up in an electric field due to charge separated in the insulator. The simplest case of a material experiencing a breakdown was originally thought to be that of a gas. The possible modes for breakdown in a gas were shown in Figure 2-12. The breakdown can be manifested in any number of ways depending on the voltage characteristics. For liquids and solids the situation can be just as complicated. For example, in solids with voids, the voids break down as a small gas would under the applied voltage and the total behavior of the material is a mixture of the solid behavior and the small gaseous portion. These are called partial discharges in solids (Bartnikas, 1987). In this case, the solid behaves perfectly linearly, but the gas in needle shaped voids breaks down when the voltage across the gas is exceeded even though the stress in the solid material has not yet reached breakdown. Depending on the density of the voids, this can lead to very complicated situations.

Tests are usually relied on to provide some insight into the behavior of materials, various techniques have been developed which take into consideration the unique properties of solid, liquid or gaseous materials.

The fluence required for breakdown in an internal situation like we have just described will be the minimum fluence required, since we have assumed there is no leakage. So we do not typically expect internal discharges unless the fluence is $> 5.5 \times 10^{11}$ e/cm^2. For materials with low breakdown voltage thresholds and with perverse geometries and dielectric properties, discharges may be seen at lower fluences. Nonetheless, we would not expect internal discharges unless the material was a good insulator or an isolated conductor which had experienced a fluence greater than 5.5×10^{11} e/cm^2.

3.3.1. Buried Charge Breakdowns

In the situation where charges have sufficient energy to penetrate below the surface of a dielectric and become trapped while the dielectric surface is maintained near zero, strong electric fields will exist in the material. This can lead to electric fields inside the material large enough to cause breakdowns. The field can even change sign inside the material. Breakdowns within and on the material can be avoided if the material is conductive enough. There is some work currently pursuing conductive polymers (Conwell, 1987), but most commonly used dielectrics on spacecraft are good insulators. An estimate of the conductivity required to eliminate the danger of buried charge and surface discharges can be made as follows.

The differential equation relating currents and fields for a linear dielectric in one dimension is:

$$\varepsilon \frac{dE(x,t)}{dT} + g(x)E(x,t) = J(x) \qquad (3\text{-}17)$$

where ε is the dielectric constant, $g(x)$ is the conductivity at depth x, $E(x,t)$ is the electric field, and $J(x)$ is the current density. The solution to this equation, assuming $J(x)$ and $g(x)$ are independent of time, is

$$E(x,t) = E_0(x) \exp\left[\frac{g(x)t}{\varepsilon}\right] - \left[\frac{J(x)}{g(x)}\right] \times \left(1 - \exp\left\{1 - \exp\left[\frac{-g(x)t}{\varepsilon}\right]\right\}\right)$$

(3-18)

where $E_0(x)$ is the field at t=0. At long times this reduces to the form E=J/g -- a simple Ohm's law response. Thus the flux, J, into and out of the dielectric can be used to estimate the conductivity, g, required to eliminate internal discharges.

The current density, J, during substorms is typically in the range 0.1 to 1.0 nA/cm^2, giving a value of ~1 x 10^{-15} mho/cm for the minimum allowable dark conductivity assuming the breakdown field is 10^5 V/cm.

3.3.2 Minimum Discharge

In gaseous discharges the breakdown depends on the product of the pressure of the gas, P, and the separation of the electrodes, d. At values of Pd approaching a total vacuum the breakdown voltage is fairly high, but as the pressure increases, the breakdown voltage drops. At some value of Pd the breakdown voltage reaches a minimum, and begins to rise. Early rocket flights with exposed high voltages experienced breakdowns as the rocket passed through this minimum breakdown region; that is, for a fixed separation between the high voltage electrodes, as the pressure dropped, the breakdown voltage fell until there was a breakdown. The breakdown occurred at some high altitude when the pressure times the separation of the electrodes was above the Paschen curve. This dependence was shown in Figure 3-6. The minimum is called the Paschen minimum and the curve is called the Paschen curve. Breakdowns would be expected when the voltage across the gap between the metal electrodes exceeds the Paschen curve.

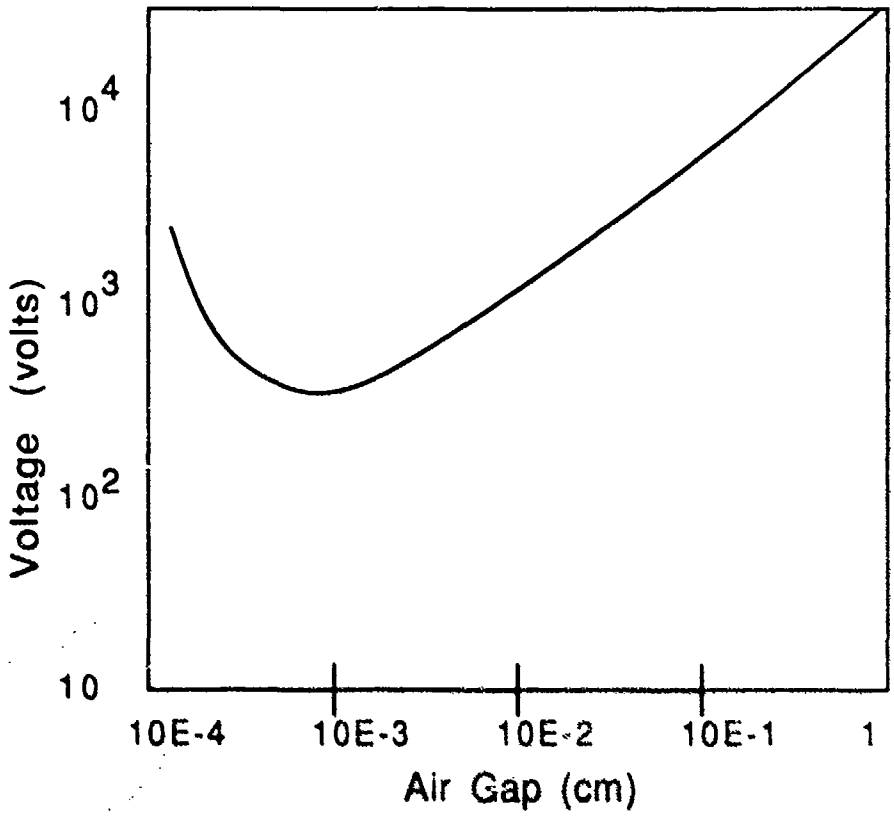

Figure 3-6. Paschen Curve for Breakdown in Air (Sessler, 1980)

3.3.3 Electrode Geometry

The details of a Paschen curve for any gas depend on the shape of the electrodes separated by the gas. As the electrodes get sharper, the local electric field gets higher and the breakdown voltage drops. Similarly the breakdown in solid dielectrics is influenced by the shape of nearby conductors and the charge distribution on and within the dielectric. For many experimental studies it is convenient to divide the configuration into the simple geometric categories shown in Figure 3-7. The energy and peak voltage in the breakdown pulse even for the same material are strongly influenced by the geometry. In general, floating metal configurations give the largest and narrowest pulses; breakdowns in dielectrics surrounded by metal give the smallest and broadest pulses; breakdowns involving one free surface give intermediate results.

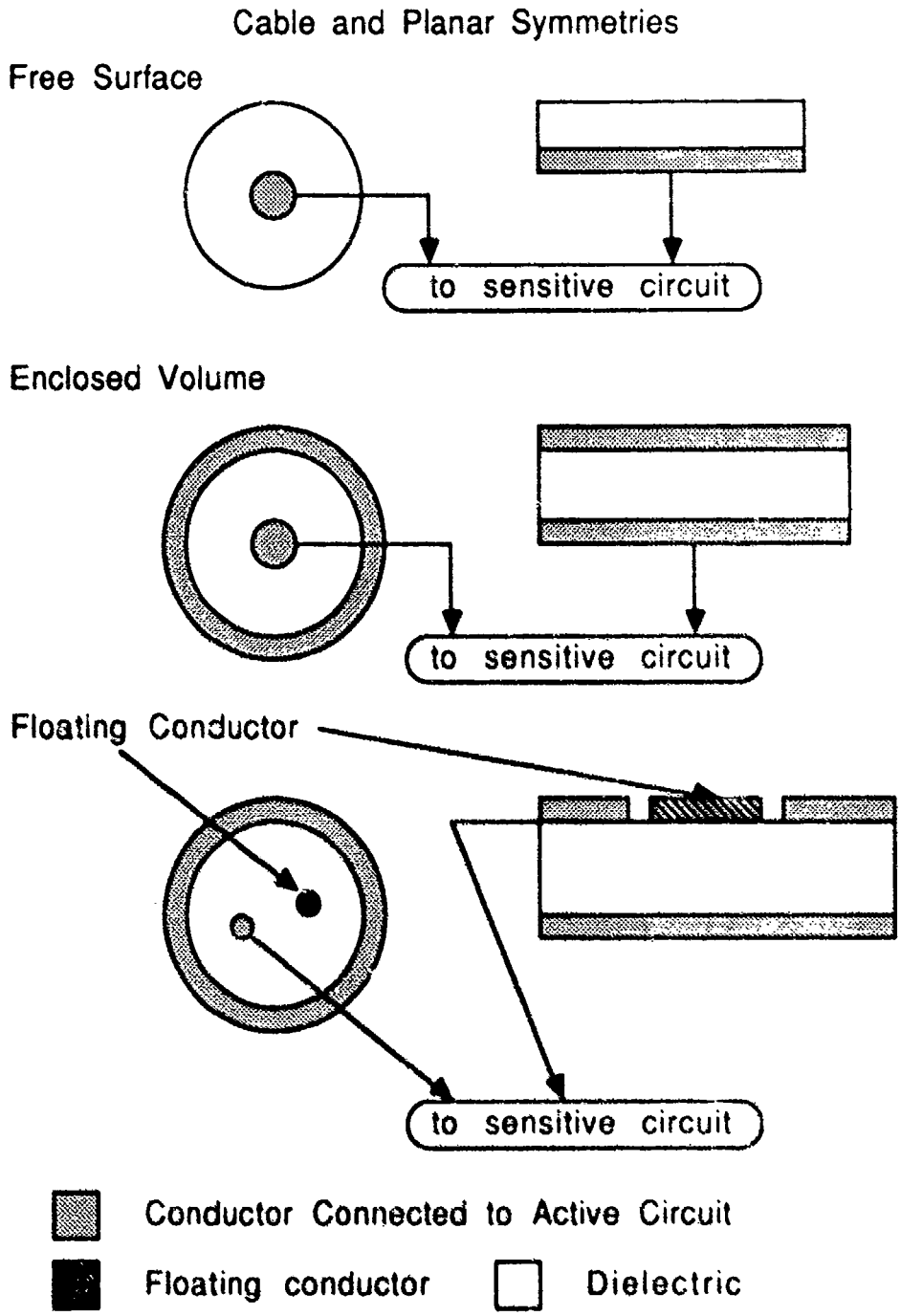

Figure 3-7. Internal Discharge Configurations Used on Internal Discharge Monitor

3.4. Calculation of Internal Discharge Rates

If internal discharges cannot be eliminated entirely, the engineering concern is "how often will the discharge occur?" A feel for this number can be obtained by referring to Table 3-2 from Coakley. In this table the time required in seconds for the flux to equal 5×10^{11} e/cm^2 is estimated for different space environments and shielding. There are approximately 8.6×10^4 seconds in a day and approximately $\pi \times 10^7$ seconds per year. The shielding is

assumed to be aluminum with 2.7 g/cm^3 density. One mil is one thousandth of an inch. The fission saturated numbers ignore the first 12 hours after injection of fission electrons to allow the pumped up belts to equilibrate. Typical pulse shapes are thought to be in the range shown in Figure 3-8.

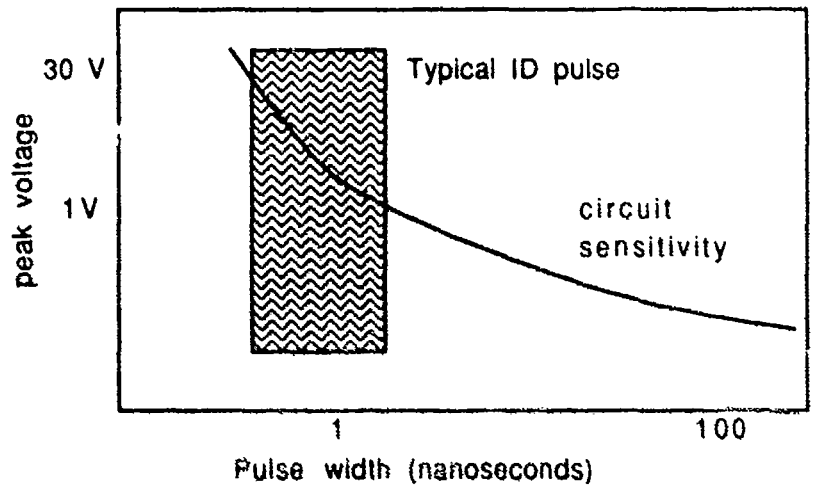

Figure 3-8. Internal Discharge Characteristics. Typical ID pulses are generated on reasonably small surface areas or in small volumes of insulators and so range from 10 to several hundred millivolts with pulse widths in nanoseconds.

Table 3-2. Time (Seconds) to Reach Minimum Internal Discharge Fluence (Coakley, 1986a)

Environment	Surface	20 mil	100 mil	250 mil
Natural				
Low earth orbit	n/a	2×10^7	5×10^8	
1/2 synchronous	n/a	1×10^6	2×10^8	1×10^{10}
1.0 synchronous	n/a	1×10^6	7×10^8	1×10^{10}
Storm				
Low earth orbit	n/a	2×10^5	5×10^6	
1/2 synchronous	10^2	7×10^4	8×10^5	1×10^8
1.0 synchronous	3×10^2	1×10^5	3×10^6	1×10^8
Fission Saturated				
Low earth orbit	???	1×10^2	1.5×10^3	
1/2 synchronous	1×10^1	2×10^3	4×10^4	1×10^6
1.0 synchronous	1×10^1	7×10^3	1.7×10^5	1.5×10^6

3.4.1. Discharge Rate Depends on Incident Flux

Internal discharges occur on and in materials with very high resistivity. For those materials, the voltage drop across the material to maintain currents on the order of those flowing in space is reasonably large. The larger the current the greater the potential difference for ideal Ohm's law materials. From this alone one would expect a flux dependence on the rate of discharge in insulating materials. Figure 3-9 shows how the assumption of an ideal Ohm's law material is helpful in determining which materials are internal discharge concerns.

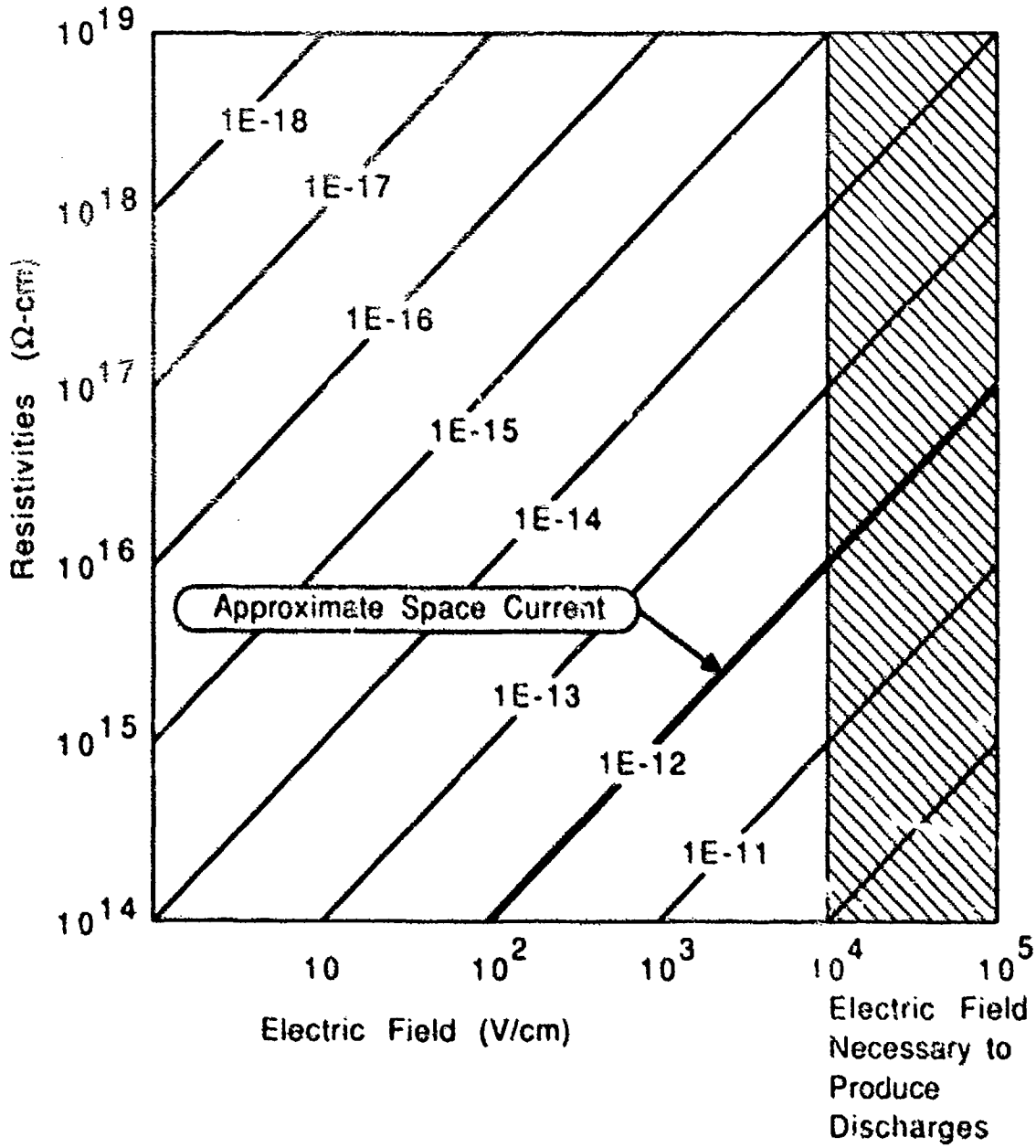

Figure 3-9. Ohm's Law Materials Versus Space Currents

3.4.2. Experimental Discharge Rates

Figure 3-10 shows some data from Coakley (1986a) on circuit board materials which indicates a flux dependence. After the initial sharp rise, the discharge rate appears to be almost linear with the flux.

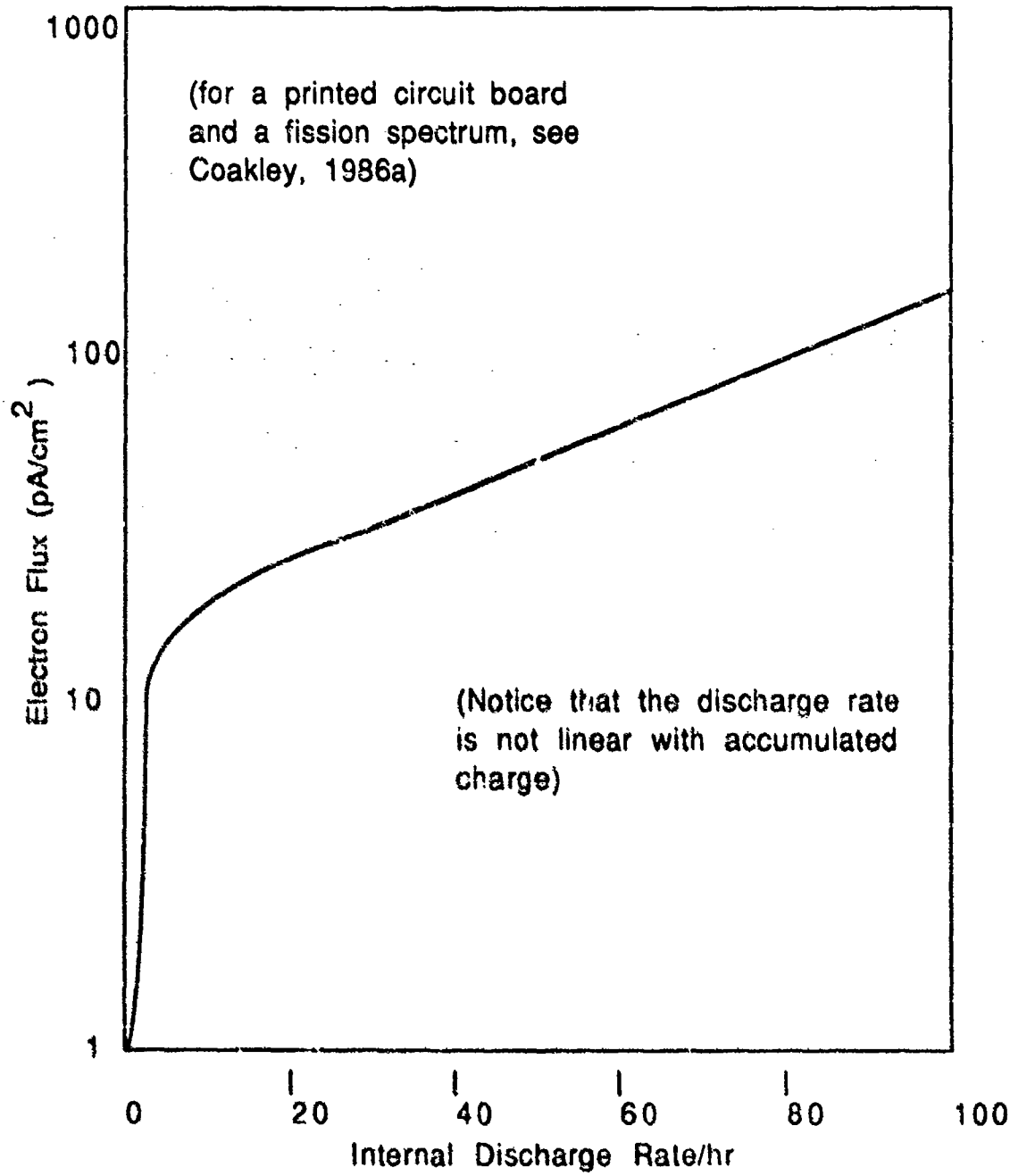

Figure 3-10. Flux Versus Discharge Rate

Some generic materials and configurations have been investigated for internal discharge characteristics. Table 3-3 is taken from the work done in preparing the internal discharge monitor for the CRRES spacecraft (Robinson, 1985).

Table 3-3 Measured Internal Discharge Pulses

Material	Thickness Shape	Min Voltage	Max Voltage
Fiberglass FR4	125 mils configuration 2	0.10	5.0
Fiberglass FR4	125 mils configuration 6	0.02	100
Fiberglass FR4	125 mils configuration 4	0.05	1.00
Fiberglass FR4	47 mils configuration 2	0.01	0.20
FEP Teflon	90 mils configuration 6	1.00	100.
FEP Teflon	90 mils configuration 4	0.02	0.20
FEP Teflon	90 mils configuration 2	0.01	0.20
PTFE	90 mils configuration 4	0.02	1.00
PTFE	90 mils configuration 2	0.03	0.20
Alumina	40 mils configuration 6	0.02	40.0

3.5. Coupling to Sensitive Circuits

Once a discharge occurs, the coupling of energy proceeds exactly as described in the discussion of surface charging and discharging. The differences between an internal discharge and a surface discharge are: the lower amount of energy usually involved, the slightly faster initial pulse, and the possibility of much closer proximity of the discharge site to a sensitive circuit.

3.6. ID Causing Environments

Internal discharges are caused when charged particles build up on a surface or in the bulk of a material inside the spacecraft to the point where a discharge occurs. Internal discharging is of concern when the fluence received is greater than approximately 10^{11} electrons per centimeter squared. For electrons to penetrate the skin of the spacecraft and so cause internal discharge their energy must be in the range of 300 keV to 5 MeV. Below about 300 keV electrons cannot penetrate the skin of a typical spacecraft. Above 5 MeV, electrons typically pass through a box of electronics, and for electronics near earth, the natural population of electrons above 5 MeV is very small. No laboratory experiments to date have produced internal discharges with current density less than 0.3 pA/cm^2. The population of electrons in most spectra is well below 0.3 pA/cm^2 above 5 MeV. Some missions (for example those to Jupiter) may have to contend with harsher environments but those tend to be specialized cases. Each mission should evaluate its mission flux independently. It is the peak flux which helps determine the likelihood of internal discharges. Figure 3-11 shows a typical environment of concern (the predicted CRRES environment an eliptical orbit from shuttle altitude to geosynchronous).

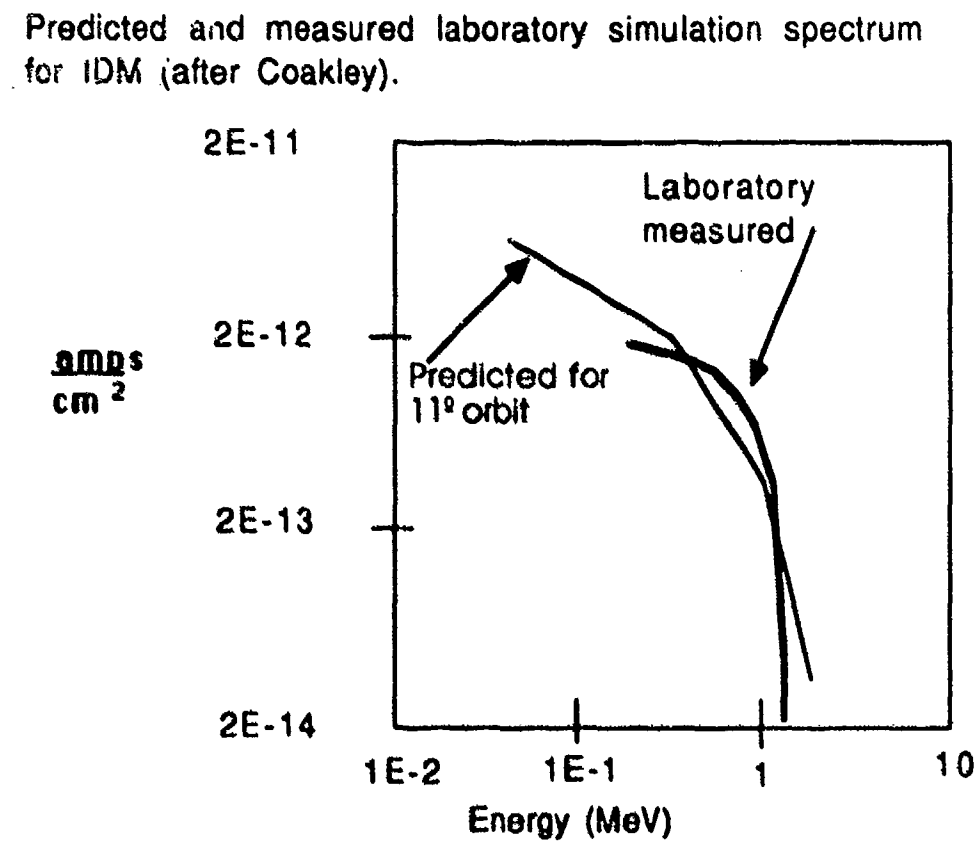

Figure 3-11 ID Space Electron Environments; Predicted and Measured Laboratory Simulation Spectrum for IDM (Coakley et al., 1985)

The environment near the earth is shown in Figure 3-12. A fission saturated environment is a good estimate of the upper bound of the penetrating electron fluence for internal charging calculations.

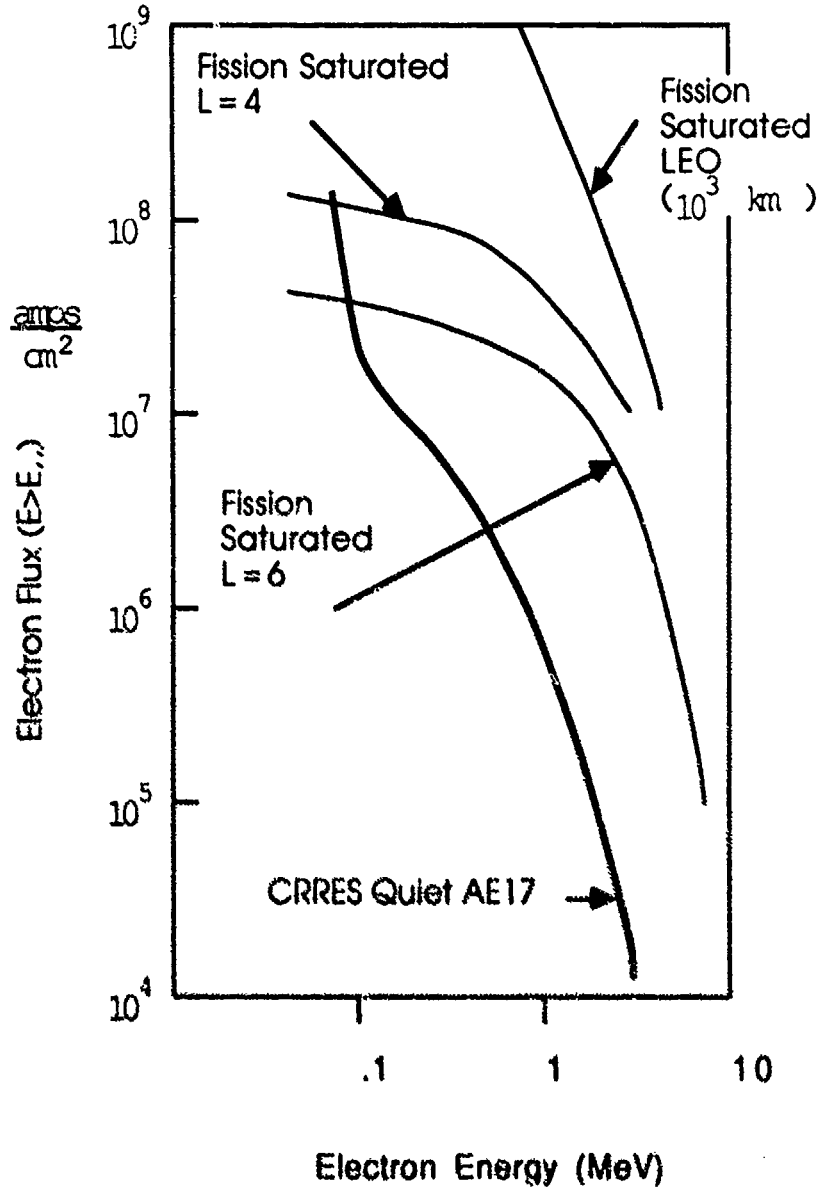

Space Electron Environments (after Coakley)

Figure 3-12. Space Electron Environments (Coakley, 1986a,b)

The time it takes for a satellite to have its internal dielectrics charged by a fluence of 5.5 x 10^{11} e/cm^2 can be estimated for different orbits around the earth as a function of the shielding between the dielectric and the surface of the spacecraft. In Table 3-4, these calculations are summarized for two orbits of interest, synchronous and half synchronous. Three shielding cases are also considered under each orbit condition, 20-, 100-, and 250-mil aluminum shielding. If the typical time required to absorb 5.5x10^{11} e/cm^2 is less than the time required to bleed off accumulated charge, internal discharge is a concern,. If the bleed-off time is short compared to the time to accumulate 5.5x10^{11} e/cm^2 then there is no concern for internal discharges.

Good insulating materials typically used in spacecraft have virgin dark conductivities on the order of 10^{-1} per ohm-centimeter. Electric fields may increase the conductivity by an order of magnitude or more. Radiation induced conductivity can increase the conductivity even higher, typically another order of magnitude. Surface conductivities are an order of magnitude higher than bulk conductivities. Ceramics in spacecraft configurations wi

store charge for an hour or so, polyimides and Teflon for several hours, and fiberglass composites (like FR4) for several days. Resistivities of some spacecraft materials are given in Table 3-1.

Table 3-4. Charging Time for ID Near Earth

20 mil shielding	Typical	Storm	Fission saturated
Low Earth orbit	2.0E+7	2.0E+5	1.0E+2
One-half synchronous	1.0E+6	7.0E+4	2.0E+3
Geosynchronous	1.0E+6	1.0E+5	7.0E+3

100 mil shielding	Typical	Storm	Fission saturated
Low Earth orbit	5.0E+8	5.0E+6	1.5E+3
One-half synchronous	2.0E+8	8.0E+5	4.0E+4
Geosynchronous	7.0E+8	3.0E+6	1.7E+5

250 mil shielding	Typical	Storm	Fission saturated
One-half synchronous	1.0E+10	1.0E+8	1.0E+6
Geosynchronous	1.0E+10	1.0E+8	1.5E+6

3.7. Summary

Internal discharges occur when charged particles, primarily electrons, penetrate into floating metal or chunks of dielectric within the spacecraft. Thus we are limited primarily to the radiation belts where there are significant quantities of high energy penetrating particles. We are primarily interested in electrons because of their long mean free paths at typical radiation belt energies in typical spacecraft structures.

Following geomagnetic storms the radiation belts can be emptied and refilled with high energy electrons. During active times like that the fluxes can reach high enough levels to cause internal discharges. The GOES 4 failure was correlated with a buildup of the high energy electron population. At Jupiter, the quiet time radiation belt is of sufficient intensity to cause ID's (see the POR in Chapter 5). Internal discharges are especially worrisome as they occur very near sensitive circuits and do not benefit from Faraday cage design. Care in removing floating metal, careful electronic design, and adequate shielding can eliminate or reduce internal discharges.

Chapter

4

SINGLE EVENT UPSETS

4.1. Single Event Upsets (SEUs) Due to Heavy Ions

Single event upsets are produced in an integrated circuit when a single particle produces a change in the digital logic. Usually these changes occur in memories, however an SEU can occur in any type of digital logic which requires information retention as part of its function. Memories especially those with a large number of bits visibly demonstrate SEUs. (A memory location is typically made up of more than one active device and connecting components.) This phenomenon became a concern in the late 1970's, although it had been predicted earlier. SEUs became a concern because advancing technology (both CMOS and bipolar) was evolving towards lower power and higher speed and consequently a smaller amount of charge involved in storing the information in the circuit. Lower power is desired for more efficient energy use. Higher speed is needed for more sophisticated programs and operational performance. Speed is a measure of the access time, the risetime, the delay time or some other parameter that measures how fast the device can perform its function. As technology has advanced, a bit in the device is represented by smaller and smaller amounts of charge. This is illustrated in Figure 4-1, which the Galileo Project used to explain to NASA management why this effect was not of concern for Voyager, but was for the Galileo spacecraft. The y-axis represents a quality factor for the device. It is the energy in picojoules involved in each operation of the device. The energy associated with each operation is the power required to operate the device divided by the time required to complete that operation. For commercial reasons, chip manufactures want chips which are faster, use a minimum of power, and hold as much information as possible. As one decreases along the y-axis, one is either increasing the speed of the device or decreasing the power (or both). The horizontal axis (x-axis) is the threshold for single event upsets for a device. The smaller this value the larger the sensitivity of the device to SEUs will be. Thus the space represented by this graph expresses two measures of "goodness" for the device: its commercial value, and its hardness to SEUs. The boxes labeled in the space are the actual performance of classes of chip technology in the recent past. Based on past performance the Galileo program hoped to estimate where the current developments in device technology were leading with respect to SEU hardness. Since commercial forces were pushing towards as low as possible a value for the energy per operation parameter it seemed clear that devices were going to become more and more sensitive to SEUs unless something was done to alert manufacturers to the danger, and to find ways to circumvent this aspect of smaller and faster devices.

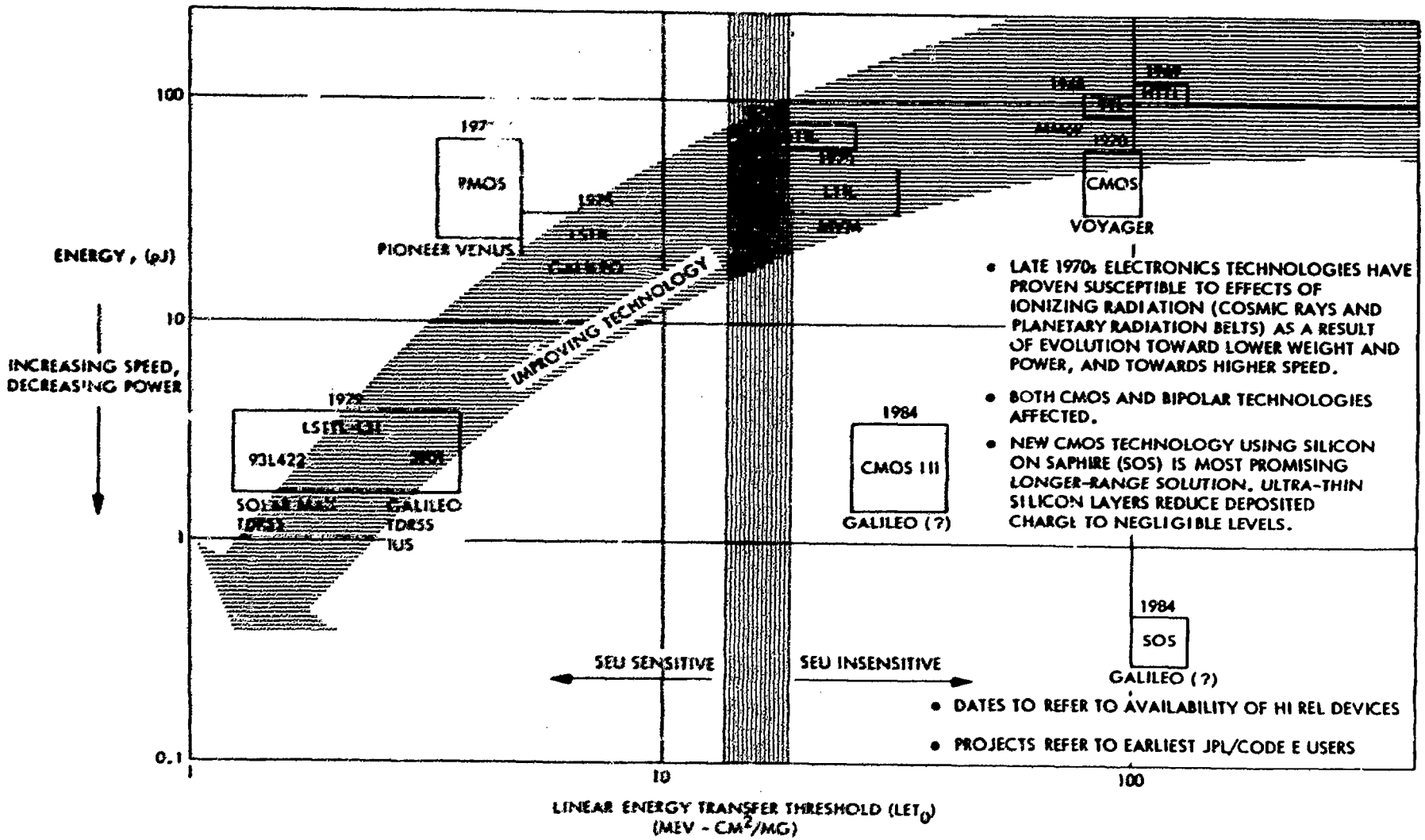

Figure 4-1 Progress in Technology Leads to SEU Concern. Power speed product versus threshold for SEU diagram.

4.1.1. Early History -- (Contributed by E. Petersen, NRL)

Wallmark and Marcus first predicted upsets in 1962. They looked at the evolution of microcircuits and pointed out that as the devices got smaller they would enter a region in which there would be upsets. This work was more or less ignored because it was too far ahead of its time. Then in 1975 Binder, Smith, and Holman published a paper in which they identified upsets in flip-flop circuits in the space environment. This work was again ignored. In 1978 Pickel and Blandford performed an analysis of the upset in dynamic circuits in space. In 1979 May and Woods showed that upset problems in newly developed 4k memory chips were caused by alpha particles, and a team from Aerospace, Hughes and JPL lead by Kolasinski used particle accelerators to test Binder et al.'s single event upset supposition. Since that time there have been many upset tests and predictions as well as upsets on satellites using sensitive parts. Upsets have occurred in all kinds of device types including TTL, CMOS, NMOS, and fast bipolar.

4.1.2. Basic Mechanism

Early experiments with SEU sensitive parts showed that to zero order, the occurrence of an SEU was a step function process with a threshold determined by the charge stored on the node in the IC representing the state of the bit. The simple argument goes that when an ionizing particle passes through the depletion region of the off node in the flip-flop circuit, the electron hole pairs left along the particle's path are separated by the electric field in the depletion region, resulting in a short current pulse at that node. If that pulse is large enough and lasts long enough, the feedback of the circuit will cause a change in the final state of the circuit. This is interpreted by the rest of the electronics as a "bit-flip" because that memory location now reads the opposite of what it did before the particle hit it. Typical flip-flop circuits are discussed later in this chapter. Figure 4-2 illustrates the passage of a heavy ion through the depletion region of the off node.

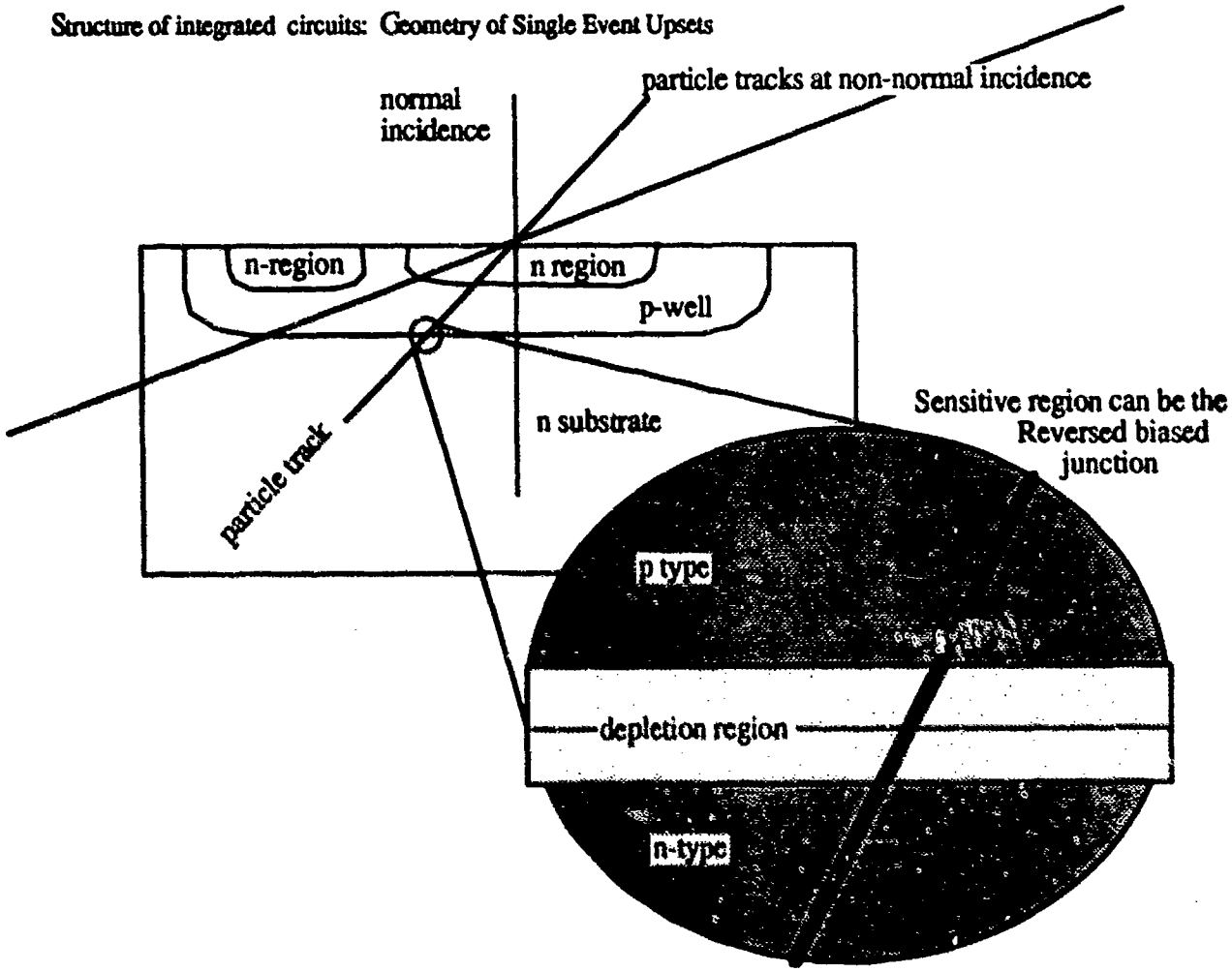

Figure 4-2. Single Event Upset Diagram

The basic SEU mechanism involves a single particle passing through the device leaving a track of electron hole pairs. When this track crosses a depletion region, the electric field in the depletion region separates the charges in the track so they do not recombine. This charge pulse can then be interpreted by the circuit as a change in state of the bit in memory represented by that circuit. The volume the particle must hit to cause an upset (the sensitive volume) is determined by the chip feature size. This determines the cross section or the probability of SEU. Figure 4-3 shows this cross section as the LET of the ionizing particle is varied. The linear energy transfer (LET) of the particle is a measure of its ability to ionize the material along its path.

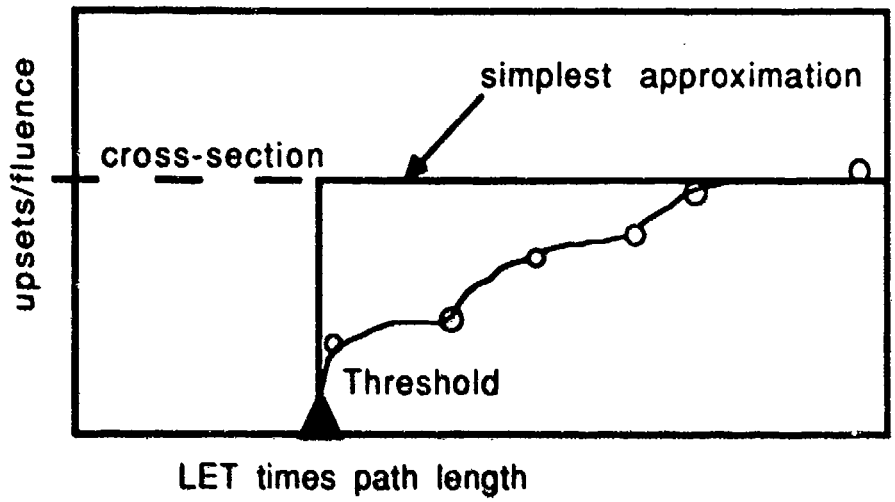

Figure 4-3. Classical Experiment Cross-Section. The two key parameters for determining the SEU rate are the threshold and the cross-section at large LET times path length. The actual cross-section as a function of LET times path length will give a more realistic, lower value of the SEU rate.

4.1.3. Linear Energy Transfer (LET)

The likelihood of an SEU occurring in a particular situation is dependent both upon the charge deposited by the incident particle and the state and characteristics of the electronic device. Let us first consider the charge depositing ability of the incident particle.

The rate of energy loss of a particle is ordinarily expressed in terms of its stopping power, dE/dx. dE is the energy lost to the incident particle in traveling a distance dx.

$$\text{LET} = \frac{dE}{dx} \qquad \text{Typical units are MeV/micron} \qquad (4\text{-}1)$$

Many times this quantity is divided by the density of the target material, so that the stopping power or linear energy transfer (LET) becomes

$$\text{LET} = \frac{1}{\rho}\frac{dE}{dx} \qquad \text{Typical units are MeV-cm}^2\text{/mg.} \qquad (4\text{-}2)$$

Figure 4-4 illustrates the typical behavior of various ions in silicon.

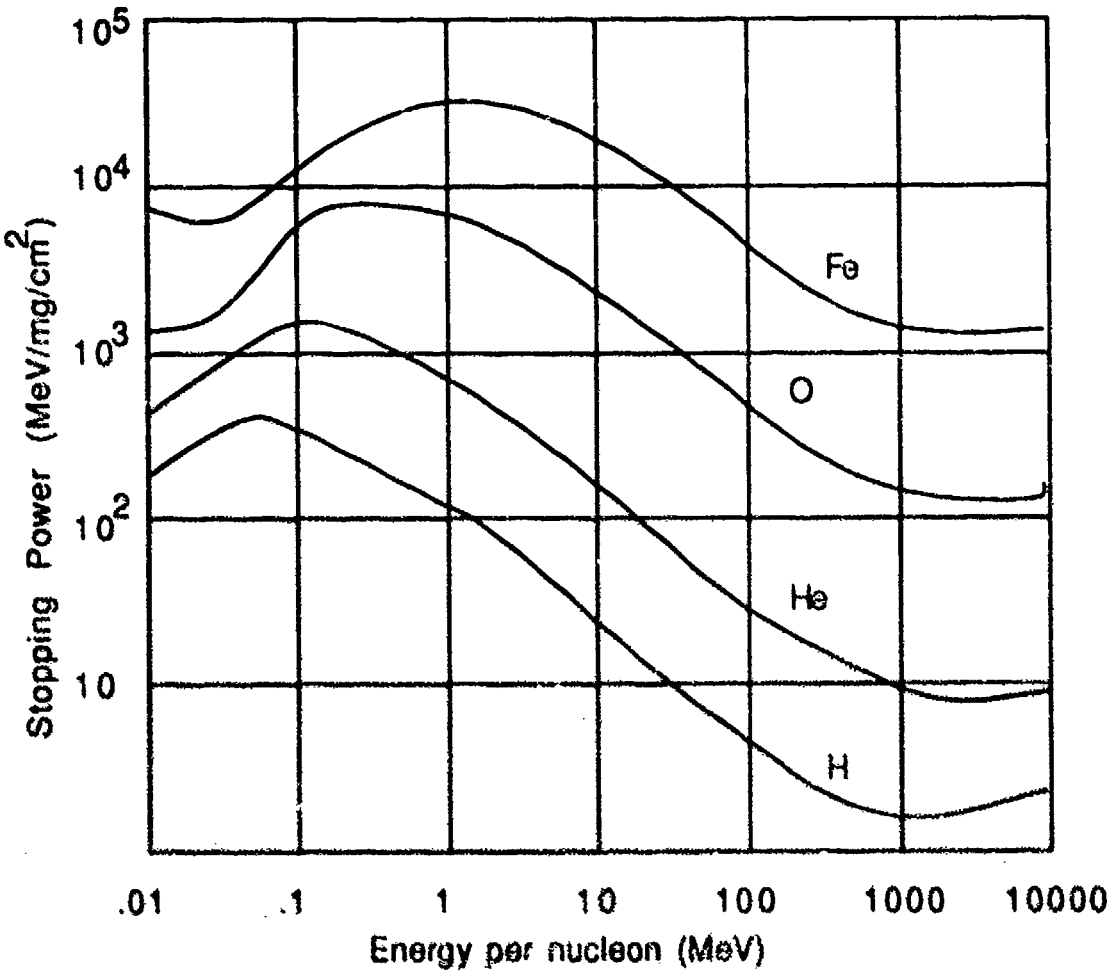

Figure 4-4. Stopping Power in Silicon

For SEU investigations the important parameter is the charge density per unit pathlength. This is related to the LET or stopping power by a factor which expresses the average energy required in a given material to produce one electron-hole pair. For silicon it takes 3.6 eV/electron-hole pair. For GaAs it takes 4.8 eV/electron-hole pair. Supposing that half of the charge is separated and contributes to the current pulse, then the factor 1.6×10^{-19} coulombs per 3.6 eV converts the energy deposited in silicon to the charge deposited in silicon.

4.1.4. Charge Required for SEU

Upsets are usually produced when the ionization produced in the chip results in a net charge which the flip-flop circuit interprets as a command to change state. On the average it takes 3.6 eV to produce an electron-hole pair in silicon. Producing electron-hole pairs provides a conductive plasma, but does not produce any net charge on a node, unless electric fields are present. When an electric field is present a significant portion of the charge available along the ionized track can be separated and collected. Silicon with a density of 2.329 g/cm^2 requires 3.6 eV/pair; GaAs with a density of 5.316 g/cm^2 requires 4.8 eV/pair.

Typical semiconductor devices (1980's) store information using a total charge in the range of 0.01 picocoulomb to 1.0 picocoulomb. In terms of late 1970s/early 1980s technology, feature sizes are on the order of one micron, and depletion depths -- the length over which electric fields exist -- are also on the order of a micron. The charges deposited in one micron of silicon for various particles with energy between 0.1 and 10^3 MeV/nucleon (typical cosmic ray energies) are shown in Figure 4-5.

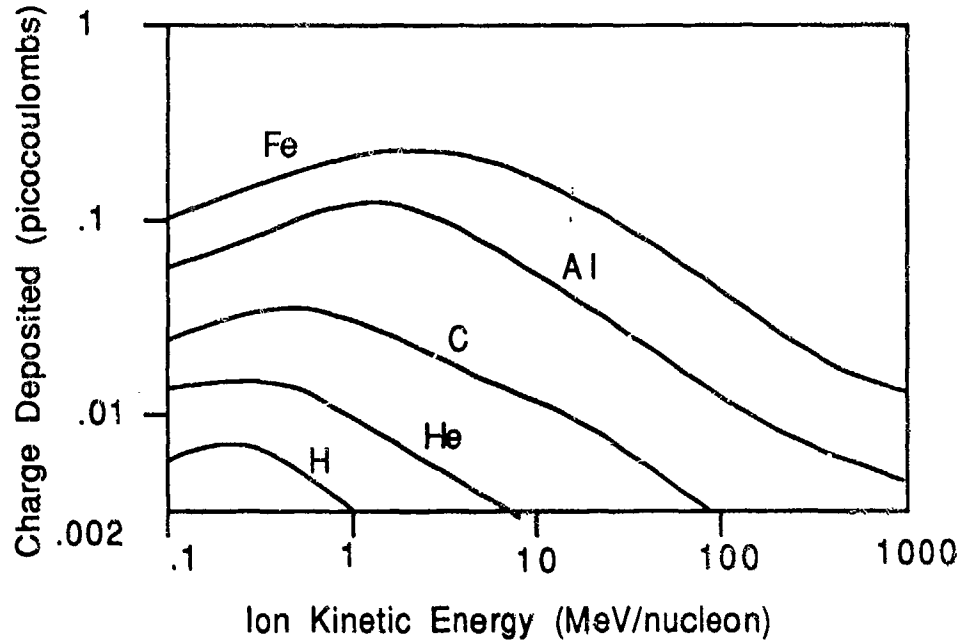

Figure 4-5. Charge Deposited in One Micron

Assuming a one micron depletion region, figure 4-5 shows all ions except hydrogen can produce more than .01 picocoulombs in the collection region and hence are of concern. Fortunately, hydrogen is not able to deliver such a charge directly. If hydrogen were able to deposit 0.01 coulomb/micron, the upset rate of those parts on space systems would increase by 10^4 to 10^5 since there are many more protons than heavy ions in cosmic rays. In a later section we will discuss the effect of non-normal incidence which has the effect of increasing the distance over which an ion can deposit charge. Funnelling (discussed below) and charge diffusion can also increase the distance over which a node can collect charge from an ion track.

As mentioned earlier charge separation takes place in the device in regions where there is an electric field present to separate the electron-hole pairs generated along the particle's track. Electric fields in semiconductors are discussed in solid state physics texts and circuit design texts (see for example, Messenger and Ash, 1986, Mead and Conway, 1980, or Ashcroft and Mermin, 1976) In Silicon technology devices are made by doping the silicon semiconductor with ions which either supply electrons or holes. Figure 4-6 is a cartoon of the junction area which is essentially free of free electrons or free holes. Electric fields generally exist only in these depletion regions. Figures 4-7 and 4-8 show the effect of "forward biasing" and "reverse biasing" on the depletion region. The sensitiv region in many devices is the reversed biased region, where the depletion thickness is large and there are large electr fields.

P-type Silicon

positive charges (holes) are majority carriers

doped with Acceptors (group III)

e.g. Boron

Negative ions are fixed in the silison lattice, holes are free to flow in the Silicon lattice

Conduction band

Fermi level

Valence Band

n- type Silicon

negative charges (electrons) are the majority carriers

doped with donors (Group V)

e.g. phosphorus, Arsenic

Positive ions become fixed in the silicon lattice, electrons are free to flow in the conduction band

Conduction band

Fermi level

Valence Band

When a junction is formed by bringing two differently doped silicons together (or doping different regions differently) the charge density in the region between the p-type and the n-type region becomes a depletion region, neither carrier type is majority. The charges rearrange themselves so there is an electric field in that region. Since there is no external electric field, the Fermi level does not change across the junction.

$$\frac{dE_f}{dx} = eE = 0$$

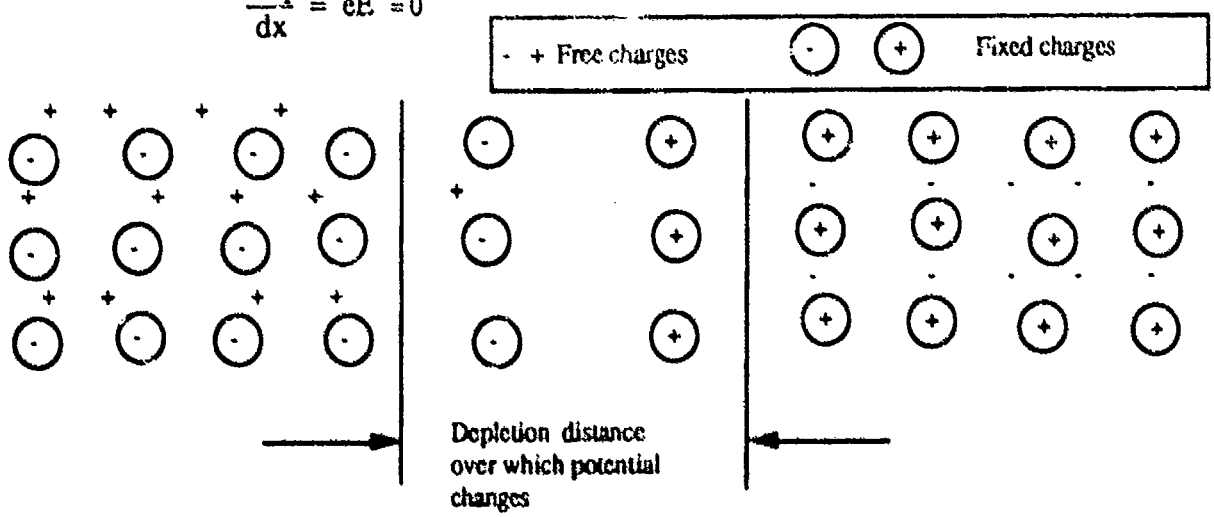

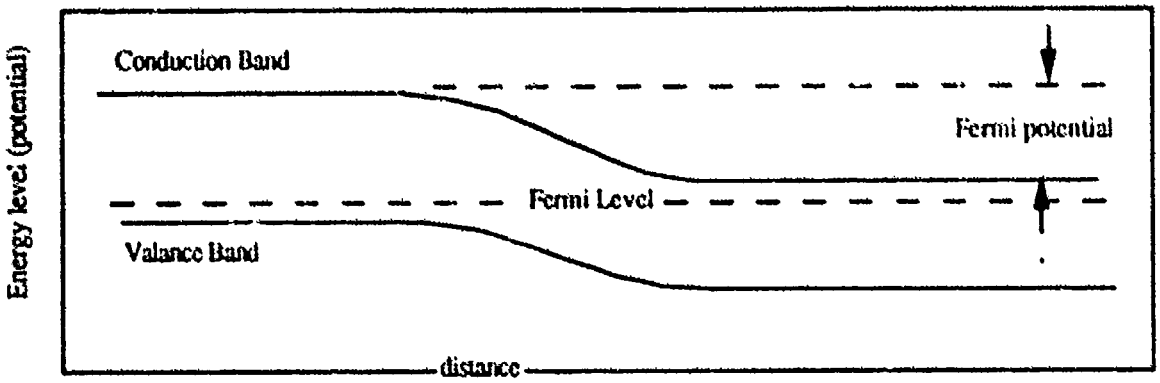

Figure 4-6. P-N Junction

FORWARD Bias: Positive bias on p type semiconductor, reduces the depletion region by forcing majority carriers tow the boundary, allows current flow across junction easily.

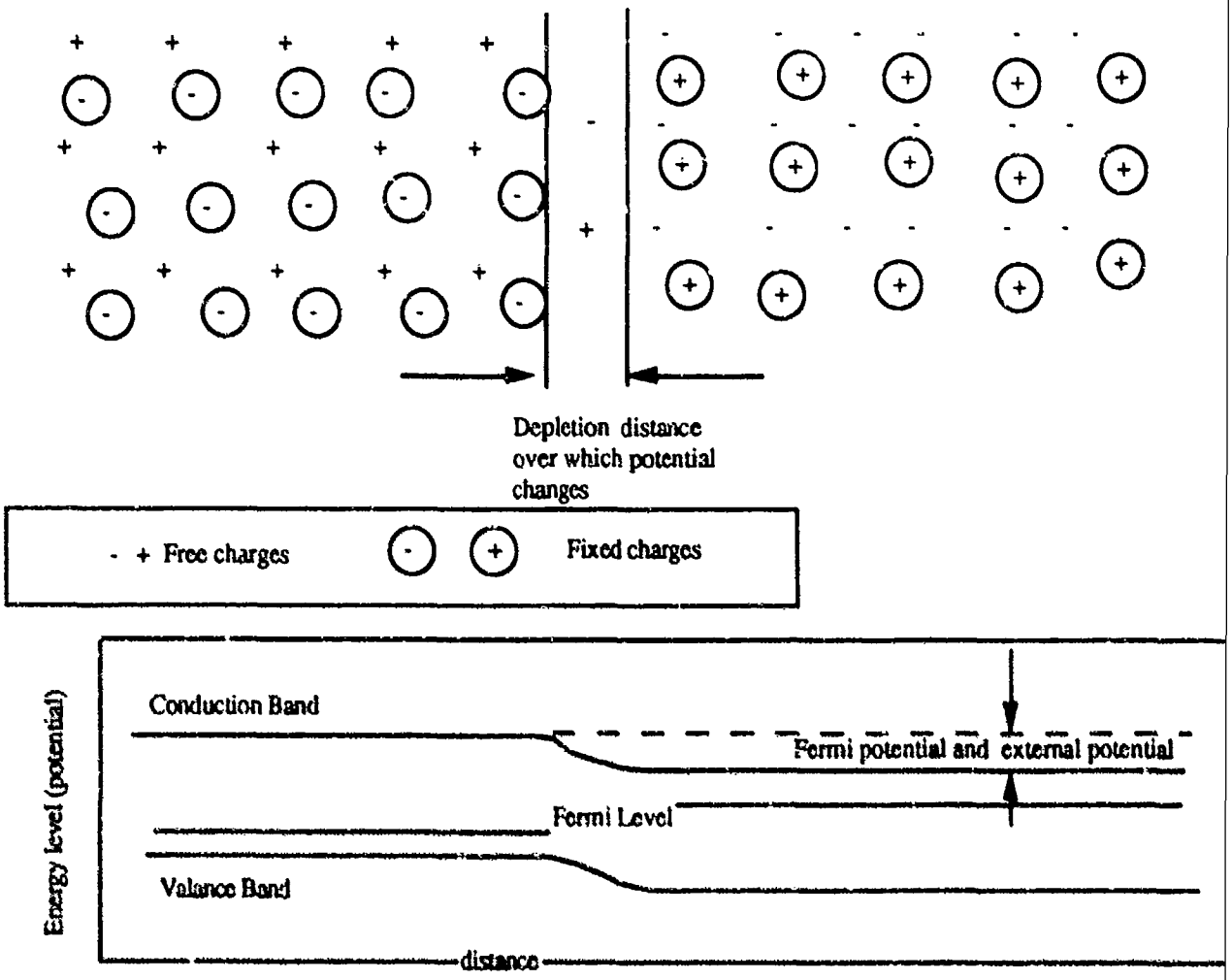

Figure 4-7. Forward Biased Junction

REVERSE Bias: negative bias on p type semiconductor, increases the depletion region by forcing majority carriers away from the boundary, tends to restrict current flow across junction.

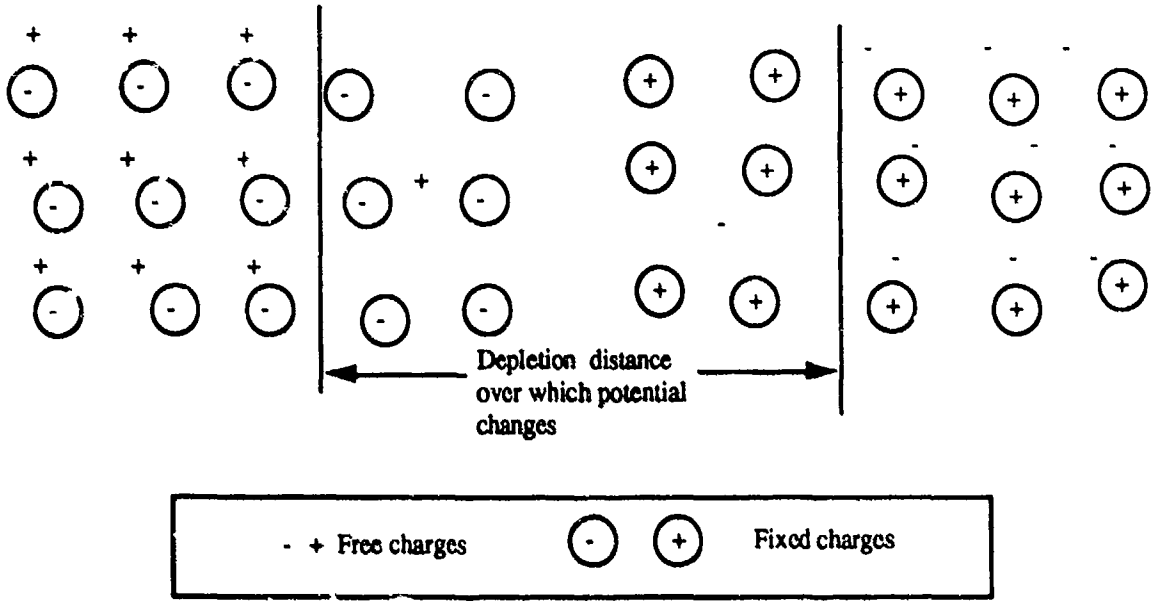

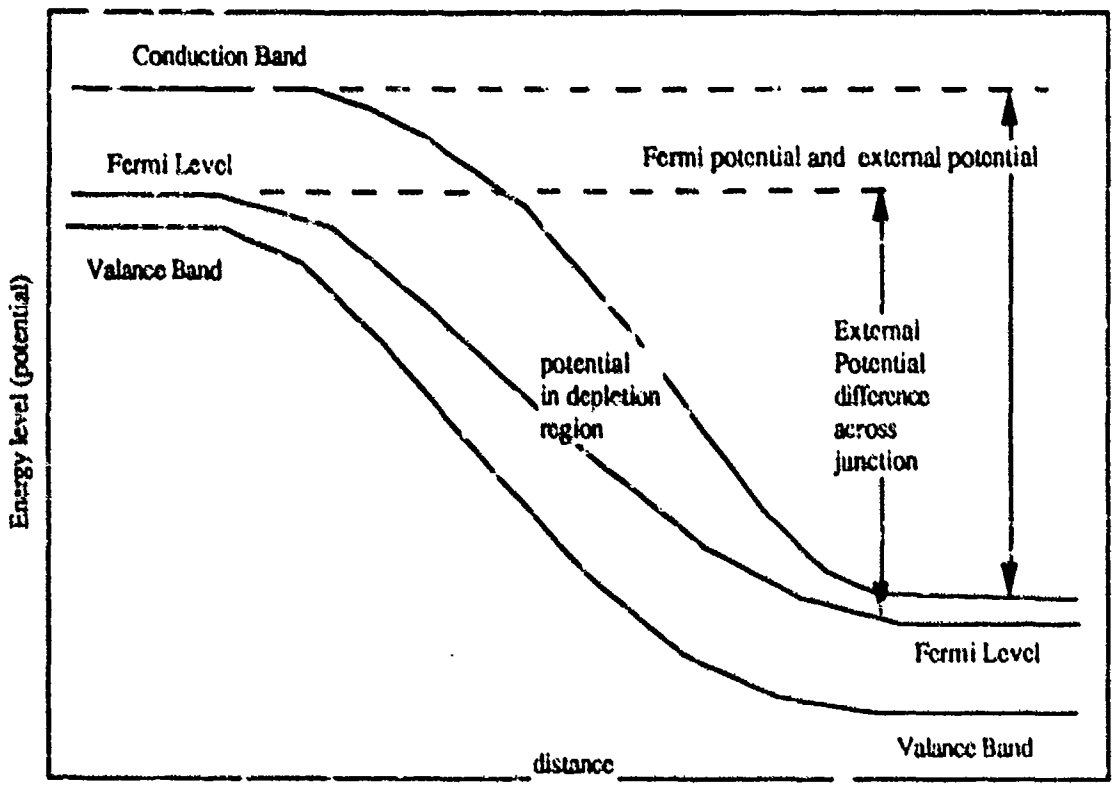

Figure 4-8. Reverse Biased Junction

4.1.5. LET and Range

The LET of a particle is dependent on the target material, in this case silicon, and the energy of the incident particle. As the energy of the incident particle increases, the deposited energy increases to a broad peak at about 1 MeV/nucleon -- called the Bragg peak. Beyond that, the ability of the particle to deposit energy decreases to a very broad minimum near the point at which particles become relativistic. At very high relativistic energies there is a gentle rising in the stopping power with energy.

The range, R, of a particle is defined as the distance a particle will travel before stopping in a material.

$$\frac{dE}{dx} = \frac{dE}{dx} \quad ; \quad \text{or} \qquad dx = \frac{dE}{(dE/dx)}$$

therefore

$$\int_0^R dx = R = \int_E^0 \frac{dE}{(dE/dx)} \qquad (4\text{-}3)$$

where R is the range and E is the initial energy of the particle.

Since dE/dx is given as a function of energy one may integrate the stopping power curve to obtain the range of a particle in a material. Northcliffe and Schilling (1970), Ziegler (1980), Litmark and Ziegler (1980) have produced compilations of stopping powers and ranges for a number of ions and targets. Janni (1982) has listed stopping powers and ranges for protons. The stopping power and range for protons in Silicon from Janni are summarized in table 4-8 at the end of this chapter. Using the energy range relation, the effects of shields or overlayers can easily be taken into account. Given an initial particle of specified energy, the total range indicates how far that particle will penetrate the target material. If the target material is thicker than the range, the incident will not penetrate the target. If the material is thinner, the incident particle will degrade in energy by an amount such that its range after exiting the material plus the distance it traveled in the thin target material is the range it had at its original energy. If the stopping power were constant with energy the new energy would be just the fraction of the total range left to the incident particle, but the stopping power is a function of energy, and must be taken into account.

It is important to consider the effects of shielding and overlayers in SEU calculations. Degrading a particle's energy will actually increase its LET if the initial particle has an energy above the Bragg peak. Section 4.2.1.2.2 emphasizes the importance of including shielding in SEU calculations.

4.1.6. Funnelling

Without an electric field or differences in electron and hole mobility to separate the charge along an ion's track, there would be no net charge at a circuit node. A process called "funnelling" can add to the total charge collected at a node in the circuit. Funnelling refers to the extension of the electric field which is usually confined to the depletion layer into the silicon beyond the depletion region. This is illustrated in figure 4-9. When this happens the electron-hole pairs which normally recombine or very slowly diffuse into the depletion region are rapidly separated by the electric field and add to the total charge collected after the ion passes through the chip.

Although the total charge collected when a funnel plays a role may be several times that expected from the path in the depletion region alone, the pulse still rises and falls in fractions of a nanosecond as it did when no funnel formed. Recent work has shown additional complications. For very heavy ionizing particles leaving a dense track, recombination becomes important, decreasing the collected charge. For some structures that have very high electric fields, charge multiplication takes place, increasing the collected charge. For other devices the charge collected by diffusion is important.

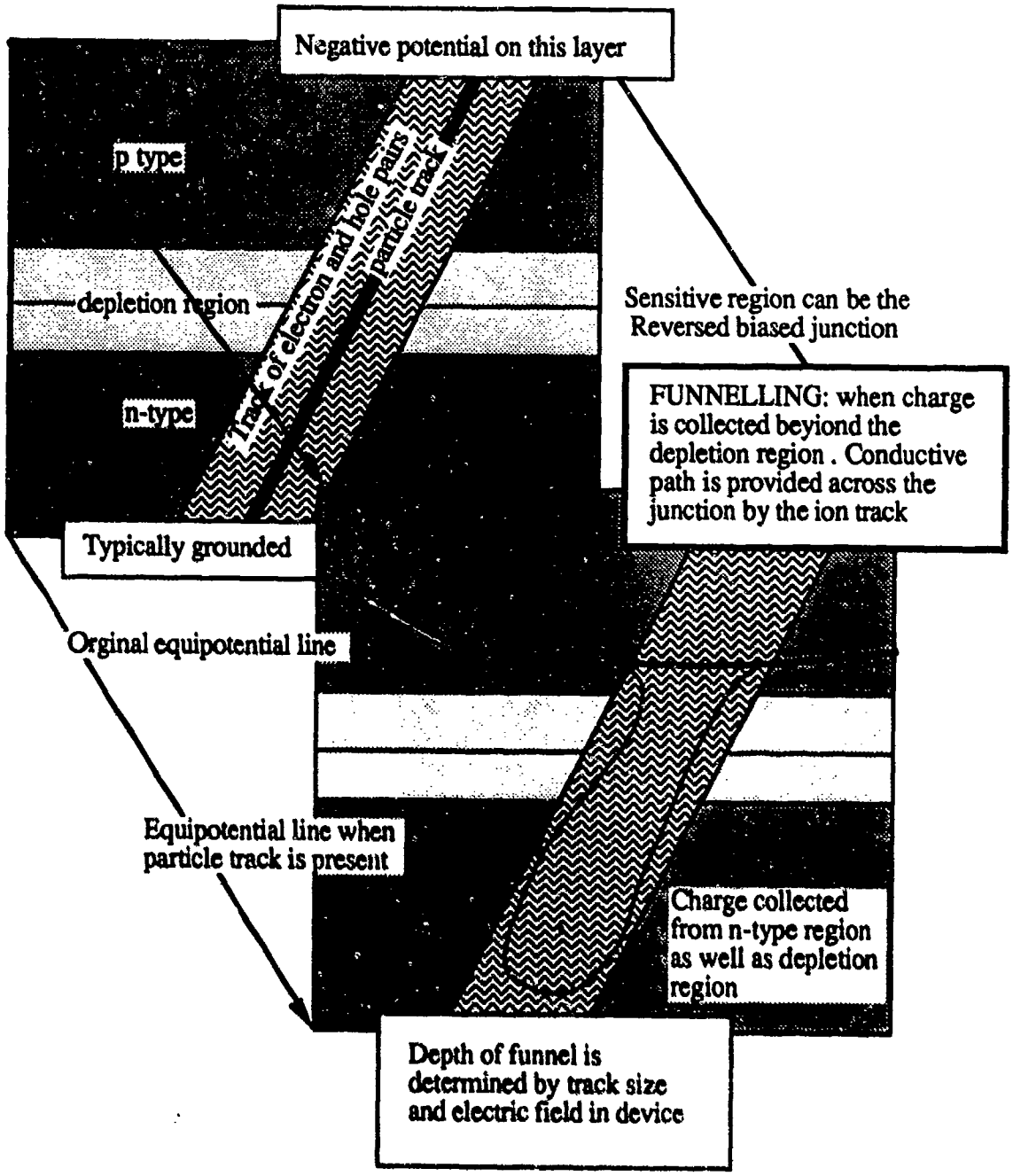

figure 4-9 Charged Track Funnel Formation

4.1.7. Current Pulse

The current injected at a node in the flip-flop circuit is the sum of the prompt charge -- that is the charge deposited and separated in the depletion region, the charge "sweep up" in the funnel, and the charge which diffuses relatively slowly from the remainder of the ions' path into the depletion region. The prompt and funnelled charges are separated and collected very quickly, on the order of a fraction of a nanosecond. The delayed diffusion component takes from one to hundreds of nanoseconds to finally be collected. The total cosmic ray pulse injected at the node of the circuit is then a sharply rising pulse with a rapid decay in a nanosecond or less, followed by a long, slow, small

current representing the collection of charge which is diffusing from the ion track to the node. A realistic SEU current pulse has a sharp rise and fairly fast fall time with most of the charge collected in less than a nanosecond (see Figure 4-10). So long as the pulse width is considerably less than the circuit response time, the critical charge is independent of the shape of the pulse. For example, Pickel frequently uses a trapezoidal pulse with a rise time of .0 ns and a full width at half maximum of 0.09 ns (Pickel, 1983).

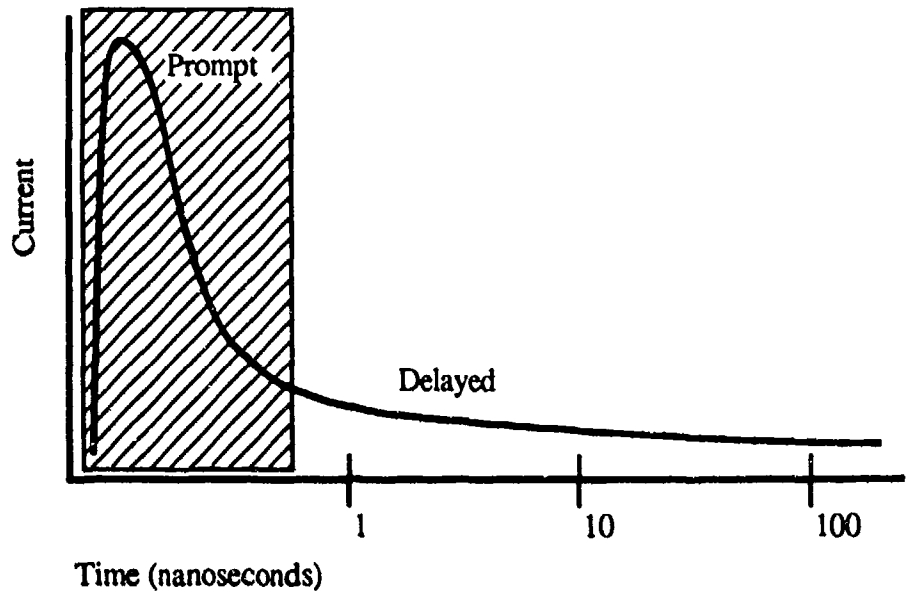

Figure 4-10. Ion Current Pulse

4.1.8. Advancing Technology

One of the important parameters in determining the speed and power used by a device on a chip is the feature size. The smaller the feature size the faster the processing speed and the smaller the power required to maintain the memory. Intuitively one would also guess the smaller the threshold for SEUs. The charge stored on a node should behave like the capacitance of the node =A/d where A is the area of the device. For constant d, the dept of the depletion region, the critical charge ought to go as the feature size to the second power.

Figure 4-11 shows the critical charge plotted as a function of a feature size for a number of different technologies. The critical charge essentially follows the simple scaling rule $Q \sim 1/L^2$ over a wide range of device technologies and feature sizes, L. This underlies the trends in technologies discussed earlier at the beginning of thi chapter.

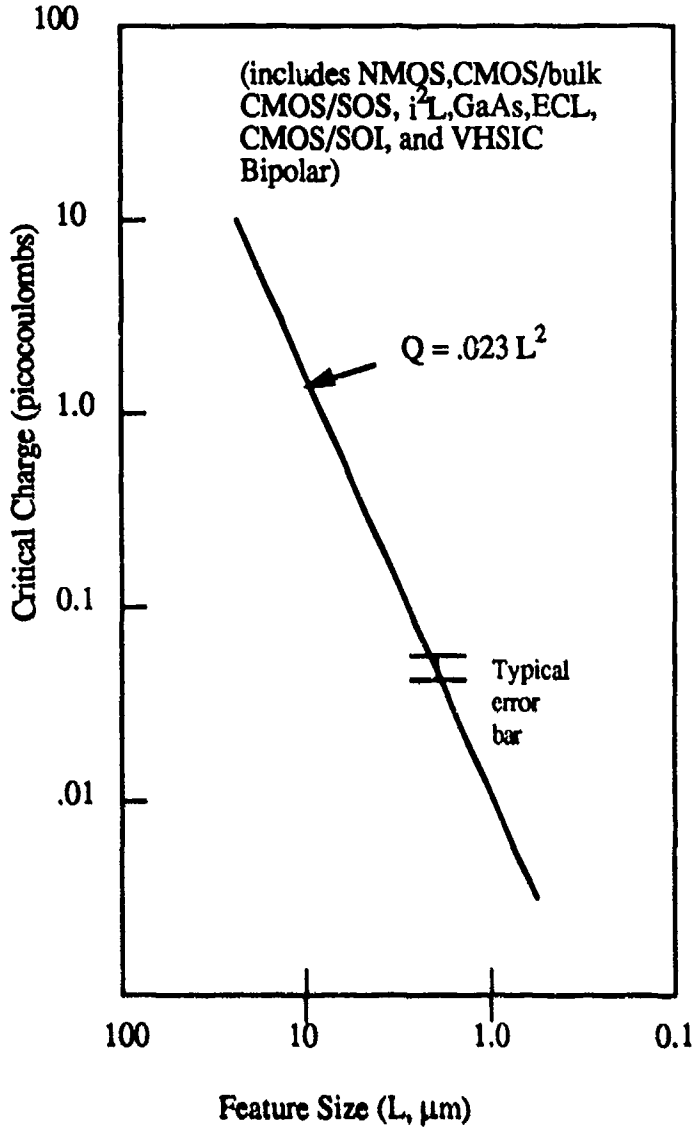

Figure 4-11. Sensitivity Versus Feature Size (Petersen, private communication, 1987)

4.1.9. Upset Mechanisms -- Circuit Analysis

A detailed consideration of the circuitry involved is always needed in evaluating the response of a circuit to an ionizing particle. Simple experimental measurements are clouded by the existence of more than one sensitive region, memory cells which have a sensitivity that depends on the state of the cell, complex shapes of the sensitive volume, funnelling, and the inherent shielding of the chip when testing at non-normal angles of incidence.

Memory devices can be broadly categorized as: (1) charge storage devices, (2) voltage storage devices, or (3) current steering devices. Devices which store charge for their memory, e.g., dynamic RAMs and charge coupled devices, determine their memory state by the presence or absence of charge. Voltage storage devices e.g., static RAMs or CMOS RAMs, determine their memory state by the voltage which is present at certain nodes in a flip-flop circuit. Bipolar devices determine their memory state by steering currents such that certain transistors are in an "on" state. Common bipolar technologies for memory and processor applications include transistor-transistor logic, TTL, and integrated injection logic, I^2L. All of these devices have some susceptibility to single event upsets (Pickel, 1983). Nichols (1987) ranks current technologies as follows:

least susceptible	CMOS/SOS
	CMOS
	standard bipolar
	Low power Schottky bipolar
most susceptible	NMOS DRAMs

He also notes that PMOS is susceptible to SEUs. It is important to remember that single event upsets can occur in any type of digital logic which involves state retention.

4.1.9.1. Charge Storage and Dynamic RAM

In a dynamic RAM (figure 4-12), the bit is stored as charge on the gate capacitance of the "storage transistor," Q_2. The read, Q_1, and write, Q_3, transistors are used to read, write and refresh the charge on the node representing the bit. Normally the decay time for charge to leak off the gate capacitance is on the order of 2 milliseconds. If charge left along an ion track neutralizes enough of the charge on the storage capacitor, the refresh circuit will replace the one with a zero and a bit error will have occurred. In this case the ion does not need to interact solely with the depletion region and charges diffusing into the gate region may have enough time to influence the response of the circuit.

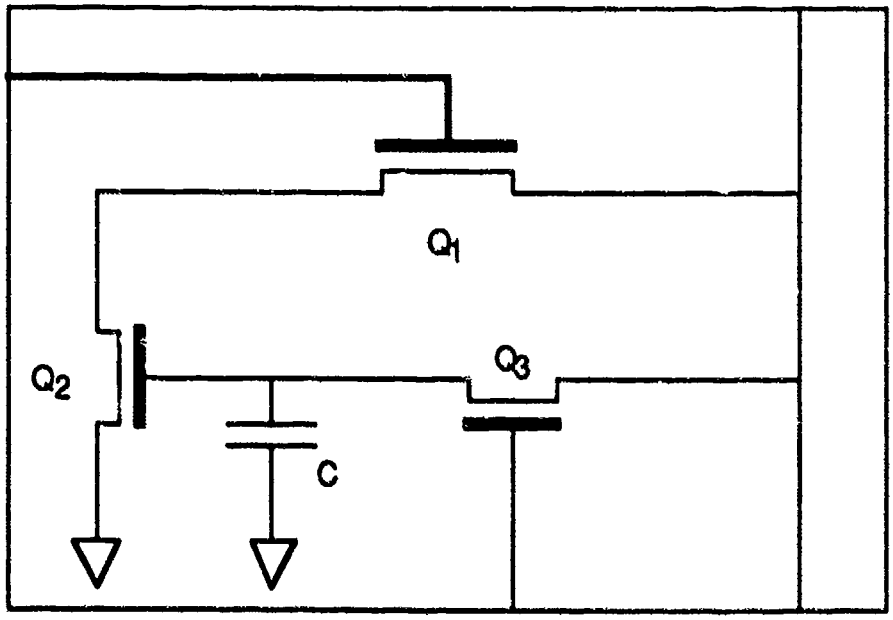

Figure 4-12. A Dynamic RAM Storage Cell, in Particular, an N-Channel 3-Transistor Cell Composed of a Storage Transistor, Q_1, and Write and Read Transistors. Positive charge is stored on the gate capacitance of the storage transistor, C. Electrons collected from ionization in the junction of the write transistor, Q_3, are a loss of charge from the storage node. When the charge loss exceeds some critical charge, a bit error occurs. The refresh circuitry reads the stored charge to refresh it, but refreshes it to the wrong state.

4.1.9.2. Voltage Storage

The storage mechanism for CMOS memory is the voltage state of the two cross-coupled inverters. This is illustrated in figure 4-13. The sensitive junctions are the drains of the off transistors. In this case there are two sensitive junctions, the drain at P1 and the drain at N2. Ionization at these junctions will put a voltage disturbance on the circuit node and can cause the other inverter to change state initiating the "bit flip" and single event upset.

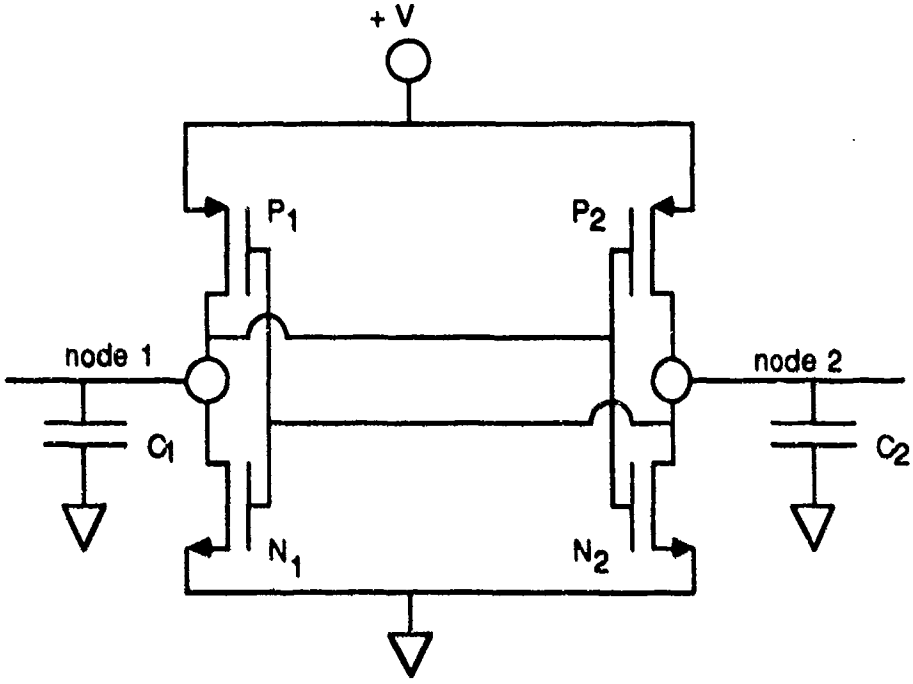

Figure 4-13. CMOS Memory Cell Circuit. P_1 and N_2 are on. Sensitive junctions are the off junctions

In this case there is a race condition which determines the final state. If there has been enough charge deposited by the ion track, the final state of the memory cell will be the opposite of what it was originally. Figures 4-14 and 4-15 show SPICE calculations by C. Chu at Caltech of the voltage on the node representing the bit in two cases, first where there was not enough charge to cause a bit flip (figure 4-14), and second when there was (figure 4-15). In both cases the voltage on the node goes high, but only in the second case is the feedback strong enough to drive the node to the opposite state. The passage of a heavy ion through the device is modeled in SPICE putting a pulse on the node . The pulse height and pulse width are varied to produce different total charges on the node. When the charge is rapidly placed on the node the circuit changes state. A pulse with a longer pulse but the same total charge width might not cause a change of state.

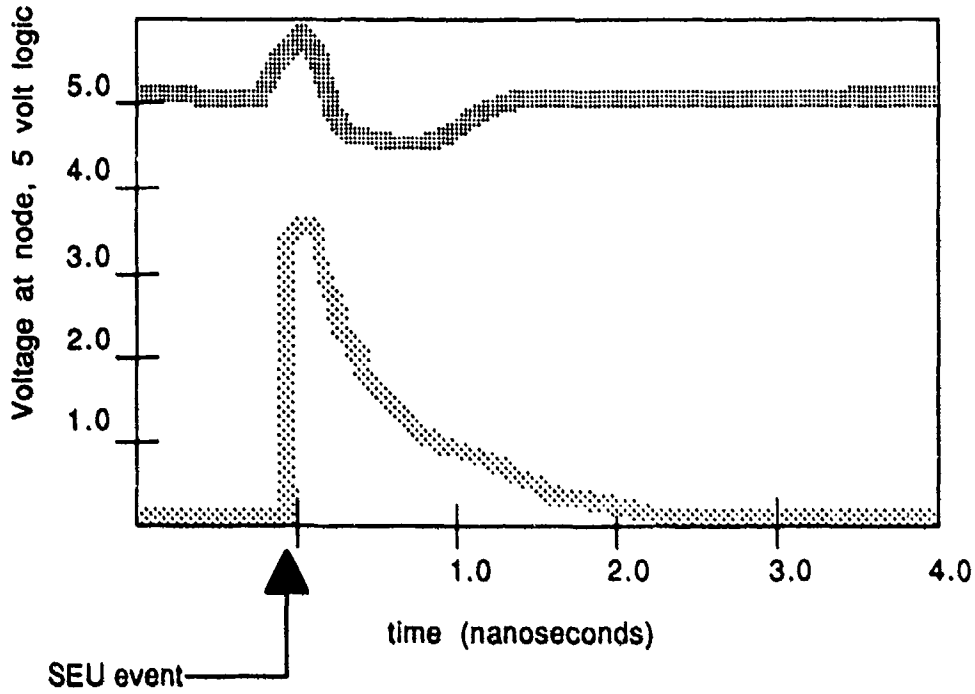

Figure 4-14. SPICE Simulation of non-SEU

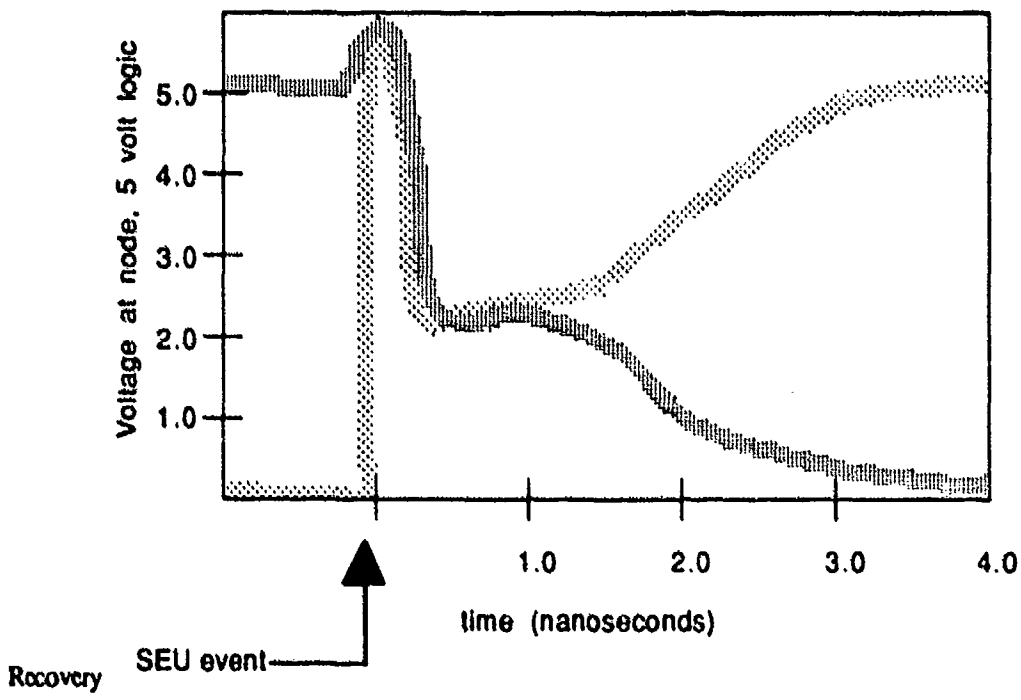

Figure 4-15. SPICE Simulation of SEU

4.1.9.3. Current Steering and I^2L

The I^2L gate consists of a vertical npn transistor and a lateral pnp transistor which are merged such that the collector of the lateral transistor and the base of the vertical transistor are a common region. The mechanism for an error in these devices, bipolar I^2L, is ionization within an "off" p-n junction which results in a current pulse being applied to a circuit node. If the voltage on that node becomes sufficient to cause a change in the state transistor, then an "off" transistor can go "on" resulting in a signal being applied to a feedback path and a flip-flop changing state. Figure 4-16 shows the cosmic ray current source and lumped node capacitance and resistance.

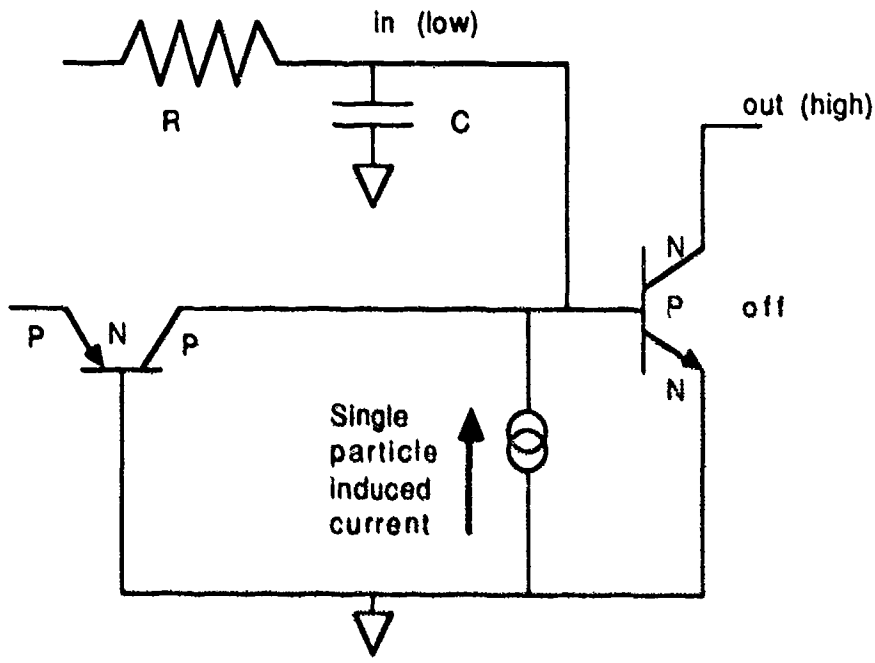

Figure 4-16. I^2L Gate Circuit (Pickel, 1983)

4.2 Calculation of SEU Rate

Once the circuit sensitivity is known the upset rate is calculated by evaluating an integral that combines the target size or cross section, the path length distribution through the charge collecting region, the distribution of ions as a function of LET and spatial parameters, and the critical charge of the device. A general formulation of the problem might be represented as,

$$\text{seu rate} = \sum_{z=1}^{z=92} \int_0^{2p} d\phi \int_0^{p} d\theta \int_{E_1}^{E_2} dE \; f_z(E,\theta,\phi)\sigma(E,\theta,\phi) \tag{4-4}$$

Here the summation of over all ion species, and the integration is over all angles and all energies (E_1,E_2). The number of ions of atomic number z, energy E, and moving in the direction indicated by the angles per unit energy.is.

$$f_z(E,\theta,\phi)$$

The probability that a particle in the given direction and with the energy E will cause an upset.is

$$\sigma(E,\theta,\phi)$$

Experiments and experience in space have shown that the ability of the particle to deposit charge, rather than its energy is the most important parameter in determining the SEU rate. Assuming that the cross section depends only on the LET of the particle, and nothing else, we write the cross section as a function of LET rather than energy, and remove if from the energy integral, and the summation over ion species. This means that the integral representation of the SEU rate can be simplified.

$$\text{seu rate} = \int_0^{2\pi} d\phi \int_0^{\pi} d\theta\, \sigma(\text{let},\theta,\phi) \sum_{z=1}^{z=92} \int_{E_1}^{E_2} dE\ f_z(E,\theta,\phi) \tag{4-5}$$

Now the limits on the energy integral are the range of energies for each ion over which the LET is equal to or greater than the LET of concern (let). With this simplification the SEU rate integration can be broken up into independent parts, representing the environment and the device characteristics. This simplifies the calculations considerably. Some work (Criswell, et al., 1987), however, indicates that this full separation is not accurate, and that there is a dependence of cross section on ion species. In the following discussion we will assume that the cross section does not depend on the ion species, and that the notion of a sensitive volume described below embodies the physics of SEU formation. Improvements to this model may be forced on us as both the technology of integrated circuits and our test methods and understanding evolves.

The second part of the integral

$$\sum_{z=1}^{z=92} \int_{E_1}^{E_2} dE\ f_z(E,\theta,\phi)$$

focuses on the environment. The energy range for each ion species is that portion of the Bragg peak such that the LET is greater than the given LET. This is shown in Figure 4-17. E_1 and E_2 are the energies between which the LET is greater than the L_0 under consideration.

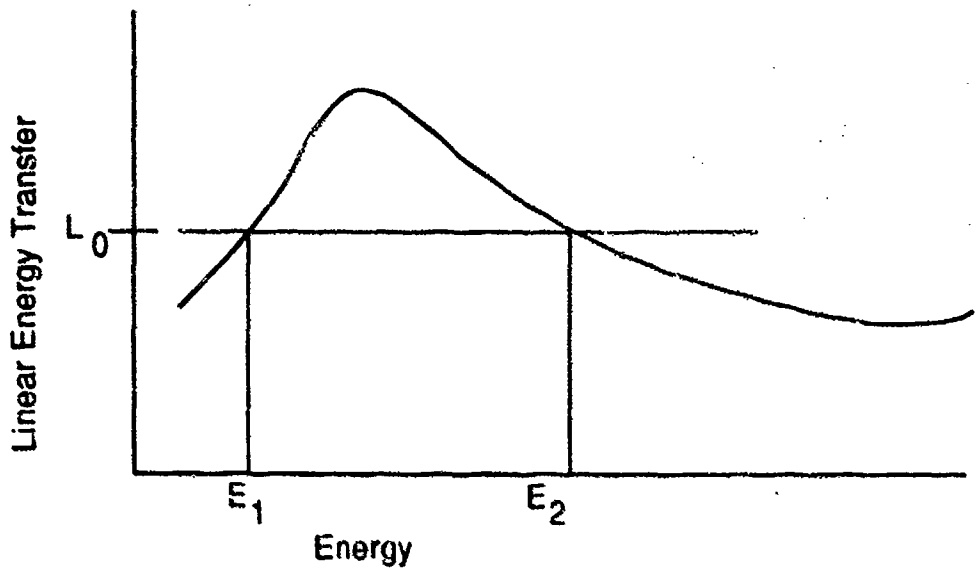

Figure 4-17. LET Distribution

This separation allows a derivation of the final rate as a simple product of the Heinrich flux and the cross section .

$$\text{seu rate} = \int_0^{2\pi} d\phi \int_0^{\pi} d\theta\, \sigma(L,\theta,\phi)\ \Phi(L) \qquad (4\text{-}6)$$

where we have let L represent the LET. In general the Heinrich flux, Φ, is calculated by summing over all energies and ion species.

$$\Phi(L) = \text{flux}(\text{let}>L_0) = \sum_{z=1}^{z=92} \int_{E_1}^{E_2} dE\ f_z(E,\theta,\phi) \qquad (4\text{-}7)$$

The energy limits of the integral are taken so that the LET is above the threshold.

The simplification which flows from understanding the behavior of the cross section is even more significant. Experiments have suggested that the cross section is in some cases a step function of LET, that is that below a certain LET value no upsets occur and that above that LET SEUs do occur. Further, as the angle of the incoming flux is varied there is a very simple relation between the cross section, LET threshold and angle. It is found for some parts at least that if the incident LET is divided by the cosine of the angle of the beam with respect to the surface and the cross section is foreshortened by a factor of the cosine of the angle, the result is the same as if you had normal incident particles with the effective LET,

$$\frac{L_{th}}{\cos\theta} = L_{eff} \qquad (4\text{-}8)$$

This allows further simplifications in calculating an upset rate. Since the angular dependence is now included in the effective LET and a simple cosine factor.

Thus the rate relations can be summarized as:

$$\text{rate} \rightarrow \int \Phi(L)\,\sigma(L_{th})\,d\Omega$$

$$L = \frac{L_{th}}{\cos\theta}$$

$$\sigma = \sigma_0 \cos\theta$$

and

$$\sigma_0 = m\,L + b$$

$$d\Omega = -d\varphi\; d\cos\theta \qquad (4\text{-}9)$$

In particular, a series of cross section and LET pairs from experimental measurements can be used to describe the cross section. Using the above equations and expressing $d\cos\theta$ in therms of dL

$$d\cos\theta = -\frac{L_{th}}{L^2}\,dL \qquad (4\text{-}10)$$

The rate equation takes the following form

$$\text{rate} \rightarrow \int_{L_1}^{L_2} \Phi(L)\,\sigma(L_{th})\,d\Omega = \frac{m\Phi(L)}{L} + \frac{b\,\Phi(L)}{2\,L^2} \qquad (4\text{-}11)$$

where the integral is carried out for each interval and evaluated at the end points of the interval in the usual manner.

This does not account for particles which hit the edge of the sensitive region. For thin sensitive regions one sometimes assumes that the cross section is proportional to the thickness times a typical dimension of the measured cross section, $\sqrt{\sigma}$ and that the solid angle for hitting the edge is roughly proportional to $t/\sqrt{\sigma}$. This results is an edge hitting contribution that goes like t*t * the Heinrich flux. To account for regions where the thickness is longer than a typical dimension on the surface of the sensitive region, the Heinrich flux is scaled by taking the Heinrich flux at the threshold LET times $t/\sqrt{\sigma}$.

Alternatively one can "understand" the observation by imagining a volume which collects charge. If this was a thin rectangular volume (such as one would suspect if the depletion region of a transistor on the chip would be) then one would observe the same "cosine law" type behavior. Physically in the most simple cses this seems to be what is going on. In that case the upset rate could be understood in terms of the distribution of pathlengths through a parallelopiped. Thus the SEU rate is of the form:

$$\text{rate} \rightarrow \sigma \int \Phi(L)\,D(d(L))\,d\Omega \qquad (4\text{-}12)$$

Here D is the distribution of pathlengths, d, through the sensitive volume. The "cross section" is now just a number in front of the integral. In practice we make the same change of variable and integrate over L rather than angle. For example Adams uses the following in his popular SEU code CREME,

$$\text{rate} = 22.5\,\pi\,\sigma\,Q_{crit}\int_{\frac{22.5\,Q_{crit}}{d_{max}}}^{L_{max}} D[d(L)]\,\text{flux}(\text{let}>L_0)\frac{dL}{L^2} \qquad (4\text{-}13)$$

where the flux is the Heinrich flux calculated in the code, the critical charge is based on the threshold LET and the thickness of the sensitive region, 22.5 is a number that keeps things in the proper units assuming that it takes 3.6 eV to create an electron-hole pair in Silicon, Q_{crit} is the critical charge (experimentally the threshold LET times the thickness of the sensitive volume), L_{max} is the largest LET for the particle environment, d_{max} is the longest distance through the sensitive volume,and L is the LET of the particle causing the upset.

$$d_{max} = \sqrt{2\sigma + t^2} \qquad (4\text{-}14)$$

4.2.1. Integral for Heinrich Curve

The cumulative LET spectrum is the summation of each integral for each ion species.

$$\text{flux}(\text{let}>L_0) = \sum_{z=1}^{z=92}\int_{E_1}^{E_2} dE\; f_z(E,\theta,\phi) \qquad (4\text{-}15)$$

where f_z is the flux as a function of energy for each ion species. This distribution is sometimes referred to as a Heinrich curve after the researcher who used it in investigating the effects of cosmic rays on genetics (Heinrich, 1977).

Referring to figure 4-4 or 4-5 , one can see that hydrogen has by far the lowest LET, or deposited charge per micron-particle among the ions. Experiments have fortunately shown that most parts are not sensitive to upsets caused by protons passing through a sensitive part of the part. This is fortunate because protons are so numerous in most radiation environments. For most parts today, protons when they are effective in causing SEUs, do so via a nuclear reaction near a sensitive volume in the part. Proton caused SEUs are discussed separately (see section 4.3) as they involve a significantly different mechanism than other ions and therefore do not fit into formalism about to be developed. In the most simple case, where the cross section and LET threshold do not depend on the angle of incidence of the incoming particle, the SEU rate is simply the cross section as a function of LET of the incoming particle integrated over the flux of particles with that LET or greater. In the case of a cross section that is a step function, the SEU rate is just the product of the cross section times the number of particles with LET greater than or equal to the threshold LET.

4.2.1.1 Environments of Concern

Setting aside proton nuclear reactions for special treatment in section 4.3, the environment which produces SEUs is the high energy ion component of the radiation environment. Although not an important contributor in most cases to the total radiation dose heavy ions are present in most radiation fields. Solar flares for example usually contain some heavy (z equal to or greater than two) ions. Even planetary radiation belts contain ions. Jupiter's radiation belts are thought to be rich in sulphur and oxygen. The earth's radiation belt included oxygen and nitrogen ions. Galactic cosmic rays include a full spectrum of all elements at very high energies (the average cosmic ray ion energy is .5 GeV/amu). SEU calculations should include heavy ions from all of these sources. The galactic cosmic ray ions are present in most missions, although they may not penetrate deeply inside planetary magnetic

fields. Solar particle events, although infrequent, produce large amounts of heavy ions at energies usually lower tha galactic cosmic rays. Missions which spend considerable time in the radiation belts of a planet may also need to consider the SEU rate produced by ions from the belts. The natural SEU causing environments are summarized in Table 4-1, where it is noted whether they experience large variations with location or time or both.

Table 4-1. Natural SEU Causing Environments

Natural environments	Strong time dependence	Strong position dependence	Comment (see note)
Galactic cosmic rays	no	no	≈1 GeV/amu $Z \geq 1$
Anomalous component	yes	no	≈20 MeV/amu He, N, O, Ne
Planetary radiation belts	yes	yes	protons; ≈50 MeV some heavy ions
Solar particle events	yes	yes	protons; ≈100 MeV; some heavy ions

Note: Galactic cosmic rays, solar flares, and trapped radiation all include ions heavier than hydrogen. Both proton-caused and heavy-ion-caused SEUs should be considered. The anomalous component refers to certain singly ionized ions which are seen occasionally at earth and increase the background flux for those ions in the 10 to 100 MeV/amu range.

4.2.1.1.1 Cosmic Radiation

Although the total number of cosmic ray particles is very small compared to the trapped radiation belts or solar flares, these particles are at very high energy. Typically cosmic ray energies are measured in GeV/amu. (An amu is an atomic mass unit; thus these particles have energies on the order of a GeV/nucleon.) Whenever a single high energy particle can influence the behavior of a spacecraft, cosmic rays will be important. In our context, cosmic rays — since they include particles of all known atomic weights and number — are of primary concern for single event upsets.

The bulk of the description to follow is taken from models constructed for SEU evaluations from Naval Research Laboratory (NRL) memoranda, "Cosmic Ray Effects on Microelectronics" Parts I through IV - NRL Reports 4506, 5099, 5402, and 5901. The reader in need of more detailed information on static cosmic radiation is referred to these and the references therein. (Adams et al., 1981; Adams et al., 1983; Tsao et al., 1984; and Adams, 1986).

4.2.1.1.1.1 Universal Abundance

All possible elements are represented in the cosmic ray spectrum. The elemental composition of these energetic particles is similar to the universal composition of matter as determined from the study of meteorites, the sun and the stars. Figure 4-18 shows the relative abundances of the elements in nature (Cameron, 1980). The major elements are hydrogen (93.6 percent) and helium (6.3 percent). The remaining 0.14 percent includes all the

rest of the elements. This is approximately the composition seen on average in galactic cosmic rays, although the actual composition varies a lot from flare to flare.

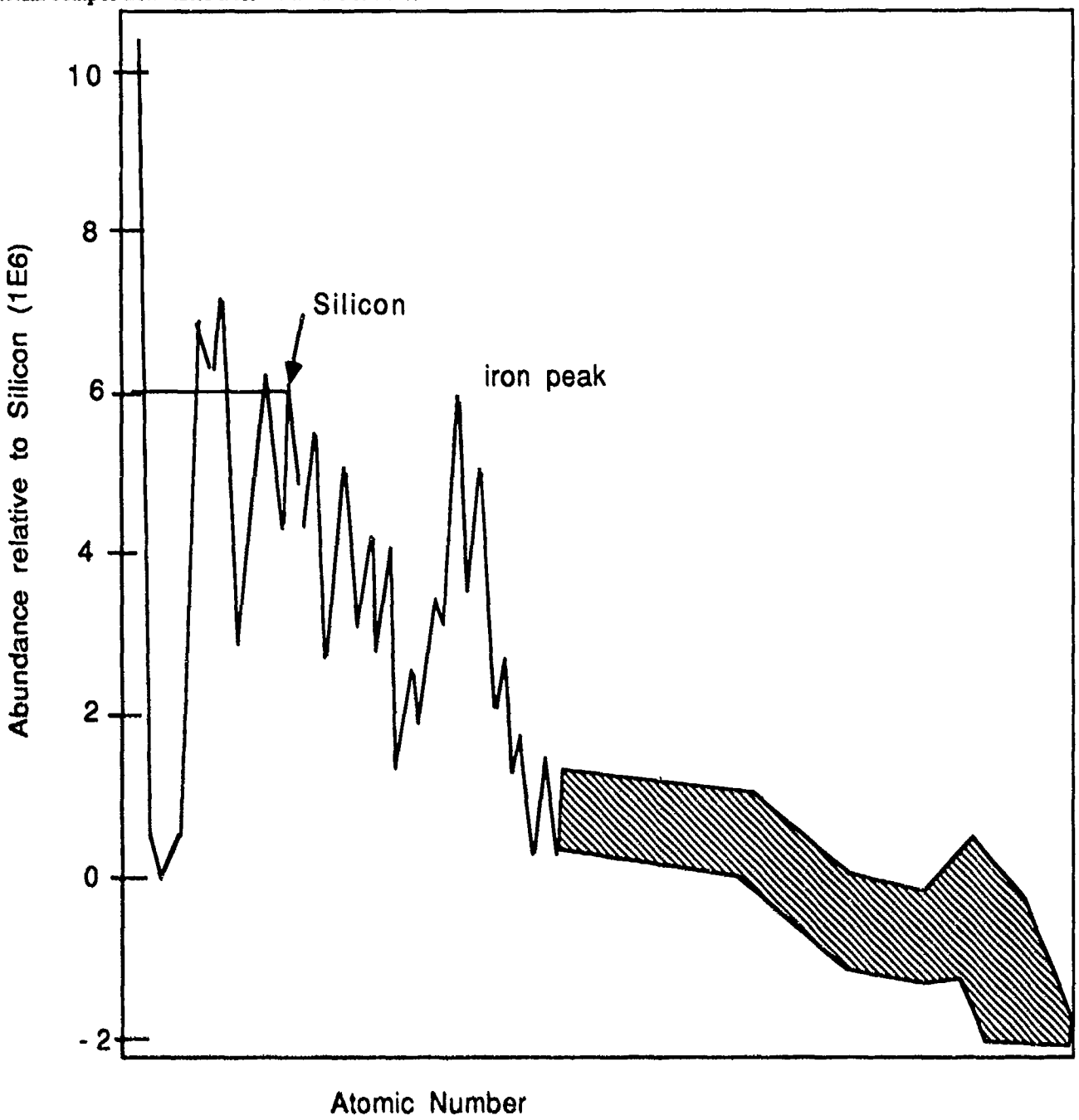

Figure 4-18. Universal Abundance. The relative abundance of chemical elements in nature relative to silicon. Based on studies of meteorites, our sun, and other stars (Cameron, 1980).

4.2.1.1.1.2 Cosmic Ray Abundance

As cosmic rays travel through the galaxy, they occasionally collide with nuclei of interstellar gas. The resulting nuclear reactions modify the initial composition of cosmic rays. Thus one would expect the observed cosmic ray abundance, which may be assumed to be identical to the "universal abundances" initially, to differ from the naturally occurring abundances because of the nuclear reactions with interstellar gas. Figure 4-19 shows the resulting cosmic ray composition at an energy of 2 GeV per nucleon relative to silicon (arbitrarily assigned a value of 10^6) (MeWaldt, private communication, 1987). The differences are thought to be explainable by nuclear reactions with interstellar gases.

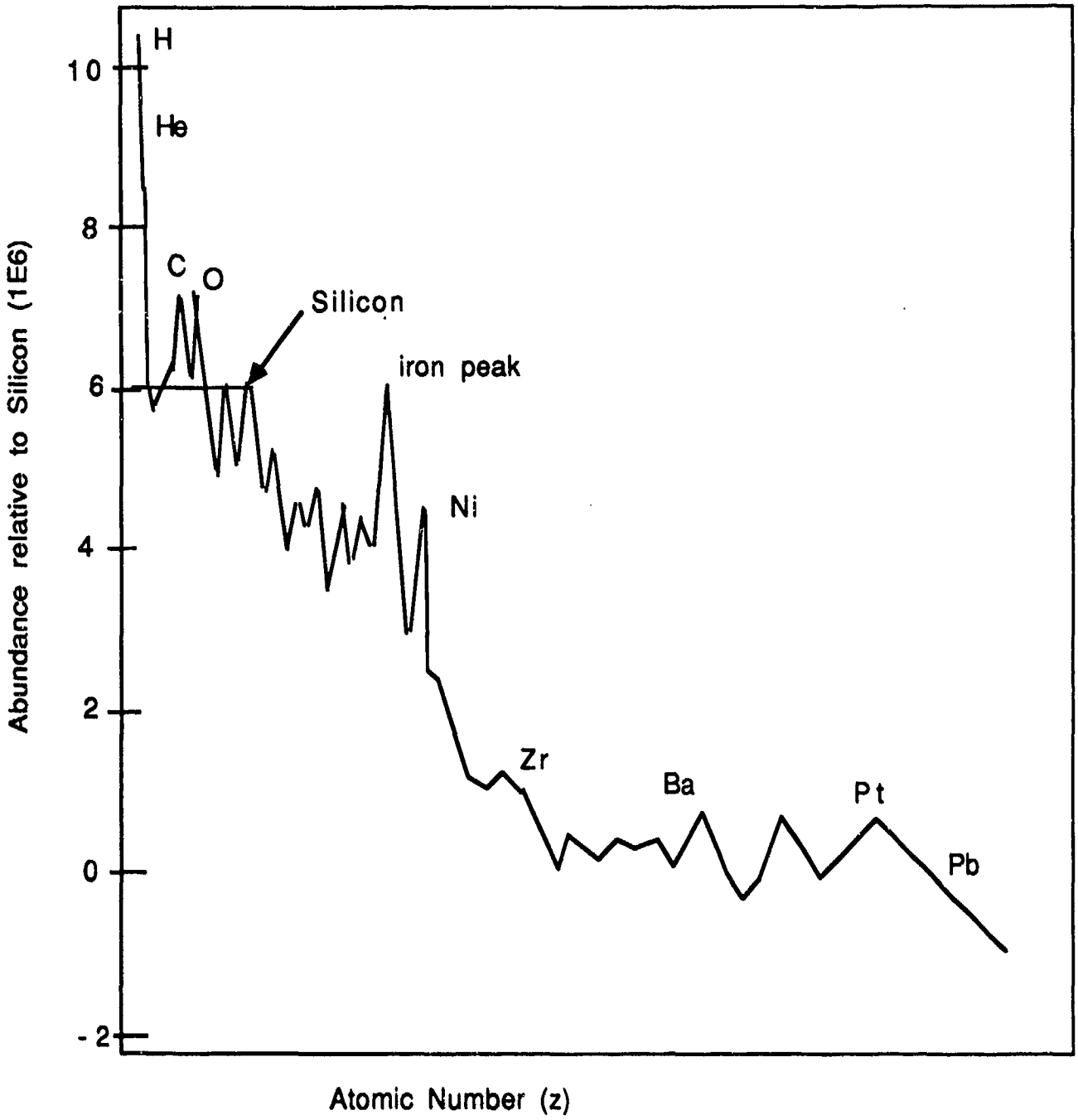

Figure 4-19 Cosmic Ray Abundance. The relative abundance of chemical elements in galactic cosmic rays (GCR) relative to silicon for fluxes with 2 GeV per nucleon. For $z < 31$ fluxes are for each element; for z between 30 and 60 they are for pairs of elements; and for $z > 60$ they are given for groups of elements (McWaldt, private communication, 1987).

4.2.1.1.1.3. Hydrogen Spectrum

The most abundant element in cosmic rays is hydrogen . Figure 4-20, from Adams, et al., 1981, shows differential energy spectrum of hydrogen (for the most part protons) for solar max, solar min, and a "90% worst case." At very high energies a simple power law with a spectral index of 2.75 is a good fit. A power law spectru of this kind could have been produced by particle acceleration in random moving magnetic fields (Fermi acceleratic The deviation below about 5 GeV/amu is thought to be due to solar modulation. The amount of solar modulatior depends on the general level of solar activity, thus one sees a variation from solar minimum to solar maximum. very low (for cosmic rays) energies, there is a considerable difference between either solar min or max conditions a the dashed line representing the "90% worst case." This worst case curve represents the highest proton spectrum observed with a 90% confidence level including protons from solar flares. This includes most so flares.

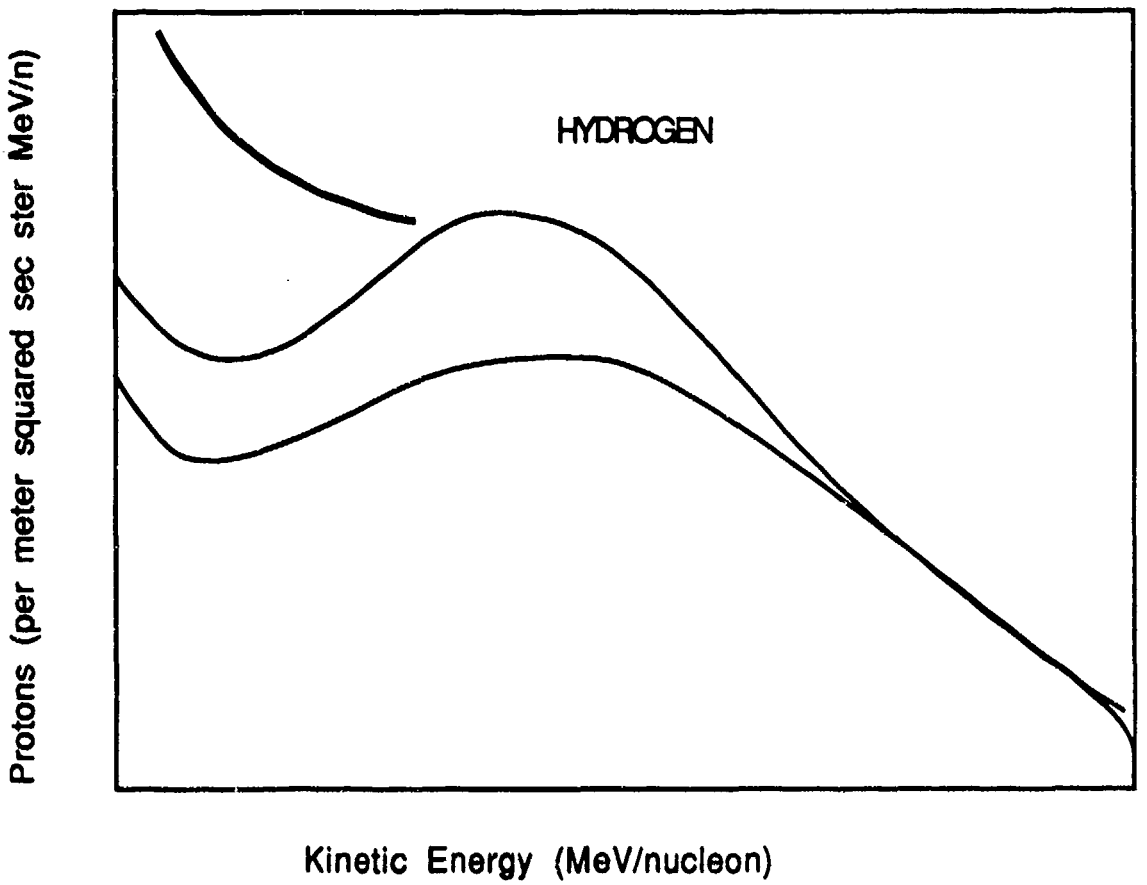

Figure 4-20. Proton Spectrum. The differential spectrum of hydrogen (Adams et al., 1981).

4.2.1.1.1.4. Helium Spectra

The differential energy spectrum of helium for solar max, solar min and the Adams 90% worst case is shown below. The cosmic-ray He abundance is approximately 15 percent of the H abundance in the energy range 200-700 MeV/u, and 5 percent above 10^4 MeV/u. Cosmic ray helium is thought to be mostly primordial materia that is only about 10% is thought to be secondary products from collisions of higher Z particles with interplanetar

gas. In Adams' model, helium is used for comparisons with other elements because it is distinct from all the singly charged particles (i.e. protons, electrons, muons, and pions all have one charge); it is plentiful; and it has a charge to mass ratio similar to the heavier elements (and hence has a similar rigidity). The Helium spectra is shown in figure 4-21

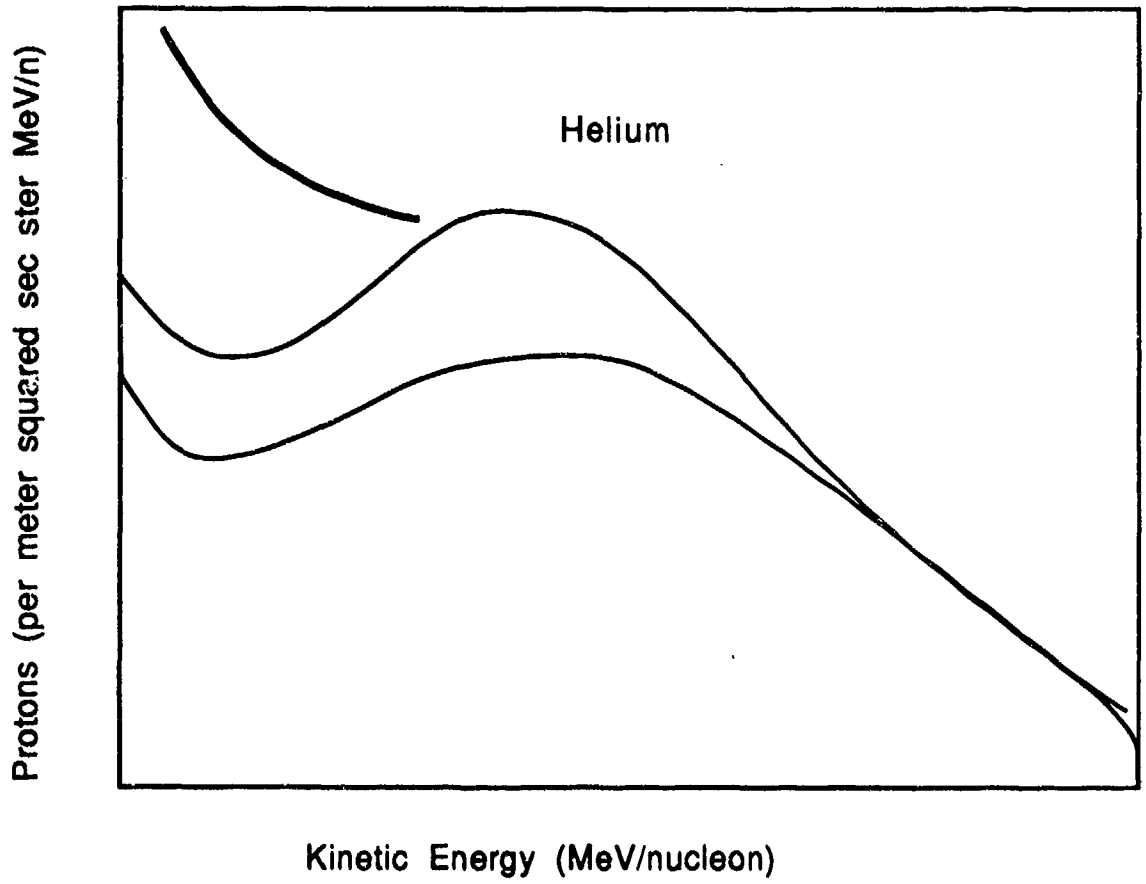

Figure 4-21. Helium Spectrum. The differential spectrum of helium (Adams et al., 1981).

4.2.1.1.1.5. Extension to Other Elements

The nuclei of hydrogen, helium, carbon, oxygen, neon, magnesium, silicon, sulfur, calcium and iron are all thought to be primarily pr .nordial. Thus one might expect them all to have similar energy spectra. Adams in constructing an easily used and yet accurate model which includes all of the important elements needed for single event upset calculations has ratioed all elements to either helium or iron. A detailed fit to the hydrogen (Figure 4-20), helium (Figure 4-21) and iron spectra (Figure 4-22) is provided along with a formula for scaling any other element to those three basic spectra. From an engineering point of view this is a good technique.

Lithium, beryllium and boron are entirely composed of secondaries and hence have a different energy dependence than helium. Nitrogen is mostly composed of secondaries but because of some surviving primaries has an energy dependence different from both helium and lithium. Adams takes these variations in the energy spectra in account by modifying the ratio to either helium or iron as a function of energy.

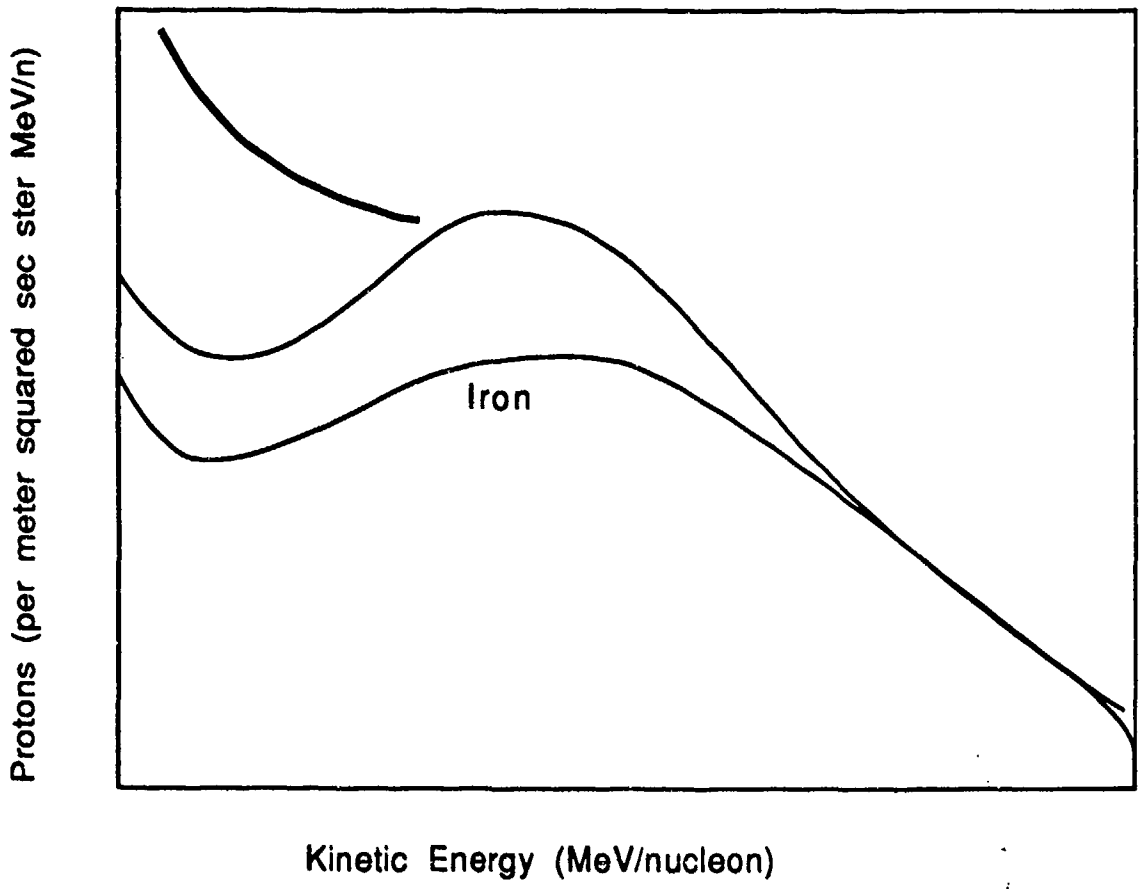

Figure 4-22. Iron Spectrum. The differential spectrum of iron (Adams et al., 1981).

4.2.1.1.1.6. The Adams Model

In the Adams model the differential energy spectra of protons (f_1), helium (f_2), and iron (f_{26}) nuclei are given below for energies above 10 MeV/amu:

$$f(E) = A(E)\sin[w(t - t_0)] + B(E) \quad (4\text{-}16)$$

where w=0.576 radians per year, t_0=1950.6 AD, t is the date of concern (in years), E is the particle energy in MeV/nucleon, and A and B are energy dependent functions given below.

$$A(E) = 0.5\,[Fmin + Fmax] \;;\; B(E) = 0.5\,[Fmin - Fmax] \quad (4\text{-}17)$$

The functions Fmin and Fmax refer to solar minimum and solar maximum conditions of the following equation and differ only by different constants in the basic equation:

$$F = (10)^m \left(\frac{E}{E_0}\right)^a \quad (4\text{-}18)$$

Here the exponent of ten, m, is defined by

$$m = C_1 (e)^{-X_2[\log_{10}E]^2} - C_2 \quad (4\text{-}19)$$

The exponent of the energy ratio is the only factor that changes from solar min to solar max. It is

$$a = a_0 \left\{ 1 - (e)^{-X_1(\log_{10}E)^b} \right\} \quad (4\text{-}20)$$

Adams' best fit parameter values for hydrogen, helium and iron are given in Table 4-2 (Adams, 1986).

Table 4-2. Basic Spectra: Parameters for Adams' Model Hydrogen (f_1), Helium (f_2), and Iron (f_{26}) Spectra

Parameter	Hydrogen	Helium	Iron
α_0	-2.20	-2.35	-2.14
E_0	1.1775E5	8.27E4	1.175E5
b	2.685	2.070	2.64
X_1 for Fmin	0.117	0.241	0.140
X_1 for Fmax	0.079	0.180	0.102
X_2	0.80	0.83	0.65
C_1	6.52	4.75	6.63
C_2	4.0	5.10	7.69

Using these three spectra shapes, the remainder of the elements are modeled using the ratios in Tables 4-3 and 4-4.

Table 4-3. Hydrogen to Nickel: Adams' Model for Galactic Cosmic Rays

Element	Ratio:	Energy dependence modeled by:
(Z):		
H (1)	-	$\equiv f_1$
He (2)	-	$\equiv f_2$
Li (3)	0.330	helium spectra, f_2, modified as
Be (4)	0.176	$f = 0.021 \times f_2$, for $E < 3$ GeV/u
B (5)	0.480	$f = 0.729E^{-0.443} \times f_2$, $E > 3$ GeV/u
C (6)	3.04 E-2	f_0
N (7)	8.7×10^{-3}	$\{\exp[-0.04(\log_{10}E-3.15)^2] + 7.6 \times 10^{-3} \exp[-0.9(\log_{10}E-0.8)^2]\} f_2$
O (8)	2.84 E-2	f_2
F (9)	6.06 E-4	f_2
Ne (10)	4.63 E-3	f_2
Na (11)	1.02 E-3	f_2
Mg (12)	6.02 E-3	$f_2\, S(E)$
Al (13)	1.07 E-3	f_2
Si (14)	4.63 E-3	$f_2\, S(E)$
P (15)	2.34 E-4	f_2
S (16)	9.30 E-4	$f_2\, S(E)$
Cl (17)	0.070	$Q(E)f_{26}$
Ar (18)	0.130	$Q(E)f_{26}$
K (19)	0.090	$Q(E)f_{26}$
Ca (20)	2.1 E-1	f_{26}
Sc (21)	0.042	$Q(E)f_{26}$
Ti (22)	0.147	$Q(E)f_{26}$
V (23)	0.070	$Q(E)f_{26}$
Cr (24)	0.140	$Q(E)f_{26}$
Mn (25)	0.100	$Q(E)f_{26}$
Fe (26)	—	$\equiv f_{26}$
Co (27)	3.4 E-3	f_{26}
Ni (28)	5.0 E-2	f_{26}

$S(E) = f_0$ for $E < 2200$ MeV/u

$S(E) = f_0\,(1 + 1.56\times10^{-5}\,(E-2200))$ for $E > 2200$ MeV/u

$Q(E) = 16\,[1 - \exp(-0.075\,E^{0.4}]\,E^{-0.33}$ (this is the so-called iron subgroup)

Table 4-4. Copper to Uranium: Ratio of Abundances to Iron for Adams' Model

Z	Element	Ratio to Iron	Z	Element	Ratio to Iron
29	Cu	6.8 E-4	61	Pm	1.9 E-7
30	Zn	8.8 E-4	62	Sm	8.7 E-7
31	Ga	6.5 E-5	63	Eu	1.5 E-7
32	Ge	1.4 E-4	64	Gd	7.0 E-7
33	As	9.9 E-6	65	Tb	1.7 E-7
34	Se	5.8 E-5	66	Dy	7.0 E-7
35	Br	8.3 E-6	67	Ho	2.6 E-7
36	Kr	2.3 E-5	68	Er	4.3 E-7
37	Rb	1.1 E-5	69	Tm	8.9 E-8
38	Sr	3.6 E-5	70	Yb	4.4 E-7
39	Y	6.8 E-6	71	Lu	6.4 E-8
40	Zr	0.7 E-5	72	Hf	4.0 E-7
41	Nb	2.6 E-6	73	Ta	3.6 E-8
42	Mo	7.1 E-6	74	W	3.8 E-7
43	Tc	1.6 E-6	75	Re	1.3 E-7
44	Ru	5.3 E-6	76	Os	5.6 E-7
45	Rh	1.5 E-6	77	Ir	3.7 E-7
46	Pd	4.5 E-6	78	Pt	7.2 E-7
47	Ag	1.3 E-6	79	Au	1.3 E-7
48	Cd	3.6 E-6	80	Hg	2.3 E-7
49	In	1.4 E-6	81	Tl	1.8 E-7
50	Sn	7.5 E-6	82	Pb	1.7 E-6
51	Sb	9.9 E-7	83	Bi	9.0 E-8
52	Te	5.7 E-6	84	Po	0
53	I	1.5 E-6	85	At	0
54	Xe	3.5 E-6	86	Rn	0
55	Cs	5.8 E-7	87	Fr	0
56	Ba	6.0 E-6	88	Ra	0
57	La	5.3 E-7	89	Ac	0
58	Ce	1.6 E-6	90	Th	9.0 E-8
59	Pr	3.0 E-7	91	Pa	0
60	Nd	1.1 E-6	92	U	5.4 E-8

4.2.1.1.1.7. Variation With Distance From the Sun

The flux of galactic cosmic rays varies with location in the solar system, with the largest observed variations being in the radial direction. The radial gradient is always positive; fluxes increase exponentially with radial distance from the sun. The magnitude of the radial gradient varies with both ion species and energy. For relativistic cosmic rays the radial gradient is expected to be just under 4 percent per AU while for cosmic ray particles below 100 MeV per nucleon the gradient is expected to be under 10 percent per AU. Figure 4-23 shows the flux of four different ions for various heliocentric distances. The latitudinal gradient is small, under 1 percent per degree, and is suspected of changing signs each half solar cycle.

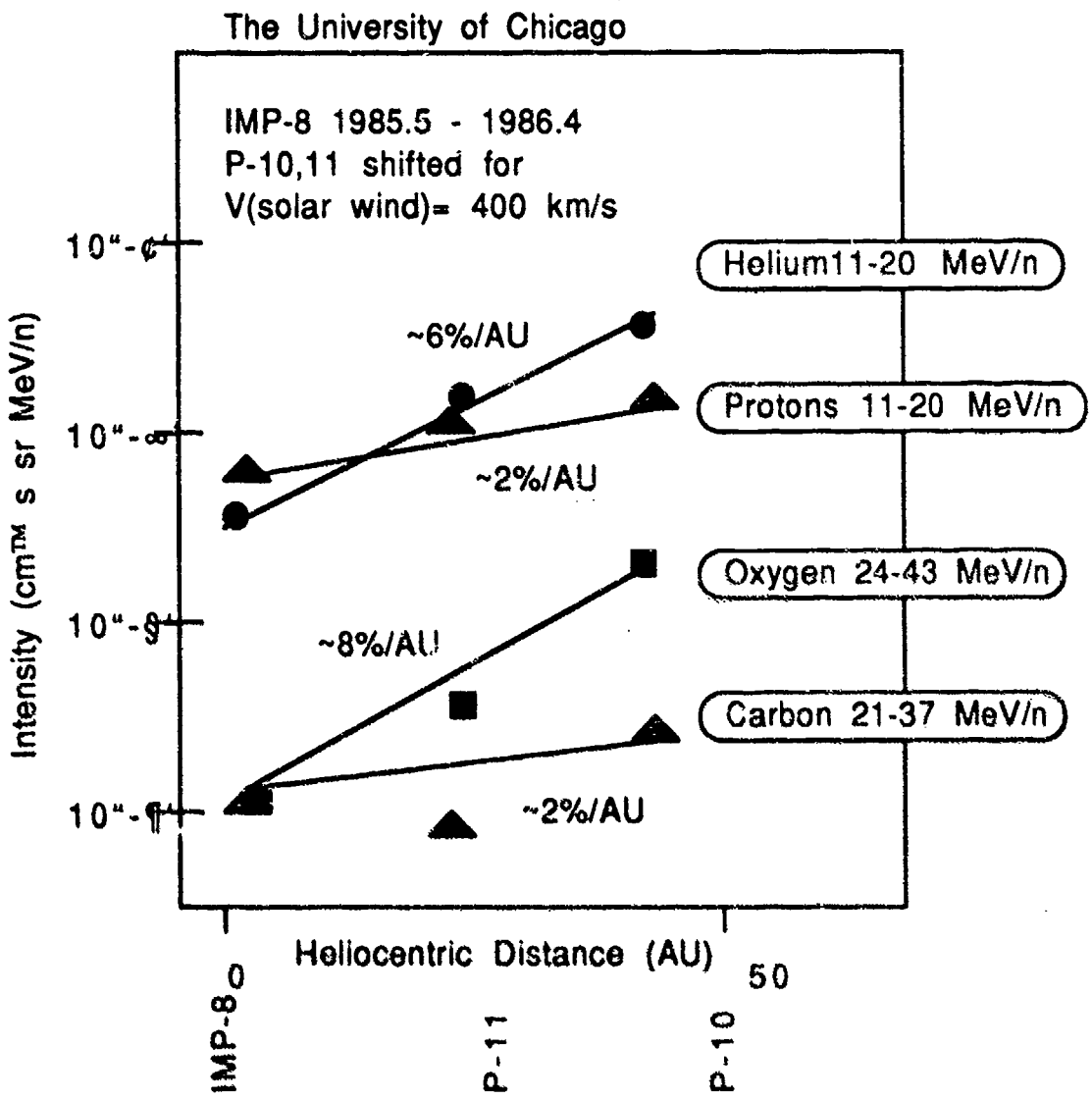

Figure 4-23. Flux Versus Heliocentric Distance: The University of Chicago (McKibben, private communication, 1987)

4.2.1.1.2 Heavy Ions in Planetary Radiation Belts

Galactic cosmic rays come to our solar system from great distances and must penetrate the outward-flowing solar wind to reach the earth. The solar wind modulates the cosmic rays by deflecting particles. Lower energy particles can be completely excluded by the solar magnetic field (see discussion of rigidity in the glossary). As a result, the cosmic rays reaching earth vary with the 11 year cycle of solar activity. At the maximum of solar activity, cosmic ray intensity is at a minimum and vice versa. The cosmic ray intensity, at moderate energies, varies by a factor of 4 to 8 depending on the energy and ion being considered (see the model of Adams et al., 1981).

The anomalous component is a curious bump or flattening in the differential energy spectra of certain ions like helium, oxygen, nitrogen and neon. This feature is strongly affected by solar modulation varying in intensity by a factor of 100 to 1000 over the 11 year solar cycle in a similar way to cosmic rays. The anomalous component is more intense at greater distances from the sun, so it is not thought to be from solar flares. The elemental and

isotopic composition of the ions suggests that these particles did not come from great distances. Fisk et al., 1974, has suggested that the anomalous component may be interstellar gas accelerated by the solar wind. Such ions would probably be singly ionized regardless of their energy. This would give them the ability to penetrate the earth's magnetic field at much lower energies than fully-ionized particles.

The species, abundances, energies and time variations of particles that are trapped in radiation belts vary greatly depending upon the planet. Planetary magnetic fields influence the particle spectrum that is observed near the planets in two ways -- first, the magnetic field of the planet shields the planet from the cosmic ray spectrum and second, it allows particles to be trapped near the planet in radiation belts.

The earth's radiation belts are populated primarily by protons and electrons; however, heavy ions have been observed around the earth and other planets. The possibility of trapped heavy ions raises a serious issue for single event upset calculations (Adams and Partridge, 1982).

4.2.1.1.2.1. Helium

Helium nuclei (mostly alpha particles) have been detected throughout the magnetosphere. The principal source of these nuclei appears to be the solar wind (Blake, 1973, and Hovestadt et al., 1978). The solar wind particles are transported down into the magnetosphere and accelerated by radial diffusion. This process was described theoretically by Cornwall (1972) and has recently been shown to describe well the helium ion population in the magnetosphere (Spjeldvik and Fritz, 1978, and Fritz and Spjeldvik, 1979). The bulk of the helium nuclei are, however, at energies too low to penetrate the walls of a spacecraft. Assuming that the anomalous component (discussed below) is singly ionized, Blake and Friesen (1977) have suggested that anomalous nuclei entering the atmosphere might be stripped in the lower geocorona, thus becoming stably trapped for periods up to a year or more. This could add heavy ions, unexpectedly, to the trapped radiation.

4.2.1.1.2.2. C, N, and O

C, N, and O have been observed in several experiments. It is by no means clear that the particles in all these observations were trapped in the magnetosphere, but in each instance the particles were forbidden direct access by the geomagnetic cutoff, so they did not come in directly from outside.

There is very little data on the actual flux of trapped helium and heavy ions above 10 MeV/u. Adams used the available data and theoretical estimates to determine the heavy ion flux above 10 MeV/u and found that there is apparently a small flux of helium nuclei and a smaller flux of heavier nuclei in the magnetosphere at all times. He also found reports of long-lasting enhancements of the low energy heavy ion flux after large solar flares, possibly due to the anomalous component.

4.2.1.1.2.3. Anomalous Particles

Some particles incident on the earth do not appear to originate outside the solar system. One component consists of high energy (up to ~20 MeV/amu) particles which appear to be co-rotating with the high speed solar wind and interplanetary field structures of the sun. Another, the "anomalous component," appears to be singly ionized particles with an energy in the range of 1 to 200 MeV/amu which is not always present near the earth (Adams et al., 1981). It appeared between 1971 and 1972 and disappeared again in the solar maximum of 1978. Jokipii et al., (1977), predict that the anomalous component appears near earth only once every other solar minimum, i.e., in ~1994. Fisk et al., 1974, predict that only atoms with a first ionization potential higher than hydrogen will display anomalous spectra, and that the ions will be singly ionized. If the anomalous component is singly ionized it will penetrate much more deeply into the earth's magnetic field. Blake and Friesen (1977) suggested that the particles of the anomalous component become stripped rapidly near their geomagnetic cutoff and consequently travel in the local mirror plane for trapped particles. Once stripped, they have a much lower magnetic rigidity and because they are moving in the local mirror plane, become more or less stably trapped. This leads to a special trapped population of oxygen, nitrogen, neon and a few other elements which comprise the anomalous component (see Table 4-5).

Anomalous cosmic rays have a radial gradient that can be as large as 15 percent per AU (is always positive) and may decrease with radial distance. The latitudinal gradient has a magnitude of 3 to 5 percent per degree and is believed to change sign in alternate solar cycles when the solar magnetic field reverses. There might also be a small 1 percent per degree longitudinal gradient.

Table 4-5. Composition of Heavy Ions

Element	Anomalous Comp.	Relative Composition (O^{16} = 1.0) Magnetosphere	Galactic CR
C	.23 ± .09	.21 ± .019	1.13 ± .03
N	.22 ± .09	.21 ± .041	.27 ± .02
O	1.0	1.0	1.0
Ne	.07 ± .04	.08 ± .02	.18 ± .01
Mg	.002 ± .002	.006 ± .004	.20 ± .01
Si	< .02	.004 ± .002	.14 ± .006
S	----	< .004	.035 ± .003
Ar	----	< .003	.013 ± .002
Fe Group	----	.05 ± .02	.084 ± .001

4.2.1.1.2.4. Planetary Radiation Belt Temporal Variations

Planetary radiation belts are relatively stable, but are influenced by solar and other activity. Solar flares and other activity produce magnetic storms, aurora and other effects at the earth. This changes the boundary conditions for diffusion into and out of the radiation belts, alters the geomagnetic cutoff of cosmic rays and influences the energy distribution in the geomagnetic tail. Some have suggested that the stable equilibrium population of the radiation belts is no radiation belts at all. This implies that the belts we see require a source to continually resupply particles that are lost in the aurora and elsewhere. Studies of the Starfish nuclear explosion underlie the dynamic nature of the radiation environment about the earth. The outer belts are more rapidly influenced by changes in the solar input than the inner magnetosphere as was seen in the examples discussed in this chapter. Most empirical models for the radiation belt consequently are long time averages which are useful only for engineering applications when applied over a period of time comparable to the averaging period of the model.

4.2.1.1.3 Solar Particle Events

A large fraction of the total flux seen over a year as calculated by a model which averages data accumulated over the last solar cycle or two will be due to a few solar particle flares. The flux received at a given location will depend on how well connected that location is with the solar event and the size of the event. It is easy to have variations of 100 in fluence at different points for the same flare. The "connection" between the flare and the point depends on the conditions between the sun and the spacecraft at the time. For a quiet solar wind of v = 430 km/s a solar flare at ± 54° west of the center of the sun as viewed from the earth will connect to the earth. Of course the time buildup and decay of the flares' intensity will be a strong function of the details of the magnetic field and currents between the flare and the satellite at the time.

At the present time it is not possible to predict the occurrence of large solar flares other than to state they will occur. Yet they will continue to dominate the production of anomalies on spacecraft. Statistical models are being developed to estimate the largest of these flares (Feynman); however, the intensity and number of very large solar flares seem to vary over many solar cycles and therefore statistical models require a very long time data base for accurate results. Most data on large solar flares is from the very recent past.

4.2.1.1.3.1. Solar Flare Particles

Adams et al., 1981, describe solar flares as follows:

"Solar flares are sudden outbursts on the visible surface (photosphere) of the sun which release huge amounts of energy. Most of this energy is radiation in UV and X-rays. A part of this energy, mostly from hard X-rays, goes into very rapid heating of the solar corona above the flare. This produces large currents and moving magnetic fields in the corona that accelerate ambient coronal material to very high energies quickly. (For a review of solar flare particle acceleration, see Ramaty et al., 1980.)

"Many of these coronal particles escape the sun and spray out into the interplanetary medium. As the particles move into the interplanetary medium they tend to be guided along the existing spiral magnetic field pattern in the ecliptic plane. As a result, both the intensity and the spectrum observed at earth depend on the relative positions of the earth and the flare on the sun. For example, a solar wind velocity of 430 km/sec produces a spiral field that connects the earth directly to points on a solar longitude line ~ 54° west of the center of the sun as viewed from earth. For flares at other positions the flux measured at earth will build up more slowly and may contain fewer high energy particles. The actual degree of "well connectedness" between the earth and the flare site depends on interplanetary conditions at the time of the flare. These conditions are highly variable and unpredictable. This may lead to variations as large as 100 in the observed flux from the same flare at different points around the earth's orbit (see Simnett, 1976)."

The maximum intensity falls off approximately as r^{-3} compared to the intensity at 1 AU (see Figure 4-24). For engineering studies, the dependence inside 1 AU has been taken as r^{-2}. This seems to be both reasonable and conservative enough for engineering design.

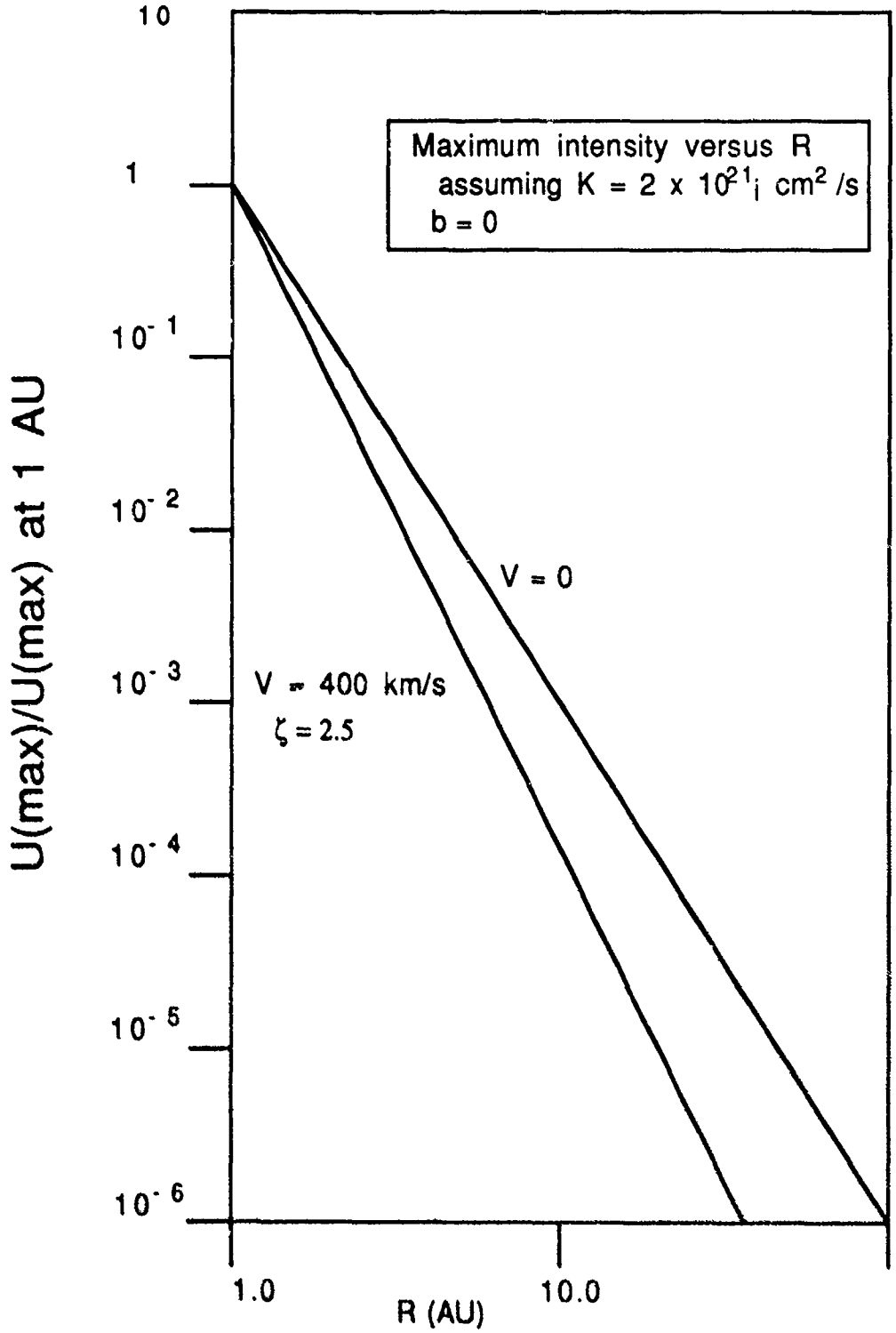

Figure 4-24. Propagation of Solar Flare

Below 400 MeV the total yearly solar flare proton fluence dominates the galactic cosmic ray contribution. Galactic cosmic rays are, however always present, whereas a single large solar flare lasting only a few days may account for half or more of the total solar fluence for the year. Figure 4-25 illustrates the typical situation.

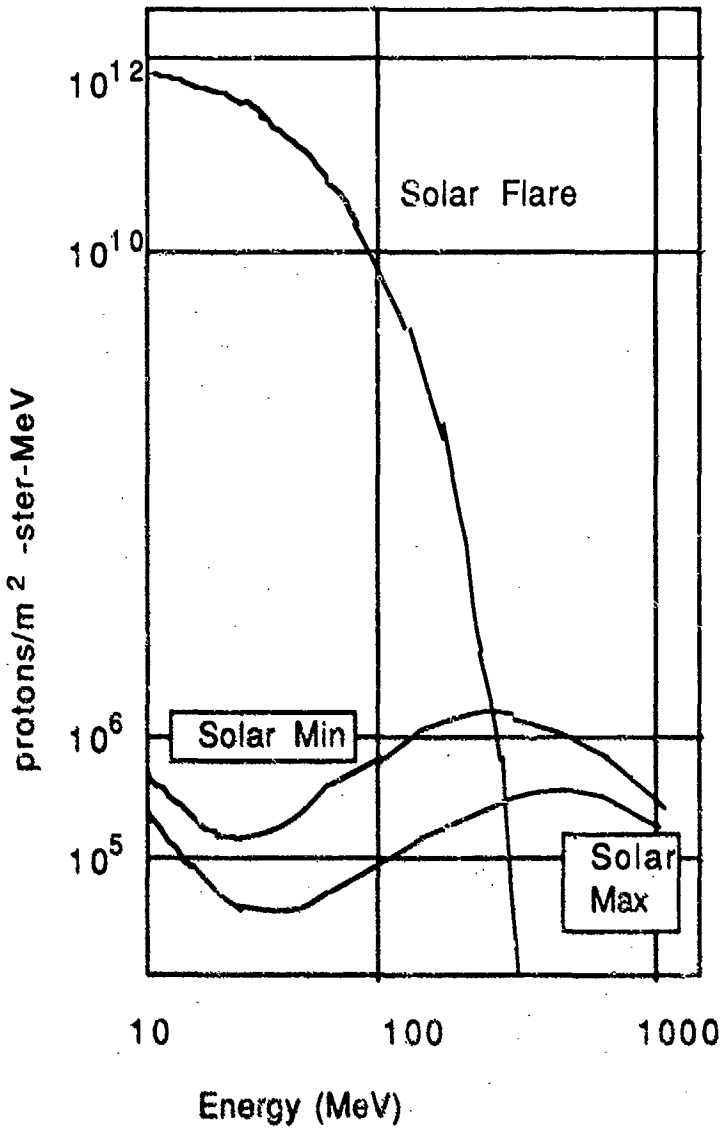

Particles

Figure 4-25. Proton differential fluence for solar flares and cosmic rays at solar minimum and solar maximum (Adams, 1987, private communication).

4.2.1.1.3.3. Solar Proton Fluxes

The event-integrated proton fluxes above 30 MeV for the major solar particle events of the 19th and 20th solar cycles are presented in Figure 4-26. This illustrates both the high variability and significance of a single flare. The peak proton flux used in Adams' model (Adams et al., 1981) for typical, worst-case, and anomalously large particle events as a function of energy is shown in Figure 4-27.

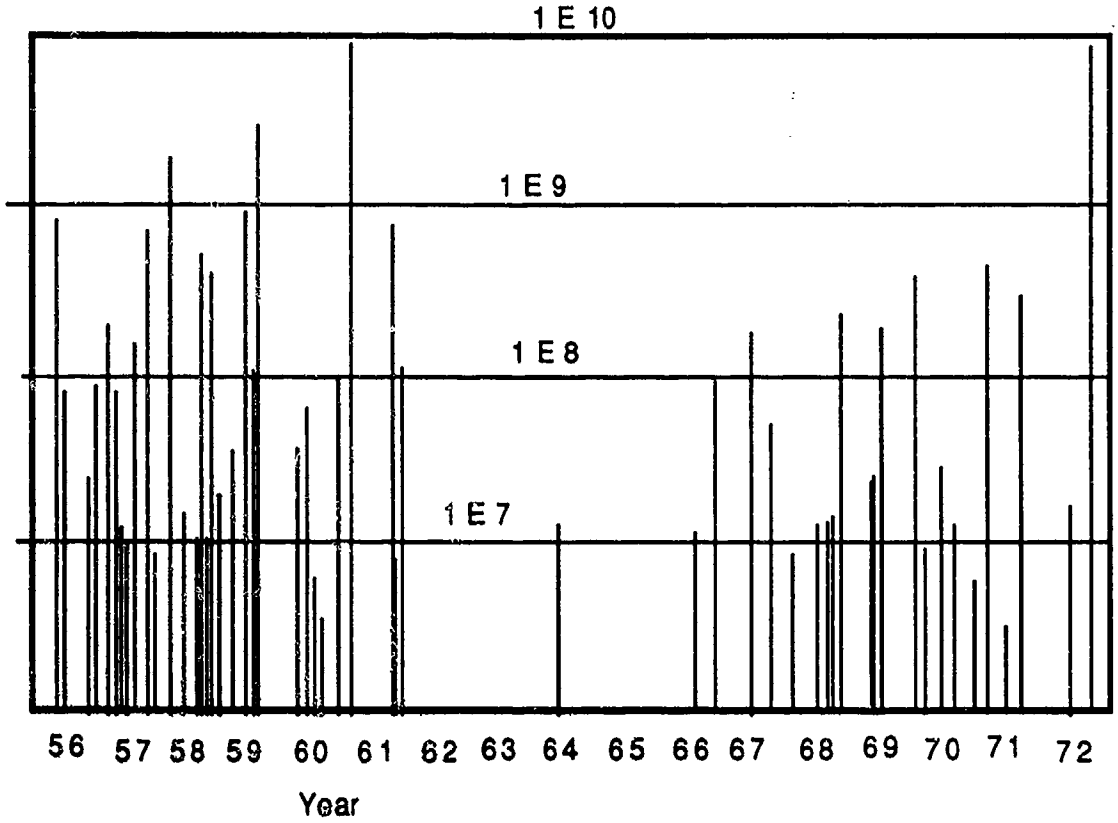

Figure 4-26. Solar Flare Occurrences: protons/cm^2 Greater Than 30 MeV. Event integrated proton fluxes above 30 MeV for major solar events (from JSC, 1987 and King, 1974).

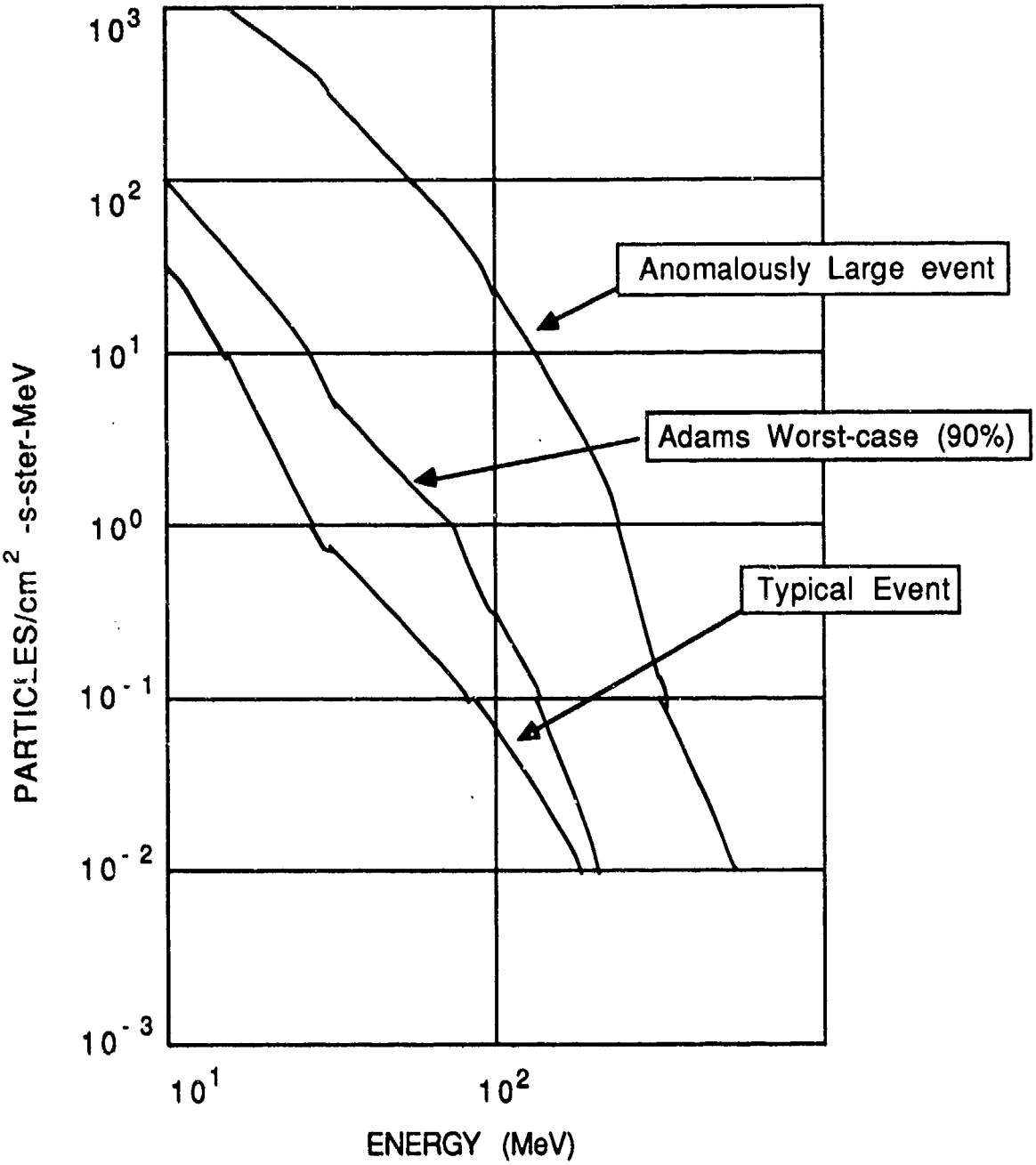

Figure 4-27. Solar Flares: Peak Proton Differential Energy Flux. Several flare spectra (from Adams et al., 1981).

4.2.1.1.3.4. Solar Energetic Particle Composition

The elemental composition of particles from solar flares is highly variable. Some cases show enormous enhancements in heavy elements. Table 4-6 gives the composition relative to hydrogen of the elements through nickel. The elements above Ni follow in Table 4-7 for the mean composition. Both mean and worst-cases (90 percent confidence level) are given. Multiply the abundance ratio from the table by the appropriate proton spectrum to get the flare spectrum of any element in the table.

In the Adams' model, the worst-case compositions of the elements from copper to uranium are obtained by multiplying the abundance ratios of Table 4-6 by:

$$1.92 \exp\left(\frac{z^{0.78}}{6.89}\right)$$

Table 4-6. Mean and Worst-Case Solar Particle Event Composition – Low Z

Element	Mean case	Worst case	Element	Mean case	Worst case
H	1	1	P	2.3×10^{-7}	1.1×10^{-6}
He	1.0×10^{-2}	3.3×10^{-2}	S	8.0×10^{-6}	5.0×10^{-5}
Li	0	0	Cl	1.7×10^{-7}	8.0×10^{-7}
Be	0	0	Ar	3.3×10^{-6}	1.8×10^{-5}
B	0	0	K	1.3×10^{-7}	6.0×10^{-7}
C	1.6×10^{-4}	4.0×10^{-4}	Ca	3.2×10^{-6}	2.0×10^{-5}
N	3.8×10^{-5}	1.1×10^{-4}	Sc	0	0
O	3.2×10^{-4}	1.0×10^{-3}	Ti	1.0×10^{-7}	5.0×10^{-7}
F	0	0	V	0	0
Ne	5.1×10^{-5}	1.9×10^{-4}	Cr	5.7×10^{-7}	4.0×10^{-6}
Na	3.2×10^{-5}	1.3×10^{-5}	Mn	4.2×10^{-7}	2.3×10^{-6}
Mg	6.4×10^{-5}	2.5×10^{-4}	Fe	4.1×10^{-5}	4.0×10^{-4}
Al	3.5×10^{-6}	1.4×10^{-5}	Co	1.0×10^{-7}	5.5×10^{-7}
Si	5.8×10^{-5}	1.9×10^{-4}	Ni	2.2×10^{-6}	2.0×10^{-5}

Table 4-7. Mean Solar Particle Event Compositions -- High Z

Element	Mean case	Element	Mean case	Element	Mean case
Cu	2.0×10^{-8}	Sn	2.0×10^{-10}	Lu	2.0×10^{-12}
Zn	6.0×10^{-8}	Sb	1.4×10^{-11}	Hf	8.0×10^{-12}
Ga	2.0×10^{-9}	Te	3.0×10^{-10}	Ta	9.0×10^{-13}
Ge	5.0×10^{-9}	I	6.0×10^{-11}	W	1.0×10^{-11}
As	3.0×10^{-10}	Xe	2.7×10^{-10}	Re	2.0×10^{-12}
Se	3.0×10^{-9}	Cs	2.0×10^{-11}	Os	3.0×10^{-11}
Br	4.0×10^{-10}	Ba	2.0×10^{-10}	Ir	3.0×10^{-11}
Kr	2.0×10^{-9}	La	2.0×10^{-11}	Pt	6.0×10^{-11}
Rb	3.0×10^{-10}	Ce	5.0×10^{-11}	Au	1.0×10^{-11}
Sr	1.0×10^{-9}	Pr	8.0×10^{-12}	Hg	1.0×10^{-11}
Y	2.0×10^{-10}	Nd	4.0×10^{-11}	Tl	9.0×10^{-12}
Zr	5.0×10^{-10}	Pm	0	Pb	1.0×10^{-10}
Nb	4.0×10^{-11}	Sm	1.0×10^{-11}	Bi	6.0×10^{-12}
Mo	2.0×10^{-10}	Eu	4.0×10^{-12}	Po	0
Tc	0	Gd	2.0×10^{-11}	At	0
Ru	9.0×10^{-11}	Tb	3.0×10^{-12}	Rn	0
Rh	2.0×10^{-11}	Dy	2.0×10^{-11}	Fr	0
Pd	6.0×10^{-11}	Ho	4.0×10^{-12}	Ac	0
Ag	2.0×10^{-11}	Er	1.0×10^{-11}	Th	2.0×10^{-12}
Cd	7.0×10^{-11}	Tm	2.0×10^{-12}	Pa	0
In	9.0×10^{-12}	Yb	9.0×10^{-12}	U	1.2×10^{-12}

4.2.1.1.3.5. Ionization State

In recent years, evidence has been accumulating that solar energetic heavy ions may not be fully ionized. This is certainly the case in the $0.5 \leq E \leq 2.5$ MeV/u energy range, as has been shown by A. Luhn et al. (1984). At the higher energies of interest here solar energetic heavy ions may not be fully ionized (as has been generally assumed up to now). Although heavy ions with energy >10 MeV/u would be fully ionized by passing through sufficient matter, the available data place only an upper limit on their path length in matter (McWaldt and Stone, 1983).

Fischer et al. (1984) report evidence that solar energetic heavy ions in the energy range $5 \leq E \leq 20$ MeV/u are not fully ionized. These authors report upper limits on the charge to mass ratio of heavy ions as low as 0.1 (this ratio is ~0.5 for fully ionized heavy ions). Breneman and Stone (1985) have obtained indirect evidence that solar energetic heavy ions in the energy range 3.5 to 50 MeV/u have the same distribution of charge states as that measured for 0.5 to 2.5 MeV/u ions by Luhn et al. (1984). These authors have shown that the systematic abundance can be understood if the charge state distributions measured by Luhn et al. are assumed for these higher energy heavy ions.

Most models assume that the SPE (solar particle event) heavy ions are fully ionized. This assumption may be incorrect from the evidence discussed above. If this is the case, the SEU rates due to SPEs will be systematically underestimated for spacecraft in low earth orbit, because geomagnetic shielding will not be as effective as the present model assumes.

Under the present circumstances, the charge state of SPEs is uncertain, so it's not clear how the models for SPEs should be altered to account for the SPE charge states. Therefore, Adams recommends continuing to use the present models. A conservative calculation can always be made by neglecting the protection afforded by the geomagnetic cutoff (i.e., assuming the geomagnetic cutoff transmission function is 1.0 for all energies).

4.2.1.2. Environment at the Spacecraft Location

The next step in evaluating the environmental part of the SEU rate is to determine the environment at the part location within the spacecraft. Planetary magnetic fields influence the number of charged particles reaching a spacecraft. This "magnetic shielding" is very different from mass shielding which degrades a particle's energy. In a magnetic field, the low energy portion of the spectra is removed, but the high energy particles are unattenuated even though they are now traveling in different directions. Inside a planet's magnetic field, one must consider both the magnetic reflection of galactic and solar cosmic rays, and particles trapped by the magnetic field (Adams and Partridge, 1982). The spacecraft's mass also influences the particle population at the part by degrading the energy o the particles as they pass through the material (see discussion on LET in section 4.5.1.5)

4.2.1.2.1. Magnetic Shielding

Earth's magnetic field serves as an extremely effective shield of low to medium energy cosmic rays. The earth's magnetic field must be penetrated by cosmic rays in order for them to reach a spacecraft in earth orbit. The magnetic field a cosmic ray must cross to reach a given point within the magnetosphere approximately determines the minimum energy it must possess. This penetrating ability is determined uniquely by the cosmic ray's momentum divided by its charge -- a quantity called the particle's rigidity (Appendix 2). To penetrate the earth's magnetic field, a particle must have sufficient magnetic rigidity (momentum per unit charge) to avoid being turned away. There is a minimum magnetic rigidity a cosmic ray must possess to arrive from a given direction at a given point in the magnetosphere. Regions in the outer magnetosphere and near the poles can be reached at much lower magnetic rigidities than are required to reach points near the earth's equator. In general, for each point in the magnetosphere and for each direction from that point, there exists a magnetic rigidity below which cosmic rays cannot arrive. This value is the geomagnetic cutoff. For magnetic rigidities above this value, cosmic rays arrive freely, almost as though no magnetic field were present.

To obtain the differential energy spectra for the various nuclei reaching the skin of a spacecraft from outsid the magnetosphere, multiply the flux in the interplanetary medium (for example, from Adams, 1986) by the transmission function. To do this, the magnetic rigidity, P (in GeV/ec) must be computed for each particle energy, E (in MeV/u), i.e.:

$$P = \left(\frac{A}{Z}\right)\left[\left(\frac{E}{1000}\right)^2 + \frac{1.86}{10^3\,E}\right]^{0.5} \qquad (4\text{-}21)$$

and then used to look up the geomagnetic cutoff transmission. Here A is the atomic mass and Z is the particle charge (in electron charges). The geomagnetic transmission at any particle energy depends on the particle's charge through its A/Z ratio. If an ion is fully stripped, then A/Z ≈ 2; however, if the ion is only singly ionized, A/Z = A Thus the rigidity of singly ionized particles will be much greater than fully ionized particles at the same energy.

4.2.1.2.2. Effect of Mass Shielding

As charged particles pass through material they lose (or gain) energy by interactions with the material. This effect is dealt with in a number of texts [Evans 1955, Fermi 1950, van Lint et al., 1980, and others]. Computer codes from Oak Ridge National Laboratory's Radiation Shielding Information Center (RSIC) and various commercial and government laboratories have been designed to calculate the flux and fluence of particles given the shielding configuration. [RISC is a good place to start if you have no in-house shielding capability. Their address is ORNL, Box X, Oak Ridge, Tenn. 37831-6362, Telephone 615-574-6176 or FTS 624-6176]. Quick one dimensional estimates can be made from a knowledge of the range energy relations of particles given in the discussion of LET earlier.

4.2.2. The Sensitive Volume

The remaining part of the SEU rate integral focuses on the part sensitivity to SEUs. The cross section information required for this part of the integration, is most easily understood by introducing the concept of a sensitive volume. Imagine a box which can collect all the charge that is released inside it. When an ion passes through that box with a constant LET the amount of charge to be collected in the box will depend on how long the path of the ion was in the box. If the box is a very thin one, the charge deposited by a path which glances from one end of the box to the other will be much greater than the charge if the ion passes straight through the thin dimension of the box. All the popular models for calculating SEU rates use the notion of a sensitive volume as the way to extrapolate from ground tests with low energy monodirectional ions to high energy omnidirectional ions.

This notion of a parallelepiped sensitive volume is the source of the so-called "cosine" law for relating the LET threshold to the normal incidence LET when tests are done by rotating the angle of the device with respect to the beam. This also allows the calculation of omnidirectional flux SEU rates, because now each angle has a unique cross section -- obtained by foreshortening the front surface cross section, and a thickness which is related to the normal thickness by $1/(\cos \phi)$. Shortly we will discuss the "path length distribution" in such a sensitive volume. The path length distribution is the number of paths through the volume as a function of the length of the path. Since the LET required by the particle to cause an upset depends on the path length through the volume, the Heinrich integral must be done for each threshold as appropriate and summed over all possible angles.

4.2.2.1. Determining the Path Length

Single particle effects including SEUs and latchups are highly dependent upon the path lengths of incident particles within sensitive device regions. For example, a sensitive region that is cubical has path lengths that vary from zero to the square root of three times the thickness of the sensitive volume, whereas a flat geometry can have path lengths that vary from zero to many orders of magnitude times the thickness of the sensitive region. Since the path length in the sensitive volume model determines the range of particles that can cause an upset, the shape of the sensitive volume is a very important consideration in determining the upset rate. Sensitive volumes which admit long path lengths will respond to lower Z particles at glancing angles while sensitive volumes which do not allow long path lengths will not respond to low Z particles. For most devices in the early 80's the thickness of the sensitive region was small compared to the linear dimensions of the cross section. This meant that the sensitive volume was a parallelepiped. This shape for the sensitive volume gives the measured LET threshold an apparent angular dependence. Most experimenters take advantage of this effect, by assuming a rectangular sensitive volume and using the $1/(\cos \theta)$ dependence to determine the threshold. When a normally incident particle does not cause an upset, the chip is rotated in the beam. If upsets occur at the angle then the threshold is $LET_1/\cos \theta$, where LET_1 is the LET of the particle at the sensitive region, and θ is the angle the chip makes with respect to the beam (see Figure 4-28).

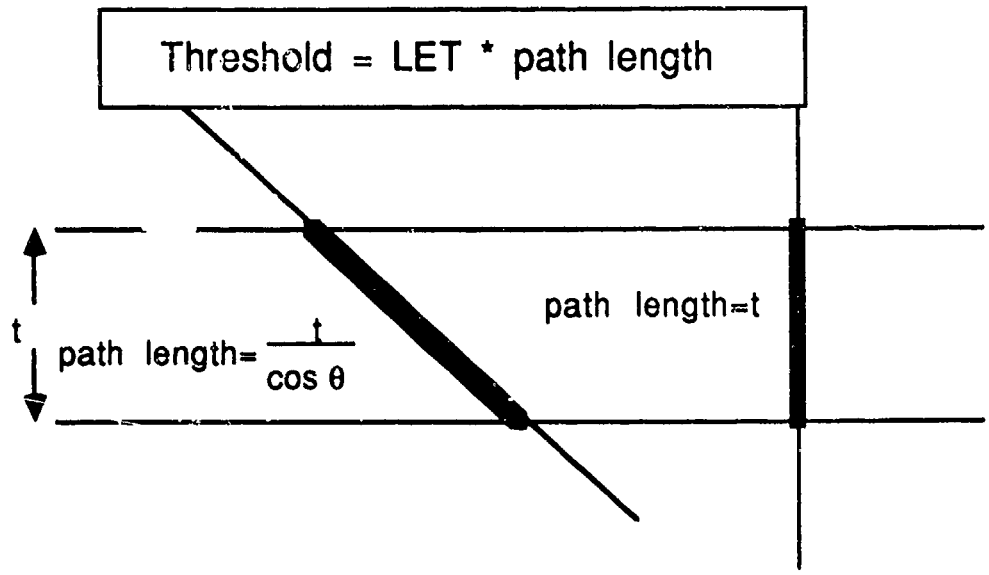

Figure 4-28. The Cosine Law

Currently, most single particle effect modeling assumes that all sensitive regions can be modeled as parallelepipeds, and take the measured cross section as an approximation to the normal area of the sensitive region parallelepiped. The actual thickness of the sensitive region of the device is then the thickness of the parallelepiped. This thickness can be determined experimentally by varying the ion species and energy of the incident particles and noting the SEU rate. Many times the depletion depth is taken as the thickness of the sensitive volume, when this is known, or it can be determined from doping profiles. When the actual device sensitive thickness is unknown, the thickness can be estimated by taking the thickness within the range of a likely thickness that produces the worst case upset rate.

For all single particle effects, the question of effective sensitive region as opposed to actual sensitive region must be considered. For example, a thin geometry might allow low LET-induced upsets but straggling might counteract this by not allowing the particles to remain within the sensitive region long enough for adequate charge collection. In addition, the slower charge collection from diffusion from outside the sensitive region might have to be included depending upon the circuits' behavior. The "charge funnelling effect" can either increase the effective size of the sensitive region or increase the rate and flux of outer charge collection. The actual geometries are not generally parallelepipeds as modeled and the LET will not remain constant. All of these effects can impact the actual path length distribution.

If the physical effects just mentioned can either be included in a simple geometrical model or shown to be of minor importance, then the path length distribution calculation reduces to a mathematical problem. The mathematical portion of this problem has been investigated by a number of researchers in recent years. Petroff derived the differential path length distribution for a parallelepiped. Shapiro, Petersen and Adams (1982) showed the equivalence of Petroff's equations with the integral path length distribution used by Pickel and Blandford (1980), calculated some examples for SEUs and discussed some of the approximations being used. Bendel (1984) greatly simplified Petroff's equations and investigated the characteristics of the distribution. Various forms of the Petroff equations along with other techniques are included in the current SEU models being used. Figure 4-29 shows a typical chord length distribution. In this case the spikes characteristic of a path through the volume in the direction of one of the sides of the box show up at 10 and 20 (the box dimensions).

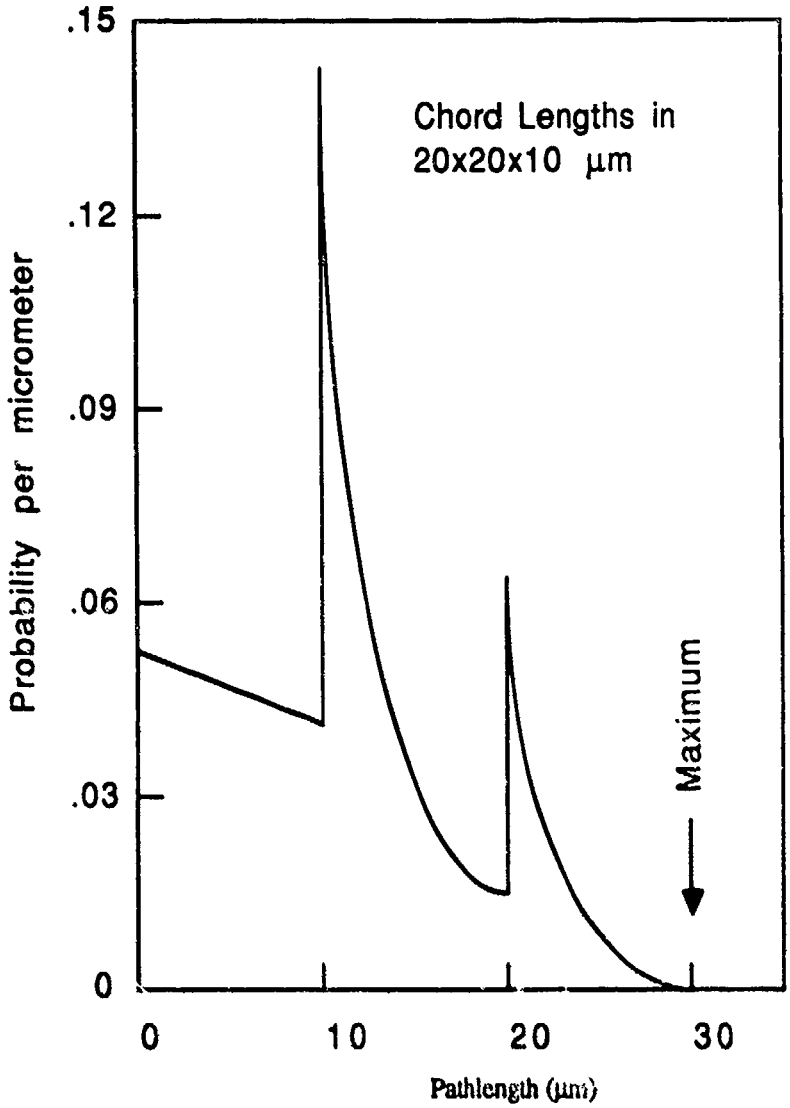

Figure 4-29. Path Length Distribution Function (Bender, 1984)

4.2.4. Part Data

The key component in predicting SEU rates is obtaining information about the part. The SEU rate is very dependent upon the technology and design of the circuit. The best situation is when there is a complete analysis of the part coupled with experimental SEU verification, e.g. Zoutendyck et al.'s (1985) analysis of the AM2901B part. Predictions of SEU rates are usually based upon limited analysis: a simulation of the part and/or accelerator testing to determine threshold LET and cross-section.

Transient circuit analysis determines the critical charge of the part if the equivalent circuit parameters are known or can be estimated. The circuits are modeled by computer simulation using programs such as SYSCAP or SPICE. The cosmic ray is simulated by application of a current pulse from a generator that is placed in parallel with the appropriate junction in the circuit. The current pulse amplitude is then varied to find the threshold for memory state change;. The critical charge is given by the time integral of the minimum current pulse to cause error.

Some only believe test results. Chapter 8 deals with SEU tests which determine the threshold(s), and cross section for SEU. If the threshold is low enough, both proton and heavy ion test results are needed to determine the SEU rate. A comprehensive SEU test plan will include if necessary temperature, frequency, voltage, and particle effects, and determine latch-up susceptibility.

4.2.5. Available SEU Rate Calculations

The following sections present two of the most popular techniques for calculating the SEU rate. The first, Petersen (1983) estimates the SEU rate based on the sensitive volume. The second, Adams (1981), includes a number of the factors we have discussed in this section. In all of these calculations the effects of shielding both by the mass surrounding the device, and by the magnetic field surrounding the spacecraft need to be included.

4.2.5.1. Petersen Approximation

If the critical charge and the dimensions of the sensitive region are known then the SEU rate can be approximated by the following formula:

$$R \propto \frac{a\,b\,c^2}{(Q\ \text{critical})^2} \qquad (4\text{-}22)$$

where a and b are the dimensions of the sensitive region that are perpendicular to the normal and c is the depth of the sensitive region. The proportionality constant will be dependent on the technology and the environment.

Since the critical LET is simply the critical charge divided by the depth of the sensitive region, the approximate rate can be given in terms of the device area and the critical LET as:

$$R \propto \frac{\text{device area}}{(\text{LET critical})^2} = \frac{\text{limiting cross-section}}{(\text{LET critical})^2} \qquad (4\text{-}23)$$

For geosynchronous galactic cosmic ray fluxes the error rate becomes,

$$R = 5 \times 10^{-10}\ \frac{\sigma\ [\text{microns}^2]}{\text{LET}\left[\frac{\text{picocoulombs}}{\text{micron}}\right]} \qquad (4\text{-}24)$$

where σ is the limiting cross-section (ab), and LET is the threshold LET = Qc, Q is the critical charge and c is the thickness of the sensitive region.

4.2.5.2. Detailed Calculation -- Adams, 1981

When upsets are caused by intensely ionizing particles originating outside the spacecraft, these particles generally pass through the sensitive volume of the memory cell at a high velocity, so that their rate of ionization or linear energy transfer (LET) does not change over the dimensions of that sensitive volume. This means that the LET spectra can be used to estimate upset rates. One method for estimating the upset rate is,

$$\text{rate} = 22.5\,\pi\,\sigma\,Q_{crit}\int_{\frac{22.5\,Q_{crit}}{d_{max}}}^{L_{max}} D[d(L)]\,\text{flux}(\text{let}>L_0)\frac{dL}{L^2} \qquad (4\text{-}25)$$

where,

$\text{flux}(\text{let}>L_0)$ is the integral LET spectrum inside the spacecraft in particles/m^2 ster s,

L is the LET in MeV cm^2/g,

the largest pathlength of the sensitive volume is $d_{max} = \sqrt{2\sigma + t^2}$

t is the thickness of the sensitive volume

D(d(L)) is the differential path length distribution of particles passing through the sensitive volume in cm^2/g,

σ is the surface area of the sensitive volume in m^2,

Q_{crit} is the minimum electrical charge (in picocoulombs) that must be generated by the ionizing particle to cause an upset,

$L_{max} = 1.05 \times 10^5$ MeV cm^2/g, the highest LET any stopping ion can deliver, and

22.5 is the constant required to get the units right assuming 3.6 eV per electron hole pair.

The relationship between LET and path length is $\rho = 22.5\ Qcrit/L$.

To use the rate equation given above for estimating upset rates, the LET spectrum inside the spacecraft must be calculated from the particle fluxes in the natural space environment. The constant 22.5 is the conversion from picocoulombs to MeV assuming 3.6 eV per hole-electron pair.

Adams, 1986, presents detailed results of SEU calculations. Figures 4-30 and 4-31 show some of his results. Notice that low critical charge devices can have very significant SEU rates.

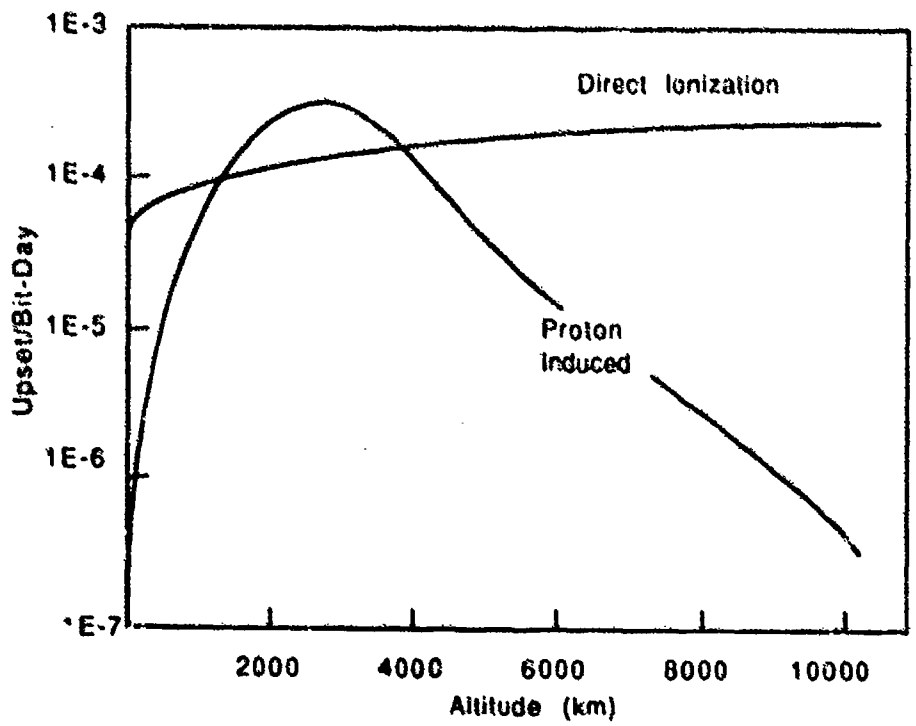

Figure 4-30 SEU Rate for 2901B (Adams, 1986)

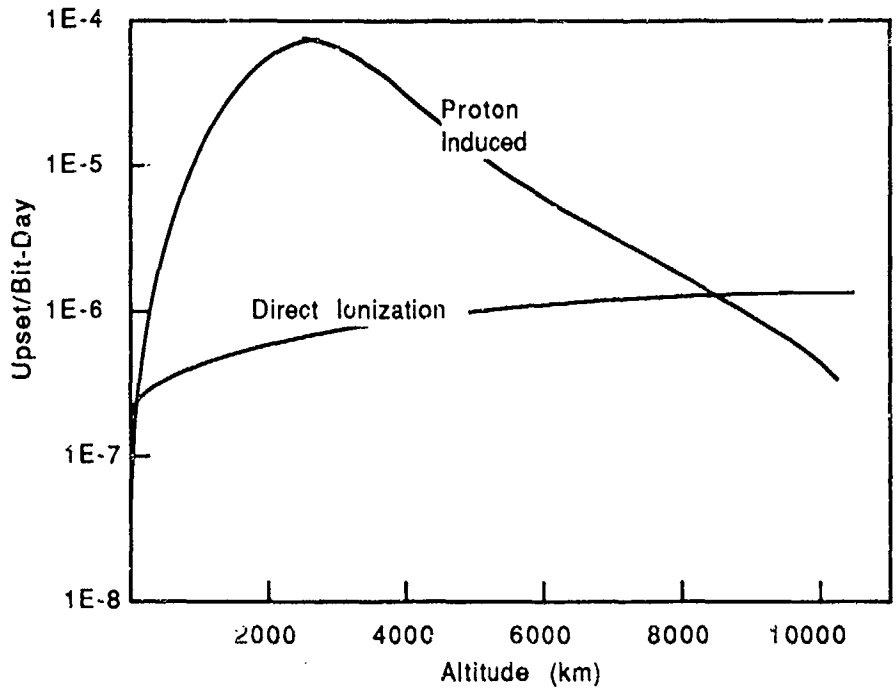

Figure 4-31. SEU Rate for SBP9989 (Adams, 1986)

The calculated SEU rates are for an AMD2901B. The device is assumed to be uniformly shielded by 0.1 inch of aluminum and in a 60° inclination circular orbit. The SEU rate is plotted versus orbital altitude, separately, for upsets that result from nuclear reaction caused by protons and upsets that result from the direct ionization of heavy ions (taken from Adams, 1986). The sensitive volume is taken to be 80x80x3 micrometers with a critical charge of 0.25 picocoulomb

Shown is a second example of calculated SEU rates. Conditions are identical to the 2901B calculation in the previous figure. Notice the large difference in the relative importance of proton induced SEUs and heavy ion induced SEUs. The sensitive volumes/critical charges for the SBP9989 are: 100x10x1.8/0.36(30%), 10x10x1.8/0.10(70%), 1x1x1.8/0.02(70%). Each of the last two sensitive volumes is only sensitive 15% of the time. This reflects the reduced cross section with which these low values of critical charge are observed.

4.2.5.3. Comparative Part Technologies

Each technology will need to be investigated to determine its SEU sensitivity. Nichols, 1987, has presented his assessment of today's technologies, Messenger and Ash, 1986, (p. 299, Table 7-3), give a very interesting table of SEU rate calculations (geosynchronous error rates vary from 10^{-9} to almost 10^{-3} errors per day bit). Guidelines are useful, but cannot substitute for detailed knowledge of the parts used on your mission.

4.3. Single Event Upsets Due to Protons

4.3.1. Introduction

Protons can cause SEUs either by direct ionization or by nuclear reactions which produce energetic heavy ions within the sensitive volume which cause the SEU. For that matter any particle which can produce recoiling heavy ions can cause SEUs. Protons at glancing angles will produce SEUs if their LET is high enough, and they are not deflected from the sensitive volume. No devices yet flown have been upset in this manner. However, a number of devices tested have proven susceptible to proton upsets via nuclear reactions.

SEUs caused by proton nuclear reactions involve a two-step process, first the proton must undergo a nuclear scattering. Second that scattering has to occur close enough to the sensitive region for the reaction products, alpha

particles, silicon atoms, etc., to reach and deposit enough charge in the sensitive region to cause the SEU. Assuming this mechanism is correct, proton caused SEUs will not be significant unless the heavy ion threshold is below about 8 Mev-cm^2/gm. This is because silicon has a Bragg peak at 17 MeV-cm^2/gm.Since the likelihood of producing Silicon knock-on ions at the Bragg peak is rare, an LET of 8 Mev-cm^2/gm is a reasonable rule of thumb. The probability (cross section) for proton collision is a strong function of energy -- rising rapidly as the energy increases. The proton flux is usually also a strong function of energy -- falling rapidly as the energy increases. Thus the proton SEU rate is a delicate function of energy.

Proton fluxes are discussed in more detail in the chapters on the environment (two and three). Typically, the cumulative proton flux for both flares and trapped protons can be fitted with a power law or perhaps several power laws for the energy region of interest.

$$\Phi = \Phi_0 (E)^{-P_1} \quad ; \quad E_1 > E > E_2 \quad \text{etc.} \quad (4\text{-}26)$$

The proton flux at the part is based on the energy-range relations given in Table 4-8. Computer codes exist which use proton cross sections to calculate proton fluxes behind one, two, or three dimensional configurations.

4.3.2. Semi-Empirical Proton SEU Cross-Section

The proton-induced upset cross-section is typically zero for proton energies below 15 to 20 MeV. Bendel and Petersen (1983) have suggested a semiempirical proton upset cross section as a function of an experimentally determined parameter A (E and A are in MeV),

$$\sigma = \left(\frac{24}{A}\right)^{14} \left(1 - e^{-0.18\left(\frac{18}{A}\right)^{1/4}(E-A)^{1/2}}\right)^4 \quad (4\text{-}27)$$

where σ is in 10^{-12} upsets-cm^2 per proton (Bendel and Petersen, 1983). After measuring the cross-section for proton upsets as a function of energy, A is determined by fitting the experimental data to the above equation. A is like a threshold, but is not strictly related to the threshold for nuclear reactions in the classical sense. If a great number of measurements are available, other fits or even numerical integration could be used to calculate the proton-induced upset rate.

4.3.3. Proton Upset Rate

The total proton upset rate is

$$\text{Rate} = \int_A^{\infty} \sigma(E) \times \frac{d\Phi}{dE} dE \quad (4\text{-}28)$$

The lower limit, A, is either the empirical parameter A given in the Bendel-Petersen formulation above or the threshold for the onset of proton-induced upsets.

Table 4-8. Stopping Power and Range of Protons (Janni, 1982)

Proton Energy MeV	LET Energy Loss MeV/g/cm^2	Proton Range mg/cm^2	Microns
.01	297.95	.034	.146
.0125	328.05	.048	.174
.02	412.5	.0579	.248
.025	456.2	.068	.293
.030	485.7	.0779	.334
.04	517.3	.0964	.414
.07	522.1	.151	.647
.1	491.7	.208	.894
.125	462.5	.259	1.113
.2	390.6	.433	1.86
.3	326.4	.711	3.05
.4	283.6	1.04	4.45
.7	211.1	2.27	9.74
1.	171.5	3.85	16.5
1.25	150.6	5.40	23.2
2.	110.7	11.3	48.3
3.	84.0	21.7	93.1
4.	68.4	34.9	149.8
7.	45.3	89.9	386.
10.	34.5	156.	713.
12.5	29.1	245.	1052.
20.	20.2	559.	2400.
30.	14.7	1147.	4920.
40.	11.7	1912.	8240.
70.	7.62	5167.	22177.
100.	5.84	9703.	41643.
125.	4.97	14345.	61567.
200.	3.63	32.3 gm/cm^2	138.480 mm
300.	2.86	63.6	273.
400.	2.47	101.3	434.9
700.	1.99	239.	1026.
10^3	1.81	398.	1707.
10^4	1.84	5530.	23736.

Chapter

5

The Lessons of History

5.1. Introduction

Perhaps the best argument for including the consideration of environmentally produced anomalies in the design of a space system is a good example of how the anomaly affected the operation of a system that did not design to exclude the environmental effect. In this chapter is a collection of reports on various systems that have been affected by environmentally caused anomalies. Table 5-1 summarizes a number of the known anomalies and their suspected causes. In almost every case, these space systems were pioneers which helped define the anomaly, and so should be looked on with gratitude for their pioneering work rather than as examples of designs which neglected good engineering practice. Technology is sometimes its own worst enemy in that environmentally produced effects that were insignificant for one technology are performance-threatening for an advanced technology.

Table 5-1 Spacecraft and Anomalies

System	Anomaly	Comment
Voyager 1	Power-on Resets	Internal Discharges (Leung, et al., 1980)
SCATHA	34 Pulses detected	4 attributed to ID; remainder to surface discharges
DSP	False flag from star sensor	Possible ID
DSCS II	Spin up/Amplified gain change power switching events	Correlated with geomagnetic activity
GPS	Clock shift False command	Made S/C non-operational in 1980, correlated with ID ID suspected as cause
INTELSAT III and IV	Spin up	
Skynet 2B	Telemetry	Partially correlated with A index and eclipses
ANIK	Power downs	
CTS	Short circuit noise bursts power inverter shutdown	Moderate substorm several hours earlier
Meteosat	Status changes	Correlated with geomagnetic indices
GOES 4 and 5	Upsets and failure	Environmental cause suspected; Loss of GOES 4 thought to be due to ID
Solar Max mission	93L422 part SEU	10 upsets/year in triply redundant majority vote RAM

5.2. GPS Operations -- contributed by Michael O'Brine, Air Force

During the past few years there appears to be a clear qualitative correlation between high solar activity and repeatable upsets occurring on board GPS space vehicles. In general we have noted that 3 to 5 days following sustained high solar activity certain upsets are possible. Most of these upsets have had serious consequences to space vehicle health, mission accomplishment, or both.

The first type of serious upset involves the space vehicle solar array drive electronics. This system autonomously steers the solar arrays normal to the sun to assure adequate power generation to support vehicle electrical loads. In April 1983 both solar array drives on Navstar 1 went into hold mode (i.e. not tracking) without being commanded to do so. This anomaly, which occurred while the vehicle was out of view, eventually caused the solar arrays to drift far enough off the sun to cause a negative power balance. This in turn caused protective timers on board to turn off all non-essential electrical loads after one hour, leading to loss of vehicle attitude control. The time required to safe the vehicle and return it to proper three-axis stabilization was two months, during which time the mission payload was non-functional.

This same upset occurred again on 8 November 1986, when one solar array drive on Navstar 11 went into hold mode without command. Fortunately, in this case the orbit conditions were more favorable, so the arrays did not go very far off the sun and loadshed (that is the turning off of all the experiments so that the attitude control electronics can be maintained in the face of a decreasing power source) did not occur. This type of upset remains a potential threat to future GPS Block I operations. The solar array drive electronics on GPS Block II space vehicles have been redesigned with latching relays to eliminate this problem.

Another serious upset related to high solar activity has been a series of uncommanded re-tunes of the on-board atomic frequency standard on Navstar 6. This problem has also occurred to a lesser extent on Navstar 2. The impact of this problem is to make the on-board navigation payload unusable until the frequency standard is brought back to its original tuning value by ground command. Switching frequency standards on Navstar 6 have reduced this problem.

High solar activity is also apparently related to upsets in the navigation signal baseband on all on-orbit GPS vehicles. When this occurs the navigation ranging codes transmitted by the vehicle to users become unsynchronized, making the vehicle unusable for navigation until ground intervention restores normal operation. This upset occurs randomly on all GPS vehicles.

In addition to the above examples, there are also a number of less serious upsets which seem related to solar activity. These include uncommanded resets of the on-board electromagnets and uncommanded reconfigurations of the telemetry PCM encoder. Payload operation is not affected by these problems.

In summary, while no GPS space vehicle has been lost or permanently damaged due to solar related upsets, there have been some close calls. In addition, navigation service to users has been interrupted on occasion due to these problems. A clearer understanding of these phenomena is required to prevent their occurrence on future spacecraft.

5.3. Voyager's Power On Resets

The Voyager 1 spacecraft experienced 42 power-on-resets (PORs) within the Flight Data Subsystem (FDS) during its passage through the radiation belts of Jupiter. The Voyager FDS is an on-board computer system containing a volatile memory system. During the design of this system it was recognized that power line undervoltage transients could cause malfunctions of the memory and hence uncontrolled computer operations. To avoid this situation, a circuit was added which sensed the voltage and sent a command to start the POR sequence if an undervoltage condition was detected. The power-on-reset sequence consists of stopping the processing, stopping the internal FDS clock, reinitializing the computations if necessary, waiting a minimum period of time, and restarting the processing if the undervoltage condition had ceased. Unfortunately in packaging this circuit for Voyager, the circuitry which sensed the undervoltage condition was separated from the command receiver which initiates the power down and power on sequence. This means that a wire connecting the undervoltage circuits and the command receivers ran through the system cabling. Subsequent testing on the ground verified that noise pulses in this cable bundle would produce the POR sequence seen at Jupiter. The sensitivity of the command receiver to pulses in the cable bundle is seen below in Figure 5-1.

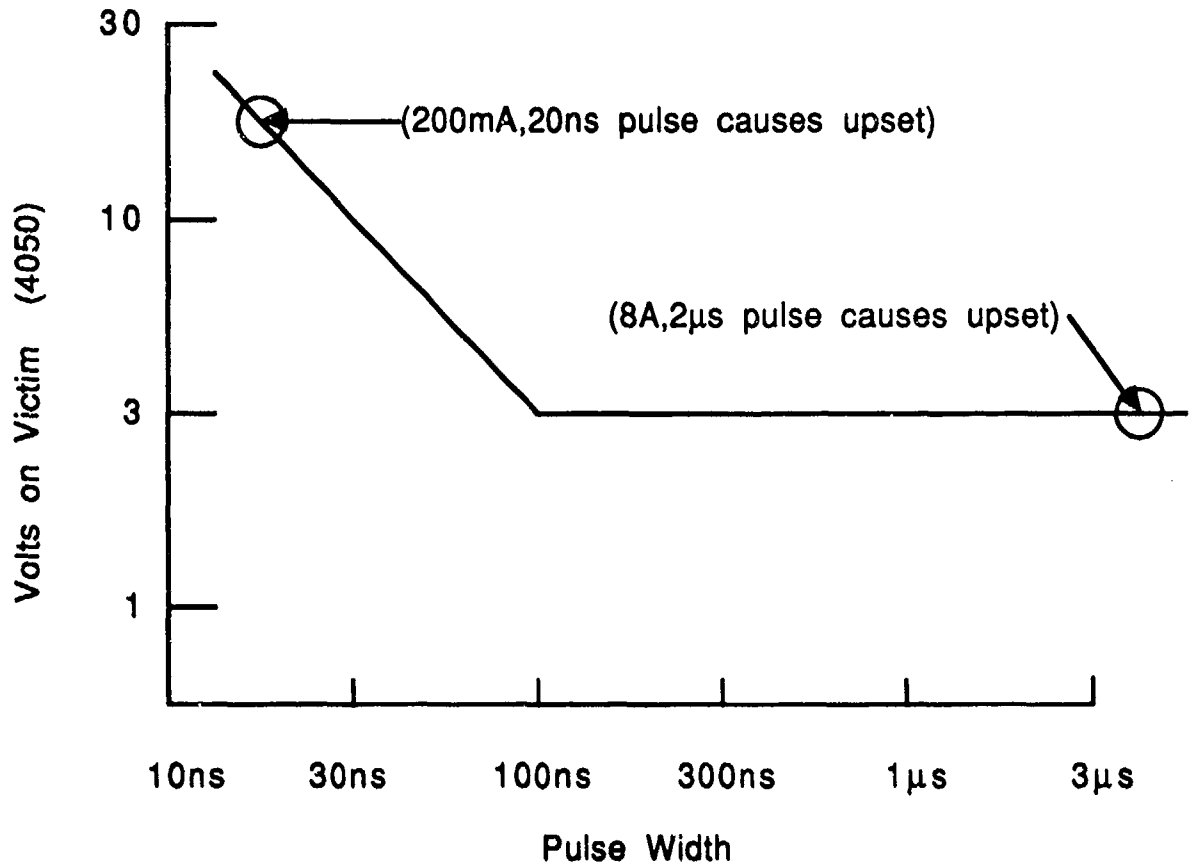

Figure 5-1. Sensitivity of Command Receiver to Noise Spikes

5.3.1. Effect of POR

Each time this happens a discrepancy of at least 175 milliseconds between the FDS clock and the spacecraft clock occurs. So the original indications of a problem were slight but important differences in camera angles for the pictures taken at Jupiter. This was eventually traced back to the scenario just outlined.

Attention now focused on the manner in which a noise spike could be generated to affect this cable bundle. Many of the mechanisms known to produce noise pulses were investigated -- surface charging, thruster firings, spacecraft mode changes by commands, velocity and wake effects, and single event upsets. None of these seemed particularly plausible; however, as seen in Figure 5-2, the unusual distribution of PORs correlates amazingly well with the high energy electron spectrum seen by Voyager 1.

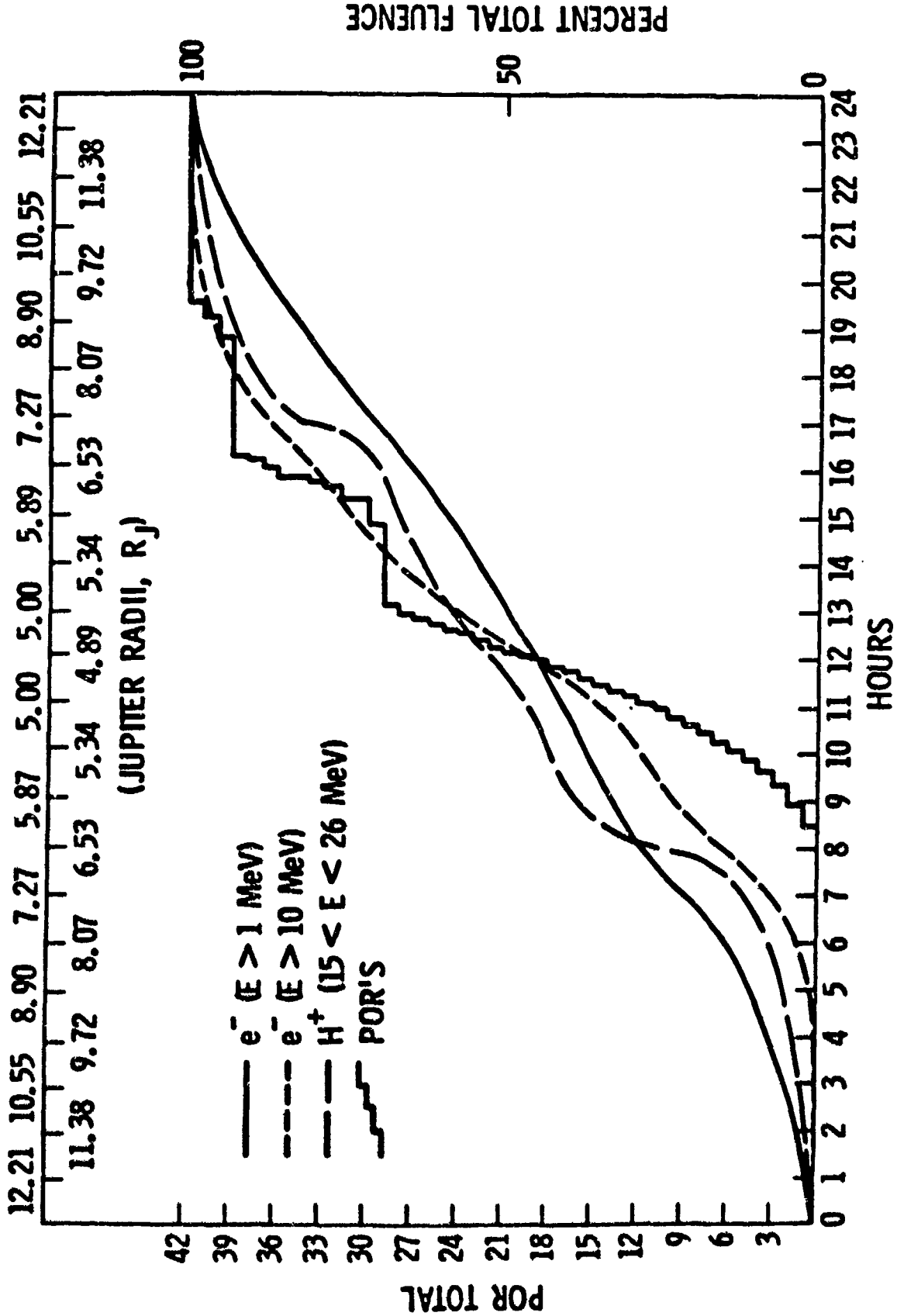

Figure 5-2. Correlation of PORs With High Energy Electron Environment

5.3.2. Environmental Correlation

Such a correlation indicated that the higher energy electrons were depositing enough charge within the spacecraft in a short enough period of time to cause a discharge. Ground test with Voyager flight spare cable bundles verified the occurrence of energetic electron caused noise spikes. Two classes of spikes were observed; some very short pulses which resulted in about one volt across a 50 ohm impedance, and some very short pulses with amplitudes near 100 volts. The higher voltages were due to short segments of wire that were inadvertently left floating in the wire bundle. These floating wires could have been spares that were not used, or the lead wires left on small connectors and not removed when the full number of connectors were not used for the bundle. Peak voltages as high as 100 volts with pulse widths of 500 nanoseconds or less such as those observed in ground tests cannot be ruled out for Voyager. Internal discharges such as these are thought to be the most likely cause of PORs on Voyager 1. The extremely harsh electron environment near Jupiter, shown below, (figure 5-3) makes internal discharging particularly likely since cables in thinly shielded areas will see higher electron fluxes than they would near other planets.

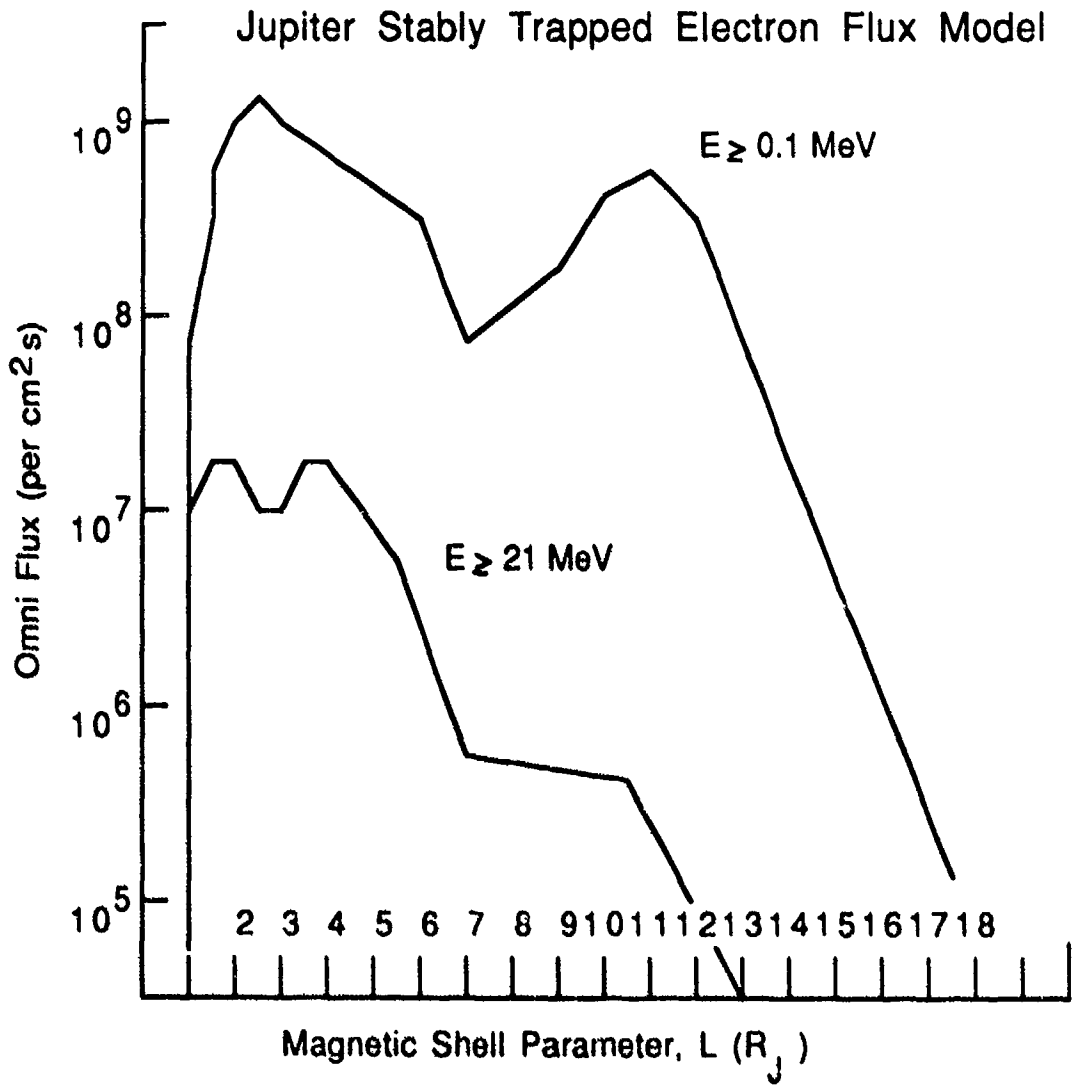

Figure 5-3. Jupiter's High Energy Spectra

5.4. GOES 4 and 5 Anomalies -- Winfred Farthing, GSFC

The Geostationary Operational Environmental Satellite, GOES-4 was launched on 9 September 1980; GOES-5 on 22 May 1981. The primary instrument, an atmospheric sounder, on both GOES-4 and GOES-5 is the Visible and Infrared Spin Scan Radiometer (VISSR). This instrument observes the earth using the spin of the spacecraft to scan in the east-west direction. A mirror is stepped to produce scans in the north-south direction. There are eight channels of data taken in different spectra regions covering the visible and infrared regions of the spectrum.

Subsystems aboard GOES-4 and -5 have shown numerous instances of anomalous changes in state corresponding to false commands. Table 5-2 covers a 15 month period for GOES-4 and a 6 month period for GOES-5. There were 27 anomalous commands recorded during that period, 14 on GOES-5 and 13 on GOES-4. The first anomaly observed on GOES-4 (29 March 1981) was an uncommanded stepping of the VISSR mirror. Simultaneously the gain in one of the visible channels (number six) had an uncommanded gain step. On 1 April 1981, the mirror again began uncommanded stepping. Ground magnetograms examined shortly after these anomalie showed evidence of substorm activity, suggesting that these anomalies were environmentally induced. Initial suspicions focused on surface charging as the cause of these anomalies. A search of the instrument for a site of differential charging revealed that part of the VISSR second stage radiation cooler was ungrounded. The inner member of this assembly was grounded through a wire which went into the VISSR electronics package. It was proposed that charge built up on the ungrounded radiator until a breakdown occurred across the insulating epoxy bonding the two parts together. The resulting current surge was then conducted through the ground wire into the VISSR electronics. Tests performed on the GOES-5 spacecraft which at that time was awaiting launch at the eastern test range (ETR) confirmed that the radiator was indeed ungrounded. GOES-5 was modified to ground the radiator. GOES-5 did not experience this particular command anomaly, but has experienced a number of "phantom commands."

Table 5-2. GOES 4 and 5 Anomalies

DATE	SPACECRAFT	UNIVERSAL TIME	ECLIPSE TIME	COMMAND NUMBER(S)	COMMAND NUMBER(S)
3/29/87	GOES-4	11:42:00	08:32 TO 09:34	301/334 AND 302	STEP SCAN ON (PRIMARY OR REDUNDANT COMMAND) VISIBLE CHANNEL 6 GAIN STEP
4/1/81	GOES-4	09:55:31	08:33 TO 09:34	331/334	STEP SCAN ON
4/1/81	GOES-4	10:10:22	08:33 TO 09:34	301/334 AND 302	STEP SCAN ON (PRIMARY OR REDUNDANT CMD) VISIBLE CH.6 GAIN STEP
4/13/81	GOES-4	09:03:17	NO ECLIPSE	331/334	STEP SCAN ON (PRIMARY OR REDUNDANT CMD)
4/14/81	GOES-4	11:36:35	NO ECLIPSE	331/334	STEP SCAN ON (PRIMARY OR REDUNDANT CMD)
4/17/81	GOES-4	08:38:22	NO ECLIPSE	331/334	STEP SCAN ON (PRIMARY OR REDUNDANT CMD)
4/19/81	GOES-4	12:35:22	NO ECLIPSE	331/334	STEP SCAN ON (PRIMARY OR REDUNDANT CMD)
4/20/81	GOES-4	14:35:22	NO ECLIPSE	331/334	STEP SCAN ON (PRIMARY OR REDUNDANT CMD)
4/21/81	GOES-4	14:45:44	NO ECLIPSE	030	VDM HALF RESOLUTION
4/24/81	GOES-4	09:40:33	NO ECLIPSE	331/334	STEP SCAN ON (PRIMARY OR REDUNDANT CMD)
4/26/81	GOES-4	08:36:27	NO ECLIPSE	331/334	STEP SCAN ON (PRIMARY OR REDUNDANT CMD)
8/20/81	GOES-5	08:21:58	NO ECLIPSE	301	CH. 7 GAIN STEP (FROM 2 TO 3)
8/23/81	GOES-5	11:08:05	NO ECLIPSE	301	CH. 7 GAIN STEP (FROM 2 TO 3)
8/28/81	GOES-5	05:20:39	NO ECLIPSE	301	CH. 7 GAIN STEP (FROM 2 TO 3)
8/29/81	GOES-5	10:17:01	NO ECLIPSE	301	CH. 7 GAIN STEP (FROM 2 TO 3)
9/11/81	GOES-5	12:01:39	0426-0527	301	CH. 7 GAIN STEP (FROM 2 TO 3)
9/12/87	GOES-5	10:47:33	0425-0527	301	CH. 7 GAIN STEP (FROM 2 TO 3)
10/2/81	GOES-4	14:49:41	0819-0923	030	VDM HALF RESOLUTION
10/10/81	GOES-5	07:11:03	0421-0511	301	CH. 7 GAIN STEP (FROM 2 TO 3)
10/10/81	GOES-5	08:35:55	0421-0511	301	CH. 7 GAIN STEP (FROM 2 TO 3)
10/11/81	GOES-5	07:46:22	0423-0510	301	CH. 7 GAIN STEP (FROM 2 TO 3)

Table 5-2. GOES 4 and 5 Anomalies (Cont'd)

DATE	SPACECRAFT	UNIVERSAL TIME	ECLIPSE TIME	COMMAND NUMBER(S)	COMMAND NUMBER(S)
10/12/81	GOES-5	08:57:35	0425-0507	301	CH. 7 GAIN STEP (FROM 2 TO 3)
10/21/81	GOES-5	09:14:00	NO ECLIPSE	301	CH. 7 GAIN STEP (FROM 2 TO 3)
11/12/81	GOES-5	10:58:00	NO ECLIPSE	301	CH. 7 GAIN STEP (FROM 2 TO 3)
11/23/81	GOES-5	06:46:11	NO ECLIPSE	301	CH. 7 GAIN STEP (FROM 2 TO 3)
11/23/81	GOES-5	10:58:36	NO ECLIPSE	301	CH. 7 GAIN STEP (FROM 2 TO 3)
11/23/87	GOES-4	12:10:16	NO ECLIPSE	331/334	STEP SCAN ON

5.5. GOES-4 Failure -- contributed by Daniel Wilkinson, National Geophysical Data Cente

The Visual Infrared Spin-Scan Radiometer (VISSR) on board the western Geosynchronous Operational Environmental Satellite (GOES-4), failed at 0445 UT, November 26, 1982, as a series of intense storms descended on the California coast. The VISSR maps the earth and its cloud cover day and night and allows the tracking and forecasting of severe storm systems. This failure of the VISSR on board GOES-4 deprived weather forecasters of a important means of tracking the nighttime progress of life-threatening storms as they moved across the Pacific.

The cause of this critical satellite failure is of great interest to the National Oceanic and Atmospheric Administration (NOAA), operators of the GOES network. A study now in progress should resolve the reason for failure and determine whether solar activity caused it. Figure 5-4 was prepared at the National Geophysical Data Center in Boulder, Colo., in response to a call for information about the earth's space environment at the time of th GOES-4 failure.

All GOES spacecraft carry a Space Environment Monitor (SEM) instrument package containing an X-ray sensor, a three-component magnetometer, and a particle detector. Together these instruments provide continuous monitoring of the space environment at the satellite's altitude. SEM data from selected satellites are received and processed for archiving at the Space Environment Laboratory in Boulder. When GOES-4 failed at 135 W longitude the reference satellite for SEM archival purposes was GOES-2, located at 108 W longitude. The proximity of the two satellites suggested that their local environments were similar, and selected data from representative GOES-2 channels were reproduced for November 25-26, 1982.

The top frame of Figure 5-4 shows the prominent X4.5 solar flare reported by the Space Environment Services Center at 0229 UT. Owing to the intensity of the flare and the history of its associated sunspot region, forecasters at that center immediately posted a proton event warning.

Close inspection of the middle frame shows that indeed the fast, high energy protons in the 110-500 MeV range began arriving at the satellites approximately 45 minutes before failure, with slower protons arriving in quantity a few minutes after failure. Counts of electrons trapped at geostationary altitude, 6.67 earth radii, often sho a quiet-time daily variation, a variation that produces lower electron counts in the UT morning than in the UT evening. The electron curve does not drop to quiet-time values on the morning of November 26, indicating the satellite environment contained a significant electron flux at the time GOES-4 failed. Lacking spectral information for electrons, however, we can give no detailed interpretation of their importance.

The magnetometer's three field components are defined as follows: H_p is parallel to the satellite spin axis and is perpendicular to the satellite's orbital plane; H_E lies parallel to the satellite-earth line and points earthward; H is perpendicular to both H_P and H_E, and points westward. No magnetic storm activity was indicated when GOES-4 failed. Note, however, the correlation between the H curves and the electron curve.

This display of the SEM data does not determine the cause of the GOES-4 failure. It does nevertheless rais the question of solar activity as a contributing factor. According to NASA Headquarters, there are currently 86

surveillance and communications satellites in geostationary orbit, representing a U.S. investment in the tens of billions of dollars. An investment of this size will eventually stir renewed interest in Solar-Terrestrial relationships.

[Space environment data from the GOES system have been archived continuously since July 1974 and are available for sale through the Solar-Terrestrial Physics Division of the National Geophysical Data Center -- an organization known internationally as World Data Center A for Solar-Terrestrial Physics. Inquiries should be addressed to the National Geophysical Data Center, NOAA Code E/GC2, 325 Broadway, Boulder, CO 80303 (telephone 303-497-6136).]

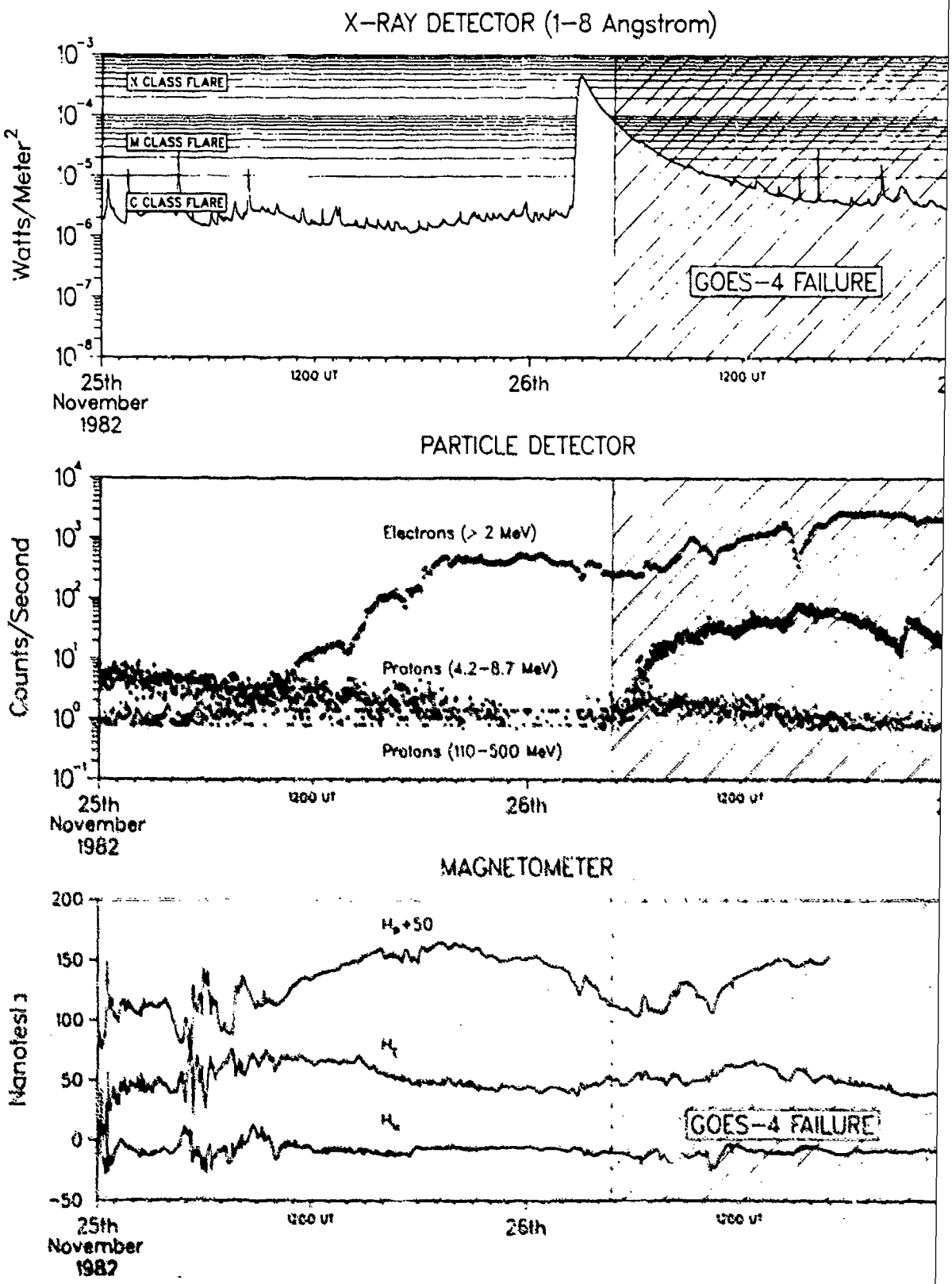

Figure 5-4. Correlation of Failure With Environment

5.6. Los Alamos Anomaly Studies -- contributed by Dan Baker, Los Alamos National Laboratory

The Space Plasma Physics Group of the Earth and Space Sciences Division at Los Alamos National Laboratory has available to it data from a number of instruments in orbit. When investigating anomalies of spacecraft, especially at geosynchronous orbit they often begin with the high-energy electron data at geosynchronous orbit. Figure 5-5 illustrates how helpful such data are in identifying the source of anomalies. In this case star tracker upsets occur only on those occasions when the high energy flux exceeds a certain level. This indicates some sort of internal charging anomaly (see Figure 5-5).

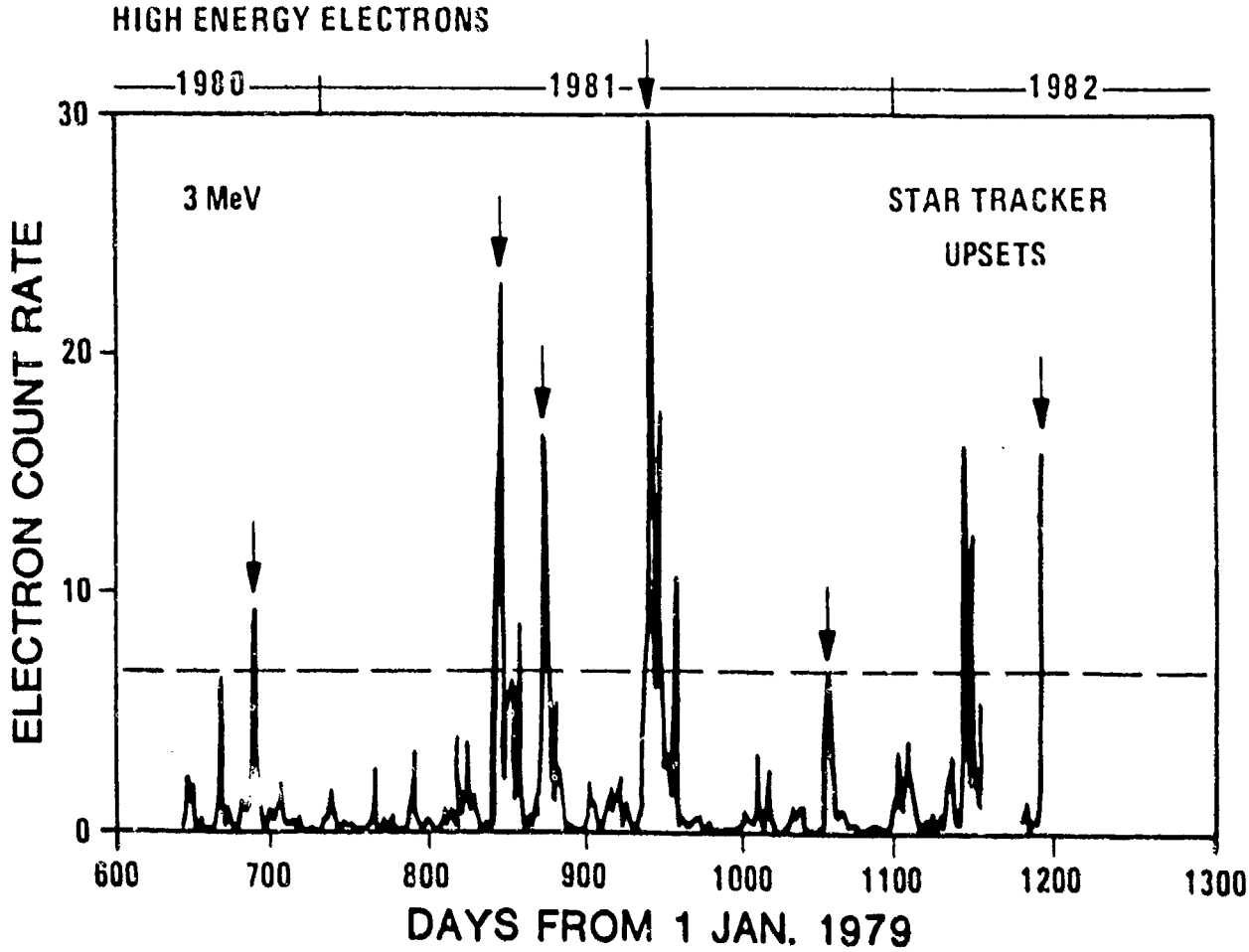

Figure 5-5. Electron Count Rate Versus Upsets

5.8 Operational Impact

From an understanding of surface charging/discharging, internal charging/discharging, and SEU phenomena gained from the previous chapters and the adverse effects these have had on operating space assets as discussed in the previous chapter, it is clear that something must be done to avoid the adverse effects on space systems of the environments responsible for surface and internal charging and single event upsets. Literally thousands of anomalies have been experienced in recent years. Each succeeding generation of electronics has seemingly brought a higher degree of susceptibility to these phenomena than those before. This is not surprising because the goal of improved technologies is to "do more with less," that is to make electronics faster, using less power, and controlling more. This translates into having smaller amounts of charge representing more information than ever before. Thus, smaller disruptions are more likely to disturb electronics. These anomalies will not disappear unless the scientific

and engineering communities understand and allow for what is truly unavoidable, and avoid what can be avoided. In the remainder of this chapter, the impacts due to surface and internal charging/discharging and SEU will be discussed along with operational techniques which are required for space systems which are not successful in eliminating susceptibility to these problems. In general, of course, it would be better to have space systems which are completely insensitive to the environment. Engineering for immunity will be discussed in chapter 7.

5.8.1 Surface Charging

The occurrence of charging on the surface of a spacecraft produces effects that can be divided into two areas: (1) engineering problems due to discharges resulting from the surface charging, (2) the corruption of measurements due to the charged surfaces.

Operational work-arounds for these anomalies include reloading memories, toleration of noisy data, switching to redundant units, and restarting sequences. In cases where attitude control and station keeping are concerned, it may require real time updating of attitude control commands. If the discharge rate is low enough this may only mean an occasional correction. In some cases the discharge merely results in a "flutter" of the control system which is automatically corrected when the system is updated automatically. Predictions of expected charging periods are helpful in this case so that the spacecraft can be monitored more closely during periods of expected discharges. For example when a spacecraft enters or emerges from eclipse, surface and internal discharges are more likely than during sunlit times. Periods of solar activity or solar flares are also times in which operational alertness is essential for spacecraft with known susceptibility to environmental anomalies.

5.8.1.1. Engineering Concerns -- Discharges

The engineering problems in the power subsystem show up as transients on the power line, loss of power if the plasma density in the region of the solar cells is too high, discharges on exposed high voltage electrodes, damage to solar cell structures and erosion of the regions near the discharge points, and reduction of the efficiency of solar cells by the reattraction of contamination to solar cell covers. Most of these effects result in a slow degradation of the system as the transients are typically damped out by the heavy filtering of the power subsystem. In that case a graceful degradation in the operations of the system occurs. When sudden discharges or shorts occur in the power system, however, the operator may have to power down and then power up the space system to restore the system to a known operating position.

Communications subsystems are affected by transients in the received or transmitted signals, disturbances or destruction of sensitive electronics at the transmit and receive points in the system (especially those parts of the electronics exposed to the environment in the receive or transmit antennas), power loss due to phenomena such as multipacting which is related to surface charging through the plasma properties of the ambient environment and the potential of exposed contacts in the communications system, and power loss due to the problems mentioned in the power subsystem. In many cases switching to a redundant system will restore normal operation to the system. However, care must be exercised if one part of the redundant system has been damaged or responds in an unusual way. Careful planning before launch based on a detailed understanding of the space system and reasonable ground tests usually is needed for confident response to real-time space situations.

Attitude control, data processing and other subsystems are affected by surface charging and related phenomena primarily through transient signals transmitted from the discharge sites through the cabling of the system to the victim circuit. Most spacecraft built today rely in part on a Faraday shield design which tends to provide good isolation between the electronics and the environment outside. Careful and complete EMC testing usually eliminates coupling of transients caused by surface charging to the electronics inside the Faraday shield; however, the requisite feed throughs and openings in the structure of the spacecraft allow for some transmission of transients from the exterior to the electronics inside. Currents from one major part of the structure to another (for example the spinning and despun parts of a communications spacecraft couple easily to electronics inside the spacecraft. Anytime a transient could be responsible for the observed anomaly, surface charging needs to be considered as a possible cause. Promptly characterizing and reporting such anomalies will help determine whether they are environmentally caused or indicate another problem.

5.8.1.2. Charged Surface Concerns

For some applications, only when a discharge occurs is there a concern. In other cases, the fact that a surface or surfaces are charged is a concern directly. For example if you have an instrument that is attempting to measure the low energy part of the plasma environment, even uniform charging of the spacecraft to some potential with respect to the ambient environment will distort the flux of electrons available for analysis to the instrument. Surfaces at different potentials with respect to each other and the space environment will further complicate the analysis of the instrument measurements. The charging and discharging of surface elements as they are exposed to the sun and shadow easily generate currents that can affect sensitive sensors or electronics. An earth sensor was affected in this way on an early communication satellite (Wadham, 1986) even though there was no violent discharge in the usual sense. The alternate charging and discharging of the sensor's body produced unwanted signals in the sensor circuit. This is one reason that the sun-system-earth angle is interesting in diagnosis of anomalies. Any periodic behavior in synchronism with spin periods or rotation periods may indicate this type of charging/discharging phenomenon.

5.8.2. Internal Discharge

Internal charging/discharging presents a similar situation to that just described under surface charging, except the point of charging or discharging is now located inside the Faraday cage, and is therefore more likely to couple directly to the victim circuit. Thus a much smaller discharge in terms of total energy or charge is of concern since the coupling efficiency is much greater. The mechanism is slightly different for internal discharges in that no photocurrents are present. When transients or discharges are capable of producing the anomalous behavior under investigation but no surface charging exists, internal charging/discharging in lightly shielded cables or electronics should be investigated. Near earth internal charging events tend to be irregular both because the flux required to produce them is usually present only sporadically, and because the time to discharge once the flux is present is a random variable.

No anomalies have yet been attributed to internal charging without a discharge, but one can imagine a particularly sensitive circuit where large volumes of charged dielectric influence measurements.

5.8.3. Single Event Upsets

Single event upsets (SEUs) always occur in the memory parts of integrated circuits. Whenever there are mistaken commands or data, single event upsets are a possible cause. When single event upsets are suspected, the parts holding or processing the anomalous data should be investigated to see if any of those parts involved are SEU sensitive. First consult the data on parts already tested by various organizations. In general one would expect SEUs to be a very random occurrence. However, there are cases (solar flares, magnetic shielding, and heavy ion radiation belts) which increase or decrease the likelihood of SEUs. Once the parts' sensitivity is established, the environment will determine the expected SEU rate. Any peculiarities in occurrence are important in distinguishing the various possible causes of an anomaly. Cycles in the occurrence of anomalies should be examined for operational cycles as well as environmental dependence. Sometimes certain activities are more sensitive to the detection of an anomaly than others. Power cycling, data processing cycles, etc., can superimpose behavior on an anomaly rate which has little or nothing to do with the environmental cause of the anomaly. It is especially important in SEU investigations to understand the operational variables in determining the anomaly cause. Operationally, once SEUs are known to be occurring, the usual procedure is to correct the mistaken bits of information by reloading part or all of the memory. Although not discussed in this text, single particles can cause hardware failures. In evaluating a failure or anomaly, single particles from cosmic rays or trapped heavy ion belts need to be considered especially as integrated circuits get smaller and faster.

5.9. Obtaining Environmental Data and Reporting Anomalies

Environmental data is available through either the DOD or civilian groups listed below.

5.9.1. Air Weather Service

The Air Weather Service, through its staff weather officers and staff meteorologists, provides both real time and historical data and analyses to meet the requirements of any Air Force project. This is typically done through Support Assistance Requests (SARs). If the data or models are lacking, action can be taken to obtain the required data or capability. In addition, customers are encouraged to contribute data from their systems to further enhance the general database. A real time database of observed or suspected anomalies at the Air Force Global Weather Central, based upon operators' reports not only encourages participation by others but also enhances the confirmations of environmentally induced anomalies.

Air Force Global Weather Central (AFGWC) through AFGWC/WSE provides real time operational support in both 24 hour center and tailored support modes. USAFETAC provides retrospective analysis for those programs doing anomaly investigations with a long time history. Contact the appropriate military officers to obtain this support.

5.9.1.1. Air Weather Service Support Organization

The Air Weather Service support organization is organized into two groups, staff weather officers and staff meteorologists.

5.9.1.1.1. Staff Weather Officers (SWOs)

SWOs are collocated with major Air Force commands. For example, the HQ 4th Weather Wing stationed in Colorado Springs supports North American Aerospace Defense Command, Unified U. S. Space Command and Air Force Space Command. Staff weather officers obtain data for operational use.

5.9.1.1.2. Staff Meteorologists

Staff meteorologists (Staffmets) are collocated with Air Force Systems Command Product Divisions and Laboratories. For example Detachment 50, 2nd Weather Squadron is located at Space Division.

Staff meteorologists obtain data to assist system designers, developers, and engineers in overcoming environmental problems. Staffmets should be used early in each program so that the systems can be designed with due consideration to environmentally induced anomalies.

5.9.1.2. Real Time Monitoring System

Both ground-based and satellite data is collected at AFGWC. The actual data is collected in near real time and is available soon thereafter. A database is maintained for a number of days at AFGWC before it is shipped to USAF Environmental Technical Application Center (USAFETAC) for permanent storage.

5.9.2. NOAA Space Environmental Laboratory -- Reporting Anomalies

The Space Environment Service Center (SESC) provides a real time support and forecast service for operations that are affected by solar-geophysical activity. Their number (24 hours a day 7 days a week) is (303) 497-3171. This is an evolving service, but anticipates providing real time data for anomaly investigations and near real time data for up to one month in the past. It is coordinated with the National Geophysics Data Center (below). When reporting an anomaly the following information is typically asked for:

Customer name, organization and spacecraft
Start and stop time of the anomaly
Location of the spacecraft
Any usual or unusual operations
Description of the anomaly
Any communications problems
Satellite local time, and Sun-vehicle-earth angle

5.9.3. National Geophysical Data Center

The National Geophysical Data Center (NGDC) supports retrospective data request and analysis. A database of spacecraft anomalies is maintained at the Solar-Terrestrial Physics Division of the NGDC in Boulder, Colorado. It includes the date, time, location, and other pertinent information about incidents of spacecraft operational irregularities which are suspected to be due to the environment. These events range from minor operational problems which can be easily corrected to permanent spacecraft failures. The data base includes spacecraft anomalies in interplanetary space and in near-earth orbit. The majority of the data base comes from geostationary spacecraft. About 1600 anomalies have been reported as of June 1987. The data base includes data from several nations. The database is maintained on an IBM compatible personal computer in a dBase III type file. To facilitate access to the information, custom software has been written to perform a full range of functions for managing, displaying, and analyzing the contents. The Spacecraft Anomaly Manager (SAM) software has the added benefit of
encouraging operators to report their anomalies in a uniform, ready-to-use format. Satellite operators can use SAM to create a database containing only their anomalies and forward the data to NGDC (address in Appendix 3) on a floppy disk for inclusion in the master archive.

Histograms of local time, and seasonal frequency show distinct patterns for spacecraft susceptible to static charge buildup and subsequent discharge. SAM includes functions to display anomaly collections versus local time and season. The figures in Appendix 3 show these functions for the GOES satellite.

The data and software are currently available on two IBM compatible floppy disks for the nominal cost of $30 per disk. Contributors of anomaly data may obtain the disks on a data exchange basis.

5.10. Unreported Anomalies

One of the most fruitful collaborations is between those that study the environment and those operating spacecraft in that environment. More than providing engineers with essential data needed to improve future designs, it alerts operations to environmental concerns and provides essential clues to understanding the environment itself. One of the hopes for this text is that it will bring together these two groups in ways that will advance the goals of both groups. Unreported anomalies are a loss to both the spacecraft operators involved and to their larger communities. The effort required to report and analyze an anomaly yields a better understanding of the spacecraft, its operations, and the behavior of the environment, and suggests better engineering techniques for future designs.

Chapter

6

Engineering for Immunity

6.1 Organizing for Success

This chapter presents the concepts needed to conduct a successful design and fabrication of a space system, which properly considers the possibility of the environment inducing anomalies via surface charging or discharging, internal charging or discharging and single event upsets. It is most desirable that any hardness or immunity assurance plan be implemented at the very outset of the program. This alerts everyone involved with the program that immunity to ESD, Internal Discharge and SEU must be considered in all appropriate trade-off studies.

There is no sure "fix" for any one of these anomaly causing phenomena, nor does a solution for one necessarily provide a solution for the other two. Such a cure-all does not currently exist. However, there are mitigation techniques, circumvention methods, and design approaches which can and are being employed to minimize the deleterious effects of surface charging/discharging, internal charging/discharging, and SEU on satellite systems. The timely adaptation of the practices and procedures outlined in this chapter can achieve this goal.

A successful assurance plan begins at the inception of the program and is carried through every trade-off and system design decision. The only sure fix for any anomaly producing phenomenon is careful attention to the phenomenon throughout the program. It may not be possible to simultaneously fix every problem, however the early awareness of each phenomenon and careful consideration of its impact and importance enable a program to find the engineering solutions which will best meet each program's unique needs. The recent experience of the design of the Galileo spacecraft illustrates this point. When the parts for the attitude and control system were first chosen, single event upsets were not widely known or appreciated. Improvements in the size and speed of microelectronics were driving microelectronic parts in the direction of increasing sensitivity to single event upsets. When this fact became known, new parts were required to meet both the old requirements for memory, total dose radiation hardness, speed, and the new requirement of SEU hardness.

The keystone of engineering for immunity is a well thought out immunity program. This program will be as individual as the design team and the project. The plan should begin with the management structure already in use by the design team. By building on the familiar management structure, environmental design consideration responsibilities can be added to the appropriate design groups, or cost centers as necessary. This makes immunity to environmental effects the same as any other system problem. Consequently environmental concerns will compete with other considerations at the design level, for the limited resources in time, money, and effort.

One way to organize a large system effort is to develop a series of project documents which spell out what is going on. These not only relate the technical requirements and methods of analysis, but describe the manner in which various organizations within the parent organization operate. With the possible exception of a "skunk works," all projects need documents to know how to respond to requirements. "It's not what you don't know, but

what you don't do" that determines the success of a program. Every Sunday morning quarterback knows exactly what you should have done and why you should have known to do it. The trick is doing all the things you know have to be done. Project documents can outline the plan for avoiding problems.

The key to getting all of the activities done which need doing in a complex undertaking is to put the responsibility for each task with the person who can perform that task. It is important to tailor the task to fit the players. All involved should understand what is required of them, how they are going to do it, and whom they are going to give their results to.

Project documents if carefully thought out are one way to do this. It certainly isn't the only way, but for a large project involving many people with finite capacities for remembering what they need to do, it certainly is a good way to do it. (It certainly makes the job of finding out after the fact how things were done easier.) Project documents codify requirements, and institutionalize operating procedures.

The assurance program is nothing more than making sure that the above process is thought through, and is being followed.

In the table below (Table 6-1) are some documents which can be incorporated into system design and planning thinking.

Table 6-1. Guidelines/Military Standards

High Voltage Standards/Handbooks	
MIL-STD-1540	Test Requirements for Space Vehicles
MIL-STD-1541	EMC Requirements for Space Systems
EMC and EMI	
DoD-STD-1686	ESD Control Program for Protection of Electrical and Electronic Parts
DoD Handbook 263	ESD Control Handbook for Protection of Electrical and Electronic Parts
	AFSC Design Handbook 1-4, Electromagnetic Compatibility

Problems can be thought of as having a cause, a medium through which the problem is transmitted and a victim. The system approach to eliminating problems is to look at each element of this path and decide what combination of actions is required to eliminate the problem (see Figure 6-1). Requirements describe the threat. Sometimes the environment can be changed. For example, don't launch during a large solar flare, or, don't fly through the radiation belts.

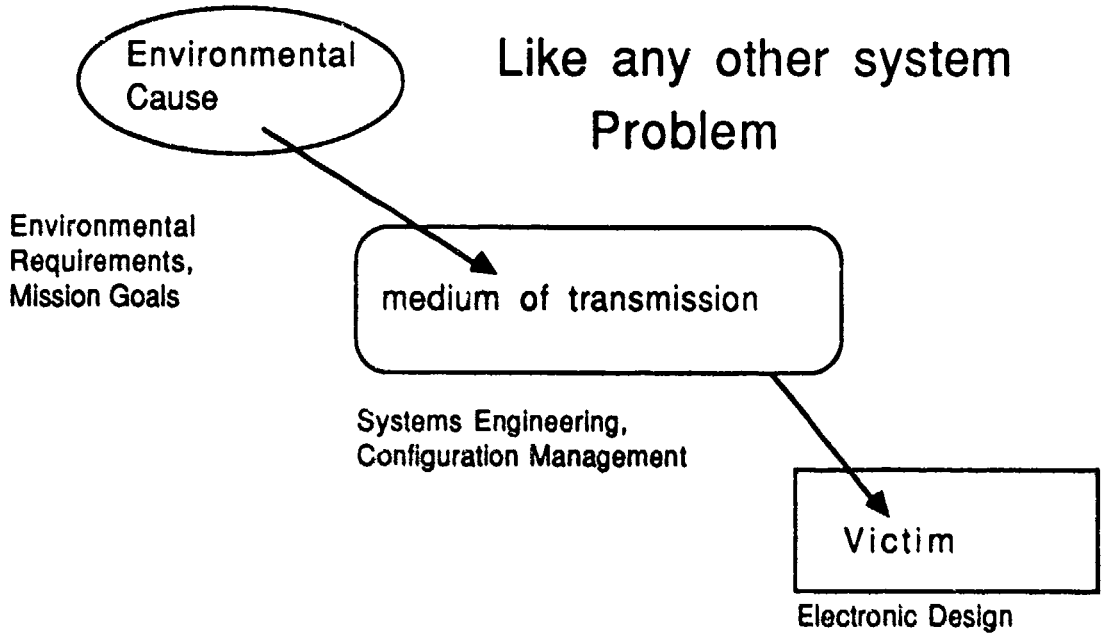

Figure 6-1. Cause-Transmission-Victim Chart

A number of possibilities exist in the configuration and system engineering areas to control the transmission of the environmental effects. The final line of defense is at the victim's level. For example the circuit design itself may be made immune to the effect. This approach, to make the radiation problem look like any other system problem so that it could be attacked on all three levels in a coordinated manner, benefits from the ideas of the entire design team.

System and subsystem reviews provide the program with the visibility to ascertain whether or not immunity is being designed into the system. Reviews are convenient milestones for logging the acceptance of the hardness program and philosophy by the contractors. Reviews tend to force specialists in the environment, hardness technology, and the designers to work together to satisfy the system requirements.

The reviewing process should be continuous in order to minimize the impact on scheduling and cost. The timely discovery of a problem provides the most options for solution of the problem. Replacement parts, testing programs, additional shielding, circuit redesign, and if required, spec deviations all take time. Hence it is important to closely review all systems for immunity to ESD, ID, and SEU on a continuing basis.

Quality Assurance (QA) must be an integral part of any immunity/hardness program. This must be done at the fabrication site during the fabrication process.

When establishing a parts reliability program the question of immunity to ESD, ID, and SEU must now be taken into account. Any approved piece parts list will have to show how the manufacturer rates each part for immunity to anomalous upsets. In cases where this cannot be done, then the contractor must assess the situation and inform the customer of how it will impact his parts reliability program.

Once the system is built and operating, it is too late to make design changes, but there are operational changes that can perhaps improve a situation. To discover these operational changes it is necessary to understand how the system works and was designed, the environment the system is in, and the interaction of the environment with the system.

Any anomalies experienced by a system should be reported as soon as possible so that future systems can avoid similar situations, and other operators can benefit from your experience. Appendix 4 lists groups which are interested in sharing and collecting anomaly data.

6.2. Immunity to ESD

The phenomenon of charging has been discussed in chapter 2 and is fairly well understood. At first, a simple-minded solution seems obvious; don't allow a charge buildup which can result in a subsequent discharge (ESD) large enough to produce an anomaly to any spacecraft system. This of course suggests "grounding" all potential sources for ESD. This is easier said than done, since there are so many interactions between the various systems, sub-systems and structures that must be considered. In the guidelines that follow, a number of options are presented.

6.2.1. Design Assessment

Use the NASA Charging Analyzer Program (NASCAP) or similar analytic technique to evaluate a given design. This is to be done in a preliminary fashion to isolate possible discharge sites by computing charging behavior for a few time steps (about one half-dozen 100 second time steps should be sufficient). The analysis of an "as built," or "as planned" system is usually more than worth the cost of the analysis in insuring that the designers actually do what they planned to do. Surface charging can be minimized by materials selection and re-evaluation. The final choice of exterior materials must be an iterative process since both thermal and electrostatic requirements must be considered. Qualification for electrostatic surface cleanliness should be conducted by analysis for both substorm and average conditions. Testing can be limited to the determination of any unknown properties of materials selected. As part of the charging analysis, the designer should evaluate the impact of possible surface discharges on system performance. This can be done with one of the available coupling codes (e.g., SEMCAP). This philosophy considers only surface charging and possible discharges. There exists also the possibility of discharges due to the high energy particle charging of interior cables. This is discussed under internal discharges.

There are several excellent handbooks on spacecraft charging. Much of the material in this section is taken from the handbook of Purvis, Garrett, Whittlesey, and Stevens (1984), and Vampola, Mizera, Koons, Fennell, and Hall (1985). Assessment begins with the determination of the environment, usually a worst case according to some criteria. Then analysis using the environment helps locate the trouble spots in the design. This is followed by trade-offs between the various materials, configurations etc. that are used in the design versus the risks, costs, etc. involved with the various options which can be used in designing the system.

There are two forms of charging of concern in designing a space system: absolute and differential. For absolute charging, the satellite charges as a whole; the dielectric surface voltages are "locked" to the ground voltage. This type of charging depends on the capacitance of the system as a whole to free space, and the plasma currents to the spacecraft. It occurs very rapidly (fractions of seconds) during eclipse charging events when the plasma current is not balanced by the photocurrent, and more slowly in the sunlight. Differential charging depends on the capacitance of one part of the spacecraft to another and the relative current between the two surfaces. Differential charging usually occurs slowly (minutes) on spacecraft in homogeneous isotropic plasmas. Differential charging results in a difference in potential between one part of the spacecraft and another. Differential charging can change the absolute charging level of the satellite by influencing trajectories near the spacecraft body. In some instances a relatively small patch of highly charged material will create a small potential hill in front of the rest of the spacecraft and thereby prevent photocurrents from escaping. In that case the entire spacecraft sinks to a very negative potential, although the differential charging is less than would be expected from simple calculations ignoring the barrier effect.

Satellite configuration plays a key role in charging behavior. For isotropic environments, a spinning satellite usually has a lower spacecraft potential (a few hundred volts) in sunlit charging events than one with large areas continually in the shade. A three-axis stabilized satellite can have large negative spacecraft potentials (a few thousand volts) in sunlit charging environments. Any shaded dielectric can induce large differential voltages. For both configurations differential charging is limited by the three-dimensional barrier effect. In eclipse charging, the voltage buildup is controlled by the secondary yield of the dielectrics, rather than photoemission. Anisotropic fluxes coupled with the peculiarities of the spacecraft configuration may influence both differential and absolute charging.

The mission of the satellite determines the extent to which one must control charging interactions. Nonscientific satellites typically don't need to control the absolute potential, and their only concern is with differential charging when it leads to discharges which affect spacecraft operation. It is important to note that large absolute charging levels can (through field emission from sharp points) lead to discharges and thus be of vital engineering concern. For a scientific satellite absolute charging should be controlled.

In considering the mission, configuration, and both absolute and differential charging concerns, the worst case environment usually determines the surface charging design. There is considerable debate on just what that worst case is. Gussenhoven and Mullen (1982) suggested four criteria: (a) the measured environment which produces the largest vehicle frame (ground) to plasma potential difference, (b) the environment which produces the largest differential potential between adjacent spacecraft surface materials, (c) the hottest plasma environment encountered at geosynchronous orbit, and (d) the environment which causes the greatest number of satellite anomalies.

Chapter two described some recommended worst case charging environments which can be used in assessing system sensitivity to surface charging

When a discharge occurs, charge is redistributed around the spacecraft. At one time investigators felt that large areas of charged dielectric would discharge to space, i.e. a blowoff of charge from the body of the spacecraft. Subsequent opinion (see Purvis et al., 1984) maintains that only a small portion of the charge actually leaves the surface in typical spacecraft discharges.

Purvis, et al. (1984) recommend calculating the discharge transient parameters as follows:

Voltage: Use a square wave approximation of the voltage transient, assuming the voltage pulse rises to the equilibrium ground potential of the spacecraft, remains at that voltage for the duration of the voltage pulse, and then returns to zero.

Current: The current pulse is also approximated by a square pulse where the total charge is made up of two parts -- the charge that is lost to space, and the charge that is redistributed within the dielectric.

Current to space: The charge lost to space is estimated to be

$$\Delta Q_1 = C_1 \, |V_0| \text{ (coulombs)} \quad (6\text{-}1)$$

where C_1 is the satellite to space capacitance (typically picofarads) and $|V_0|$ is the absolute value of the satellite ground voltage at time of discharge.

Currents in the Dielectric: Based on ground tests with grounded substrates which give unrealistically high transfer of charge to space, Purvis et al. (1984) recommend assuming that only 1 percent of the total charge stored on the dielectric surface is involved in this portion of the discharge process. This arbitrary assumption stresses the fact that the discharge is limited to a small dielectric area. Of this one percent, 1/3 is lost to space and 2/3 remains on the dielectric or neutralizes the polarization charge:

$$\Delta Q_2 = KC_2 \, |\Delta V_2| \text{ (coulombs)} \quad (6\text{-}2)$$

where:

$K = 0.003$	is the fraction of total charge lost to space
C_2	is the capacitance across the small portion of the dielectric involved in the discharge
$\lvert\Delta V_2\rvert$	is the absolute value of differential voltage at the discharge site just before the discharge

The total charge lost is:

$$\Delta Q = \Delta Q_1 + \Delta Q_2 \text{ (coulombs)} \quad (6\text{-}3)$$

and the current pulse is:

$$I = \frac{\Delta Q}{\Delta t} \text{ (amps)} \quad (6\text{-}4)$$

The pulse width (Δt) is uncertain, but is on the order of tens of picoseconds. Experiments with grounded substrates indicate that the maximum duration varies as the dielectric area from which charge has been removed. Using this relationship, Δt can be approximated as:

$$\Delta t \sim 0.02(0.01\ A)^{0.5}\ (\mu sec) \qquad (6\text{-}5)$$

where A is the dielectric area in cm^2.

Once the transient pulses expected have been estimated, coupling of the pulse to sensitive circuits can be estimated. There are a number of EMC-type techniques available to do this. Most involve estimating capacitances and inductances from one point to another within the spacecraft, and can be quite complex. Part sensitivity to transients is also difficult to estimate, although methods are available for the persistent. Military Design Handbooks on EMC as well as the Don White series of texts on EMC deal at great length with this part of the process of assessing system sensitivity. The chain of the calculation is to start with the charging environment, estimate the conditions at breakdown, estimate the resulting pulse amplitude and location, estimate the coupling to the victim circuit, and (based on the victim circuit's sensitivity to the pulse) assess the system response.

By careful selection of the materials used in a spacecraft the ESD problem can be reduced or eliminated. For example, the use of grounded conductive coatings and the avoidance of Teflon as an interior dielectric can go a long way in eliminating ESD problems. However, thermal design considerations may restrict the choices available for surfaces. Careful trade-off studies which weigh both the charging and thermal considerations are needed.

The best way to avoid differential charging of spacecraft surfaces is to make all surfaces conductive and grounded to the spacecraft structure. By conductive we mean conductive enough to equalize the currents expected around the spacecraft. Usually the currents in space are small so a resistance which is fairly high by electronic standards may be adequate. However, typical spacecraft surface materials such as Mylar, Kapton, Teflon, fiberglass, glass, quartz, or other dielectric materials, do not usually meet spacecraft charging conductivity desires. In some areas (areas adjacent to antennas operating at less than 1 GHz, or areas where material contamination or thermal control is critical) conductive coatings may be out of the question. In other cases indium tin oxide (ITO) coatings or other techniques should be considered.

The following recommendations are taken from Purvis et al., 1984.

"To discharge surfaces that are being charged by space plasmas, a high resistivity to ground can be tolerated because the plasma charging currents are small. The following guidelines are recommended:

"(1) Conductive materials (e.g., metals) must be grounded to structure with the smallest resistance possible

$$R < \frac{10^9}{A},\ \Omega$$

where A is the exposed surface area of the conductor in square centimeters.

"(2) Partially conductive surfaces (e.g., paints) applied over a conductive substrate must have a resistivity-thickness product

$$rt \leq 2 \times 10^9,\ \Omega\text{-}cm^2$$

where r is the material resistivity in ohm-centimeters and t is the material thickness in centimeters.

"(3) Partially conductive surfaces applied over a dielectric and grounded at the edges must have material resistivity such that

$$\frac{rh^2}{t} \leq 4 \times 10^9,\ \Omega\text{-}cm^2$$

where r and t are as above and h is the greatest distance on a surface to a ground point, in centimeters.

"These guidelines depend on the particular geometry and application. A simplified set of guidelines is supplied for early design activities:

"(1) Isolated conductors must be grounded with less than 10^6 Ω to structure.

"(2) Materials applied over a conductive substrate must have bulk resistivities of less than 10^{11} Ω-cm.

"(3) Materials applied over a dielectric area must be grounded at the edges and must have a resistivity less than 10^9 'ohms per square.' ('Ohms per square' is defined as the resistance of a flat sheet of the material measured from one edge of a square section to the opposite edge. It can be seen that the size of the square has no effect on the numeric value.)

"These requirements are more strict than the preceding relations, which include effects of spacecraft geometry.

"In all cases the usage or application process must be verified by measuring resistance from any point on the material surface to structure. Problems can occur. For example, one case was observed where a nonconductive primer was applied underneath a conductive paint; the paint's conductivity was useless over the insulating primer.

"All grounding methods must be demonstrated to be acceptable over the service life of the spacecraft. It is recommended that all joint resistances and surface resistivities be measured to verify compliance with these guidelines. Test voltages should be at least 500 V. Grounding methods must be able to handle current bleed-off from ESD events, vacuum exposure, thermal expansion and contraction, etc. As an example, painting around a zero radius edge or at a seam between two dissimilar materials could lead to cracking and a loss of electrical continuity at that location.

"By the proper choice of available materials the differential charging of spacecraft surfaces can be minimized. At present, the only proven way to eliminate spacecraft potential variations is by making all surfaces conductive and tying them to a common ground.

"Surface coatings in use for this purpose include conductive conversion coatings on metals, conductive paints, and transparent partially metallic vacuum-deposited films, such as indium tin oxide. Table 6-2 describes some of the more common acceptable surface coatings and materials with a successful use history. Table 6-3 describes other common surface coatings and materials that should be avoided if possible.

"The following materials have been used to provide conducting surfaces on the spacecraft:

Table 6-2. Surface Coatings and Materials Acceptable for Spacecraft Use (from Purvis et al., 1984, p. 13)

Material	Comments
Paint (carbon black)	Work with manufacturer to obtain paint that satisfies ESD conductivity requirements of Section 3.1.2 from Purvis, et al. (1984) and thermal, adhesion, and other needs
GSFC NS43 paint (yellow)	Has been used in some applications where surface potentials are not a problem (apparently will not discharge)
Indium tin oxide (250 nm)	Can be used where some degree of transparency is needed; must be properly grounded; for use on solar cells, optical solar reflectors, and Kapton
Zinc ortho-titanate paint (white)	Possibly the most conductive white paint; adhesion difficult without careful attention to application procedures
Alodyne	Conductive conversion coatings of magnesium, aluminum, etc., are acceptable

Table 6-3. Surface Coatings and Materials to be Avoided for Spacecraft Use (from Purvis et al., 1984, p. 13)

Material	Comments
Anodyze	Anodizing produces a high-resistivity surface; to be avoided. The surface is thin and might be acceptable if analysis shows stored energy is small
Fiberglass material	Resistivity is too high
Paint (white)	In general, unless a white paint is measured to be acceptable, it is unacceptable
Mylar (uncoated)	Resistivity is too high
Teflon (uncoated)	Resistivity is too high. Teflon has a demonstrated long-time charge storage ability and causes catastrophic discharges
Kapton (uncoated)	Generally unacceptable, due to high resistivity. However, in continuous-sunlight applications if less than 0.13 mm (5 mils) thick, Kapton is sufficiently photoconductive for use
Silica cloth	Has been used as antenna radome. It is a dielectric, but because of numerous fibers, or if used with embedded conductive materials, ESD sparks may be individually small
Quartz and glass surfaces	It is recognized that solar cell cover slides, optical surfaces, and second-surface mirrors have no substitutes that are ESD acceptable. Their use must be analyzed and ESD tests performed to determine their effect on neighboring electronics

"(1) Vacuum-metalized dielectric materials in the form of sheets, strips, or tiles. The metal-on-substrate combinations include aluminum, gold, silver, and Inconel on Kapton, Teflon, Mylar, and fused silica.

"(2) Thin, conductive front-surface coatings, especially indium tin oxide on fused silica, Kapton, Teflon, or dielectric stacks

"(3) Conductive paints, fog (thin paint coatings), carbon-filled Teflon, or carbon-filled polyester on Kapton (shielded black Kapton)

"(4) Conductive adhesives

"(5) Exposed conductive face sheet materials (graphite/epoxy or metal)

"(6) Etched metal grids or bonded (or heat embedded) metal meshes on nonconductive plastic film tapes

"Because of the variety in the configuration and properties of these materials, there is a corresponding variety in the applicable grounding techniques and specific concerns that must be addressed to insure reliable in-flight performance.

"The following practices have been found useful:

"(1) Conductive adhesives should be used to bond fused silica, Kapton, and Teflon second-surface mirrors to conductive substrates that are grounded to structure. If the substrate is not conductive, metal foil or wire ground links should be laminated in the adhesive and bolted to structure. Only optical solar reflectors (OSRs) with conductive (Inconel) back surfaces should be used.

"(2) When conductive adhesives are used, the long-term stability of the materials system must be verified, particularly conductivity in vacuum after thermal cycling, compatibility of the materials (especially for epoxy adhesive) in differential thermal expansion, and longterm resistance to galvanic corrosion.

"(3) Metalized Teflon is particularly susceptible to electrostatic discharge degradation, even when grounded. Avoid using it. If there is no substitute for a specific application, the effects of electromagnetic interference (EMI), contamination, and optical and mechanical degradation must be evaluated.

"(4) Paints should be applied to grounded, conductive substrates. If this is not possible, their coverage should be extended to overlap grounded conductors.

"(5) Ground tabs must be provided for free-standing (not bonded down) dielectric films with conductive surfaces.

"(6) Meshes that are simply stretched over dielectric surfaces are not effective: they must be bonded or heat sealed in a manner that will not degrade or contaminate the surface.

"(7) There are several techniques for grounding thin, conductive front-surface coatings such as indium tin oxide, but the methods are costly and have questionable reliability. The methods include welding of ground wires to front-surface metal welding contacts, front-surface bonding of coiled ground wires (to allow for differential thermal expansion) by using a conductive adhesive, and chamfering the edges of OSRs before ITO coating to permit contact between the coating and the conductive adhesive used to bond the OSR to its substrate.

"Grounding techniques for OSRs include chamfering edges and bonding or welding of ground wires. Bonding down solar cell covers with conductive adhesive is not applicable. For multilayer insulation (MLI), extending the aluminum foil tab to the front surface is suitable.

"If the spacecraft surface cannot be made 100 percent conductive, an analysis must be performed to show that the design is acceptable from an ESD standpoint. Note that not all dielectric materials have the same charging or ESD characteristics. The choice of dielectric materials can significantly affect surface voltage profiles. For example, it has been shown (Bever and Staskus, 1981) that cesium-doped microsheet charges to much lower potentials under electron irradiation than fused silica, and it therefore may be preferred as a solar array cover slide material.

"An adequate analysis preceding the selection of materials must include spacecraft analysis to determine surface potentials and voltage gradients, spark discharge parameters (amplitude, duration, frequency content), and EMI coupling. The cost and weight involved in providing adequate protection (by shielding and electrical redesign) could tilt the balance of the trade-off to favor the selection of the newer, seemingly less reliable (optically) charge control materials that are more reliable from spacecraft charging, discharging, and electromagnetic interference points of view.

"The 'proven' materials have their own cost, weight, availability, variability, and fabrication effects. In addition, uncertainties relating to spacecraft charging effects must be given adequate consideration. Flight data have shown apparent optical degradation of standard, stable thermal control materials (e.g., optical solar reflectors and Teflon second-surface mirrors) that is far in excess of ground test predictions, part of which could be the result of charge-enhanced attraction of charged contaminants. In addition, certain spacecraft anomalies and failures may have been reduced or avoided by using charge control materials.

"Ironically, after an extensive effort to have nearly all of the spacecraft surface conductive, the remaining small patches of dielectric may charge to a greater differential potential than a larger area of dielectric would. On the shadowed side of a spacecraft, a small section of dielectric may be charged rapidly while the bulk of the spacecraft remains near zero potential because of photoemission from sunlit areas.

"A spacecraft with larger portions of dielectric may have retarding electric fields because the dielectric diminishes the effects of the photoemission process. As a result, the spacecraft structure potential may go more negative and thus reduce the differential voltage between the dielectric and the spacecraft.

"The lesson to be learned is that all dielectrics must be examined for their differential charging. Each dielectric region must be assessed for its breakdown voltage, its ability to store energy, and the effects it can have on neighboring electronics (disruption or damage) and surfaces (erosion or contamination).

"Other means to reduce surface charging exist but are not well developed and are not in common usage. One suggestion for metallic surfaces is an oxide coating with a high secondary electron yield. This concept, in a NASCAP computer program simulation, reduced the absolute charging of a spacecraft dramatically and reduced differential charging of shaded Kapton slightly. Any selected materials should be carefully analyzed to insure that they do not create problems of their own and that they work as intended over their service lives."

6.2.1.3. Grounding

Since ungrounded conductors when they discharge produce large current and voltage transients, all conducting elements, surface and interior, should be tied to a common electrical ground, either directly or through a resistor. The following detailed instructions on grounding are from the spacecraft charging handbook of Purvis, et al. (1984).

"All structural and mechanical parts, electronics boxes, enclosures, etc., of the spacecraft should be electrically bonded to each other. All principal structural elements should be bonded by methods that assure a direct-current (dc) resistance of less than 2.5 mΩ at each joint. The collection of electrically bonded structural elements is referred to as "structure" or structure ground. The objective is to provide a low-impedance path for any ESD-caused currents that may occur and to provide an excellent ground for all other parts of the spacecraft needing grounding. If structure ground must be carried across an articulating joint or hinge, a ground strap, as short as possible, should carry the ground across the joint. Relying on bearings to serve as a ground path is risky. Structural ground should be carried across using slip rings dedicated to the structural ground path, some at each end of the slip ring set. The bond to structure should be achieved within 15 cm of the slip ring on each end of the rotating joint. Slip rings chosen for grounding should be away from any slip rings carrying sensitive signals.

"All spacecraft surface (visible, exterior) materials should be conductive in an ESD sense (section 3.1.2 of Purvis, et al., 1984). All such surface materials should be electrically bonded (grounded) to the spacecraft structure. Because they are intended to drain space charging currents only, the bonding requirements are less severe than those for structural bonding. The dc impedance to structure should be compatible with the surface resistivity requirements: that is, less than about 10^9 Ω from a surface to structure. The dc impedance must remain less than 10^9 Ω over the service life of the bond in vacuum, under temperature, under mechanical stress, etc.

"All wiring and cabling exiting the shielded 'Faraday cage' portion of the spacecraft (section 3.1.3 of Purvis et al., 1984) should be shielded. Those cable shields and any other cable shields used for ESD purposes should be bonded to the Faraday cage at the entry to the shielded region as follows:

"(1) The shield should be terminated 360° around a metal shielded back shell, which is in turn terminated to the chassis 360° around the cabling.

"(2) The shield ground should not be terminated by using a pin that penetrates the Faraday cage and receives its ground inside the shielded region.

"(3) A mechanism should be devised that automatically bonds the shield to the enclosure/structure ground at the connector location, or a ground lug that uses less than 15 cm of ground wire should be provided for the shield and procedures that verify that the shield is grounded at each connector mating should be established.

"The other end of the cable shield should be terminated in the same manner. The goal is to maintain shielding integrity even when some electronics units must be located outside the basic shielded region of the spacecraft.

"Signal and power grounds require special attention in the way they are connected to the spacecraft structure ground. For ESD purposes a direct wiring of all electrical/electronics units to structure is most desirable. In particular, one should not have separate ground wires from unit to unit or from each unit to a single point on the structure.

"If the electronic circuitry cannot be isolated from power ground, signal ground may be referenced to structure with a large (>10 kΩ) resistor. Once again, box-to-box signals must be isolated to prevent ground loops. This approach must be analyzed to assure that it is acceptable from an ESD standpoint.

"In some cases it is necessary to run signal and power ground lines in harnesses with other space vehicle wiring. This should be avoided where possible and limited where considered necessary. Excessively long runs of signal ground lines should be eliminated."

6.2.1.4. Cable Harness and Routing

Cables form the most common coupling path from the discharge site to the victim circuit. Care should be taken in the layout and bundling of cables not to provide easy coupling from the exterior to sensitive circuits. Filtering and careful documentation of the actual layout of cables will both help prevent anomalies and aid in the analysis of any anomalies experienced in space.

6.2.1.5. Faraday Cage Shielding

The key to providing immunity to surface discharges is the concept of a Faraday cage. Discharges, fields, potentials, etc. outside the cage do not affect anything inside the cage. In practice, penetrations and non-ideal materials compromise the behavior of an ideal Faraday cage, but the concept is still very useful. The spacecraft structure, electronic component enclosures, and electrical cable shields should be used to provide an electrically

continuous shielded surface around all electronics and wiring. The primary spacecraft structure should be designed as an electromagnetic-interference-tight shielding enclosure -- a Faraday cage. This (1) prevents entry of space plasma into the spacecraft interior, (2) shields the interior electronics from any radiated noise from discharges on the exterior of the spacecraft. Generally shielding should provide 40 dB of attenuation or more for radiated electromagnetic fields associated with surface discharges. A 1-mm thickness of aluminum or magnesium will do this if it is as free from holes and penetrations as possible. The effect of penetrations to the shield can be minimized by feedthroughs, meshes, and baffles where penetrations are necessary.

Although the metalization on multilayer insulation is insufficient to provide adequate shielding, properly grounded thermal blankets can be used to increase the shielding effectiveness of the spacecraft. Aluminum honeycomb structures and aluminum face sheets provide significant attenuation.

Some equipment must be placed outside the main body of the spacecraft, e.g., science instruments mounted on booms. The cables exterior to the Faraday cage should be shielded to extend the Faraday cage to those electronic enclosures exterior to the main body. Cable shields have been fabricated from aluminum or copper foil, sheet, or tape. Shields should be terminated when they enter the spacecraft structure from the outside and carefully grounded at the entry point. Braid shields on wires should be soldered to any overall shield wrap and grounded at the entrances to the spacecraft. Conventional shield grounding through a connector pin to a spacecraft interior location should not be used because this provides a convenient antenna. The unwanted pulse can be used to broadcast its signal within the Faraday cage.

Care exercised with the shielding and cabling in the design of the spacecraft greatly increases the immunity to surface and internal discharges.

6.2.2. Mitigation Techniques

Current limiting, filtering, and error detection and correction techniques can be used to mitigate the effects of both internal and surface discharges.

6.2.2.1. Current Limiting

No matter how careful one is in the design of a system, it may be that pulses will appear on the inputs to electronic boxes. The military has an extensive experience base from hardening electronics to EMP and SGEMP. The current limiting technique developed for these threats is also effective for both internal and surface discharges.

6.2.2.2. Filtering

Electrical filtering is a well known method of protecting circuits from discharge-induced upsets. The usual criterion suggested for filtering is to eliminate noise below a specific time duration (i.e., above a specific frequency). On the Communications Technology Satellite (CTS), in-line transmitters and receivers were used that effectively eliminated noise pulses of less than 5-μs duration. Other filtering concepts include diodes which clamp the peak voltage below a preset value.

6.2.2.3. Error Detection/Correction

Providing error detection and correction software in the system is another way of designing in immunity. This technique is discussed in a little more detail under the topic of fault tolerance in the SEU section.

6.2.2.4. Plasma Contactors contributed by Tod Williamson -- Hughes Research Labs

A number of experiments have demonstrated convincingly that emitting a low-density plasma from an on-board plasma source, i.e., a "plasma contactor," can offer protection of geosynchronous-Earth-orbit (GEO) spacecraft against both differential charging of exterior dielectrics and net charging of the spacecraft frame (Olsen, 1985, Cohen and Lai, 1982, and Purvis and Bartlett, 1980). (The term plasma contactor was first coined by Mario Grossi of the Harvard Smithsonian Institution.) This "active" approach to electrostatic-discharge (ESD) prevention offers the important advantage of freeing the spacecraft designer from difficult thermal/ESD trade-offs. In the case of scientific spacecraft, having a plasma contactor on board permits operation at local space-plasma potential, revealing charged-

particle populations to on-board spectrometers that otherwise would be hidden by even small amounts of vehicle frame charging. Plasma contactors are also used to serve two other applications: (1) lowering the electrical impedance of electrodynamic tethers by making "contact" with the space plasma (Patterson and Wilbur, 1987, Katz and Parks, 1985) and (2) clamping the potential of spacecraft that emit charged-particle beams close to space-plasma potential (Burch, 1986).

6.2.2.4.1. Requirements for ESD Prevention

For ESD prevention, a plasma contactor must be capable of producing a sufficiently dense plasma in the near vicinity of the spacecraft that the diffusion-limited flux of contactor-produced ions to a charged spacecraft surface exceeds the space-plasma electron flux (assuming negative charging). For small spacecraft, this requirement can be met with a simple hollow-cathode/keeper type of contactor, as was successfully demonstrated on ATS-6 (Olsen, 1985). Figure 6-2 shows the ATS-6 spacecraft and the effect of a neutralizer during a charging event. Notice that the equilibrium potential is near zero only during the charging event, and that both before and after the neutralizer was on, the spacecraft was charging. Larger spacecraft (with more than a few square meters of surface exposed to the

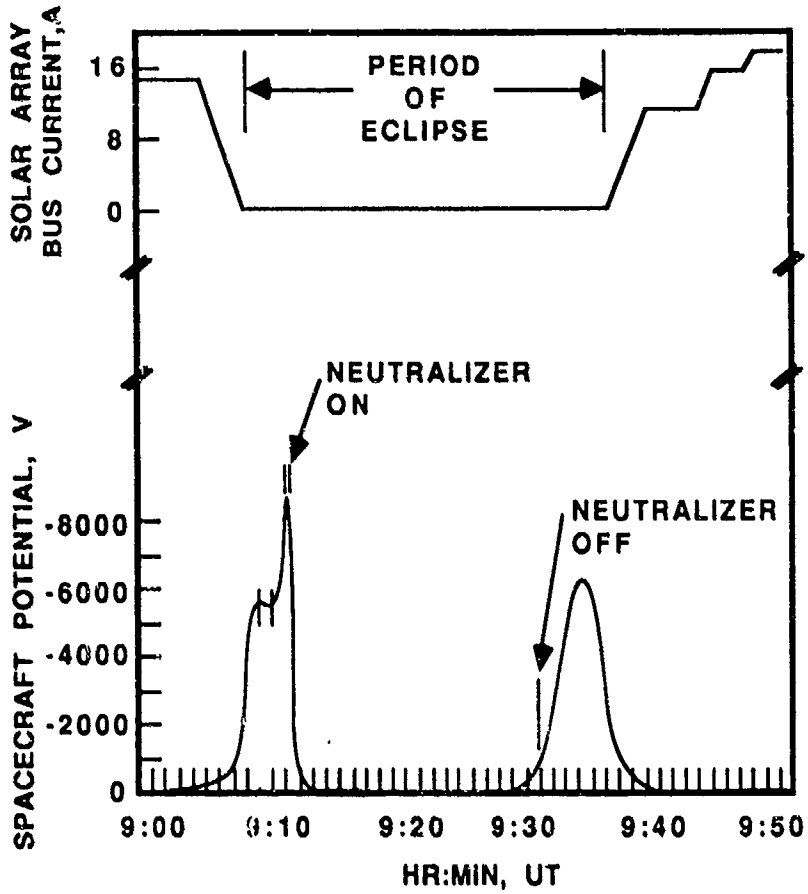

Figure 6-2. Neutralizer Discharge During Eclipse

~3-microamp-per-square meter space-plasma electron flux) require larger ion currents than can be provided by the hollow-cathode/keeper devices. To provide this additional ion-current capability, modern plasma contactors employ small Penning-type discharge chambers to increase the fractional ionization of the weakly ionized plasma from a hollow-cathode/keeper device. The operation of plasma contactors of this enhanced type is described in the next section.

6.2.2.4.2. Plasma Contactor Operation

The technology of plasma contactors is derived from an ion propulsion space flight and ground-life test heritage. A plasma contactor system is shown schematically in Figure 6-3; it consists of a plasma source, a gas-feed system, and a power-processor/controller. The plasma source contains two distinct discharge regions: one between the cathode and keeper electrode, and one between the cathode and anode. A magnetic field is imposed between the cathode and anode, to maximize the number of collisions electrons experience before they reach the anode. The magnetic field strength is adjusted so that the impedance that it presents to electron flow results in an electron energy (about 25 eV) that is favorable for ionizing collisions. The magnetic-field geometry is designed to produce a large fraction of these ionizing collisions in the vicinity of the exit orifice, so that recombination losses on the discharge-chamber walls are minimized.

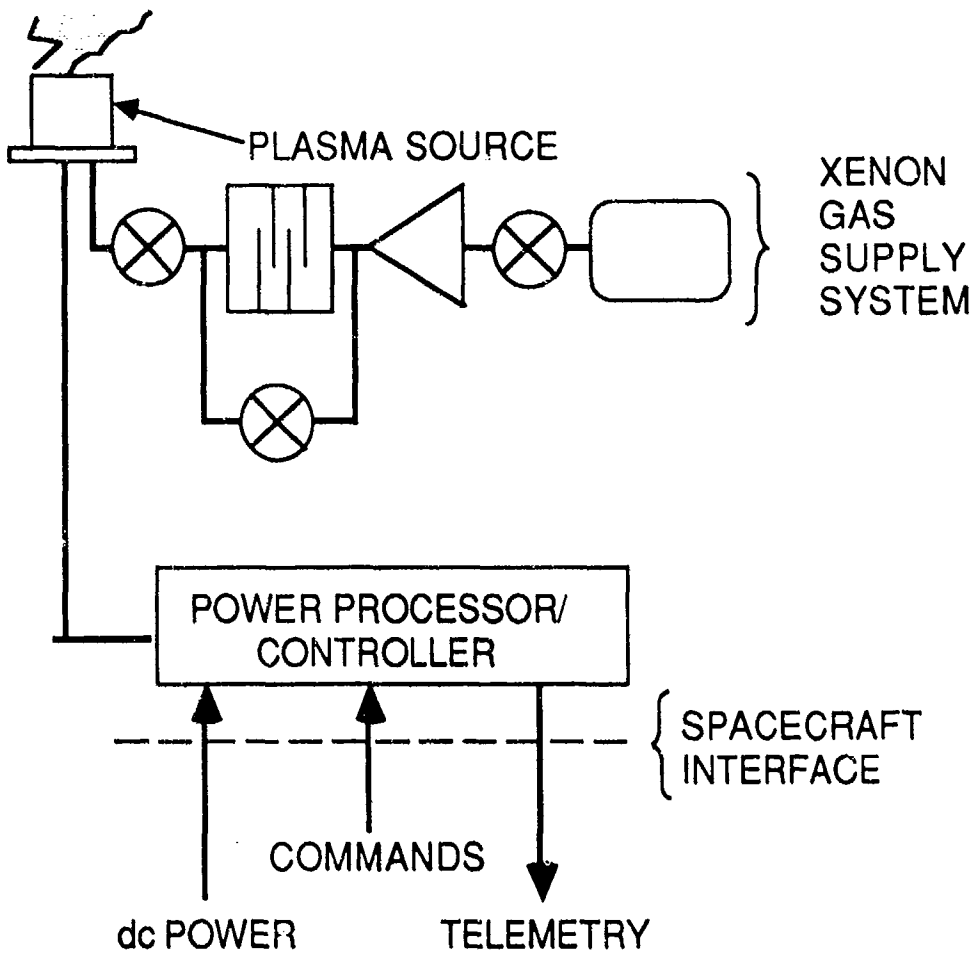

Figure 6-3. Plasma Contactor

Plasma densities of the order of 10^{17} m^{-3} are characteristically produced in Penning-discharge plasma sources. Since this plasma has a potential close to anode potential, ions leave the discharge plasma under the impetus of the anode-to-space-plasma potential difference. The electrons that leave the source are those from the high-energy tail of the Maxwell-Boltzmann distribution in the discharge that are energetically able to overcome the electrostatic barrier that is presented by the same potential difference. The greater electron mobility and larger temperature (a few eV vs. 0.1 eV for the ions) overcome this disadvantage.

The particular plasma source that is illustrated below, in Figure 6-4, was designed specifically for ESD avoidance on GEO spacecraft. It operates on a flow of 0.5 standard cm^3 per minute (about 2.2×10^{17} atoms/s) of xenon gas and requires a total power of less than 10 W. For applications in which larger ion currents are needed --

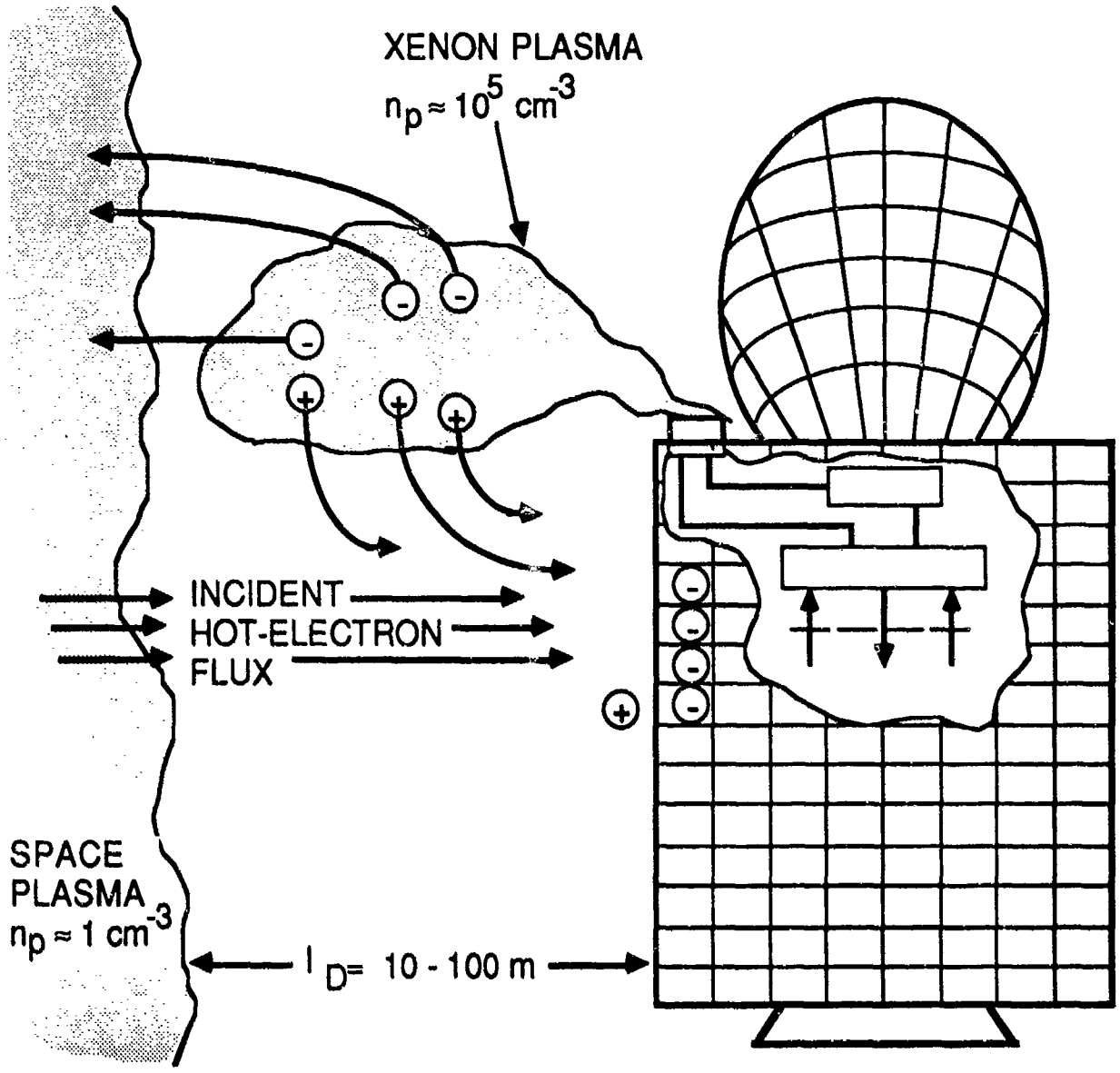

Figure 6-4. SPACECLAMP

for example, experiments in which charged-particle beams are ejected from the spacecraft (Raitt et al., 1982, Obayashi, 1984) -- larger plasma contactors are available by straightforward modification of existing ion-thruster designs. A 25-cm (anode diameter) ring-cusp plasma contactor that is capable of producing 4 A of ion current is shown below in Figure 6-5. This plasma contactor design is based on an advanced xenon ion-propulsion system (XIPS) which is being developed for station-keeping application on large communications satellites.

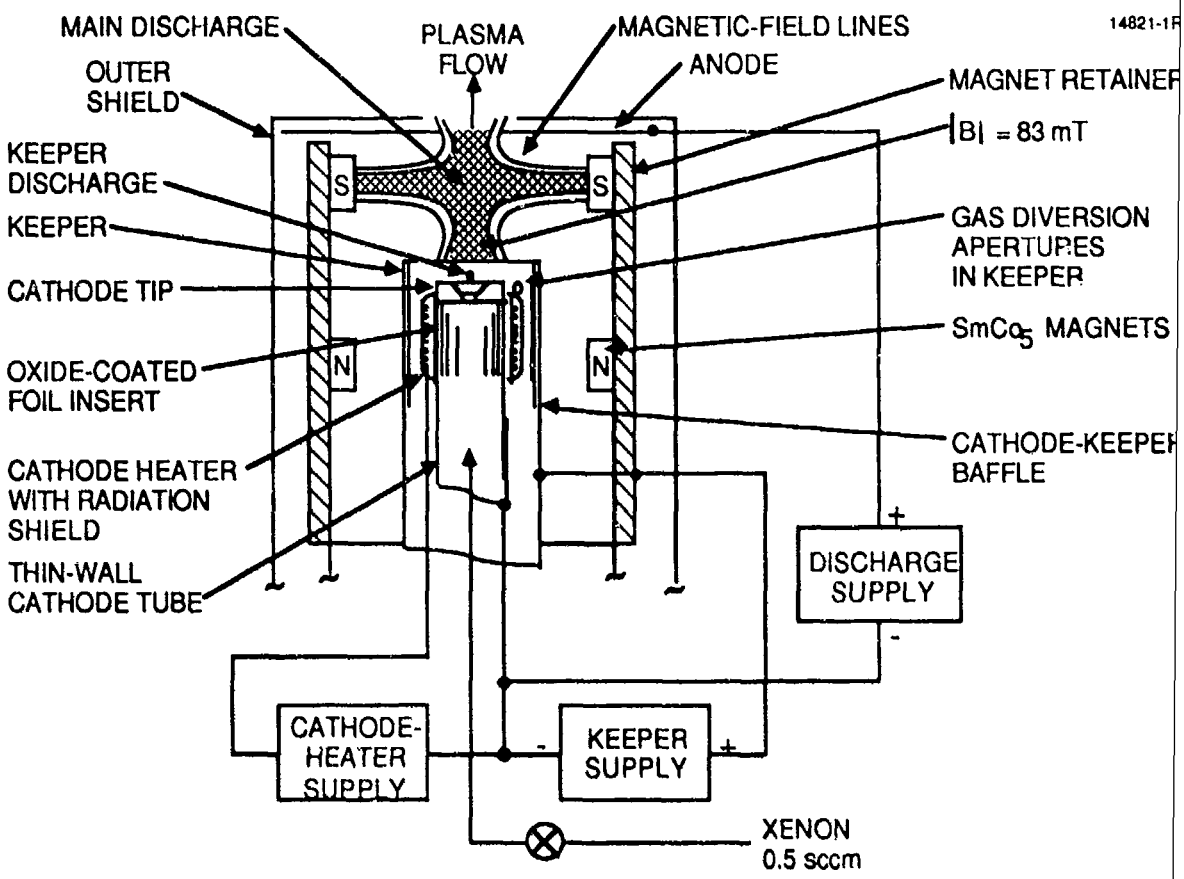

Figure 6-5. 25-cm Plasma Contactor

6.2.2.4.3. Current Bias Relations

The ion current that is produced by a plasma contactor depends upon the potential difference between the plasma source and the external plasma: it typically reaches a maximum when the source is a few volts above space plasma potential. Figure 6-6 below shows a current-voltage characteristic of the SPACECLAMP contactor. The measured floating potential is about 14 V. For ESD prevention, this small potential offset would be unimportant on scientific spacecraft a bias power supply would be needed to establish a zero floating potential.

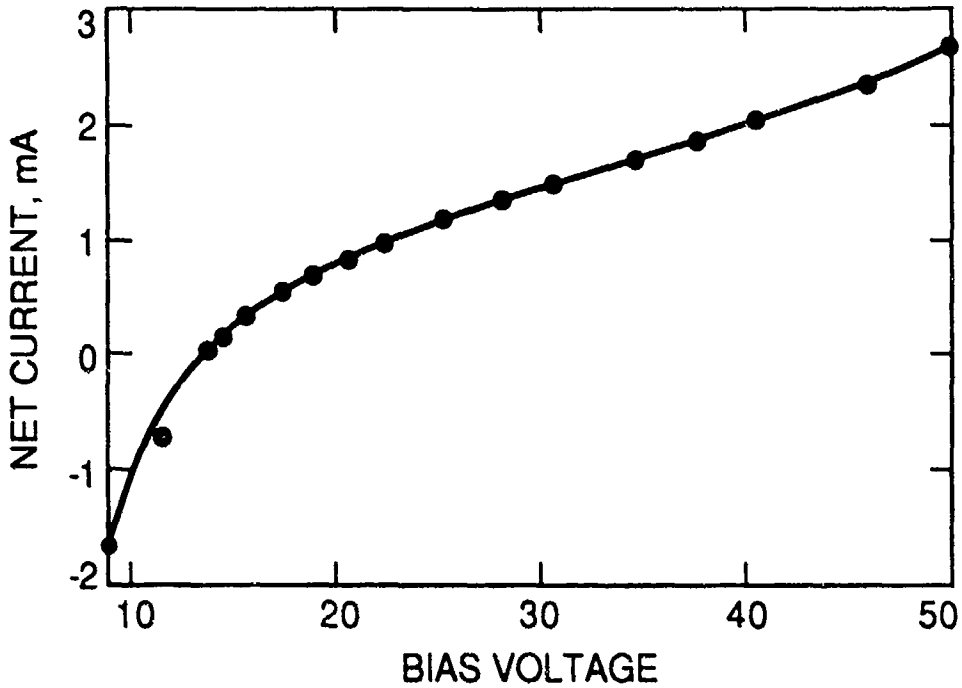

Figure 6-6. SPACECLAMP Current

An interesting feature of the relationship measured between the current and the bias is that positive currents above 2 mA are shown, while the SPACECLAMP contactor has a maximum ion production of 1 mA. The additional current consists of electron collection from the background plasma. The electron-collection capability, which illustrates the bidirectional nature of the plasma-contacting process, is beneficial on spacecraft that actively emit negative charge.

For ESD prevention, a plasma contactor could be operated continuously, or it could be activated only when a threatening environment is detected. The former option is obviously the simplest, but it carries a penalty in that the gas tankage and plasma-source lifetime must be adequate for the entire duration of the spacecraft service life. While plasma sources similar to those discussed here have demonstrated lifetimes in excess of 15,000 hr, the longer plasma-source lifetimes that would be required by many contemporary spacecraft have not been demonstrated. The alternative approach, of using instrumentation to detect a threatening environment or the onset of spacecraft charging and automatically activating the plasma contactor only when needed, is attractive because of its gas-, power-, and lifetime-sparing qualities. Available plasma contactors are described in the appendix.

6.2.3. Methods of Circumvention

Sometimes, in spite of the best intentions, a space system is flown that has weaknesses, and is subject to anomalies. In those cases, circumvention techniques can be developed to avoid real problems and to enable the system to provide the service it was designed to provide. Circumvention techniques include redundancy, monitoring, and operational changes to avoid, modify, or respond to the impact of an anomaly.

Many systems provide some level of redundancy in the hardware so that when one side of the system fails or is upset, it can be turned off and a duplicate system turned on. This is an excellent way to circumvent anomalies when the rate of failure or upset is not too high. Operator or automatic action to switch from one redundant unit to another is sometimes the best way to maintain a space system's capability.

Other times operator intervention involves a detailed understanding of the nature of the anomaly to perform the proper corrective action. Examples of this might be reloading a memory or resetting a switch to restore operation.

Some transients are never noticed. For example a star sensor which takes a number of readings on a star's location and averages them before acting on the result might not be bothered by one extremely wrong data point due to a transient. Designs which operate on average conditions or require redundant data from the environment are less susceptible to upsets then ones which operate on single pieces of information.

Real-time predictions of the environment can benefit corrective operator action by predicting periods of increased activity and hence need for alertness. Onboard monitoring of the environment can go even further in alerting operators to the likelihood of upsets or anomalies.

6.2.4. Quality Control

Proper handling, assembly, inspection, and test procedures should be instituted to insure the electrical continuity of the space vehicle grounding system. The continuity of the space vehicle electrical grounding system i of great importance to the overall design susceptibility to spacecraft charging effects. In addition it will strongly affect the integrity of the space vehicle electromagnetic capability (EMC) design. Proper handling and assembly procedures must be followed during fabrication of the electrical grounding system. All ground ties should be carefully inspected and dc resistance levels should be tested during fabrication and again before delivery of the space vehicle. A final check of the ground system continuity during preparation for space vehicle launch is desirable.

In addition to insuring that the spacecraft is assembled the way it was designed, careful documentation of how it was built will help in the analysis and correction of any anomalies. This is especially true with cable layou surface conductors, grounding, and other system aspects. Some manufacturers even recommend documenting by filming the system in various stages of completion. In the repair of the Solar Max mission undocumented thermal blanket spacers prevented the Solar Max mission capture device from working as planned (private communication, N. John Stevens, 1986).

6.2.5. Cost-Effectiveness

The effects of designing in immunity for surface charging/discharging are:

1. Reduced operational costs
2. Reduced outages
3. Simplification of data analysis and hence reduced cost for data analysis or more data analyzed.

The effectiveness of the hardness approach implemented is highlighted for military space systems in the ODAP reports; for NASA and commercial systems, incentive fees for performance or successful completion of a mission highlight immune designs.

6.2.6. Subsystem Guidelines

In addition to the general guidelines given above, Purvis, et al. (1984) provide some specific advice for subsystems in providing immunity to surface charging. These are given below.

6.2.6.1. Solar Panel Grounding

"Solar array panels and substrates should be electrically grounded to the structure. Solar array panels and conductive sections of substrates and honeycomb should be grounded to each other with grounding jumpers and the entire network grounded to the space vehicle structure with less than 2.5-mΩ dc resistance per joint. Deployable panels on three-axis-stabilized vehicles can be grounded to the structure through slip rings where necessary. A ground wire can be used to bond together each lateral strip or row of solar cells.

6.2.6.2. Solar Panel Fabrication

"Solar array panels should use materials and fabrication techniques to minimize electrostatic discharge effects. Solar panel back surfaces, edges, and honeycomb should be grounded conductors. Conductive black paint i suitable for the rear surface of the solar panel. Solar panel edges can be wrapped with grounded conductive tape. Th front surface of the solar array consists of nonconductive cover slides and gaps sometimes potted with nonconductiv adhesive for electrical design reasons. The potting thickness should be the minimum required. The front surfaces o

cover slides may be coated with a conductive, transparent coating of grounded indium tin oxide if required. Such coatings typically reduce transmissions by 5 to 10 percent and are generally used when absolute charging must be controlled.

6.2.6.3. Power System Electrical Design

"Power system electrical design should incorporate features to protect against transients due to electrical discharge. Spark discharges from solar arrays should be anticipated, and the electrical design of the power system just provide adequate protection. The following design practices will help in reducing the effects of such spark discharges.

"(1) Clamp solar array wiring, preferably at the entry to the spacecraft Faraday cage, but definitely before it enters the power supply.

"(2) If solar array wiring is not clamped at the entry point to the Faraday cage, shield the wiring from that point to the power supply.

"(3) Use solar array diodes with forward current ratings that anticipate expected ESD transient currents.

"(4) Perform analysis and testing to verify the power system electrical design for survivability or immunity to spacecraft charging effects.

6.2.6.4. Mechanical and Structural

"In addition to the general guidelines, the following specific guideline applies: Conductive honeycomb and face sheets should be electrically grounded to the structure.

"Aluminum honeycomb substructures require special consideration for electrical grounding. Techniques for grounding conductive honeycomb and face sheets include rivets, copper wires, and metal inserts.

"Care should be taken to establish ground ties at several locations on the honeycomb structure and to maintain ground continuity through all honeycomb parts and face sheets. For example, a recommended method of using copper wires involves sewing the wires transversely at shallow inclination angles through the honeycomb (making contact with several of the cell walls). The wires should be installed at maximum intervals of 30 cm across the structure. Electrical inspection of grounding interfaces for honeycomb structures applies.

6.2.6.5. Thermal Blankets

"All metalized surfaces in multilayer insulation (MLI) blankets should be electrically grounded to the structure. The metalized multilayer surfaces should be electrically grounded to each other by ground tabs at the blanket edges. Each tab should be made from a 2.5-cm-wide strip of 0.005-cm-thick aluminum foil. The strip should be accordion folded and interleaved between the blanket layers to give a 2.5- by 2.5-cm contact area with all metalized surfaces and the blanket front and back surfaces. Nonconductive spacer or mesh material must be removed from the vicinity of the interleaved tab. The assembly should be held in place with a metallic nut and bolt that penetrates all blanket layers and captures 2.0-cm-diameter metallic washers positioned on the blanket front and back surfaces and centered in the 2.5- by 2.5-cm tab area. The washers may have different diameters, with the inner surface of the smaller washer recessed to insure maximum peripheral contact area between the interleaved foil strip and each metalized blanket surface. The tab should be grounded to structure by a proven technique such as a wire that is as short as possible (15 cm maximum) or conductive Velcro.

"The following practices should be observed during blanket design, fabrication, handling, installation, and inspection:

"(1) Verify layer-to-layer blanket grounding during fabrication.

"(2) After installation, verify less than 10-Ω dc resistance between blanket and structure.

"(3) Close blanket edges (cover, fold in, or tape) to prevent direct irradiation of inner layers.

"(4) Do not use crinkled, wrinkled, or creased metalized film material.

"(5) Handle blankets carefully to avoid creasing of the film or possible degradation of the ground tabs.

"(6) If the blanket exterior is conductive (paint, indium tin oxide, 'fog'), make sure that it contacts the ground tab.

6.2.6.6. Thermal Control Louvers

"Ground the blades of thermal control louvers. A fine wire with minimal torque behavior or a fine slip brush can do the job with acceptable torque constraints.

6.2.2.7. Antenna Grounding

"Antenna elements should be electrically grounded to the structure. Implementation of antenna grounding will require careful consideration in the initial design phase. All metal surfaces, booms, covers, and feeds should b grounded to the structure by wires and metallic screws (dc short design). All waveguide elements should be electrically bonded together with spot-welded connectors and grounded to the spacecraft structure. These elements must be grounded to the Faraday cage at their entry points. Conductive epoxy can be used where necessary, but dc resistance of about 1 Ω must be verified by measurements.

6.2.6.8. Antenna Apertures

"Spacecraft RF antenna aperture covers should be ESD conductive and grounded. Charging and arcing of dielectric antenna dish surfaces and radomes can be prevented by covering them with grounded ESD-conductive material. Antenna performance should be verified with the ESD covering installed.

6.2.6.9. Antenna Reflector Surfaces

"Grounded, conductive spacecraft charge control materials should be used on antenna reflector rear surfaces Appropriate surface covering techniques must be selected. Applicable methods include conductive meshes bonded t dielectric materials, silica cloth, conductive paints, or non-conductive (but charge bleeding) paints overlapping grounded conductors.

6.2.6.10. Transmitters and Receivers

"Spacecraft transmitters and receivers (command line and data line) should be immune to transients produc by electrostatic discharge. Transmitter and receiver electrical design must be compatible with the results of spacect charging effects. The EMI environment produced by spacecraft electrostatic discharge should be addressed early in t design phase to permit effective electrical design for immunity to this environment. The transmitter, receiver, and antenna system should be tested for immunity to ESDs near the antenna feed. The repetition rate should be selecte to be consistent with estimated arc rates of nearby materials.

6.2.6.11. Attitude Control

"Attitude control electronics packages should be insensitive to ESD transients. See Table IV [Purvis et a (1984), p. 16]. Attitude control systems often require sensors that are remote from electronics packages for Farada shielding. This presents the risk that ESD transients will be picked up and conducted into electronics. Particular care must be taken to insure immunity to ESD upset in such cases.

6.2.6.12. Deployed Packages

"Deployed packages should be grounded by using a flat ground strap extending the length of the boom to the vehicle structure. Several spacecraft designs incorporate dielectric booms to deploy payloads. The payload electrical system may still require a common ground reference, or the experiment may require a link to some electr potential reference. In these cases it is recommended that a flat ground strap be used to carry this ground tie to the vehicle structure. Electrical wiring extending from the deployed payload to the spacecraft interior must be carried inside or along the dielectric booms. This wiring should be shielded and the shield grounded at the package end an at the Faraday cage entrance.

6.2.6.13. Ungrounded Materials

"Specific items that cannot be grounded because of system requirements should undergo analysis to assure specified performance in the spacecraft charging environment. Certain space vehicles may contain specific items or materials that must not be grounded. For example, a particular experiment may have a metallic grid or conducting plate that must be left ungrounded. If small, these items may present no unusual spacecraft charging problems; however, this should be verified through analysis.

6.2.6.14. Deliberate Surface Potentials

"If a surface on the spacecraft must be charged (detectors on a science instrument, for example), it should be recessed or shielded so that the perturbance in surface electrostatic potentials is less than 10 V. Scientific instruments with the need for exposed surface voltages for measurement purposes, such as Faraday cups, require special attention to insure that the electrostatic fields they create will not disrupt adjacent surface charging or cause discharges by their operation. They can be recessed so their fields at the spacecraft surface are minimal or shielded with grounded grids. An analysis may be necessary to insure that their presence is tolerable from a spacecraft charging standpoint."

6.2.7. Summary -- Surface Charging

A specific implementation of a surface charging might include the following:

1. Perform a spacecraft charging analysis to determine surface potentials, and notify designers of possible arcs and their characteristics. Based on their thermal and electrical properties select materials which meet thermal requirements, but have as high an electrical conductivity as possible. Utilize grounded conductive coatings wherever possible. Ground conductive coating on optics. Cover any radomes with ESD-conductive (resistivity $<10^{10}$ ohm-cm) and ground coating. Test all non-standard materials for discharge characteristics.

2. Review bonding techniques and test to determine their current carrying capabilities. Establish grounding requirements to insure a maximum potential difference between any two points of the spacecraft of less than ten volts. (Establish a maximum resistance between any two points on the spacecraft ground plane of less than 10 milliohms.) Use Faraday cage construction for all basic spacecraft design and all electronic boxes. Bond all metallic and conductive structures together -- allow no ungrounded conductors on the surface. Allow no surface dielectric (resistivity $> 10^{14}$ ohm-cm) with areas (0.5 cm^2) which when discharged are great enough to cause the system a problem. All cables should be shielded and electrically tied to structural ground. All electronic boxes have low impedance (<2.5 mΩ) to structure. Thermal blankets are bonded to structure with aluminum bound straps. Thermally isolated structures must have at least two bond straps.

Typical Bond Strap Requirements:

Bond Area	Number of Groundstraps
<25 cm^2	None
25 cm^2 to 100 cm^2	One-if a signal cable passes within 3 inches of the thermal blanket; none otherwise.
100 cm^2 to 900 cm^2	2
900 cm^2 to 8000 cm^2	3
8000 to 16000 cm^2	4
Each additional 8000 cm^2	1 additional groundstrap

3. Use special filtering of exposed circuits at the entry point into spacecraft. Provide a conductive path to structure for all circuitry. Isolate primary and secondary windings of transformers. Ground radiation spot shields. Avoid Teflon as an interior or exterior dielectric. Use low pass filters on interface circuits. Use as low a speed logic as possible. Provide a bleed path for trace areas > 3.2 cm^2 on circuit boards. Provide a bleed path for isolated wires > 25 cm long. Use SEMCAP to estimate coupling of discharge to cables. EMI filters should be modified when circuit analysis indicates a problem. Where possible use a high voltage logic interface between boxes to increase noise level required to couple into box.

By attending to the surface design (1), the electrical grounding (2), and the circuit sensitivity (3) in a systems approach, surface charging/discharging problems can be minimized if not avoided.

6.3. Immunity to Internal Discharges

The simplest way to design for immunity to internal discharges (ID) is to either prevent the charging from taking place or dissipate any charge buildup in a manner which does not produce any upsets to circuitry.

6.3.1. Design Assessment

Assessing a system's susceptibility to internal discharges proceeds along a line parallel to the assessment just described for surface charging. First, the environment is evaluated to determine the current of penetrating charged particles. Chapter 3 describes some of the environments of concern to internal charging. This information is coupled with the material properties and configuration to determine the likelihood of discharges. Then the characteristics of the discharge are estimated and the pulse is coupled to the victim circuit. The results of the coupling are then compared to the sensitivity of the victim to determine the extent of the problem.

The principal environment of concern for internal discharge assessment is the penetrating charged particle environment. This usually means high energy electrons. In chapter 4 it was pointed out that internal discharges occur above a certain current level to the volume under consideration. This is because the charging rate is usually balanced by a leakage rate of some sort no matter how small. Charged particle transport codes typically can estimate the total charge transported to a volume, and this number together with the capacitance of the volume indicates the likelihood of a discharge. When the electric field exceeds 10^4 to 10^5 volt/cm discharges are likely to occur. As before the geometry of the charge distributions plays a central role. This is especially true for floating metal pieces.

Since internal discharges occur near their most likely victim circuits, the easiest and most conservative estimate of coupling is to consider direct injection of the charge available into the sensitive circuit. Of course, this will not occur every time there is a discharge, but this is the most likely way in which an anomaly would be introduced by internal discharging. Internal discharges tend to be very short (on the order of one nanosecond or less), and except for floating metal, less than one volt into a fifty ohm impedance circuit. Floating metal configurations have produced voltage of up to one hundred volts in laboratory tests.

The sensitivity of the victim circuit is crucial to understanding the reaction of a subsystem to internal discharges. With many of the circuits investigated so far it requires voltages on the order of hundreds of millivolts for even the most sensitive circuit to respond. Typically the transient must produce voltages on the order of the circuit's operating voltage for tens of nanoseconds to produce an anomaly. However the natural impedances and capacitances in the circuit tend to stretch internal discharges to the point where they can influence circuitry especially when large discharges occur.

Careful material selection can eliminate many internal charging problems. Somewhat leaky materials may provide very adequate electrical isolation in an electronics sense, but still provide good leakage for the charge that might build up due to the small high energy current which causes internal charging.

The first rule is to make sure there are no floating conductors anywhere in the spacecraft. Any loose metalization should be screened out of the design and fabrication process. Checkpoints should be established and closely monitored for such ungrounded metal.

All cables should be shielded or grounded and/or current limiting devices employed in the circuitry. Be careful that ungrounded wires are not left in a cable bundle. Sometimes extra wires were placed in a bundle with the idea that they would eventually be used, and not removed when they were not needed in the final design. The easiest check on this type of oversight is at the connector. Every pin should be used or grounded. Sometimes each lead is supplied with several inches of lead wire so the total amount of ungrounded wire could be significant for even a single ungrounded pin.

All circuit boards should be fabricated in such a way as to be free of loose metalization and/or ungrounded pins or connectors. Inspections for same should be made a routine fabrication requirement.

Assigning to QC the task of monitoring the design rules decided on by the system to eliminate internal discharges is an effective way of assuring project management that every step decided on is actually taken. QC deals with the "as built" status of the system, so any misapplied or forgotten steps are more obvious. Careful instructions to QC will eliminate oversights and mistakes that sometimes result in an ID sensitive system.

6.3.2. Mitigation Techniques

Although internal discharges tend to be much smaller than surface charges, unfortunately they occur inside the Faraday cage, and therefore are not affected by the Faraday cage. However, internal discharges tend to be very short, and therefore filtering techniques which discriminate against short pulse can be very effective. When the pulse is "stretched" by the coupling mechanism, its energy content tends to be small, reducing the likelihood of serious problems. Circuits designed to respond only to well controlled inputs also discriminate against internal discharges as well as random noise.

Another approach to mitigating the effects of ID type anomalies is to design into each system/subsystem a method of detecting any such upsets and an automatic means of self-correction. Parity checking, fixed program checks (programs that calculate a known answer using a known algorithm), and checks against a golden memory have been used as error detectors. This technique would undoubtedly lead to increased cost and complexity But if implemented at the beginning of a program the cost impact would be very small. Retrofitting such a technique might be expensive. This points up the importance of designing for immunity from the beginning. In the appropriate circumstance, error detection and correction methods can be very effective. Fault tolerant procedures are discussed under SEU immunity.

Onboard system monitoring for any internal discharges which might occur could be an integral part of any EDAC (electronic data and control) program. However, monitoring alone will serve no useful purpose, unless it is coupled with a procedure to mitigate the effects of internal discharges on satellite systems. Monitoring internal discharges (perhaps detecting noise pulses, changes in status, or even charge buildup inside test samples) only provides indications of the rate of ID, and may not provide any indication of specific ID caused upsets, although there should be a strong correlation when sampled over a sufficiently long time. Monitoring can, however eliminate ID as a suspected cause when no correlation is found over a long period. It is probably easier to eliminate internal discharges than to monitor them and react appropriately.

6.3.3. Methods of Circumvention

For satellite systems which have not been designed against ID type anomalies there are operational procedures which can be implemented to "work around" these upsets and minimize their systems impact. The exact details of such procedures would have to be tailored to fit each satellite's capabilities and the user's needs .

Circumventing any upsets from internal discharges by operational methods benefits from real-time predictive information about the state of "space weather". Onboard monitors are even more valuable in such cases because they give on the spot information about the actual environment the spacecraft is experiencing. The exact nature of these ground based responses will depend on an understanding of the nature of the anomaly and the space system. Once sensitive subsystems have been identified, the appropriate response can be made.

It seems clear that the most cost-effective way to engineer immunity to internal discharges into any spacecraft is to build the hardware so that charge buildup and subsequent internal discharges do not occur. By specifying materials that do not build up large potentials, requiring all metal to be grounded, and thorough EMC testing and design, the source of internal discharges can be eliminated. The filtering and shielding used for surface discharge immunity generally contribute to internal discharge immunity as well but the main attack on this problem has to be in eliminating the source and reducing circuit sensitivity.

6.4. Immunity to SEU

Single event upsets were essentially unknown when electronics systems were made up of discrete components. Modern electronic systems however are full of small low-powered fast electronics which are sensitive to single particles. The capability and desirability of using such parts from a system point of view make the immunity engineering approach less amenable to a systems approach than either of the other two anomalies we are discussing. For single event upsets, attention centers on making the part itself immune to SEUs or at least lowering its SEU rate to an acceptable level.

6.4.1. Available Part Data

For single event upset immunity a program should start with an approved parts list. This list should limit the number and types of parts available to the designers to accomplish the mission. If all of the parts on the approved parts list are SEU free, there will be no SEU problem. Usually, unfortunately, the capability required to perform the mission dictates that fast low powered parts be used. These parts tend to have non-zero SEU rates. So it is very important to estimate early what the SEU rate for each part is and ask each system what SEU rate it can tolerate. Since SEU testing of parts on the ground is a long and expensive process, a program should attempt to take advantage of the work of other programs in this area. SEU testing is discussed in 6.5.3. Below are listed some of the sources of SEU data which exist:

6.4.1.1. JPL/NASA Ground Test Radiation Data Bank

This data bank is becoming computerized and is accessible by phone (Martin et al., 1986).

6.4.1.2. IEEE Transactions on Nuclear Science

See especially the December issue each year where the proceedings are reported of the Nuclear Science Radiation Effects conference.

6.4.1.3. Defense Nuclear Agency (DNA) Hardness Assurance Advisory Committee

This group is a good source especially when you are dealing with military requirements.

6.4.1.4. DASIAC

DASIAC: DoD Nuclear Information and Analysis Center operated by Kaman Science Tempo Division, 816 State Street, P.O. Drawer QQ, Santa Barbara, California 93102, (805) 965-0551. The Electronics Radiation Response Information Center (ERRIC) has radiation data on many parts.

6.4.1.5. Various MIL Specs

Defense Electronics Supply Center (DESC) maintains a qualified parts list (QPL). The MIL specs relating to how you should test are in MIL-S-750 for semiconductors and MIL-P-883B for ICs.

6.4.2 Programs for Developing SEU Hard Parts

Where it is not possible to select hardened parts, then parts selection should be made with hardenability in mind. For example, experience has shown that certain parts can, through technology transfer, be adapted to meet SEU requirements and still retain their desirable characteristics. However, it should be noted that this is a path which is both expensive and risky.

In purchasing and stockpiling parts, always consider processing control and reliability. Manufacturers in an effort to give better service to their customers and to increase their efficiency continually "improve" their processes, and may inadvertently degrade radiation hardness in the process. Therefore, it is not at all unreasonable to at least monitor, and perhaps even control the process for the parts of interest to your program. One of the techniques for hardening parts to SEUs has been the use of cross-coupled resistors in each RAM cell, as described in chapter 4.

6.4.3 Fault Tolerant Solutions

(From viewgraphs of George Gilley (Aerospace) and Michael Sievers (Fail-Safe Technology Corp) - DNA/DARPA SEU Symposium, 20 April 1983.)

Fault tolerance is a method which will allow the system to continue to operate as specified, even if faults occur. Fault tolerance requires protective redundancy, and autonomous fault detection, isolation and recovery. Protective redundancy means that the system must be capable of switching between independent units which are

protected from each other so that a fault in one does not propagate to the other, or inhibit transfer to the other. A fault tolerant system must have a way to discover the fault, isolate where in the system the fault occurred and recover from the fault.

Intelligent operators have historically provided an incredible amount of fault tolerance in systems which they monitor and control. Recent efforts have been directed towards making the hardware itself, independent of the operator, fault tolerant. Today most "fault tolerant" systems are ones which are presumed to operate autonomously without operator intervention. Indeed with the advent of missions/systems/parts which can suffer irrecoverable damage in times shorter than the time required for data transmission to the operator, on-line autonomous fault tolerance is needed.

Fault tolerance is based on good fault avoidance practice. Known fault susceptible parts or subsystems should be avoided. Fault tolerance involves fault detection, fault diagnosis, and recovery. Fault detection can involve operator action as well as on-line autonomous detection. Recovery can be either fully operational or in a degraded mode.

On-line fault detection includes self-checking circuits, and various error codes. Historically Hamming codes have been used in data transmission as error detection schemes. Many times error detection is coupled with error correcting if the number of errors is limited, and the code not only recognizes an error, but specifically what the correction is.

Diagnosis is invoked by the fault-detection scheme. It has the responsibility to isolate the software, hardware, or combination of software and hardware which has failed. Once isolated, the failed unit needs to be replaced. There are many strategies available in the recovery phase. Standby sparing, system reset, retry, reload, masking, safe shutdown, safe reduced operation, or some combination of the previous modes are all possible options available to the system designer. But without a specific system and specific mission requirements, it is difficult if not impossible to cast a generic solution.

Fault tolerance sometimes involves significant costs -- in both hardware and software. The useful throughput of the system is also reduced as additional program execution is normally required in fault tolerant systems.

There are a number of schemes of hardware redundancy which allow fault tolerance: dual redundant, dynamic redundancy, reconfiguration (replacement of failed components with spares), N-modular redundant systems, and error correcting codes. Each scheme needs to be evaluated for its intended mission with regard to reliability, lifetime, and cost. A fault tolerant system cannot be effectively designed in an ad hoc way, it must be carefully thought through so that each item, spare, redundant module, etc. plays a useful role in protecting the system from all possible faults. Each year the IEEE holds an "International Symposium on Fault Tolerant Computing." This conference is an excellent resource for many aspects of fault tolerant design. In addition there are a number of texts on fault tolerance, reliable system design, and related topics which provide a great deal of detail on the advantages and disadvantages of various schemes.

6.4.4. Methods of Circumvention -- System Level

Following the main line of immunity of SEU hard parts, there are several methods which might possibly help an SEU problem. Among these are watchdog timers, shielding, error detection and correction at the system level (various kinds of redundant systems, voting schemes, etc.), and operational work-arounds (memory loads, restarting, etc.).

For a low enough SEU rate, a timer which expects a signal from the computer or restarts the system will prevent errors from stopping processing, although the data itself might be suspect. The timing interval is chosen so that no more than one error is expected during the timing interval.

Although shielding to attenuate the heavy ion or proton particle flux is not very effective for galactic cosmic rays it can make a difference for lower energy heavy ions when they can make a significant contribution to the total SEU rate.

Alert operators will restart, or even reload memories after suspected SEUs are experienced. For some operating spacecraft, memory reloads have become common practice to account for SEU sensitive designs.

Ultimately, the project or system designer eliminates SEUs using the most cost-effective ways he can to ensure:

1. Reduction in outage times
2. Increased reliability

3. Enhanced probability of mission success
4. Increased system lifetime.

The system designer's options range from SEU immune parts to fancy error detecting and correcting circuits. The most cost-effective way of designing the system to be SEU immune will depend on setting priorities for ensuring immunity, and for methods which are to be used in achieving that immunity.

6.5 Testing

The final step which proves that the complete system does not respond unfavorably to ESDs, IDs, or SEUs is system testing. Extensive testing before launch helps assure the system will not experience any difficulty in space. Testing is a check on the design, the workmanship, and the reliability of the system. Proper testing, coupled with an understanding of the interaction of the space system with the environment, should give the system designers and users confidence in the immunity of their system. Table 6-4 summarizes the testing required for a full analysis of SEUs,surface, and internal charging/discharging.

Table 6-4 Anomaly Testing Summary

Concern	Test
Surface charging	Material characterization: aging tests surface secondary emission photoconductivity radiation induced conductivity backscattering coefficient
Surface Discharges	EMC testing (general) surface discharge testing: capacitive coupling arc injection arc radiation
Internal Discharges	EMC testing (general) material/configuration testing detailed subsystem testing
SEU Testing	Part characterization Error simulation: software testing hardware test

On a fundamental level, determining the part or material behavior is basic to understanding its response in the environment. For integrated circuits concerned with SEUs, this means discovering the part's sensitivity to heavy ions and protons. For surface charging, material testing determines the secondary emission yield, photoemission characteristics, conductivity, and aging characteristics of the material so that charging calculations can be done. For both internal and surface discharges, material testing helps determine the probability and the characteristics of the discharge.

6.5.1. Surface Charging Testing

Before any assessment of the charging state of a space system, one needs to know the response to the environment of the materials used. For surface charging/discharging we will assume that the environment for the system has been established by measurement and theory and includes a significant plasma environment. It may not be clear at the outset exactly what comprises a "significant" plasma environment. Material tests in the specified environment will show whether the environment is "significant."

Much of the early characterization of spacecraft materials was done in simple vacuum chambers with a monoenergetic electron source at one end and the sample at the other end. Typically the sample was mounted on a plate that was grounded through a microammeter. In this way, the current leaking through the sample was measured. Non-contacting voltage probes were passed in front of the samples to measure the voltage of the sample surface. By varying the accelerating voltage on the electron gun from 1 to 30 keV, the material under test was characterized. Tests of this kind gave a good engineering understanding of the material properties, but not a complete scientific analysis. Discharges, if any, were the main objective of this type of experiment and were detected by sudden currents through the ammeter and by noting the change in voltage of the surface before and after sudden changes in the current. Materials which did not discharge in an electron beam test at 20 keV with beam current densities of 10 nA/cm^2 were usually deemed "safe" from a surface discharge point of view. Later Mizera et al. (1980, 1981), and Mizera and Boyd (1982), based on SCATHA charging results, showed that low flux tests were also important. At lower fluxes, the conductivity of the material is low enough to allow high charge accumulation on the samples; while at higher fluxes, the radiation induced conductivity may allow sufficient charge to bleed off to prevent discharges.

Test facilities for engineering tests of this type have been developed at several aerospace companies, NASA/Lewis Research Center, JPL, and the Aerospace Corporation. Some of these facilities are very complete and allow simultaneous exposure to electrons, ions, and ultraviolet radiation [Leung et al., 1981].

A nagging question that raises doubt for both photoemission and secondary emission and, hence, the charging process, is the passage of time. Both photoemission and secondary electron emission depend on the state of the surface of the material and to some degree on the chemical nature of the material. Certainly the surface of the material is influenced by the history of the material. Here the word "history" is meant to encompass all of the events that happen to the material. Radiation damage, thermal cycling, outgassing, and many other effects change the condition of the material, and this whole process is referred to as aging. A full analysis of the charging of a spacecraft includes the effects of aging. Although most analyses done so far for spacecraft ignore aging effects, the long missions now under consideration make aging concerns of more importance.

Another nagging question is the effect of the handling and processing of the material used on spacecraft. Typical scientific measurements are made on carefully prepared pure samples so that the results are not influenced by any contamination. Although spacecraft materials are typically cleaned and handled carefully, the detailed behavior can be different from pure materials. For example, the secondary yield for pure aluminum and that for aluminum with a thin oxide are different in detail. The buildup of the oxide layer can be observed as a change with time of the secondary emission of a pure aluminum sample. Studies of thermionic emitters for cathodes in electron tubes showed wide variations depending on trace elements or impurities in the material. Most spacecraft material tests have been done with "as received" materials, rather than specially prepared ones. For this reason, it is sometimes desirable to perform sensitivity studies to determine when variations in material properties impact charging/discharging analysis.

6.5.2. Internal Charging Testing

Testing materials for internal charging involves a simulation in which the charge deposited in the material simulates the charge which would accumulate during the spacecraft's flight. Simulations have shown that it is important to reproduce the rate as well as the total charge deposited for accurate results. Internal discharge tests require penetrating electrons. The electron range needs to be sufficiently deep to deposit charge in the region(s) thought to be sensitive to discharge. The flux needs to be chosen so that the charge built up in the sensitive volume is comparable to that expected on the mission. To meet both of these conditions may require long testing times on 2–3 MeV electron accelerators. When this is not acceptable because of accelerator scheduling and/or costs, short tests might be designed. Then one must address the question of how conservative the test should be. For internal

charging, the higher the rate the more likely there will be discharges if the radiation induced conductivity is small. An analysis of shortened engineering tests should include both the likelihood of a higher internal electric field due to the high flux of trapped electrons, and the additional loss of trapped electrons due to radiation induced conductivity. Many of the tests for the Galileo spacecraft were done using monoenergetic beams and only simulated the total charge deposited and the rate. Coakley et al. (1982) simulated the spectra as well.

Internal discharge tests can be divided into two classes, generic materials and spacecraft subsystems. The materials investigated for the internal discharge monitor are examples of generic materials. Tests for Galileo and other systems involved the irradiation of small pieces of hardware -- relays, specific circuit boards, small assemblies of various kinds -- in which the tests served to show the behavior of that particular collection of things. Spacecraft subsystem tests are very good engineering tests, and tend to underline the generic guidelines. For example generic tests show clearly the danger of flying ungrounded areas of metal that are well insulated by good dielectrics such as circuit boards. Specific subsystem tests revealed ungrounded metal areas which discharged. The advantage of subsystem testing is of course that it shows not only if there is a discharge, but if that discharge makes any difference to the operation of the subsystem. From a short term engineering point of view, it may be perfectly all right for a discharge to occur, if it does not affect the operation of the system. Discharges over long periods of time may degrade operations or even lead to failure. Testing subsystem by subsystem tends to be expensive, so that our recommendation is for generic tests wherever possible. Generic testing permits the generation of design rules, which can then be used to evaluate specific hardware to assure that it complies.

In chapter 4, the results of ground testing of a selection of internal discharging configurations and materials were presented. The configurations were generally chosen to represent situations with one free surface, situations bounded with grounded-by-metal enclosures (cables, capacitors, etc.), and situations where metal volumes were well insulated from ground. Those experiments considered planar and cylindrical geometries. Real geometries are of course more complex and may influence the detailed results. As usual, good engineering judgment is needed to determine the proper response in a given situation.

6.5.3. Single Event Upset Testing

Recently single-event upset testing has become necessary. As steps are being taken to address this issue, designs are becoming less susceptible to single event upsets. The work reported in the IEEE conference each July (and reported in the December issue of *Transactions on Nuclear Science*) has chronicled the progress in this area in the last few years.

Device sensitivity to single event upsets is generally believed to be due to the charge generated along the path a heavy ion takes through a sensitive region in a device. This was discussed in chapter 4. Modern electronics has combined in a single chip many functions and elements. Therefore intelligent testing requires a careful consideration of the device before the testing actually begins. This can begin with a study of the device with the purpose of identifying the bistable elements in it which may be susceptible to upset. Once these elements are found, hardware and software are needed to exercise these elements in a test to determine their state, so one can determine if an SEU has occurred. If possible, it is good to allow only one SEU per measurement cycle. This allows determination of the location of the SEU as one region may be more sensitive than another. Some experimenters use a "gold" pattern that is stored in an identical device with a reference pattern installed to which the device under test (DUT) is continually compared. The hardware for SEU testing is indicated in Figure 6-7. Key features of this design were provision for vacuum and the turning of the parts to the incident beam to allow particles to enter the sensitive region at non-normal incidence. Studies in which the temperature can be selected are also becoming popular. Typical data is shown in cartoon form in figure 6-8.

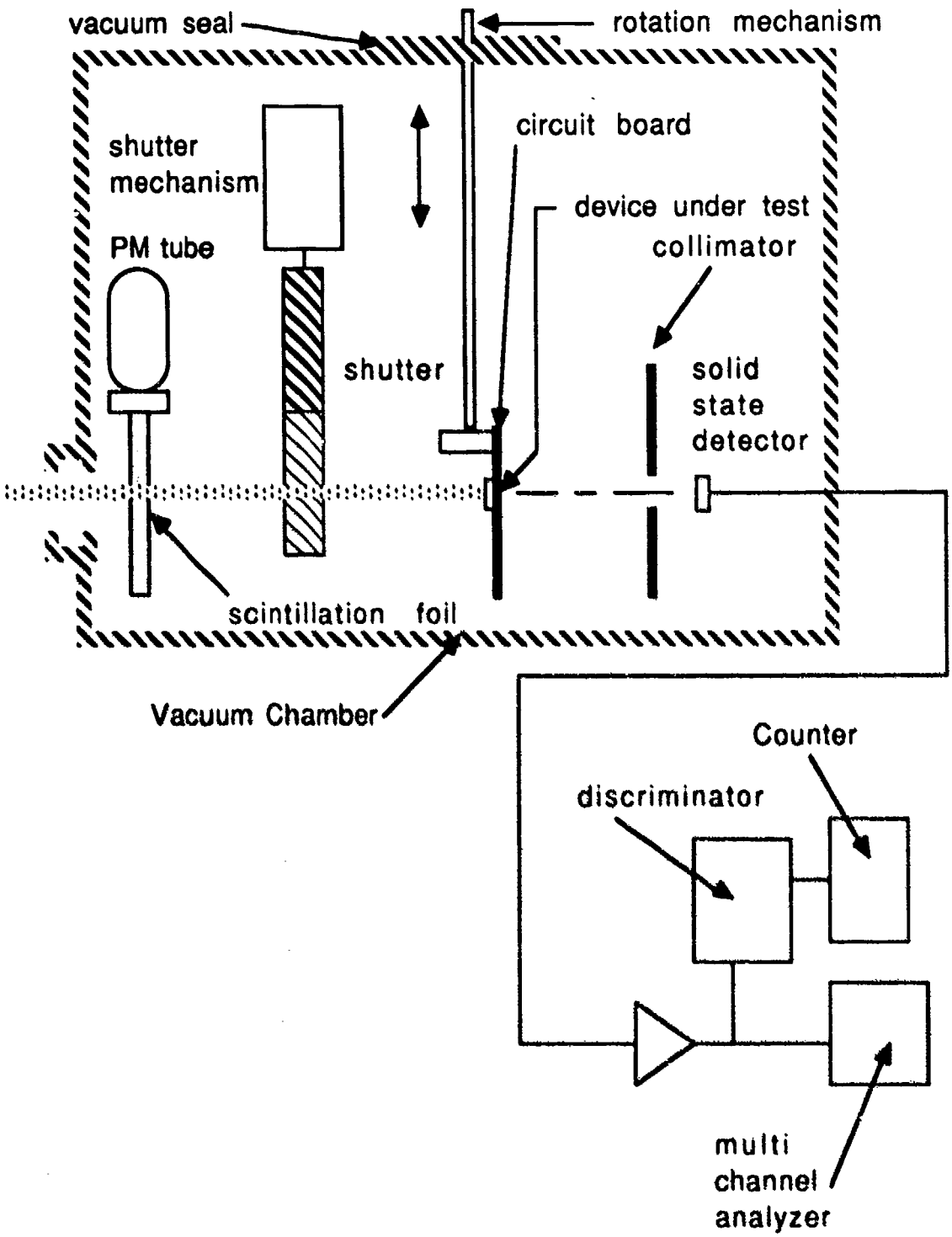

Figure 6-7 Test Apparatus. Photomultiplier output used to monitor the beam during SEU testing. Solid state detector provides accurate beam diagnostics for set up. Shutter commanded in or out of beam. Device under test can be raised or lowered as well as rotated. Device under test performance is monitored and compared to "gold chip" (not exposed to beam)

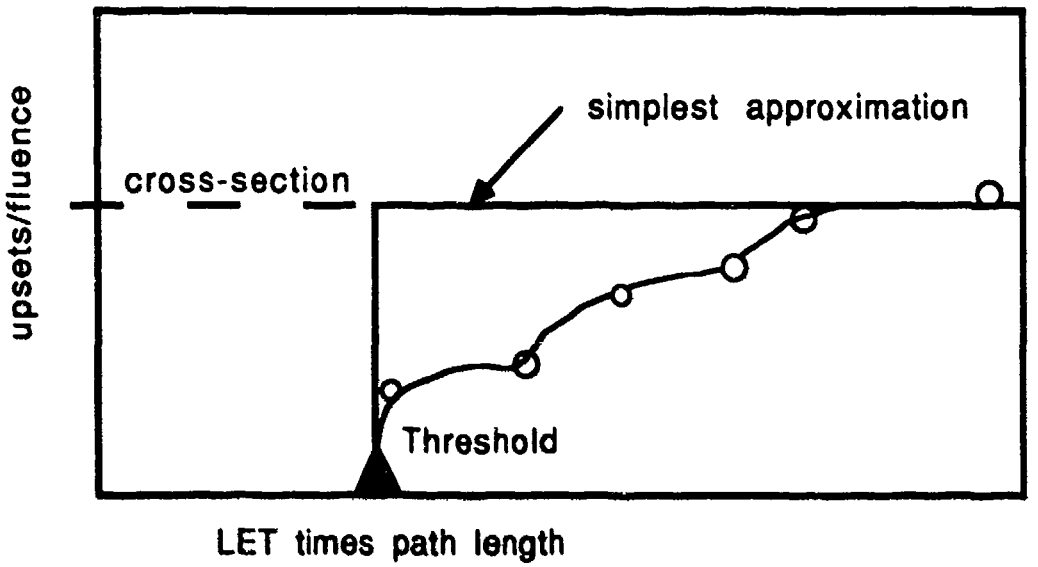

Figure 6-8 Typical Parameterization of SEUs. The two key parameters for determining the SEU rate are the threshold and the cross section at large LET times path length. The actual cross section as a function of LET times path length will give a more realistic lower value of SEU rate

The sequence of events in an SEU test needs to be well thought out. Experienced test directors have thought through in advance the purpose and methods needed to get data for their projects and are able to adapt t flow of the experiment to the project needs and the limits of the accelerator and its schedule. Such a plan is sh in Figure 6-9 or an early Galileo test. Some of the early steps insure that the beam is behaving as expected b retesting a part known to be sensitive to SEU. Variations in voltage on the part allow examination of the thr as a function of voltage. One would expect the threshold to be lower for parts operated at low voltage. Thus first test has the largest possibility of measuring SEUs at normal incidence. If none are observed, the angle o beam with respect to the plane of the chip is varied to increase the "effective LET" through the sensitive regio upsets occur readily, the search for the threshold continues by using lower LET particles. It is usually important obtain a cross section and a threshold for SEU events so that the program can predict the maximum SEU rates particular mission. If possible it is highly desirable to determine as clearly as possible the charge collection mechanism and the "sensitive volume" as described in chapter 4. his includes an estimate of the thickness o sensitive region, and the number of active regions involved in the test.

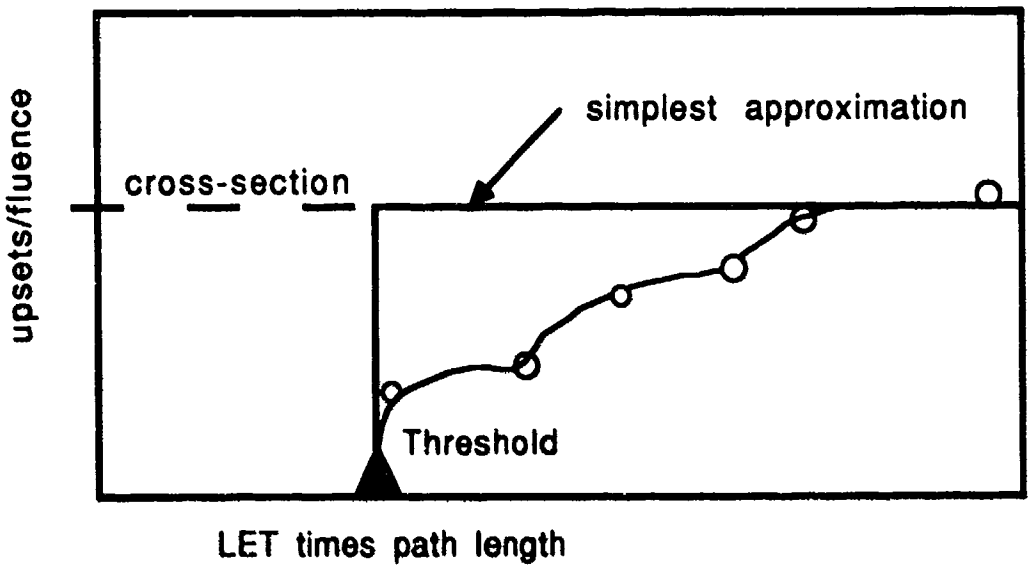

Figure 6-8 Typical Parameterization of SEUs. The two key parameters for determining the SEU rate are the threshold and the cross section at large LET times path length. The actual cross section as a function of LET times path length will give a more realistic lower value of SEU rate

The sequence of events in an SEU test needs to be well thought out. Experienced test directors have thought through in advance the purpose and methods needed to get data for their projects and are able to adapt the flow of the experiment to the project needs and the limits of the accelerator and its schedule. Such a plan is shown in Figure 6-9 or an early Galileo test. Some of the early steps insure that the beam is behaving as expected by retesting a part known to be sensitive to SEU. Variations in voltage on the part allow examination of the threshol as a function of voltage. One would expect the threshold to be lower for parts operated at low voltage. Thus the first test has the largest possibility of measuring SEUs at normal incidence. If none are observed, the angle of the beam with respect to the plane of the chip is varied to increase the "effective LET" through the sensitive region. I upsets occur readily, the search for the threshold continues by using lower LET particles. It is usually important t obtain a cross section and a threshold for SEU events so that the program can predict the maximum SEU rates for particular mission. If possible it is highly desirable to determine as clearly as possible the charge collection mechanism and the "sensitive volume" as described in chapter 4. his includes an estimate of the thickness of the sensitive region, and the number of active regions involved in the test.

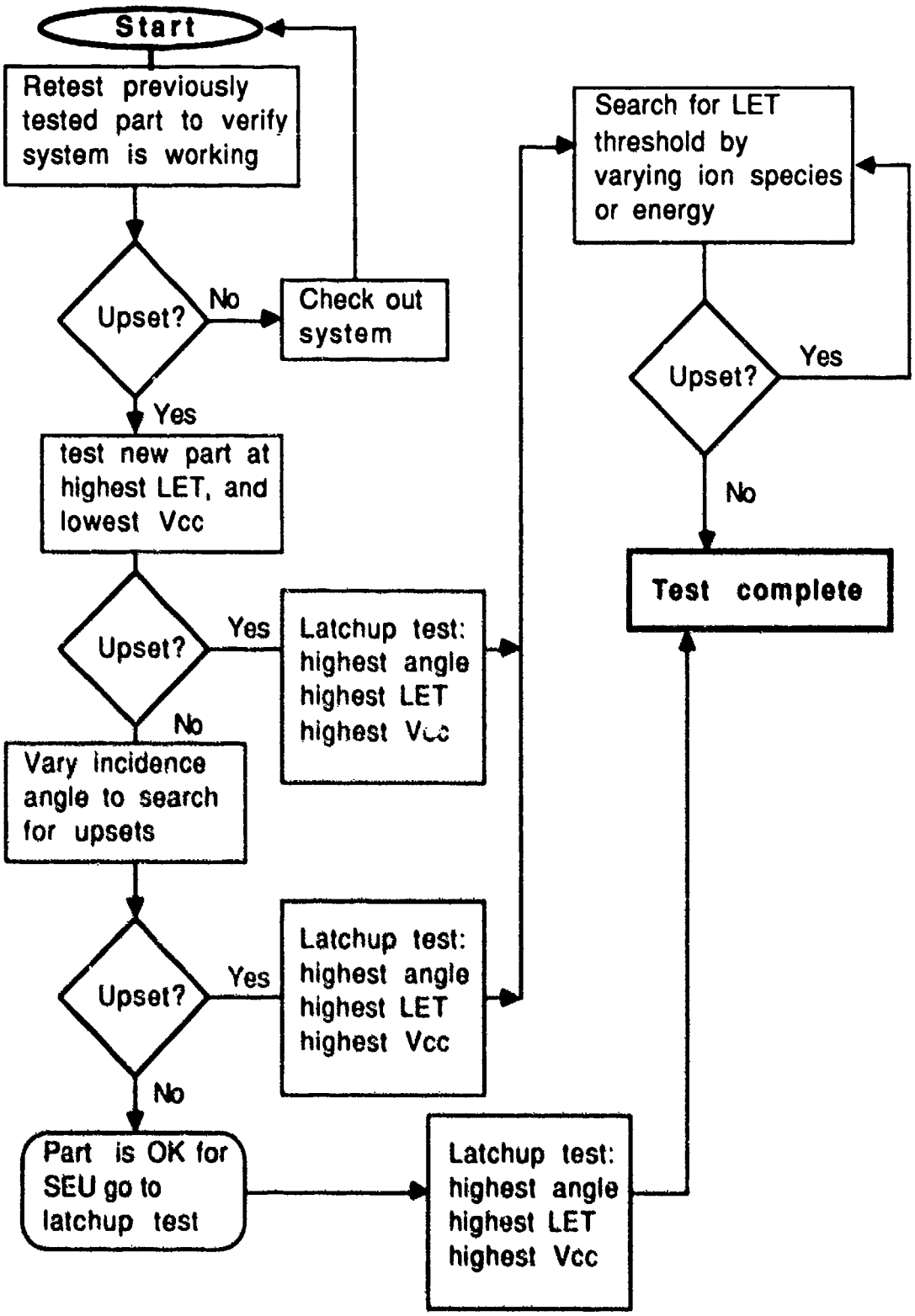

Figure 6-9 Test Flow Diagram

Figure 6-7 is a schematic representation of a test setup used to measure SEU sensitivity. Measurements are performed in experiments using heavy ions, in which a uniform beam hits the device. One observes the upset cross section as function of the energy loss of the particles. The upset cross section will be the number of upsets per particle/cm^2 hitting the device. This has units of area, so the term "cross section" seems appropriate. As the energy loss of the particles is increased, the particles cross a threshold for upset. Above this threshold the upset rate increases rapidly until all particles can deposit enough charge to cause upsets. At this point, the entire active area of the device succumbs to upsets at a limiting cross section called σ. The LET threshold L_0 occurs when the charge deposited equals the critical charge, so that L_0 may be combined with an assumed collection depth (d) in calculating the critical charge: $Q = L_0 d$.

Measurements of critical charge enable us to compare the sensitivity of various devices. This cannot be done by comparing critical charges alone. Instead, the sensitivity is stated in terms of upset rate in a reference environment. The upset sensitivity can be calculated as a function of the geometry and the critical charge.

A full parts characterization is designed to obtain an upset cross section versus LET. Two key experimental parameters are a high LET (for example ~300 MeV krypton with an LET =35 MeVcm^2/mg) cross section and the threshold LET for the onset of SEU. If the most ionizing beam used does not induce upsets at an angle up to 70° from the perpendicular, it is reasonable to assume there will be no upsets in interplanetary space.

It is worth noting here that the angle of the test beam, part bias, clocking parameters, and pattern configuration are important variables for all tests. The selection of ion species (usually krypton, argon, oxygen, neon, and carbon) and their energies dictate what the LET of the beam is. Because of the increased path length of oblique beams in the sensitive volume (those beams impinging at an angle θ with respect to the perpendicular), the effective LET threshold is often found by varying the beam angle, according to the relation

$$\text{LET(effective)} = \text{LET(ion)} \sec\theta \quad \text{for} \quad \theta \leq 60 \text{ degrees}$$

If a calculation of SEU rates for a known environment is required, then both LET threshold and high LET cross section data are required.

The range of one or two MeV/amu heavy ions is very short (a few microns), so the tests are conducted in a vacuum and the device lids are removed. In applying test results for parts where the sensitive volume is beneath passivation and other layers, it is important to account for the energy and LET changes that occur in getting to the sensitive volume. Tests with particles which stop in or before the sensitive volume are suspect.

Studies of temperature variations are becoming an integral part of SEU testing. Any system expected to operate at a temperature significantly higher than 20°C should, as a minimum, compare the effects of temperature for a selected number of parts. A difference in applied bias does have a profound effect on SEU response. For "soft error" testing, parts at a lower bias are most susceptible to upset; for latchup testing the opposite is true. Clock rates have a noticeable (but not enormous) effect on SEU rates. The pattern configuration usually does not affect the SEU response except occasionally near the LET threshold.

Proton tests are a straightforward variation of heavy ion testing. Usually much higher fluxes and fluences in terms of particles/cm^2 are required in proton testing, unless direct ionization by protons in the sensitive region can cause upsets. In those cases, proton tests along the most sensitive direction are desired, with beams with sufficient range to cross the sensitive volume.

Once the beam requirements and the appropriate accelerator have been selected for meeting the desired test objectives, it is time to implement the test. The beam line from the irradiation source is collimated and aligned with a vacuum chamber. Usually the test chamber is located remotely (e.g., behind shielding walls) from the tester/counter and dosimetry electronics. A test board and a beam scintillator/photomultiplier assembly located in the vacuum chamber are used to monitor and align the beam.

Testers range from slow manual counting of individual upsets to sophisticated computer video displays depicting upsets positioned according to their location on the chip. Current systems will have millisecond electronic reset capability, a variety of pattern configurations (e.g., checkerboard, all ones, all zeros), provisions for testing separate subsets of complex devices (e.g., flag registers, I/O latches, etc.), variable bias capability, variable clock frequencies, etc. Some tests will also have temperature control and automatic logging of bit flips and beam parameters.

The test boards are designed to hold several devices under test (DUTs), drivers, buffers, and detection electronics (e.g., a comparison test of a DUT response with that of an unirradiated reference device). The boards are mounted in such a way as to permit translational motion (selection of devices) and rotation (to change beam angle of incidence) without requiring the vacuum in the chamber to be broken.

The beam dosimetry for the requisite low ion fluxes (10^3 to 10^6 ions/cm^2/s) utilizes a scintillator to count each ion. The beam may pass through a very thin (microns) foil whose thickness is chosen to give the proper light amplitude to correspond with the beam's LET, or it may pass through an annulus which permits part of the beam to stream unimpeded onto the DUT while the outer portion is stopped by a thick scintillator. The light is then piped to a photomultiplier tube (PMT). A discriminator is used to reject all noise pulses and pass all pulses caused by the beams. Certain limits are imposed on the maximum beam intensity to prevent saturation of the PMT. In addition, beam control will include procedures for measuring ion energy and establishing beam uniformity.

A number of facilities have been used in SEU testing. Table 6-6 is a typical list. Usually tests with heavy ions are done first and if necessary proton tests follow.

Table 6-6. Test Facilities

Machine	Location	Typical Particles
88" Cyclotron	U.C. Berkeley	O, Ar, Kr, 4 MeV/nuc
BEVELAC	U.C. Berkeley	Fe 1 GeV/nuc
Van de Graff	Caltech	He, O
Cyclotron	NRL or U.C. Davis	< 50 MeV protons and neutrons
Cyclotron	Harvard Univ.	130 MeV protons
Cyclotron	Indiana Univ.	<200 MeV protons
TRIUMPH	British Columbia	400 MeV protons
CERN	Switzerland	600 MeV protons
SIN	Switzerland	590 MeV protons
AGS test beam	Brookhaven	4 GeV protons

Tests using radioactive Californium can also provide valuable insight into the sensitivity of parts (Reier, 1986, Mapper et al., 1985, Blandford and Pickel, 1985, Stephen, 1984a,b). Californium tests take advantage of the spectrum of high energy heavy ions resulting from Californium's spontaneous fission.

6.5.4 How Many Tests Are Enough?

Since SEUs occur relatively rarely, it is important to understand the statistics involved in their measurement. Test time can be very expensive and the number of actual SEUs induced in the devices under test (DUT) quite small. Statistical variations play an important role in setting the safety margin between the "average device response" and the design point. Variations can be characterized by two classes.

1. The distribution within the population. This is due to the physics of the parts and processing, etc. and represents a fundamental limit for the part and response. Safety margins can be smaller if the population distribution is narrower.
2. The uncertainty in our knowledge of the population distribution is due to the limits on the size of the test sample.

Both variations are important and play a role in determining the sampling philosophy of a program. For example, limiting the population to a single manufacturer, a single code lot, or selected diffusion lots results in distributions which one would expect to be well defined with small standard deviations. This is why single buys with careful screening are used in programs where high assurance is needed. Large sampling from such a controlled distribution should result in the smallest variation from both the population distribution and the uncertainty in our knowledge.

To estimate the mean and standard deviation of a population, one makes a series of measurements. Based on a series of N measurements the mean is estimated by

$$\text{Mean} = M = \frac{1}{N} \sum_{n=M}^{n=1} x(n)$$

with a standard deviation estimated from

$$\text{variance} = \sigma^2 = \frac{1}{N-1} \sum_{n=N}^{n=1} \{M - x(n)\}^2$$

Many times, especially in textbooks, the true population is assumed to have the form of a normal distribution with a precisely defined mean and variance (note the standard deviation is the square root of the variance)

$$P_y)dy = \frac{1}{2\pi\sigma^2} (e)^{-(x(n)M)^2/2\sigma^2} dx$$

For other situations, other distributions (e.g. exponential, gamma, Weilbull, etc.) may be more appropriate. So although most examples assume a normal distribution, one should remain alert for data which violate this assumption.

6.5.5. EMC Tests

Testing for surface discharges and internal discharges is best done in conjunction with standard EMC testing and evaluation. Surface and internal discharges represent a specific source of radiated and conducted noise which the system must tolerate in order to perform. Normal EMC procedures such as those in the EMC handbooks should be followed. When systems or subsystems are tested they need to exercise all of their modes, and should be configured so that the test setup does not induce anomalies that would not occur in the real situation.

Ideally subsystem testing is identical to that of the normal environmental qualification test:

(1) Subject the spacecraft to a specified environment that is representative of that expected plus any engineering margins.
(2) Have a design qualification test sequence that exercises all elements of the hardware, and all modes of the system.
(3) Establish a flight qualification and flight acceptance philosophy.

Some programs have a separate qualification model which is tested to the full extent and duration environments (plus margins), while the flight hardware is tested only to the full levels but not to the full duration. This insures the design is adequate (the qualification test) and that the workmanship is adequate on the actual flight hardware (flight acceptance). In other cases, only one set of hardware will be built and one must weigh the desirability of extensive ground testing with the possibility of over-testing or stressing the flight hardware so that it fails in flight. When there is only one piece of hardware for both qualification and flight, the tests are referred to as protoflight tests. Generally extensively tested hardware (even if it has had to be repaired) has performed better than inadequately tested hardware. One flight systems program manager at JPL has commented that he has never seen a spacecraft fail in flight due to excessive ground tests, but he has seen flight failures due to inadequate ground testing.

In space, the flight spacecraft will be electrically isolated from ground and bombarded with electron, ion, and extreme ultraviolet radiation levels. Systems should operate without upset throughout this phase. Such an environment could be simulated on the ground, but the costs in facilities, schedule, and engineering would be high. Therefore, spacecraft charging tests usually take the form of assessing unit or spacecraft immunity to electrical discharge transients. The appropriate discharge sources are based on separate estimates of discharge parameters (location, duration, frequency, and amplitude).

Arc discharge tests are both simple to do and useful checks on the closure of the Faraday shield design. Even in cases where discharges are not expected to occur, radiated energy from portable arc discharge simulators

provides a quick, convenient, EMC-type check-out during systems testing. Injected and capacitively coupled tests, however, should be carefully planned and executed. Comparisons of predicted versus actual arc discharge characteristics and tested versus predicted response complete the verification of the system, and prepare operators for any anomaly investigations required in the future.

ESD test techniques are not well established because: the system itself dictates what the proper test should be, each system response is influenced by so many details, and the arc source itself is stochastic. It is important, therefore, to understand the various parameters which affect arc generation and coupling to the system. A spacecraft with a completely conducting exterior surface should not experience any surface discharges. Discharge testing on its surface therefore would not be appropriate; however, verifying the soundness of its Faraday shield for external sources (e.g. lightning) with an arc discharge radiating energy might be very appropriate. Some of the important considerations in designing discharge tests are:

(1) Spark occurrence and location:
   a) Will the expected environment cause discharges?
   b) What kinds of discharges are expected? (The types of discharges one might expect are described below.)
   c) What are the return current paths?

(2) Characterization of discharge region:
   a) What are the background radiated fields or structural currents?
   b) What are the area, the thickness, and the dielectric strength of the material?
   c) What is the total charge involved in the event?

(3) Characterization of discharge:
   a) What is the breakdown voltage?
   b) What is the current or voltage wave form: rise time, width, fall time, and rate of rise
   c) What is the impedance of discharge?

(4) Characterization of coupling to spacecraft:
   a) What is the location of discharge and coupling of the discharge to the spacecraft?
   b) How is the discharge source grounded?
   c) What is the return path for coupled current?
   d) What are the possible victim circuits?

In the fourth question we are concerned with exactly how the discharge current flows about the spacecraft. How is the discharge coupled to the rest of the spacecraft? Possible answers are: capacitively, inductively, or through directly connected conductive path(s). Discharges come in different varieties. These have been colorfully described as blowoff, punch-through, and flashover. In blowoff, charge is released to space from the surface of the discharge. Eventually charge balance is achieved, but initially there is a net flow of charge away from the spacecraft body. This causes current throughout the entire structure of the spacecraft. Blowoff is simulated by setups in which the return current from the discharge is far away from the injection point or the coupled point. A large capacitively coupled discharge simulation in which the capacitor and the spacecraft both use the test facility ground might be used to simulate this kind of discharge.

Punch-throughs are small breakdowns which sometimes leave a small puncture in the dielectric. Currents flow from the trapped charge to its image charge on the other side of the dielectric. Except for the energy radiated away from the breakdown there are no large current flows outside the immediate region of the punch-through. Punch-throughs are simulated by the radiated emission of a self-contained discharge. This type of simulation is good for surface discharge tests and quick EMC tests. Usually the radiated emission has no effect on a spacecraft unless there is a serious fault in its immunity to electromagnetic noise. However, even though punch-throughs themselves are not expected to be a problem, and are seldom observed, they apparently can instigate blowoff discharges which are more likely to cause problems for space systems.

Flashovers occur when the charge on the surface neutralizes its image charge either through a punch-through or across an edge. Flashovers involve a large surface area and therefore large total charge. Since this charge is moving about, large currents can be induced in other parts of the spacecraft. This type of discharge is simulated by specific current paths through or around the spacecraft. For example, if an antenna is expected to discharge along an edge, the assumed current path might involve the antenna, the antenna mast, and the spacecraft body. A large metal sheet paralleling the antenna might simulate the charge buildup, and this capacitor might be referenced to a ground,

for both the metal sheet and the antenna, at the base of the antenna. The discharge would then be assumed to short out the metal sheet to its ground, allowing currents to flow from the antenna structure to the base of the antenna, with possible coupling to the main spacecraft body.

Each region and discharge mechanism needs to be evaluated individually. For example, one might begin by estimating the capacitance, C, of the region of concern using the surface area, dielectric thickness, and dielectric constant. If one then assumes the breakdown occurs across the thinnest part of the dielectric, the dielectric strength of the material provides an estimate of the breakdown voltage (punch-through). In other cases, the breakdown at an edge (flashover) might be assumed. For an edge breakdown, the breakdown of a vacuum might be more appropriate. The total energy involved in the discharge is estimated by

$$E = \frac{C V^2}{2} \quad (6\text{-}6)$$

where C is the capacitance and V is the voltage.

Experiments in the laboratory have determined that peak current in the discharge scales as the square root of the area involved in the discharge. Flashover discharges occur with rise times on the order of the distance over which the flashover travels divided by one third of the speed of light. Blowoff discharges involve the capacitance to free space and velocities of a plasma cloud on the order expected by electrons accelerated by the electric field just before breakdown. The variability seen experimentally in the magnitudes and durations of discharges suggests that the same region may discharge in more than one manner, and/or that several different regions are involved in discharging. Vampola et al. (1985) have summarized their results from measured discharges on the SCATHA spacecraft. A total of 77 pulses occurred on 35 separate days, which included both surface discharges and internal discharges. Some of the measured surface charging pulses far exceeded the response of the pulse monitor to the Military Standard 1541 (MIL-STD-1541) test pulses. This implies that unthinking application of MIL-STD-1541 may not provide adequate testing of a space system.

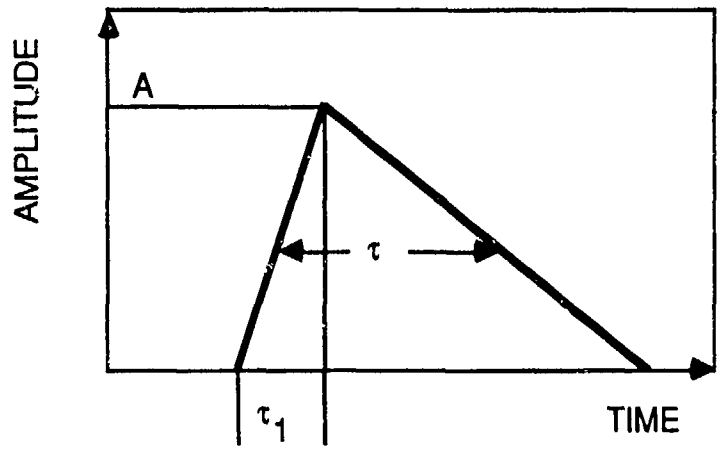

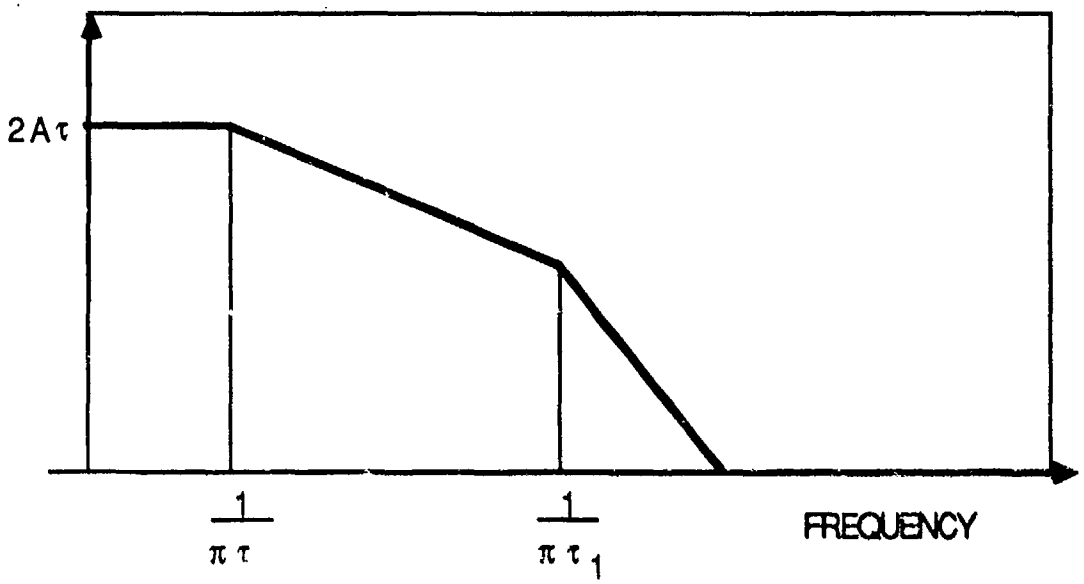

SOURCE	τ_1	τ	$1/\pi\tau$	$1/\pi\tau_1$	A	$2A\tau$
LIGHTNING	0.05 µs	20 µs	17 kHz	650 kHz	50 kA	2 kA/kHz
EMP	10 ns	250 ns	1.3 MHz	30 MHz	100 kV/m	50 VkHz/m
ESD	1 ns	150 ns	2 MHz	300 MHz	5 A	1.5 A/MHz
ID	0.1 ns	10 ns	30 MHz	3 GHz	0.2 A	4 A/GHz

(after Mardiguian, 1985)

Figure 6-10. Typical Discharges

Since a discharge of any kind is compared to a lightning stroke, Figure 6-10 (Mardiguian, 1985) compares the energy content as a function of frequency for several of the more popular discharges, including surface and internal discharges.

Michel Mardiguian (1985) points out that an ESD or surface discharge simulator does much more than just explore the weakness of the system to static discharges. He states, "Although the ESD test cannot pretend to replace the traditional method, the wideband field which flashes produce all at once reveals many of the same weak spots that classical EMI tests explore:

1. improper circuit board layout -- poor or missing decouplings, long runs far from their return trace, etc.
2. missing or loose ground connections
3. uncontrolled ground loops and parasitic capacitances
4. improperly terminated cable shields and poor connector bonding
5. shield discontinuities, etc.

Even more, an ESD test is usually very simple to run and is often ideally suited to field testing."

The MIL-STD-1541 arc source is available in several commercial versions and is easily made in an EMC lab. It can be used as a general EMC tool, as well as the specific surface charging simulator discussed below.

Military Standard 1541 (MIL-STD-1541) describes an arc source which is commonly used. The schematic and usage instructions extracted from MIL-STD-1541 are presented in Figure 6-11. The arc source is easily manufactured and provides some of the parameters necessary to simulate a discharge event. The only adjustable parameter for the MIL-STD-1541 arc source is the discharge voltage. The rise time, pulse width, and fall time are more or less constant. The discharge voltage is varied by adjusting the discharge gap and, if necessary, the dc supply to the discharge capacitor. The peak current and energy vary with the discharge voltages. This permits some degree of flexibility in planning tests, but not enough to cover all circumstances.

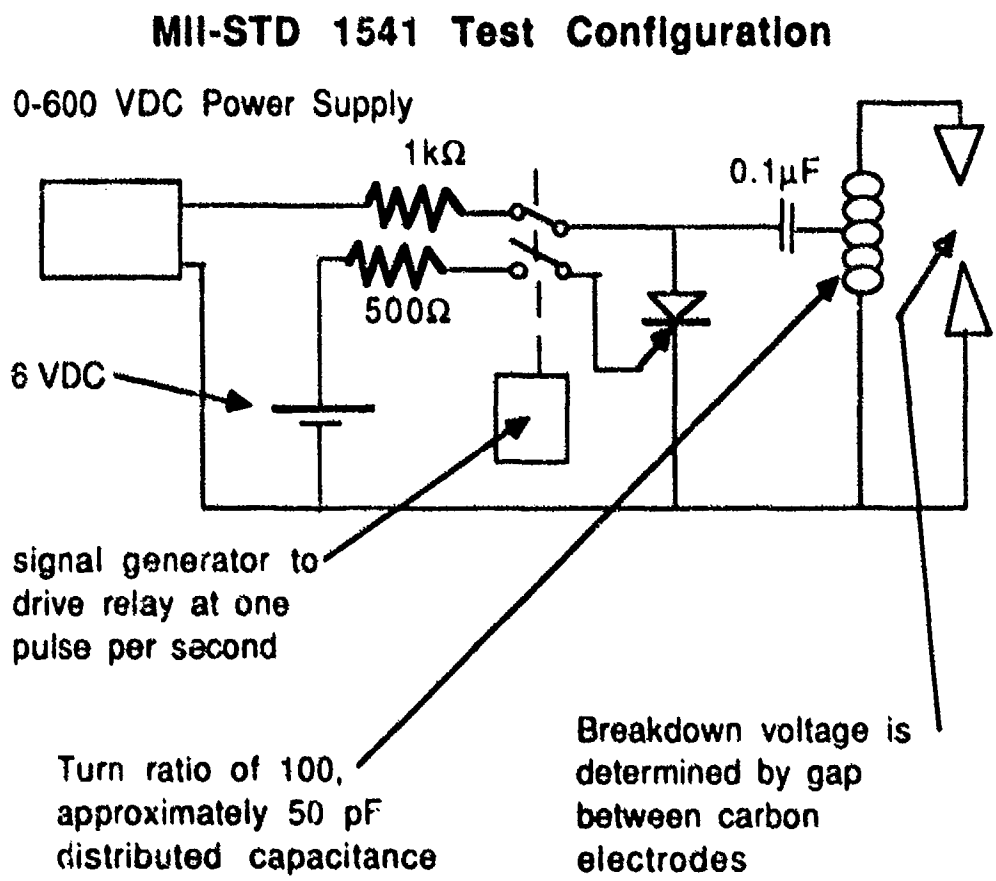

Figure 6-11 MIL-STD-1541 Test Configuration

A flat-plate capacitor is useful in several circumstances. A flat-plate capacitor can be used to approximate flashovers or blowoffs on thermal blanket areas, calibration targets, or nonconductive paints. The flat-plate capacitor permits a widespread discharge to simulate the physical path of current flow. This can be significant where cabling or circuitry is near the area in question. Also, the large size of the capacitor acts as an antenna during discharge and thus produces significant radiated fields.

Several parameters can be varied: the area, the voltage on the plate, and the dielectric thickness. These affect the capacitance, the discharge current, and the energy. The discharge voltage of the flat plate can be controlled by using a needlepoint discharge gap at the plate's edge, calibrated to break down before the dielectric, or some sort of switching circuit. This also affects discharge energy.

Rather than build a capacitor using the spacecraft as one plate, regular capacitors can be used to simulate the charge buildup in a given area, or regular capacitors can be used to supplement the charge stored on a flat plate arrangement. However, some capacitors have a high internal resistance and will not provide the fast rise times and peak currents.

Although in nature the occurrence of discharges is a random process, testing requires repeatable and controllable discharges. Switches are used to achieve repeatable and commandable discharges in some testing. The types of switches used in discharge testing range from spark gaps to electronics. A wide variety of switches are available to initiate arc discharges. At low voltages, semiconductor or mechanical switches can be used. The problem with mechanical switches is their "bounce." A bounce of the contact may result in non-uniform pulses; in some cases two or more discharges will be generated in a few milliseconds. Mercury-wetted switches can alleviate this problem somewhat.

The MIL-STD-1541 arc source uses a silicon controlled rectifier (SCR) to initiate the spark activity on the primary of a step-up transformer. The circuit is designed to produce a high voltage at an air spark gap on the transformer's secondary. The gap then breaks down, initiating the discharge.

For high-voltage switching in air, a gap made of two pointed electrodes can be used as the discharge switch. The tips are placed toward each other and adjusted so that the distance between them corresponds to the desired breakdown voltage. In air, this calibration is typically 1 mm/kV. The gap should be tested and adjusted before the test. A two parallel gap system is useful when the breakdown voltage is to be varied during the test. One gap is set for the maximum discharge voltage allowed and fixed; the second gap is then varied as the test progresses. Since the gaps are in parallel across the high voltage, the breakdown voltage of the system is determined by the lower breakdown voltage of the two gaps. The fixed gap acts as a safety gap preventing discharges from exceeding the maximum breakdown voltage desired. Calibrated gas discharge tubes can also be used as the safety gap, or when only fixed breakdown voltages are to be used in a test. Discharge tubes have faster rise times than needlepoint breakdowns in air, and are very repeatable. Their large dimensions make them better radiators of electromagnetic noise than simple air gaps.

A discharge produces a wide spectrum of radiated electromagnetic energy. Discharges from any source can affect the operation of a spacecraft. Discharge tubes or needlepoint gaps are effective in producing a wide spectrum of radio noise to verify the immunity of a system to RF interference and to check the susceptibility of scientific instruments.

To simulate blowoff or flashover events, current must be injected directly into locations on the spacecraft. One way to do this is to use a point on the spacecraft as one electrode in the breakdown gap. When planning this type of test, the spacecraft surface can be protected by a temporary metallic fitting at the location of the discharge test. This test is more severe than the radiated test, but better simulates the actual current injection at the discharge point. Depending on the return path used for the discharge gap this type of test simulates an event which places either large current flow about the spacecraft or only fairly local currents.

As described earlier, blowoff events can be simulated by metal plates or foil placed over the region of concern. Using any of the methods already discussed, the capacitor made up of the plate or foil as one side and the spacecraft as the other is discharged and the resulting structural currents induced to verify the immunity of the system. As with tests using the spacecraft as one electrode in a spark gap, tests which use the spacecraft as one plate of a capacitor depend crucially on how the return current flows. Causing that flow to traverse the entire length and breadth of the spacecraft is very different from a test in which the return path is as short as possible and confines currents to the area local to the foil. A number of current paths need to be considered and different parts of the spacecraft system need to be tested. A too remote return path may overtest the system, while a too short and local path may undertest the system. Here again, a detailed understanding of your system and the environment must be used to design and implement the test.

For internal charging and local surface charging concerns it occasionally is prudent to expose the subsystem of concern to penetrating electrons directly or to an energetic plasma. Such tests should be carefully designed not to overstress the subsystem, not to allow the measurements of the anomalous behavior to be the cause of the anomalous behavior, and yet to prove the subsystem will operate when exposed to the environment. For example, Leung and Robinson (1982) tested a number of Galileo subsystems and components for internal charging effects. In some cases, the results of these tests removed concerns which would have required considerable redesign effort.

System level testing involves large crews of people, costly facilities, a significant fraction of the funding, and is the first and last time the entire system is realistically exercised before launch. System level testing provides the most reliable determination of the expected performance of a space vehicle in the environment.

For surface charging concerns, discharges at the system level should duplicate the coupling paths which will be important in space. However, both internal discharges and SEU tests at the system level are difficult to plan and carry out. Therefore, surface and internal discharge testing may require testing on a representation of the spacecraft before exposing the flight spacecraft, to insure that there will be no inadvertent overstressing of flight units.

A detailed test plan must be developed that defines test procedures, instrumentation, test levels, and parameters to be investigated. Test techniques will probably involve current flow in the spacecraft structure. Tests can be conducted in ambient environments, but screen rooms with electromagnetic dampers are recommended. MIL-STD-1541 system test requirements and radiated electromagnetic interference testing are considered to be a minimal sequence of tests.

The spacecraft should be isolated from ground. Instrumentation must be electrically screened from the discharge test environment and must be carefully chosen so that instrument response is not confused with spacecraft response. The spacecraft and instrumentation should be on battery power to avoid ground loops. Complete spacecraft telemetry should be monitored. Full functional tests, if possible, are good. Voltage probes, current probes, E and H shield current monitors, and other sensors should be installed at critical locations. Sensor data should be transmitted with fiber optic data links for best results. Oscilloscopes and other monitoring instruments should be capable of resolving the expected fast response to the discharges (≤250 MHz).

The test levels should be determined from analysis and test of discharging behavior in the substorm environment. Purvis et al. (1984) recommend full level testing, with test margins, for structural, engineering, or qualification models of spacecraft. The test measurements (structural currents, harness transients, upsets, etc.) are the key system responses that are to be used to validate predicted behavior. Some manufacturers reduce test levels for flight hardware to avoid overstressing anything. It can be argued that there have been more in-flight failures due to insufficient testing than overtesting, although thorough development testing gives one confidence in shortening or lessening flight-unit testing.

6.5.5.1. Tests Designed Specifically for Surface Charging

Surface discharges have been bothersome to spacecraft designers for a long enough period so that test practices are being developed. Below is the section on system testing for surface charging effect from Purvis et al. (1984). This is followed by an abstract of the test actually done on INTELSAT VI by Tucker (1987). ESA is currently carrying out experiments to validate its model response to surface discharges (Granger and Ferrante, 1987).

"Spacecraft testing is generally performed in the same fashion as unit testing; a test plan of the following sort is typical:

"(1) The MIL-STD-1541 radiated test is applied around the entire spacecraft.

"(2) Spark currents from the MIL-STD-1541 arc source are applied through spacecraft structure from launch vehicle attachment points to diagonally opposite corners.

"(3) ESD currents are passed down the length of booms with cabling routed along them (e.g., sensor booms or power booms). Noise pickup into cabling and circuit disruption are monitored.

"(4) Special tests are devised for special situations. For example, dielectric regions such as quartz second-surface mirrors, Kapton thermal blankets, and optical viewing windows should have ESD tests applied on the basis of their predicted ESD characteristics.

"The spacecraft ESD testing configuration ideally simulates a 100 percent flight-like condition. This may be difficult because of the following considerations:

"(1) Desire for ESD diagnostics in the spacecraft

"(2) Nonfunctioning power system

"(3) Local rules about grounding the spacecraft to facility ground

"(4) Cost and schedules to completely assemble the spacecraft for the test and later disassemble it

"(5) The possible large capacitance to ground of the spacecraft in its test fixture

"(6) ESD coupling onto nonflight test cabling

"To obtain more information about circuit response than can be obtained by telemetry, it is common to measure induced voltages due to the ESD test sparks at key circuits. If improperly implemented, the very wires that access the circuits and exit the spacecraft to test equipment (e.g., oscilloscopes) will act as antennas and show noise that never would be present without those wires.

"Two approaches have been used with some success. The first is using conventional oscilloscope probes, with great care. Long oscilloscope probes (3 m) were procured from Tektronix. For the circuits being monitored, a small "tee" breakout connector was fabricated and inserted at the connector nearest the circuit. Two oscilloscope probes were attached to each circuit's active and return wires and the probe tips were grounded to satellite structure in the immediate vicinity of the breakout tee. The probe grounds were less than 15 cm from the probe tip. The signal was measured on a differential input of the oscilloscope. Before installation, the probes were capacitively compensated to their respective oscilloscope preamplifiers, and it was verified that their common-mode voltage rejection was adequate (in short normal good practice). The two probe leads were twisted together and routed along a metal structure inside the satellite until they could be routed out of the main chassis enclosure. They were then routed (still under thermal blankets) along the structure to a location as remote as possible from any ESD test location and finally were routed to the oscilloscope. The oscilloscopes were isolated from building ground by isolation transformers. Clearly, this method permits monitoring only a few circuits.

"A second method of monitoring ESD-induced voltage waveforms on internal circuits is the use of battery-powered devices that convert voltages to light-emitting diode (LED) signals. The LED signals can be transmitted by fiber optics to exterior receiver devices, where the voltage waveform is reconstructed. As with the oscilloscope probes, the monitoring device must be carefully attached to the wires with minimal disturbance to circuit wiring. The fiber optic cable must be routed out of the satellite with minimal disturbance. The deficiency of such a monitoring scheme is that the sending device must be battery powered, turned on, and installed in the spacecraft before spacecraft buildup and must operate for the duration of the test. The need for batteries and the high power consumption of LEDs severely restrict this method.

"Another proposed way to obtain circuit response information is to place peak-hold circuitry at key circuits, installed as described above. This method is not very useful because the only datum presented is that a certain peak voltage occurred. There is no evidence that the ESD test caused it, and there is no way to correlate that voltage with any one of the test sequences. For analysis purposes, such information is worthless.

"Spacecraft using solar cells or nuclear power supplies often must use support equipment power supplies for ground test activities and, thus, are not totally isolated from ground. In such cases, the best work-around is to use an isolated and balanced output power supply with its wires routed to the spacecraft at a height above ground to avoid stray capacitance to ground. The power wires should be shielded to avoid picking up stray radiated ESD noise; the shields should be grounded at the support equipment end of the cable only.

"To simulate flight, the spacecraft should be isolated from ground. Normal test practice dictates an excellent connection to facility ground. For the purposes of this test a temporary ground of 0.2 to 2 MΩ or more will isolate the spacecraft for the purposes of the ESD test. Generally, 0.2 to 2 MΩ, is sufficient 'grounding' for special test circumstances of limited duration and can be tolerated for the ESD test.

"Often testing is done in the most compact form possible, attempting to interleave several tasks at one time or to perform tasks in parallel. This practice is incompatible with the needs of ESD testing and must be avoided. A thermal vacuum test, for example, is configured like the ESD test, but has numerous (nonflight) thermocouple leads penetrating from the interior to the exterior of the spacecraft. These leads can act as antennas and bring ESD-caused noise into satellite circuitry, where it never would have been.

"If stray capacitance to facility ground is present during the ESD test, it will modify the flow of ESD currents. For a better test the spacecraft should be physically isolated from facility ground. It can be shown that raising a 1.5-m-diameter spherical satellite 0.5 m off the test flooring reduces the stray capacitance nearly to that of an isolated satellite in free space. A dielectric (e.g., wood) support structure can be fabricated for the ESD test and will provide the necessary capacitive isolation.

"One method of reducing ESD coupling to and from the spacecraft on nonflight test wiring is the use of ferrite beads on all such wiring."

6.5.5.2. INTELSAT VI Tests

On the INTELSAT VI spacecraft [Tucker, 1987], battery powered sensors, optical fiber links, and high speed single shot recording equipment were combined with lumped element circuit models to design a test simulating surface discharges. The bandwidth of the optical link was suggested by the predictions of the lumped element model. Optical links are required to avoid direct coupling of the discharge energy into sensitive regions of the spacecraft via cables used only to instrument the test. Sensors and their optical transmitters were located at points of interest about the spacecraft. The discharge source was chosen to be an 18.5 kV pulser with an effective capacitance of 60 picofarads, delivering a 10 millijoule pulse. The pulser was placed at different locations to explore the system's sensitivity to discharges. Over 166,000 pulses were injected into the INTELSAT flight model to test the design and validate the lumped element model of the spacecraft. The measured results agreed well with the predictions of the lumped element model. The measured responses at various locations have characteristics which indicate where discharges are occurring. If voltage and current sensors were flown on the spacecraft, analysis using the lumped element model would be very useful in monitoring the spacecraft health and response to the environment.

The key to good tests is adequate modeling prior to testing. Adequate modeling maximizes the information obtained in testing, and assures the system that over-testing/stressing will not occur.

In applying the discharge source, Figure 6-12 care needed to be taken with the switch initiating the discharge. (Air gaps have been used for MIL-STD-1541, but repeatability is sometimes considered a problem.) INTELSAT VI testers chose instead to use a triggered source. A triggered spark gap was selected because of its short rise time and good repeatability. In the Hughes injector, a high voltage source was used to charge up a 60 pF capacitor. The energy on this capacitor was then discharged through a triggered spark gap to the spacecraft. With this test setup, the rise time of a typical discharge pulse was 7 ns. The high voltage used in the tests ranged from 6 to 18 kV; the injected energy ranged as high as 20 mJ. A simplified schematic of the Hughes INTELSAT VI arc source is shown in Figures 6-12, 6-13, and 6-14.

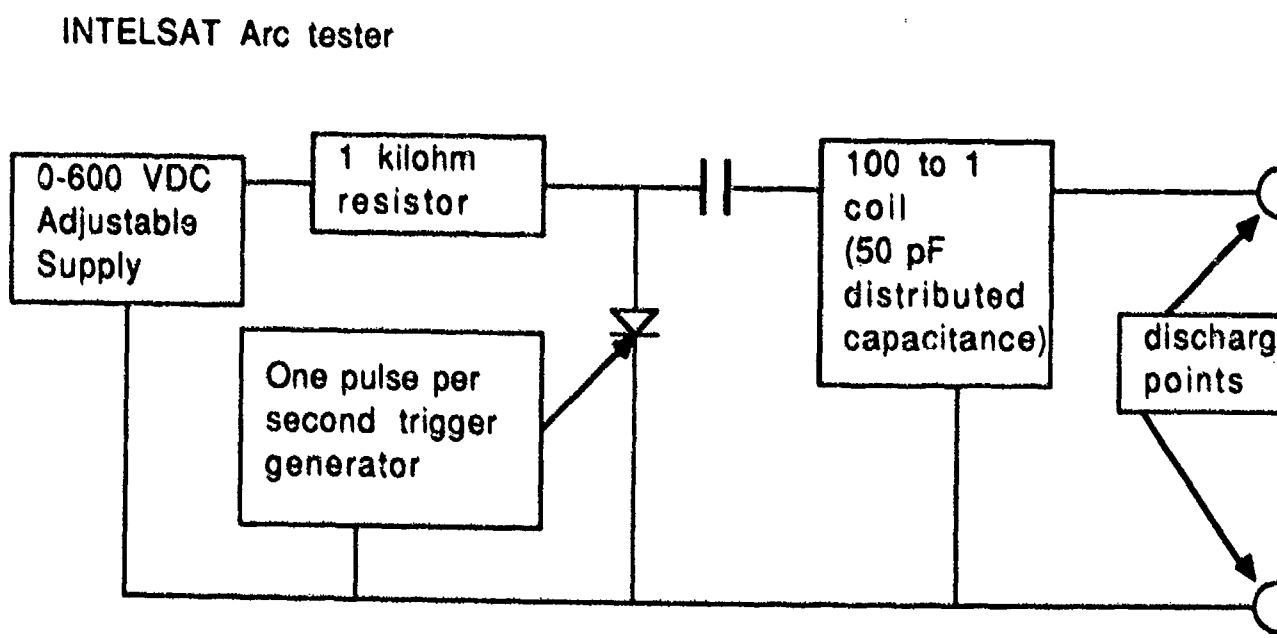

Figure 6-12. INTELSAT Source

Direct Injection Test to Various Points on Spacecraft

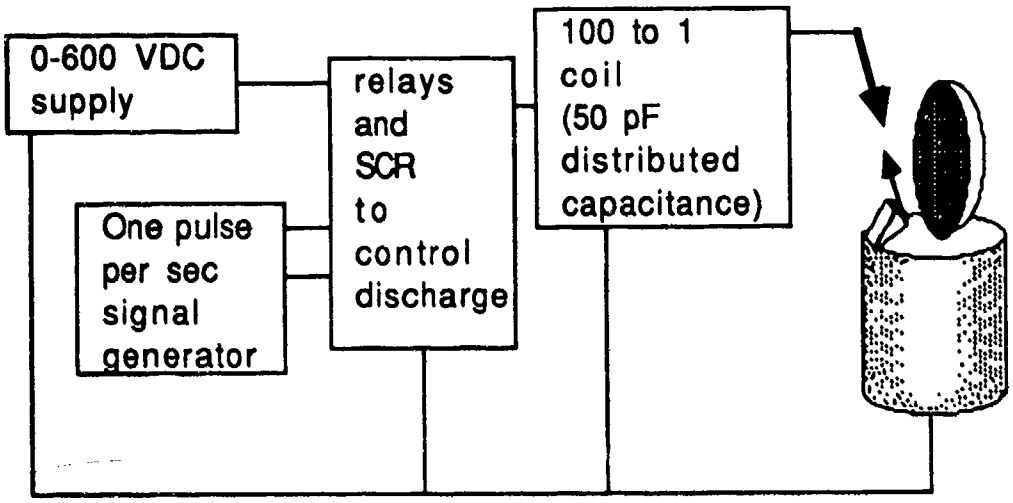

Figure 6-13. INTELSAT IV Tests

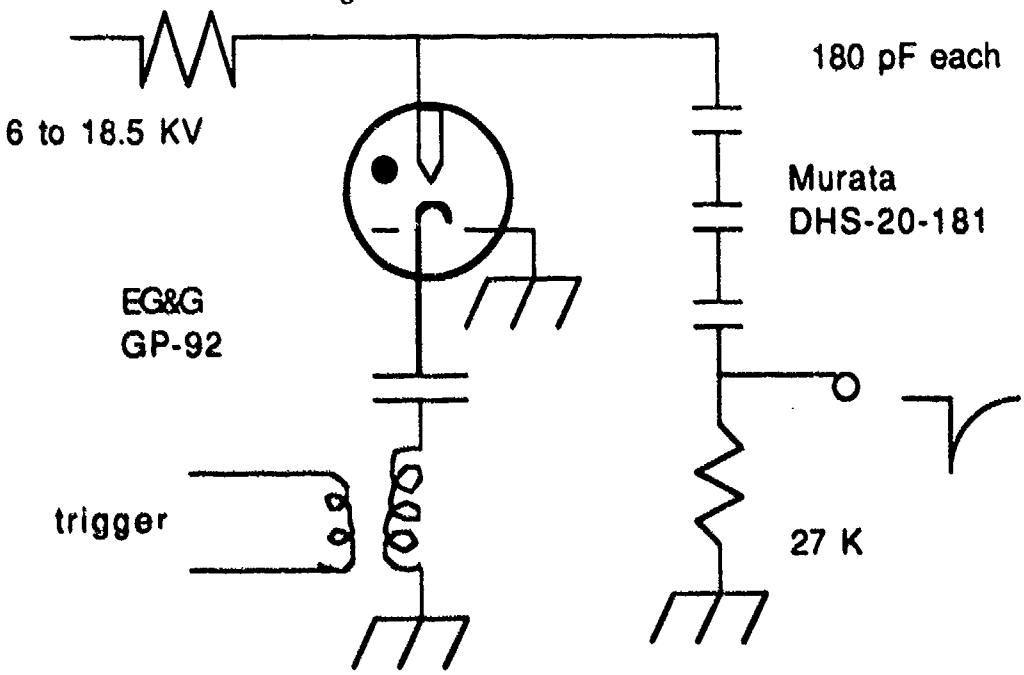

Figure 6-14. INTELSAT VI Trigger (after Tucker, 1987)

6.5.5.3. Tests Designed Specifically for Internal Charging

Since internal charging is a large effect where it occurs and is small outside of the box, it is difficult to provide a test which will produce large enough signals inside the box without overstressing components outside the box. For this reason most internal charging experiments are done at the subsystem level. Perhaps small controlled

arc sources coupled to test control by fiber optics and monitored with fiber optic coupled sense circuits will allow accurate internal discharge tests at a system level in the future.

6.6. A Final Word

The analysis, testing and monitoring needed to eliminate internal discharging surface charging/discharging and single event upset caused anomalies is available. There are many different approaches which can be adapted to each program.

Appendix

1

General References

A1.1 Conference Proceedings

Solar Wind
Solar Wind (NASA SP 308): A conference held at Pacific Grove California, 21-26 March 1971.

IUGG, 18th General Assembly
Contributions in Solar-Planetary Relationships, U. S. National Report 1983-1986, published by the American Geophysical Union.

IUGG, 19th General Assembly
Contributions in Solar-Planetary Relationships, U. S. National Report 1983-1986, published by the American Geophysical Union.

A1.2 Spacecraft Charging

1977

AFGL-TR-77-0051//NASA TMX 73537, C. P. Pike and R. R. Lovell, Editors, Proceedings of the Spacecraft Charging Technology Conference, AFGL, Hanscom AFB, MA, 24 February 1977.

1978

NASA Conference Publication 2071//AFGL-TR-79-0082, R. C. Finke and C. P. Pike, Editors, Spacecraft Charging Technology, AFGL, Hanscom AFB, MA, 1978.

1980

NASA Conference Publication 2182 // AFGL-TR-81-0270, N. John Stevens and C. P. Pike, Editors, Spacecraft Charging Technology, AFGL, Hanscom AFB, MA, 1980.

1983

NASA Conference Publication 2359/AFGL-TR-85-0018, C. K. Purvis and C. P. Pike, co-chairs, Spacecraft Environmental Interactions Technology 1983, 1985.

A1.3 Government Documents

AFGL, 1985
Handbook of Geophysics and the Space Environment, A. S. Jursa, scientific editor, Air Force Geophysics Laboratory, Hanscom AFB, MA, 1985.

JPL, 1986
Space Technology Plasma Issues in 2001, JPL Publication 86-49, H. Garrett, J. Feynman, S. Gabriel editors, Jet Propulsion Laboratory, Pasadena, CA, 1 Oct. 1986.

JSC, 1987
Space Station Program Natural Environmental Definition for Design, Space Station Program Office, Johnson Space Center, Houston, TX, January 15, 1987.

A1.4 Individual References

Adamo and Nanevicz, 1976

R. C. Adamo and J. E. Nanevicz, "Spacecraft-Charging Studies of Voltage Breakdown Processes on Spacecraft Thermal Control Mirrors. Spacecraft Charging by Magnetospheric Plasmas," A. Rosen, ed., Prog. Astronaut. Aeronaut., Vol. 47, MIT Press, MA pp. 225-235, 1976.

Adams, 1986

James H. Adams Jr.," Cosmic Ray Effects on Microelectronics, Part IV," NRL Memorandum Report 5901, Naval Research Laboratory, Washington, D.C., 1986.

Adams and Partridge, 1982

J. H. Adams Jr. and K. Partridge, "Do Trapped Heavy Ions Cause Soft Upsets on Spacecraft?," NRL Memorandum Report 4846, Naval Research Laboratory, Washington, D.C., October 1982.

Adams et al., 1981

J. H. Adams Jr., R. Silberberg, and C. H. Tsao, "Cosmic Ray Effects on Microelectronics, Part I: the Near-Earth Particle Environment," NRL Memorandum Report 4506, Naval Research Laboratory, Washington, D.C., August 1981.

Adams et al., 1983

J. H. Adams Jr., J. R. Letaw, and D. F. Smart, "Cosmic Ray Effects on Microelectronics, Part II: the Geomagnetic Cutoff Effects," NRL Memorandum Report 5099, Naval Research Laboratory, Washington, D.C., May 1983.

Akasofu and Fry, 1986

S.-I. Akasofu and C. D. Fry, "Heliospheric Current Sheet and its Solar Cycle Variations," Journal of Geophysical Research - Space Physics, Vol. 91, p. 13679, 1986.

Alfven and Falthammar, 1963

H. Alfven and C.G. Falthammar, Cosmical Electrodynamics, Clarendon Press, Oxford, 1963.

Anderson, 1981

Physics Vade Mecum, Herbert L. Anderson, Editor-in-Chief, American Institute of Physics, New York, 1981.

Bartnikas, 1987

R. Bartnikas, "1987 Whitehead Memorial Lecture: A Commentary on Partial Discharge Measurement and Detection," IEEE Transaction on Electrical Insulation, Vol. EI-22, No. 5, pp. 629-653, 1987.

Beers et al., 1979

B. L. Beers, V. W. Pine, H. C. Hwang, H. W. Bloomberg, D. L. Lin, M. J. Schmidt, and D. J. Strickland, First Principles Numerical Model of Avalanche-Induced Arc Discharges in Electron-Irradiated Dielectrics, SAI-102-79-002, Science Applications, NASA Contract NAS3-21378, NASA CR-159560, Lewis Research Center, Ohio, 1979.

Bendel, 1984

W. L. Bendel, Length Distribution of Chords Through a Rectangular Volume, NRL Memorandum Report 5369, July 1984.

Bendel and Petersen, 1983

W. L. Bendel and E. L. Petersen, "Proton Upset in Orbit," IEEE Transaction on Nuclear Science, Vol. NS-30, pp. 4481-4485, 1983.

Bever and Staskus, 1981

R. S. Bever and J. Staskus, "Tank Testing of a 2500-cm^2 Solar Panel," Spacecraft Charging Technology 1980, NASA CP-2182, pp. 211-227, 1981.

Binder et al., 1982
D. Binder, E. C. Smith, and A. B. Holman, "Satellite Anomalies from Galactic Cosmic Rays," IEEE Transactions on Nuclear Science, Vol. NS-29, p. 2085, 1982.

Blake and Friesen, 1977
J. B. Blake and L. N. Friesen, 15th International Cosmic Ray Conference, Vol. 2, p. 341, 1977.

Blandford and Pickel, 1985
J. T. Blandford Jr. and J. C. Pickel, "The use of CF-252 to determine parameters for SEU rate calculation," IEEE Transactions on Nuclear Science, Vol. NS-32, pp. 4282-4286, December 1985.

Breneman and Stone, 1985
H. H. Breneman and E. C. Stone, "Solar and Photospheric Abundance from Solar Energetic Particle Measurements," Astrophysical Journal, Vol. 299, pp. L57-L61, 1985.

Brundin, 1963
C. L. Brundin, "Effects of charged particles on the motion of an earth satellite," AIAA Journal, Vol. 1, pp. 2529-2538, 1963.

Burch, 1986
J.L. Burch, "Space Plasma Physics Results from Spacelab I," J. Spacecraft and Rockets, Vol. 23, p. 331, 1986.

Cameron, 1980
A. C. W. Cameron, Elementary and Nuclidic Abundances in the Solar System, Harvard-Smithsonian Center for Astrophysics Preprint Series No. 1357, 1980.

Carpenter, 1966
D. L. Carpenter, J. Geophysical Research, Vol. 71, p. 693, 1966.

Cauffmann, 1973
D. P. Cauffmann, "Ionization and Attraction of Neutral Molecules to a Charged Spacecraft," SAMSO-TR-73-263, SAMSO, Los Angeles, CA, 1973.

Chen, 1974
Francus F. Chen, Introduction to Plasma Physics, Plenum Press: New York, NY, 1974.

Coakley, 1986a
P. Coakley, Assessment of Internal ECEMP with emphasis for producing interim Design Guidelines, J200-86-1133/2266, JAYCOR report, JAYCOR, San Diego, CA, June 1986.

Coakley, 1986b
P. Coakley, ECEMP Test Specification for Electronic Hardware, for Air Force Contract F29601-82-C-0023, JAYCOR Report, JAYCOR, San Diego, CA, 12 Dec. 1986.

Coakley et al., 1982
P. Coakley, B. Kitterer, and M. Treadaway, "Charging and Discharging Characteristics of Dielectric Material Exposed to Low- and Mid-Energy Electrons," IEEE Trans. Nucl. Sci., Vol. NS-29, pp. 1639-1643, December 1982.

Coakley et al., 1985
P. Coakley, M. J. Treadaway, and P. A. Robinson Jr., "Low Flux Laboratory Test of the Internal Discharge Monitor (IDM) Experiment intended for CRRES," IEEE Transactions on Nuclear Science, Volume NS-32, Number 6, pp. 4066-4072, December 1985.

Cohen and Lai, 1982
H.A. Cohen and S. Lai, "Discharging the P78.2 Satellite using Ions and Electrons," AIAA paper no. 82.0266, presented at AIAA 20th Aerospace Sciences Meeting, Orlando, FL, Jan. 11-14, 1982.

Comstock, 1969
G. M. Comstock, Astrophysical Journal, Vol. 155, p. 619, 1969.

Conwell, 1987
E. M. Conwell, "Transpirt in Polyacetylene," IEEE Transactions on Electrical Insulation, Vol. EI-22, No. 5, pp. 591-627, 1987.

Cornwall, 1968
J. M. Cornwall, "Diffusion Processes Influenced by Conjugate Point Wave Phenomena," Radio Science, Vol. 3, p. 740, 1968.

Cornwall, 1972
J. M. Cornwall, "Radial Diffusion of Ionized Helium and Protons: A Probe for Magnetospheric Dynamics," J. Geophys. Res., Vol. 77, p. 1756, 1972.

Cotts and Reyes, 1985
David B. Cotts and Zolla Reyes, SRI International, New Polymeric Materials Expected to have Superior Properties for Space-based Uses, RADC-TR-85-129, Final Technical Report, RADC, Bedford, MA, July 1985. **ADA160285**

Criswell, et al., 1987
T. L. Criswell, D. L. Oberg, J. L. Wert, P. R. Measel, and W. E. Wilson, "Measurement of SEU Thresholds and Cross Sections at Fixed Incident Angles," IEEE Transactions on Nuclear Science, Vol. NS-34, Dec. 1987, pp. 1316-1321.

CRC, 1977
Handbook of Chemistry and Physics, Chemical Publishing Company, 58th Edition, 1977.

Cummings et al., 1968
W. D. Cummings, J. N. Barfield, and P. J. Coleman Jr., "Magnetospheric substorms observed at the Synchronous Orbit," J. Geophysical Research, Vol. 73, pp. 6687-6698, 1968.

DeForest, 1972
S. E. De Forest, "Spacecraft Charging at Synchronous Orbit," J. Geophys. Res., Vol. 77, pp. 651-659, Feb. 1, 1972.

Edmonds, 1985
Larry Edmonds, Final Report: Cosmic Ray Environment Model for Earth Orbit, JPL Publication 84-98, Jet Propulsion Laboratory, Pasadena, CA, 1985.

Edmonds, 1987
L. Edmonds, Boundary Value Problem for the Solution of Magnetic Cutoff Rigidities and Some Special Applications, JPL Publication 87-9, Jet Propulsion Laboratory, Pasadena, CA, 1987.

EOS, 1986
EOS, Vol. 67, No. 24, Cover, 17 June 1986.

Evans, 1955, 1982
R. D. Evans, The Atomic Nucleus, McGraw-Hill, 1955 and Kliegler Publishing, 1982.

Falthammar, 1968
C. G. Falthammar, "Radial Diffusion by Violation of the third Adiabatic Invariant," Earth's Particles and Fields, editor B.M. McCormac, Reinhold, New York, NY, p. 157, 1968.

Fan et al., 1966
C. Y. Fan, G. Gloeckler, and J. A. Simpson, Physical Review Letters, Vol. 17, p. 329, 1966.

Fermi, 1950
Enrico Fermi, Nuclear Physics, Revised Edition, (course notes compiled by Jay Orear, A. H. Rosenfeld, and R. A. Schluter, Midway reprint 1974), University of Chicago Press, Chicago, IL, 1950.

Feynman, 1985
J. Feynman, "Chapter 3: Solar Wind" in Handbook of Geophysics and the Space Environment, Air Force Geophysics Laboratory, A. S. Jura, Editor, Document Accession Number ADA16700, National Technical Information Service, Springfield, VA, 1985.

Fischer et al., 1984
S. Fischer, M. Vandas, K. Kudels, S. N. Kuznetsov, and V. N. Lutsenko, "Determination of the Effective Charge of Solar Cosmic Ray Nuclei Using the Earth's Magnetic Field," Advances in Space Research, Vol. 4, pp. 169-172, 1984.

Fisk et al., 1974
L. A. Fisk, B. Kpzlovsky, and R. Ramaty, Astrophysical Journal (Letters), Vol. 190, pp. 135-137, 1974.

Frederick, 1985
R. A. Frederick, "Solar Wind and the Magnetosphere -- Space Environment Forecaster Course," also "Spacecraft Operations," part of the same course, AFGWC, Bedford, MA, March 1985.

Frederickson, 1974
A. R. Frederickson, "Radiation Induced Electrical Current and Voltage in Dielectric Structures," AFCRL-TR-74-0582, Physical Sciences Research Papers, No. 613, Air Force Cambridge Research Laboratories, Bedford, MA, 1974. **ADA007670**

Freier and Waddington, 1968
P. S. Freier and C. J. Waddington, Physical Review, Vol. 175, p. 1641, 1968.

Freier et al., 1979
P. S. Freier, J. Young, C. J. Waddington, R. Fickle, C. Gilman, and W. R. Scarlett, Proc. 16th Intl. Cosmic Ray Conf., Vol. 1, p. 316, 1979.

Fritz and Spjeldvik, 1979
T. A. Fritz and W. N. Spjeldvik, "Simultaneous Quiet Time Observations of Energetic Radiation Belt Protons and Helium Ions: the Equatorial a/p Ratio Near 1 MeV," Journal of Geophysical Research, Volume 84, No. A6, pp. 2608-2618, June 1979.

Fritz and Wilden, 1976
T. A. Fritz and B. Wilden, "Substorm Generated Fluxes of Heavy Ions at the Geostationary Orbit," Magnetospheric Particles and Fields, editor B.M. McCormac, Reidel Publishing Co., Dordrecht, Holland, 1976.

Garcia-Munoz et al., 1975
M. Garcia-Munoz, G. M. Mason, and J. A. Simpson, Astrophysical J., Vol. 202, p. 265, 1975.

Garrett, 1979
H. B. Garrett, "Review of Quantitative Models of the 0 to 100 keV Near Earth Plasma," Reviews of Geophysics, Vol. 17, pp. 397-417, 1979.

Garrett, 1981
H. B. Garrett, "The Charging of Spacecraft Surfaces," Rev. Geophys., Vol. 19, No. 4, pp. 577-616, Nov. 1981.

Gerhard-Multhaupt, 1987
R. Gerhard-Multhaupt, "Electrets: Dielectric with Quasi-permanent Charge or Polarization," IEEE Transaction of Electrical Insulation, Vol. EI-22, No. 5, pp. 531-554, 1987.

Gleick, 1987
James Gleick, Chaos Making a New Science, Viking, New York, NY, 1987.

Granger and Ferrante, 1987

J. P. Granger and J. G. Ferrante, "Electrostatic-Discharge Coupling in Spacecraft Electronics," ESA Journal, Vol. 11, pp. 19-30, 1987.

Grard, 1973
R. J. L. Grard, "Properties of the Satellite Photoelectron Sheath Derived from Photoemission Laboratory Measurements," J. Geophys. Res., Vol. 78, pp. 2885-2906, June 1, 1973.

Grier and Stevens, 1979
N. Grier and N. J. Stevens, "Plasma Interaction Experiment (PIX) Flight Results," Spacecraft Charging Technology 1978, NASA CP-2071, pp. 295-314, 1979.

Grier, 1985
N. Grier, "Plasma Interaction Experiment II (PIX-II): Laboratory and Flight Results," Spacecraft Environmental Interaction Technology 1983, pp. 333-348, 1985.

Gurevich and Dimant, 1975
A. V. Gurevich and Y. S. Dimant, "Flow of a rarefied plasma around a disk," Geomagn. Aeron. (USSR, English Translation), Vol. 15, pp. 183-190, 1975.

Gurevich et al., 1970
A. V. Gurevich, L. P. Pitaevskii, and V. V. Smirnov, "Ionospheric Aerodynamics," Soviet Physics Usp., Vol. 99, No. 1-2, p. 595, 1970.

Gussenhoven and Mullen, 1982
M. S. Gussenhoven and E. G. Mullen, "A Worst Case Spacecraft Charging Environment as Observed by SCATHA, 24 April 1979," AIAA 20th Aerospace Sciences Meeting, January 11-14, 1982.

Gussenhoven et al., 1985
M. S. Gussenhoven, E. G. Mullen, and R. C. Sagalyn, "CRRES/SPACERAD Experiment Descriptions," AFGL-TR-85-0017, Environmental Research Paper, AFGL, Hanscom AFB, MA, January 25, 1985. **ADA160504**

Hall, 1977
David F. Hall, "Spacecraft Charging/contamination Experiment on SCATHA," p. 699, Proceedings of the Spacecraft Charging Technology Conference, AFGL TR-77-0051, **ADA045459**

Haymes, 1971
Robert C. Haymes, Introduction to Space Science, John Wiley and Sons, Inc., New York, NY, 1971.

Heinrich, 1977
W. Heinrich, "Calculation of LET-spectra of heavy Cosmic Ray Nuclei at Various Absorber Depths," Radiation Effects, Vol. 35, pp. 143-148, 1977.

Hess and Mead, 1968
W. N. Hess and G. D. Mead, Introduction to Space Science, Gordon and Breach, New York, NY, 1968.

Inouye, 1976
G. T. Inouye, "Spacecraft Potentials in a Substorm Environment," Progress in Astronautics and Aeronautics: Spacecraft Charging by Magnetospheric Plasma, edited by A. Rosen, AIAA, New York, Vol. 47, pp. 103-120, 1976.

Jackson, 1962
J. D. Jackson, Classical Electrodynamics, John Wiley and Sons, New York, NY, 1962.

Jacobs, 1970
J. A. Jacobs, Geomagnetic Micropulsations, Springer-Verlag, New York, NY, 1970.

Janni, 1982

J. F. Janni, "Proton Range-Energy Tables, 1 keV-10GeV, Part 1," Atomic Data and Nuclear Data Tables, Volume 27, pp. 150-339, March/May 1982, "Proton Range-Energy Tables, 1 keV-10GeV, Part 2," Atomic Data and Nuclear Data Tables, Volume 27, pp. 341-529, July/September 1982.

Jemiola, 1978

J. M. Jemiola, editor. Proceedings of the USAF/NASA International Spacecraft Contamination Conference, AFML-TR-78-190/NASA CP-2039, USAF Academy, Colorado Springs, CO, March 1978.

Jemiola, 1980
J. M. Jemiola, "Spacecraft Contamination - A Review," Progress in Astronautics and Aeronautics, Vol. 71, pp. 680-706, 1980.

Jokipii et al., 1977
J. R. Jokipii, E. H. Levy, and W. B. Hubbard, "Effects of Particle Drift on Cosmic Ray Transport. I. General Properties, Application to Solar Modulation," Astrophysical Journal, Vol. 213, p. 861, 1977.

JSC, 1987
Space Station Program Natural Environment Definition for Design, NASA/Lyndon B. Johnson Space Center, Houston, TX, 15 January 1987.

Juliusson, 1974
E. Juliusson, Astrophysical Journal, Vol. 191, p. 331, 1974.

Juliusson et al., 1973
E. Juliusson, Proc. 13th Intl. Cosmic Ray Conf., Vol. 1, pp. 178-183, 1973.

Jursa, 1985
Handbook of Geophysics and the Space Environment, Adolph Jursa, Editor, Air Force Geophysics Laboratory, Air Force Systems Command, United States Air Force, available from National Technical Information Service Document, accession number ADA 167000, 1985.

Kolasinski, 1979
W. A. Kolansinski, J. B. Blake, J. K. Anthony, W. E. Price, E. C. Smith, "Simulation of Cosmic Ray Induced Soft Errors and Lathchup in Integrated Circuit Computer Memories," IEEE transactions on Nuclear Science, TNS volume 20, No. 6 pp. 5087-5091 (1979)

Katz and Parks, 1985
I. Katz and D.E. Parks, "Theory of Plasma Contactors for Electrodynamic Tethered Satellite Systems," presented at Tether Applications in Space Program Review, 17-18 July 1985.

Katz and Penfold, 1952
L. Katz and A. S. Penfold, "Range-Energy Relations for Electrons and the Determination of Beta-Ray End Point Energies by Absorption," Reviews of Modern Physics, Vol. 24, p. 28, 1952.

Katz et al., 1984
I. Katz, D. L. Cooke, D. E. Parks, and M. J. Mandell, "Three Dimensional Wake Model for Low Earth Orbit," Journal of Spacecraft and Rockets, Vol. 21, p. 125, 1984.

Katz et al., 1986
I. Katz, M. Mandell, G. Jungeward, and M. S. Gussenhoven, "The Importance of Accurate Secondary Electron Yields in Modeling Spacecraft Charging," J. Geophysical Research, Vol. 91, No. A13, pp. 13739-13744, 1986.

Kaye, 1986
G. W. C. Kaye, Tables of Physics and Chemistry Constants and some Mathematical Functions, 15th Edition, Longman, NY, 1986.

Kennel and Petschek, 1966
C. F. Kennel and H. E. Petschek, "Limit on stably trapped particle fluxes," J. Geophysical Research, Volume 71, pp. 1-28, 1966.

Kennerud, 1974
K. L. Kennerud, High Voltage Solar Array Experiments, Boeing Aerospace Company, NASA Contract NAS3-14364, NASA CR-121280, 1974.

King, 1974
J. H. King, "Solar Proton Fluences for 1977-1983 Space Missions," Journal of Spacecraft and Rockets, Vol. 11, No. 6, pp. 401-408, June 1974.

Knecht and Shuman, 1985
Knecht and Shuman, "Chapter 4: The Geomagnetic Field," Handbook of Geophysics and the Space Environment, Adolph Jursa, Editor, Air Force Geophysics Laboratory, Air Force Systems Command, United States Air Force, available from National Technical Information Service Document, accession number ADA 167000, 1985.

Koons, 1982
H. C. Koons, "Summary of Environmentally Induced Electrical Discharges on the P78-2 (SCATHA) Satellite," AIAA 20th Aerospace Sciences Meeting, January 11-14, 1982.

Lanzerotti et al., 1978
L. J. Lanzerotti, D. C. Webb, and C.W. Arthur, "Geomagnetic Field Fluctuations at Synchronous Orbit, 2. Radial Diffusion," J. Geophys. Res., Vol. 83, p. 3866, 1978.

Leech and O'Gallagher, 1978
H. W. Leech and J. J. O'Gallagher, "The Isotopic Composition of Cosmic-Ray Helium From 123 to 279 MeV per Nucleon: A New Measurement and Analysis," Astrophysical. J., Vol. 221, p. 1110, 1978.

Leung and Robinson, 1982
P. Leung and P Robinson, "Jovian Radiation and Charging Environment Considerations for Galileo," AIAA paper 82-0118, 20th Aerospace Sciences Meeting, Orlando, Florida, January 11-14, 1982.

Leung et al., 1986
P. Leung, A. C. Whittlesey, H. B. Garrett, and P. A. Robinson Jr., "Environment-Induced Electrostatic Discharges as the Cause of Voyager 1 Power-On Resets," Journal of Spacecraft and Rockets, Volume 23, No. 3, pp. 323-330, May/June 1986.

Leung et al., 1981
M. S. Leung, M. B. Tueling, and E. R. Schnauss, Effects of Secondary Electron Emission on Charging, Aerospace Report No. TOR-0081(6470-02)-2, prepared for Space Division Air Force Systems Command, Contract No. F04701-80-C-0081, 30 July 1981.

Levy, 1985
Leon Levy, "A new understanding of Breakdowns in the day sections of Geosynchronous Orbit," Centre d'Etudes et de Recherches de Toulouse, working paper, private communication, March 1985.

Levy et al., 1986
L. Levy, D. Sarrail, J. P. Philippon, J. P. Catani, and J. M. Fourquet, "Sur la Possibilite de Charge Differentielle de Plusieurs Kilovolts dans le Secteur Jour de l'Orbite Geosynchrone," AGARD Conference proceedings, No. 406, The Aerospace Environment at High Altitudes and its implications for Spacecraft Charging and Communications, June 1986.

Luhn et al., 1984
A. Luhn, B. Klecker, D. Movestact, G. Gloeckler, F. M. Ipavich, M. Scholer, C. Y. Fan, and L. A. Fisk, "Ionic Charge States of N, Ne, Mg, Si, and S in Solar Particle Events," Advances in Space Research, Vol. 4, pp. 161-164, 1984.

Lund, 1980
N. Lund, Bulletin of the American Physical Society, Vol. 25, p. 563, 1980.

Lyons and Moore, 1981
L. R. Lyons and T. Moore, "Effects of Charge Exchange on Distribution of Ionospheric Ions Trapped in the Radiation Belts near Synchronous Orbit," J. Geophys. Res., Vol. 86, p. 5885, 1981.

Lyons and Thorne, 1973
L. R. Lyons and R.M. Thorne, "Equilibrium Structure of Radiation Belt Electrons," J. Geophys. Res., Vol. 78, p. 2142, 1973.

Mapper et al., 1985
D. Mapper, T. K. Sanderson, J. H. Stephen, J. Farren, L. Adams, and R. Harboe-Sorensen, "An experimental study of the effect of absorbers on the LET of the fission particles emitted by Cf-252," IEEE Transactions on Nuclear Science, Vol. NS-32, pp. 4276-4281, 1985.

Mardiguian, 1985
Michel Mardiguian, "The ESD Simulator, an EMI Engineer's Multifaceted Friend," EMC Technology, pp. 55-61, January/March, 1985.

Martin et al., 1986
K. E. Martin, M. K. Gauthier, J. R. Coss, A. V. Dantas, and W. E. Price, Total-Dose Radiation Effects Data for Semiconductor Devices 1985 Supplement, JPL Publication 85-43 (Consisting of Volume I, Volume II part A, and Volume II part B), Jet Propulsion Laboratory, Pasadena, CA, May, 1986.

Massaro and Ling, 1979
M. J. Massaro and D. Ling, "Spacecraft Charging Results for the DSCS-III Satellite," Spacecraft Charging Technology 1978, NASA Conference Publication 2071/AFGL-TR-79-0082, pp. 158-178 AFGL, Hanscom AFB, MA, 1979. **ADA084626**

Massaro et al., 1977
M. J. Massaro, T. Green, and D. Ling, "A Charging Model for Three Axis Stabilized Spacecraft," Proceedings of the Spacecraft Charging Technology Conference, AFGL TR-77-0051/NASA TMX-73537, AFGL, Hanscom AFB, MA, 1977. **ADA045459**

May and Woods, 1979
T. C. May and M. H. Woods, "Alpha-particle-induced Soft Errors in Dynamic Memories," IEEE Transactions in Electron Devices, Vol. ED-26, No. 1, pp. 2-9, 1979.

McCormac, 1966
Billy M. McCormac, editor, "Radiation Trapped in the Earth's Magnetic Field," D. Reidel Co. Dordrecht-Holland, Gorden and Breach, New York, 1966

McCoy et al., 1980
J. E. McCoy, A. Knoradi, and O. K. Garriott, "Current Leakage for Low Altitude Satellites," Space Systems and Their Interactions with Earth's Space Environment, Progress in Astronautics and Aeronautics, H. B. Garrett and C. P. Pike editors, AIAA, New York, NY, Vol. 71, pp. 523-553, 1980.

McDonald et al., 1974
F. B. McDonald, M. A. I. Van Hollebeke, J. H. Trainor, N. Lai, and W. R. Weber, Astrophysical Journal Letters, Vol. 187, pp. L105-108, 1974.

McIlwain, 1961
C. E. McIlwain, "Coordinates for Mapping the Distribution of Magnetically Trapped Particles," J. Geophys. Res., Vol. 66, p. 3681, 1961.

Messenger and Ash, 1986
G. C. Messenger and M. S. Ash, The Effects of Radiation on Electronic Systems, Van Nostrand Reinhold Co., New York, NY, 1986.

McWaldt and Stone, 1983
R. A. Mewaldt and E. C. Stone, "A Search for Deuterium, Tritium, and ^{3}He in Large Solar Flares," Bull. of the Am. Phys. Soc., Vol. 28, p. 742, 1983.

Mizera and Boyd, 1982

P. F. Mizera and G. M. Boyd, "A Summary of Spacecraft Charging Results," AIAA 20th Aerospace Sciences Meeting, January 11-14, 1982.

Mizera et al., 1980
P. F. Mizera, H. C. Koons, E. R. Schnauss, D. R. Croley Jr., H. K. A. Kan, M. S. Leung, N. J. Stevens, F. Berkopec, J. Staskus, W. L. Lehn, and J. E. Nanewics, "First results of material charging in the space environment," Appl. Phys. Lett., Vol. 37, No. 3, 1 August 1980.

Mizera et al., 1981
P. F. Mizera, M. S. Leung, and H. K. A. Kan, Laboratory and Space Results from the SSPM Experiment, Aerospace Report no. TOR-0081(6505-02)-3, prepared for Space Division Air Force Systems Command, Contract no. F04701-80-C-0081, 15 July 1981.

Nakada and Mead, 1965
M. P. Nakada and G.D. Mead, "Diffusion of Protons in the Outer Radiation Belt," J. Geophys. Res., Vol. 70, p. 4777, 1965.

Nanevicz, et al., 1978
J. E. Nanevicz, R. C. Adamo, B.L. Beers, "Characterization of Electromagnetic Signals Generated by Electrical Breakdown of Spacecraft Insulating Materials," pp. 868-875 NASA Conference Publication 2071//AFGL-TR-79-0082, R. C. Finke and C. P. Pike, Editors, Spacecraft Charging Technology, AFGL, Hanscom AFB, MA, 1978. (also see Nanevicz in Rosen 1976) ADA084626

Neugebauer and Davis, 1978
M. Neugebauer and R. W. Davis, editors, A Close-Up of the Sun 1 Sept. 1978, JPL Publication 78-70, Jet Propulsion Laboratory, Pasadena, CA, 1978.

Nichols, 1987
D. K. Nichols, Trends in Electronic Parts Susceptibility to Single Event Upset Space Station Environment, JPL D-4785 (internal document), Jet Propulsion Laboratory, Pasadena, CA, September 1987.

Northcliffe and Schilling, 1970
L. C. Northcliffe and R. F. Schilling, "Range and Stopping Power tables for Heavy Ions," Nuclear Data Tables, Vol. A7, pp. 233-463, 1970.

Northrop, 1963
T. G. Northrop, The Adiabatic Motion of Charged Particles, Interscience, New York, NY, 1963.

Obayashi, 1984
T. Obayashi, N. Kawashima, K. Kuriki, M. Nagatomo, K. Ninomiya, S. Sasaki, and M. Yanagisawa, "Space Experiments with Particle Accelerators," Science, Vol. 225, p. 195, 1984.

Olsen, 1980
R. C. Olsen, "Differential and Active Charging Results from the ATS Spacecraft," PhD Thesis Univ of Calif, San Diego, 1988

Olsen, 1983
R. C. Olsen, "A Threshold Effect for Spacecraft Charging," J. Geophys. Res., Vol. 88, pp. 493-499, Jan. 1, 1983.

Olsen, 1985
R. C. Olsen, "Experiments in Charge Control at Geosynchronous Orbit -- ATS-5 and ATS-6," J. Spacecraft and Rockets, Vol. 22, p. 254, 1985.

Olsen and Whipple, 1977
R. C. Olsen and E. C. Whipple, Active Experiments in Modifying Spacecraft Potential: Results from ATS-5 and ATS-6, Contract NAS 5-23481, University of California, San Diego, May 1977-Feb 1979.

Ormes and Weber, 1965

J. F. Ormes and W. R. Weber, "Measurement of the primary proton and helium spectra and their modulations using a balloon-borne Cerenkov-scintillation counter," Proceedings 9th International Conference Cosmic Rays, London, Vol. 1, p. 349, 1965.

Orth et al., 1978
C. D. Orth, A. Buffington, G. F. Smoot, and T. S. Mast, "Abundances and Spectra for Cosmic Ray Nuclei From Lithium to Iron for 2 to 150 GeV per Nucleon," Astrophysical Journal, Vol. 226, p. 1147, 1978.

Papadopoulos, 1984
K. Papadopoulos, "On the Shuttle Glow (The Plasma Alternative)," Radio Sci., Vol. 19, p. 571, 1984.

Parker, 1957
E. N. Parker, "Newtonian Development of the Dynamical Properties of Ionized Gases of Low Density," Physical Review, Vol. 107, pp. 924-933, 1957.

Parker, 1963
E. N. Parker, Interplanetary Dynamical Processes, Interscience, 1963.

Parker, 1978
L. W. Parker, "Differential charginig and sheath asymmetry of nonconducting spacecraft due to plasma flow," Journal of Geophysical Research, Vol. 83, pp. 4873-4876, 1978.

Parker, 1979
L. W. Parker, "Plasma Sheath Effects and Equilibrium Voltage Distributions of Large High-power Satellite Solar Arrays," Spacecraft Charging Technology 1978, edited by R. C. Fink and C. P. Pike, NASA Conference Publication 2071, AFGL-TR-79-0082, pp. 341-357, 1979. **ADA084626**

Parker, 1980
L. W. Parker, "Plasmasheath-photosheath Theory for Large High-voltage Space Structures," in Space Systems and Their Interactions with Earth's Space Environment, Progress in Astronautics and Aeronautics, H. B. Garrett and C. P. Pike editors, AIAA, Vol. 71, pp. 477-522, 1980.

Parker and Murphy, 1967
L. W. Parker and B. L. Murphy, "Potential buildup on an electron emitting ionospheric satellite," Journal of Geophysical Research, Vol. 72, p. 1631, 1967.

Patterson and Wilbur, 1987
M.J. Patterson and P.J. Wilbur, "Plasma Contactors for Electrodynamic Tethers," Aerospace America, p. 32, Feb. 1987.

Petersen, 1983
E. L. Petersen, "Single Event Upsets in Space: Basic Concepts," Tutorial Short Course, IEEE Nuclear and Space Radiation Effects Conference, 1983.

Pickel, 1983
J. C. Pickel, "Single Event Upset Mechanisms and Predictions," Tutorial Short Course, IEEE Nuclear and Space Radiation Effects Conference, 1983.

Pickel and Blandford, 1978
J. C. Pickel and J. T Blandford, "Cosmic Ray Induced Errors in MOS Memory Cells," IEEE Trans. Nuc. Sci., Vol. NS-25, pp. 1166-1171, December 1978.

Pickel and Blandford, 1980
J. C. Pickel and J. T. Blandford, "Cosmic-Ray-Induced Errors in MOS Devices," IEEE Trans. Nucl. Sci., Vol. NS-27, p. 1066, 1980.

Price et al., 1973
P. B. Price, J. H. Chan, D. O'Sullivan, and A. Thompson, 13th International Cosmic Ray Conference, Vol. 1, p. 146, 1973.

Prochaska, 1980
R. Prochaska, Geomagnetic Index Calculation and Use at AFGWC, AFGWC/TN-80/002, HQ Air Force Global Weather Central, Offutt AFB, NE, April 1980.

Pruett, 1980
R. G. Pruett, "A Comparison of DMSP and NTS-2 Dosimeter Measurements With Predictions," J. of Spacecraft and Rockets, May/June 1980.

Purvis and Bartlett, 1980
C. K. Purvis and R. O. Bartlett, "Active Control of Spacecraft Charging," in Space Systems and their Interactions with the Earth's Space Environment, H.B. Garrett and C.P. Pike, eds., American Institute of Aeronautics and Astronautics, 1980.

Purvis et al., 1984
C. K. Purvis, H. B. Garrett, A. C. Whittlesey, and N. J. Stevens "Design Guidelines for Assessing and Controlling Spacecraft Charging Effects," NASA Technical paper 2361, September 1984.

Pyle, 1981
K. R. Pyle, private communication to J. Adams, quoted in Adams, 1981.

Raitt et al., 1982
W.J. Raitt, et al., "Early Experiments in Charged Particle Beams from the Space Shuttle," AIAA paper no. 82-0083, presented at AIAA 20th Aerospace Sciences Meeting, Orlando, FL, Jan. 11-14, 1982.

Ramaty et al., 1980
R. Ramaty, S. A. Colgatye, G. A. Dulk, P. Honig, J. W. Knight, R. P. Lin, D. B. Melrose, F. Orrall, C. Paizis, P. R. Shapiro, D. F. Smith, and M. Van Hollebeke, Proceedings of the Second Skylab Workshop on Solar Flares, Chapter 4, Boulder, Colorado, 1980.

Reames and Fichtel, 1967
D. V. Reames and C. E. Fichtel, Physical Review, Vol. 162, p. 1291, 1967.

Reier, 1986
M. Reier, "The use of Cf-252 to measure latchup cross sections as a function of LET," IEEE Transactions on Nuclear Science, Vol. NS-33, pp. 1641-1645, 1986.

Reiff et al., 1980
P. H. Reiff, J. W. Freeman, and D. L. Cooke, "Environmental Protection of the Solar Power Satellite," in Space Systems and Their Interactions with Earth's Space Environment, Progress in Astronautics and Aeronautics, Vol. pp. 554- 576, B. Garrett and C. P. Pike editors, AIAA, New York, NY, 1980.

Riddell and Passenheim, 1982
J. R. Riddell and B. C. Passenheim, "Electrical Conductivity of Spacecraft Thermal Control Dielectrics," FLTSACOM Experimentation Memo #165, AFWL, SGEMP-M-5160, Albuquerque, NM, 1982 .

Robinson, 1985
Paul Robinson Jr., "Internal Discharge Analysis," IEEE 1985 Annual Report, Conference on Electrical Insulation and Dielectric Phenomena, pp. 432-440, 1985.

Robinson and Holman, 1977
P. A. Robinson Jr. and A. B. Holman, "Pioneer Venus Spacecraft Charging Model," Proceedings of the Spacecraft Charging Technology Conference, edited by C. P. Pike and R. R. Lovell, AFGL-TR-0051, pp. 297-308, AFGL, Hanscom AFB, MA, 1977. **ADA045459**

Roederer, 1968

J. G. Roederer, "Experimental Evidence on Radial Diffusion of Geomagnetically Trapped Particles," Earth's Particles and Fields, Editor, B.M. McCormac, p. 143, Reinhold, New York, NY, 1968.

Roederer, 1970
J. G. Roederer, Dynamics of Geomagnetically Trapped Radiation, Springer-Verlag, New York, NY, 1970.

Rose, 1987
M. F. Rose, "Electrical Insulations and Dielectrics in the Space Environment," IEEE Trans. on Electrical Insulations, Vol. EI-22, No. 5, pp. 555-571, 1987.

Ryan et al., 1972
M. J. Ryan, J. F. Ormes, and V. K. Balasubrahmanyan, Physical Review Letters, Vol. 28, p. 985, 1972.

Samir and Jew, 1972
U. Samir and H. Jew, "Comparison of theory with experiment for electron density distribution in the near wake of an ionospheric satellite," J. Geophysical Research, Vol. 77, pp. 6819-6827, 1972.

Sauer, 1984
H. H. Sauer, An Atlas of Polar Cap Energetic Particle Observations, NOAA/ERL/SEL-3, -4 Technical Report U.S. Dept. of Commerce, Boulder, Colorado, (note Vol 1: Tiros: 1 Jan 79 – 28 Feb 81, Vol 2: NOAA/6 : 8 July 79 – 10 May 83), 1984.

Scarlett et al., 1978
W. R. Scarlett, P. S. Freier, and C. J. Waddington, Ap. Space Sci., Vol. 59, p. 301, 1978.

Schultz and Lanzerotti, 1974
M. Schultz and L. J. Lanzerotti, Particle Diffusion in the Radiation Belts, Springer-Verlag, New York, NY, 1974.

Sessler, 1980
G. M. Sessler, editor, Electrets (Topics in Applied Physics), Springer-Verlag, Berlin, West Germany, 1980.

Shane, 1977
Douglas F. Shane, "Spacecraft Charging Technology Conference, p78-2," AFGL TR-77-0051, Proceedings of the Spacecraft Charging Technology Conference, C. P. Pike and R. R. Lovell, Editors, pp. 25–35, AFGL, Hanscom AFB, MA, 1977. ADA045459

Shapiro et al., 1982
P. Shapiro, E. L. Peterson, and J. H. Adams, "Calculation of Cosmic-Ray Induced Soft Upsets and Scaling in VLSI Devices," NRL Memorandum Report 4864, Naval Research Laboratory, Washington, D.C., August 1982.

Sharp et al., 1970
R. D. Sharp, E. G. Shelley, and R. G. Johnson, "Preliminary Results of a Low Energy Particle Survey at Synchronous Altitude," Journal of Geophysical Research, Vol. 75, p. 6092, 1970.

Shawhan, 1982
S. D. Shawhan, "Description of the Plasma Diagnostic Package (PDP) for the OSS-1 Shuttle mission and JSC plasma chamber test in conjunction with the Fast Pulse Electron Gun (FPEG)," Artificial Particle Beams in Space Plasma Studies, edited by B. Grandal, Plenum, New York, NY, pp. 419-429, 1982.

Simnett, 1976
G. M. Simnett, "Solar Cosmic Radiation During August 1972," Space Science Reviews, Vol. 19, p. 579, 1976.

Simon et al., 1979
M. Simon, H. Spiegelhauer, W. K. H. Schmidt, F. Siohan, J. F. Ormes, V. K. Balasubrahmanyan, and J. F. Arens, 16th Intl. Cosmic Ray Conf., Vol. 1, p. 352, 1979.

Smart and Shea, 1985
D. F. Smart and M. A. Shea, "Chapter 6, Galactic Cosmic Radiation and Solar Energetic Particles," Handbook of Geophysics and the Space Environment, Adolph S. Jursa scientific editor, Air Force Geophysics Laboratory, Air Force Systems Command, United States Air Force, 1985. ADA167000

Smith et al., 1973
L. H. Smith, A. Buffington, G. F. Smoot, L. W. Alvarez, and W. A. Washlig, Astrophysical Journal, Vol. 180, p. 987, 1973.

Smith et al., 1986
R. A. Smith, C. K. Goertz, and W. Grossman, "Thermal catastrophe in the plasma sheet boundary," Geophys, Res. Letrs, 13, pp.1380-1383, December 1986

Soop, 1972
M. Soop, "Report on photosheath calculations for the satellite GEOS," Planetary Space Science, Vol. 20, p. 859, 1972.

Soop, 1973
M. Soop, "Numerical calculations of the perturbation of an electric field around a spacecraft," Photon and Particle Interactions with Surfaces in Space, edited by R. J. L. Grard, D. Reidel Publishing Company, Hingham, MA, p. 127, 1973.

Soraas and Davis, 1968
F. Soraas and L. R. Davis, Temporal Variations of the 10 keV to 1700 keV Trapped Protons Observed on Satellite Explorer 26 During First Half of 1965, NASA TMX-63320, NASA/Goddard Space Flight Center, Maryland, 1968.

Spitzer Jr., 1962
L. Spitzer Jr., Physics of Fully Ionized Gasses, Interscience, New York, NY, 1962.

Spjeldvik, 1977
W. N. Spjeldvik, "Equilibrium Structure of Equatorially Mirroring Radiation Belt Protons," J. Geophys. Res., Vol. 82, p. 2801, 1977.

Spjeldvik, 1979
W. N. Spjeldvik, "Expected Charge States of Energetic Ions in the Magnetosphere," Space Science Reviews, Vol. 23, p. 499, 1979.

Spjeldvik and Fritz, 1978
W. N. Spjeldvik and T. A. Fritz, "Theory of Charge States of Energetic Oxygen Ions in the Earth's Radiation Belts," J. Geophys. Res., Vol. 83, No. A4, p. 1583, 1978.

Spjeldvik and Fritz, 1981
W. N. Spjeldvik, and T. A. Fritz, "Observations of Energetic Helium Ions in the Earth's Radiation Belts During a Sequence of Geomagnetic Storms," J. Geophys. Res., Vol. 86, p. 2317, 1981.

Spjeldvik and Rothwell, 1983
W. N. Spjeldvik and P.L. Rothwell, "The Earth's Radiation Belts," Environmental Research Paper No. 854, AFGL-TR-83-0240, Air Force Geophysics Laboratory, MA, 1983.ADA142673

Stassinopoulos, 1980
E. G. Stassinopoulos, "The Geostationary Radiation Environment," J. Spacecraft and Rockets, Vol. 17, pp. 145-152, 1980.

Stephen et al., 1984a
J. H. Stephen, T. K. Sanderson, D. Mapper, J. Farren, R. Harboe-Sorensen, and L. Adams, "A comparison of Heavy Ion Sources used in Cosmic Ray Simulation Studies of VLSI circuits," IEEE Transactions on Nuclear Science, Vol. NS-31, pp. 1069-1072, 1984.

Stephen et al., 1984b
J. H. Stephen, T. K. Sanderson, D. Mapper, M. Hardman, J. Farren, L. Adams, and R. Harboe-Sorensen, "Investigation of Heavy Particle Induced Latch-up, using a Calfornium-252 Source, in CMOS SRAM's and PROMs," IEEE Transactions on Nuclear Science, Vol. NS-31, pp. 1207-1211, 1984.

Sternglass, 1957

E. J. Sternglass, "Theory of Secondary Electron Emission by High Speed Ions," Phys. Rev., Vol. 108, No. 1, pp. 1-12, Oct. 1, 1957.

Stevens, 1980
N. J. Stevens, "Space Environmental Interactions with Biased Spacecraft Surfaces," in Space Systems and Their Interactions with Earth's Space Environment, Progress in Astronautics and Aeronautics, Vol. 71, H. B. Garrett and C. P. Pike editors, AIAA, New York, NY, pp. 455-476, 1980.

Stevens, 1982
N. J. Stevens, "Design Practices for Controlling Spacecraft Charging Interactions," NASA Technical Memorandum 82781, prepared for the 20th Aerospace Sciences Meeting, January 11-14, 1982.

Stevens et al., 1978
N. J. Stevens, C. K. Purvis, and J. V. Staskus, "Insulator Edge Voltage Gradient Effects in Spacecraft Charging Phenomena," IEEE Trans. Nucl. Sci., Vol. NS-25, pp. 1304-1312, Dec. 1978.

Stix, 1962
Thomas H. Stix, The Theory of Plasma Waves, McGraw-Hill, New York, New York, 1962.

Stormer, 1955
C. L. Stormer, The Polar Aurora, Clarendon Press, Oxford, England, 1955.

Sturman, 1981
J. C. Sturman, "Development and Design of Three Monitoring Instruments for Spacecraft Charging," NASA Technical Paper 1800, September 1981.

Tsao et al., 1984
C. H. Tsao, R. Silberberg, J. H. Adams Jr., and J. R. Letaw, "Cosmic Ray Effects on Microelectronics, Part III: Propagation of Cosmic Rays in the Atmosphere," NRL Memorandum Report 5402, Naval Research Laboratory, Washington, D.C., August 1984.

Tucker, 1987
G. H. Tucker (Geraco Engineering), "ESD Response Measurements in a Satellite Environment," 9th Annual Electrical Overstress/Electrostatic Discharge Symposium, Orlando, Florida, 29 Sept - 1 Oct 1987.

Vampola et al., 1985
A. L. Vampola, P. F. Mizera, H. C. Koons, J. F. Fennell, and D. F. Hall, The Aerospace Spacecraft Charging Document, The Aerospace Company, Los Angeles, CA, Report SD-TR-85-26, June 1985.

van Lint et al., 1980
V. A. J. van Lint, T. M. Flanagan, R. E. Leadon, J. A. Naber, and V. C. Rogers, Mechanisms of Radiation Effects in Electronic Materials, Volume 1, Wiley-Interscience, New York, NY, 1980.

Vette, 1966
J. I. Vette, Volume I: Inner Zone Protons and Electrons, NASA SP-3024, 1966.

Von Rosenvinge et al., 1969
T. T. Von Rosenvinge, W. R. Weber, and J. F. Ormes, Astrophys. Space Sci., Vol. 5, p. 342, 1969.

Wadham, 1986
P. N. Wadham, "The effects of electrostatic discharge phenomena on Telesat's domestic communication satellites," The Aerospace Environment at High Altitudes and its Implications for Spacecraft Charging and Communications, AGARD Conference Proceedings, No. 406, pp. 25-1 to 25-10, 1986.

Wallmark and Marcus, 1962

J. T. Wallmark and S. NM Marcus, "Minimum Size and Maximum Packing Density of Nonredundant Semiconductor Devices," Proceedings of IRE,286 (1962)

Webber and Lenzniak, 1973
W. R. Webber and J. A. Lezniak, J. Geophysical Research, Vol. 78, p. 1979, 1973.

Webber and Ormes, 1967
W. R. Webber and J. F. Ormes, Journal of Geophysical Research, Vol. 72, p. 5957, 1967.

Webber et al., 1973
W. R. Webber, J. A. Lezniak, and J. Kish, Proc. 13th Intl. Cosmic Ray Conf., Vol. 1, p. 248, 1973.

Whipple Jr., 1965
E. C. Whipple Jr., "The Equilibrium Electric Potential of a Body in the Upper Atmosphere and in Interplanetary Space," NASA TM X-55368, 1965.

Whipple Jr., 1981
E. C. Whipple Jr., "Potentials of Surfaces in Space," Rep. Prog. Phys., Vol. 44, pp. 1197-1250, Nov. 1981.

Wilkenfeld et al., 1981
J. Wilkenfeld, C. Mallon, and J. Horne, "Conduction and Charge storage in electron irradiated Spacecraft Insulators," RADC TR-81-198, Rome Air Development Center Technical Report, July 1981. ADA104796

Williams, 1983
D. J. Williams, "The earth's Ring Current: Causes, Generation, and Decay," Space Science Reviews, Vol. 34, pp. 223-234, 1983.

Williams, 1985
D. J. Williams, "Dynamics of the Earth's Ring Current: Theory and Observation," Space Science Reviews, Vol. 42, pp. 375-396, 1985.

Williams, 1987
D. J. Williams, Ring Current and Radiation Belts, U. S. National Report to International Union of Geodesy and Geophysics 1983-1986, pp. 570-578, 1987.

Ziegler, 1980
J. F. Ziegler, "Handbook of Stopping Cross Sections for Energetic Ions in all Elements," Volume 5 of The Stopping and Ranges of Ions in Matter, Pergamon Press, New York, NY, 1980.

Zoutendyck et al., 1985
J. A. Zoutendyck, L. S. Smith, G. A. Soli, P. Thieberger, and H. E. R. Wegner, "Single-event Upset Model Verification and Threshold Determination using Heavy ions in a Bipolar Static RAM," IEEE Transc. on Nuclear Science, Vol. NS-32, No. 6, pp. 4164-4169, December 1985.

A1.5 Bibliography

Al'pert, 1983

Ya L. Al'pert, The Near-Earth and Interplanetary Plasma, Volumes 1 (General Properties and Fundamental Theory) and 2 (Plasma Flow, Plasma Waves and Oscillations), Cambridge University Press, ISBN 0 521 24364 5 and ISBN 0521 24601 6, 1983.

Avdienko, 1977

A. A. Avdienko, "Surface breakdown of solid dielectrics in vacuum. I. Characteristics for breakdown of insulators along the vacuum surface," Sov. Phys. Tech. Phys., Vol. 22(8), August 1977.

Balmain and Hirt, 1980

K. G. Balmain and W. Hirt, "Dielectric Surface Discharges, Dependence on Incident Electron Flux," for presentation at the IEEE Radiation Effects Conference, 1980.

Balmain et al., 1982

K. G. Balmain, M. Gossland, and R. D. Reeves, "Optical Measurement of the Velocity of Dielectric Surface Arcs," prepared for presentation at the IEEE Nuclear and Space Radiation Effects Conference, Las Vegas, Nevada, 1982.

Barlett et al., 1976

R. H. Barlett, G. A. Fulk, R. S. Lee, and R. C. Weingart, "Temperature Dependence of X-Ray-Induced Photoconductivity in Kapton and Teflon," prepared for the IEEE Annual Conference on Nuclear Space Radiation Effects, July 7, 1976.

Beers et al., 1981

B. L. Beers, V. W. Pine, and S. T. Ives, "Internal Breakdown of Charged Spacecraft Dielectrics," IEEE Trans. Nucl. Sci., Vol. NS-28, pp. 4529-4534, December 1981.

Beers et al., 1982

B. L. Beers, V. W. Pine, and S. T. Ives, Continued Development of a Detailed Model of Arc Discharge Dynamics, BEERS 1-82-16-23, Beers Associates; NASA Contract NAS3-2253, NASA CR-167977, 1982.

Beers et al., 1985

B. L. Beers, R. E. Daniell, and T. N. Delmer, "A Simple Model of Electron Beam Initiated Dielectric Breakdown," Spacecraft Environmental Interactions Technology 1983, NASA CP 2359/AFGL-TR-85-0018, pp. 591-598, 1985. **ADA202020**

Bernstein, 1979

W. Bernstein, H. Lenibach, P. J. Kellogg, S. J. Mosnson, and T. Hallinan, "Further Laboratory Measurements of the Beam-Plasma Discharge," Journal of Geophysical Research, Vol. 84, No. A12, Dec. 1, 1979.

Bouquet et al., 1979

F. L. Bouquet, W. E. Price, and D. M. Newell, "Designer's Guide to Radiation Effects on Materials for use on Jupiter Fly-Bys and Orbiters," IEEE Transactions on Nuclear Science, Vol. NS-26, No. 4, August 1979.

Bradford, 1979

J. N. Bradford, "A Distribution Function for Ion Track Lengths in Rectangular Volumes," J. Appl. Phys., Vol. 50, p. 3799, 1979.

Briet, 1986

R. Briet, ASCAT: Aerospace Spacecraft Charging Analysis Technique, Report TOR-0086(6508-10)-1, The Aerospace Corp., Los Angeles, CA, 24 Sept. 1986.

Bronshteyn and Protsenko, 1970
I. M. Bronshteyn and A. N. Protsenko, "Inelastic Electron Scattering and the Secondary Electron Emission of Insulators, "Radio Engineering and Electronic Physics, Vol. 15, No. 4, 1970.

Chen, 1965
F. F. Chen, Electric Probes. Plasma Diagnostic Techniques, R. H. Huddlestone and S. L. Leonard, eds., Academic Press, pp. 113-200, 1965.

Chenette and Dietrich, 1984
D. L. Chenette and W. F. Dietrich, "The Solar Flare Heavy Ion Environment for Single Event Upsets: A Summary of Observations over the Last Solar Cycle, 1973-1983," IEEE Transactions on Nuclear Science, Vol. NS-31, No. 6, pp. 1217-1222, December 1984.

Coakley et al., 1983
P. G. Coakley, N. Wild, and M. J. Treadaway, "Laboratory Investigation of Dielectric Materials Exposed to Spectral Electron Environments (1 to 100 keV)," IEEE Trans. Nucl. Sci., Vol. NS-30, pp. 4605-4609, December 1983.

Coffey et al., 1975
H. T. Coffey, J. E. Nanevicz, and R. C. Adamo, Photoconductivity of High-Voltage Space Insulating Materials, SRI Report for NASA/Lewis Research Center, OH, October 1975.

Coleman, 1969
R. Coleman, "Random Paths through Convex Bodies," J. Appl. Prob., Vol. 6, p. 430, 1969.

Cuddihy, 1987
E. F. Cuddihy, "A concept for the Intrinsic Dielectric Strength of Electrical Insulation Materials," IEEE Transactions of Electrical Insulations, Vol. EI-22, No. 5, pp. 573-589, 1987.

DeForest and McIlwain, 1971
S. E. DeForest and C. W. McIlwain, "Plasma Clouds in the Magnetosphere," J. Geophys. Res., Vol. 76, pp. 3587-3611, June 1, 1971.

de La Cotardiere, 1987
P. de La Cotardiere, Larousse Astronomy, Facts on File, New York, NY, 1987.

Dessler and Parker, 1959
A. J. Dessler and E. N. Parker, "Hydromagnetic Theory of Geomagnetic Storms," Journal of Geophysical Research, Vol. 64, pp. 2239-2252, 1959.

Eagles and Belanger, 1976
A. E. Eagles and V. J. Belanger, Conductive Coatings for Satellites, Technical Report AFML-TR-76-233, General Electric Space Division, Final Report for Period 15 May 1975 to 30 June 1976, Valley Forge, PA, Dec. 1976.

Eagles et al., 1977
A. E. Eagles, L. J. Amore, V. J. Belanger, and R. E. Schmidt, Spacecraft Static Charge Control Materials, Technical Report AFML-TR-77-105, Part I, General Electric Space Division, Report for Period 17 Feb. 1976 to 16 Feb. 1977, June 1977.

Eagles et al., 1977
A. E. Eagles, R. E. Schmidt, L. J. Amore, and V. J. Belanger, Transparent Antistatic Satellite Materials, Technical Report AFML-TR-77-174, Part I, General Electric Space Division Report for Period 17 June 1976 to 16 June 1977, October 1977.

Eagles et al., 1978
A. E. Eagles, R. E. Schmidt, L. J. Amore, and V. J. Belanger, Transparent Antistatic Satellite Materials, Technical Report AFML-TR-77174, Part II, General Electric Space Division Report for Period 17 June 1977 to 16 June 1978, July 1978.

Edmonds, 1986
L. Edmonds, Approximations Useful for the Prediction of Electrostatic Discharges for Simple Electrode Geometries, JPL Publication 86-36, Jet Propulsion Laboratory, Pasadena, CA, August 15, 1986.

Fellas, 1980
C. N. Fellas, "An Arc-Free Thermal Blanket for Spacecraft Use," IEEE 1980 Annual Conference on Nuclear and Space Radiation Effects, 15-18 July 1980.

Fennel et al., 1983
J. F. Fennel, et al., "A Review of SCATHA Satellite Results: Charging and Discharging," Spacecraft/Plasma Interactions and Their Influence on Field and Particle Measurements, A. Pedersen, T. D. Guyenne, and J. Hunt, eds., ESA-SP-198, European Space Agency, Noordwijk, The Netherlands, pp. 3-11, 1983.

Feynman et al., 1984
J. Feynman, D. A. Hardy, and E. G. Mullen, "The 40 keV Electron Durable Trapping Region," Journal of Geophysical Research, Vol. 89, pp. 1517-1526, March 1984.

Flanagan et al., 1979
T. M. Flanagan, R. Denson, C. E. Mallon, M. J. Treadaway, and E. P. Wenaas, "Effect of Laboratory Simulation Parameters on Spacecraft Dielectric Discharges," for presentation at 1979 IEEE Conference on Space and Nuclear Radiation Effects, July 17-20, 1979.

Forbes and Garrett, 1975
J. M. Forbes and H. B. Garrett, "Variations in the Atmospheric Neutral Density at 145 km," Planet. Space Sci., Vol. 23, pp. 1399-1404, 1975.

Forbes and Garrett, 1978
J. M. Forbes and H. B. Garrett, "Seasonal-Latitudinal Structure of the Diurnal Thermospheric Tide," Journal of the Atmospheric Sciences, Vol. 35, No. 1, January 1978.

Forbes and Garrett, 1979
J. M. Forbes and H. B. Garrett, "Theoretical Studies of Atmospheric Tides," Reviews of Geophysics and Space Physics, Vol. 17, No. 8, pp. 1951-1981, November 1979.

Forbes and Garrett, 1979
J. M. Forbes and H. B. Garrett, "Solar Tidal Wind Structures and the E-Region Dynamo," J. Geomag. Geoelect., Vol. 31, pp. 173-182, 1979.

Frederick, 1987
R. A. Fredericks, Glossary for the Solar-Geophysical Environment, pamphlet 87-001, Office of the Staff Meteorologist, Air Force Satellite Control Facility, CA, January 1987.

Frederickson, 1982
A. R. Frederickson, "Electrostatic Charging and Discharging in Space Environments," Proceedings: Tenth International Symposium on Discharges and Electrical Insulation in Vacuum, IEEE, 1982.

Frederickson, 1985
A. R. Frederickson, "Discharge Pulse Phenomenology," Spacecraft Environmental Technology 1983, NASA Conference Publication 2359/AFGL-TR-85-0018, pp. 483-509, 1985. **ADA202020**

Garrett, 1980
H. B. Garrett, "Spacecraft Charging: A Review from Space Systems and Their Interactions with Earth's Space Environment," edited by Henry B. Garrett and Charles P. Pike, Progress in Astronautics and Aeronautics, Vol. 71, 1980.

Garrett and Forbes, 1978
H. B. Garrett and J. M. Forbes, "Tidal Structure of the Thermosphere at Equinox," Journal of Atmospheric and Terrestrial Physics, Vol. 40, pp. 657-668, 1978.

Garrett and Forbes, 1979
H. B. Garrett and J. M. Forbes, "Time Evolution of Ion Contaminant Clouds at Geosynchronous Orbit," Geophysical Research Letters, Vol. 6, No. 12, Dec. 1979.

Garrett and Spitale, 1985
H. B. Garrett and G. C. Spitale, "Magnetospheric Plasma Modeling (0-100 keV)," J. Spacecraft, Vol. 22, No. 3, May-June 1985.

Garrett et al., 1980
H. B. Garrett, D. C. Schwank, P. R. Higbie, and D. N. Baker, "Comparison Between the 30- to 80-keV Electron Channels on ATS 6 and 1976-059A During Conjunction and Application to Spacecraft Charging Prediction," Journal of Geophysical Research, Vol. 85, No. A3, pp. 1155-1162, March 1, 1980.

Garrett et al., 1981
H. B. Garrett, D. D. Schwank, and S. E. Deforest, "A Statistical Analysis of the Low-Energy Geosynchronous Plasma Environment--I. Electrons," Planet. Space Sci., Vol. 29, No. 10, pp. 1021-1044, 1981.

Garrett et al., 1981
H. B. Garrett, D. C. Schwank, and S. E. Deforest, "A Statistical Analysis of the Low-Energy Geosynchronous Plasma Environment--II. Ions," Planet. Space Sci., Vol. 29, 1981.

Garrett et al., 1986
H. Garrett, J. Feynman, and S. Gabriel, editors, Space Technology Plasma Issues in 2001, JPL Publication 86-49, Jet Propulsion Laboratory, Pasadena, CA, October 1986.

Giddingd et al., 1985
A. E. Giddingd, F. W. Hewlett, R. K. Treece, D. K. Nichols, L. S. Smith, and J. A. Zoutendyck, "Single Event Upset Immune Integrated Circuits for Project Galileo," IEEE Transactions on Nuclear Science, Vol. NS-32, pp. 4159-4163, December 1985.

Gilley and Sievers, 1983
George Gilley (Aerospace) and Michael Sievers (Fail-Safe Technology Corp.), DNA/DARPA SEU Symposium, private communication, 20 April 1983.

Gilligan et al., 1976
J. E. Gilligan, T. Yamauchi, R. E. Wolf, and C. Ray, Electrically Conductive Paints for Satellites, IIT Research Institute, IL, Dec. 1976.

Glassford and Liu, 1984
A. P. M. Glassford and C. K. Liu, "Characterization of Contamination Generation Characteristics of Satellite Materials, Volume II," AFWAL-TR-83-4126, Wright-Patterson AFB, Ohio, 1984.

Goldstein and DeForest, 1976
R. Goldstein and S. E. DeForest, "Active Control of Spacecraft Potentials at Geosynchronous Orbit, Spacecraft Charging by Magnetospheric Plasmas," A Rose, ed., Prog. Astronaut. Aeronaut., Vol. 47, pp. 169-181, MIT Press, MA, 1976.

Goodman et al., 1980
S. H. Goodman, D. P. Salisbury, R. W. Rosser, and J. A. Zelik, Low Outgassing Conductive Adhesives Part II, Technical Report AFML-TR-78-193, Hughes Aircraft Company - Aerospace Groups, El Segundo, CA, January 1980.

Grard, 1973
R. J. L. Grard, Photon and Particle Interactions with Surface in Space, D. Reidel Publ. Co., Dordrecht, Holland, 1973.

Grard et al., 1983
R. J. L. Grard, K. Knott, and M. R. Pedersen, "Spacecraft Charging Effects," Space Sci. Rev., Vol. 34, pp. 289-304, Mar. 1983.

Hall and Fote, 1979
D. F. Hall and A. A. Fote, Preliminary Flight Results from P78-2 (SCATHA) Spacecraft Contamination Experiment, ESA Symposium on Spacecraft Materials held at ESTEC, 2-5 October 1979, ESA SP-145, ESA, Noordwijk, The Netherlands, Dec. 1979.

Heirtzler et al., 1987
J. R. Heirztler, editor, Contributions in Solar-Planetary Relationships, U. S. National Report 1983-1986, Nineteenth General Assembly, International Union of Geodesy and Geophysics, Vancouver, British Columbia, Canada, August 9-22, 1987.

Henrich, 1973
V. E. Henrich, "Fast, Accurate Secondary-Electron Yield Measurements at Low Primary Energies," The Review of Scientific Instruments, Vol. 44, No. 4, April 1973.

Herron et al., 1972
B. G. Herron, J. R. Bayless, and J. D. Worden, "High Voltage Solar Array Technology," AIAA paper no. 72-443, AIAA 9th Electric Propulsion Conference, April 17-19, 1972.

Inouye, 1981
G. T. Inouye, "Brushfire Arc Discharge Model," Spacecraft Charging Technology 1980, NASA Conference Publication 2182/ AFGL-TR-81-0270, pp. 133-162, 1981.ADA114426

Inouye and Sellen, 1978
G. T. Inouye and J. M. Sellen Jr., "A Proposed Mechanism for the Initiation and Propagation of Dielectric Surface Charges," presented at the Symposium on the Effects of the Ionosphere on Space and Terrestial Systems, Arlington, VA, 24-26 January 1978. (Further elaborated in TRW internal memo M2-142-80, 1980.)

James et al., 1983
D. E. James, editor, Contributions in Solar-Planetary Relationships, U. S. National Report 1979-1982, Eighteenth General Assembly, International Union of Geodesy and Geophysics, Hamburg, Federal Republic of Germany, August 15-27, 1983.

Janzen, 1975
J. Janzen, "On the critical conductive filler loading in antistatic composites," Journal of Applied Physics, Vol. 46, No. 2, Feb. 1975.

Kamen et al., 1979
R. E. Kamen, A. B. Holman, N. J. Stevens, and F. D. Berkopec, "Design Guidelines for Control of Spacecraft Charging," Spacecraft Charging Technology 1978, NASA CP-2071, pp. 817-818, 1979.

Kanaya and Kawakatsu, 1972
K. Kanaya and H. Kawakatsu, "Secondary electron emission due to primary and backscattered electrons," J. Phys. D: Appl. Phys., Vol. 5, 1972.

Kanaya and Okanaya, 1972
K. Kanaya and S. Okanaya, "Penetration and energy-loss theory of electrons in solid targets," J. Phys. D: Appl. Phys., Vol. 5, 1972.

Kashat and Klein, 1977

I. Kashat and N. Klein, "Current runaway in insulators affected by impact ionization and drift," J. Appl. Phys., Vol. 48, No. 12, Dec. 1977.

Katz and Parks, 1982

I. Katz and D. E. Parks, "Space Shuttle Orbiter Charging," AIAA 20th Aerospace Sciences Meeting, January 11-14, 1982.

Katz et al., 1977

I. Katz, et al., "NASCAP, A Three Dimensional Charging Analyzer Program for Complex Spacecraft," IEEE Trans. Nucl. Sci., Vol. NS-24, pp. 2276-2280, Dec. 1977.

Katz et al., 1977

I. Katz, D. E. Parks, M. J. Mandell, J. M. Harvey, D. H. Brownell, S. S. Wang, and M. Rotenberg, A Three Dimensional Dynamic Study of Electrostatic Charging in Materials, NASA CR-135256, S-Cubed Report SSS-R-77-3367, 1977.

Katz et al., 1979

I. Katz, J. J. Cassidy, M. J. Mandell, G. W. Schnuelle, D. G. Steen, D. E. Parks, M. Ratenberg, and J. M. Alexander, Extension, Validation, and Application of the NASCAP Code, SSS-R-79-3904, Systems Science and Software, NASA Contract NAS 3-21050, NASA CR-159595, 1979.

Katz et al., 1980

I. Katz, M. J. Mandell, D. E. Parks, and G. W. Schnuelle, "A Theory of Dielectric Surface Discharges," presented at 1980 IEEE Annual Conference on Nuclear and Space Radiation Effects, July 15-18, 1980.

Katz et al., 1983

I. Katz, et al., "NASCAP Simulations of Spacecraft Charging of the SCATHA Satellite," Spacecraft/Plasma Interactions and their Influence on Field and Particle Measurements, A. Pedersen, D. Guyenne, and J. Hunt, eds., European Space Agency, Noordwijk, The Netherlands, pp. 109-114, 1983.

Kaufman and Robinson, 1979

H. R. Kaufman and R. S. Robinson, Interaction of High Voltage Surfaces with the Space Plasma, prepared for Lewis Research Center, Ohio, NASA CR-159731, Grant NSG 3196, May 1979.

Kellerer, 1971

A. M. Kellerer, "Considerations on the Random Traversal of Convex Bodies and Solutions for General Cylinders," Rad. Rev., Vol. 47, p. 359, 1971.

Klein and Solomon, 1976

N. Klein and P. Solomon, "Current runaway in insulators affected by impact ionization and recombination," Journal of Applied Physics, Vol. 47, No. 10, October 1976.

Knott, 1972

K. Knott, "The Equilibrium Potential of a Magnetospheric Satellite in an Eclipse Situation," Planet. Space Sci., Vol. 20, pp. 1137-1146, Aug. 1972.

Laframboise, 1982

J. G. Laframboise, Theory of Spherical and Cylindrical Langmuir Probes in a Collisionless Maxwellian Plasma at Rest, UTIAS-100, Univ. Toronto, Toronto, Canada, 1982.

Laframboise, 1982

J. G. Laframboise, "Is There a Good Way to Model Spacecraft Charging in the Presence of Space-Charge Coupling, Flow, and Magnetic Fields?," Proc. Workshop on Natural Charging of Large Space Structures in Near-Earth Polar Orbits, Air Force Geophysics Laboratory, Massachusetts, September 1982.

Laframboise, 1984

J. G. Laframboise, "Calculation of Secondary-Electron Escape Currents from Inclined Spacecraft," Proc. USAF/NASA Spacecraft Environmental Interactions Technology Conference, 1984.

Laframboise et al., 1982

J. G. Laframboise, R. Godard, and M. Kamitsuma, "Multiple Floating Potentials, Threshold-Temperature Effects, and Barrier Effects in High-Voltage Charging of Exposed Surfaces on Spacecraft," Proc. Internat. Symp. on Spacecraft Materials in Space Environment, Toulouse, France, Publications Branch, European Space Agency, Noordwijk, The Netherlands, 8–11 June 1982.

Leadon et al., 1978

R. E. Leadon, A. L. Weiman, and R. C. Keyser, "Electrical Simulation of Electrostatic Discharges in Dielectrics," presented at the 1978 IEEE Annual Conference on Nuclear and Space Radiation Effects, July 18-21, 1978.

Le Jeune and Magnolia, 1973

W. R. Le Jeune and L. R. Magnolia, Characteristics of Magnetospheric Substorms and Their Effects Upon Spacecraft: A Selected Bibliography, TRW Systems Group, Redondo Beach, CA, Oct. 1973.

Leung, 1985

Philip Leung, Characterization of EMI Generated by the Discharge of a 'VOLT' Solar Array, JPL Publication 85-82, Jet Propulsion Laboratory, Pasadena, CA, November 1985.

Lezniak and Webber, 1978

J. A. Lezniak and W. R. Webber, "The Charge Composition and Energy Spectra of Cosmic-Ray Nuclei From 3000 MeV per Nucleon to 50 GeV per Nucleon," Astrophysical Journal, Vol. 223, p. 676, 1978.

Littmark and Ziegler, 1980

U. Littmark and J. F. Ziegler, "Handbook of Range Distributions for Energetic Ions in all Elements, Volume 6 of The Stopping and Ranges of Ions in Matter," Edited by J. F. Ziegler, Pergamon Press, New York, NY, 1980.

Liu and Glassford, 1983

C. K. Liu (Incorrectly listed as Kiu on some reports) and A. P. M. Glassford, "Characterization of Contamination Generation Characteristics of Satellite Materials, Volume I," AFWAL-TR-83-4126, 1983.

Lovell et al., 1976

R. R. Lovell, et al., "Spacecraft Charging Investigation; A Joint Research and Technology Program, Spacecraft Charging by Magnetospheric Plasmas," A Rosen, ed., Prog. Astronaut. and Aeronaut., Vol. 47, MIT Press, MA, pp. 3-14, 1976.

Makhov, 1976

A. F. Makhov, "An empirical relation for the secondary electron emission of solids," Sov. Phys. Solid State, Vol. 17, No. 8, 1976.

Mandell, et al., 1978

M. J. Mandell, I. Katz, G. W. Schnuelle, P. G. Steen, and J. C. Roche, "The Decrease of Effective Photocurrents due to Saddle Points in Electrostatic Potentials near Differentially Charged Spacecraft," IEEE Transactions on Nuclear Science, Vol. NS-25, p. 1313, 1978.

McPherson et al., 1975

D. A. McPherson, D. P. Cauffman, and W. R. Schober, "Spacecraft Charging at High Altitudes: SCATHA Satellite Program," Journal of Spacecraft and Rockets, Vol. 12, No. 10, pp. 621-626, October 1975.

Moore, et al., 1981
T. E. Moore, R. L. Arnoldy, J. Feynman, and D. A. Hardy, "Propagating Substorm Injection Fronts," Journal of Geophysical Research, Vol. 86, pp. 6713-6727, August 1981.

Mullen and Gussenhoven, 1982
E. G. Mullen and M. S. Gussenhoven, "High-Level Spacecraft Charging Environments Near Geosynchronous Orbit," AFGL-TR-82-0063, Environmental Research Papers, No. 771, 11 February 1982. **ADA118791**

Mullen et al., 1980
E. G. Mullen, H. B. Garrett, D. A. Hardy, and E. C. Whipple, "P78-2 SCATHA Preliminary Data Atlas," AFGL-TR-80-0241, AFGL, Hanscom AFB, MA, 11 August 1980. **ADA094122**

Mullen et al., 1981
E. G. Mullen, M. S. Gussenhoven, and H. B. Garrett, "A Worst Case Spacecraft Environment as Observed by SCATHA on 24 April 1979," AFGL-TR-81-0231, Environmental Research Papers, No. 751, 31 July 1981. **ADA108680**

Nichols, 1985
D. K. Nichols, Trends in Electronic Parts Susceptibility to Single Event Upset Space Station Environment, JPL D-2767 internal document, Jet Propulsion Laboratory, Pasadena, CA, September 1985.

Olsen, 1980
R. C. Olsen, "Modification of Spacecraft Potentials by Thermal Electron Emission on ATS-5," Journal of Spacecraft and Rockets, AIAA report 81-4348, p. 527, 1980.

Olsen, 1981
R. C. Olsen, "Modification of Spacecraft Potentials by Plasma Emission," Journal of Spacecraft and Rockets, AIAA report 81-4287, p. 462, 1981.

Olsen and Purvis, 1983
R. C. Olsen and C. K. Purvis, "Observations of Charging Dynamics," Journal of Geophysical Research, Vol. 88, p. 5657, 1983.

Olsen et al., 1981
R. C. Olsen, C. E. McIlwain, and E. C. Whipple, Jr., "Observations of Differential Charging Effects on ATS-6," J. Geophys. Res., Vol. 86, pp. 6809-6819, Aug. 1, 1981.

Parker and Whipple Jr., 1967
L. W. Parker and E. C. Whipple, "Theory of a Satellite Electrostatic Probe," Ann. Phys., Vol. 44, pp. 126-161, Aug. 1967.

Parker and Whipple Jr., 1970
L. W. Parker and E. C. Whipple, "Theory of Spacecraft Sheath Structure, Potential, and Velocity Effects on Ion Measurements by Traps and Mass Spectrometers," J. Geophys. Res., Vol. 75, pp. 4720-4733, Sept. 1, 1970.

Pickel and Blandford, 1982
J. C. Pickel and J. T. Blandford, "Cosmic-Ray-Induced Errors in MOS Devices," IEEE Trans. Nucl. Sci., Vol. NS-29, p. 2122, (material in appendix summarizing work of M. D. Petroff on path length distributions), 1982.

Pruett, 1982
R. Pruett, "Impact of the Space Particle Environment on Current Air Force Space Division Programs," AIAA report 82-0114, AIAA 20th Aerospace Sciences Meeting, Orlando, FL, January 11-14, 1982.

Purvis, 1979
C. K. Purvis, Jupiter Probe Charging Study, NASA TP-1263, Washington, D.C., Jan. 1979.

Purvis, 1980
C. K. Purvis, "Configuration Effects on Satellite Charging Response," AIAA Paper 80-0040, Jan. 1980.

Rosen, 1976
A. Rosen, editor, "Spacecraft Charging by Magnetospheric Plasma," Prog. Astronaut. Aeronaut., Vol. 47, MIT Press, MA, 1976.

Rothwell et al., 1976
P. L. Rothwell, et al., "Simulation of the Plasma Sheath Surrounding a Charged Spacecraft, Spacecraft Charging by Magnetospheric Plasmas," A. Rosen, ed., Prog. Astronaut. and Aeronaut., Vol. 47, MIT Press, MA, pp. 121-133, 1976.

Schmidt, 1980
R. E. Schmidt, Charging Control Satellite Materials, Technical Report AFWAL-TR-80-4017, Part I, General Electric Space Division, Report for Period 1 Aug. 1978 to 31 Oct. 1979, March 1980.

Shaw et al., 1976
R. R. Shaw, J. E. Nanevicz, and R. C. Adamo, "Observations of Electrical Discharges Caused by Differential Satellite Charging, Spacecraft Charging by Magnetospheric Plasmas," A. Rose, ed., Prog. Astronaut. Aeronaut., Vol. 47, MIT Press, MA, pp. 61-76, 1976.

Sprour, 1983
J. R. Sprour, "Basic Mechanisms of Radiation Effects on Electronic Materials, Devices, and Integrated Circuits," Tutorial Short Course, IEEE 1983 Nuclear and Space Radiation Effects Conference, 1983.

Stern, 1978
D. Stern, Solar-Terrestrial Programs: A Five-Year Plan, Solar Terrestrial Programs Office, NASA, Washington, D.C., 1978.

Sternglass, 1950
E. J. Sternglass, "Secondary Electron Emission and Atomic Shell Structure," Phys. Rev., Vol. 80, No. 5, pp. 925-926, Dec. 1, 1950.

Sternglass, 1954
E. J. Sternglass, "Backscattering of Kilovolt Electrons from Solids," Phys. Rev., Vol. 95, No. 2, pp. 345-358, July 15, 1954.

Stettner and Marks
R. Stettner and R. Marks, Physical Modeling of Spacecraft Discharge Processes and Associated Electron Blowoff, Mission Research Corporation, Santa Barbara, California.

Stevens
N. J. Stevens, High Voltage System - Plasma Interaction Summary, TRW, Inc., Space and Technology Group-System Integration Laboratory, undated.

Stevens and Purvis, 1980
N. J. Stevens and C. K. Purvis, "NASCAP Modeling Computations on Large Optics Spacecraft in Geosynchronous Substorm Environment," NASA TM-81395, 1980.

Strunk and White, 1979
William Strunk Jr. and E. B. White, The Elements of Style, Third Edition, MacMillan, New York, NY, 1979.

Townsend et al., 1982
R. E. Townsend, R. W. Cannata, R. D. Prochaska, G. E. Rattray, and J. C. Holbrook, Source Book of the Solar-Geophysical Environment, AFGWC/TN-82/002, AFGWC, Offutt AFB, NE, August 1982.

Treadaway et al., 1979
M. J. Treadaway, et al., "The Effects of High-Energy Electrons on the Charging of Spacecraft Dielectrics," IEEE Trans. Nucl. Sci., Vol. NS-26, pp. 5102-5106, Dec. 1979.

Vanderschueren and Linkens, 1977
J. Vanderschueren and A. Linkens, Nature of transient currents in polymer, Laboratory of Physical Chemistry, University of Liege, Sart-Tilman, B-4000 Liege, Belgium, Dec. 1977.

Wallmark and Marcus, 1962
J. T. Wallmark and S. M. Marcus, "Minimum Size and Maximum Packing Density of Nonredundant Semiconductor Devices," Proceedings of the IRE, p. 286, 1962.

Webb and Williams, 1979
J. B. Webb and D. F. Williams, "Hopping conduction in thin films of tetrathiotetracene," J. Phys. C: Solid State Phys., Vol. 12, 1979.

Webber et al., 1979
W. R. Webber, E. C. Stone, and R. E. Vogt, 16th Intl. Cosmic Ray Conf., Vol. 5, p. 357, 1979.

Whipple Jr., 1976
E. C. Whipple Jr., "Theory of the Spherically Symmetric Photoelectron Sheath: A Thick Sheath Approximation and Comparison with the ATS Observation of a Potential Barrier," J. Geophys. Res., Vol. 81, pp. 601-607, Feb. 1, 1976.

Whipple Jr. and Parker, 1969
E. C. Whipple Jr. and L. W. Parker, "Theory of an electron trap on a charged spacecraft," J. Geophys. Res., Vol. 74, pp. 2962-2971, June 1, 1969.

Whipple Jr. and Parker, 1969
E. C. Whipple Jr. and L. W. Parker, "Effects of Secondary Electron Emission on Electron Trap Measurements in the Magnetosphere and Solar Wind," J. Geophys. Res., Vol. 74, pp. 5763-5774, Nov. 1, 1969.

Whittlesey, 1978
A. C. Whittlesey, "Voyager Electrostatic Discharge Protection Program," International Symposium on Electromagnetic Compatibility, Proceedings, IEEE, pp. 377-383, 1978.

Wilkenfeld et al., 1982
J. M. Wildenfeld, B. L. Harlacher, and D. Mathews, Development of Electrical Test Procedures for Qualification of Spacecraft Against EID, Vol. 2: Review and Specification of Test Procedures, IRT-8195-022-1, IRT Corp., NASA Contract NAS3-21967, NASA CR-165590, 1982.

Willis and Skinner, 1973
R. F. Willis and D. K. Skinner, "Secondary Electron Emission Yield Behavior of Polymers," Solid State Commun., Vol. 13, No. 6, pp. 685-688, Sept. 15, 1973.

Yadlowsky, et al., 1980
E. J. Yadlowsky, R. C. Hazelton, and R. J. Churchill, "Characteristics of Edge Breakdowns on Teflon Samples," presented at 1980 Annual Conference on Nuclear and Space Radiation Effects, July 15-18, 1980.

Zinsser, 1985
William Zinsser, On Writing Well, Third Edition, Harper and Row, New York, NY, 1985.

Appendix

2

Glossary

A index

A daily index of geomagnetic activity derived as the average of the eight 3-hourly a indices.

a index

A 3-hourly "equivalent amplitude" index of local geomagnetic activity; "a" is related to the 3-hourly K index according to the following scale:

K	0	1	2	3	4	5	6	7	8	9
a	0	3	7	15	27	48	80	140	240	400

absorption

The dissipation of radio wave energy into heat. As a wave passes through an ionized medium, it forces free electrons to oscillate (positive ions are much less mobile and can be ignored). Collisions with particles in the medium convert wave energy into heat. In the ionosphere, this process is most effective at D region altitudes, where the product of free electron density and collisional frequency is a maximum. (Also see attenuation.)

active region

A region on the sun where transient features (such as sunspots, plages, filaments, and flares) are observed. These features are characterized by enhancements of the local solar magnetic field.

AE index

A geomagnetic index of the auroral electrojet, which measures the maximum range of excursion (both positive and negative) from quiet levels; measured at a given universal time by using the combined data from a worldwide ring of high-latitude magnetic observatories. AU (A upper) refers to the greatest positive deviation from the quiet time reference and AL (A lower) to the most negative. By definition AE = AU - AL. AO refers to the mean of AU and AL: AO = 1/2(AU + AL).

AFGWC

Air Force Global Weather Central: the forecast center operated by the Air Force at Offutt AFB, Nebraska. It monitors and forecasts both atmospheric weather and the space environment.

Alfven wave

A transverse wave in magnetized plasma characterized by a change of direction of the magnetic field (rather than a change of intensity). An Alfven wave travels with a speed $C_A(2) = [B^2/(4\pi mn)]^{1/2}$, where B is the magnetic field strength, m is the mass of an ion (proton in plasma of ionized hydrogen), and n is the number density of ions (which in a singly ionized plasma equals the number density of electrons). The Alfven number in a plasma moving at speed C is C/C_A, the analog of the Mach number in a neutral gas. For average conditions in the solar wind, C_A = 50 to 100 km/s. The bulk velocity of the solar wind typically exceeds 300 km/s and is thus "superalfvenic," as well as supersonic.

angstrom

A unit of length equal to 1×10^{-8} centimeters. Used chiefly to express short (optical) wavelengths.

anomalous propagation

The propagation of radio waves through the atmosphere along a path different from that expected as a result of the normal 4/3 radians curvature caused by standard tropospheric refraction. Less bending than normal is known as subrefraction. More bending than normal includes superrefraction, ducting, or trapping.

A_p index

An averaged planetary A index based on data from a set of specific stations. The official A_p index is determined at the Institut fur Geophysik at Gottingen, F.R.G.

a_p,A_p

Indices that provide a linear measure of the level of disturbance of the planetary geomagnetic field. A_p is a 24-hour index, and a_p is a 3-hour index. Both indices range from 0 to 400. (Also see K, K_p, and K_m.) The following descriptive terms apply to both a_p and A_p:

Level:

0 - 6 Quiet
7 - 14 Unsettled
15 - 29 Active
30 - 49 Minor Storm
50 or higher Major Storm

apogee

The point on the path of an earth-orbiting satellite farthest from the earth. The general term for any planet is apoapsis. Apsis is the point in an orbit which is either farthest or closest to the center of attraction. Aphelion is the farthest point for comets from the sun.

Appleton anomaly

Two areas of enhanced F Region electron density centered at +20 and -20 degrees geomagnetic latitude, and extending in local time from noon to midnight. Their origin is a horizontal transport of free electrons by high altitude winds, from which the electrons are produced over equatorial latitudes (by solar radiation) and over auroral latitudes (by particle precipitation). Also known as "subequatorial ridges," they are characterized by strong horizontal electron density gradients and thus are a source of "non-great circle propagation." They are most distinctive near the equinoxes at average levels of geomagnetic activity. During high geomagnetic activity the ridges tend to merge into a single ridge over the equator. Near the summer and winter solstices a single, broad ridge is found in the winter hemisphere midlatitudes, a phenomenon called the "Winter Anomaly."

attenuation

This term includes all power losses experienced by a radio wave. Absorption is only one component of attenuation. Other components include: free space loss due to beam spreading, beam focusing/defocusing (for example power loss in a duct is small), scatter loss, etc. (Also see absorption.)

AU

Astronomical unit: the mean earth-sun distance, 1.496×10^{11} meters (214.94 solar radii).

aurora

Sporadic radiant emission from the upper atmosphere over middle and high latitudes. Precipitating charged particles (electrons and, to a lesser extent, protons) are guided by the earth's geomagnetic field into the higher latitudes. These particles collide with atmospheric gases, which become excited or ionized. When the atoms and molecules return to a normal energy state, electromagnetic energy (radio, infrared, visible, or ultraviolet radiation) is emitted. Auroras are most intense, and are observed furthest equatorward, at times of geomagnetic storms.

auroral electrojet

An electric current that flows in the auroral zone at E layer altitudes. It is most intense during geomagnetic disturbances, and ultimately owes its origin to a convective motion of charged particles in the magnetotail.

auroral oval

A roughly elliptical area in which aurora may be occurring at a particular time. The auroral activity is generally most intense, and extends furthest equatorward, in the midnight sector (since the precipitating particles causing aurora come from the magnetotail). An oval band around each geomagnetic pole ranging from about 75 deg magnetic latitude at local noon to about 67 deg magnetic latitude at midnight under average conditions. It is the locus of structured auroras and widens to both higher and lower latitudes during the expansion phase of magnetic substorms.

auroral zone

A roughly circular band around either geomagnetic pole, over which auroral activity is most often seen. The band's center lies about 23 degrees of latitude from the geomagnetic pole, and has a width of about 12 degrees.

auroral zone absorption (AZA)

During a geomagnetic storm, ultraviolet and x-ray auroral emissions in the E Region can cause an increase in the electron density of the underlying D Region. The result is an increase in absorption of radio signals transiting the auroral zone. (Also see D Region.)

autumnal equinox

The equinox that occurs in September.

Bartel's rotation number

The serial number assigned to 27-day rotation periods of solar and geophysical parameters. Rotation 1 in this sequence was assigned arbitrarily by Bartel to begin in January 1833, and the count has continued by 27-day intervals to the present. (For example, rotation 2000 began on 12 November 1979, rotation 2030 on 30 January 1982.) The 27-day period was selected empirically from the observed recurrence of geomagnetic activity attributed to corotating features on the sun. The sun has a rotation period (as seen from the earth) of 27.27 days; therefore, solar longitude slowly drifts with respect to the Bartel rate. Solar rotation serial numbers do not coincide with Bartel rotation numbers because of this difference in rotation rate and also because the initial solar rotation serial number was assigned (by Carrington) to begin on a different date.

bow shock

A collisionless shock wave in front of the magnetosphere arising from the interaction of the supersonic solar wind with the earth's magnetic field.

butterfly diagram

A plot of observed sunspot latitude versus time. This diagram, which resembles a butterfly, shows the tendency of solar active regions to drift from high to low latitudes during a sunspot cycle.

C event

(See solar flare.) The least energetic type of solar flare, as defined by the peak x-ray emission observed in the 1–8 angstrom band. For a C event, peak emission is between 1.0 and 9.9 x 10^{-3} ergs/cm^2/sec. For example, C5.3 means peak emission was 5.3 x 10^{-3} ergs/cm^2/sec. (Also see M and X events.)

c9 index

A daily index of geomagnetic activity derived from the daily C_p index. The index ranges from 0 to 9, 9 representing "most disturbed."

Carrington longitude

A system of fixed longitudes rotating with the sun. Carrington longitude is widely, but imprecisely used to mean heliographic longitude. (See solar coordinates.)

chromosphere

The layer of the solar atmosphere lying between the photosphere and the transition region and the corona. The chromosphere is not visible to the naked eye, but is the source of the strongest absorption lines in the solar spectrum including hydrogen and the H and K lines of calcium, and is the source of the red (chromium) color often seen around the rim of the moon during total solar eclipses.

conjugate points

Two points on the earth's surface at opposite ends of a geomagnetic field line.

continuum storm (CTM)

General term for solar radio noise lasting for hours and sometimes days, in which the intensity varies smoothly with frequency over a wide range in the meter and decimeter wavelengths.

convection

The bulk transport of plasma (or gas) from one place to another, in response to mechanical forces (for example, viscous interaction with the solar wind) or electromagnetic forces.

coordinated universal time

By international agreement, the local time at the prime meridian, which passes through Greenwich, England. Therefore, it is also known as Greenwich mean time, or sometimes simply universal time. There are 24 time zones around the world, which are labeled alphabetically. The time zone centered at Greenwich has the double designation of A and Z. Especially in the military community, coordinated universal time is often referenced as Z or ZULU time.

corona

The outermost layer of the solar atmosphere. A greatly extended region of low density and high temperature, the corona extends far out into interplanetary space, becoming the solar wind.

coronal hole

A region of low density and open magnetic field lines in the solar corona. Holes may persist for several months, and are a primary source of the high speed solar wind streams observed near the earth. As such, they are closely related to the occurrence of recurrent geomagnetic storms.

corpuscular radiation

See "particulate radiation."

corrected geomagnetic coordinates

The spherical "geomagnetic coordinate" system is based on approximating the earth's actual magnetic field by a centered dipole (bar magnet). A slightly better fit with the actual field is achieved if the dipole axis is offset from the earth's center by about 450 kilometers toward a location in the Pacific Ocean (15.6N, 150.9E). This "eccentric dipole" axis intersects the surface at 81N, 85W and 75S, 120E. The non-spherical, corrected geomagnetic coordinate system is based on this eccentric dipole. (Also see geomagnetic coordinates.)

cosmic radio noise

Radio waves from extraterrestrial sources.

cosmic rays

Very high energy particulate radiation which permeates interstellar space. Cosmic rays are measured at the earth's surface by a "Neutron Monitor," an instrument capable of detecting secondary neutrons produced by collisions between cosmic rays and atmospheric gases. "Galactic cosmic radiation" originates outside the solar system, and is modulated by solar activity. During periods of high solar activity, counting rates on neutron monitors fall (known as a Forbush decrease), due to an increase in the shielding effect of the disturbed solar wind and geomagnetic field. (See "rigidity" for more explanation on the shielding of particles by a magnetic field, as well as the discussion in chapter 2 on single particle motions and Stormer orbits. "Solar cosmic rays" are produced by the most energetic solar flares; in these instances, counting rates on neutron monitors are observed to rise (known as a "ground level event").

C_p index

A daily index of geomagnetic activity obtained from the A_p index. The range of C_p is 0 to 2.5, 2.5 representing the most disturbed.

critical frequency

The limiting radio frequency below which radio waves are reflected by, and above which they penetrate through, an ionized medium (such as an ionospheric layer) at vertical incidence. Also known as the "plasma frequency."

CRRES

Combined Release Radiation Effects satellite.

cusp(s)

In the magnetosphere, two regions near magnetic local noon and approximately 15 deg of latitude equ rward of the north and the south magnetic poles. The cusps mark the division between geomagnetic field lines on the sunward side (which are approximately dipolar, but somewhat compressed by the solar wind) and the field lines in the polar cap that are swept back into the magnetotail by the solar wind. "Cusp" implies conical symmetry around the axis of the bundle of converging (Northern Hemisphere) or diverging (Southern Hemisphere) field lines. In practice, "cusp" and "cleft" are often used interchangeably. However, "cleft" implies greater extension in longitude (local time) and hence a wedge-shaped structure.

D region (D layer)

A daytime layer in the ionosphere between about 50 and 90 kilometers altitude. During solar flares, the D layer may be enhanced and lowered by an increased flux of x-ray radiation from the sun. The D layer is responsible for most radio wave absorption. Major "absorption" events include: short wave fades (SWF), auroral zone absorption (AZA), and polar cap absorption (PCA). The same physical process causes the dissipation of radio wave energy in each event. However, the events differ by the source of the ionizing radiation, location, and time scale:

Event	Source	Location	Time Scale
SWF	Flare X-Rays	Sunlit Hemisphere	Tens of Minutes
AZA	Electrons from the Magnetotail	Auroral Zones	Hours
PCA	Flare Protons	Polar Caps	Hours - Days

declination

(1) The angular distance of an astronomical body north (+) or south (-) of the celestial equator. (2) In geomagnetic applications, the angle between true north and the horizontal component of the local geomagnetic field.

differential flux

The differential flux j(E) denotes the number of particles of energy E per unit energy interval, per unit area, per unit time, per unit solid angle of observation, passing through an area perpendicular to the viewing direction. It is approximately obtained from the count rate of a physical detector measuring the flux of particles between energy E and E + dE, geometric factor G, and solid angle of view dW through the relationship

$$j(E) = \frac{C}{(G * dE * dW\ 8\ dt)}$$

where C is the number of detector counts in time dt. This approximate definition assumes that the flux is isotropic, constant over the energy range of the detector channel, and time-independent over the accumulation time dt.

differential rotation

Refers to the variation of solar rotation rate with latitude. Low solar latitudes rotate faster (about 13 degrees per day) than high latitudes (about 10 degrees per day).

dipole equator

The dipole or "dip equator" is defined by where the earth's magnetic field lines are inclined zero degrees to the earth's surface. The dip equator does not correspond exactly to the "geomagnetic equator," since the dip system includes local variations in the near earth magnetic field. The dip poles, known as the "North, or South, Magnetic Poles (NMP, SMP)," are where magnetic field lines are inclined 90 degrees to the earth's surface. They lie a considerable distance from the geomagnetic poles. (Also see geomagnetic coordinates.)

Pole	Lat.	Long.
NMP (dip NP)	76N	101W
Geomagnetic NP	79N	70W
SMP (dip SP)	66S	141E
Geomagnetic SP	79S	110E

DMSP

Defense meteorological satellite program. A series of high inclination, low altitude spacecraft designed to monitor weather and the near earth space environment (especially in the auroral zones).

Doppler shift

A displacement in the observed frequency of a radiated signal caused by relative motion between an emitter and a receiver.

DSCS

A military communications satellite.

Dst index

A geomagnetic index describing variations in the equatorial ring current. It is computed from the H-components at approximately four near-equatorial stations at hourly intervals. At a given time, the Dst index is the average of a storm time variation over all longitudes. An index of 50 is considered significant, and an index of 200 or more is associated with middle-latitude auroras. The reference level is chosen to be statistically zero on internationally designated quiet days.

E region (E layer)

The ionospheric region between 90 kilometer altitude and about 120 to 140 kilometers. At night this layer virtually disappears, except at auroral latitudes (where it is partially maintained by precipitating particles).

eccentric dipole

See "corrected geomagnetic coordinates."

ECEMP

Electron Caused Electromagnetic Pulse is a term used to describe internal charging and spacecraft charging discharges. It is sometimes used in the limited sense of discharges on cables and circuit boards inside the spacecraft.

ecliptic

The great circle made by the intersection of the plane of the earth's orbit with the celestial sphere. (Less properly, the apparent path of the sun around the sky during the year.)

EDP

Electron density profile: the variation in the density of free electrons with altitude. It represents a vertical sounding of the ionosphere.

electrojet

(1) Auroral: A current that flows in the ionosphere in the auroral zone driven by magnetospheric convection. (2) Equatorial: A thin electric current layer in the ionosphere over the dip equator, driven by the dynamic action of westward electron motion at about 100 to 115 km altitude.

EMI

Electromagnetic interference.

EP

Energetic particle data are provided by a series of geostationary satellites operated by the Air Force. Electrons ranging from 30 keV to 2 MeV, and protons from 50 keV to 150 MeV, are measured.

ephemeris

An astronomical almanac listing solar coordinates and the positions of the sun and other heavenly bodies at regular intervals in time.

equatorial electrojet

An ionospheric electric current at E region altitudes (between 100 and 120 kilometers), centered over the "dipole equator" and roughly 10 degrees latitude in width. It is driven by the dynamic action of a daytime westward drift of free electrons across geomagnetic field lines.

equinox

One of the two points of intersection of the celestial equator and the ecliptic. The sun passes through the vernal equinox on about 21 March and through the autumnal equinox on about 22 September.

erg

The cgs unit of energy (1 erg = 1×10^{-7} joule).

ESD

Electrostastic discharge (ESD) covers any breakdown. The "static" is misleading as a discharge is hardly static. ESD is used for everything from discharges produced when people contact metal objects after crossing a wool rug to high voltage breakdowns. ESDs need to be eliminated in the manufacturing as well as the operation of spacecraft. This text deals only with ESD produced by environmental charging. In the manufacture of electronics, ESDs from the people assembling the parts due to charge buildup on their bodies have been known to damage parts. The term ESD covers all of these effects.

EUV

See extreme ultraviolet.

eV

Electron volt. A unit of energy (1 eV = 1.602×10^{-19} joule). The kinetic energy acquired by an electron accelerated through an electrical potential difference of one volt.

extraordinary mode

One of the two modes of propagation of electromagnetic waves in a magnetic plasma. For propagation along the direction of the magnetic field, it is the mode for which the electric vector rotates in the same sense that an electron gyrates about the field. For propagation perpendicular to the magnetic field, the electric vector oscillates perpendicular to the primary magnetic field. (See also ordinary mode.)

extreme ultraviolet

A portion of the electromagnetic spectrum from approximately 100 to 1000 angstroms in wavelength.

extremely low frequency (ELF)

That portion of the radio frequency spectrum from 30 to 3000 hertz.

F layer trough

An area of depleted F region electron density often found in the night sector just equatorward of the auroral oval. There is a particularly steep horizontal electron density gradient between the trough and oval, which causes "non-great-circle propagation" and focusing of radio waves.

F region (F layer)

The ionospheric region between about 130 and roughly 1000 kilometer altitude. The F region is responsible for most of the refraction suffered by radio waves as they transit the ionosphere. It is subdivided into the F2 and the F1 regions. The F2 layer is usually the densest (in terms of electron density) region of the ionosphere and persists throughout the night. The F1 layer, often thought of as a ledge in the "electron density profile" at the bottom of the F layer, occurs only in daylight.

$F_{10.7}$

The solar radio flux observed at a wavelength of 10.7 cm (2800 MHz) by the Ottawa Radio Observatory at 1700Z daily (local noon). Normally reported in "solar flux units" (1 sfu = 1×10^{-22} webers/meter^{2}hertz). The variation of the 10.7 cm radio flux is closely associated with enhanced thermal radiation from "active regions" and thus the overall level of solar activity.

$F_{10.7}$ bar

The 90 day running mean value of the 1700Z Ottawa $F_{10.7}$.

filament

A mass of relatively high density, low temperature gas suspended in the upper chromosphere or the lower corona by magnetic fields. It is seen as a ribbonlike absorption feature against the solar disk. (Also see prominence.)

flare

(1) A sudden, short-lived brightening of a localized region in the solar chromosphere. Flares nearly always occur in the plage of an active region, and are usually only visible in monochromatic light. They are classified according to area (0,1,2,3,4) and brightness (F,N,B), and/or by x-ray intensity (C,M,X). The x-ray classification scheme is as follows:

C event - The least energetic type of solar flare, as defined by the peak x-ray emission observed in the 1-8 angstrom band. For a C event, peak emission is between (1.0 and 9.9) x 10^{-3} erg/cm^2/sec. For example, C5.3 means peak emission was 5.3 x 10^{-3} erg/cm^2/sec.

M event - A moderate solar event as defined by an x-ray burst with a peak emission between (1.0 and 9.9) x 10^{-2} erg/cm^2/sec.

X event - A major solar flare, as defined by an x-ray burst with peak emission in excess of 1.0 x 10^{-1} erg/cm^2/sec. For example, X3.5 means the peak emission was 3.5 x 10^{-1} erg/cm^2/sec.

(2) A sudden eruption of energy on the solar disk lasting minutes to hours, from which radiation and particles are emitted. Flare classification is based on size at the time of maximum brightness in H-alpha. One square degree is equal to $(1.214 \times 10^4 \text{ km})^2 = 48.5$ millionths of the visible solar hemisphere.

fluence

Time integrated flux.

flux

The amount of something (protons, x-rays, radio energy, etc.) passing through a specified area in a given time period.

fmin

The minimum reflected frequency observed by a vertical incidence (VI) ionosonde. It depends on the electron density in the ionosphere (mostly D layer), ionosonde power and sensitivity, and the amount of radio noise. (Also see LUF.)

foE

"Critical frequency" (for the ordinary or "o" wave) of the solar (ultraviolet) produced E layer. It is the highest frequency returned by that layer at vertical incidence, and thus provides a measure of that layer's maximum electron density.

foEs

"Critical frequency" (for the ordinary or "o" wave) of the sporadic E layer. It is the highest frequency reflected by that layer at vertical incidence, and thus depends on enhancements in the E layer's electron density caused by non-solar sources (such as particle precipitation, wind shear, or meteor ionization).

foF2

"Critical frequency" (for the ordinary or "o" wave) of the F2 layer. It is the highest ordinary wave polarization frequency returned by that layer at vertical incidence, and thus provides a measure of that layer's maximum electron density. (Also see MUF.)

forbush decrease

See cosmic rays.

Fraunhofer spectrum

The system of dark lines due to absorption in the solar and terrestrial atmospheres, superimposed on the continuous solar spectrum.

gamma

A unit of magnetic field strength (1 gamma = 1×10^{-5} gauss = 1 nanotesla). The average surface strength of the geomagnetic field is about 1/2 gauss, while the average strength of the interplanetary magnetic field (IMF) is roughly 6×10^{-5} gauss (or 6 gamma).

gauss

A unit of magnetic induction named after Carl Friedrich Gauss (1777-1855) who first developed a method for accurately determining the absolute value of a magnetic field. In 1838 Gauss expressed the earth's magnetic field in a spherical harmonic series, the coefficients of which are called Gauss coefficients, $1G = 10^{-4}T$.

geomagnetic coordinates

A system of spherical coordinates (geomagnetic latitude and longitude). The system is based on approximating the actual magnetic field of the earth by a centered dipole (bar magnet) field. The axis of the dipole passes through the earth's center, but is inclined about 11 degrees to the earth's rotational axis. Intersection of this axis with the earth's surface defines the Geomagnetic North Pole (at 78.5N, 110E). (Also see corrected geomagnetic coordinates and dipole equator.)

geomagnetic cutoff

The geomagnetic cutoff is a measure of the rigidity (see rigidity) required to penetrate the earth's magnetic field to the given location. The geomagnetic cutoff was first estimated by Stormer in 1930 using a dipole approximation for the earth's magnetic field. He showed that the cutoff, that is the rigidity, of a particle external to the earth's magnetic field required for it to reach the earth's surface at a given latitude and longitude was:

$$\text{rigidity} = P = \frac{60}{r^2 \dfrac{\left[1 - \sqrt{(1 - \cos \quad \cos^3 \lambda)}\ \right]^2}{(\cos \quad \cos \lambda)^2}}$$

where P is the rigidity in GeV/ec for positive particles, r is the radial distance from the dipole center in earth radii, λ is the latitude in dipole coordinates, and is the angle which the trajectory makes with magnetic west.

geomagnetic elements

The components of the geomagnetic field at the surface of the earth. These elements are usually denoted thus in the literature:

X - the northward component

Y - the eastward component

Z - the vertical component, reckoned positive downward

H - the horizontal intensity of magnitude $\sqrt{(X^2 + Y^2)}$

F - the total intensity $\sqrt{(H^2 + Z^2)}$

I - the inclination (or DIP) angle, $\tan^{-1}$ (Z/H)

D - the declination angle, $\tan^{-1}$ (Y/X)

However, in SESC use, the northward and eastward components are often called the H and D components, where the D component is expressed in gammas and is derived from D (the declination angle) using the small angle approximation so that the D component = H (the correct horizontal intensity) multiplied by D (the declination angle, expressed in radians).

geomagnetic field

The magnetic field observed in and around the earth. The intensity of the magnetic field at the earth's surface is approximately 0.32 gauss at the equator and 0.62 gauss at the north pole (the place where a compass needle points vertically downward). The geomagnetic field is dynamic and undergoes continual slow secular changes as well as short-term disturbances (see geomagnetic storm). The geomagnetic field can be approximated by a dipole field, with the axis of the dipole offset to the earth's rotational axis. Geomagnetic dipole north is near 78.3N, 69W (near Thule, Greenland).

geomagnetic local time

Time as measured in the geomagnetic coordinate system. Geomagnetic local time at a location is computed from local midnight on the basis that 15 degrees of geomagnetic longitude is 1 hour of time.

geomagnetic storm

(1) A widespread disturbance of the geomagnetic field. A storm is normally defined as being in progress when the a_p index is 30 or higher. A geomagnetic storm results when an enhanced stream of solar plasma strikes the magnetosphere, causing a disruption in various electric currents in the magnetotail. Sporadic geomagnetic storms are caused by particle emissions from solar flares and disappearing filaments (also known as eruptive prominences). Recurrent geomagnetic storms are caused by discontinuities in the solar wind associated with Solar Storm Boundaries in the IMF, or high speed particle streams from coronal holes. In general, recurrent storms are weaker, show a slower onset, but last longer than sporadic storms.

(2) A worldwide disturbance of the earth's magnetic field, distinct from regular diurnal variations. A storm is precisely defined as occurring when the daily A_p index exceeds 29.

Minor geomagnetic storm: A storm for which the A_p index was greater than 29 and less than 50.

Major geomagnetic storm: A storm for which the A_p index was greater than 49 and less than 100.

Severe geomagnetic storm: A storm for which the A_p index was 100 or more.

Initial phase: Of a geomagnetic storm, that period when there may be an increase of the middle-latitude horizontal intensity (H) (see geomagnetic elements) at the surface of the earth. The initial phase can last for hours (up to a day), but some storms proceed directly into the main phase without showing an initial phase.

Main phase: Of a geomagnetic storm, that period when the horizontal magnetic field at middle latitudes is generally decreasing, owing to the effects of an increasing westward-flowing magnetospheric

ring current. The northward component can be depressed as much as several hundred gammas in intense storms. The main phase can last for hours, but typically lasts less than 1 day.

Recovery phase: Of a geomagnetic storm, that period when the depressed northward field component returns to normal levels. Recovery is typically complete in one to two days, but can take longer.

geosynchronous

Any equatorial satellite with an orbital velocity equal to the rotational velocity of the earth, and thus a period of 23 hours, 56 minutes. Geosynchronous altitude is near 6.6 earth radii from the earth's center (i.e 35,782 kilometers, 22,235 statute miles, or 19,321 nautical miles, above the earth's surface). To also be geostationary, the satellite must satisfy the additional restriction that its orbital inclination be exactly zero degrees. The net effect is that a geostationary satellite is virtually motionless with respect to an observer on the ground.

GOES

Geostationary Operational Environmental Satellite: A series of satellites designed to monitor weather and the near earth space environment. They provide observations of energetic particles and x-rays, and are operated by NOAA (National Oceanic and Atmospheric Administration).

GPS

Global positioning satellite.

gradual commencement

The commencement of a geomagnetic storm that has no well-defined onset. (See also sudden commencement.)

granulation

The tops of small scale convective cells, seen in the sun's photosphere, which are responsible for the mottled appearance of the sun as seen in white light.

ground level event (GLE)

A sudden increase in secondary neutrons measured by a ground based "Neutron Monitor." GLEs are important as indicators that a very energetic solar flare has occurred and a PCA event and geomagnetic stor are almost certain to follow. (Also see cosmic rays.)

group speed

The speed (v_g) at which energy (or information carrying signals) travels; always less than the speed of ligh

$$v_g = \frac{d\omega}{dk}$$

where ω is the angular frequency, and k is the wave number (2π over the wavelength). For light waves, th relation between ω and k is

$$w = \frac{c\ k}{n(k)}$$

where n is the index of refraction and c is the speed of light. So,

$$v_g = \frac{c}{\left[n + \omega\left(\frac{dn}{d\omega}\right)\right]}$$

(Also see phase speed. When the index of refraction does not depend on ω, the phase velocity and the grou velocity are the same numerical value.)

H alpha line

An absorption line located at 6563 angstroms in the red end of the visible electromagnetic spectrum. Most chromospheric features, such as solar flares, are normally observed at this wavelength. (Also see monochromatic light.)

hertz

A unit of frequency equal to one cycle per second.

HF

High frequency. The 3-30 MHz radio wave band. Normally used for long distance communication by refraction in the F region of the ionosphere and reflection from the D layer in the ionosphere.

high-speed stream

A feature of the solar wind having velocities that are about double the average solar wind values. The densities of high-speed streams are less than for average solar wind. High-speed streams are believed to originate in coronal holes.

homologous flares

Solar flares that occur repetitively in the same active region, with essentially the same position and with a common pattern of development.

IAGA

International Association of Geomagnetism and Aeronomy.

IC

Integrated circuit.

ID

Internal discharges.

IDM

Internal discharge monitor.

IGRF

International Geomagnetic Reference Field.

IMF

Interplanetary magnetic field. The magnetic field carried with the solar wind. The IMF originates with the large scale photospheric magnetic fields found on the sun's surface. (See Chapter 2 for further explanation.)

integral flux

The integral flux J(E) is literally the integral, with respect to E, of the differential flux j(E); hence its name. It denotes the number of particles of energy equal to or greater than E per unit area, per unit solid angle, per unit time, passing through an area perpendicular to the viewing direction. It is obtained by integrating the differential flux with respect to energy, or, given a detector that counts all particles of energy equal to or greater than some threshold energy E, with geometric factor G and solid angle of view dW, it is obtained from

$$J(>E) = \frac{C}{(GdWdt)}$$

where C is the number of counts in time dt.

inversion line

See neutral line.

ion-acoustic waves

Longitudinal waves in a plasma are similar to sound waves in a neutral gas. Amplitudes of electron and ion oscillations are not quite the same, and the resulting Coulomb repulsion provides the potential energy to drive the waves.

ionosonde

An instrument used to produce a sounding of free electron density in the ionosphere. Short pulses are transmitted, usually at vertical incidence (VI), scanning in frequency from about 1 to 20 MHz over about a five minute cycle. Delay time between pulse transmission and echo reception is recorded as a function of frequency. Such a plot is known as an ionogram. The ionogram can also be labelled with virtual height and free electron density. Virtual height is the apparent altitude of reflection assuming pulses travel at light speed. The group speed times half the delay time equals the virtual height. Free electron density (in $\#/cm^3$) is equal to the critical frequency (f_0, in kilohertz) divided by nine, squared; i.e., $Ne = (f_0/9)^2$.

ionosphere

That portion of the earth's upper atmosphere where ions and electrons are present in quantities sufficient to affect the propagation of radio waves. Normally, the ionosphere extends down to about 50 kilometers altitude, but at certain times and locations it reaches even lower. Variations of electron density with height led to the subdivision of the ionosphere into the D, E, and F regions (or layers).

ionospheric storm

(1) A disturbance in the ionosphere which may follow a geomagnetic storm. During an ionospheric storm the free electron density in the F2 layer is typically enhanced for a few hours, then becomes depleted for up to several days.

(2) A disturbance in the F region of the ionosphere, which occurs in connection with geomagnetic activity. In general, there are two phases of an ionospheric storm, an initial increase in electron density (the positive phase) lasting a few hours, followed by decrease lasting a few days. At low latitudes only the positive phase is seen. Individual storms can be quite varied and their behavior depends on geomagnetic latitude, season, and local time. The phases of an ionospheric storm are not coincident with the initial and main phases of a geomagnetic storm.

IPP

Ionospheric penetration point. The geographic point over which a radio wave passes through an altitude of 350 kilometers while in transit between a ground station and a satellite.

K, K_p, K_m

A 3-hour dimensionless quasi-logarithmic index that provides a measure of the level of disturbance of the geomagnetic field. Without a subscript, the index refers to the deviation of the most disturbed horizontal component relative to an assumed quiet day curve for the recording site. The K index ranges from 0 (very quiet) to 9 (violently disturbed). The "p" subscript denotes a planetary, as opposed to a single station, index. K_p is generated in Gottingen, West Germany, based on the K index from 12 or 13 stations distributed around the world. The K_p index has been derived routinely since 1932. GWC estimates K_p and A_p indices using data from six North American stations. The K_p index ranges from 0° to 9°, with 27 one-third unit steps (0°, 0+, 1-, 1°, 1+, 2-, etc.). (Also see a_p, A_p.) K_m is similar to K_p but based on a more symmetric global array of stations.

Kelvin-Helmholtz instability

A mechanism often invoked to explain phenomena at the magnetopause (and sometimes the plasmapause), especially the observed magnetic pulsations. The quasi-laminar flow of two magnetized plasmas on opposite sides of the surface that divides them (for example, the magnetopause) can develop into turbulent flow within a few proton gyroradii of the boundary if the number density and the relative velocity of the two plasmas are high enough to meet certain conditions. The microinstabilities that develop within one proton gyroradius of the boundary transfer momentum across the boundary, thus giving rise to the equivalent of a tangential viscous force. Meanwhile, larger turbulent cells "rolling" off the layer because of this friction can be the source of circularly or elliptically polarized magnetic pulsations.

LEO

Low Earth orbit.

LET

Linear energy transfer.

limb

The edge of the solar disk, corresponding to the level at which the solar atmosphere becomes transparent to visible light.

limb darkening

For certain solar spectral lines, a lessening of the intensity of the line from the center to the limb caused by the existence of a temperature gradient in the sun. At the center we see to much deeper and hotter layers than we do near the limb, where our line of sight enters the solar atmosphere at an oblique angle.

lobes

Two regions (north and south) inside the magnetotail separated by the neutral sheet.

LUF

Lowest usable frequency. The lowest frequency that allows reliable long range HF radio communication by ionospheric refraction. It is a function of D region absorption, transmitted power, receiver sensitivity, and other equipment parameters.

M event

(See solar flare.) A moderate solar event as defined by an x-ray burst with a peak emission between (1.0 and 9.9) x 10^{-2} erg/cm^2/sec. (Also see C and X events.)

magnetic bay

A relatively smooth excursion of the H (horizontal) component (see geomagnetic elements) of the geomagnetic field away from and returning to quiet levels. Bays are "positive" as H increases or "negative" as H decreases.

magnetogram

A plot showing the amplitude of one or more vector components of a magnetic field versus space or time. Solar magnetograms are a graphic representation of solar magnetic field strengths and polarity.

magnetometer

An instrument used to record the strength and orientation of the geomagnetic field as observed at a particular point on, or near, the earth's surface.

magnetopause

The boundary surface between the solar wind (with its embedded interplanetary magnetic field) and the earth's magnetosphere. At the magnetopause, the pressure due to the magnetic field and particles of the earth equals the pressure (magnetic plus particle) of the solar wind. In practical terms, the magnetic field pressure of the earth equals the particle pressure from the solar wind, as these are the dominate terms in the relation.

magnetopause current sheet

An electric current sheet that more or less coincides with the magnetopause.

magnetosheath

The region between the bow shock and the magnetopause. This region is characterized by a very turbulent plasma. Along the sun-earth axis, the magnetosheath is about two earth radii thick. As the solar wind passes through the bow shock on the day side, its velocity becomes subsonic. Along the flanks of the magnetopause it is supersonic.

magnetotail

The portion of the magnetosphere in the anti-solar direction. In the magnetotail, geomagnetic field lines are drawn out to great distances by the flow of the solar wind past the earth. The magnetotail is divided into two lobes. In the north lobe, magnetic field lines are directed toward the earth; while in the south lobe, they are directed away. These two lobes are separated by a relatively narrow neutral plasmasheet of hot, dense plasma. High currents can flow in the plasma separating the two lobes. This allows the magnetic field to "reverse" in this region.

Maunder minimum

An approximately 70-year interval during the 17th and 18th centuries when practically no sunspots were observed on the sun.

MeV

Million electron volts: A unit of energy (1 MeV = 1.602×10^{-3} joule).

MHz

Megahertz: A unit of frequency equal to a million cycles per second.

monochromatic light

Pertaining to a single wavelength or, more commonly, to a very narrow band of wavelengths.

MUF

Maximum usable frequency. The highest frequency that allows reliable long range HF radio communication by ionospheric refraction. It depends on the of F2 (or equivalently, the F2 region maximum electron density) at the control point and the angle of incidence with which a radio wave enters the ionosphere. Frequencies higher than the MUF do not suffer sufficient ionospheric refraction to be bent back toward the earth, i.e., they are transionospheric.

multipath

Implies a radio wave splits and follows several paths to a receiver. Since the paths may be of different lengths, the arrival time and phase via each path will differ. The result may be intermittent fading and/or reinforcement of the signal received.

NASA

National Aeronautics and Space Administration.

NASCAP

NASA Charging/Analyzing Program.

neutral line

A line separating solar magnetic fields of opposite polarity. Neutral line analysis of an active region indicates its magnetic complexity and flare producing potential. Neutral line is a misleading term, since it implies no magnetic field. Usually a strong field is present, but it is parallel to the sun's surface (a transverse field), rather than perpendicular (a longitudinal field). A more accurate term for a neutral line is an inversion line.

neutral point

A point of zero magnetic field within the magnetotail of the earth.

neutral sheet

The boundary separating the northern and southern lobes in the magnetotail. In this region the magnetic field reverses in the magnetotail.

neutron monitor

An instrument used for ground based detection of secondary neutrons produced during collisions between cosmic rays and atmospheric molecules or atoms.

NGDC

National Geophysical Data Center.

non-great-circle propagation

Radio waves tend to propagate along the shortest distance between two points on the earth, a great circle path. Horizontal gradients in ionospheric electron density will cause refraction in a horizontal plane, resulting in non-great-circle propagation. Strong horizontal gradients are associated with the equatorward boundary of the auroral oval (especially in the night sector), the subequatorial ridges, and the sunrise terminator. (Also see F layer trough.)

NSSDC

National Space Science Data Center.

ordinary ("o") wave

The presence of the earth's magnetic field in the ionosphere causes a linearly polarized radio wave to split into two circularly polarized components. These components rotate in opposite senses, an ordinary ("o") and an extraordinary ("x") wave. The "o" wave deviates less than the "x" component in propagation characteristics from what is expected in the absence of a magnetic field.

ordinary mode

One of the two modes of propagation of electromagnetic waves in a magnetic plasma. For propagation along the direction of the magnetic field, it is the mode for which the electric vector rotates in the opposite sense that an electron gyrates about the field. For propagation perpendicular to the magnetic field, the electric vector oscillates parallel to the primary magnetic field. (See also extraordinary mode.)

particulate radiation

Radiation consisting of particles, specifically atomic particles such as protons (hydrogen nuclei), electrons, neutrons, and alpha particles (helium nuclei). Also known as corpuscular radiation.

PCA

Polar cap absorption. An anomalous condition of the polar ionosphere where HF and VHF (3-300 MHz) radio waves are absorbed and LF and VLF (3-300 kHz) radio waves are reflected at lower altitudes than normal. PCAs generally are associated with major solar flares. PCAs begin a few hours after the event and reach a maximum within a day or two of onset. Some energetic solar flares emit streams of protons, which can gain direct access to the polar caps via cusps in the magnetosphere. High energy (mostly 5 to 15 MeV) protons will penetrate to D layer altitudes before colliding with atmospheric gases, and causing an increase in ionization. This increase in free electron density causes a corresponding increase in absorption of HF radio waves transiting the polar caps. A PCA event is defined by the amount of absorption of cosmic radio noise at 30 MHz seen by a riometer at Thule, Greenland. The PCA threshold is about 2 dB of absorption at 30 MHz for daytime and 0.5 dB at night. This threshold allows for additional ionization caused by solar ultraviolet radiation. In practice, PCAs are taken to be simultaneous with proton events. Transpolar radio paths may be disturbed for days or weeks following a proton event. (Also see D region.)

penumbra

The gray portion of a sunspot that may surround the black umbra. It is the portion of a spot where magnetic fields are less intense, causing the temperature (and thus brightness) of the sunspot to be closer to that of the overall photosphere.

perigee

The point in an orbit of closest approach to earth. A more general term used for any planet is periapsis.

perihelion

That point on the orbit of a sun-orbiting body nearest to the sun.

phase speed

The speed (vp) at which a wave pattern moves

$$vp = \frac{\omega(k)}{k}$$

For radio waves, vp = c/n, where c = speed of light in a vacuum and n = index of refraction. In matter, the phase speed can be more than c, since it is essentially a mathematical concept, not a physical quantity like group speed. If the phase speed also depends on the frequency of a wave, the material is said to be dispersive (for example, the ionosphere is a dispersive medium). (Also see group speed and refraction.)

photosphere

The visible surface of the sun as seen in white light; it is the location of sunspots.

pitch angle

The angle between the velocity vector of a charged particle and the direction of the ambient magnetic field.

plage

A region in the solar atmosphere where chromospheric plasma is concentrated by intense magnetic fields. Plages are denser, hotter, and brighter than the overall chromosphere. Nearly all flares occur in the vicinity of a plage.

plasma

An ionized gas, i.e., a gas composed of ions and free electrons.

plasma frequency

The characteristic frequency of free plasma oscillations. An electron travels away from an ion until its kinetic energy is overcome by the Coulomb attraction, and it falls back. The frequency of this oscillation is given by $f^2 = 4\pi ne^2/m$, where n is the local plasma density, e is the charge of an electron, and m is the electron mass. See critical frequency.

plasma sheet

A sheet of hot (high energy), dense plasma running down the center of the magnetotail. The plasma sheet normally remains beyond geosynchronous orbit, except when it is forced inward during geomagnetic disturbances. (Also see magnetotail.)

plasmasphere

A region of cool (low energy), dense plasma surrounding the earth. It may be considered an extension of the ionosphere. Like the ionosphere, it tends to corotate with the earth. The inner Van Allen radiation belt lies in the plasmasphere.

polar cap

The area poleward of the auroral oval within about 20 degrees of the geomagnetic poles. It is susceptible to direct bombardment by high energy solar particles deflected by our geomagnetic field and guided in through cusps in the magnetosphere.

polar cusps

Funnel-like features in the magnetosphere over the noontime sector of the auroral oval.

polarimeter

An instrument used to measure the total electron content (TEC) along a path between a ground station and a satellite equipped with a VHF beacon, preferably geostationary.

polarization

The polarization of an electromagnetic wave is defined as the plane of vibration of its electric field. An electromagnetic wave is a transverse wave consisting of an electric and a magnetic field. The two fields oscillate in phase, but are perpendicular to each other and to the direction of propagation. Polarization is defined in terms of the electric field because the existence of point electric charges (and lack of point magnetic charges) means the electric field will interact more strongly with matter than will the magnetic field.

pore

A very small sunspot without a penumbra.

prominence

A mass of relatively high density, low temperature gas suspended in the upper chromosphere or the lower corona by magnetic fields. It is seen as a bright, ribbonlike emission feature against the dark of space above the solar limb.

proton event

By definition, the measurement of at least 10 protons/cm s ster at energies greater than 10 MeV, by the primary SESC geosynchronous satellite. (See polar cap absorption.)

proton flare

Any flare producing significant fluxes of greater than 10 MeV protons in the vicinity of the earth.

pulsation

A rapid fluctuation of the geomagnetic field having periods from a fraction of a second to tens of minutes and lasting from minutes to hours. There are two main patterns: Pc (a continuous, almost sinusoidal pattern), and Pi (an irregular pattern). Pulsations occur at magnetically quiet as well as disturbed times. Pcs are grouped, according to their physical and morphological properties, into five categories:

Pc1 (periods 0.2-5 s) may occur in bursts (pearls), or in consecutive groups of pulsations with sharply decreasing frequency.

Pc2 (periods 5-10 s) do not seem to be physically related to Pc1 or Pc3.

Pc3 (periods 10-45 s) occur over a wide range of latitudes.

Pc4 (periods 45-150 s) are also known as Pc II or Pc^0.

Pc5 (periods 150-600 s) are sometimes called giant micropulsations.

Q Qe

The Q index is a 15 minute index of geomagnetic activity intended for high latitude (auroral) stations. Q is the largest deviation scaled from the undisturbed level for the two horizontal components. This differs from the K index, which is scaled from the largest relative difference. The range of Q is from 0 to 11. The 15 minute periods are centered at HH:00, HH:15, HH:30, and HH:45. The relation between the deviation in gammas and Q is given below.

Q	deviation (gammas)
0	<10
1	10 to 20
2	20 to 40
3	40 to 80
4	80 to 140
5	140 to 240
6	240 to 400
7	400 to 660
8	660 to 1000
9	1000 to 1500
10	1500 to 2200
11	>2200

Qe - Q is an index used to specify the size of the auroral oval. Theoretically, $Q = 2K_p - 0.35$. Qe is an estimate of what the Q index would have to be to account for the observed extent of the auroral oval as seen by DMSP optical or particle sensors. Qe ranges from about -4 to +12.

quiet day curve (QDC)

Especially in connection with the components of the geomagnetic field (see geomagnetic elements), the trace expected in the absence of activity. The K index and Q index are measured from deviations relative to the QDC.

rad

A unit of absorbed radiation dose, equal to the radiation that imparts to the absorbing material 100 ergs of energy per gram.

radar aurora

Radar returns reflected by ionization caused by particle precipitation in or near the auroral oval. The strength of radar auroral returns is aspect dependent.

radiation belts

The region of the magnetosphere roughly 1.2 to 6 earth radii above the equator in which charged particles (electrons with energies ~0.1 to 500 MeV, and trace quantities of heavier ions) are trapped by the geomagnetic field. The outer boundary is near the magnetopause on the sunward side (10 earth radii under normal quiet conditions) and at about 6 earth radii on the nightside. The nightside boundary is ill-defined

because of the phenomenon of quasi-trapping, whereby particles that are trapped in the outer part of the belt on the sunward side, when carried by their drift motions to the nightside, can become temporarily untrapped.

radio burst

A sudden, transient enhancement of solar radio emission over background levels. Usually associated with an active region or flare.

radio emission

Emission of the sun in radio wavelengths from centimeters to decameters, under both quiet and disturbed conditions. Some patterns, known variously as noise storms, bursts, and sweeps, have been named as described below. These types of emissions are subjectively rated on an importance scale of 1 to 3, 3 representing the most intense.

Type I. A noise storm composed of many short, narrowband bursts in the metric range (300 - 50 MHz) of extremely variable intensity. The storm may last from several hours to several days.

Type II. Narrowband emission that begins in the meter range (300 MHz) and sweeps slowly (tens of minutes) toward decameter wavelengths (10 MHz). Type II emissions occur in loose association with major flares and are indicative of a shock wave moving through the solar atmosphere.

Type III. Narrowband bursts that sweep rapidly (seconds) from decimeter to decameter wavelengths (500 - 0.5 MHz). They often occur in groups and are an occasional feature of complex solar active regions.

Type IV. A smooth continuum of broadband bursts primarily in the meter range (300 - 30 MHz). These bursts are associated with major flare events beginning 10 to 20 minutes after the flare maximum, and can last for hours.

RAM

Random access memory.

Rayleigh-Taylor instability

A fluted or ripple-like instability that can develop on a surface and propagate along it. This instability is often invoked to explain phenomena in the ionosphere and magnetosphere.

reconnection

A process, important in systems of magnetized plasmas, by which differently directed field lines link up, allowing topological changes of the magnetic field to occur, determining patterns of plasma flow, and resulting in conversion of magnetic energy to kinetic and thermal energy of the plasma. Reconnection is invoked to explain the acceleration of the plasmas that are observed in solar flares, magnetic substorms, and elsewhere in the solar system.

refraction (ionospheric)

Ionospheric radio wave refraction is a change in the direction of propagation due to passing obliquely through the interface between two areas of differing free electron density (and thus index of refraction). Since the amount of bending also depends on the frequency of the radio wave, the ionosphere is said to be dispersive. For a given angle of incidence, higher frequencies are bent less than lower frequencies.

refraction (tropospheric)

Tropospheric radio wave refraction is a change in the direction of propagation due to passing obliquely through the interface between two areas of differing pressure, temperature, or moisture content. Since the amount of bending does not depend (to any significant degree) on the frequency of the radio wave, the troposphere is said to be non-dispersive. Below the VHF band, the index of refraction in air is very close to that in a vacuum (i = 1), and we can ignore tropospheric refraction compared to ionospheric refraction. However, ionospheric refraction decreases with increasing frequency. In the VHF band, both are comparable in magnitude; while in the UHF and super high frequency (SHF) bands, tropospheric refraction dominates.

relativistic

Particles with sufficient energy to move at speeds which are an appreciable fraction (10 percent or more) of the speed of light.

REM

Roentgen equivalent man. The dose of ionizing radiation equal to the absorbed dose in rads multiplied by the total quality factor for the radiation concerned.

RFI

Radio frequency interference. For example, interference caused by a solar radio burst.

rigidity

A measure of how easily a particle is deflected by a magnetic field. It is the momentum per unit charge. In gaussian units it is pc/Ze. If a particle of momentum p is directed towards a uniform magnetic field, its equation of motion in the plane perpendicular to the magnetic field will be:

$$\frac{d(p)}{dt} = \frac{Ze}{c(V \times B)} \qquad \text{or} \qquad \frac{mv^2}{r} = \frac{Zev}{cB}$$

this is simply r = (pc/(Ze)) * (1/B), that is, the penetration of the particle into the magnetic field is inversely proportional to the strength of the magnetic field and directly proportional to the momentum per unit charge in the parentheses. That expression (pc/(Ze)) is termed the rigidity of the particle. Using the normal relativistic relations between kinetic energy and total energy and momentum the rigidity can be expressed as

$$\text{rigidity} = \frac{A}{(Ze)\sqrt{(T^2 + 2m_0c^2\,T)}}$$

where T is the kinetic energy of the particle per unit mass, and m_0c^2 is the unit mass rest energy. In general, the rigidity is a useful concept when the major force on a particle is the magnetic field because the equation of motion can be expressed as the time rate of change of the rigidity being the cross-product of the unit vector in the direction of the rigidity and the magnetic field .

The integral proton spectrum of a flare can be expressed as an exponential function of rigidity rather than a power function of energy. That is

$$\Phi(>P) = \Phi_0 \exp\frac{-P}{P_0}$$

where Φ_0 is the total proton fluence for the event (protons per cm^2) and P is the rigidity. P_0 is a characteristic of each individual flare. A typical number for P_0 might be 100 MV.

ring current

A westward electric current that flows above the geomagnetic equator; it is located in the outer Van Allen radiation belt. The ring current is produced by the drift (eastward for electrons and westward for protons) of trapped charged particles. This drift is superimposed on the spiraling motion of particles as they bounce between conjugate points. The ring current is greatly enhanced during geomagnetic storms by the injection of hot plasma from the magnetotail.

riometer

Relative ionospheric opacity meter. A monitor used to record the strength of high frequency cosmic radio noise received at ground level. A decrease in power represents an increase in ionospheric opacity or absorption. Riometers can detect short wave fade (SWF), auroral zone absorption (AZA), and polar cap absorption (PCA) events. (Also see D region.)

RSTN

Radio Solar Telescope Network. The system of standardized, computer-controlled solar radio telescopes operated by the USAF. Standard frequencies monitored are 15400, 8800, 4995, 2695, 1415, 410, and 245 MHz. Additionally, a sweep frequency interferometric radiometer (SFIR) monitors the 25 to 75 MHz band.

SCATHA

Spacecraft charging at high altitudes.

scintillation

A rapid, random variation in amplitude and/or phase of an electromagnetic signal (usually on a satellite communication link). Scintillation effects tend to decrease with increasing frequency. Scintillation is caused by abrupt variations in electron density anywhere along the signal path, and is positively correlated with "Spread F" and (to a lesser degree) with "Sporadic E." Like Spread F and Sporadic E, it shows a clear minimum in frequency of occurrence and intensity at mid-latitudes. At low latitudes, scintillation shows its greatest range in intensity, with both the quietest and most severe of conditions being observed. At high latitudes, its frequency and intensity are greatest in the auroral oval, although it is also strong over the polar caps.

SE Asian anomaly

See South Atlantic anomaly.

SEMCAP

Specification and Electromagnetic Compatibility Program.

SEON

Solar Electro-optical Observing Network. An acronym for the combined SOON-RSTN observatory network operated by the Air Force.

SESC

Space Environment Services Center. The forecast center operated by the National Oceanic and Atmospheric Administration (NOAA) at Boulder, Colorado. It is the civilian counterpart of the Space Environmental Support Branch, Air Force Global Weather Central, Offutt AFB, Nebraska.

SESS

Space Environmental Support System. A blanket acronym referring to all components, both military and civilian, of the real-time solar geophysical monitoring and forecasting network.

SEU

Single event upset.

SFIR

Sweep frequency interferometric radiometer. An instrument used to monitor solar radio emissions in the 25 to 75 MHz band. Radio bursts in this band are produced by particle streams moving through the solar corona. Type II and IV bursts are caused by proton streams, Type III and V bursts by electron streams, and Type I bursts by trapped electrons.

SFU

Solar flux unit. A measure of emitted radio energy flux equal to 10^{-22} watts/meter^2 hertz. It is the standard unit for reporting solar radio background flux and bursts, notably $F_{10.7}$.

shock

A discontinuity in pressure, density, and particle velocity, propagating through a compressible fluid or plasma.

short wave fade (SWF)

An abrupt decrease of radio signal strength observed at frequencies above a few megahertz over long transmission paths in the sunlit hemisphere. An SWF is due to increased absorption in the lower ionosphere as a result of increased ionization. The increased ionization is caused by enhanced x-ray radiation accompanying many solar flares. An SWF is one type of sudden ionospheric disturbance (SID). (Also see D region.)

smoothed sunspot number

An average of 13 monthly RI numbers, centered on the month of concern. The 1st and 13th months are given a weight of 0.5.

solar constant

The total radiant energy received vertically from the sun, per square centimeter per unit of time, at a position just outside the earth's atmosphere when the earth is at its average distance from the sun. Radiation at all wavelengths from all parts of the solar disk is included. The solar constant's value is approximately 2.00 cal/cm^2 min = 1.37 kW/m^2 = 1.37 x 10^6 erg/cm^{2}s, and varies by 0.1%.

solar coordinates

Specifications for a location on the solar surface. The location of a specific feature on the sun (for example, a sunspot) is complicated by the fact that there is a tilt of 7° 15' between the ecliptic plane and the solar equatorial plane, as well as a true wobble of the solar rotational axis. (Only twice a year are the solar north pole and the celestial north pole in apparent alignment.) Consequently, to specify a location on the solar surface, three coordinates (p, B_0, L_0) are used to define a grid. Daily values for the coordinates at UT (universal time) are listed in the Astronomical Almanac, published annually by the U.S. Naval Observatory. The terms used to refer to the coordinates are defined as follows:

P-Angle (or P): The position angle between the geocentric north pole and the solar rotational north pole measured eastward from geocentric north. The range in P is ±26.31°.

B_0: Heliographic latitude of the central point of the apparent solar disk; also called the B-angle. The range of B_0 is ±7.23°, correcting for the tilt of the ecliptic with respect to the solar equatorial plane. Example: If (P,B) = (-26.21°, -6.54°), the heliographic latitude of the central point on the solar disk is -6.54° (the north rotational pole is not visible) and the angle between a vertical to the ecliptic and the projection of the north solar rotational pole onto the disk is 26.21° to the west.

L_0: Heliographic longitude of the central point of the apparent solar disk. The longitude value is determined with reference to a system of fixed longitudes rotating on the sun at a rate of 13.2°/day (the mean rate of rotation observed from central meridian transits of sunspots). The standard meridian on the sun is defined to be the meridian that passed through the ascending node of the sun's equator on 1 January 1854 at 1200 UT and is calculated for the present day by assuming a uniform sidereal period of rotation of 25.38 days.

Once P, B_0, and L_0 are known, the latitude, central meridian distance, and longitude of a specific solar feature can be determined as follows:

Latitude. The angular distance from the solar equator, measured north or south along the meridian.

Central meridian distance (CMD). The angular distance in solar longitude measured from the central meridian. This position is relative to the view from earth and will change as the sun rotates; therefore, this coordinate should not be confused with heliographic positions that are fixed with respect to the solar surface.

Longitude. The angular distance from a standard meridian (0° heliographic longitude), measured from east to west (0° to 360°) along the sun's equator. It is computed by combining CMD with the longitude of the central meridian at the time of the observation, interpolating between ephemeris values (for 0000 UT) by using the synodic rate of solar rotation (27.2753 days, 13.2° per day).

solar cosmic rays

High energy particulate radiation emitted by extremely energetic solar flares. Preferred nomenclature is SPE. (Also see cosmic rays.)

solar cycle

The approximately 11-year quasi-periodic variation in frequency or number of solar active events. Examples of features or indices that show such variations are the sunspot number, plages, flares, and the 2800-MHz radio emission. The polarity pattern of the magnetic field shows an approximate 22-year variation.

solar flare

See flare.

solar maximum

The month(s) during the solar cycle when the 12-month mean of monthly average sunspot numbers reaches a maximum. The most recent solar maximum occurred in December 1979.

solar minimum

The month(s) during the solar cycle when the 12-month mean of monthly average sunspot numbers reaches a minimum. The most recent solar minimum occurred in June 1976.

solar rotation rate

(1) Synodic: $13.39°-2.7° \sin^2 \Phi$ per day (Φ = solar latitude).

(2) Sidereal: $14.38°-2.7° \sin^2 \Phi$ per day. The difference between sidereal and synodic rates is the earth orbital motion of 0.985° per day.

solar sector boundary (SSB)

Boundary between large scale unipolar magnetic regions on the sun's surface. SSBs are the origin of sector boundaries in the interplanetary magnetic field (IMF), which separates regions of opposite polarity (either toward or away from the sun). A sector boundary in the IMF is normally narrow, being convected past the earth in minutes or hours, compared to days to a week or so required for passage of the sector itself.

solar wind

An extension of the sun's corona into interplanetary space. The solar wind is a low density (about 8 ions/cm^3 and 8 electrons/cm^3 at 1 AU) plasma expanding at near sonic speed (300 - 900 km/s) outward from the sun. These parameters vary considerably with time, but are consistent with gross charge quasi-neutrality. The ionic constituents are chiefly protons with a small (~4%) percentage of alpha particles. The solar wind carries wave and density structures, and an embedded interplanetary magnetic field (IMF).

SOON

Solar Observing Optical Network. A system of standardized, computer-controlled solar optical telescopes operated by the Air Force. The telescopes are capable of objective white light and H alpha observations. Spectrographic observations can also be made, to include obtaining magnetograms of individual active regions.

South Atlantic anomaly

Like the SE Asian anomaly, a region of highly variable F region electron density. The earth's actual magnetic field is best approximated by a dipole (bar magnet) field offset from the earth's center by about 450 kilometers toward the Pacific Ocean. The geomagnetic field is symmetric with respect to this eccentric dipole, so the altitude at which one encounters any given value of magnetic field strength will be a minimum over the Atlantic and a maximum over the Pacific. The result is that trapped particles in the plasmasphere can more easily be precipitated in these locations, increasing the degree of ionization at F region altitudes. (Also see corrected geomagnetic coordinates.)

spacecraft charging

A term which encompasses all of the charging effects on a spacecraft due to the environment in space. Occasionally this term is used in a more limited sense of surface charging.

SPE

Solar particle event.

SPO

System Program Office.

sporadic E (Es)

Transient, localized patches of relatively high electron density occurring at E layer altitudes. Sporadic E is independent of the regular solar (ultraviolet) produced E layer. At high latitudes, Es is related to the auroral electrojet, is most common at night, and shows little seasonal dependence. At midlatitudes, Es is related to wind shear and meteor ionization, and is most common in the summer daytime. At low latitudes, Es is related to the equatorial electrojet, is most common during the daytime, and shows little seasonal dependence.

spray

Chromospheric material ejected from a solar flare with sufficient velocity that much of it can escape the sun. (Also see surge.)

spread F

Small scale inhomogeneities in the free electron density gradient at F layer altitudes. Two types of spread F are identified and named after their appearance on vertical incidence ionograms: frequency and range spread F. Spread F is most common at high and low latitudes, with a clear minimum in frequency of occurrence at the middle latitudes. It is primarly a nighttime phenomenon.

SSN

Solar sunspot number. The Wolf, or relative, daily sunspot number (R) is an index for the degree of spottiness on the sun. It is based on the number of sunspot groups (g) and individual spots (s): $R = k(10g + s)$. The k is a subjective correction factor to allow for the difference in observatory equipment, observing conditions, and observer tendencies. Sunspot number is the most frequently used index for the general level of solar activity.

SSNe

Effective solar sunspot number. A daily index used by Air Force Global Weather Central as a measure of the average state of the ionosphere with respect to ionospheric climatology. It is unrelated to the number of sunspots visible on the sun. The larger the effective SSN, the greater the degree of overall ionization in the ionosphere.

STS

Space Transportation System.

subequatorial ridges

See Appleton anomaly.

substorm

A full cycle in auroral activity, from quiet to highly active to quiet conditions. During a substorm, auroras are at their brightest and the auroral oval widens and extends equatorward. A geomagnetic storm can be thought of as a sequence of one or more substorms typically 1-3 hours in duration and separated by 2-3 hours. Each substorm corresponds to an injection of charged particles from the magnetotail into the auroral oval and the ring current. The initial substorm is caused by the arrival of a shock front in the solar wind (which may be the result of a solar sector boundary, high speed stream from a coronal hole, or a mass ejection from a flare or disappearing filament). Subsequent substorms are produced by irregularities in the post-shock plasma. (Also see geomagnetic storm.)

sudden cosmic noise absorption (SCNA)

A sudden decrease in the signal strength of cosmic radio noise. SCNA is caused by increased D region ionization due to enhanced x-ray radiation from a solar flare. SCNA is one type of sudden ionospheric disturbance.

sudden enhancement of atmospherics (SEA)

A sudden increase in the intensity of low frequency (LF) radio noise. SEAs are caused by improved D region LF reflectivity, which accompanies enhanced ionization produced by solar flare x-rays. As a result of this improved reflectivity, atmospheric signals (atmospherics) generated by distant thunderstorms arrive with amplitudes greater than normal. SEA is one type of sudden ionospheric disturbance.

sudden enhancement of signal (SES)

A sudden increase in the strength of very low frequency (VLF) signals from a distant radio transmitter. Signal enhancements of this type are due to the same phenomena as the sudden enhancement of atmospherics (SEA).

sudden frequency deviation (SFD)

A small, abrupt change in the frequency of a high frequency (HF) radio wave received from a distant transmitter. SFDs are caused by increases in the F1 and E regions ionization resulting from enhanced solar flare x-ray radiation. As the amount of ionization in the F1 and E regions increases, the exact altitude from which a particular radio wave is refracted lowers. The changing altitude causes a Doppler shift in the frequency of the received signal. SFDs are one type of sudden ionospheric disturbance, and the only one not related to increased D region ionization.

sudden ionospheric disturbance (SID)

A large, sudden increase in the amount of ionization in the ionosphere (especially the D region) over the entire sunlit hemisphere of the earth. SIDs are caused by enhanced ultraviolet and/or x-ray radiation emitted during a solar flare. SIDs include a number of ionospheric effects: sudden cosmic noise absorption (SCNA), sudden enhancement of atmospherics (SEA), sudden enhancement of signal (SES), sudden frequency deviation (SFD), sudden phase advance (SPA), and short wave fade (SWF).

sudden phase advance (SPA)

An abrupt shift in the phase of a low frequency radio signal received from a distant transmitter. Solar flare x-ray radiation causes increased D region ionization, which in turn causes an effective lowering of ionospheric reflection heights. The resulting change in path length is responsible for a phase shift. SPA is one type of sudden ionospheric disturbance.

sunspot cycle

A quasi-periodic variation in the number of sunspots. The cycle exhibits an average period of 11 years, but may be as short as 7 or as long as 17 years.

sunspots

Relatively dark regions in the solar photosphere. Seen in white light, they appear dark because they are cooler than the surrounding photospheric gases. Sunspots are characterized by strong magnetic fields, which are mainly perpendicular to the solar surface. Sunspots normally occur in magnetically bipolar groups.

surge

A stream of chromospheric gas ejected outward along magnetic field lines, but which eventually returns to the surface. (Also see spray.)

TEC

Total electron content. The total number of free electrons in a unit area column from the ground to a height well above the level of peak ionization. Commonly measured by a Faraday rotation polarimeter. TEC may not be equivalent to the actual column electron content vertically over a station, since the polarimeter measures along a slant path to a geostationary satellite, and responds only to the electron density below about 1000 kilometers.

ultraviolet (UV)

That part of the electromagnetic spectrum between 50 and 4000 angstroms.

umbra

The dark core in a sunspot. It is the portion of a sunspot where magnetic fields are most intense, causing the temperature to be coolest (about 3900 kelvin) compared to the overall photosphere (6000 kelvin). (Also see penumbra.)

Van Allen radiation belts

Magnetospheric regions of stably trapped charged particles. Near the earth, the geomagnetic field is strong and field lines are closed. As a result, the energy associated with magnetic fields dominates particle kinetic energy, and we find a region of stable particle trapping. Outside the radiation belts, the geomagnetic field is weaker and field lines are more distended or open, and so particle kinetic energy is the controlling factor. The distribution of protons led to a division of the region of stable trapping into two belts. The inner Van Allen belt has a maximum proton density near 5000 kilometers altitude; it is part of the plasmasphere and corotates with the earth. Inner belt protons are mostly high energy (MeV range) and originate from the decay of secondary neutrons created during collisions between cosmic rays and upper atmospheric particles. The outer Van Allen belt has a maximum proton density near 16,000–20,000 kilometers altitude. Outer belt protons are lower energy (about 200 keV to 1 MeV) and come from the solar wind.

vertical height

See ionosonde.

VI ionogram

Vertical incidence ionogram. A plot of critical frequency (or equivalently, electron density) versus delay time (or equivalently, altitude) obtained by a vertical incidence ionosonde.

white light (WL)

Sunlight integrated over the visible portion of the spectrum (4000–7000 angstroms) so that all colors are blended to appear white to the eye. No significant contribution from any one spectral line (or element emitting light) is implied.

white light flare

A major flare in which small parts become visible in white light. This rare continuum emission is caused by energetic particle beams bombarding the lower solar atmosphere. Such flares are usually strong x-ray, radio, and particle emitters.

winter anomaly

F region electron densities in the winter hemisphere middle latitudes (40 to 50 degrees) are enhanced by as much as a factor of four over the summer hemisphere. The phenomenon is strongest near solar maximum, and hardly noticeable near solar minimum. The anomaly is caused by the horizontal transport of free electrons by high altitude winds from where they are produced (by solar radiation) in the summer hemisphere. (Also see Appleton anomaly.)

Wolf number

An historic term for sunspot number. In 1849, R. Wolf of Zurich originated the general procedure for computing the sunspot number. The record of sunspot numbers that he began has continued to this day.

X event

See flare. A major solar flare, as defined by an x-ray burst with peak emission in excess of 1.0×10^{-1} ergs/cm^2/sec. For example, X3.5 means the peak emission was 3.5×10^{-1} ergs/cm^2/sec.

x-ray flare class

Rank of a flare based on its x-ray energy output. Flares are classified by the order of magnitude of the peak burst intensity (I) measured at the earth in the 1 to 8 angstrom band as follows:

	Peak Flux, 1 to 8 angstrom band	
Class	(in W/m^2)	(in ergs/cm^{2}s)
B	$I < 10^{-6}$	$I < 10^{-3}$
C	$10^{-6} \leq I < 10^{-5}$	$10^{-3} \leq I < 10^{-2}$
M	$10^{-5} \leq I < 10^{-4}$	$10^{-2} \leq I < 10^{-1}$
X	$I \geq 10^{-4}$	$I \geq 10^{-1}$

x-ray flare termination

The criteria for considering an x-ray event to be terminated are as follows:

Class X events: Terminate when event decays to less than 5×10^{-5} W/m^2 and remains stable (see below) for at least 4 continuous minutes, or decays to less than M1 regardless of stability.

Class M events: Terminate when event decays to less than C5 (5×10^{-6} W/m^2) or event reaches 1/2 peak and remains stable for at least 4 minutes.

Class C events: Terminate when event decays to 1/2 peak.

(Stable = change of less than 0.1 unit in 4 minutes, when 1-min averages are used.)

Zeeman effect

The name applied to the behavior of certain spectral lines in the presence of a strong magnetic field. Briefly, the lines split into three or more components of characteristic polarization: circular if the local magnetic field is parallel to the line of sight, and linear if the field is perpendicular to the line of sight. The amount of splitting is proportional to the strength of the field.

Appendix

3

Models and Committees

The Space Environment, Anomaly, and Radiation Effects Committee (pronounced sear/ek) is an ad hoc committee of civilian and DoD members designed to:

1. Facilitate the identification of environmentally induced problems on spacecraft,
2. Educate the satellite user community concerning spacecraft environmentally caused anomalies, and
3. Promote the generation of handbooks, specifications, and test procedures for use by the entire satellite community.

Current members are Dr. J. H. Allen, Dr. Peter G. Coakley, Gary Heckman, Dr. Jack Quinn, Dr. Thomas Criswell, Dr. William N. Hall, Dr. Paul R. Higbie, Dr. James I. Vette, Dr. Paul Robinson Jr., Dr. Jason Wilkenfeld, Lt. Col. George Davenport, Lt. Colette de la Barre, N. John Stevens, E. D. Zaffery, and R. Pruett.

A3.1. NASCAP Predictions -- Myron Mandell, S-Cubed, San Diego, CA

NASCAP (NASA Charging Analyzer Program) is a three-dimensional computer code which can be used to study electrostatic charging of spacecraft surfaces. It was developed for NASA and the Air Force by the S-Cubed Division of Maxwell Laboratories.

A3.1.1. Geometrical Modeling

NASCAP is a three-dimensional finite element code. Finite element means that there are several basic geometrical entities which can be combined to represent a geometrically complex object. In the case of NASCAP, elemental volumes are taken to be cubes or specific variants of cubes. Elements comprising the spacecraft can be described in terms of cubes, wedges, cylinders, and other shapes. Close to the surface of a satellite , the resolution is typically on the order of ten centimeters. Typical spacecraft dimensions are on the order of a few meters, and the electrostatic sheath enveloping a charged spacecraft may be non-spherical for several spacecraft radii. In order to keep computer storage requirements and running time reasonably small, an approach of nested rectangular grids was developed for NASCAP in which the inner region has high resolution (say 10 centimeters) and the outer region may be as large as required to include enough space to adequately represent the sheath, as well as to include long booms which may extend from the spacecraft. NASCAP accomplishes this by successive nested grid regions. The spacecraft model must fit within the inner (most detailed) grid boundary, except that thin booms may extend along

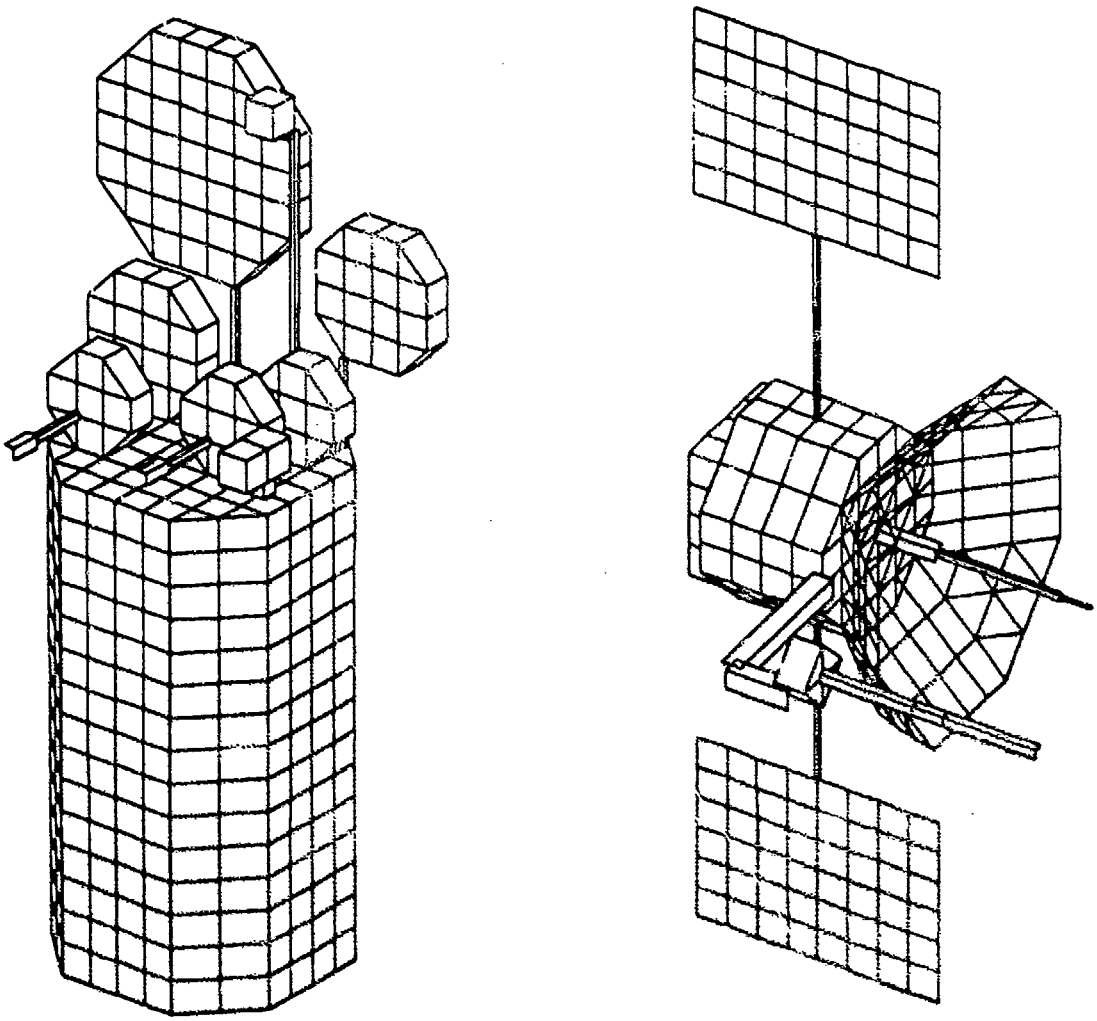

Figure A3-1. NASCAP Satellite Examples

grid lines into the outer grids. Figure A3-1 illustrates the complexity of geometry possible using these techniques. In this Figure, reasonably complex communications satellites are portrayed.

A3.1.2 Material Properties Used in Modeling

NASCAP's geometrical modeling allows a three-dimensional spacecraft representation where the surface materials can vary over the surface of the spacecraft. The material properties will help determine the charge state of each surface area and, therefore, the charge state of the entire satellite. Among the material properties used by NASCAP are secondary emission functions and bulk and surface electrical conductivities.

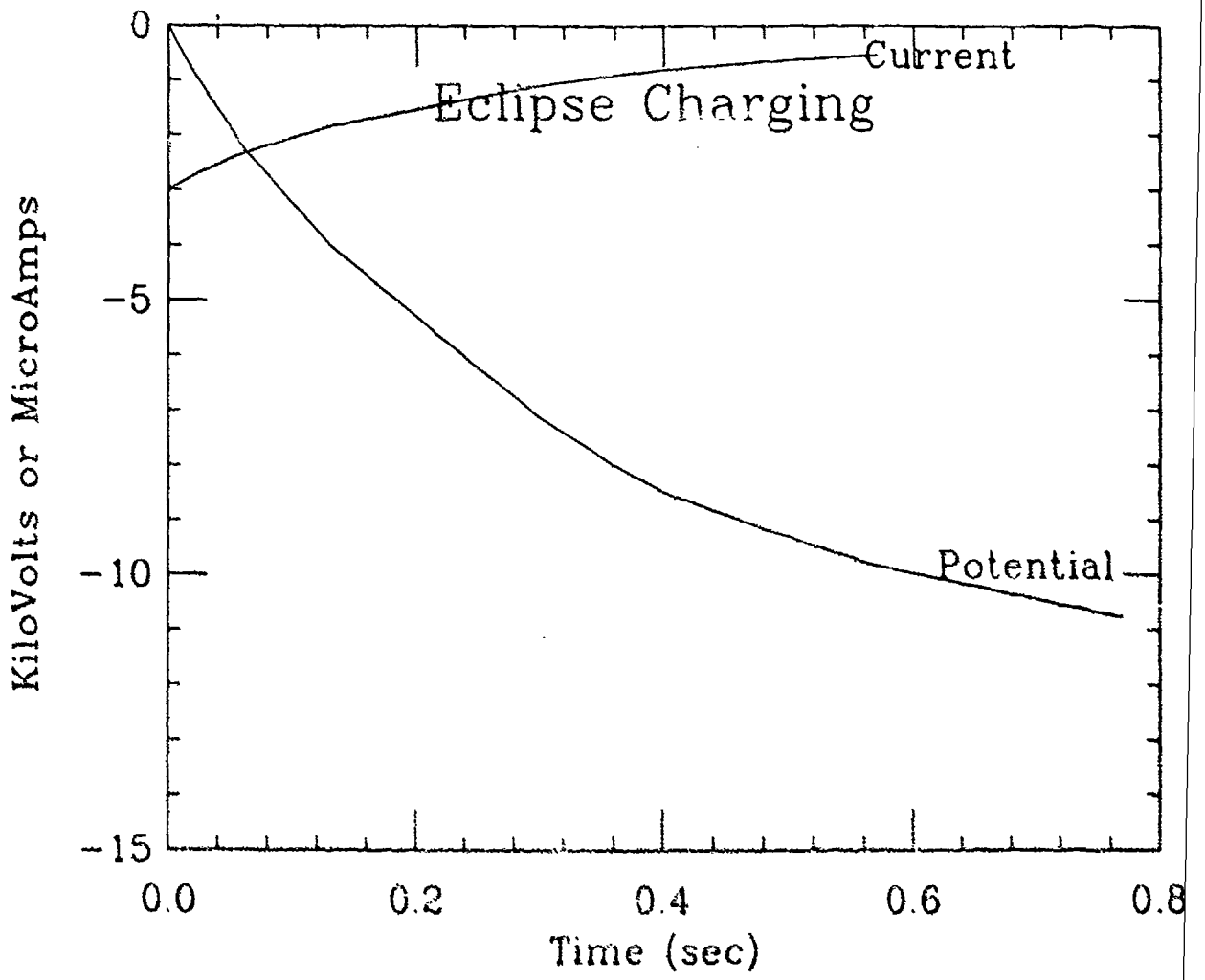

Figure A3-2. Eclipse Charging

A3.1.3 Calculations

NASCAP calculations proceed in a series of timesteps. During each timestep the net current to each surface cell and the resultant voltage is calculated. First, the currents to the surface are calculated based on the potential distribution on and about the spacecraft from the previous timestep. Then, the charge states of the surfaces and surrounding space are calculated from the potentials of the surfaces and the charging currents. Finally, the potentials are updated based on the charge distributions and the boundary conditions (charge state of the spacecraft). All processes are assumed quasi-static during a timestep, i.e., plasma wave effects are ignored. The user may perform a simulation with short timesteps (milliseconds to about a second) to obtain accurate charging dynamics, or with long timesteps (a second to a minute) to achieve steady state in a minimum number of timesteps.

Calculations may be done for Maxwellian, double Maxwellian, or directly input data representing the space plasma environment, or for laboratory environments consisting of electron and ion beams. Normally, the high energy penetrating electrons are not represented in NASCAP, which has no details on the interior structure of the spacecraft. Internal charging is usually treated outside of NASCAP.

NASCAP predictions of a spacecraft (Figure A3-3) in eclipse suddenly encountering a magnetospheric substorm show absolute potentials of about ten kilovolts, developing on the surface of the satellite in about one second. Figure A3-2 shows the spacecraft potential and current as a function of time. Here we have assumed a

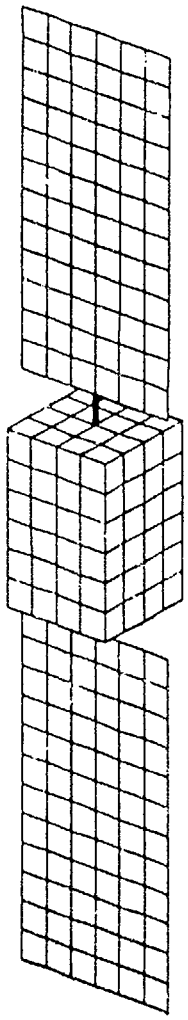

Figure A3-3. Simple Spacecraft Configuration Assumed

Maxwellian environment with electron temperature and density of 15 keV and 0.7 per cm^3, and ion temperature and density of 20 keV and 0.6 per cm^3. If we were to continue this calculation for several minutes, we would see differential charging develop on the spacecraft due to the presence of different surface materials.

During sunlight, in the same environment, a potential difference of a few kilovolts builds up between the sunlit and shaded portions of the spacecraft over a period of several minutes. Figure A3-4 shows the minimum and maximum potentials on the spacecraft surface as a function of time. While this calculation was done for a stationary spacecraft, the same type of charging will also take place on a spinning spacecraft, since such satellites normally have some surfaces which are always shaded. Figure A3-5 shows the potential distributions in space about the spacecraft for the above two calculations.

A3.1.4. NASCAP Conclusion

The NASCAP code is useful for predicting the nature and magnitude of electrostatic charging on a spacecraft due to plasma effects. This information should be used to minimize the likelihood and/or effect of electrostatic discharges. NASCAP can also be used to determine the effect of charging on science instruments attempting to measure the plasma environment. NASCAP will be particularly useful in positioning instruments where there is minimum perturbation of the environment which the instrument is trying to measure.

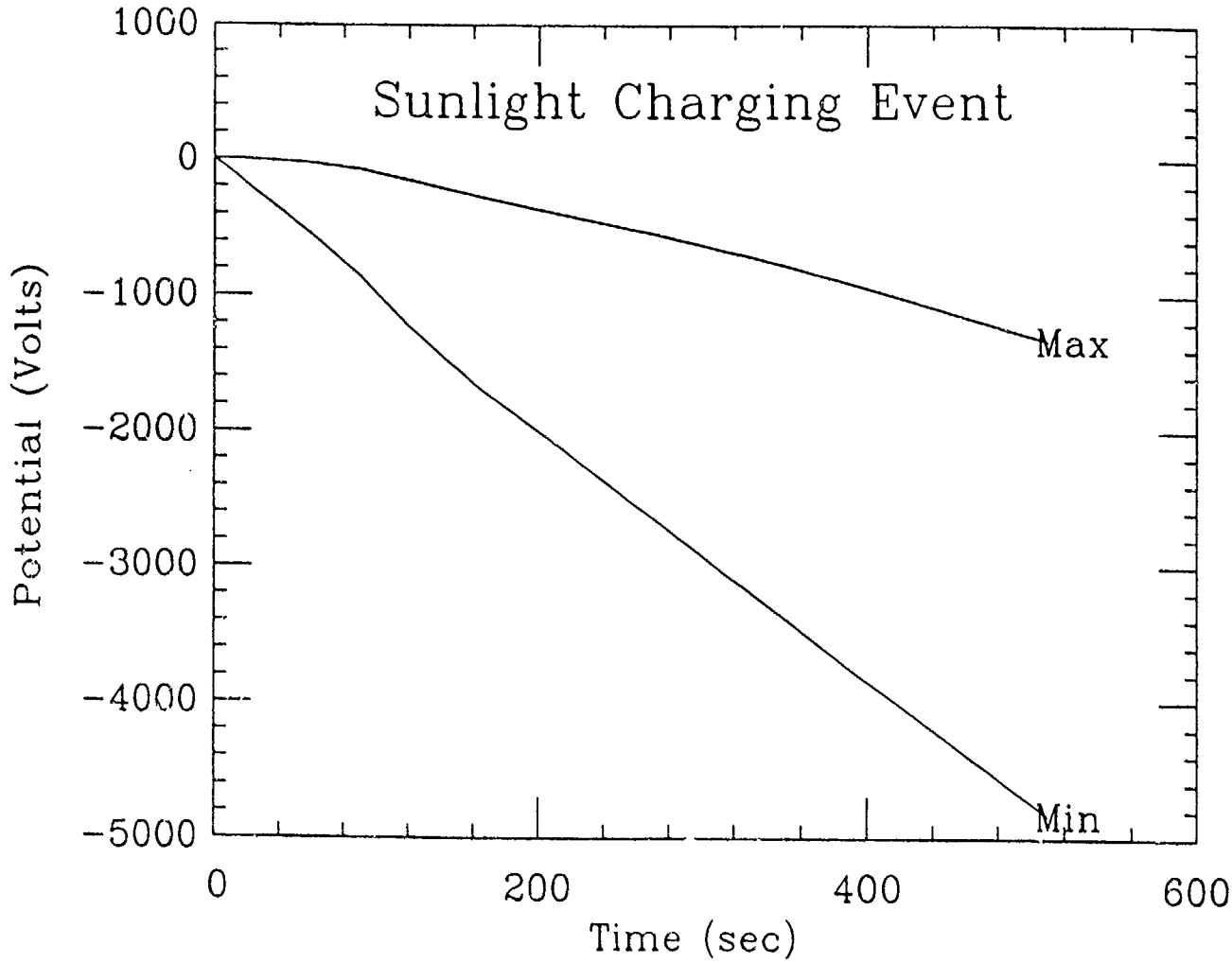

Figure A3-4. Sunlight Charging

NASCAP can be obtained by contacting NASA/Lewis Research Center, or the S-Cubed Division of Maxwell Laboratories.

A3.2. Environmental Models

A3.2.1. NASA

In 1964, a program, jointly sponsored by NASA and the USAF, was begun at The Aerospace Corporation for the express purpose of constructing model environments of geomagnetically trapped particles. This work was under the direction of Dr. James I. Vette. The first model environment was published in 1966 (Vette, 1966), *Volume I, Inner Zone Protons and Electrons*. This initial model covered protons in the energy range 5 MeV to 300 MeV, divided into four energy bands, and electrons with energies ranging from 0.3 MeV to 7.0 MeV. These maps were labeled AP1, AP2, AP3, and AP4 for protons and AE1 for electrons. The letter "A" stood for aerospace, "P" for protons and "e" for electrons. This nomenclature has continued over the years even though the work was transferred to NASA's Goddard Space Flight Center around 1967. Subsequent models and/or updates of models were

published under the NASA SP-3024 format up through Volume VII, dated 1971. Since that time, the models have been published under the cover of the National Space Science Data Center (NSSDC), but sequentially numbered up through current models AP8 and AE8.

A3.2.2. AP8

The proton model AP8, *Trapped Proton Environment for Solar Maximum and Solar Minimum*, is, and has been, the scientific community accepted proton model since it was first published in December 1976, as NSSDC 76-06. The purpose of this document is to provide a new computer-accessible model of the stably trapped proton flux with energies between 0.1 and 400 MeV.

The need for this new model arose from two main factors. First, to cover this approximate energy range, it was previously necessary to use the four separate models designated AP1, AP5, AP6, and AP7. Each of these models was derived independently, and this resulted in significant discontinuities in the energy spectra. Second, new data had become available that indicated a need for improvement in the earlier models in certain regions of space. Particularly useful in this effort were the data sets from the OV3-3 and Azur satellites.

Because most of the data used in generating AP8 were acquired around the solar minimum period 1964, this version is designated AP8MIN, epoch 1964. AP8MAX differs from AP8MIN only for altitudes less than about 1000 km and for L values less than 3.0 Earth radii.

A3.2.3. AE4, AE5, AE6, AE7, and AE8

The AE4 model of the outer radiation zone electron environment was published in 1972 (NSSDC 72-06). The inner zone electron model, AE5 was also published in 1972 (NSSDC 72-10). Both of these models were for solar maximum time periods. A model of the trapped electron population for solar minimum, both inner and outer zones, was published in 1974 (NSSDC 74-03).

In May 1976, NASA published the AE6 electron model (NSSDC 76-04). This model was intended to provide estimates of mission fluxes that spacecraft would encounter in the 1980 solar maximum time period and is an inner zone only model. In the previous solar maximum model, AE5, for the epoch 1967, the inner zone electron fluxes contained a substantial contribution from the Starfish event of July 1962. These artificial electron fluxes continuously decayed and then became insignificant after about 1970.

The AE7 electron model (outer zone) grew out of the uncertainty in the electron population above about 2 MeV. Data sets from experimental satellites with energies above 2 MeV were very sketchy and required extrapolations in order to cover the outer zone, at least out to the geosynchronous (L = 6.6) orbit. After many years of debate and data analysis, NASA introduced an "interim" outer zone electron model called AEI-7. The "I" stood for interim; there were two versions, a high and a low, hence, the terms AEI-7Hi and AEI-7Lo. These models, while never documented, were distributed to the user community around 1977 and became the outer zone electron design criteria for many satellite programs between 1977 and 1987, even though NASA model AE8 has been in existence since 1984.

AE8 was introduced to the user community, on an as requested basis, around 1984. It has a maximum and a minimum version to reflect the solar cycle and, more importantly, this model covers the trapped electron environment over the entire magnetosphere, not just the inner or outer zone.

Orbital integration comparisons between AEI-7Hi and AE8 have been made for several representative orbits and the results show that in the 3 to 5 MeV energy range the differences are dramatic. For example, in a half-synchronous (12 hour) orbit and in a low altitude polar orbit, the AEI-7Hi model yields electron fluxes which are higher than the AE8 model by about 2 orders of magnitude at 5 MeV, and about a factor of 8 higher at 3 MeV.

Because neither AEI-7 nor AE8 have been officially documented nor published by NASA, it is easy to understand why there is still some uncertainty among model users as to which electron environment should be used in the design of a spacecraft.

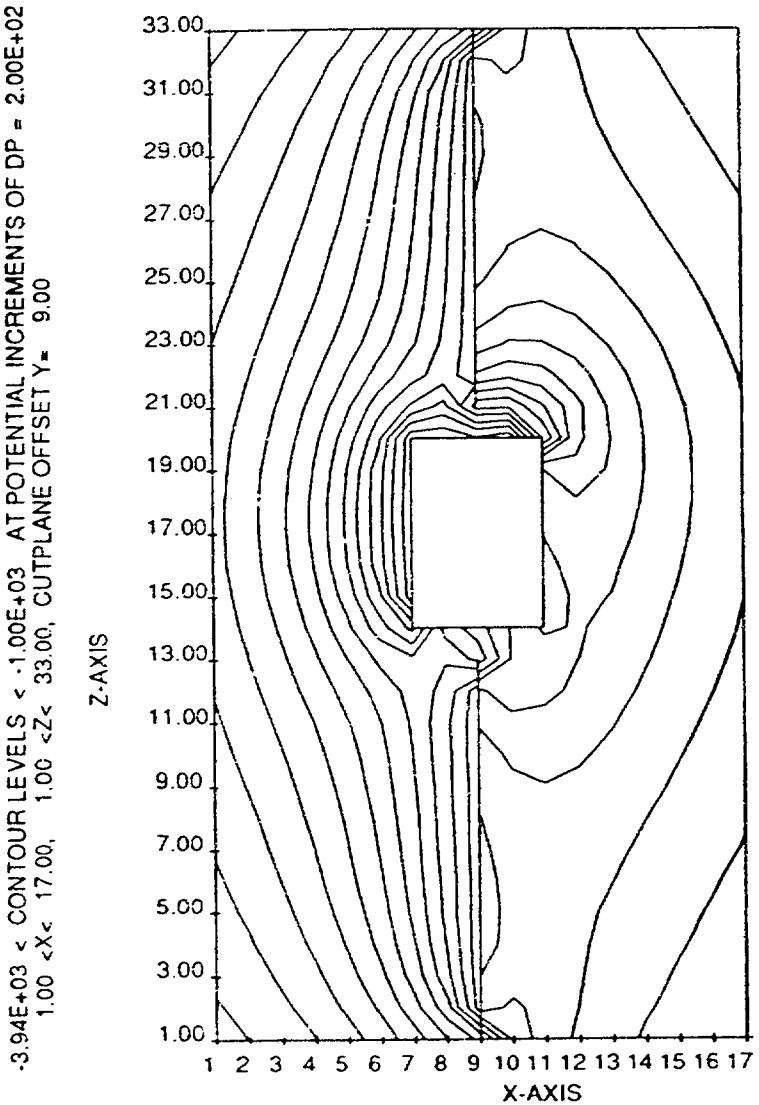

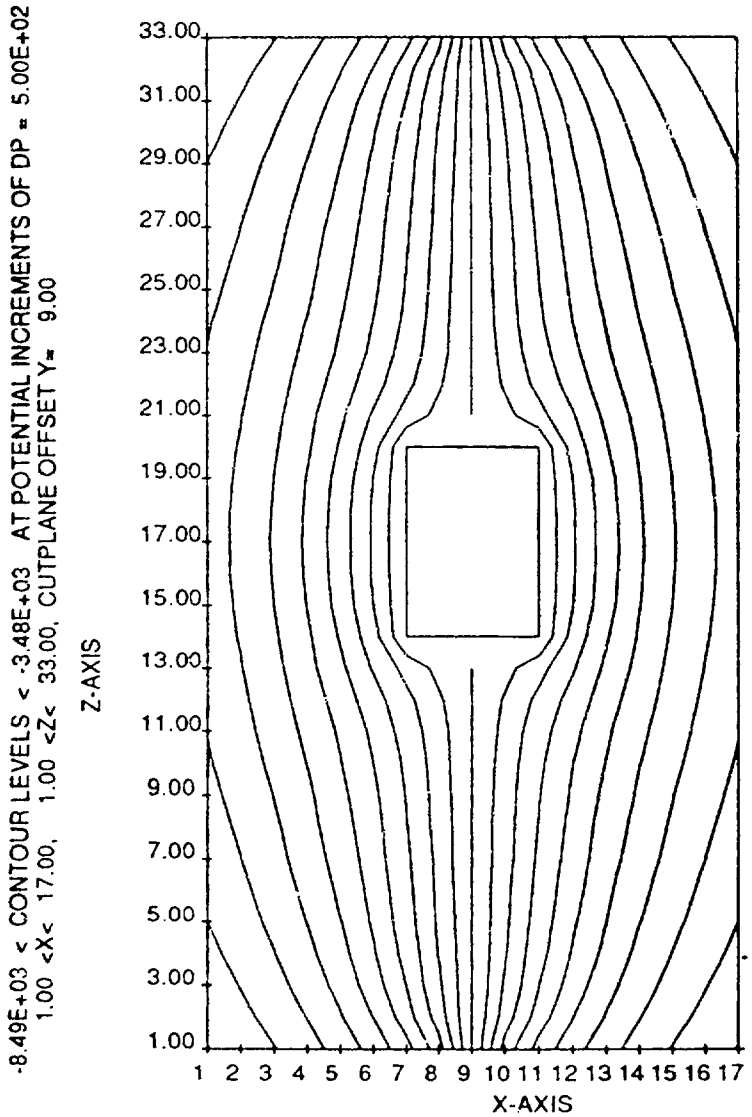

Figure A3-5. Potential Distributions

R.G. Pruett (1980) concluded that the AEI-7 electron environment predicts total doses which are higher than dosimeter measurements by factors of 3 to 6 in the NTS-2 orbit (half-synchronous). Even though the NTS-2 dosimeter data were accumulated over a one year time span, it was not a solar maximum year, and the AEI-7 model is predicated on solar maximum storm time enhancements in the electron environment. Even so, it is suggestive of an environment somewhat less severe than the AEI-7 model would predict.

It is hoped that the long term, wide ranging environmental data sets from the CRRES program will permit the construction of a more accurate electron and proton model environment; not only construction of models which are time and space averaged, but dynamic models which are capable of handling environmental needs over short times (hours to days).

A3.2.4. Orbital Integration Codes

Coincident with the development of model environments, it was recognized that programs to perform orbital integrations of the electron and proton fluxes would also be required. Hence, an Orbital Flux Integration (OFI) code was developed at GSFC. Over the years, a large, sophisticated, and complex OFI system evolved. Three such computer codes were ORB, ORP, and MODEL.

Program ORB is a simple orbit-generation and B-L conversion program used for generating orbit tapes which are used with program ORP to obtain orbital integrated fluxes. ORB is a FORTRAN IV program for IBM machines. It exists in two versions, both sharing a common MAIN program. The two versions, respectively 1 and 2, contain a Brouwer orbit generator and a Lydane orbit generator. The Brouwer generator is more suited to orbits with eccentricities greater than 0.1, while the Lydane generator is better suited to less eccentric orbits.

Program ORP simply takes the ORB output tape of any B-L orbit and combines it with the MODEL program(s) to perform orbital flux integrations.

Program MODEL is a series of data sets containing each of the NASA trapped particle environments such as AP8 and/or AE4, AE8, etc.

Documentation on MODEL and ORP is contained in NSSDC 72-11.

There are other computer programs which perform orbital integrations of either electrons or protons such as the Short Orbital Flux Integration Program (SOFIP). This code is documented in NSSDC 79-01, published in January 1979.

A3.3. AFGWC

The Air Force Global Weather Center and its officers provide environmental support within the DoD. See appropiate military offices.

Sources of real-time databases include:

(1) NOAA -- Space Environmental Laboratory
Space Environmental Services Center
325 Broadway, Boulder, Colorado 80303

(2) Christopher Balch (303) 497-3171 (24-hour and 7-day/week line)

(3) Gary Heckman

(4) AFGWC/WSE

Sources of historical databases include:

(1) AWS -- USAF/ETAC

(2) Joe Allen and Dan Wilkenson
National Geophysical Data Center
325 Broadway, Boulder, Colorado 80303
(303) 497-6215

A3.4. NGDC

Spacecraft Anomaly Data and Software
National Geophysical Data Center
Solar-Terrestrial Physics Division

A database of spacecraft anomalies is maintained at the Solar-Terrestrial Physics Division of the National Geophysical Data Center in Boulder, Colorado. It includes the date, time, location, and other pertinent information about incidents of spacecraft operational irregularities which are suspected to be due to the environment. These events range from minor operational problems which can be easily corrected to permanent spacecraft failures. The database includes spacecraft anomalies in interplanetary space and in near-earth orbit. The majority of the database comes from geostationary spacecraft. About 1600 anomalies have been reported as of June 1987. The database includes data from several nations.

The database is maintained on an IBM-compatible personal computer in a dBase-III-type file. To facilitate access to the information, custom software has been written to perform a full range of functions for managing, displaying, and analyzing the contents. The Spacecraft Anomaly Manager (SAM) software has the added benefit of encouraging operators to report their anomalies in a uniform, ready-to-use format. Satellite operators can use SAM to create a database containing only their anomalies and forward the data to NGDC (address below) on a floppy disk for inclusion in the master archive.

Histograms of local time and seasonal frequency show distinct patterns for spacecraft susceptibility to static charge buildup and subsequent discharge. SAM includes functions to display anomaly collections versus local time and season. Figures A3-6 and A3-7 show these functions for the GOES satellite.

The data and software are currently available on two IBM-compatible floppy disks for the nominal cost of $30 per disk. Contributors of anomaly data may obtain the disks on a data exchange basis. The NDGC contact is Dr. Daniel C. Wilkinson, NOAA Code E/GC2, 325 Broadway, Boulder, CO 80303, (303) 497-6137, (FTS) 320-6137, Telemail: JHALLEN.

S T A T I S T I C S - MONTHLY

Data File: DATA\ANOM4H (June 2, 1987)

Data Filter: BIRD=GOES

Date of First Anomaly: March 29, 1981

Date of Last Anomaly: October 8, 1986

Number of Days in This Interval: 2019

Mean Number of Days Between Anomalies: 17.4

Month	Anomaly Count
Jan	5
Feb	8
Mar	12
Apr	29
May	2
Jun	6
Jul	7
Aug	8
Sep	16
Oct	14
Nov	7
Dec	2
TOTAL	116

SPACECRAFT ANOMALIES by MONTH for BIRD=GOES

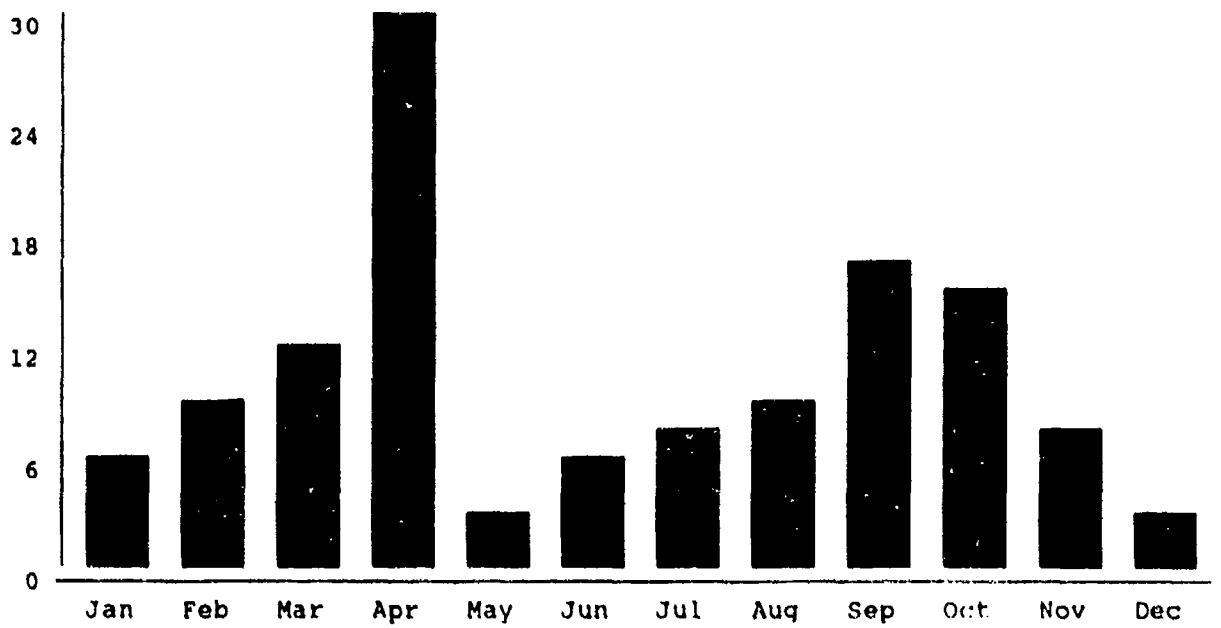

Figure A3-6. Monthly GOES Statistics

S T A T I S T I C S - LOCAL TIME

Data File: DATA\ANOM4H (June 2, 1987)

Data Filter: BIRD=GOES

Date of First Anomaly: March 29, 1981

Date of Last Anomaly: October 8, 1986

Number of Days in This Interval: 2019

Mean Number of Days Between Anomalies: 18.0

Hour (LT)	Anom Count	Hour (LT)	Anom Count
0	11	12	2
1	9	13	2
2	10	14	3
3	16	15	2
4	12	16	1
5	14	17	1
6	6	18	1
7	8	19	2
8	2	20	0
9	2	21	2
10	0	22	1
11	1	23	4
		TOTAL	112

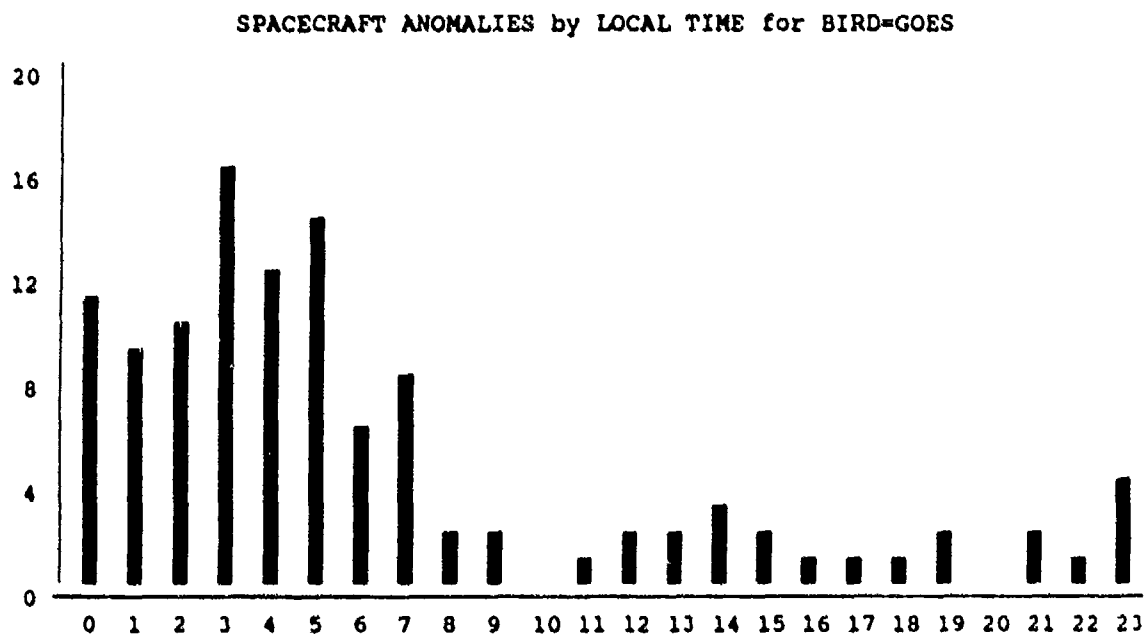

Figure A3-7. Local Time GOES Statistics

Appendix

4

Available Sensors and Detectors

This Appendix lists instrumentation which has been developed to measure the environment or monitor anomalies. It is hoped that future programs will use these or similiar instruments for local, real-time monitoring of their spacecraft and environments. Contributions by instrument developers and investigators to this section are welcomed.

A4.1 CRRES/SPACERAD Experiment Descriptions

M. S. Gussenhoven et al. (1985) describe in some detail the compliment of instruments ready to fly on the CRRES spacecraft. The SPACERAD experiments are shown in Table A4-1.

Table A4-1. SPACERAD Experiments

Experiment	Agency
Microelectronics Characteristics	NRL/ATC/FST/Telenetics
Internal Discharge Monitor	AFWL/AFGL/JPL
Total Dose Dosimeter	AFGL/Panametrics
MOS Dosimeter (Total Dose)	NRL
High Energy Electron Spectrometer	AFGL/Panametrics
Med. Energy Electron Spectrometer	Aerospace
Med. Energy Electron/Proton Spectrometer	AFGL/Aerospace
Low Energy Plasma Analyzer	AFGL/Emmanuel/Mullard
Relativistic Proton Detector	Aerospace
Proton Switches	Aerospace
Proton Telescope	AFGL/Emmanuel/MIT
Ion Composition Spectrometer	Aerospace/Max Planck
Low Energy Ion Comp. Spectrometer	Aerospace/LASL
Heavy Ion Telescope	Aerospace/LASL
Fluxgate Magnetometer	AFGL/Schonstedt
Search Coil Magnetometer	AFGL/U. of Iowa

Thermal Plasma Probe	AFGL/U. C. Berkeley/Analytx/Regis College
Passive Plasma Sounder	AFGL/U. of Iowa

It is highly recommended that those seeking experiments to fly include the CRRES instruments in their evaluations.

A4.2 SOPA Detector (Synchronous Orbit Particle Analyzer)

supplier

Richard Belian, (505) 667-9714, Los Alamos National Laboratory, P. O. Box 1663, Los Alamos, New Mexico 87545.

purpose

The SOPA is a charged particle analyzer for space use. It measures fluxes of energetic electrons, protons, alpha particles, and other ions in a satellite's locale to monitor the space environment.

method of operation

The detector consists of three solid state telescopes "looking" in three different directions relative to the spacecraft spin axis. Each telescope consists of a thick back detector, 3000 micrometers, and a thin, 4 micrometers, front detector with a collimated 12° field of view.

advantages/uniqueness of instrument

The SOPA is designed to monitor electrons from 50 keV up to ~2MeV, protons from 50 keV up to ~50MeV, and alpha particles from 500 keV up to 1.3 MeV. It also monitors carbon, nitrogen, and oxygen ions uniquely and all particles with Z > sulpher and all particles with Z > strontium above certain energies. Finally, the SOPA has a very high resolution E by dE/dx capability which provides a ΔED1-ΔED2 matrix.

results

Particle identification and energy.

weight

<11.5 lb does not include data handling electronics.

size

7" x 12" x 6"

power

4.0 watts

commands

On/off; PHA mode select; separate enable/disable for each of the six solid state detectors; in-flight calibrate.

output data

Particle identification and energy rate channels, pulse height pairs for E by dE/dx.

special features

High time resolution; protons, electrons, and alpha particles for all three telescopes are sampled every 0.640 seconds. High energy resolution (10 electron channels, 12 proton channels, and 5 carbon, nitrogen, and oxygen channels). The ΔED1-ΔED2 matrix is 1024 x 1024 channels covering ~0 to 60MeV on each axis.

A4.3 Plasma Spectrometer

supplier

Samuel J. Bame, (505) 667-5308, (FTS) 843-5308, Los Alamos National Laboratory, P. O. Box 1663, Los Alamos, New Mexico 87545.

purpose

The Plasma Spectrometer is a detector system used to monitor the plasma environment surrounding its host satellite to evaluate the effect of the environment on spacecraft systems and other instrumentation onboard. The measurements can be used to determine the spacecraft charge potential. Electrons and ions are measured from 1 eV to 40 keV over ~94% of the 4π space surrounding the spacecraft.

method of operation

Plasma particles that enter a curved plate electrostatic analyzer are bent into six channel electron multipliers (CEM) by use of decaying voltage waveforms on the analyzer plates. Making use of the spacecraft spin, electrons and ions are detected in six polar angle ranges extending between +70° and −70°, and in 24 azimuthal angle ranges scanned during one spacecraft rotation. Individual energy sweeps are divided into 40 energy intervals.

advantages/uniqueness of instrument

This instrument is designed to measure both electrons and ions with one lightweight package in order to conserve spacecraft resources. Both particle species are detected in a single analyzer by means of a unique voltage switching of the CEM front end bias. The sensor package, including power supplies, but without its logics system (composed of three cards), weighs 7.3 pounds and uses 3.5 watts. A simple modification, which includes the logic cards in the package would increase the weigh by −1.5 pounds.

results

Full time monitoring of the plasma environment of the spacecraft and the spacecraft charge level.

weight

<8.8 pounds

size

Fits within a 6" x 6.5" x 12" volume, including logic cards.

power

4.0 watts, including logics.

commands

On/off; four mode selects; CEM high voltage level selects; four power supply on/offs; calibrate.

output data

The output data count matrices of electrons and ions composed of counts at 40 energy levels from CEMs measured in 24 energy sweeps during a spacecraft revolution. Various combinations such as integration over the six CEMs or telemetering every-other-counts-sample can be used to reduce bit rate requirements.

special features

Ions and electrons from 1 eV to 40 keV are measured using one lightweight package containing a single electrostatic analyzer and one set of channel electron multipliers. Future models are being developed which will allow comprehensive measurements to be made over most of 4π space from a 3-axis stabilized spacecraft.

A4.4 Pulse Monitor

supplier

Dr. Harry C. Koons, (213) 336-6519, The Aerospace Corporation, P. O. Box 92957, Los Angeles, California 90009.

description

The Pulse Analyzer measures the amplitude of electromagnetic emissions in the time domain from 14 ns to 16 ms. The measurements are made on four sensors: (1) a loop antenna around the space vehicle command distribution unit, (2) a wire in a typical space vehicle cable bundle, (3) an external short dipole antenna, and (4) a digital command line to the Pulse Analyzer package. The primary objective is to verify that electrical discharges are occurring on the vehicle. Secondary objectives are to measure the pulse amplitudes and shapes produced by the discharges. The signal

processor may be switched by ground command to any subset of the four sensors. It then steps automatically through the selected sensors, monitoring each in turn for 16 seconds. When a signal exceeds the threshold, its amplitude is sampled 16 times to determine the shape of the pulse. The 16 samples may be spaced logarithmically or linearly. The minimum spacing is 14 ns. There are eight commandable options. The amplitude is measured by a bank of 245 discriminators -- 12 positive and 12 negative. The range of the voltage measurement is 5 mV to 2 V. The signal from each sensor can be attenuated to place it within this range. The voltage threshold, timing sequence, and attentuation can be independently set for each sensor. The instrument is commanded by a 22-bit serial digital command. Only the seven least significant bits of the command are used. One pulse shape measurement is made each 1/2 second. In addition, there are four counters which count the number of times in one second that each of four preselected thresholds are exceeded. There are also three analog housekeeping measurements which monitor power and temperature.

weight

2 kg

size

9" x 10"x 2"

power

10.9 watts

data requirements

256 bits/sec

A4.5 SSPM

supplier

Dr. Harry C. Koons, (213) 336-6519, The Aerospace Corporation, P. O. Box 92957, Los Angeles, California 90009.

description

The Satellite Surface Potential Monitor (SSPM) measures the charging potentials and currents associated with plasma interactions with typical spacecraft materials. The SSPM measures the front surface potential of an isolated sample of material by directly measuring the back surface voltage. Each sample is surrounded by a gold frame which is grounded to chassis. Behind the center of each sample is a vibrating reed electrometer which has been calibrated to give the front surface potential from a measurement of the back surface potential. Current through the sample is measured by a high impedance electrometer. Each sample is approximately 6 inches square.

weight

3.3 kg

size

13" x13" x 2"

power

4 watts

data requirements

96 bits /sec

A4.6 2d Plasma Analyzer

supplier

Dr. J. F. Fennell, (213) 336-7075, The Aerospace Corporation, P. O. Box 92957, Los Angeles, California 90009.

description

The 2d Plasma Analyzer is a toroidal design which measures electrons and ions over 180° to 360° in a plane, depending on the configuration used. The field of view is fan shaped and, on a spinning spacecraft, will provide a three-dimensional measurement of the plasma distributions. The energy range covered is 50 eV to 30 keV and the geometric factor is on the order of 10^3 cm^2 sr keV. The supporting digital electronics and satellite interface (DPU) is in a separate package.

weight

5 kg for sensor, 2.3 kg for DPU

size

26 x 21 x 25 cm, DPU 26 x 21 x 8 cm

power

12 watts

data requirements

2275 bps

A4.7 1D Plasma Analyzer

supplier

Dr. J. F. Fennell, (213) 336-7075, The Aerospace Corporation, P. O. Box 92957, Los Angeles, California 90009.

description

The unidirectional Plasma Analyzer is a self-contained unit which measures electrons and ions in the energy range 50 eV/q to 30 keV/q within a 20° x 20° field of view. The sensor, analog, and digital electronics, plus the satellite interface, are contained in one package.

weight

4.5 kg

size

26 x 21 x 17 cm

power

6.5 W

data requirements

300 bps

A4.8 Internal Discharge Monitor

supplier

Dr. Paul Robinson Jr., (818) 354-3882, Jet Propulsion Laboratory, 4800 Oak Grove Drive, Pasadena, California 91109.

purpose

The pupose of the Internal Discharge Monitor (IDM) is to detect and record discharges in samples that build up a charge due to penetrating radiation. Each sample is enclosed in its own RF-tight minibox so that the instrument does not detect transients other than those from the sample. There is a thin cover which allows most high energy electrons to penetrate, but excludes low energy particles.

method of operation

A nanosecond response time event detector registers which sample in the sample tray of 16 samples discharged. Results are telemetered down at a very slow rate. IDM was originally designed to fly on CRRES, which is well instrumented to allow correlation of discharges with the environment.

advantages/uniqueness of instrument

This instrument does not record very many false events. This is due in part to the careful isolation of each sample. Samples should be chosen for the mission. For example, typical materials from the spacecraft itself could be flown along with well calibrated materials from previous flights.

results

Results are discharges for each sample as a function of time. The threshold trigger can be crudely set.

weight

38 pounds for 16 samples

size

12.5" x 10.875" x 9.675"

power

10 watts

data requirements

2 bps; commands: on/off, attenuate each channel, calibrate; output data: sample which discharged, S/C clock.

special features

Future models will include a high speed digitizer to capture pulse height and shape information.

A4.9 FMDS: An Automatic Plasma-Contactor System for Spacecraft Potential Control

supplier

Ben Shuman at the Air Force Geophysics Laboratory, (617) 377-3991, or Ron Robson at Hughes Research Laboratories, (213) 317-5391.

summary

The Flight Model Discharge System (FMDS) is a unique spacecraft-charging-control system which automatically monitors environmental parameters that indicate the development of a charging hazard and activates the SPACECLAMP plasma source to protect the spacecraft in the event a hazard is detected. FMDS is intended for service on geosynchronous-Earth-orbit (GEO) spacecraft.

introduction

As described in Chapter 7, it has been demonstrated that the operation of a small onboard plasma source, called a plasma contactor, can prevent spacecraft charging, thereby avoiding ESD hazards and affording new potential-control capability to scientific spacecraft. To employ a plasma contactor in practice, however, requires either that the plasma contactor be operated continuously for the life of the spacecraft, or that some form of electronic intelligence be added to enable the system to determine when the contactor should be activated. The former (continuous-operation) approach requires both unnecessarily massive tankage of the plasma contactor's working gas and an unnecessarily long plasma-contactor lifetime. The latter (intelligent-system) approach offers substantial advantages not only of reduced tankage and operating-lifetime requirements, but also of operational flexibility and autonomy. In this Appendix, we briefly describe the design and operating characteristics of the intelligent spacecraft-charging control system being built at Hughes Research Laboratory (Contract No. F19628-83-C 0143). The system is called the Flight Model Discharge System (FMDS).

Figure A4-1 shows a block diagram of the FMDS, and Figure A4-2 shows its physical layout. The system consists of a Hughes SPACECLAMP plasma contactor, which provides: the surface- and frame-neutralizing flow of low-energy plasma; a number of sensors, which measure environmental properties; and a microprocessor-based controller, which interprets the sensor data to identify the presence of a charging hazard and operates the plasma contactor through its associated power supplies and gas-feed system. This idea was described in Chapter 7; here we describe the sensors, controller, and operation of the FMDS.

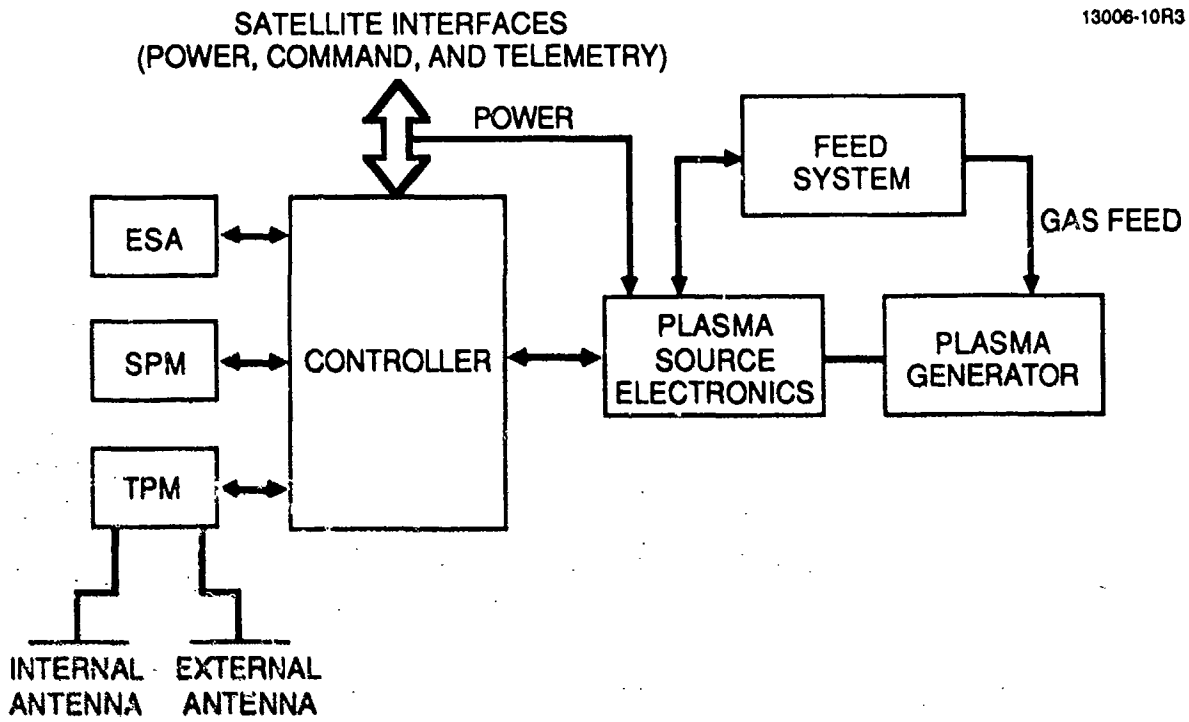

Figure A4-1. SPACECLAMP Block Diagram

A4.9.1 FMDS Environmental Sensors

The sensors carried on FMDS are similar (with the exception of the transient pulse monitor (TPM), which is a new, novel design) to proven instruments that were carried on the SCATHA (P78-1) spacecraft, but they have less resolution and greater simplicity. They include electrostatic ion and electron energy analyzers (iESA and eESA, respectively), two surface potential monitors SPMs, and a TPM. The functions of these instruments are listed in Table A4-2.

In a stereotypical charging event, the sequence of events might be as follows: (1) a magnetic substorm develops, with the attendant injection of high-energy electrons into the locale of the spacecraft; (2) surface dielectrics charge; (3) the spacecraft frame potential goes negative; and, (4) arcing begins on the spacecraft surface. Referring to Table A4-2, it is clear that there is a one-to-one correspondence between this chain of events and the capabilities of the instruments present in the FMDS: each instrument is capable of detecting events corresponding to a particular phase of the development of the charging event. The eESA detects the change in the electron-energy spectrum corresponding to the hot-electron injection that identifies the beginning of the charging hazard. The SPMs, which measure the potential of isolated dielectrics relative to frame potential, detect differential charging. The iESA can detect frame charging because no ions will be

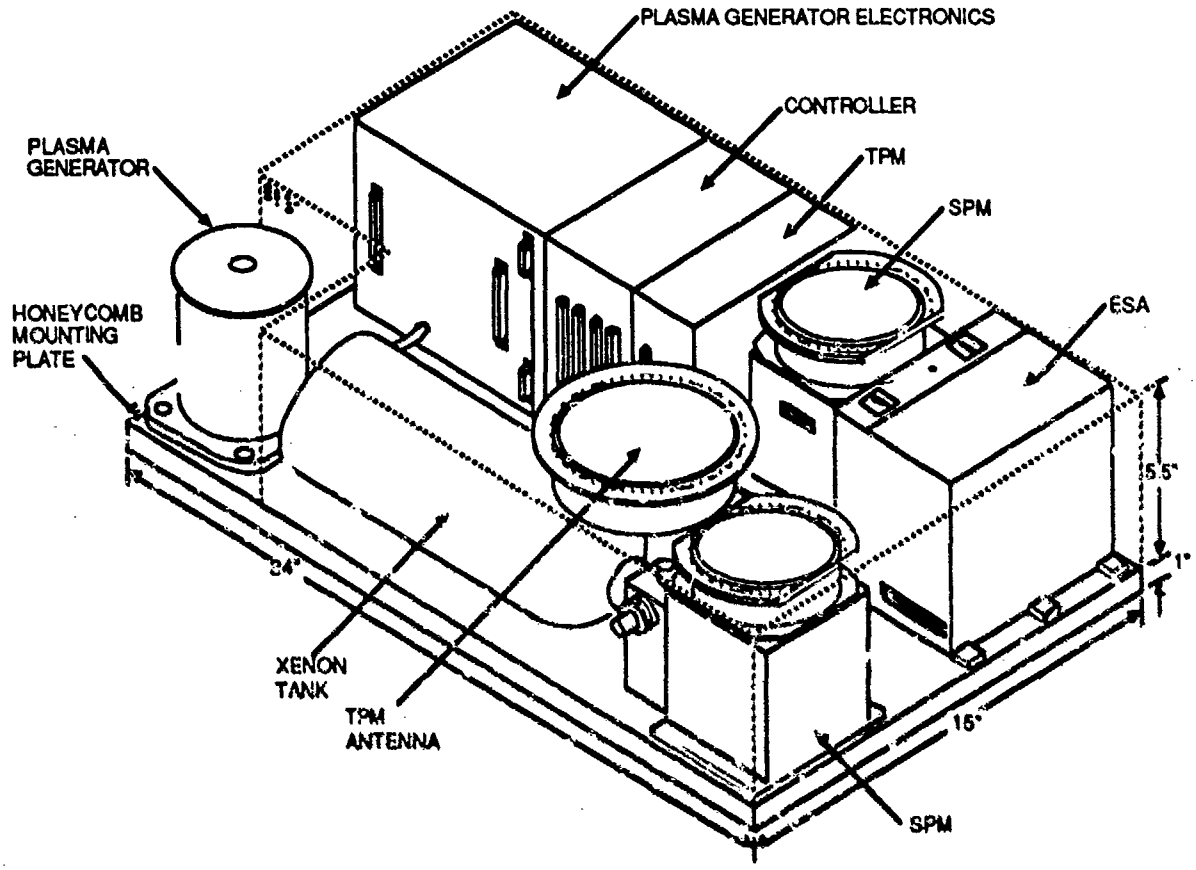

Figure A4-2. FMDS Layout

present in the "impossible region" of the spectrum with energies below that corresponding to the frame potential. Finally, the TPM identifies surface arcing by measuring the amplitude of electrical transients both inside and outside the Faraday cage of the spacecraft. If two signals are time-coincident, and the outside signal has large amplitude, it is judged to be the signature of an ESD event.

Table A4-2. FMDS Instrument Functions

Instr.	Property Measured	Charging Hazard
eESA	Electron energy spectrum	Substorm onset
iESA	Ion energy spectrum	Spacecraft charging
SPM	Potential of isolated dielectric	Differential charging
TPM	Electric field inside and outside spacecraft	Surface ESD

A4.9.2 FMDS Controller

The FMDS controller is a microprocessor-based device that serves three principal functions:

(1) it processes instrumental data to decide when a charging hazard is present,

(2) it turns the SPACECLAMP plasma contactor on and off as required, and

(3) it provides telemetry data to the spacecraft and accepts and executes commands received from the spacecraft.

The FMDS controller normally operates in a 4-second cycle, during which it acquires data from all of the instruments, executes algorithms to determine if a charging hazard is present, assures that the plasma contactor is in the desired operating mode, sends telemetry to the spacecraft if it is requested, and looks for commands being sent from the spacecraft. In this automatic mode, FMDS is completely autonomous, requiring no spacecraft or ground activity to protect the spacecraft from charging. A number of other modes are also available, which include the capability for manual operation of the SPACECLAMP plasma contactor from the ground.

Commands to the FMDS controller are used to change the operating mode, to power instruments up and down or mask them off from consideration in the charging algorithms, to change decision points and thresholds in the charging and SPACECLAMP-control algorithms, and, if desired, to rewrite the algorithms themselves. This command capability affords tremendous capability to fine-tune FMDS operations while it is in service on orbit.

A4.10 Concluding Comments

FMDS is a unique charging-control system which automatically monitors environmental signals that indicate the development of a charging hazard and activates the SPACECLAMP protective device in the event a hazard is detected. (SPACECLAMP is capable of ignition in less than a second; it is shut down after a preset time period if there is no remaining evidence of a charging environment.)

*U.S. GOVERNMENT PRINTING OFFICE: 1989-600-000/00031